Investigating Angiotensin II in Cardiac Remodelling and the Counter-Regulatory Actions of Angiotensin-(1-9)

Katrin Nather BSc(Hons) MRes

Submitted in fulfilment of the requirements for the degree of Doctor of Philosophy to the College of Medical, Veterinary and Life Sciences, University of Glasgow

Research conducted at the British Heart Foundation Glasgow Cardiovascular Research Centre, Institute of Cardiovascular and Medical Sciences, College of Medical, Veterinary and Life Sciences, University of Glasgow, U.K.

November 2016

Author's declaration

I declare that this thesis has been written entirely by myself and is a record of work performed by me at the University of Glasgow BHF Cardiovascular Research Centre in the Institute of Cardiovascular and Medical Sciences under the supervision of Dr Stuart A. Nicklin and Dr Christopher M. Loughrey. This thesis has not been submitted previously for a higher degree. A subset of *in vivo* data presented in this thesis was generated by Lauren Wills as part of an MRes student project. Histological sections and blood pressure data of 2 week low dose Ang II-infused mice were provided by Dr Monica Flores-Munoz and rat serum was provided by Dr Delyth Graham.

Acknowledgements

First and foremost, I would like to thank my supervisors Chris and Stu who have been fantastic supervisors and who have helped me throughout the years not only to develop as a scientist but also as a person. Thanks for always taking time to provide me with your help and guidance not only in scientific but also personal matters. I would also like to thank Professor Rhian Touyz for her help and guidance and for facilitating the many great opportunities for fundraising and public engagement I was able to take part in.

A big thank you also to everyone in the Level 4 lab who had to endure my frequent rants about cleanliness and tidiness. Thanks especially to Nicola and Gregor who done such a great job in managing the lab and helping out when I needed help. I wish you all the best for your future endeavours. Thanks to my office buddies Charlotte, Weihong, Caron and Ashley for the banter, help and support. A massive thank you to my bestie Lauren for the many evenings of hilarious banter and for helping me out during her Master's project. I hope I have been able to teach you some useful things!

Special thanks goes to my better half Kris whose endless patience and support especially while writing this thesis is beyond words. Thank you for putting up with my never-ending moaning that I am so stressed. One day, I won't be! Thank you also to Kris' family for their help and support throughout the years.

My final thanks goes to my family; my sister, Martin and little Emily and above all my parents without whom I would have never accomplished what I have today and who made it possible for me to move to Britain to study. I can only imagine how hard it must have been to let your child off to foreign lands. Thank you for your endless support in the good and bad times. This thesis is dedicated to you. I love you.

Table of contents

List of tables

List of figures

List of publications, presentations and awards

Publications

He W, McCarroll CS, **Nather K**, Elliott EBA, Nicklin SA, Loughrey CM. The cathepsin-L inhibitor CAA0225 protects against myocardial ischaemia-reperfusion injury. Heart 2015;101:A1 (Meeting Abstract)

McCarroll CS, He W, Foote KK, **Nather K**, Fattah C, Elliott EBA, Cochrane A, Bowman P, Bell M, Kubin T, Braun T, Nicklin SA, Cameron ER, Loughrey CM. Runx1 deficiency protects against adverse cardiac remodelling following myocardial infarction Heart 2015;101:A3 (Meeting Abstract)

Nather K, Flores-Muñoz M, Wills L, Touyz RM, Loughrey CM, Nicklin SA. Angiotensin-(1-9) Reverses Cardiac Dysfunction in a Model of Angiotensin II-Induced Hypertensive Heart Disease by Acting as a Positive Inotrope. Hypertension. 2015;66:AP109 (Meeting Abstract)

Nather K, Flores-Muñoz M, Touyz RM, Loughrey CM, Nicklin SA. Angiotensin II Mediates Microvascular Rarefaction In Vivo and Exacerbates Endothelial-To-Mesenchymal Transition In Vitro. Hypertension. 2015;66:AMP02 (Meeting Abstract)

Nather K, Flores-Muñoz M, Wills L, Touyz RM, Loughrey CM, Nicklin SA. Angiotensin-(1-9) reduces cardiac dysfunction in a model of angiotensin II-induced hypertensive heart disease. Heart. 2015;101:A108-A109 (Meeting Abstract)

McCarroll D, Elliott EB, **Nather K**, Morrison LJ, Loughrey CM. Extracellular cathepsin-L alters Ca2+ transient amplitude and sarcoplasmic reticulum Ca2+ content in adult rat cardiomyocytes. Biophysical Journal. 2013;104:436a (Meeting Abstract)

Presentations

Council on Hypertension 2015, Washington, DC, 16-19th September, 2015: Angiotensin-(1-9) reverses cardiac dysfunction in a model of angiotensin II-induced hypertensive heart disease by acting as a positive inotrope (Poster)

Angiotensin II mediates microvascular rarefaction in vivo and exacerbates endothelial-to-mesenchymal transition in vitro (Moderated poster)

Joint British Atherosclerosis/British Society of Cardiovascular Research Late Spring Meeting 2015, Manchester, United Kingdom, 8-9th June 2015: Angiotensin-(1-9) reduces cardiac dysfunction in a model of angiotensin II-induced hypertensive heart disease (Poster)

British Heart Foundation 4 Year PhD Student Conference, Cambridge, United Kingdom, 26th March 2015: Angiotensin-(1-9) reduces angiotensin II-induced cardiac dysfunction (Talk)

Awards

Council on Hypertension 2015, On site poster competition award winner.

Definitions/abbreviations

1/2 K 1/2 C	1/2 Kidney, 1/2 Clip
AA	Arachidonic acid
ACE	Angiotensin converting enzyme
ACE-I	Angiotensin converting enzyme inhibitor
Ang I	Angiotensin I
Ang II	Angiotensin II
Ang-(1-7)	Angiotensin-(1-7)
Ang-(1-9)	Angiotensin-(1-9)
ANP	Atrial natriuretic peptide
ARB	Angiotensin type 1 receptor blocker
AT_1R	Angiotensin type 1 receptor
AT_2R	Angiotensin type 2 receptor
BCA	Bicinchoninic acid
BFA	Brefeldin A
BNP	Brain natriuretic peptide
BP	Blood pressure
BSA	Bovine serum albumin
C21	Compound 21
CaMKII	Calcium-calmodulin kinase II
cAMP	Cyclic adenosine monophosphate
CD31	Cluster of differentiation 31
cGMP	Cyclic guanosine monophosphate
CHD	coronary heart disease
CICR	Ca^{2+} induced Ca^{2+} release
CNS	Central nervous system
Ct	Cycle threshold
CTGF	Connective tissue growth factor
CVD	Cardiovascular disease
Cx-43	Connexin-43
Cx-45	Connexin-45
DAG	Diacyglycerol
DDR2	Discoid domain receptor 2
DiI	1,1'-Dioctadecyl-3,3,3',3'-Tetramethylindocarbocyanine Perchlorate
DMEM	Dulbecco's Modified Eagle Medium

DMSO	Dimethyl sulfoxide
DOCA	Deoxycorticosterone acetate
dP/dt_{max}	Maximal rate of pressure increase
dP/dt_{min}	Maximal rate of pressure decrease
dsDNA	Double stranded DNA
EC	Endothelial cell
EC coupling	Excitation-contraction coupling
ECM	Extracellular matrix
EDTA	Ethylenediaminetetraacetic acid
EF	Ejection fraction
EGF	Epidermal growth factor
EGFR	Epidermal growth factor receptor
EGTA	Ethylene glycol-bis(ß-aminoethyl ether)-N,N,N',N'-tetraacetic acid
EMT	Epithelial-to-mesenchymal transition
EndMT	Endothelial-to-mesenchymal transition
eNOS	Endothelial nitric oxide synthase
ERK	Extracellular signal–regulated kinases
ESCRT	Endosomal sorting complex responsible for transport
ET-1	Endothelin-1
FAK	Focal adhesion kinase
FAM	Fluorescein amidite
FBS	Fetal bovine serum
FFR	Force–frequency relationship
FGF-1	Fibroblast growth factor 1
FITC	Fluorescein isothiocyanate
FS	Fractional shortening
FSP1	Fibroblast specific protein 1
GPCR	G-protein coupled receptor
GSK-3ß	Glycogen synthase kinase-3ß
HCAEC	Human coronary artery endothelial cells
HDAC	Histone deacetylase
HR	Heart rate
HEPES	4-(2-hydroxyethyl)-1-piperazineethanesulfonic acid
HF	Heart failure
HHD	Hypertensive heart disease
HRP	Horse radish peroxidase

Hsp	Heat shock protein
HW/TL	Heart weight/ tibia length
I_{Ca}	L-type Ca^{2+} current
ICAM-1	Intercellular Adhesion Molecule 1
IGF	Insulin-like growth factor
IGF-1R	Insulin-like growth factor 1 receptor
I_{k1}	Inward rectifier K^+ current
I_{kr}	Rapid delayed rectifier K^+ current
I_{ks}	Slow delayed rectifier K^+ current
IL-6	Interleukin 6
I_{Na}	Rapid Na^+ current
IP3	Inositol-1,4,5-trisphosphate
IRAP	Insulin-regulated aminopeptidase
I_{to}	Transient outward K^+ current
IVSd	Interventricular septum diastole
IVSs	Interventricular septum systole
JAK/STAT	Janus kinase/ signal transducers and activators of transcription
JNK	c-Jun N-terminal kinase
KH	Krebs-Henseleit
LA	Left atrium
LTBP	Latent TGFß binding protein
LV	Left ventricle
LVDP	Left ventricular developed pressure
LVEDD	Left ventricular end diastolic diameter
LVEDP	Left ventricular end diastolic pressure
LVESD	Left ventricular end systolic diameter
LVESP	Left ventricular end systolic pressure
LVFWd	Left ventricular free wall diastole
LVFWs	Left ventricular free wall systole
LVP	Left ventricular pressure
MAP	Mean arterial pressure
MAPK	Mitogen-activated protein kinase
MCP-1	Monocyte chemoattractant protein-1
MEF-2	Myocyte enhancer factor 2
MEK	MAPK/ERK kinase
MEM	Minimum essential medium

MI	Myocardial infarction
min	Minutes
MLCK	Myosin light chain kinase
MLP	Muscle LIM protein
MMP	Matrix metalloproteinase
MV	Microvesicle
MVB	Multivesicular body
NCD	Non-communicable disease
NCX	Sodium-calcium exchanger
NEP	Neutral endopeptidase , neprilysin
NFAT	Nuclear factor of activated T-cells
NFκb	Nuclear factor κb
NHE	Sodium hydrogen exchanger
NO	Nitric oxide
Nox	NADPH oxidase
NPR	Natriuretic peptide receptor
NRCF	Neonatal rat cardiac fibroblasts
NRCM	Neonatal rat cardiomyocytes
NTA	Nanoparticle tracking analysis
PBS(T)	Phosphate buffered saline (tween)
PDGF	Platelet derived growth factor
PDGFR	Platelet derived growth factor receptor
PDLIM5	PDZ And LIM Domain 5
PECAM-1	Platelet endothelial adhesion molecule-1
PFA	Paraformaldehyde
PGH2	Prostaglandin H2
PI3K	Phophoinositide 3-kinase
PKB	Protein kinase B
PKC	Protein kinase C
PKD	Protein kinase D
PKG	Protein kinase G
PLA2	Phospholipase A2
PLB	Phospholamban
PLC	Phospholipase C
POP	Prolylendopeptidase
PP	Protein phosphatase
PV-loop	Pressure-volume loop

qPCR	Quantitative polymerase chain reaction
RA	Right atrium
RAS	Renin-angiotensin-system
rhACE2	Recombinant human ACE2
ROS	Reactive oxygen species
RQ	Relative quantity
RV	Right ventricle
RyR	Ryanodine receptor
s	Seconds
SA node	Sinoatrial node
SEM	Standard error of the means
SERCA	Sarco/endoplasmic reticulum Ca2+-ATPase
SHR	Spontaneously hypertensive rat
SHRSP	Stroke prone spontaneously hypertensive rat
SM22-α	Smooth muscle 22-α
SORBS2	Sorbin And SH3 Domain Containing 2
SR	Sarcoplasmic reticulum
TAK1	TGFß activated kinase 1
TBS(T)	Tris-buffered saline (tween)
TGF	Transforming growth factor
TGFßRI	TGFß receptor I
ThxA2	Thromboxane A2
TIMP	Tissue inhibitors of metalloproteinase
Tlr4	Toll like receptor 4
TNF	Tumor necrosis factor
TOP	Thimet oligopeptidase
Tsp-1	Thrombospondin-1
VASP	Vasodilator-stimulated phosphoprotein
VE-cadherin	Vascular endothelial-cadherin
VEGF	Vascular endothelial growth factor
VSMC	Vascular smooth muscle cell
WGA	Wheat Germ Agglutinin
WKY	Wistar Kyoto rat
αMHC	α-myosin heavy chain
αSMA	α-smooth muscle actin
ßAR	ß-adrenergic receptor
ßMHC	ß-myosin heavy chain

Summary

Cardiovascular diseases (CVDs) including, hypertension, coronary heart disease and heart failure are the leading cause of death worldwide. Hypertension, a chronic increase in blood pressure above 140/90 mmHg, is the single main contributor to deaths due to heart disease and stroke. In the heart, hypertension results in adaptive cardiac remodelling, including LV hypertrophy to normalize wall stress and maintain cardiac contractile function. However, chronic increases in BP results in the development of hypertensive heart disease (HHD). HHD describes the maladaptive changes during cardiac remodelling which result in reduced systolic and diastolic function and eventually heart failure. This includes ventricular dilation due to eccentric hypertrophy, cardiac fibrosis which stiffens the ventricular wall and microvascular rarefaction resulting in a decrease in coronary blood flow albeit an increase in energy demand. Chronic activation of the renin-angiotensin-system (RAS) with its effector peptide angiotensin (Ang)II plays a key role in the development of hypertension and the maladaptive changes in HHD. Ang II acts via the angiotensin type 1 receptor (AT_1R) to mediate most of its pathological actions during HHD, including stimulation of cardiomyocyte hypertrophy, activation of cardiac fibroblasts and increased collagen deposition. The counter-regulatory axis of the RAS which is centred on the ACE2/Ang-(1-7)/Mas axis has been demonstrated to counteract the pathological actions of Ang II in the heart and vasculature. Ang-(1-7) *via* the Mas receptor prevents Ang II-induced cardiac hypertrophy and fibrosis and improves cardiac contractile function in animal models of HHD. In contrast, less is known about Ang-(1-9) although evidence has demonstrated that Ang-(1-9) also antagonises Ang II and is anti-hypertrophic and anti-fibrotic in animal models of acute cardiac remodelling. However, so far it is not well documented whether Ang-(1-9) can reverse established cardiac dysfunction and remodelling and whether it is beneficial when administered chronically. Therefore, the main aim of this thesis was to assess the effects of chronic Ang-(1-9) administration on cardiac structure and function in a model of Ang II-induced cardiac remodelling. Furthermore, this thesis aimed to investigate novel pathways contributing to the pathological remodelling in response to Ang II.

First, a mouse model of chronic Ang II infusion was established and characterised by comparing the structural and functional effects of the infusion of a low and

high dose of Ang II after 6 weeks. Echocardiographic measurements demonstrated that low dose Ang II infusion resulted in a gradual decline in cardiac function while a high dose of Ang II induced acute cardiac contractile dysfunction. Both doses equally induced the development of cardiac hypertrophy and cardiac fibrosis characterised by an increase in the deposition of collagen I and collagen III. Moreover, increases in gene expression of fibrotic and hypertrophic markers could be detected following high dose Ang II infusion over 6 weeks. Following this characterisation, the high dose infusion model was used to assess the effects of Ang-(1-9) on cardiac structural and functional remodelling in established disease.

Initially, it was evaluated whether Ang-(1-9) can reverse Ang II-induced cardiac disease by administering Ang-(1-9) for 2-4 weeks following an initial 2 week infusion of a high dose of Ang II to induce cardiac contractile dysfunction. The infusion of Ang-(1-9) for 2 weeks was associated with a significant improvement of LV fractional shortening compared to Ang II infusion. However, after 4 weeks fractional shortening declined to Ang II levels. Despite the transient improvement in cardiac contractile function, Ang-(1-9) did not modulate blood pressure, LV hypertrophy or cardiac fibrosis.

To further investigate the direct cardiac effects of Ang-(1-9), cardiac contractile performance in response to Ang-(1-9) was evaluated in the isolated Langendorff-perfused rat heart. Perfusion of Ang-(1-9) in the paced and spontaneously beating rat heart mediated a positive inotropic effect characterised by an increase in LV developed pressure, cardiac contractility and relaxation. This was in contrast to Ang II and Ang-(1-7). Furthermore, the positive inotropic effect to Ang-(1-9) was blocked by the AT_1R antagonist losartan and the protein kinase A inhibitor H89.

Next, endothelial-to-mesenchymal transition (EndMT) as a novel pathway that may contribute to Ang II-induced cardiac remodelling was assessed in Ang II-infused mice *in vivo* and in human coronary artery endothelial cells (HCAEC) *in vitro*. Infusion of Ang II to mice for 2-6 weeks resulted in a significant decrease in myocardial capillary density and this was associated with the occurrence of dual labelling of endothelial cells for endothelial and mesenchymal markers. *In vitro* stimulation of HCAEC with TGFβ and Ang II revealed that Ang II

exacerbated TGF-induced gene expression of mesenchymal markers. This was not correlated with any changes in SMAD2 or ERK1/2 phosphorylation with co-stimulation of TGFβ and Ang II. However, superoxide production was significantly increased in HCAEC stimulated with Ang II but not TGFβ.

Finally, the role of Ang II in microvesicle (MV)-mediated cardiomyocyte hypertrophy was investigated. MVs purified from neonatal rat cardiac fibroblasts were found to contain detectable Ang II and this was increased by stimulation of fibroblasts with Ang II. Treatment of cardiomyocytes with MVs derived from Ang II-stimulated fibroblasts induced cardiomyocyte hypertrophy which could be blocked by the AT_1R antagonist losartan and an inhibitor of MV synthesis and release brefeldin A. Furthermore, Ang II was found to be present in MVs isolated from serum and plasma of Ang II-infused mice and SHRSP and WKY rats.

Overall, the findings of this thesis demonstrate for the first time that the actions of Ang-(1-9) in cardiac pathology are dependent on its time of administration and that Ang-(1-9) can reverse Ang II-induced cardiac contractile dysfunction by acting as a positive inotrope. Furthermore, this thesis demonstrates evidence for an involvement of EndMT and MV signalling as novel pathways contributing to Ang II-induced cardiac fibrosis and hypertrophy, respectively. These findings provide incentive to further investigate the therapeutic potential of Ang-(1-9) in the treatment of cardiac contractile dysfunction in heart disease, establish the importance of novel pathways in Ang II-mediated cardiac remodelling and evaluate the significance of the presence of Ang II in plasma-derived MVs.

Chapter 1 – General Introduction

1.1 The heart

The heart is a two-sided pump that operates in series to distribute blood across all organs. The right pump consists of the right atrium (RA) and ventricle (RV) which deliver blood into the pulmonary circulation for oxygenation. The oxygenated blood then enters the left atrium (LA) and is propelled through the systemic circulation via the left ventricle (LV) (the left pump). Cardiac contraction is initiated by electrical impulses from specialised cells residing in the sinoatrial node located in the RA. In a concerted manner, the impulse then travels through the cardiac muscle leading to cardiac contraction (Boulpaep, 2009). The cardiac muscle is composed of cardiomyocytes, the primary contractile cells providing the mechanical force necessary for cardiac contraction. Although cardiomyocytes occupy the bulk volume of the entire myocardium, they only account for up to one third of the cell population in the adult human heart with cells such as fibroblasts, endothelial cells (ECs) and vascular smooth muscle cells (VSMC) accounting for the remainder (Vliegen *et al.*, 1991). The cell populations in the heart are dynamically regulated by environmental factors and differ between species with larger animals proposed to have a smaller proportion of cardiomyocytes and a larger number of fibroblasts (Banerjee *et al.*, 2007). As such the adult rat heart consists of 27 % cardiomyocytes, 63 % fibroblasts and 5 % other cell types (such as ECs and VSMCs) (Banerjee *et al.*, 2007) while a recent study has demonstrated that the mouse heart contains 32 % cardiomyocytes, 12 % fibroblasts, 55 % ECs and 5% VSMCs (Pinto *et al.*, 2016). Cardiac fibroblasts are the main cell type involved in the maintenance of the extracellular matrix (ECM) providing a structural network ensuring proper cardiac form and function (Souders *et al.*, 2009). ECs and VSMCs form the network of coronary blood vessels which ensure adequate delivery of nutrients and oxygen to the cardiomyocytes. Due to its vital function in maintaining blood flow, oxygen and nutrient supply to all organs within the body, cardiovascular diseases (CVDs) with failure of the heart as a pump are some of the most common causes of morbidity and mortality. Understanding the physiological processes that maintain normal cardiac function and the pathophysiological processes contributing to CVDs is essential for developing novel therapies to maintain pump function.

1.2 Cardiovascular Disease

In 2012, CVDs including coronary heart disease (CHD), cerebrovascular disease, hypertension and heart failure (HF) were the leading cause of death amongst non-communicable diseases (NCD) accounting for 46.2 % of all NCD deaths (WHO, 2014b). Amongst CVDs, hypertension is one of the most common risk factors for premature death around the world. It is estimated that complications of hypertension accounted for approximately 45 % of deaths due to heart disease and stroke (WHO, 2013, WHO, 2014b).

1.2.1 Hypertension

Hypertension is defined as repeatedly elevated blood pressure (BP) above 140/90 mmHg. New guidelines have classified the severity of hypertension into stages according to which treatment is administered: pre-hypertensive (>120/80 mmHg), Stage 1 (≥140/90 mmHg), Stage 2 (≥160/100 mmHg) and severe hypertension (≥180/110 mmHg). People diagnosed with stage 1 or stage 2 hypertension generally require confirmation of BP *via* repeat measures and ambulatory monitoring before anti-hypertensive treatment is administered while patients with severe hypertension receive treatment at the time of presentation (Nadella and Howell, 2015). The World Health Organisation estimated that in 2008 approximately 40 % of people aged over 25 were diagnosed with hypertension which was equivalent to approximately 1 billion people worldwide (WHO, 2013). World health statistics in 2014 estimated the global prevalence of hypertension as 23.4 % in men and 24 % in women (WHO, 2014a). Albeit the general notion that CVDs are diseases of high-income countries, hypertension is most prevalent in low- and middle-income countries where the risk of death due to CVDs is more than double that of high-income countries (WHO, 2014b). The prevalence of hypertension increases with age and it has been estimated that approximately 90 % of people who are normotensive at the age of 55-65 will develop hypertension by the age of 80-85 (Vasan *et al.*, 2002, Burt *et al.*, 1995).

Hypertension is a multifactorial disease and depending on the underlying cause for high BP can be classified either as essential or secondary hypertension involving either primary largely unidentified genetic and environmental predispositions or secondary identifiable underlying causes. Essential

hypertension accounts for approximately 95 % of all cases of hypertension while hypertension secondary to other diseases accounts for the remainder. Essential hypertension is defined as hypertension of unknown cause and is thought to occur as a result of genetic predisposition and environmental factors such as obesity, high alcohol or salt intake, smoking, diabetes and aging (Carretero and Oparil, 2000). In most cases hypertension can be controlled effectively by non-pharmacological methods such as changes in lifestyle and pharmacologically by anti-hypertensive medication. However, approximately 15-30 % of patients with hypertension suffer from resistant hypertension where BP remains uncontrolled despite extensive anti-hypertensive therapy (Pimenta and Calhoun, 2012). Resistant hypertension is defined as an increased BP above 140/90 mmHg despite treatment with at least three anti-hypertensive drugs which normally include an angiotensin converting enzyme-inhibitor (ACE-I) or angiotensin type 1 receptor blocker (ARB) (Section 1.3.5), a calcium channel blocker and a thiazide diuretic (Myat *et al.*, 2012). The risk of developing an adverse cardiovascular event is doubled in patients with resistant hypertension compared to patients with controlled BP highlighting the need for new anti-hypertensive strategies to tackle resistant hypertension in the population (Daugherty *et al.*, 2012). Chronic elevations in BP lead to progressive development of end organ damage predominantly affecting the heart, kidney, brain, blood vessels and the eye and may result in severe consequences such as heart and renal failure (Nadella and Howell, 2015). In the heart, hypertension predisposes to the development of hypertensive heart disease (HHD) which contributes to the progression to HF.

1.2.2 Hypertensive heart disease

HHD describes the structural changes in the heart in response to chronic increases in BP. Classically, the development of HHD is thought of as the thickening of the LV wall and an increase in LV mass resulting in diastolic dysfunction. Subsequently, after a series of remodelling events in the heart, the LV dilates, ejection fraction (EF) decreases and HF develops (Drazner, 2011). However, it is now recognised that concomitant with an increase in LV mass during HHD there is a significant degree of cardiac fibrosis and microvascular disease resulting in increased cardiac stiffness, diastolic dysfunction and decreased coronary blood flow whilst there is an increase in cardiac oxygen demand (Frohlich *et al.*, 1992, Frohlich, 1999). The adverse remodelling in

response to hypertension is equally influenced by haemodynamic and non-haemodynamic factors which include genetic influences and neurohormonal systems. In particular, the renin-angiotensin-system (RAS) is of special interest due to the ability of pharmacological antagonists of the RAS to mediate regression of LV hypertrophy in HHD.

The incidence of LV hypertrophy is directly related to the incidence of hypertension although only 15-20 % of hypertensive patients present with LV hypertrophy on echocardiographic assessment (Levy *et al.*, 1990). Next to age, LV hypertrophy is a strong predictor of adverse cardiovascular outcomes in patients with hypertension. The Framingham study has demonstrated that the relative risk for development of subsequent CVD was 1.49 and 1.57 for every 50 g/m increment in LV mass for men and women, respectively (Levy *et al.*, 1990). The risk of death due to CVD doubled in patients with LV hypertrophy and similarly, LV hypertrophy significantly increases the risk of ventricular arrhythmias, cerebrovascular disease and sudden death (Levy *et al.*, 1990, Verdecchia *et al.*, 2001, Levy *et al.*, 1987). In particular, chronic untreated HHD is thought to predispose to the development of HF which may manifest as diastolic (congestive) or systolic HF, both of which have been demonstrated in advanced models of HHD (Brooks *et al.*, 2010, Regan *et al.*, 2015).

1.2.3 Heart Failure

HF is classically described as the inability of the heart to produce an adequate cardiac output for the perfusion of peripheral organs and the failure to accommodate venous return (Kemp and Conte, 2012). Compensatory mechanisms to maintain tissue perfusion include increasing cardiac output *via* the Frank-Starling mechanism, neurohormonal activation to increase mean arterial pressure (MAP) and cardiac remodelling to accommodate the increasing stresses on the heart. Although initially compensatory, these changes quickly become maladaptive and participate in a vicious cycle of worsening HF (Kemp and Conte, 2012). HF is associated with a poor prognosis with a 5-year mortality rate of approximately 65 % (Jhund *et al.*, 2009). HF can be subdivided into two categories, systolic and diastolic HF which affects 60 % and 40 % of patients with HF, respectively (Federmann and Hess, 1994). Systolic HF and diastolic HF are predominantly distinguished by EF where an EF ≤40 % indicates systolic

dysfunction and an EF ›40 % may indicate diastolic dysfunction and describes HF patients with preserved EF (Kemp and Conte, 2012). Systolic HF is generally caused by the loss of functional myocardium usually seen in ischaemic heart disease or after a myocardial infarction (MI). This leads to a reduction in cardiac output and general hypoperfusion (Federmann and Hess, 1994). Additionally, due to impaired myocardial contraction, there is an increase in ventricular volume and LV end diastolic pressure (LVEDP) which in turn increases the pressure in the pulmonary capillaries resulting in pulmonary congestion and the typical signs of HF (Kemp and Conte, 2012). LV systolic dysfunction may also be a result of chronic uncontrolled BP although it has only been observed in late stage HHD (Vasan and Levy, 1996). In contrast, hypertension and HHD are a major cause of diastolic dysfunction and subsequent diastolic HF and can be found in 90 % of patients with LV hypertrophy (Mandinov *et al.*, 2000). In diastolic HF, the passive stiffness of the ventricle is significantly increased resulting in impaired relaxation and early filling of the ventricle during diastole (Zile *et al.*, 2004). This leads to a reduction in LV end diastolic volume with increased LVEDP resulting in a decreased stroke volume and decreased cardiac output. Additionally, atrial enlargement and impaired atrial contractile function further contribute to the reduction in cardiac output in advanced stages of the disease (Mandinov *et al.*, 2000).

1.3 The classical renin-angiotensin-system

The classical RAS is an important endocrine system involved in the acute regulation of BP, renal function, fluid and electrolyte balance. Renin was first discovered more than 100 years ago as a heat labile substance in kidney extracts that led to a sustained increase in BP (Tigerstedt and Bergman, 1898). It was later identified that not renin but a pressor substance other than renin mediated acute increases in BP and this lead to the discovery of Angiotensin I (Ang I) and Ang II (then called hypertensin) in 1954 (Skeggs *et al.*, 1954). The discovery of the enzyme responsible for Ang II formation, ACE, soon thereafter established the concept of the RAS as a single system involved in the regulation of BP and fluid balance (Skeggs *et al.*, 1956). Since then our understanding of the RAS has expanded greatly and it is now recognised that next to its function in BP regulation, the RAS participates in numerous other physiological processes including digestive, neuronal, sensory, dermal and immune functions (Paul *et*

al., 2006). Next to its physiological actions, extensive research on the RAS and its effector Ang II has also documented its involvement in a wide range of diseases, particularly CVDs including hypertension, CHD, HF, MI and kidney disease (Nicholls and Robertson, 2000). In this aspect, the development of ARBs and ACE-I in the 1980s is termed as one of the greatest advances in cardiovascular medicine whose impact still persists until today (Ferrario, 2006).

The classical enzymatic cascade of the endocrine RAS begins with the release of renin into the circulation from juxtaglomerular cells triggered in response to a decrease in renal perfusion pressure. Renin then cleaves liver-derived angiotensinogen to form the decapeptide Ang I which then in turn is cleaved by ACE predominantly located in the lung epithelium to form Ang II (Figure 1-1).

The discovery of RAS components in various tissues, including the heart, kidney and brain have led to the characterisation of local tissue-specific RAS that acts independently of the endocrine systemic RAS (Paul *et al.*, 2006). In this respect, independent Ang II forming systems involving cathepsin G, kallikrein and chymase have been described in tissues including the heart, kidney, blood vessels and immune cells which are distinct from the renin- and ACE-dependent systemic formation of Ang II in the regulation of BP (Urata *et al.*, 1990b, Owen and Campbell, 1998, Rykl *et al.*, 2006, Ihara *et al.*, 1999, Sasaguri *et al.*, 1995). Thus, for example, in human blood vessels it is estimated that 60 % of the generated Ang II is derived *via* non-ACE pathways and in the human heart, the serine protease chymase accounts for up to 80 % of the locally produced Ang II (Urata *et al.*, 1990a, Urata *et al.*, 1990b, Okunishi *et al.*, 1993).

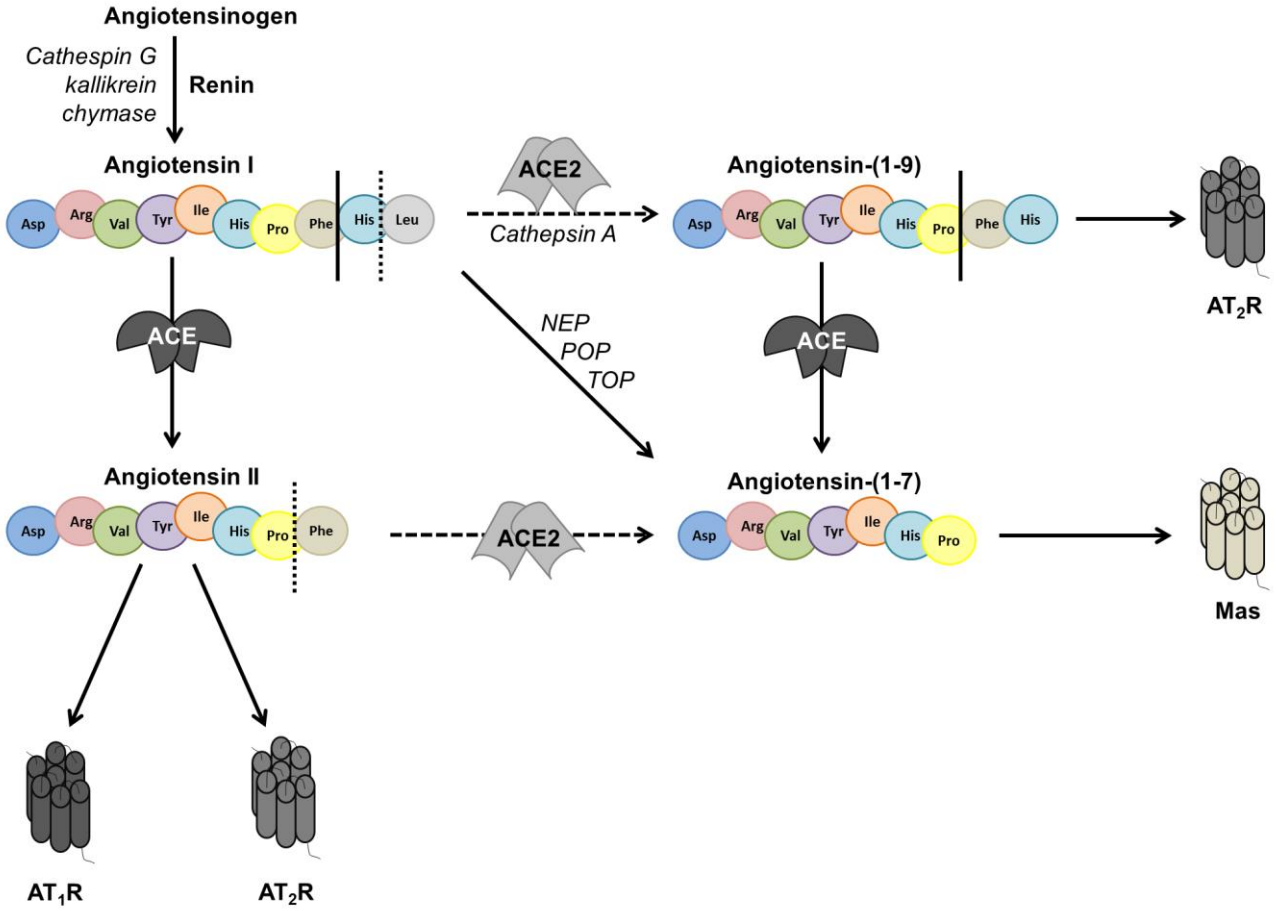

Figure 1-1. The classical and counter-regulatory RAS.
In the classical RAS, renin converts angiotensinogen to Ang I which is then further cleaved by ACE to form Ang II. Ang II can then act either on the AT_1R or the AT_2R. In the counter-regulatory axis, ACE2 cleaves Ang I and Ang II to form Ang-(1-9) and Ang-(1-7), respectively. Ang-(1-7) binds the Mas receptor while Ang-(1-9) binds the AT_2R. Alternative pathways for the production of Ang I, Ang-(1-7) and Ang-(1-9) exist. Ang-(1-7)= angiotensin-(1-7), Ang-(1-9)= angiotensin-(1-9), Ang I= angiotensin I, Ang II= angiotensin II, AT_1R= angiotensin type 1 receptor, AT_2R= angiotensin type 2 receptor, NEP= neprilysin, POP= prolyl endopeptidase, TOP= thimet oligopeptidase.

1.3.1 ACE

ACE was first isolated in 1956 and was then termed hypertensin converting enzyme (Skeggs *et al.*, 1956). ACE is a zinc dipeptidyl carboxypeptidase and mediates the formation of Ang II from Ang I by the cleavage of the His-Leu dipeptide from the C-terminus. ACE is the major enzyme for the systemic conversion of Ang I to Ang II (Urata *et al.*, 1990a), however, unlike renin, ACE is not substrate-specific and can cleave other substances such as bradykinin, ß-amyloid and gonadotropin-releasing hormone (Bernstein *et al.*, 2013). Ang II is not cleaved further by ACE and acts as a natural inhibitor providing an additional regulatory mechanism to maintain adequate Ang II levels (Masuyer *et al.*, 2012). In mammals, two distinct isoforms of ACE exist, the somatic tissue ACE (sACE) and germinal ACE (gACE) that is solely expressed in male testes. Although derived from the same gene, sACE has two active sites while gACE only consists of a single active site which is achieved by different promoter activities (Coates, 2003). sACE is an ectoenzyme and is anchored to the plasma membrane *via* a C-terminal transmembrane domain although ACE may also be shed from the plasma membrane by the action of secretases (Coates, 2003). ACE mRNA can be detected in all major tissues (Rivière *et al.*, 2005); it is however particularly abundant in pulmonary ECs, the intestine and renal brush border membranes (Fuchs *et al.*, 2008, Rivière *et al.*, 2005). The two catalytic sites in sACE are formed by the N- and C-domains which share approximately 55 % sequence identity (Bernstein *et al.*, 2013). Importantly, the enzymes differ in the substrate specificities. Both domains bind and hydrolyse bradykinin with equal efficiencies. Although both domains also bind Ang I with equal affinities, the C-domain has a 3x higher catalytic activity making it the major site of Ang I conversion (Wei *et al.*, 1991).

1.3.2 Ang II

Ang II is the octapeptide formed by the cleavage of the terminal His-Leu residues from Ang I *via* ACE. Circulating plasma Ang II levels in humans vary widely, ranging between 5-50 pg/mL (Roig *et al.*, 2000, van Kats *et al.*, 1997, Vilas-Boas *et al.*, 2009). The half-life of Ang II is estimated to be 30 s, however Ang II can be accumulated in tissues such as the heart, kidney and adrenal glands and this prolongs its half-life to approximately 15 min due to protection from endothelial

proteases (van Kats *et al.*, 1997). Ang II has pleiotropic effects in a variety of tissues that concertedly contribute to the physiological regulation of BP. When renal perfusion pressure falls, renin is released from the kidney to initiate the regulation of BP to normalise renal blood flow. Thus, in the vasculature, Ang II causes vasoconstriction of small arteries raising total peripheral resistance. In the kidney, Ang II stimulates increased renal sodium re-absorption *via* the release of aldosterone from the adrenal glands. Additionally, the Ang II-induced release of anti-diuretic hormone from the pituitary gland stimulates anti-diuresis (Kaschina and Unger, 2003). These concerted actions result in an increase in blood volume and BP which in turn normalises renal perfusion and decreases renin release, restoring homeostasis. In the heart, Ang II increases cardiac contractility and heart rate (HR), however, long term stimulation of cardiomyocytes by Ang II over days and weeks results in cardiac hypertrophy (Masaki *et al.*, 1998, Gusev *et al.*, 2009). Ang II mediates its effects by binding to two distinct receptors, the angiotensin type 1 receptor (AT_1R) or the angiotensin type 2 receptor (AT_2R). Both receptors are seven transmembrane G-protein coupled receptors (GPCRs), however, they differ substantially in their signal transduction pathways and physiological outcomes (Sections 1.3.3& 1.3.4). Ang II mediates most of its physiological and pathological effects *via* the AT_1R while signalling through the AT_2R counteracts these responses (Table 1-1).

Table 1-1.Physiological actions of the angiotensin receptors

AT_1R	AT_2R
Vasoconstriction	Vasodilation
Salt/water retention	Decreased proliferation
Aldosterone release	Apoptosis
Sympathetic facilitation	Natriuresis
Cell growth/proliferation	Cell differentiation
Stimulation of thirst	

1.3.3 Angiotensin type 1 receptor

The AT_1R is a 41 kDa seven-transmembrane GPCR located on chromosome 3 in humans (Dinh *et al.*, 2001). In contrast, rodents possess two isoforms of the AT_1R, the AT_1R_{1A} and the AT_1R_{1B} which are located on chromosome 17 and 2 respectively and share 94 % sequence homology (Iwai and Inagami, 1992, Lewis *et al.*, 1993). The AT_1R_{1A} is widely expressed in the kidney, lungs, heart, brain, vasculature and liver while the AT_1R_{1B} is confined to endocrine organs such as the adrenal gland, the pituitary gland and testes (Gasc *et al.*, 1994, Martin *et al.*, 1995). Pharmacologically, the two receptors are indistinguishable (Martin *et al.*, 1995) and knockout experiments *in vivo* have demonstrated that the receptors may largely be functionally redundant although the AT_1R_{1A} is the predominant form involved in the regulation of BP (Chen *et al.*, 1997, Ito *et al.*, 1995). Di-sulphide bridge formation between four cysteine residues in the extracellular domain of the receptor is crucial for the tertiary structure of the receptor and the transmembrane domain and extracellular loop are important for Ang II binding to the receptor (Dinh *et al.*, 2001). The cytoplasmic tail contains numerous serine and threonine phosphorylation sites which play an important role in the modulation and internalisation of the AT_1R. Like many other GPCRs, the AT_1R is subject to desensitisation following stimulation. This process involves the phosphorylation of the AT_1R by G protein kinases followed by the recruitment of ß-arrestins (commonly ß-arrestin 1 and ß-arrestin 2) and the internalisation of the agonist-receptor complex into clathrin coated pits (Rajagopal *et al.*, 2010). The AT_1R is recycled back to the cell membrane while Ang II is targeted to lysosomes (Hein *et al.*, 1997). Uncoupling of the receptor from G protein signalling occurs rapidly within seconds to minutes and following 10 min Ang II stimulation, receptor density may decrease by 50 % before reaching a new steady-state (Hein *et al.*, 1997, Guo *et al.*, 2001). Expression of the AT_1R is under tight regulation by its agonist Ang II and while acute stimulation may lead to an increase in AT_1R expression, chronic Ang II stimulation leads to receptor down-regulation (Ichihara *et al.*, 2001, Lassègue *et al.*, 1995, Ichiki *et al.*, 2001). Numerous growth factors and cytokines such as epidermal growth factor (EGF), Nitric oxide (NO), mineralocorticoids and low density lipoprotein have been shown to affect AT_1R expression which may contribute to disease processes in various disorders (Kaschina and Unger, 2003).

Activation of the AT_1R by Ang II results in the activation of signalling cascades that are either G protein dependent ($G_{q/11}$, G_i and $G_{12/13}$) or G protein independent (Hunyady and Catt, 2006) (Table 1-2). However, as more data emerges distinctions between signalling pathways have become blurred highlighting the complex inter-related signalling cascades that are activated upon AT_1R stimulation. Additionally, AT_1R signal transduction and the resulting physiological and pathological effects have become increasingly complex with the characterisation of receptor transactivation cascades and homo- and heterodimer formation. In monocytes, Factor XIIIA transglutaminase mediates cross-linking of AT_1R resulting in enhanced Ang II signal transduction which may contribute to atherosclerosis development (AbdAlla *et al.*, 2004). In contrast, the formation of heterodimers with the AT_2R counteracts Ang II signalling through the AT_1R (AbdAlla *et al.*, 2001). Heterodimer formation has also been reported with the bradykinin B_2 receptor which enhanced AT_1R G protein activation and has been suggested to contribute to hypersensitivity to the vasopressor effects of Ang II in various CVDs (AbdAlla *et al.*, 2000). AT_1R-ß-adrenergic receptor (ßAR) complexes have also been observed and inhibition of either receptor with specific antagonists resulted in diminished responsiveness of either receptor (Barki-Harrington *et al.*, 2003). Furthermore, in VSMC Ang II mediates the transactivation of EGF receptors (EGFR), platelet derived growth factor receptor (PDGFR) and Insulin-like growth factor 1 receptor (IGF-1R) and it has been demonstrated that their activation is indispensable for Ang II-induced VSMC proliferation, hypertrophy and redox-signalling (Kelly *et al.*, 2004, Touyz *et al.*, 2003, Bokemeyer *et al.*, 2000, AbdAlla *et al.*, 2005).

Table 1-2. AT_1R signalling pathways.

Target	Second messenger	Pathways	Effect	References
PLC	IP_3, DAG, PKC, Ca^{2+}	MLCK phosphorylation Na^+/H^+ phosphorylation ↑PI3K, ↑ERK1/2 ↑*c-fos, c-jun, c-myc, Egr-1*	Vasoconstriction Cell proliferation ↑Cardiac contractility	(Liang *et al.*, 2010) (Kanaide *et al.*, 2003) (Sadoshima and Izumo, 1993b) (Mehta and Griendling, 2007) (Olson *et al.*, 2008)
PLD	phosphatidic acid, DAG, PKC,	Ca^{2+} mobilisation NADPH oxidation Activation of tyrosine kinases	Vasoconstriction VSMC proliferation Aldosterone secretion	(Qin *et al.*, 2010) (Touyz and Berry, 2002)
PLA_2	AA, prostaglandins (PGI_2, PGE_2), $ThxA_2$, PGH_2	MAPK activation Ca^{2+} mobilisation	Vasodilation/Vasoconstriction Cell proliferation	(Dulin *et al.*, 1998) (Touyz and Berry, 2002) (Griendling *et al.*, 1994)
Nox (Nox1, Nox2, Nox4)	ROS	NO scavenger ↑NFkb, ↑AP1, ↑Nrf2 ↑p38 MAPK/ERK/JNK	Inflammation Hypertrophy	(Drummond and Sobey, 2014) (Griendling *et al.*, 1994)
ß-arrestins		↑Src/eNOS/MAPK	↓ Blood pressure ↑Cardiac contractility	(Violin *et al.*, 2010) (Tohgo *et al.*, 2002)
Tyrosine kinases (Src, FAK, Pyk2 PDGFR, EGFR, IGFR		↑Ras/Raf/MAPK ↑PLC ↑Akt/PKB ↑p38 MAPK	Cytoskeletal reorganisation Focal adhesion formation Cell migration Cell proliferation	(Hunyady and Catt, 2006) (Bokemeyer *et al.*, 2000) (Kelly *et al.*, 2004)
Jak/STAT		↑*c-fos, c-jun, c-myc, Erg-1, VL-30*	Cardiac hypertrophy Inflammation VSMC proliferation Angiotensinogen synthesis	(Marrero *et al.*, 1995) (Booz *et al.*, 2002)

1.3.4 Angiotensin type 2 receptor

The AT_2R is a 41 kDa seven transmembrane receptor encoded by the *Agtr2* gene located on the X chromosome both, in humans and rodents (Dinh *et al.*, 2001). The receptor binds Ang II with equal affinity to the AT_1R (Flores-Muñoz *et al.*, 2011), however, it only shares 34 % sequence homology with the AT_1R and belongs to the group of atypical seven transmembrane receptors that predominantly signal independently of G proteins (Mukoyama *et al.*, 1993). The AT_2R is highly expressed during foetal development but expression rapidly decreases postnatally and in the adult, AT_2R can predominantly be detected in the heart, brain, adrenal glands and kidney (Mukoyama *et al.*, 1993, Wang *et al.*, 1998). AT_2R expression is re-activated during cardiac pathology such as MI, HF and atherosclerosis (Nio *et al.*, 1995, Tsutsumi *et al.*, 1998, Sales *et al.*, 2005). Factors that may contribute to this upregulation are insulin and IGF while growth factors such as PDGF and EGF downregulate AT_2R expression (Kambayashi *et al.*, 1996). Similarly, Ang II negatively regulates AT_2R expression (Ouali *et al.*, 1997). Unlike the AT_1R, the AT_2R does not get internalised upon agonist binding and can demonstrate constitutive activation (Hein *et al.*, 1997, Widdop *et al.*, 2002). The physiological actions of the AT_2R antagonise Ang II signalling through the AT_1R and as such it has been demonstrated to mediate vasodilation, natriuresis, negative inotropic and chronotropic effects (Castro-Chaves *et al.*, 2008, Kemp *et al.*, 2014, Tsutsumi *et al.*, 1999). The signalling cascades activated by the AT_2R are diverse but are so far not well understood. Three main signalling cascades have been proposed to be activated by the receptor: NO release and cyclic guanosine monophosphate (cGMP) formation, phospholipase A_2 (PLA_2) stimulation and protein phosphatase activation (Table 1-3). In similarity to the AT_1R, the AT_2R has also been demonstrated to form heterodimers with the B_2 receptor which modulates phosphoprotein signalling leading to an enhancement of NO and cGMP synthesis (Abadir *et al.*, 2006). Heterodimer formation with the AT_1R inhibits AT_1R signalling and decreased heterodimer formation correlates with an increase in Ang II sensitivity (AbdAlla *et al.*, 2001). Investigations of Ang II binding to the AT_2R revealed that Ang II binding is not dependent on specific ligand-receptor interactions and the receptor exists in a “relaxed” state suggestive of a constitutively active receptor (Miura and Karnik, 1999). This was confirmed in VSMC and epithelial cells where AT_2R expression mediated cellular apoptosis independently of Ang II (Miura and Karnik, 2000).

Despite the demonstration that activation of the AT_2R antagonises the pathological signalling of Ang II at the AT_1R, the role of the AT_2R in CVD remains unclear as studies investigating the loss or gain of function of AT_2R have demonstrated controversial results. Thus, ventricular specific overexpression of the AT_2R induced dilated cardiomyopathy characterised by a decrease in cardiac contractile function, significant chamber dilation and cardiomyocyte hypertrophy (Yan *et al.*, 2003). This was found to be due to the chronic activation of signalling pathways involved in pathological hypertrophy and HF, including protein kinase c (PKC)-α, PKC-ß, extracellular signal-regulated kinase (ERK)1/2 and $p70^{s6k}$ (Yan *et al.*, 2003). Additionally, isolated cardiomyocytes showed a significant depression in fractional shortening (FS) concomitant with a decrease in peak Ca^{2+} amplitude which was accompanied by a significant increase in phospholamban (PLB) expression and a decrease in the sarco/endoplasmic reticulum Ca^{2+} ATPase (SERCA)/PLB ratio (Nakayama *et al.*, 2005). Cardiomyocytes of AT_2R overexpressing mice are generally found to be larger compared to those of wildtype littermates (Nakayama *et al.*, 2005, Yan *et al.*, 2003). *In vitro* overexpression of the AT_2R in neonatal cardiomyocytes using adenoviral-mediated gene transfer caused constitutive growth of cardiomyocytes in the absence of ligand that was resistant to inhibition by the AT_2R antagonist PD123319 or the mitogen-activated protein kinase (MAPK) inhibitor PD98059 (D'Amore *et al.*, 2005). Previously, Senbonmatsu *et al.* (2003) proposed a novel AT_2R signalling pathway mediating cardiomyocyte hypertrophy *in vivo* and *in vitro* (Senbonmatsu *et al.*, 2003). This involves the activation of the promyelocytic zinc finger protein by the AT_2R which results in the increased expression of p85α, phosphoinositide 3-kinase (PI3K) and $p70^{s6k}$ (Senbonmatsu *et al.*, 2003). A role for the AT_2R in cardiac hypertrophy was also confirmed in *Agtr2* knockout mice which failed to increase cardiomyocyte size following chronic pressure overload and Ang II infusion potentially through a decrease in $p70^{s6k}$ (Senbonmatsu *et al.*, 2000, Ichihara *et al.*, 2001). Interestingly, cardiac fibrosis was also absent in *Agtr2*$^{-/Y}$ mice, suggesting a role for the AT_2R in collagen deposition.

In contrast, in a different strain of mice with cardiac specific overexpression of the AT_2R, the AT_2R abolished Ang II-induced cardiac fibrosis but not cardiac hypertrophy *via* activation of the bradykinin-NO system (Kurisu *et al.*, 2003).

Similarly, lentiviral-mediated overexpression of the AT_2R postnatally prevented Ang II-mediated increases in ventricular wall thickness and interstitial fibrosis while the fibrotic response to aortic banding was exacerbated in *Agtr2*$^{-/y}$ mice (Falcón *et al.*, 2004, Akishita *et al.*, 2000). Similar observations were made in the model of MI where deletion of the AT_2R exacerbated the progression to HF and significantly decreased survival (Adachi *et al.*, 2003) while lentiviral gene transfer or moderate transgenic AT_2R overexpression prevented HF progression post-MI by reducing post-myocardial remodelling and improving contractile function in a mechanism involving increased endothelial nitric oxide synthase (eNOS) expression and downregulation of NADPH oxidase (Nox) 2 (Metcalfe *et al.*, 2004, Xu *et al.*, 2014). Interestingly, in AT_2R transgenic mice it was noted that the resulting cardiac phenotype was directly related to the degree of transgene expression (Xu *et al.*, 2014, Nakayama *et al.*, 2005, Yan *et al.*, 2003). Thus, for example, in MI, moderate AT_2R expression improved functional outcomes while high expression of the transgene worsened recovery (Xu *et al.*, 2014). Similarly, myocyte contractile dysfunction was worst at the highest level of transgene expression (Nakayama *et al.*, 2005). This suggest that the contrasting reports on the role of the AT_2R in CVD is in part due to the experimental approaches to manipulate the AT_2R *in vivo* and highlights that the cardiovascular outcome of AT_2R activation may be largely governed by its relative expression levels in relation to other RAS components.

Table 1-3. AT_2R signalling pathways

Target	Second messenger	Pathways	Effect	References
NO/cGMP	Bradykinin	Caspase 3 NHE3 internalisation Na^+/H^+ exchanger inhibition	Vasodilation ↑Apoptosis ↓Blood pressure ↑Natriuresis ↑Angiogenesis ↓ Contractility	(Kemp *et al.*, 2014) (Castro-Chaves *et al.*, 2008) (Munk *et al.*, 2007) (Dimmeler *et al.*, 1997) (Tsutsumi *et al.*, 1999)
PLA_2	AA, 11,12-epoxyeicosatrienoic acid	↓Erk, ↓IL-6, ↓NFkb, ↑K_{Ca}	↑Natriuresis ↓Inflammation Vasodilation	(Rompe *et al.*, 2010) (Arima *et al.*, 1997)
Phosphatases	MKP-1, PP2A, SHP-1	↓ERK, ↑JNK ↑BCL-2 dephosphorylation I_{to} inhibition	↓cell proliferation, ↑apoptosis APD prolongation	(Bedecs *et al.*, 1997) (Horiuchi *et al.*, 1997) (Caballero *et al.*, 2004)
$G_{i/o}$	↓cAMP	↓Akt, ↓eNOS, ↑MKP-1	↓endothelial migration/ tube formation ↑apoptosis ↑,↓fibrosis	(Benndorf *et al.*, 2003) (Yamada *et al.*, 1996) (Mifune *et al.*, 2000)

1.3.5 ACE inhibitors and angiotensin type 1 receptor blockers

The first natural ACE-I was isolated in the 1960s from the venom of the Brazilian arrowhead viper and this led to the development of synthetic peptides inhibiting ACE (Ferreira, 1965). Captopril was the first ACE-I to be introduced in 1981 and since then 17 ACE-I were licensed for clinical use (Zaman *et al.*, 2002). In contrast, with the release of losartan in 1995, ARBs are one of the newest classes of drugs available for the treatment of hypertension and CVDs (Ripley and Hirsch, 2010). To date, eight ARBs have been licenced for clinical use, the most recent one being azilsartan medoxomil in 2011 (Paulis *et al.*, 2012). ACE-I act by binding to the catalytic site of ACE and thereby preventing hydrolysis of its substrates. The prevention of Ang I cleavage to form Ang II following acute administration of ACE-I significantly reduces the plasma levels of Ang II and aldosterone while plasma renin activity and Ang I are increased due to the loss of negative feedback (Chen *et al.*, 2010, Juillerat *et al.*, 1990). In contrast, ARBs act by blocking the binding of Ang II to the AT_1R and thereby prevent pathological signalling through the AT_1R (Ripley and Hirsch, 2010). Despite different modes of action, both drugs mediate their BP lowering activity by decreasing vasopressin release, sympathetic activation, total peripheral resistance and increasing renal blood flow thereby promoting sodium and water excretion (Atlas, 2007).

Several large clinical trials have demonstrated that ACE-I and ARB therapy significantly improves symptoms and cardiac function while dramatically reducing morbidity and mortality in patients with hypertension, HF, post-MI cardiac dysfunction and CHD (Zaman *et al.*, 2002, Yusuf *et al.*, 2000). Next to the haemodynamic alterations, both, ARBs and ACE-I have also been demonstrated to mediate regression of LV hypertrophy and cardiac fibrosis in animal models of hypertension and small short-term clinical studies (Kim *et al.*, 1995, Brilla, 2000, Lip, 2001, Schwartzkopff *et al.*, 2000, Boldt *et al.*, 2006, Tokuda *et al.*, 2004, Devereux *et al.*, 2004, López *et al.*, 2001, Díez *et al.*, 2002, Kawasaki *et al.*, 2007, Kawano *et al.*, 2005a). However, data from large scale long-term studies are lacking to identify the physiological relevance of this observation. Nevertheless, this suggests that ACE-I and ARB may be beneficial in targeting cardiac remodelling in CVD.

In recent years, research has focussed on the development of novel ACE-I and ARBs. This includes the development of C-selective ACE-I such as lisW-S which reduces side effects due to inhibition of bradykinin degradation (Burger *et al.*, 2014) and ARBs with selective agonism on the AT_1R such as TRV120027. TRV120027 selectively activates ß-arrestin signalling at the AT_1R thereby increasing cardiac contractile performance and mediating cardioprotection (Violin *et al.*, 2010, Kim *et al.*, 2012, Boerrigter *et al.*, 2011, Boerrigter *et al.*, 2012). Additionally, a novel approach is suggesting to harness the beneficial effects of the counter-regulatory RAS in the treatment of CVDs with development of AT_2R agonists to engage counter-regulatory signalling pathways. Compound (C)21 was the first non-peptide agonist synthesised for the AT_2R in 2004 and has been extensively employed to assess the physiological functions of the AT_2R (Steckelings *et al.*, 2011). Although no clear evidence has been published on the anti-hypertensive actions on C21 (Kemp *et al.*, 2014, Bosnyak *et al.*, 2010, Rehman *et al.*, 2012) it has been demonstrated to preserve cardiac function post-MI by reducing infarct size and prevent adverse cardiac remodelling (Kaschina *et al.*, 2008, Lauer *et al.*, 2014). Specifically, C21 has been demonstrated to significantly improve cardiac EF, contractility and relaxation by preventing cardiac dilatation, the development of severe cardiac fibrosis and normalising the expression of markers of inflammation (Lauer *et al.*, 2014, Kaschina *et al.*, 2008, Rehman *et al.*, 2012). This data highlights C21 and the engagement of the AT_2R in general as a potential new therapeutic target for the treatment of adverse cardiac remodelling. A clinical trial to investigate the potential of C21 in pulmonary fibrosis is to get underway this year (Pharma, 2016) and another AT_2R agonist MP-157 developed by a Japanese company is currently being tested in a Phase I clinical trial for its safety and tolerability (NHS, 2011).

1.4 Cardiac remodelling in CVD

1.4.1 Cardiac hypertrophy

Cardiac hypertrophy is an adaptive mechanism of the heart to compensate for increased cardiac wall stress due to increased cardiac workload. It can be classed as physiological when it occurs in healthy individuals in response to exercise or pregnancy and is not associated with cardiac damage or scarring. In

contrast, pathological hypertrophy results, for example, from chronic pressure or volume overload and MI. Unlike physiological hypertrophy, pathological hypertrophy is associated with the re-expression of foetal genes [e.g. ß-myosin heavy chain (ßMHC), atrial natriuretic peptide (ANP) and brain natriuretic peptide (BNP)], alterations in the proteins required for excitation-contraction (EC) coupling and changes to the energetic and metabolic state of the cell (Kehat and Molkentin, 2010). There are two types of hypertrophy, concentric and eccentric hypertrophy (Figure 1-2). Eccentric hypertrophy is usually associated with chronic volume overload or ventricular remodelling following MI (Chen *et al.*, 2011). It is characterised by an increase in the internal LV diameter and concomitant wall thinning. Cardiomyocyte contractile units are assembled in series leading to an increase in cell length while cell width remains unchanged or decreases. This increases the shortening capacity of cardiomyocytes and helps maintain ventricular function (Kehat and Molkentin, 2010). In contrast, concentric hypertrophy usually occurs in response to chronic pressure overload (Izumiya *et al.*, 2006). Macroscopically, concentric hypertrophy is characterised by an increase in LV wall thickness without a change in LV chamber size. Microscopically, cardiomyocyte contractile units are assembled in parallel leading to a net increase in cell width. Concentric hypertrophy may progress to eccentric hypertrophy in the progression towards HF (Kehat and Molkentin, 2010).

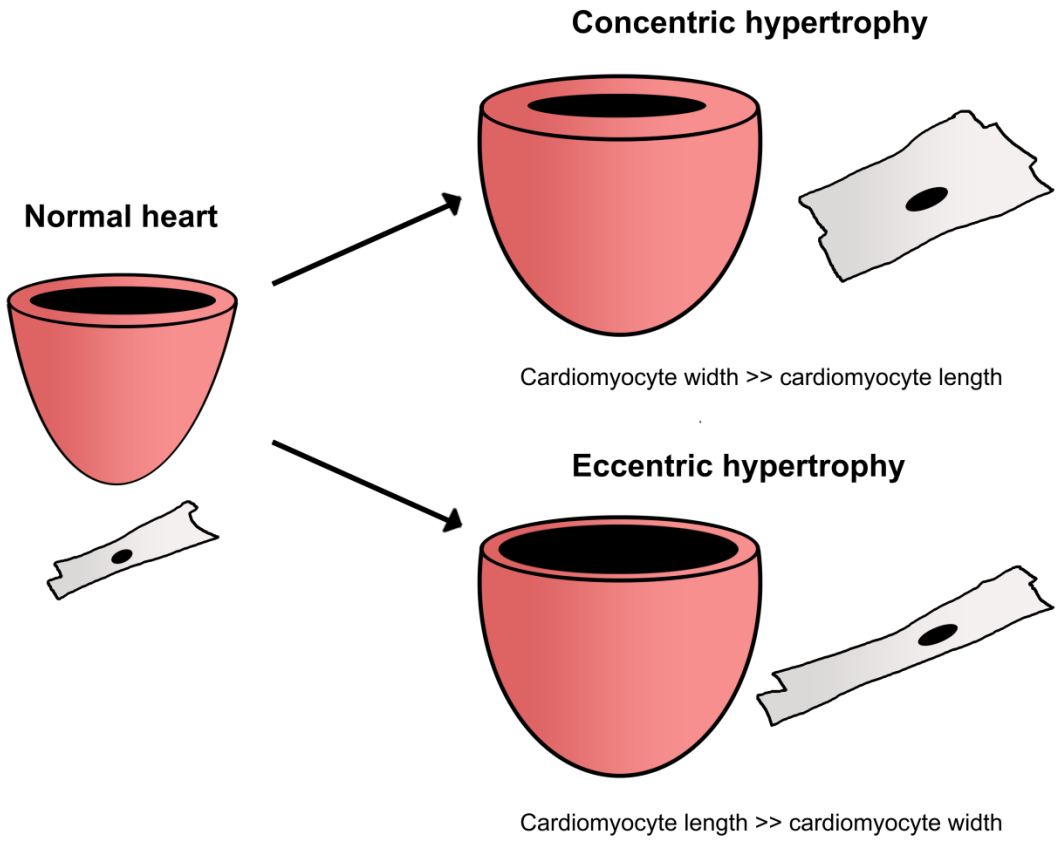

Figure 1-2. Patterns of cardiac hypertrophy.
Concentric hypertrophy is characterised by an increased left ventricular wall thickness without an increase in chamber size. Microscopically, cardiomyocytes increase in width by assembly of new contractile units in parallel. Eccentric hypertrophy is characterised by dilatation of the heart where the internal diameter of the ventricle increases to a greater degree than wall thickness. Microscopically, cardiomyocytes assemble new contractile units in series resulting in a greater increase in cell length than cell width.

1.4.1.1 Molecular mechanisms of cardiomyocyte hypertrophy

Since cardiomyocytes are terminally differentiated, cardiomyocytes respond to hypertrophic stimuli with an increase in protein synthesis which increases cell size and the re-expression of foetal genes that adjust cardiomyocyte function to the altered workload (Sadoshima and Izumo, 1993a). Broadly, there are two types of hypertrophic stimuli, mechanical and neurohormonal factors (e.g. Ang II, endothelin-1 [ET-1], growth factors) which induce a spectrum of intracellular signalling pathways that either stimulate or inhibit pro-hypertrophic gene expression (Figure 1-3).

Cardiomyocytes directly respond to increased myocardial stretch *via* an internal sensory apparatus. Although not well characterised this is thought to involve cell surface ß-integrins and its effector kinase focal adhesion kinase (FAK), the $ß_1$-integrin interacting protein melusin and the Z-disc protein muscle LIM protein (MLP) which transduce changes in cell stretch to the intracellular cytoskeleton and mediate hypertrophic gene expression (Shai *et al.*, 2002, Peng *et al.*, 2006, Heineke and Molkentin, 2006, Brancaccio *et al.*, 2003, Knöll *et al.*, 2002). Additionally, stretch-induced ion channels have also been suggested to participate in the activation of hypertrophic signalling pathways by increasing intracellular Ca^{2+} and activating the sodium hydrogen exchanger (NHE) leading to MAPK activation (Tatsukawa *et al.*, 1997, Yamazaki *et al.*, 1998).

Pro-hypertrophic neurohormonal factors mediate their effects by binding to seven-transmembrane GPCRs coupled to the $G_{q/11}$ subclass of G proteins. Activation of the $G_{q/11}$ subunit has been demonstrated to be a necessary event for the induction of pathological hypertrophy (Heineke and Molkentin, 2006). This subunit couples to the activation of phosphoplipase C (PLC) ß which mediates the formation of diacylglycerol (DAG) and inositol-1,4,5-trisphosphate (IP_3) (Heineke and Molkentin, 2006). IP_3 mediates the release of Ca^{2+} from internal calcium stores by binding to the IP_3 receptor. This has been associated with the activation of the calcineurin-nuclear factor of activated T-cells (NFAT) pathway and calcium-calmodulin kinase II (CaMKII)-dependent inactivation of histone deacetylase (HDAC) II and activation of the transcription factor myocyte enhancer factor 2 (MEF-2) (Wu *et al.*, 2006). DAG participates in the activation of PKC and especially PKCε has been demonstrated to play a role in pathological

cardiac hypertrophy (Dorn and Force, 2005). Additionally, PKC can activate protein kinase D (PKD) which phosphorylates HDAC II and results in its nuclear export thereby disinhibiting hypertrophic gene expression (Vega *et al.*, 2004).

The MAPK pathway is a central pathway involved in cardiac hypertrophy (Mutlak and Kehat, 2015). MAPK signalling pathways consist of a series of kinases that lead to the phosphorylation of the effector kinases p38, ERK1/2 and c-jun N-terminal kinase (JNK) (Heineke and Molkentin, 2006). ERK1/2 signalling in particular has been demonstrated to be important for concentric hypertrophy by enhancing transcriptional activation of NFAT, AP-1 and GATA-4 (Sanna *et al.*, 2005, Bueno *et al.*, 2000). In contrast, overexpression of ERK5 in mice precipitated ventricular dilatation and eccentric cardiac remodelling suggesting that the type of cardiac hypertrophy is in part regulated by specific MAPK activation (Nicol *et al.*, 2001).

Hypertrophic signalling is counteracted in part by activation of p38, JNK and glycogen synthase kinase (GSK)-3β which phosphorylate NFAT and other transcription factors and prevent nuclear translocation (Heineke and Molkentin, 2006). In particular, inhibition of GSK-3β is a convergence point for many hypertrophic signalling pathways induced by a variety of stimuli (Dorn and Force, 2005). Additionally, the natriuretic peptides ANP and BNP are natural inhibitors of cardiac hypertrophy and are increased in response to pathological hypertrophy in an attempt to counteract detrimental remodelling. ANP and BNP bind to natriuretic peptide receptors (NPRs) which are linked to activation of guanylyl cyclase and the formation of cGMP. Increases in cGMP have been suggested to activate protein kinase G (PKG) 1 which inhibits L-type Ca^{2+} channels thereby blocking calcineurin-dependent activation of NFAT (Barry *et al.*, 2008).

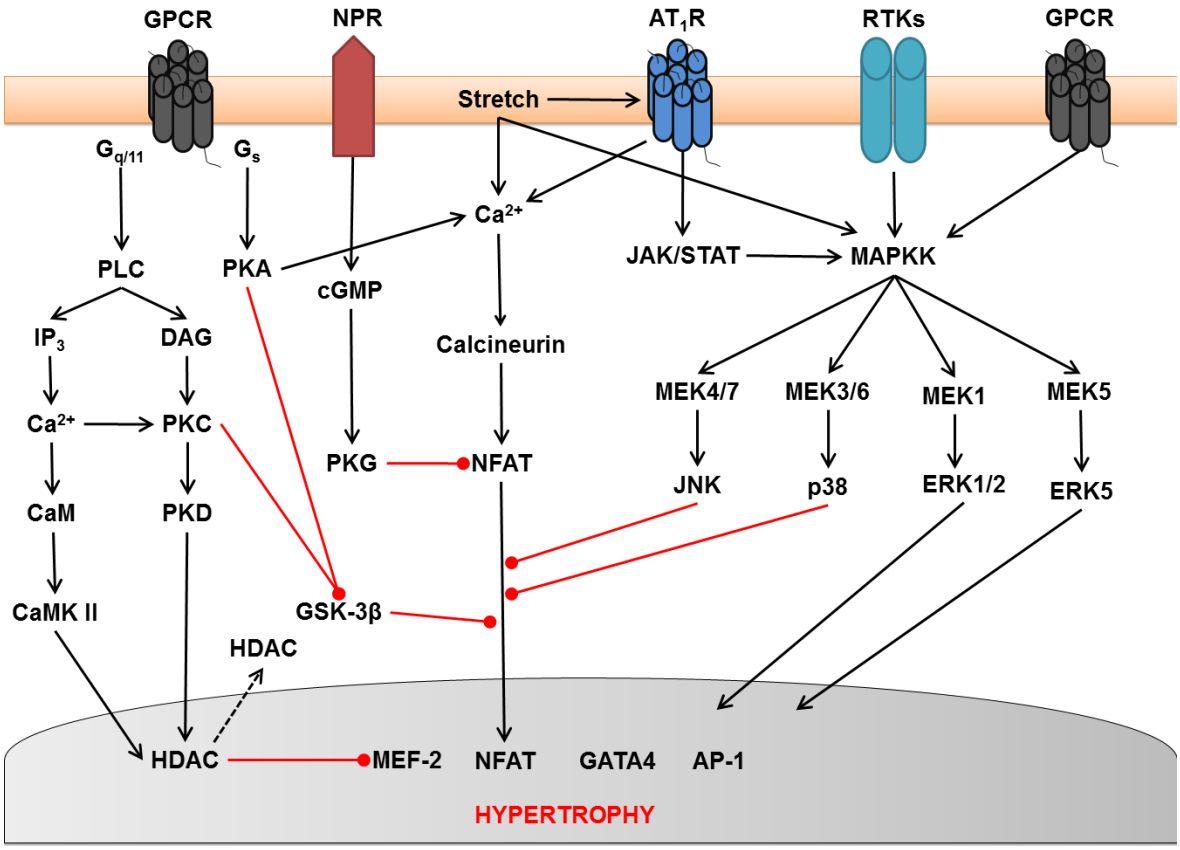

Figure 1-3. Hypertrophic signalling pathways.
Cardiac hypertrophy can be induced by a variety of signals at the cell membrane resulting in the activation of the nuclear pro-hypertrophic transcription factors MEF-2, NFAT, GATA4 and AP-1. This includes G-protein coupled receptors signalling *via* $G_{q/11}$ and Phospholipase C to mediate the nuclear export of HDAC disinhibiting MEF-2 transciptional activity. Similarly, AT_1R-, receptor tyrosine kinase or G-protein mediated activation of the MAP kinase pathway, specifically ERK1/2 and ERK5 can activate pro-hypertrophic gene expression. Furthermore, cellular stretch may activate hypertrophic signalling either indirectly *via* AT_1R activation or directly by increasing intracellular calcium and promoting the nuclear localisation of NFAT. Cellular hypertrophy can be inhibited by promoting the cytoplasmic retention of transcription factors such as NFAT. This is mediated by natriuretic peptide mediated activation of PKG, activation of the MAP kinases JNK or p38 and GSK-3β. Especially inhibition of GSK-3β *via* PKA or PKC is a main convergence point of pro- hypertrophic signalling pathways. AP-1= activator protein 1, AT_1R= angiotensin type 1 receptor, CaM= calmodulin, CaMK II= calcium calmodulin kinase II, DAG= Diacylglycerol, ERK= extracellular signal regulated kinase, GPCR= G protein coupled receptor, GSK-3β= glycogen synthase kinase 3β, HDAC= histone deacetylase, IP_3= inositol-1,4,5-trisphosphate, JAK= janus kinase, JNK= c-jun N-terminal kinase, MEF-2= myocyte enhancer factor 2, MEK= mitogen-activated protein kinase, NFAT= nuclear factor of activated T-cells, NPR= Natriuretic peptide receptor, PKC= protein kinase C, PKD= protein kinase D, PLC= phospholipase C, RTK= receptor tyrosine kinase, STAT= signal transducers and activators of transcription. Red lines with filled circle indicate inhibition. Black arrows indicate activation. Adapted from Heineke & Molkentin (2006), Dorn & Force(2005) and Shah & Mann (2011).

1.4.1.2 Role of Ang II in cardiomyocyte hypertrophy

Ang II signalling is one of the main mediators of cardiac hypertrophy in CVDs. Evidence demonstrates that Ang II mediates a direct pro-hypertrophic effect on the heart which is independent of its pressor effect (Gusev *et al.*, 2009). Ang II stimulation of cardiomyocytes directly induces early response genes such as *c-fos*, *c-jun*, *c-myc* and *Egr-1* which precede the re-expression of foetal genes such as ß-MHC, BNP, ANP and skeletal actin within 24 h (Kim *et al.*, 1995). During Ang II infusion *in vivo,* cardiomyocyte hypertrophy is evident in as little as three days when hypertension is not yet fully developed highlighting the potent pro-growth effect of Ang II on cardiomyocytes (Kim *et al.*, 1995). The signalling pathways involved in Ang II-induced hypertrophy have been widely studied unravelling a complex signalling network that involves the cross-activation of various other growth factor pathways including transforming growth factor (TGF)ß, ET-1, EGF, interleukin (IL)-6 and aldosterone (Figure 1-4). Pro-hypertrophic signalling pathways activated by Ang II binding to the AT_1R include G_q mediated activation of PLC, PLD, PLA_2 and the subsequent activation of PKC, Rho/ Rock, c-Src, MAPKs and Nox (Sadoshima and Izumo, 1993b, Peng *et al.*, 2016, Nakagami *et al.*, 2003, Aoki *et al.*, 2000, Bendall *et al.*, 2002). Additionally, mechanical stretch has also been shown to induce the autocrine release of Ang II and ET-1, and it has also been demonstrated that signalling at the AT_1R can be activated by mechanical stretch in the absence of its ligand highlighting that mechanical stretch synergistically induces hypertrophic signalling *via* conventional receptor-mediated pathways and cytoskeletal mechanosensors (Zou *et al.*, 2004).

The dependency for cross-activation of growth factor signalling pathways in Ang II-induced cardiac hypertrophy has been demonstrated in $TGFß_1$ knockout mice where chronic Ang II infusion failed to elicit cardiac remodelling and cardiac dysfunction observed in wildtype mice (Schultz *et al.*, 2002). Similarly inhibition of the TGFß receptor I (TGFßRI) completely abolished the hypertrophic response to Ang II stimulation (Watkins *et al.*, 2012). Ang II stimulates TGFß mRNA in isolated cardiomyocytes and fibroblasts which acts in an autocrine and paracrine mechanism to stimulate cardiomyocyte growth by activating TGFß activated kinase 1 (TAK1) (Gray *et al.*, 1998, Everett *et al.*, 1994, Koitabashi *et al.*, 2011). Similarly, it has been demonstrated that Ang II stimulates the autocrine and

paracrine release of IL-6 from cardiomyocytes and fibroblasts which activates the cardiomyocyte Janus kinase/ signal transducers and activators of transcription (JAK/STAT) pathway leading to cell growth (Sano *et al.*, 2000b, Sano *et al.*, 2000a). Additionally, it has been demonstrated that Ang II stimulation induces the release of ET-1 from ECs, fibroblasts and cardiomyocytes in a PKC-dependent manner and Ang II-induced protein synthesis can be blocked by the addition of an ET_A receptor antagonist (Ito *et al.*, 1993). Interestingly, the hypertrophic response to Ang II infusion is blunted in mice with endothelial-specific ET-1 deletion indicating an important paracrine role of non-myocyte cells in Ang II induced-hypertrophy (Adiarto *et al.*, 2012). A role for EGFR transactivation was demonstrated in a transgenic mouse model expressing an AT_1R incapable of transactivating EGFR (Zhai *et al.*, 2006). Ang II-induced phosphorylation of EGFR failed to induce cardiomyocyte hypertrophy and induction of foetal genes *via* the activation of Erk1/2 and Akt (Zhai *et al.*, 2006, Peng *et al.*, 2016). Aldosterone has also been suggested to participate in Ang II-induced cardiac hypertrophy which is demonstrated by the ability of aldosterone antagonists to inhibit cardiomyocyte growth (Matsui *et al.*, 2004). Stimulation of cardiomyocytes with aldosterone revealed a potent pro-hypertrophic effect that is mediated by the activation of ERK1/2, PKC and JNK (Okoshi *et al.*, 2004).

Ang II has also been increasingly linked to the induction of oxidative stress *via* the activation of Nox. Reactive oxygen species (ROS) have been demonstrated to play a role in Ang II-induced cardiac hypertrophy as induction of the foetal gene program can be prevented by antioxidants. In mice with deletion of $gp91^{phox}$ (Nox2), Ang II fails to induce cardiac hypertrophy (Byrne *et al.*, 2003, Bendall *et al.*, 2002). The activation of Nox by Ang II is likely due to pathways involving Rho/Rock and ERK1/2 (Higashi *et al.*, 2003, Nakagami *et al.*, 2003, Laplante *et al.*, 2003), however, downstream mechanisms of ROS-mediated induction of cardiac hypertrophy need to be elucidated but this is likely to involve Akt and nuclear factor (NF)κb activation (Higuchi *et al.*, 2002, Hingtgen *et al.*, 2006).

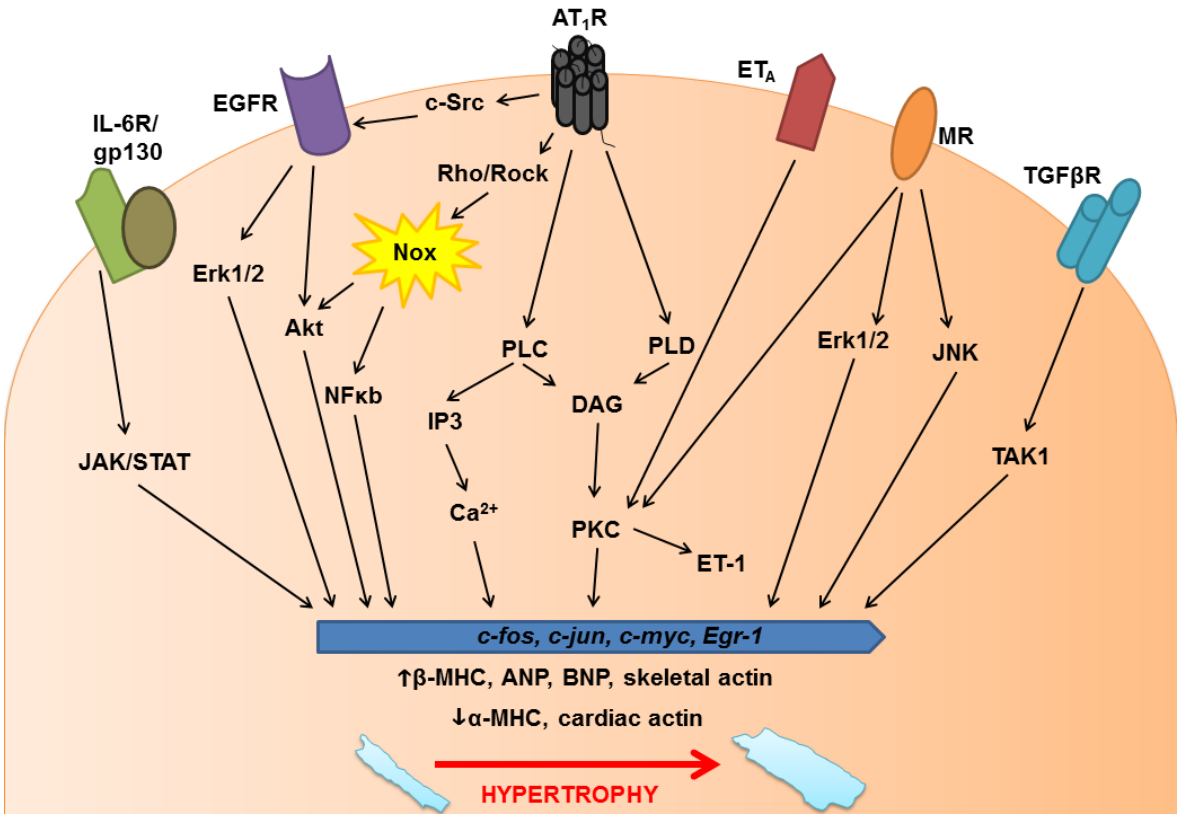

Figure 1-4. Hypertrophic signalling pathways activated by Ang II.
Ang II mediated cellular hypertrophy is complex and involves the cross-activation of various other growth factor pathways. Direct activation of the AT_1R by AngII can result in the activation of the phospholipase C and D pathways resulting in the release of intracellular Ca^{2+} and PKC activation which in turn activate the early response genes *c-fos, c-jun, c-myc* and *Egr-1*. Furthermore, AT_1R mediated activation of Rho/Rock and increased Nox activity can promote pro-hypertrophic gene expression via Akt and NFκb signalling. AT_1R activation mediates the cross-activation of the EGFR via c-src and promotes the release of IL-6, ET-1, aldosterone and TGFβ which in turn contribute to pro-hypertrophic signalling by activation of the JAK/STAT pathway, ERK1/2, JNK and TAK1. α/β-MHC= α/β myosin heavy chain, ANP= atrial natriuretic peptide, AT_1R= angiotensin type 1 receptor, BNP= brain natriuretic peptide, DAG= diacylglycerol, EGFR= epidermal growth factor receptor, ERK1/2= extracellular signal regulated kinase, ET_A= endothelin receptor A, ET-1= endothelin-1, IP_3= inositol-1,4,5-trisphosphate, JAK/ STAT= janus kinase/ signal transducers and activators of transcription, JNK= c-jun N-terminal kinase, MR= mineralocorticoid receptor, NFκB= nuclear factor κB, PKC= protein kinase C, PLC= phospholipase C, PLD= phospholipase D, TAK1= TGFβ activated kinase 1, TGFβR= TGFβ receptor.

1.4.2 Fibrosis

1.4.2.1 The extracellular matrix and the role of cardiac fibroblasts

The cardiac ECM comprises approximately 20 % of the total cardiac volume in humans and provides a highly organised 3 dimensional network surrounding and connecting individual cardiomyocytes (Vliegen *et al.*, 1991, Porter and Turner, 2009). Its main function is to provide mechanical support for cardiomyocytes and assist in the distribution of mechanical forces; however, the ECM has also been demonstrated to harbour a variety of growth factors, cytokines and chemokines (Souders *et al.*, 2009). The ECM predominantly consists of fibrillar collagens with collagen type I (80 %) and type III (10 %) being the most abundant (Brown *et al.*, 2005). Less abundant ECM molecules include collagen type IV which forms the cardiomyocyte basement membrane, collagen type V, type VI, laminin and fibronectin. Fibrillar collagens are synthesised as pro-collagens which are secreted into the ECM and proteolytically cleaved to remove the N- and C-terminal domains forming mature collagen which is then incorporated into collagen fibrils (Bishop and Laurent, 1995). Type I collagen predominantly forms large thick parallel fibres and has a tensile strength as high as steel (Collier *et al.*, 2012). In contrast, collagen type III forms thin fibrillar networks with lower stiffness and contributes to tissue elasticity (Collier *et al.*, 2012). The myocardial collagen network is organised in a hierarchical order containing 1) the endomysium, an intricate network of small fibrils surrounding individual cardiomyocytes; 2) the perimysium, collagen sheaths surrounding bundles of cardiomyocytes and collagen struts that connect individual cardiomyocytes and blood vessels; and 3) the epimysium which encapsulates entire muscle bundles (Brown *et al.*, 2005). Especially the organisation of the perimysial collagen fibres in parallel to the cardiomyocytes serves to prevent overstretching of the cardiomyocytes and contributes to the elastic recoil during diastole facilitating ventricular filling (Janicki and Brower, 2002). Due to the high tensile strength of fibrillar collagen and its close contact with cardiomyocytes, it is thought that the collagen network contributes to the maintenance of the size and shape of the cardiac chambers and directly impacts cardiac contractile performance (Janicki and Brower, 2002). This is exemplified in MI where the near complete loss of the collagenous membrane in the scar weakens the scar and makes it susceptible to spontaneous rupture as it cannot withstand the increase in

pressure during systole (Fang *et al.*, 2008, Heymans *et al.*, 1999). Additionally, a clear link has been established between cardiac collagen content and the passive stiffness of the heart which thereby impacts on cardiac relaxation and diastolic filling (Badenhorst *et al.*, 2003, Kitamura *et al.*, 2001, Jalil *et al.*, 1989). Maintenance of the ECM is therefore of special significance in CVDs which are associated with a dysregulation of ECM homeostasis and may directly contribute to disorganisation of cardiac structure and impaired contractile function.

Fibroblasts are the main connective tissue cell found in the heart and are responsible for the deposition and maintenance of the cardiac ECM. In the mouse heart it has been suggested that fibroblasts constitute approximately 12-26 % of the cardiac cell population while in rats this has been demonstrated to be as high as 70 % (Banerjee *et al.*, 2007, Pinto *et al.*, 2016). In humans, comparable studies are missing, however it has previously been estimated that connective tissue cells constitute approximately 70 % of cells within the heart (Vliegen *et al.*, 1991). Cardiac fibroblasts are identified by their flat spindle-shaped cell morphology and are distinguished from other cell types within the heart by their lack of a basement membrane (Souders *et al.*, 2009). In the myocardium, fibroblasts are located in the endomysium surrounding cardiomyocytes and are organised into three-dimensional networks forming connections with other fibroblasts, the ECM and cardiomyocytes (Goldsmith *et al.*, 2004). This arrangement allows fibroblasts to contract the endomysial collagen network thereby exerting mechanical force on cardiomyocytes (Souders *et al.*, 2009). Although fibroblasts have usually been viewed as a homogeneous cell type with similar functions in all tissues, it has emerged that fibroblasts form a heterogeneous cell population with different phenotypes and functions across different tissues (Souders *et al.*, 2009). In the heart, fibroblasts can be primarily be identified by their expression of discoid domain receptor 2 (DDR2) and the calcium binding protein S100A4 (fibroblast specific protein 1;FSP1) (Goldsmith *et al.*, 2004, Strutz *et al.*, 1995).

The key function of cardiac fibroblasts in the normal heart is the maintenance of the ECM and to preserve a tight balance between synthesis and degradation of the collagen matrix (Porter and Turner, 2009). In response to stimulation with growth factors such as TGFβ and Ang II, fibroblasts increase their synthesis of

fibrillar collagen (Kawano *et al.*, 2000, Leivonen *et al.*, 2005). In contrast, matrix degradation is regulated by the expression of matrix metalloproteinases (MMPs) and tissue inhibitors of metalloproteinases (TIMPs). Cardiac fibroblasts express the collagenases MMP1 and MMP13, the gelatinases MMP2 and MMP9 and a membrane-bound MMP which can be activated in response to chemical, physical or environmental signals to regulate collagen matrix degradation (Porter and Turner, 2009, Stacy *et al.*, 2007). TIMP1 and TIMP2 are primarily expressed in cardiac fibroblasts and oppose the actions of MMPs (Min *et al.*, 2004, Porter and Turner, 2009). The balance of MMP:TIMP ratio is an important determinant of ECM homeostasis and disturbance of this balance during cardiac disease contributes to disease progression (Martos *et al.*, 2007, López *et al.*, 2006).

In addition to its key role in ECM homeostasis, cardiac fibroblasts can actively contribute to cardiac electrophysiology. In the myocardium, cardiac fibroblasts couple to cardiomyocytes through connexin-43 (Cx-43) and connexin-45 (Cx-45) allowing the transduction of electrical signals between the two cells (Goldsmith *et al.*, 2004). Although fibroblasts are electrically inactive, they are excellent conductors and it has been suggested that fibroblasts form bridges between myocytes that would otherwise be separated and thereby synchronise the spontaneous activity in distant cardiomyocytes (Gaudesius *et al.*, 2003). This may have important implications in CVDs where enhanced coupling between fibroblasts and myocytes predisposes to severe cardiac arrhythmias (Miragoli *et al.*, 2007).

1.4.2.2 Mechanisms of cardiac fibrosis

A hallmark of cardiac remodelling is an alteration in myocardial stiffness which has been attributed to cardiac fibrosis (Badenhorst *et al.*, 2003, Jalil *et al.*, 1989). In animal models an increase in myocardial collagen has been demonstrated to contribute to diastolic dysfunction and eventually culminate in diastolic HF (Mukherjee and Sen, 1993, Kitamura *et al.*, 2001, Doering *et al.*, 1988, Westermann *et al.*, 2011). In contrast, the degradation of the collagen matrix has been associated with chamber dilatation and progression to systolic HF (Martos *et al.*, 2007, Iwanaga *et al.*, 2002, López *et al.*, 2006). Pathological fibrosis in patients is characterised by widespread deposition of collagenous ECM equally affecting the non-hypertrophic RV and the hypertrophied LV (Berk *et al.*,

2007). Fibrotic lesions can either be characterised as scars resulting from myocyte necrosis and concomitant reparative (replacement) fibrosis or as perivascular and interstitial collagen deposits which present a type of reactive fibrosis with the increased deposition of collagen fibres in the myocardium in the absence of myocyte necrosis (Weber *et al.*, 1989).

Perivascular and interstitial fibrosis arises from the transient infiltration of leukocytes into the adventitia of coronary arterioles resulting in the activation of local myofibroblasts and the deposition of dense collagen fibres around the vessel. Myofibroblasts are characterised by the expression of the contractile protein α-smooth muscle actin (SMA) which corresponds with the acquisition of a proliferative, pro-migratory and secretory phenotype (Porter and Turner, 2009). The extensive remodelling eventually ensnares neighbouring cardiomyocytes which undergo load-dependent atrophy (Figure 1-5)(Xia *et al.*, 2009).

Myocyte necrosis in the hypertensive heart is a leading cause of replacement fibrosis and scarring resulting in impaired cardiac contractile function and diastolic stiffness (Weber *et al.*, 2013). In animal models of hypertension, such as the Goldblatt model of renovascular hypertension or Ang II infusion, myocyte necrosis occurs acutely and is visible as early as 2 days following hypertensive stimulation (Tan *et al.*, 1991, Brilla *et al.*, 1990). In hypertensive hearts, cardiomyocyte necrosis occurs as a result of Ca^{2+} overload due to the persistent activation of ßAR or other cytotoxic factors such as Ang II, triggering the opening of the mitochondrial permeability transition pore and subsequent necrotic cell death (Whelan *et al.*, 2010). The rupture of cardiomyocytes and the spillage of intracellular contents into the extracellular space releases damage-associated molecular patterns which lead to the activation of the innate immune system, subsequent infiltration of immune cells, and myofibroblast activation (Figure 1-5) (Campbell *et al.*, 1995, Zhang *et al.*, 2015). Activated macrophages engulf the necrotic myocytes and are a major source of pro-fibrotic mediators such as Ang II and $TGFß_1$ at the sight of injury which mediate the activation of fibroblasts to myofibroblasts (Kitazono *et al.*, 1995, Assoian *et al.*, 1987, Westermann *et al.*, 2011, Bai *et al.*, 2013).

In the diseased heart, myofibroblasts are the major cell type involved in the turnover of the collagen matrix. Myofibroblasts are important in the normal

wound repair process as they contribute to the contraction of the wound edges, promote scarring and maintain the integrity of the healing scar (Gabbiani, 2003). Once the scar has matured myofibroblasts usually undergo apoptosis, however, activated myofibroblasts persist in the remodelled myocardium and fail to undergo apoptosis which contributes to progressive cardiac fibrosis and transition to HF (Desmoulière *et al.*, 1995, Willems *et al.*, 1994). Myofibroblasts contribute to the pro-fibrotic remodelling by an increase in the synthesis and deposition of collagen and by altering the turnover of the ECM. In the initial stages of cardiac remodelling, increased synthesis of ECM proteins is the predominant process leading to fibrotic deposits within the heart (Berk *et al.*, 2007). In response to TGFß$_1$, myofibroblasts increase the synthesis of collagen type I and III which leads to the *de novo* deposition of collagens in the ECM contributing to scar formation (Wang *et al.*, 2006). Additionally, in later stages of remodelling, matrix degradation may occur in response to increased ECM synthesis. This is mediated by altering the balance between MMPs and TIMPs secreted by myofibroblasts and this may in itself contribute to excess fibrosis by activating a cycle of degradation and repair within the myocardium (Berk *et al.*, 2007). Most importantly, the new collagen matrix differs from the native ECM with highly cross-linked collagen I ,as it is deposited in hypertensive hearts, being degraded at a slower rate than collagen III favouring the net accumulation of a stiffer collagen matrix (Rucklidge *et al.*, 1992). A critical role for MMPs is demonstrated in the observation that mice deficient in MMP2 or MMP9 are protected against adverse cardiac remodelling following pressure overload (Matsusaka *et al.*, 2006, Heymans *et al.*, 2005). Increased circulating MMP2 and MMP9 levels have been correlated with deterioration of heart function and the transition to HF highlighting the therapeutic potential for altering ECM degradation to treat adverse cardiac remodelling (Martos *et al.*, 2007, Iwanaga *et al.*, 2002, López *et al.*, 2006).

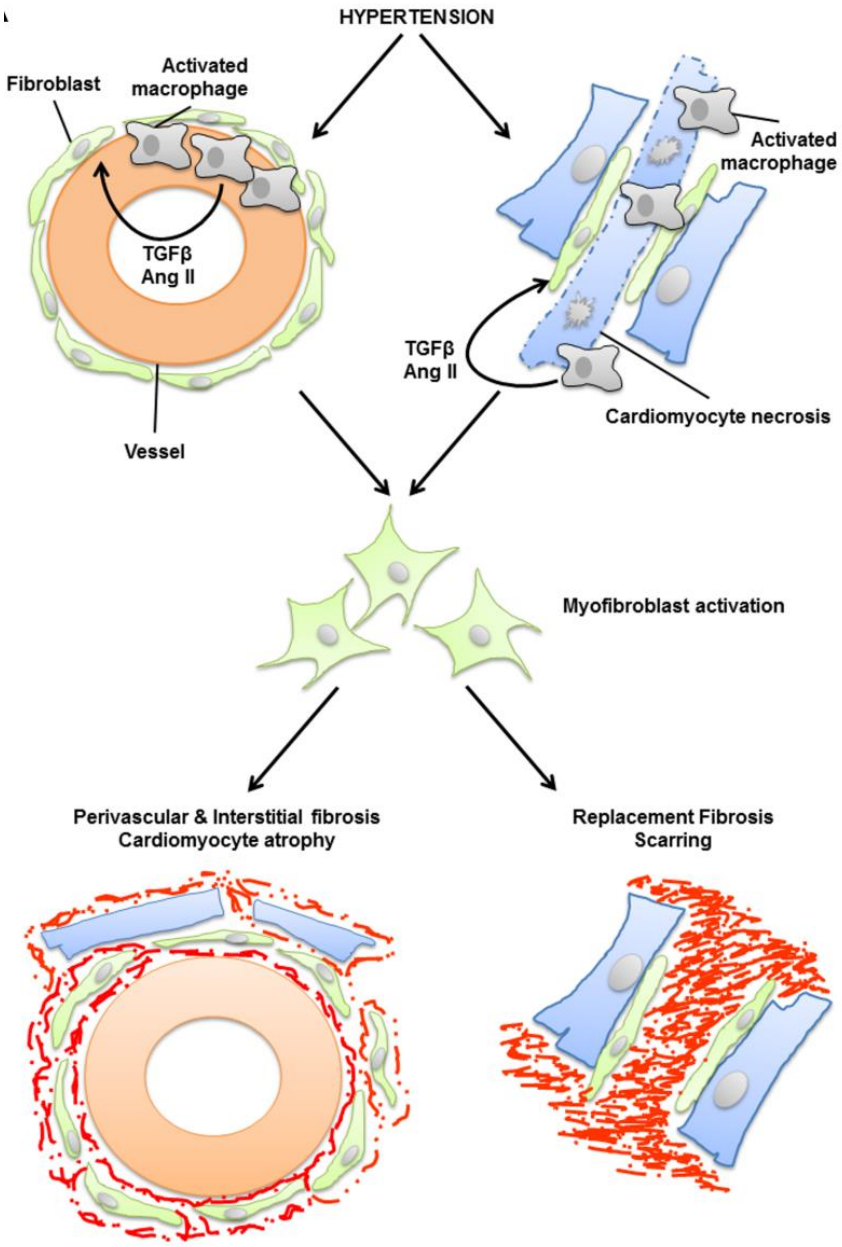

Figure 1-5. Fibrotic remodelling in the hypertensive heart.
Schematic of the stages of fibrotic remodelling in the heart leading to perivascular/ interstitial and replacement fibrosis. Perivascular fibrosis (left) results from the transient infiltration of leukocytes into the adventitia and the subsequent activation of resident fibroblasts to myofibroblasts. Replacement fibrosis (right) occurs as a result of cardiomyocyte necrosis, the subsequent infiltration of macrophages and activation of fibroblasts to myofibroblasts replacing cardiomyocytes with collagen fibres. Ang II= angiotensin II, TGFβ= transforming growth factor β.

1.4.2.3 Role of Ang II in cardiac fibrosis

Ang II is one of the main orchestrators of fibrotic signalling in the heart and has been demonstrated to induce fibroblast differentiation, proliferation and collagen secretion (Porter and Turner, 2009).

In vivo the fibroproliferative response to Ang II infusion peaks within 2-4 days of infusion and correlates with the early occurrence of cardiomyocyte necrosis although fibroblast proliferation may persist for up to 2 weeks (Campbell *et al.*, 1995, McEwan *et al.*, 1998). Activation of fibroblasts to myofibroblasts by Ang II occurs rapidly and involves activation of PKC and Nox (Bai *et al.*, 2013) (Figure 1-6). Additionally, in isolated cardiac fibroblasts Ang II is a potent mitogen and mediates an increase in DNA and protein synthesis within 24 h (Schorb *et al.*, 1993). This is mediated by an increase in AP-1 mediated transcription and increased DNA binding activity of *c-jun* and *c-fos* heterodimers (Sadoshima and Izumo, 1993a, Puri *et al.*, 1995, Crabos *et al.*, 1994). MAPK activity is one of the main signalling molecules involved in the increased protein and DNA synthesis in response to Ang II (Grohé *et al.*, 1998). Pathways involved in activating the MAPK pathway have been shown to involve PLC-mediated activation of PKC, ROS-mediated activation of PKC and tyrosine kinases and EGFR transactivation (Crabos *et al.*, 1994, Olson *et al.*, 2008, Chintalgattu and Katwa, 2009, Seta and Sadoshima, 2003). Additionally, Ang II has been demonstrated to mediate prepro-ET-1 mRNA synthesis in isolated fibroblasts and ET-1 can act in an autocrine manner to increase fibroblast proliferation *via* the ET_A receptor (Fujisaki *et al.*, 1995) (Figure 1-6).

Although the effects of Ang II on fibroblast proliferation and differentiation are directly mediated by Ang II signalling in the heart, Ang II-induced ECM expression is largely mediated by the autocrine and paracrine release of connective tissue growth factor (CTGF) and $TGF\beta_1$ (Kupfahl *et al.*, 2000, Che *et al.*, 2008).

$TGF\beta_1$ is the major cytokine mediating tissue fibrosis and directly induces the expression of collagen type I and type III by nuclear translocation of SMAD2/SMAD3. The TGFβ superfamily consists of over 30 members including the TGFβs, BMPs, activins, inhibins, nodal, myostatin, growth/ differentiation factors and anti-Müllerian hormone (Leask and Abraham, 2004). $TGF\beta_1$, $TGF\beta_2$

and TGFß$_3$ are the prototypes of the TGFß superfamily and play a key role in wound healing and fibrotic processes in the adult. TGFß receptors consist of a heteromeric complex consisting of one of seven TGFß type I (the activator) and one of five TGFß type II receptor (the propagator) (Massagué, 2012). TGFßs exclusively binds to the type I receptor TGFBR1 (also known as ALK5) and the type II receptor TGFBR2. This results in the phosphorylation of SMAD2/SMAD3 and their translocation to the nucleus where they activate pro-fibrotic gene expression (Figure 1-7). TGFß-induced ECM expression in fibroblasts is largely dependent on the activation of SMAD3 as TGFß$_1$ fails to induce collagen I expression in the absence of SMAD3 (Chen *et al.*, 1999). However, it has been demonstrated that TGFß-induced ECM expression may additionally require the activation of p38, ERK1/2 or PKC highlighting the complexity in TGFß-mediated transcriptional responses (Figure 1-7) (Sato *et al.*, 2002, Leivonen *et al.*, 2005, Mulsow *et al.*, 2005).

Stimulation of fibroblasts with Ang II leads to the upregulation of CTGF and TGFß mRNA within 1 h of stimulation which involves EGFR transactivation, RhoA, Nox, ERK1/2 and PKC activation leading to *c-fos, Egr-1* and AP-1 mediated transcription (Kawano *et al.*, 2000, Moriguchi *et al.*, 1999, Tang *et al.*, 2009, Rupérez *et al.*, 2003, Che *et al.*, 2008, Iwanciw *et al.*, 2003). Autocrine TGFß signalling in fibroblasts furthermore induces the secretion of tumour necrosis factor (TNF)α and IL-6 which synergistically exacerbate Ang II-induced collagen secretion (Sarkar *et al.*, 2004). In VSMC, a TGFß-independent pathway of collagen synthesis has also been demonstrated where Ang II mediates the early phosphorylation of SMAD2/3 independent of TGFß signalling (Wang *et al.*, 2006). Additionally, Ang II drives excess collagen deposition by modulating collagenase activity in the heart. Thus, it has been demonstrated that Ang II decreases the activity of MMP-1, MMP-2 and MMP-9 while increasing TIMP-1 thereby leading to a net increase in interstitial collagen (Brilla *et al.*, 1994, Min *et al.*, 2004, Stacy *et al.*, 2007) (Figure 1-6).

Next to the effects of Ang II on resident fibroblasts, it has also been demonstrated that Ang II can mediate the recruitment of various fibroblast precursors from the circulation and the myocardium itself. CD133$^+$ hematopoietic progenitor cells were detected in the myocardium within 1 day of Ang II infusion preceding the excess deposition of ECM (Sopel *et al.*, 2011).

Additionally, $CD43^+/CD45^+$ monocytic fibroblasts were detected in hearts from Ang II-infused mice (Haudek *et al.*, 2006). The appearance of these cells was dependent on monocyte chemoattractant protein (MCP)-1 expression and deletion of MCP-1 prevented $CD34^+/CD45^+$ fibroblast accumulation and cardiac fibrosis in response to Ang II infusion (Haudek *et al.*, 2006). Furthermore, TGFß is a main mediator of endothelial-to-mesenchymal transition (EndMT) during which ECs transdifferentiate into mesenchymal cells such as fibroblasts and VSMCs (Garside *et al.*, 2013). In the heart this process has been demonstrated to contribute up to 30 % of activated fibroblasts in the heart (Zeisberg *et al.*, 2007b). A role for Ang II is emerging in the process which is addressed in detail in Section 5. Overall, this demonstrates the importance of blood-borne and bone-marrow derived fibroblasts in the pathogenesis of Ang II-induced cardiac fibrosis.

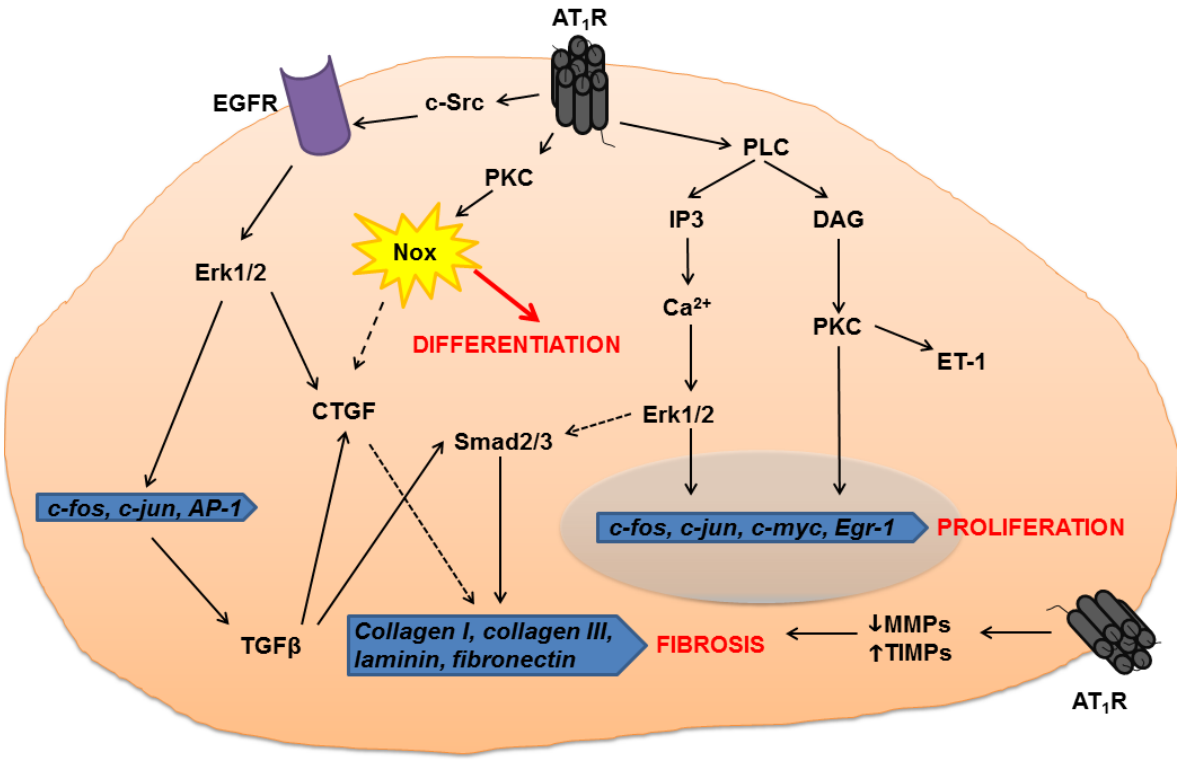

Figure 1-6. Fibrotic signalling pathways activated by Ang II in cardiac fibroblasts. Activation of the AT_1R in cardiac fibroblasts directly mediates fibroblast activation and differentiation *via* the activation of PKC and Nox signalling. In contrast, activation of the phospholipase C pathway with the activation of Erk1/2 and PKC results in the activation of early response genes (*c-fos, c-jun, c-myc, Egr-1*) and fibroblast proliferation. Collagen synthesis and deposition in response to Ang II signalling is indirectly mediated *via* the release of TGFβ and CTGF mediated by cross-activation of the EGFR, Erk1/2 and early response genes. TGFβ mediates the activation of Smad2/3 and thereby directly affects matrix gene expression and cellular fibrosis. Alternatively, AT_1R signalling can regulate fibrosis *via* the alteration in the gene expression of MMPs and TIMPs in cardiac fibroblasts. AT_1R= angiotensin type 1 receptor, CTGF= connective tissue growth factor, DAG= diacylglycerol, EGFR= epidermal growth factor receptor, ERK1/2= extracellular signal regulated kinase 1/2, ET-1= endothelin 1, IP_3= inositol-1,4,5-trisphosphate, MMP= matrix metalloproteinase, PKC= protein kinase C, PLC= phospholipase C, TGFβ= transforming growth factor β, TIMP= tissue inhibitor of metalloproteinase 1. Broken lines indicate incomplete pathway.

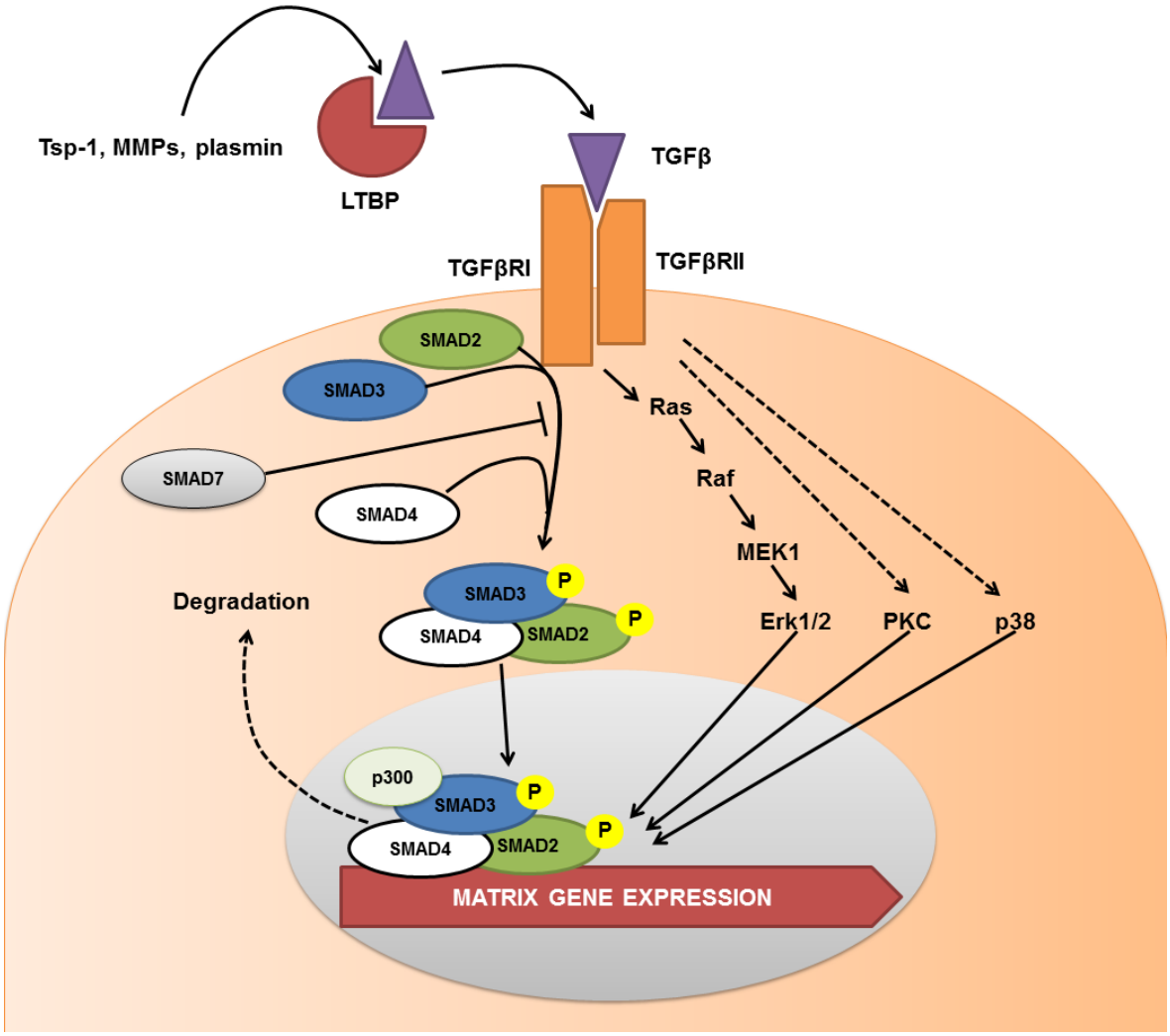

Figure 1-7. TGFβ signalling pathway for matrix gene synthesis.
TGFβs are synthesised as inactive precursors bound to latent TGFβ binding protein (LTBP) sequestered in the ECM and are activated by proteolytic cleavage of LTBP by MMPs, plasmin or thrombospondin-1. Upon binding of TGFβ to the type II receptor, phosphorylation of the type I receptor allows phosphorylation of SMAD transcription factors. Once phosphorylated, they form a trimeric complex with the common mediator SMAD4 and translocate to the nucleus to activate matrix gene expression. SMADs themselves are weak transcriptional activators and form complexes with other co-factors such as p300. SMAD signalling is terminated by phosphorylation by GSK-3β which targets SMADs for ubiquitination. Inhibitory SMAD7 competes with SMAD4 for SMAD2/3 binding and promotes TGFBR1 receptor degradation thereby inducing negative feedback**.** Erk1/2= extracellular signal regulated kinase 1/2, LTBP= latent TGFβ binding potein, MEK1= mitogen activated protein kinase 1, MMP= matrix metalloproteinase, PKC= protein kinase C, TGFβRI= type I TGFβ receptor, TGFβRII= type II TGFβ receptor, Tsp-1= thrombospondin-1. Broken lines indicate incomplete pathway.

1.5 The counter-regulatory renin-angiotensin-system

The discovery of a novel ACE-homologue, ACE2, which can hydrolyse Ang I and Ang II to biologically active peptides that can counteract Ang II signalling has built the basis for the characterisation of the counter-regulatory axis of the RAS (Figure 1-1) (Donoghue *et al.*, 2000, Tipnis *et al.*, 2000). The counter-regulatory RAS is predominantly defined by the ACE2/Angiotensin-(1-7)/Mas axis where ACE2 mediates the conversion of Ang II to Angiotensin-(1-7) [Ang-(1-7)] which binds to Mas to mediate its biological effects. Additionally, ACE2 hydrolyses Ang I to form Angiotensin-(1-9) [Ang-(1-9)] which can be further broken down to Ang-(1-7) by ACE (Donoghue *et al.*, 2000, Tipnis *et al.*, 2000). Ang-(1-9) has recently been demonstrated to be an active peptide and mediate its effects by binding to the AT_2R (Flores-Muñoz *et al.*, 2011). Ang-(1-9) may also be formed from Ang I *via* the actions of carboxypeptidase A or cathepsin A while prolylendopeptidase (POP), neutral endopeptidase (neprilysin, NEP) and thimet oligopeptidase (TOP) can convert Ang I directly to Ang-(1-7) (McKinney *et al.*, 2014).

Increasing evidence suggests a beneficial role of the counter-regulatory RAS not only in curtailing Ang II signalling but also to counteract pathological remodelling in a broad range of CVDs (Iwai and Horiuchi, 2009). The discovery of additional new Ang II metabolites with biological function forms an increasingly complex regulatory network of cardiovascular homeostasis.

1.5.1 ACE2

ACE2 was first described in 2000 by two independent research groups (Donoghue *et al.*, 2000, Tipnis *et al.*, 2000). ACE2 is a zinc metalloproteinase which shares 40 % sequence homology with the N- and C- terminal domains of ACE (Tipnis *et al.*, 2000). Additionally, ACE2 has a 48 % sequence homology in its cytoplasmic and transmembrane domains with the non-catalytic protein collectrin which has been demonstrated to play a role in the kidney and pancreas (Lambert *et al.*, 2008). In humans as well as in rodents, the *Ace2* gene is localised on the X chromosome (Tipnis *et al.*, 2000). ACE2 has one catalytic domain that functions as a carboxypeptidase by cleaving a single carboxyl-residue from its substrates and which is insensitive to ACE-I (Donoghue *et al.*, 2000). ACE2 cleaves Ang II to

Ang-(1-7) at very high efficiency and to a lesser extent Ang I to Ang-(1-9) despite a 5x lower affinity for Ang I than ACE (Rice *et al.*, 2004). Additionally, ACE2 has been demonstrated to cleave neurotensin, kinetensin, and des-Arg-bradykinin but not bradykinin itself (Donoghue *et al.*, 2000). ACE2 expression is highly confined to the heart, kidney and testes and small amounts can be detected in the liver and digestive tract (Donoghue *et al.*, 2000, Tipnis *et al.*, 2000, Rivière *et al.*, 2005). In the heart, ACE2 expression is mainly found in the ECs of intra-cardiac vessels, however, expression on cardiomyocytes and fibroblasts susceptible to cardiac pathology has also been demonstrated (Donoghue *et al.*, 2000, Gallagher *et al.*, 2008, Goulter *et al.*, 2004). The high expression of ACE2 in the heart together with its ability to degrade Ang II and generate Ang-(1-7) has been demonstrated to counteract Ang II in the heart and vasculature suggesting a crucial role for ACE2 in cardiovascular homeostasis. This is confirmed by the observation of severely impaired cardiac contractile function in *ace2*$^{-/-}$ mice that can be rescued by deletion of ACE suggesting a crucial role for Ang II imbalance in the pathology of *ace2*$^{-/-}$ mice (Crackower *et al.*, 2002). Further evidence has been presented where lentiviral-mediated overexpression of ACE2 in cardiomyocytes prevented cardiac dysfunction and cardiac remodelling in the SHRSP and following MI (Der Sarkissian *et al.*, 2008, Díez-Freire *et al.*, 2006). Interestingly, transgenic or adeno-associated viral-mediated cardiomyocyte-specific overexpression of ACE2 has also been demonstrated to result in severe cardiac fibrosis, cardiac conduction abnormalities and sudden death (Masson *et al.*, 2009, Donoghue *et al.*, 2003). While this may in part be due to the artificial increase in ACE2 in cells that usually have low ACE2 levels, this suggests that that the role of ACE2 in the heart is complex and likely dependent on other factors in the RAS.

Since ACE2 is found downregulated in many CVDs, a new strategy in the development of novel treatments for CVDs suggests that the enhancement of ACE2 activity may harbour beneficial effects. This has been approached by the use of recombinant human (rh)ACE2 and ACE2 activators. Animal studies with rhACE2 demonstrated prevention of adverse remodelling in response to Ang II infusion and a partial rescue of cardiac function, reversal of cardiac hypertrophy and fibrosis and prevention of ventricular dilatation in a model of pressure-overload induced HF suggesting therapeutic potential of rhACE2 in CVD (Zhong *et*

al., 2010). The ACE2 activator xanthenone was demonstrated to decrease BP and increase cardiac contractility and relaxation and reduce cardiac fibrosis in the SHR and streptozotocin-induced diabetic rats equally either *via* oral administration or minipump infusion (Hernández Prada *et al.*, 2008, Murça *et al.*, 2012). The beneficial effects of increased ACE2 activity may be due to the decrease in plasma Ang II levels and an increase in Ang-(1-7) formation which has been observed in plasma and interstitial and perivascular fibroblasts (Lo *et al.*, 2013, Ferreira *et al.*, 2011) highlighting their therapeutic potential. However, little is yet known about ACE2 biology and the safety of these applications. As such, infusion of rhACE2 in mice resulted in the formation of antibodies (Wysocki *et al.*, 2010) although this was not observed in humans (Haschke *et al.*, 2013). Furthermore, it has been demonstrated that xanthenone fails to activate ACE2 *in vivo* and *in vitro* and that it mediates similar anti-hypertensive effects in ACE2-null mice (Haber *et al.*, 2014)

1.5.2 Ang-(1-7)

Ang-(1-7) is a heptapeptide that is generated by the cleavage of the terminal phenylalanine residue from Ang II by ACE2 (McKinney *et al.*, 2014). Ang II hydrolysis is the major pathway involved in Ang-(1-7) formation in the human heart with an approximate production rate of 2718 pg/mL which can be completely abolished by the administration of ACE-I (Zisman *et al.*, 2003). Alternatively, Ang-(1-7) may also be produced *via* hydrolysis of Ang-(1-9) by ACE or directly from Ang I *via* the actions of POP, NEP and TOP (Santos *et al.*, 1992, Yamamoto *et al.*, 1992, Pereira *et al.*, 2013). Plasma Ang-(1-7) levels in healthy individuals have been estimated to range between 17.1-25.5 pg/mL and these may increase up to 3-fold during disease (Vilas-Boas *et al.*, 2009, Yamada *et al.*, 1998a). The half-life of Ang-(1-7) in the circulation is estimated to be 10 s before it is further metabolised to the inactive peptide Ang-(1-5) by ACE (Yamada *et al.*, 1998a). Hence, treatment with ACE-I and ARBs can significantly increase Ang-(1-7) levels and this property has been suggested to contribute to the beneficial effects of ACE-I and ARBs in CVD (Ishiyama *et al.*, 2004). Ang-(1-7) signalling antagonises most actions of Ang II in various tissues by inhibiting cell proliferation, migration, vasoconstriction and inflammation (Iwai and Horiuchi, 2009). Originally, it was thought that these effects were mediated through angiotensin receptors, however, binding studies demonstrated that Ang-(1-7) has

very low binding affinities for the AT_1R and AT_2R, although at high concentrations it shows functional selectivity for the AT_2R (Rowe *et al.*, 1995, Bosnyak *et al.*, 2011). Using ligand-binding studies, it was demonstrated that the orphan GPCR Mas functions as the receptor for Ang-(1-7) and mediates its beneficial effects in the vasculature and kidney (Santos *et al.*, 2003). Mas expression can be detected in the heart, kidney, testes, brain, vasculature, liver and adipose tissue correlating with the beneficial effects of Ang-(1-7) observed in these tissues (Alenina *et al.*, 2008, Passos-Silva *et al.*, 2013). Mice lacking Mas demonstrate impaired endothelial function, hypertension, impaired cardiac contractile function and increased cardiac ECM deposition highlighting an important role in cardiovascular homeostasis (Rabelo *et al.*, 2008, Xu *et al.*, 2008, Santos *et al.*, 2006). Despite the well described biological actions of Ang-(1-7), the underlying signalling pathways still remain elusive. It has been widely demonstrated that Ang-(1-7) activates the PI3K-Akt pathway *in vivo* and *in vitro* coupling to an increase in eNOS activity and NO generation (Sampaio *et al.*, 2007b, Dias-Peixoto *et al.*, 2008). Additionally, Ang-(1-7) inhibits the growth promoting MAPK pathway and thereby may antagonise the pathological effects of Ang II (Sampaio *et al.*, 2007a).

The effects of Ang-(1-7) in the cardiovascular system have been extensively studied. In a model of MI, Ang-(1-7) has been shown to be increasingly produced in the peri-infarct region and the degree of Ang-(1-7) significantly correlated with the rise in LVEDP (Averill *et al.*, 2003). Continuous intravenous infusion of Ang-(1-7) following MI for 8 weeks attenuated the development of HF by improving cardiac contractile function and normalising coronary flow by improving endothelial function (Loot *et al.*, 2002). The cardioprotective effect of Ang-(1-7) has been mainly attributed to its anti-hypertrophic and anti-fibrotic properties. Thus, Grobe *et al.* (2007) showed that the co-infusion of Ang-(1-7) with Ang II *via* subcutaneous osmotic minipumps in rats for 4 weeks prevented the development of Ang II-induced cardiac hypertrophy and interstitial fibrosis independent of an effect on BP (Grobe *et al.*, 2007). In a similar manner, the cardiac specific overexpression of Ang-(1-7) *via* an Ang-(1-7) fusion protein strategy in transgenic rats (VII-7) was able to prevent cardiac hypertrophy, fibrosis and downregulate the expression of molecular markers of cardiac remodelling (ANP, BNP, TGFβ) (Mercure *et al.*, 2008). This protective effect was

attributed to an increase in cardiac phosphatase activity by up-regulation of SHP-2 and dual specific phosphatase-1 which decreased mitogenic signalling pathways including ERK1/2, c-src kinase and p38 (Mercure *et al.*, 2008, McCollum *et al.*, 2012a). In deoxycorticosterone acetate (DOCA)-salt loaded rats expressing an Ang-(1-7) fusion protein (TG(A1-7)3292), Ang-(1-7) preserved cardiac contractile function by preventing the downregulation of SERCA2A and inhibiting the excessive dephosphorylation of PLB by protein phosphatase (PP)1 thereby increasing Ca^{2+} transient amplitude (de Almeida *et al.*, 2015). These beneficial effects generally occur in the absence of a hypotensive effect although some studies demonstrate BP lowering effects of Ang-(1-7). Thus, for example, intravenous infusion of Ang-(1-7) in the SHR but not Wistar Kyoto rat (WKY) decreased plasma vasopressin levels and induced natriuresis and diuresis thereby lowering BP (Benter *et al.*, 1995). Similarly, in fructose-fed rats, Ang-(1-7) infusion for 2 weeks reversed cardiac remodelling and normalised BP, an effect that was associated with a reduction in the phosphorylation of ERK1/2, JNK1/2 and p38 (Giani *et al.*, 2010). *In vitro* experiments confirm the direct anti-hypertrophic and anti-fibrotic actions of Ang-(1-7) on cardiomyocytes and fibroblasts where Ang-(1-7) decreases growth factor-induced ^{3}H-thymidine incorporation by downregulating MAPK signalling and up-regulating dual-specific phosphatase-1 (Tallant *et al.*, 2005, Iwata *et al.*, 2005, McCollum *et al.*, 2012b). Additionally, Ang-(1-7) modulates the tissue expression and activity of mitogen-activated MMPs and TIMPs *in vivo* and *in vitro* favouring collagen degradation and preventing adverse cardiac remodelling (Pei *et al.*, 2010, Pan *et al.*, 2008). The vast array of studies highlights the important role of Ang-(1-7) as a regulator of pathological cardiac remodelling which harbours potential as a new target in the treatment of hypertension and HF (Lee *et al.*, 2013).

As a result, a recent strategy is investigating the potential to directly deliver Ang-(1-7) to confer cardioprotection. So far this strategy has been hampered by the short half-life of Ang-(1-7) in the circulation. The development of a cyclic form of Ang-(1-7) where a thioether bridge links the amino acids 4-7 was largely protected against degradation by ACE and other proteases *in vivo* and *in vitro* while retaining its functional activity even when applied orally (Kluskens *et al.*, 2009, de Vries *et al.*, 2010, Durik *et al.*, 2012). In a similar manner, an oral formulation of Ang-(1-7) encapsulated in hydroxylprolyl ß-cyclodextrin conferred

cardioprotective effects in a model of MI and improved indices of cardiac function and ventricular geometry (Marques *et al.*, 2012). Although this study did not investigate the stability of encapsulated Ang-(1-7) in the circulation these data indicate that the direct delivery of modified counter-regulator peptides with enhanced half-life may hold therapeutic potential in the treatment of adverse cardiac remodelling.

1.5.3 Ang-(1-9)

Ang-(1-9) is a decapeptide that is generated by the cleavage of the terminal leucine residue from Ang I by ACE2 (Tipnis *et al.*, 2000, Donoghue *et al.*, 2000). Alternatively, in heart homogenates, Ang-(1-9) may also be generated *via* carboxypeptidase A/ cathepsin A-dependent hydrolysis of Ang I (Jackman *et al.*, 2002, Kokkonen *et al.*, 1997, Garabelli *et al.*, 2008). Cathepsin A is more abundant in atria whereas in ventricles carboxypeptidase A has been suggested to contribute up to 80 % of the Ang-(1-9) forming activity (Jackman *et al.*, 2002, Garabelli *et al.*, 2008). In fact, in heart homogenates of wildtype mice, Ang-(1-9) was the major metabolite of Ang I conversion and in failing human hearts 85 % of Ang I is metabolised to equivalent levels of Ang-(1-9) and Ang II (Kokkonen *et al.*, 1997). Ang-(1-9) can be further metabolised to Ang-(1-7) by ACE and it was originally thought that Ang-(1-9) mediates its beneficial effects in the vasculature by conversion to Ang-(1-7). However, Ang-(1-9) has been suggested to act as an endogenous inhibitor of ACE because it is a substrate of ACE itself (Donoghue *et al.*, 2000). ACE binds Ang-(1-9) and Ang I with similar affinities (Rice *et al.*, 2004), however, the catalytic efficacy of ACE at Ang-(1-9) is low and it has been demonstrated that Ang-(1-9) is hydrolysed 18x slower than Ang I supporting endogenous ACE inhibition by Ang-(1-9) that has also been observed in cardiac homogenates (Rice *et al.*, 2004, Chen *et al.*, 2005, Kokkonen *et al.*, 1997).

In contrast to Ang-(1-7), Ang-(1-9) was recognised as an active peptide only very recently and its functional effects are only just emerging. One of the first studies to demonstrate that Ang-(1-9) is an active peptide and acts independently of Ang-(1-7) investigated the role of Cathepsin A in the release of Ang-(1-7) and Ang-(1-9) from heart homogenates (Jackman *et al.*, 2002). In this study, the authors demonstrated that Cathepsin A is a major enzyme involved in

the formation of Ang-(1-9) from Ang I. Additionally, they demonstrated that in the presence of ACE, Ang-(1-9) potentiated the effect of bradykinin at the B_2 receptor and significantly increased the release of NO and arachidonic acid (AA). This effect was more pronounced with Ang-(1-9) and because the concentrations of Ang-(1-9) employed were below concentrations that would significantly inhibit ACE and increase bradykinin it was concluded that Ang-(1-9) is active *per se* and not broken down to Ang-(1-7) (Jackman *et al.*, 2002). In a later study this observation was extended to show that Ang-(1-9) was more potent than Ang-(1-7) to promote the re-sensitisation of the B_2 receptor which was thought to be due to allosteric modulation of the ACE-B_2 receptor complex by Ang-(1-9) (Chen *et al.*, 2005). A first functional link between Ang-(1-9) and cardiac function was that 1 week following MI in rats, the levels of ACE and ACE2 activity significantly increased concomitant with a significant elevation of circulating Ang II and Ang-(1-9) levels (Ocaranza *et al.*, 2006). Following 8 weeks however, ACE2 and Ang-(1-9) were significantly decreased and this could be prevented by treatment with the ACE-I enalapril which significantly elevated the bioavailable Ang-(1-9) but not Ang-(1-7), suggesting that Ang-(1-9) partially mediated the preservation of cardiac function with enalapril treatment following MI (Ocaranza *et al.*, 2006). The authors extended this finding in one of the first studies to demonstrate a direct effect of Ang-(1-9) on cardiac remodelling *in vivo* and *in vitro* (Ocaranza *et al.*, 2010). Continuous administration of Ang-(1-9) *via* osmotic minipumps for 2 weeks following MI prevented ventricular dilatation, preserved cardiac function and inhibited the development of cardiomyocyte hypertrophy (Ocaranza *et al.*, 2010). The anti-hypertrophic actions of Ang-(1-9) were corroborated *in vitro* where Ang-(1-9) dose-dependently prevented hypertrophy of neonatal rat cardiomyocytes stimulated with either norepinephrine or IGF-1. This effect was not blocked by the Mas receptor antagonist A779 further confirming that Ang-(1-9) is not broken down to Ang-(1-7) and that the actions of Ang-(1-9) are independent of the Mas receptor (Ocaranza *et al.*, 2010).

A subsequent study clearly separating the actions of Ang-(1-7) and Ang-(1-9) was the identification of the receptor for Ang-(1-9) (Flores-Muñoz *et al.*, 2011). Using radioligand binding, it was demonstrated that Ang-(1-9) was able to compete with radiolabelled Ang II at the AT_2R albeit at a lower overall affinity than Ang II (Flores-Muñoz *et al.*, 2011). Using H9c2 cardiomyocytes this observation was

confirmed and demonstrated that Ang-(1-9) prevented Ang II-induced cardiomyocyte hypertrophy and this effect could be blocked by the AT_2R antagonist PD123319. More importantly, although Ang-(1-7) and Ang-(1-9) have been demonstrated to mediate similar anti-hypertrophic effects, this study provided a clear delineation of the actions of Ang-(1-7) and Ang-(1-9) (Flores-Muñoz *et al.*, 2011). First, the addition of the ACE-I captopril did not abolish the anti-hypertrophic effect of Ang-(1-9), indicating that its actions are independent of its breakdown to Ang-(1-7). Second, this study demonstrated that Ang-(1-7) and Ang-(1-9) engaged their anti-hypertrophic effects *via* distinct receptors with the effects of Ang-(1-7) being inhibited by the Mas receptor antagonist A779 but not the AT_2R antagonist PD123319 while the effects of Ang-(1-9) were insensitive to A779. Additionally, the anti-hypertrophic actions of Ang-(1-7) were partially mediated *via* bradykinin while those of Ang-(1-9) were not (Flores-Muñoz *et al.*, 2011).

Despite the identification of the AT_2R as the receptor for Ang-(1-9), the mechanism by which Ang-(1-9) mediates beneficial effects remains elusive. In the stroke prone spontaneously hypertensive rat (SHRSP), Flores-Muñoz *et al.* (2012) demonstrated that the infusion of Ang-(1-9) over 4 weeks via osmotic minipumps at the pre-hypertensive stage improved aortic endothelial function due to an increased NO bioavailability (Flores-Munoz *et al.*, 2012). Similarly direct application of Ang-(1-9) to pre-contracted aortic rings elicited a vasodilatory response at picomolar concentrations of Ang-(1-9) and this was inhibited by the NOS inhibitor L-NAME (Ocaranza *et al.*, 2014). It is possible that this effect is mediated by potentiation of bradykinin as seen in cardiac homogenates (Jackman *et al.*, 2002), however, Ang-(1-9) has also been linked to an increase in Nox4 which can induce vasodilation *via* hydrogen peroxide release (Flores-Munoz *et al.*, 2012). In atrial preparations Ang-(1-9) has been demonstrated to enhance stretch induced ANP release *via* the AT_2R-PI3K-Akt-eNOS-GC pathway (Cha *et al.*, 2013). This presents one possible pathway by which Ang-(1-9) may mediate its anti-hypertrophic actions *in vivo* and *in vitro*. Next to its anti-hypertrophic actions, Flores-Muñoz *et al.* (2012) also demonstrated that Ang-(1-9) prevented the development of cardiac fibrosis in the SHRSP which was due to a reduction in collagen I gene expression by Ang-(1-9) (Flores-Munoz *et al.*, 2012). Additionally, Ang-(1-9) could directly inhibit

serum-induced cardiac fibroblast proliferation and reduce collagen I gene expression below that of unstimulated cells suggesting that Ang-(1-9) may improve cardiac remodelling *via* its actions on various cell types in the heart (Flores-Munoz *et al.*, 2012).

In a recent study by Ocaranza *et al.* (2014) the authors induced hypertension in rats either *via* Ang II infusion or renal artery clipping for two to four weeks prior to the administration of Ang-(1-9) *via* osmotic minipumps for a further 2 weeks (Ocaranza *et al.*, 2014). In this study design, the authors for the first time demonstrated an anti-hypertensive effect of Ang-(1-9) which was mediated *via* the AT_2R. Furthermore, Ang-(1-9) was able to reverse established cardiac hypertrophy and fibrosis in both models of hypertension, although whether this is due to a reduction in BP or directs actions of Ang-(1-9) on the heart was not addressed in this study (Ocaranza *et al.*, 2014). In a second study by Zheng *et al.* (2015) Ang-(1-9) was administered to streptozotocin-induced diabetic rats which had normal BP but developed cardiomyopathy (Zheng *et al.*, 2015). Untreated rats had significant cardiac hypertrophy and fibrosis while treatment with Ang-(1-9) reversed cardiac remodelling and significantly decreased markers of cardiac fibrosis (TGFβ, collagen I) and cardiac hypertrophy (β-MHC, BNP). Furthermore, Ang-(1-9) was shown to directly affect cardiac function and preserved indexes of cardiac contractility and relaxation, normalised LVEDP and EF. The authors hypothesised that this was due to a reduction in Nox activity, a decrease in inflammatory markers (NFkB, TNFα, IL-1β) and ACE inhibition with reduced Ang II levels further strengthening the counter-regulatory actions of Ang-(1-9) (Zheng *et al.*, 2015).

Interestingly, despite the beneficial effects of Ang-(1-9) in the heart and vasculature, one study has reported that Ang-(1-9) through the AT_1R mediates pro-thrombotic effects on platelets and this is dependent on the conversion of Ang-(1-9) to Ang II *via* a yet unknown carboxypeptidase (Kramkowski *et al.*, 2010, Drummer *et al.*, 1988). This highlights that further research is needed to understand the extensive physiological actions of the counter-regulatory RAS in order to modulate therapeutic approaches. Overall, these data demonstrate that Ang-(1-9) mediates beneficial effects on acute cardiac remodelling in various models of cardiac disease and suggests that it would be a good new therapeutic target for the treatment of adverse cardiac remodelling in CVD. However,

clinically relevant longitudinal data on the effects of Ang-(1-9) in established cardiac disease still needs to be established.

1.6 Hypothesis and aims

The counter-regulatory RAS axis peptide Ang-(1-9) demonstrates therapeutic potential in the treatment of CVDs. So far, studies have only investigated acute reversal or prevention of adverse cardiac remodelling by Ang-(1-9). Whether Ang-(1-9) is beneficial when administered chronically is unknown.

Therefore, it was hypothesised that chronic administration of Ang-(1-9) to a mouse model of Ang II-induced cardiac remodelling and dysfunction would attenuate adverse cardiac remodelling and improve cardiac function by a direct effect on the heart.

The principal aim of this thesis was to assess the effects of chronic Ang-(1-9) delivery on cardiac functional and structural parameters in a model of Ang II-induced cardiac remodelling and to investigate novel pathways by which Ang II contributes to adverse cardiac remodelling. This was addressed by the following experimental aims:

1) Develop a mouse model of chronic Ang II-infusion and characterise associated cardiac structural and functional parameters.

2) Assess the changes in structural and functional parameters with Ang-(1-9) infusion in the Ang II-infusion model and identify direct effects of Ang-(1-9) on cardiac contractility in the isolated rat heart

3) Identify new mechanisms of Ang II-induced cardiac remodelling by investigating the role of Ang II in EndMT and defining the role of microvesicles in Ang II-induced hypertrophy.

Chapter 2 – Materials and Methods

2.1 Solutions and buffers

ADS buffer, pH 7.35 (in mM): 116 NaCl, 20 4-(2-hydroxyethyl)-1-piperazineethanesulfonic acid (HEPES), 1 NaH_2PO_4, 5.5 Glucose, 5 KCl, 0.8 $MgSO_4$

Krebs-Henseleit solution, pH 7.4 (in mM): 120 NaCl, 20 HEPES, 5.4 KCl, 0.52 NaH_2PO_4, 3.5 $MgCl_2$-$6H_2O$, 20 taurine, 10 creatine, 11.1 glucose anhydrous.

10x Phosphate-buffered saline (PBS), pH 7.4 (in mM): 1370 NaCl, 27 KCl, 100 Na_2HPO_4, 18 KH_2PO_4

ROS phosphate buffer, pH 7.4 (in mM): 50 KH_2PO_4, 1 ethylene glycol tetraacetic acid (EGTA), 150 sucrose.

ROS lysis buffer, pH 7.4 (in mM): 50 KH_2PO_4, 1 EGTA, 150 sucrose, 153 x 10^{-6} aprotinin, 2.1 x 10^{-3} leupeptin, 1.46 x 10^{-3} pepstatin, 1 PMSF.

Sodium citrate buffer, pH 6 (in mM); 11.4 Tri-sodium citrate, 500 µL Tween-20/L.

10x Tris-buffered saline (TBS), pH 7.4 (in mM): 1369 NaCl, 27 KCl, 247 Tris base

Tyrode's solution (in mM): 116 NaCl, 20 $NaHCO_3$, 0.4 Na_2HPO_4, 1 $MgSO_4$-$7H_2O$, 5 KCl, 11 glucose anhydrous, 1.8 $CaCl_2$.

Western lysis buffer (in mM): 50 Tris-HCl pH7.4, 50 NaF, 1 $Na_4P_2O_7$, 1 EGTA, 1 Ethylenediaminetetraacetic acid (EDTA), 1 % (v/v) Triton-X 100, 1 DTT, 1 Na_3VO_4, 0.1 PMSF, 250 mM mannitol, 1 x complete mini protease inhibitor cocktail tablet (for 10 mL solution) (Roche, Burgess Hill, UK), 1 x phosSTOP phosphatase inhibitor cocktail tablet (for 10 mL solution) (Roche, Burgess Hill, UK).

Western transfer buffer (in mM): 192 Glycine, 25 Tris base, 0.01 % SDS, 200 mL Methanol/L

2.2 Cell culture

All cell culture was performed aseptically in sterile class II laminar flow hoods (Thermo Fisher, Paisley, UK) and cells were maintained in humidified incubators at 37 ºC and 5 % CO_2/95 % O_2. All tissue culture reagents were purchased from Gibco (Thermo Fisher, Paisley, UK) unless otherwise indicated.

H9c2 cells are an immortalised cell line of cardiomyoblasts derived from BDIX embryonic rat heart tissue (Hescheler *et al.*, 1991). H9c2 cells were purchased from Public Health England (Salisbury, UK). Cells were maintained in T150 cm^2 cell culture flasks in minimum essential media (MEM) supplemented with 10 % (v/v) fetal bovine serum (FBS), 2 mM L-glutamine, 100 U/mL penicillin and 100 µg/mL streptomycin and sub-cultured at 60-70 % confluence.

Primary human coronary artery endothelial cells (HCAEC) are derived from the right and left coronary artery of a single donor. As important regulators of coronary blood flow, they are especially useful for *in vitro* studies of atherosclerosis and hypertension. Cryopreserved HCAEC were purchased from PromoCell (Heidelberg, Germany) and maintained in T75 cm^2 cell culture flasks in Endothelial Cell Medium MV (PromoCell, Heidelberg, Germany) supplemented with 100 U/mL penicillin and 100 µg/mL streptomycin and the provided supplement mix containing 5 % (v/v) fetal calf serum, 0.4 % (v/v) endothelial cell growth supplement, 10 ng/mL recombinant human EGF, 90 µg/mL heparin and 1 µg/mL hydrocortisone. Cells were sub-cultured when reaching 90-100 % confluence. Experiments were performed in basal growth medium (endothelial cell medium MV with 2mM L-glutamine, 100 U/mL penicillin, 100 µg/mL streptomycin and 1 mM sodium pyruvate). Cells were used between passages 2-10.

2.2.1 Cell subculture

Once cells reached the desired confluence, cells were passaged. After removal of medium from a confluent flask, cells were washed twice with sterile 1x PBS before the addition of 1x trypsin-EDTA and incubation at 37 ºC for approximately 5 min or until cells were detached. Once detached, approximately 8-10 mL of complete media was added to the flask to neutralise the trypsin and prevent

over-digestion of the cells. The flask was washed several times with the media before transferring it to a sterile tube and centrifugation at 480 g for 5 min. The supernatant was decanted and the pellet re-suspended in fresh media before plating in new flasks. Primary neonatal fibroblasts were usually split 1:2- 1:3 while H9c2 cells were sub-cultured 1:3-1:8. HCAEC were seeded at a density of 7.5x 10^5 cells in a T75 cm^2 flask.

In order to seed cells at a specified density, cells were counted after re-suspension. For this, 10 µL of the suspension were added into a haemocytometer and the cells were counted in the 4 quadrants made up of 16 squares each to determine the mean number of cells across all 4 quadrants. Since each of the quadrants measures 1 mm x 1 mm and the distance between the coverslip is 0.1 mm, one quadrant fits a volume of 0.1 µL. Therefore, the number of cells is:

$$\frac{\text{cells}}{\text{mL}} = \text{mean of 4 quadrants x } 10^4$$

To determine the volume of cell suspension required for the desired seeding density, the following formula was used:

$$\text{required volume (µL)} = \frac{\text{required density}}{\text{number of cells per µL}}.$$

2.2.2 Cryopreservation

For cryopreservation and long-term storage, cells were prepared as outlined in section 2.2.1. After centrifugation and removal of the supernatant, cells were re-suspended in an appropriate volume of complete cell culture media supplemented with 10 % (v/v) dimethyl sulfoxide (DMSO) to achieve an approximate density of 1x 10^6 cells/mL. The media was then aliquoted into 1 mL cryopreservation tubes which were placed into a freezing container filled with 100 % isopropanol and placed into a -80 ºC freezer for 24 h. This method allows a cooling rate of approximately -1 ºC/minute to -80 ºC and prevents cell rupture by rapid freezing. After 24 h, frozen cells were transferred to liquid nitrogen storage tanks for long term storage.

To recover cells from liquid nitrogen, cells were rapidly defrosted by placing into a water bath at 37 ºC. The cell suspension was then transferred into a flask containing fresh pre-warmed cell culture medium and incubated for 24 h at 37 ºC and 5 % CO_2 to allow cells to adhere to the culture plastic. The cell culture medium was then replaced to remove residual DMSO.

2.2.3 Neonatal rat cardiomyocyte and fibroblast isolation and culture

Neonatal rat cardiomyocytes (NRCM) and fibroblasts (NRCF) were isolated from 3-7 day old WKY rats by enzymatic digestion. This is a two-step process where hearts are initially subjected to enzymatic digestion to free cardiac myocytes and fibroblasts. The isolated cells are then purified by differential plating on different substrates; poly-L-lysine for fibroblasts and gelatin for cardiomyocytes.

Neonatal rat pubs were killed by decapitation and hearts were quickly excised *via* thoracotomy and placed into cold sterile ADS buffer (Figure 2-1 A-C). The hearts were then transferred into a sterile laminar flow hood where the lungs, surrounding connective tissue and atria were dissected and the ventricles were placed into a Petri dish with ADS buffer. Using fine scissors, hearts were cut into small pieces until homogenised (Figure 2-1 D). The pieces were then drawn up with a Pasteur pipette and transferred into a sterile 100 mL Duran bottle. The ADS buffer was carefully removed by tapping the bottle against the bench to collect the heart pieces at the bottom. For the first digestion, 10 mL of enzyme mix containing pancreatin (Sigma, Dorset, UK) and collagenase type II (Worthington Chemicals, US) at a final concentration of 0.6 mg/mL was added to the heart pieces and incubated in a shaking water bath at 37 ºC and 180 strokes/min for 5 min. This initial digestion allows the breakdown of excess connective tissue to release the cells (Louch *et al.*, 2011). After 5 min of digestion, the enzyme was removed and discarded. Stepwise enzymatic digestion was then performed as laid out in Table 2.1. After each digestion, the digestion mix was removed from the heart pieces, transferred to a sterile falcon tube containing 2 mL of FBS and centrifuged at 210 g for 5 min to pellet the released cells and remove the enzyme. The supernatant was decanted and the pellet carefully re-suspended in 4 mL of FBS by gentle tapping. The cell suspensions from every digestion step were pooled in one Falcon tube which was placed into

the incubator at 37 ºC and 5 % CO_2 after every step. The lid was loosened to allow gas exchange. After the final digestion, the digestion mix was directly added to the falcon tube containing the cell suspension and centrifuged at 210 g for 6 min to pellet the cells. This pellet contains a mixture of cardiac cells that were isolated by the enzymatic digestion but the biggest fraction is made up of cardiomyocytes and fibroblasts. To remove adherent, non-myocytes from the cells suspension and isolate cardiac fibroblasts, the cells were pre-plated on poly-L-lysine (Sigma, Dorset, UK) coated 100 mm cell culture dishes. For this, the pellet was re-suspended in an appropriate volume of plating media (Table 2.2) and 1 mL of cell suspension was added to each dish to make up a total volume of 10 mL. Generally, one dish was used for every two hearts in the initial digestion. The plates were then placed into the incubator at 37 ºC and 5 % CO_2 for 90 min to allow adhesion of cardiac fibroblasts (Figure 2-1 E).

Once fibroblasts adhered to the dish, each dish was gently washed using a Pasteur pipette to remove the non-adherent cells. The supernatant was collected in a 50 ml Falcon tube and 5 ml of plating media was added to each dish. The wash step was repeated and the supernatant transferred into the 50 ml falcon tube. If a significant number of floating cells could still be seen under the microscope, the wash step was repeated for a third time. After the final wash, 10 mL of plating media was added to each dish and cardiac fibroblasts incubated at 37 ºC and 5 % CO_2.

To count the number of cardiomyocytes in the supernatant, 10 µL of the suspension was added to a haemocytometer and counted as described in Section 2.2.1. Since neonatal cardiomyocytes do not proliferate (Ahuja *et al.*, 2007), cells cannot be sub-cultured and need to be plated out directly for use. For experimentation, cardiomyocytes were plated out at an assay dependent density into 1 % gelatin coated cell culture plates and allowed to adhere overnight at 37 ºC and 5 % CO_2. The next day, most of the cardiomyocytes will have adhered to the dish and can be seen beating (Figure 2-1 F). The plating media was removed and cells were washed with 1x PBS to remove further cell debris before proceeding with the experimental protocol.

For long-term storage, the cardiomyocytes were plated into 60 mm cell culture dishes coated with 1 % gelatin at a density of 6-7 x 10^6 in a final volume of 4 mL

and allowed to attach overnight at 37 ºC and 5 % CO_2. The next day, the plating media was removed and cells were washed with 1x PBS before the addition of maintenance media (Table 2.3). Maintenance media contains no serum to reduce the growth of contaminating fibroblasts. After a further day in maintenance media, cardiomyocytes were then trypsinized and frozen for long-term storage as outlined in section 2.2.2.

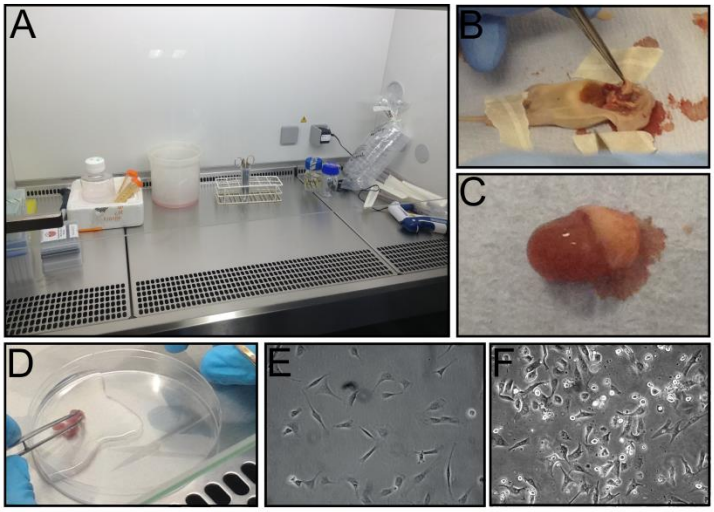

Figure 2-1. Neonatal cardiomyocyte and fibroblast isolation experimental setup and heart preparation.
(A) Setup of the isolation reagents and equipment under the laminar flow hood. (B, C) Image of the excision of the neonatal heart. (D) Mincing of the hearts using fine scissors. Example images of (E) NRCF and (F) NRCM after 24 h in culture.

Table 2.1 Digestion steps

Digest	Volume of enzyme mix (mL)	Time (min)	Strokes/min
1	10	5	180
2	10	20	160
3	8	25	150
4	8	25	150
5	6	15	160
6	6	10	150

Table 2.2 Plating media composition

	mL/500mL	Final concentration
DMEM	340	68 % (v/v)
M199	85	17 % (v/v)
Horse serum	50	10 % (v/v)
FBS	25	5 % (v/v)
Penicillin/ Streptomycin	5	100 U/mL / 100 µg/mL

Table 2.3 Maintenance media composition

	mL/500mL	Final concentration
DMEM	400	80 % (v/v)
M199	100	20 % (v/v)
Penicillin/ Streptomycin	5	100 U/mL / 100 µg/mL

2.3 Endothelial-to-Mesenchymal Transition

For induction of EndMT, HCAEC were plated into fibronectin-coated cell culture plates at 3x 10^5 cells/well and 6.4x 10^4 cells/well for 6-well and 12-well plates, respectively. 6-well plates were used for protein extraction and 12-well plates were used for RNA analysis. Cells were allowed to attach overnight and were then starved in 0.5 % FBS (v/v) basal growth medium for 24 h. Cells were then stimulated with 10 ng/mL TGFß$_1$ or TGFß$_2$ (Peprotech, London, UK), 100 nM or 1 µM Ang II (Sigma, Dorset, UK) alone or in combination in 2 % FBS (v/v) basal growth medium for up to 15 days. Medium was re-placed every second day and cells were re-stimulated. AT_1R, AT_2R and SMAD2/3 were blocked by addition of 1 µM losartan (Sigma Dorset, UK), 500 nM PD123319 (Sigma, Dorset, UK) or 1 µM SB525334 (Tocris, Bristol, UK) 15 min prior to stimulation. At the end of the protocol, cells were lysed for protein and RNA extraction as outlined in Section 2.8 and 2.9.

2.3.1 Time-course stimulations

For assessment of signalling pathways, HCAEC were plated into fibronectin coated cell culture plates at a density of 3x 10^5 cells/well and allowed to adhere overnight. Cells were then starved in serum free basal growth medium for 24 h and then stimulated with 10 ng/mL TGFß$_1$ or 1 µM Ang II alone or in combination for 5, 15, 30 and 60 min and lysed for protein extraction as described in Section 2.9. Unstimulated cells served as control.

For analysis of superoxide production, HCAEC were plated into fibronectin coated cell culture plates at a density of 2x 10^5 cells/well and allowed to adhere overnight. Cells were starved in 0.5 % FBS (v/v) basal growth medium overnight. The next day, cells were stimulated with 10 ng/mL TGFß$_1$ or 1 µM Ang II alone or in combination in serum free basal growth medium for 1, 5 and 30 min. Inhibitors of Rac1/2 (EHT1864, 10 µM; Tocris, Bristol, UK), Nox1 (ML171, 1 µM; Tocris, Bristol, UK) and Nox1/4 (GKT137831, 1 µM; provided by GenKyotex, Geneva, Switzerland) were added 30 min prior to stimulation. Following stimulation, cells were placed on ice and washed twice in ice-cold PBS. Cells were then lysed in 80 µL ROS Lysis buffer using a cell scraper and the lysate was kept on ice until use.

2.3.2 Lucigenin assay

Prior to use, the Orion Microplate Luminometer (Titertek Berthold, Pforzheim, Germany) was pre-heated to 37 ºC. In a white 96-well plate, 50 µL sample was combined with 100 µL ROS buffer and 75 µL 16.6 µM Lucigenin (Sigma, Dorset UK). The plate was read in the luminometer for basal luminescence. Each well was read 30x 1 s. 25 µL 1 mM NADPH (Tocris, Bristol, UK) were then added to each well and the plate read again to determine NOX activity levels. Protein concentration was determined in the remaining (10 µL) sample using the BCA assay (Section 2.9.2). Relative superoxide production was then determined with the following calculation:

$$O_2^- \text{ production} = \frac{\text{mean activity luminescence - mean basal luminescence}}{\text{µg protein in 50 µL}}$$

2.4 Microvesicles

2.4.1 Microvesicle conditioned medium

NRCF were isolated and cultured as outlined in Section 2.2.3. 2-3 flasks of NRCF cultured in a 150 cm^2 cell culture flask were passaged at a ratio of 1:3 or 1:2, respectively, into six 150 cm^2 cell culture flasks. Once confluent, cells were placed into a total of 18 mL serum free Dulbecco's Modified Eagle Medium (DMEM), supplemented with 100 U/mL penicillin and 100 µg/mL streptomycin. Three flasks were then stimulated with 1 µM Ang II while the other three flasks were left untreated (control) for 48 h. To inhibit microvesicle (MV) secretion, Brefeldin A (BFA) was used as an inhibitor of the endosomal secretory pathway (Islam *et al.*, 2007). Due to its global effect on cellular secretion, BFA is cytotoxic over long term and only allows stimulation for a maximum of 24 h. Thus, NRCF were treated with 5 µg/mL BFA in the presence or absence of 1 µM Ang II and stimulated for 24 h.

In a similar manner, H9c2 cells were cultured as outlined in Section 2.2. One flask of H9c2 cells was passaged 1:6 into six 150 cm^2 cell culture flask. Once 70 % confluence was reached, cells were placed into 18 mL serum free MEM, supplemented with 100 U/mL penicillin and 100 µg/mL streptomycin and three

flasks were stimulated with 1 μM Ang II while the other three were left untreated for 48 h.

2.4.2 Microvesicle isolation

Serial centrifugation and ultracentrifugation is the most common procedure employed for the isolation of MVs and exosomes in currently published literature (Pironti *et al.*, 2015, Lyu *et al.*, 2015). This method is based on the knowledge that the larger the size of a particle, the lower the centrifugation speed needed to sediment the particle. Therefore, by increasing centrifugation speed, particles are gradually excluded from the preparation. Initially, cells, debris and large apoptotic bodies are removed by low-speed centrifugation before pelleting larger MVs commonly called microparticles by centrifugation speeds between 10,000–20,000 g (Witwer *et al.*, 2013). Alternatively, the preparation may be clarified by passing it through, for example, a 0.2 μm filter and exclude vesicles by size (Théry *et al.*, 2006). Once cleared of cell debris and other contaminating vesicles, small MVs can then be pelleted by ultracentrifugation with speeds ranging between 100,000–120,000 g. While ultracentrifugation is a cost effective way to purify MVs, it fails to achieve an absolutely pure MVs population as the size and density of vesicles is largely dependent on their cargo and small vesicles may pellet at low speeds if they are located near the bottom of the tube (Witwer *et al.*, 2013). Furthermore, due to their lipophilic nature, MVs tend to aggregate which interferes with separation by vesicle size and the high speeds of centrifugation tends to sediment protein aggregates and other contaminants. To further purify the MV population from contaminants, vesicles can be floated on a 30 % sucrose gradient which will effectively separate protein to the bottom of the tube while MVs float on the gradient (Witwer *et al.*, 2013, Théry *et al.*, 2006).

2.4.2.1 Ultracentrifugation

MVs from cell culture media were isolated by serial centrifugation and ultracentrifugation as previously described (Théry *et al.*, 2006). A workflow of the MV purification procedure is outlined (Figure 2-2). Briefly, the MV conditioned medium was removed and transferred into 25 mL universal cell culture tubes and subjected to centrifugation at 850 g for 5 min to remove cell

debris and then passed through a 0.2 µm sterile filter to remove any particles ≥ 200 nm in size. The cleared medium was then transferred into Ultra-Clear, open-top thin-walled 16 x 102 mm ultracentrifuge tubes (Beckman Coulter, High Wycombe, UK) and then subjected to ultracentrifugation at 110,000 g at 4 ºC for 90 min in a Beckman Coulter SW 32.1 Ti swinging-bucket rotor in a pre-cooled Beckman Coulter L-80XP ultracentrifuge. The supernatant was decanted and the MVs were washed by resuspension in 1 mL ice-cold PBS. The tube was filled completely with PBS and the centrifugation step repeated. A small white pellet was visible after this centrifugation step and the MV pellet was re-suspended in 100 µL PBS and stored at -20ºC until further use.

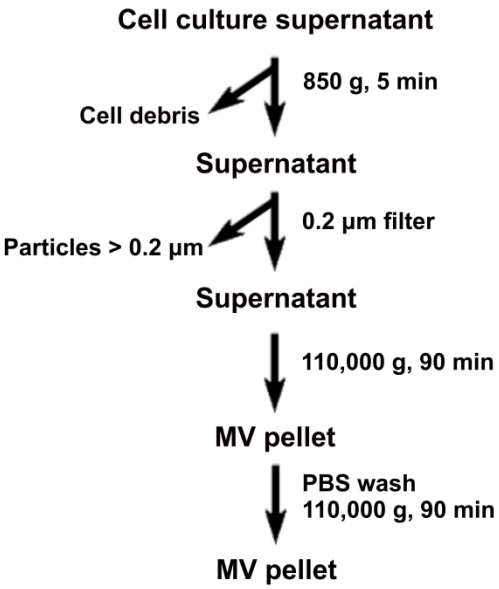

Figure 2-2. Workflow for microvesicle isolation by ultracentrifugation.

2.4.2.2 Proteinase K treatment

To remove proteins attached to the surface of MVs, MVs were treated with Proteinase K as previously described (Montecalvo *et al.*, 2012, Melo *et al.*, 2014). Proteinase K is a serine protease that can cleave proteins over a broad spectrum and allows the breakdown of proteins contained on the vesicular surface while leaving proteins contained in the vesicular lumen intact (Shelke *et al.*, 2014, Gupta and Knowlton, 2007). Proteinase K treatment was performed after the first ultracentrifugation step by resuspending the MV pellet in 500 µg/mL proteinase K followed by incubation for 1 h at 37ºC. Proteinase K was then inactivated by placing the tubes into a water bath heated to 60ºC for 10 min. Following this, ultracentrifugation was performed as described above.

2.4.2.3 Microvesicle isolation from serum and plasma

Next to ultracentrifugation, MVs and exosomes can be isolated using commercially available isolation reagents. Isolation reagents work on the basis of tying up water molecules and thereby force the less-soluble lipophilic components such as the MVs out of solution which can then be pelleted by a brief centrifugation step. Studies comparing ultracentrifugation against isolation reagents have shown that isolation reagents tend to result in a higher yield of MVs from any given volume but do not affect the cargo itself (Rekker *et al.*, 2014).

MVs were isolated from serum of Ang II-infused mice using the total exosome isolation reagent (from serum) (Thermo Fisher, Paisley, UK) according to the manufacturer's instructions. Briefly, serum was thawed at 25ºC in a water bath and then centrifuged at 2,000 g for 30 min to clear the serum of cells and other debris. 200–400 µL of clarified serum was transferred to a new tube and 0.2 volumes (i.e. 40–80 µL) of total exosome isolation reagent was added to the sample and mixed well by vortexing. Next, the sample was incubated at 4ºC for 30 min and then subjected to centrifugation at 10,000 g for 10 min at room temperature to pellet the MVs. The MV depleted supernatant was removed and stored separately and the MV pellet was resuspended in 100–200 µL PBS and stored at -20ºC until further use.

MVs were isolated from the plasma of WKY and SHRSP rats using the total exosome isolation reagent (from plasma) (Thermo Fisher, Paisley, UK) according to the manufacturer's instructions without proteinase K treatment. Briefly, plasma was defrosted at 25ºC in a water bath and then centrifuged at 2,000 g for 20 min to remove cellular debris. The supernatant was then clarified by a further centrifugation step at 10,000 g for 20 min. To dilute the plasma, 100 µL of PBS was added to 200 µL of plasma and mixed well by vortexing. Next, 0.2 volumes (60 µL) of total exosome isolation reagent was added to the sample, vortexed and incubated for 10 min at room temperature. Next, sample was centrifuged at 10,000 g for 5 min at room temperature to pellet the MVs. The plasma supernatant was removed and stored separately. The MV pellet was resuspended in 100 µL PBS and stored at -20ºC until further use.

2.4.3 Nanoparticle tracking analysis

Nanoparticle tracking analysis (NTA) is a light-scattering method for the real-time visualisation and quantification of nanoparticles in solution. It employs a focussed laser beam that is passed through the solution to illuminate the particles (Figure 2-3). The light scattered by the particles can then be visualised microscopically by a conventional microscope with a 20x objective. The microscope is connected to an electron multiplying charged coupled device camera that allows the capture of a video at 30 frames per second (Wright, 2012). The movement of particles in solution is based on the Brownian motion and the NTA software identifies and tracks each particle in each frame of a 30-60 s video (Gardiner *et al.*, 2013). Using the determined mean distance of particle movement in x and y, particle size can be calculated for a known temperature (T) and solvent viscosity (η) using a variation of the Stokes-Einstein equation:

$$\frac{\overline{(x,y)}^2}{4} = Dt = \frac{K_B T}{3\pi\eta d}$$

Where *Dt* is the particle diffusion coefficient, K_B the Boltzmann's constant and *d* the particle hydrodynamic diameter (Wright, 2012).

MVs purified from cell culture medium or animal serum and plasma were quantified using NTA. In brief, 5–10 µL of the re-suspended MVs were diluted in 1 mL PBS. Using a 1 mL syringe the sample was loaded into the sample chamber of a LM14C controller unit connected to an Andor DL-658-OEM-630 camera (Nanosight, Malvern Instruments, Malvern, UK). Videos of 60 s were recorded in duplicate for each sample. Videos were analysed using the accompanying Nanosight NTA 2.0 software with a minimal particle size of 30 nm and the gain and detection threshold adjusted accordingly to detect all particles. The determined concentration was adjusted for sample dilution and the total volume of MV suspension was noted to calculate the total number of MVs.

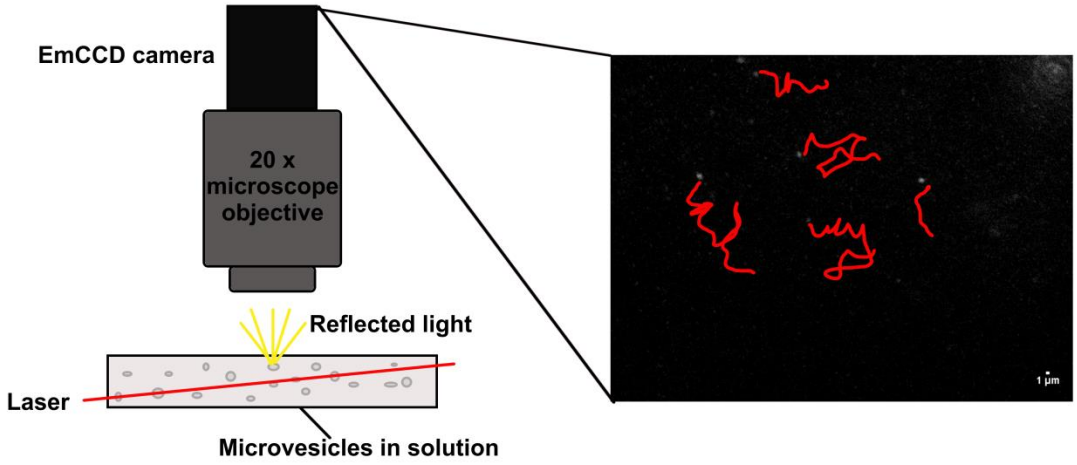

Figure 2-3. Schematic of the setup for nanosight tracking analysis.
Microvesicles in solution are placed into the sample chamber which is placed under the microscope. A laser beam is shown through the sample and the light reflected by the vesicles is captured by a 20 x microscope objective. An attached electron multiplying charged coupled device camera (EmCCD) camera captures a video of the particles moving in solution under Brownian motion and using the accompanying NTA software, the particle motion is tracked (red traces). Schematic adapted from Wright (2012).

2.4.4 Hypertrophy model

H9c2 cells were plated at a density of 1x 10^5 cells/well onto glass coverslips placed in 6-well cell culture plates and allowed to adhere overnight. The cells were then placed into 2 mL serum free MEM and were either left untreated or stimulated with 100 nM Ang II for 96 h to stimulate cardiomyocyte hypertrophy. H9c2 cells were treated with NRCF-derived MVs by dissolving MVs in 2 mL of serum free MEM followed by sterile filtration through a 0.2 µm filter. The sterile solution was then added onto H9c2 cells for 96 h. The AT_1R antagonist losartan (Sigma, Dorset, UK) was used to block the AT_1R receptor and was added at a concentration of 1 µM. In a similar manner, NRCM isolated and cultured as described in Section 2.2.3 were plated at a density of 1x 10^6 cells/well onto 1 % gelatin-coated coverslips. The next day, cells were placed into maintenance media and stimulated for hypertrophy as described above.

At the end of the protocol, cells were lysed for RNA extraction (Section 2.8) or stained with phalloidin (Section 2.5.1).

2.4.5 Labelling of NRCF with fluorescent DiI

Labelling of cells with a fluorescent dye provides an effective method for the investigation of cell proliferation, migration and adhesion (Tian *et al.*, 2013b, Progatzky *et al.*, 2013). DiI (1,1'-Dioctadecyl-3,3,3',3'-Tetramethylindocarbocyanine Perchlorate) is a member of the highly lipophilic carbocyanine dyes that exhibit strong fluorescence when incorporated into membranes (Progatzky *et al.*, 2013). When applied to the cell, the dyes diffuse laterally within the cell membrane staining the entire cell while exhibiting very low cell toxicity.

NRCF were labelled with DiI using the Vybrant DiI cell-labelling solution (Thermo Fisher, Paisley, UK) according to the manufacturer's instructions. Briefly, NRCF were trypsinised and centrifuged in a 15 mL falcon tube as described in Section 2.2.1. The cells were then resuspended in 1 mL serum free DMEM and 5 µL of Vybrant DiI labelling solution was added to the medium. Following gentle mixing, cells were incubated for 30 min at 37 °C and 5 % CO_2. Using Fluorescence-activated cell sorting, this was determined to result in ≥ 90 % labelling of NRCF

which was retained over 48 h. Cells were then pelleted by centrifugation at 480 g for 5 min and washed in PBS prior to plating.

2.4.6 Fibroblast– cardiomyocyte transwell co-culture

MV exchange between fibroblasts and cardiomyocytes was assessed by transwell co-culture. Transwell cell culture inserts consist of a 10 µm microporous polycarbonate membrane separating the top and bottom chamber and allowing the exchange of cellular signals or the migration of cells depending on pore size. A pore size of 0.4 µm prevents the migration of cells but allows the transfer of substances ≤ 400 nm, including MVs.

H9c2 cells were plated at a density of 4x 10^4 cells/well onto round glass coverslips in a 12-well plate and allowed to adhere overnight. Similarly, DiI-labelled NRCF were seeded onto the poly-L-lysine coated microporous membrane of a transwell at a density of 2x 10^4 cells. The next day, the culture media of H9c2 cells and NRCF was replaced by serum free medium and the transwell with the NRCF in the top chamber was moved over the H9c2 cells to allow MV exchange. After 48–96 h, the cells were fixed with 4 % paraformaldehyde (PFA) (Section 2.5) and mounted with Prolong Gold+ DAPI on microscope slides. MV transfer was assessed by confocal microscopy (Section 2.6) at 40x magnification and 0.7x zoom using the HeNe543 and Diode405–30 lasers to visualise DiI and DAPI, respectively. Post-processing of images was performed in Zen 2 lite black.

2.4.7 Detection of Ang II in microvesicles

2.4.7.1 Ang II ELISA

The Angiotensin II EIA Kit was purchased from Bertin Pharma (Montigny le Bretonneux, France). The ELISA is based on immobilised antigen technology which increases its sensitivity to concentrations as low as 1–2 pg/mL. Following reaction of Ang II in the sample with the monoclonal anti-angiotensin II antibody immobilised on the plate, the bound Ang II is covalently linked to the antibody by glutaraldehyde. Bound Ang II then reacts with acetylcholine esterase-conjugated anti-angiotensin II antibody and Ang II content is visualised using Ellman's reagent as substrate.

The Ang II EIA Kit was used according to the manufacturer's instructions. Briefly, 8 standards were prepared by serial dilution ranging from 125–0.98 pg/mL and 100 µL of standard, purified mouse serum and MVs were added to the pre-coated anti-Angiotensin II IgG plate. Sample less than 100 µL were adjusted to 100 µL with PBS. Untreated wells served as negative controls while a quality control of known Ang II concentration supplied with the assay served as positive control. The plate was then incubated for 1 h at room temperature with gentle agitation. Glutaraldehyde [0.5 % (v/v)] was prepared by the addition of 100 µL glutaraldehyde to 1x wash buffer and 50 µL of glutaraldehyde was added to each well and incubated with gentle agitation for 5 min. Next, borane trimethylamine was reconstituted in 5 mL 2 N HCl/Methanol (50/50, v/v) and 50 µL were added to each well and incubated for 5 min to inactivate glutaraldehyde. The plate was then washed 5 times before the addition of 100 µL anti-Angiotensin II IgG tracer. The plate was covered with a plate seal and incubated at 4ºC overnight. The tracer was then removed and the plate washed 5x prior to a 10 min incubation in 300 µL wash buffer and a further five washes with wash buffer. Next, 200 µL Ellman's reagent was added to the plate and incubated in the dark under gentle agitation for 30 min to allow colour development. Absorbance was measured at 405 nm using a Dynex plate reader (Dynex Technologies, Worthing, UK) and the supplied software Revelation 4.25. For the determination of sample concentration, the blanking value (Ellman's reagent only) was subtracted from all measurements and a standard curve with origin at x= 0 and a linear trendline was plotted. Using the linear equation, sample concentration was calculated and corrected for sample dilution if necessary. For samples with a negative concentration as determined from the standard curve Ang II concentration was assumed to be 0 pg/mL. Mean Ang II concentration was calculated by averaging all individual sample readouts measured across different ELISA plates.

2.4.7.2 Tracking of fluorescent Ang II in microvesicles

Fluorescently-labelled Ang II has previously been employed to visualise Ang II-receptor interactions and track its recycling within the cell (Hunyady *et al.*, 2002, Hein *et al.*, 1997) making it a useful tool to determine the loading of exogenous Ang II into MVs.

NRCF were labelled with Vybrant DiI as described in Section 2.4.5 and cultured in 150 cm^2 cell culture flasks until confluent. MVs were isolated from conditioned medium of NRCF stimulated with 1 µM Fluorescein amidite (FAM)-labelled Ang II (Anaspec Inc., Seraing, Belgium) (Section 2.4.1, 2.4.2.1). H9c2 cells were plated at full confluence onto round coverslips in a 12-well plate. The next day, MVs from control and Ang II-stimulated NRCF were added onto H9c2 cells in serum free medium. The cells were then placed on ice for 30 min. This reduces cellular metabolism but allows MVs to settle on the cells without being bound and internalised at the cell membrane. Subsequently, the cells were reheated by placing them at 37ºC and 5 % CO_2 for 30 min to allow MVs to bind and fuse to the cell membrane. Cells were then washed 3x in PBS prior to fixation with 1 % PFA for 20 min. Following a wash in PBS 3x, coverslips were then mounted with Prolong Gold+DAPI onto microscope slides. Slides were imaged by confocal microscopy (Section 2.6) at a magnification of 40x with a 1-1.7x zoom using a C-Apochromat 40x/1.2 x W corr lens and the Argon/2 (488), HeNe543 and Diode405-30 lasers for the detection of FAM, DiI and DAPI, respectively. Images were subsequently processed in Zen 2 lite black.

2.5 Immunocytochemistry

Immunocytochemistry (ICC) is the analysis of specific anatomical structures and localisation of proteins in isolated single cells. It differs thereby from immunohistochemistry (described in 2.7.3) which is the analysis of tissue specimens. Immunocytochemical staining involves the fixation, permeabilisation and the subsequent staining of cells with specific antibodies.

Prior to ICC, cells were cultured on coverslips as outlined in Section 2.2 and treated according to the specified experimental conditions. At the endpoint, culture medium was removed from the cells and washed with PBS three times. Cells were then fixed in 4 % paraformaldehyde for 15 min followed by 3 washes with PBS. At this stage, fixed cells could be stored at 4 ºC in PBS for later analysis. Cells were then permeabilised with 0.1 % (v/v) Triton X-100 (Sigma, Dorset, UK) in PBS for 5 min at room temperature before washing with PBST 3x 5 min. Cells were then blocked in either 10 % goat serum in PBST for single stains or 20 % goat serum in PBST for dual stains for 30 min. For this, coverslips were transferred onto a dry surface (usually the plate lid) and 150 µL blocking solution

was added to each coverslip. Coverslips were then transferred back into the culture plate and 150 µL of the appropriate antibody made up in blocking buffer (Table 2.4) was added and incubated at 4ºC overnight. Coverslips were washed 3x 5 min in PBST at room temperature and transferred back onto a dry surface before incubation with the appropriate secondary antibody made up in blocking buffer (Table 2.5) at room temperature in the dark for 1 h. Coverslips were washed 3x 5 min in PBST and mounted with Prolong Gold+DAPI (Thermo Fisher, Paisley, UK) onto glass microscope slides. Slides were allowed to dry overnight in the dark prior to imaging by confocal microscopy (Section 2.6).

Table 2.4 Primary antibodies for ICC

Antigen	Manufacturer	Host Species	Concentration	Dilution	Buffer
CD31	DAKO (JC70A)	Mouse		1:20	Blocking buffer
S100A4	Abcam (ab27957)	Rabbit	0.72 mg/mL	1:100	
αSMA	Abcam (ab5694)	Rabbit	0.2 mg/mL	1:50	

Table 2.5 Secondary antibodies for ICC

Antigen	Secondary antibody	Manufacturer	Concentration	Dilution	Buffer
CD31	Goat anti-mouse IgG Alexa Fluor 546	Thermo Scientific (A11030)	2 mg/mL	1:500	Blocking buffer
S100A4	Goat anti-rabbit IgG Alexa Fluor 488	Thermo Scientific (A11008)	2 mg/mL	1:500	
αSMA					

2.5.1 Phalloidin stain

Phalloidin is a phallotoxin found in *Amanita phalloides* (death cap mushroom). It acts by binding and stabilising filamentous (F-) actin and prevents its depolymerisation. Due to its high selectivity for F-actin, fluorescently labelled phalloidin is widely used to visualise and investigate cytoskeletal architecture.

Prior to phalloidin stain, cells were fixed with 4 % PFA as previously described in Section 2.5. Cells were then permeabilised in 0.1 % (v/v) Triton X-100 in PBS for 10 min and washed with PBS three times. Cells were then stained with 5 µg/mL fluorescein isothiocyanate (FITC) labelled phalloidin (Sigma, Dorset, UK) prepared with 1 % bovine serum albumin (BSA) in PBS at room temperature in the dark for 1 h. Cells were then washed three times with PBS and the coverslips mounted with Prolong Gold+DAPI (Thermo Fisher, Paisley, UK) onto glass microscope slides.

Images were captured by confocal imagining (Section 2.6) at 25x magnification with a 0.7x zoom and the Argon/2 and Diode405-30 to visualise phalloidin and DAPI, respectively. Images were captured from five fields of view *per* coverslip and care was taken to capture images where cell boundaries were clearly visible. Image analysis was performed using ImageJ. The scale was manually adjusted with a pre-defined macro and using the polygon lasso tool, individual cells were outlined as regions of interest and surface area was measured. Mean cell size was calculated across all measurements *per* treatment.

2.6 Confocal Microscopy

Confocal microscopy is a microscopy technique that allows the creation of true three-dimensional images of a sample. This is achieved by illuminating the sample with a laser beam and excluding out-of-focus reflected light.

The working principle of confocal microscopy is illustrated in Figure 2-4. In the confocal microscope, the sample is illuminated by a fine laser beam. The beam is passed through a pinhole and then reflects off a dichroic mirror which reflects light shorter than a certain wavelength and passes light at longer wavelength. The beam is then focussed on a small spot (1 pixel) in the sample by the

microscope objective. The emitted light passes through the dichroic mirror and is focused on a detector pinhole. The light passing through the pinhole is measured by the photomultiplier tube detector and transferred into a visual image of the section in the sample. Out-of-focus light does not enter the pinhole and therefore is eliminated. In this way, an image is generated only from the point of focus and the sample can be sectioned at multiple planes.

Confocal microscopy was carried out on a LSM 510 Meta laser scanning confocal microscope and the accompanying LSM510 software (Zeiss, Cambridge, UK). Specimens were imaged at either 25x or 40x magnification with variable zoom using a LCI Plan-neofluar 25x/ 0.8 mm KorrPh2 and C-Apochromat 40x/1.2 W corr water immersion lens, respectively. Green, red and blue flourescence were visualised using an Argon/2– 458/477/488/514 (excitation of e.g. FITC), HeNe543 (excitation of e.g. WGA) and Diode 405-30 (excitation of DAPI) laser, respectively. Images were exported as LSM files and post-processing was performed in either Zen 2 lite black (Zeiss, Cambridge, UK) or ImageJ.

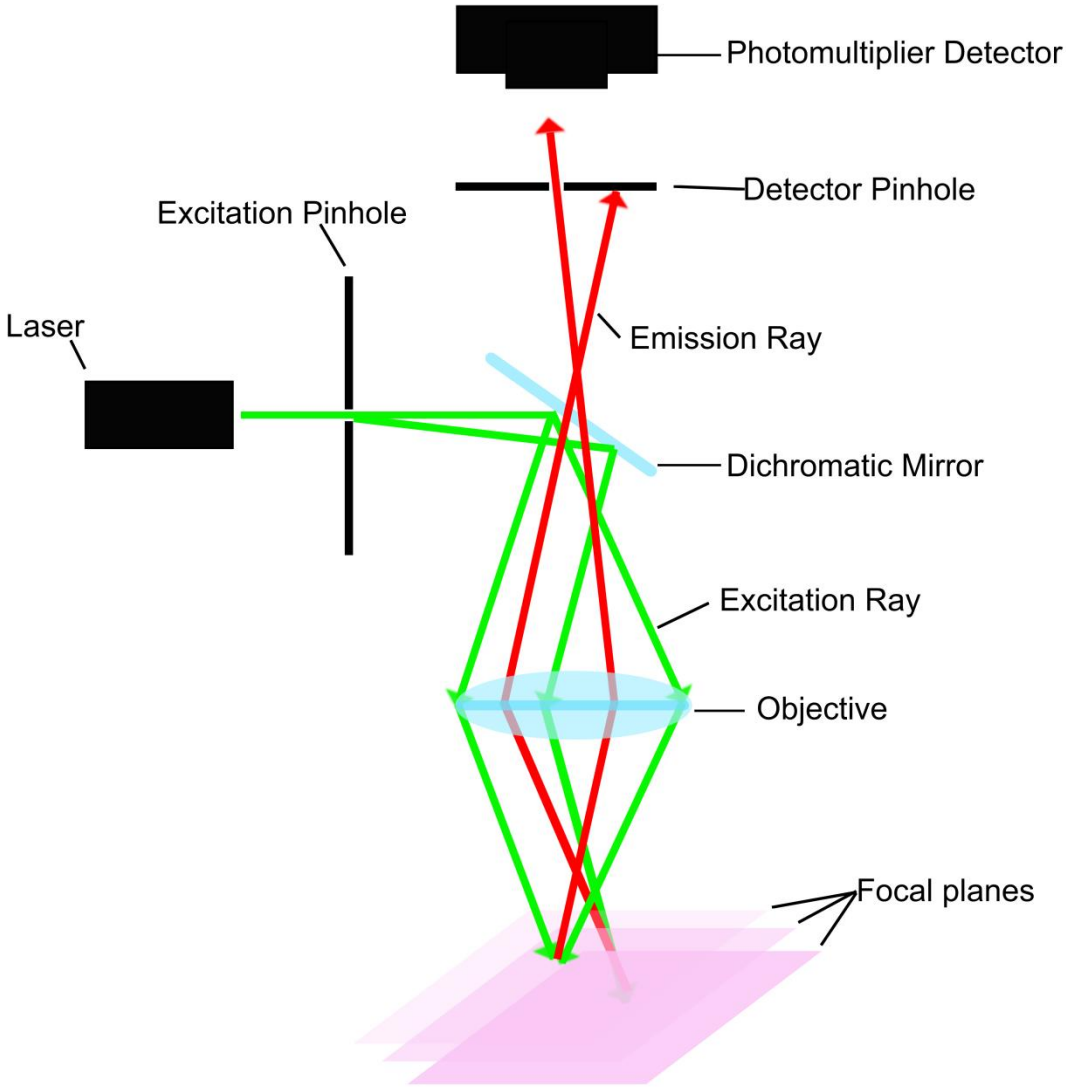

Figure 2-4. Working schematic of confocal microscopy.
The laser beam is passed through a pinhole and reflected by the dichromatic mirror before being focused on one focal plane by the objective. The reflected light is passed through the dichromatic mirror and a detection pinhole and detected by the photomultiplier. Out of focus light from other focal planes does not pass through the pinhole and is therefore discarded from the image acquisition.

2.7 Histology

2.7.1 Processing, sectioning and re-hydration

Prior to processing, fixed tissue was transferred into Shandon biopsy cassettes (Thermo Scientific, Paisley, UK) and then processed in a Shandon Excelsior tissue processor (Thermo Scientific, Paisley, UK) according to the sequence shown in Table 2.6. Once infiltrated in wax, the tissue was embedded on a Shandon Histocentre 3 (Thermo Scientific, Paisley, UK). Hearts were orientated longitudinally to visualise the full myocardial architecture. For sectioning, heart tissue blocks were chilled on ice and then sectioned on a Shandon Finesse 325 microtome (Thermo Scientific, Paisley, UK). Initially, tissue blocks were peeled in to visualise the entire cardiac chamber from which point on 5 µm serial sections were taken for staining. The sections were transferred to a waterbath at 40 ºC to flatten the tissue section before mounting on Tissue-Tek silanized microscope slides (Sakura Finetek, Thatcham, UK) and placing at 60 ºC overnight to dry the tissue.

Prior to histological staining, sections were de-paraffinised and re-hydrated by passing through histoclear and a gradient of alcohol as outlined in Table 2.7.

Table 2.6 Processing sequence for paraffin-embedded tissue sections

Solvent	Time (min)
70 % Ethanol	30
95 % Ethanol	30
100 % Ethanol	30
100 % Ethanol	30
100 % Ethanol	45
100 % Ethanol	45
100 % Ethanol	60
Xylene	30
Xylene	30
Xylene	30
Paraffin wax	30
Paraffin wax	30
Paraffin wax	45

Table 2.7 Re-hydration sequence for histology

Solution	Time (min)
Histoclear	7
Histoclear	7
100 % Ethanol	7
90 % Ethanol	7
70 % Ethanol	7
Water	5

2.7.2 Picrosirius Red

Picrosirius red is one of the most commonly used histological stains to assess collagen deposition in a variety of tissues. The stain is comprised of a solution of yellow picric acid which is a small anionic and hydrophobic dye and sirius red, a large hydrophilic acid dye which penetrate the tissue at different rates. This property leads to the characteristic stain where collagenous tissue is stained bright red and remaining tissue yellow.

After re-hydration, sections were placed into Weigert's haematoxylin (prepared by mixing equal volumes of reagent A and B) (TCS Bioscience, Buckingham, UK) for 10 min to stain the nuclei before washing under running tap water for a further 10 min. Slides were then stained in a 0.1 % sirius red solution in saturated picric acid (Pricrosirius red (F3BA)) (Sigma, Dorset, UK) in the dark for 90 min. Slides were then briefly washed in two changes of 0.01 N HCl (acidified water) by quickly dipping 3 times before de-hydration in two changes of 100 % ethanol for 3 min and two changes in histoclear for 7 min. Sections were then mounted in DPX mountant (Sigma, Dorset, UK) and dried overnight at room temperature.

2.7.3 Immunohistochemistry

Immunohistochemistry allows the detection of specific antigens in tissue sections by using antigen-specific antibodies which are then visualised by secondary enzymatic reactions or fluorescence. A workflow diagram of the steps involved in the histological staining process is shown in Figure 2-5. All incubations were performed in humidified chambers in the dark to prevent evaporation.

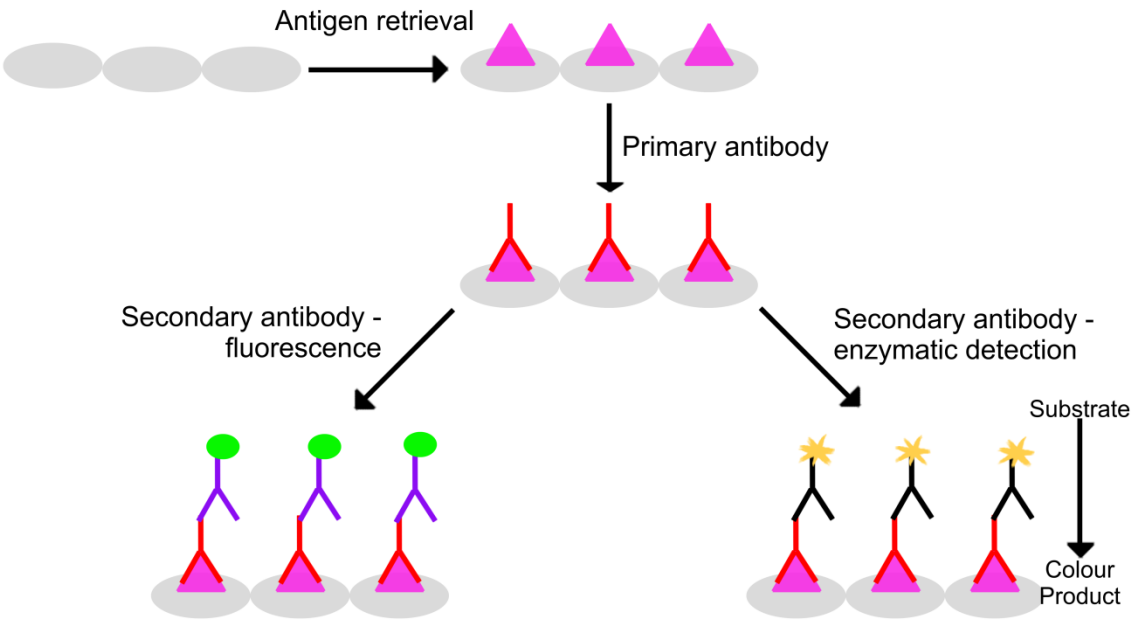

Figure 2-5. Workflow of immunohistochemical staining.
In paraffin embedded section, the antigen is unmasked by enzymatic or heat-mediated antigen retrieval. This is followed by blocking and incubation with antigen-specific primary antibody. Primary antibodies are visualised by either using fluorescently-conjugated or enzyme-conjugated secondary antibodies (raised against the host species of the primary antibody).

Prior to histological staining, tissue was processed, cut and re-hydrated as described (Section 2.7.1 and Table 2.7). This was followed by sodium citrate mediated antigen retrieval which involves boiling the sections in an acidic solution to unfold the antigen masked by the protein cross-links of the formalin fixation. Slides were placed into pre-heated sodium citrate solution and boiled for 10 min and allowed to cool for a further 20 min to allow correct re-folding of the antigen. Slides were then rinsed under running tap water for 5 min followed by two washes in 1x PBS for 5 min. Endogenous biotin activity was quenched by incubation in 3 % H_2O_2 in distilled H_2O for 15 min at room temperature followed by a 5 min wash in 1x PBS. Sections were then blocked in the appropriate blocking solution for 30-60 min as indicated (Table 2.8). Following the removal of the blocking solution by gentle tapping, sections were incubated with primary antibody prepared at the appropriate dilution in modified blocking solution at 4 ºC overnight (Table 2.8). Appropriate IgG at equal concentration was used as a negative control. For secondary enzymatic detection, sections were washed three times in PBS for 5 min followed by incubation with the appropriate secondary antibody (Table 2.9). For collagen I, enzymatic detection by 3,3'-Diaminobenzidine (DAB) staining was performed directly by using a horse radish peroxidase (HRP)–linked secondary antibody which provides a near 1:1 signal ratio to the antibody bound. For collagen III and CD31, a biotinylated secondary antibody was used and the signal was amplified by attaching HRP-linked avidin-biotin complex. Avidin has four high affinity binding sites for biotin and by binding the biotinylated secondary antibody at its unoccupied sites, the avidin-biotin complex amplifies the signal several-fold. For avidin-biotin signal amplification, the Vectastain ABC Kit (VectorLabs, Peterborough, UK) was used according to the manufacturer's instructions. Briefly, 2 drops of reagent A were mixed with 2 drops of reagent B in 5 mL PBS and incubated for 30 min at 4 ºC to allow the avidin-biotin complexes to form before applying to the tissue sections for 30 min at room temperature. Prior to colour detection with DAB, sections were washed 3x 5 min in PBS.

DAB builds the substrate for the HRP linked to the secondary antibody complex and when oxidised forms a brown precipitate at sites of primary-secondary antibody interactions. DAB was prepared according to the manufacturer's instructions of the DAB Peroxidase substrate kit (VectorLabs, Peterborough, UK).

Briefly, 2 drops of buffer, 4 drops of DAB and 2 drops of H_2O_2 were mixed in distilled water and the prepared mix was added to one slide. A stopwatch was started and the colour reaction was monitored under a microscope. Once dark brown staining was evident, the reaction was stopped by placing the slide in water. All other slides were developed according to the same protocol. Slides were then washed under running tap water before counterstaining nuclei with Harris haematoxylin (Sigma, Dorset, UK) for 30 s. Slides were rinsed for a further 5 min in tap water and then dehydrated using the reverse sequence of the re-hydration protocol (Table 2.7). Sections were mounted in DPX mountant and dried overnight.

Table 2.8 Primary antibodies for IHC

Antigen	Manufacturer	Host Species	Concentration	Dilution	Buffer	Blocking Buffer and time
CD31	Dianova (SZ31)	Rat	0.2 mg/mL	1:20	2 % rabbit serum in PBST	15 % rabbit serum PBST, 30 min
Collagen I	Abcam (ab34710)	Rabbit	1 mg/mL	1:200	4 % goat serum in 1 % BSA/PBS	6 % goat serum in 1 % BSA/PBS, 60 min
Collagen III	Abcam (ab7778)	Rabbit	1 mg/mL	1:1000	2 % goat serum in PBST	15 % goat serum in PBST, 30 min

Table 2.9 Secondary antibodies for IHC

Antigen	Secondary antibody	Manufacturer	Concentration	Dilution	Buffer	Incubation time
CD31	Biotinylated rabbit anti-rat	VectorLabs (BA-4000)	1.5 mg/mL	1:500	PBST	30 min
Collagen I	HRP goat anti-rabbit	DAKO (PO448)	0.25 mg/mL	1:100	1 % BSA/PBS	45 min
Collagen III	Biotinylated goat anti-rabbit	VectorLabs (BA-1000)	1.5 mg/mL	1:500	PBST	30 min

2.7.4 Imaging and analysis

Sections stained for picrosirius red, collagen I, collagen III and CD31 were imaged on the EVOS FL Imaging system (Thermo Scientific, Paisley, UK) or an Olympus BX41 microscope connected to a QImaging Go-3 CMOS camera. *Per* section, 5 fields of view around the entire myocardium were captured as 8-bit TIFF files.

Picrosirius red, collagen I and collagen III staining was analysed using Image-Pro Analyzer 7.0 (MediaCybernetics, Rockville, USA). The scale was set manually using a predefined macro. In all cases, the count/size menu was used to specify and select the colour and intensity of the stain and stained area was expressed as percent of total area.

CD31 staining was analysed using ImageJ (National Institute of Health, US). The scale was set manually using a predefined macro and the image was subdivided into 6 squares. Capillaries and nuclei were counted manually using the cell counter in each individual square. For capillary/cardiomyocyte ratio, the ratios of capillaries/nuclei in each individual square were averaged. For capillaries/mm^2:

$$\frac{\text{capillaries}}{mm^2} = \left(\frac{\text{sum of capillaries in all squares}}{\text{area of squares}}\right) \times 10^6$$

2.7.5 Dual Immunofluorescence

Immunofluorescence provides an alternative to enzymatic detection in paraffin embedded tissue sections and due to the variety of fluorophore colours greatly facilitates multiplexing, especially when co-localisation of certain antigens is to be determined.

Tissue sections were prepared and re-hydrated as outlined previously (Section 2.7.1 and Table 2.7) followed by antigen retrieval in 10 mM sodium citrate for 10 min as described previously (Section 2.7.3). Sections were then washed under running tap water for 10 min followed by 3x 2 min washes in TBS. Sections were blocked in TBST with 15 % goat serum for 30 min before incubation with CD31 and S100A4 or CD31 and αSMA as outlined (Table 2.10) at 4 ºC overnight.

Sections were washed 3x 5 min with TBS and then incubated with secondary antibody for 2 h at room temperature (Table 2.11). Slides were washed 3x 5 min in TBS in the dark and then treated with 0.1 % sudan black for 10 min at room temperature to remove lipofuscin-mediated autofluorescence. Sudan black was removed in three 5 min washes of TBS before staining sections with 10 µg/mL DAPI (Sigma, Dorset, UK) for 10 min. DAPI was quickly washed off in TBS before sections were mounted with Prolong Gold+DAPI (Thermo Scientific, Paisley, UK) and allowed to dry overnight. Images were captured by confocal microscopy (Section 2.6).

Co-localisation was assessed using ImageJ with the plugin Just another Co-localisation Plugin (JACoP). In both, the green and the red channel, the thresholds were manually adjusted to exclude background fluorescence and the Pearson's coefficient R and Mander's M1 and M2 coefficients were calculated. Pearson's R value is a measure of a linear relationship between both channels and ranges between -1 to +1 where -1 indicates negative correlation and 1 positive correlation or co-localisation. Mander's M1 and M2 coefficients calculate the ratio of overlap between the two channels and range from 0 to 1 (Bolte and Cordelières, 2006).

Table 2.10 Primary antibodies for immunofluorescence

Antigen	Manufacturer	Host Species	Concentration	Dilution	Buffer
CD31	Dianova (SZ31)	Rat	0.2 mg/mL	1:20	10 % goat serum in TBST
S100A4	Abcam (ab27957)	Rabbit	0.72 mg/mL	1:200	
αSMA	Abcam (ab5694)	Rabbit	0.2 mg/mL	1:100	

Table 2.11 Secondary antibodies for immunofluorescence

Antigen	Secondary antibody	Manufacturer	Concentration	Dilution	Buffer
CD31	Goat anti-rat IgG Alexa Fluor 488	Thermo Scientific (A11006)	2 mg/mL	1:500	TBST
S100A4	Goat anti-rabbit IgG Alexa Fluor 546	Thermo Scientific (A11010)	2 mg/mL	1:500	
αSMA					

2.7.6 Wheat Germ Agglutinin

Wheat Germ Agglutinin (WGA) is a plant lectin found in *Triticum vulgaris* (wheat) which preferentially binds to sugars with *N*-acetylglucosamine and *N*-acetylneuraminic acid (sialic acid) residues commonly found in membrane glycoproteins (Wright, 1984). In the myocardium, *N*-acetylglucosamine and sialic acid are especially abundant in the cardiomyocyte membrane and the t-tubular structures and in cardiac histology, fluorescently-labelled WGA is widely used to visualise the cardiomyocyte membrane and determine cardiomyocyte cross-sectional area (Savio-Galimberti *et al.*, 2008, Tsukamoto *et al.*, 2013, Bueno *et al.*, 2000).

Sections were de-paraffinised and re-hydrated as described previously (Table 2.7) before sodium citrate-mediated antigen retrieval as described previously (Section 2.7.3). Slides were allowed to cool for 20 min and washed under running tap water for 5 min followed by 1x PBS for another 5 min. Sections were blocked in 1x PBS with 1 % BSA and 5 % goat serum (VectorLabs, Peterborough, UK) for 1 h at room temperature before being incubated with 10 µg/mL Alexa Fluor 555 conjugated WGA (Thermo Scientific, Paisley, UK) prepared in the blocking solution for 1 h. Following incubation, sections were washed twice in 1x PBS for 5 min and mounted in Prolong Gold+DAPI (Thermo Scientific, Paisley, UK). Slides were protected from light and allowed to dry overnight prior to imaging by epifluorescence using an Olympus BX40 microscope connected to a QiCam 12-bit Mono Fast 1394 Cooled camera or confocal microscopy (Section 2.6).

Images were taken from 5 fields of view from each section and were analysed in ImageJ. The scale was set using a predefined macro. Cardiomyocyte cross-sectional area was measured using the region of interest tool to trace individual cardiomyocytes (Figure 2-6 B). Twenty-five cardiomyocytes were measured *per* image. Cardiomyocyte diameter was measured across the widest point of the cross-section of a cardiomyocyte (Figure 2-6 B). Forty cardiomyocytes were measured *per* image. Cardiomyocyte length was measured in longitudinal images and length was measured across the length of the cardiomyocyte (Figure 2-6 A). Up to ten cardiomyocytes were measured *per* image. Mean cell size and length was determined as the average of all measurements across all five images.

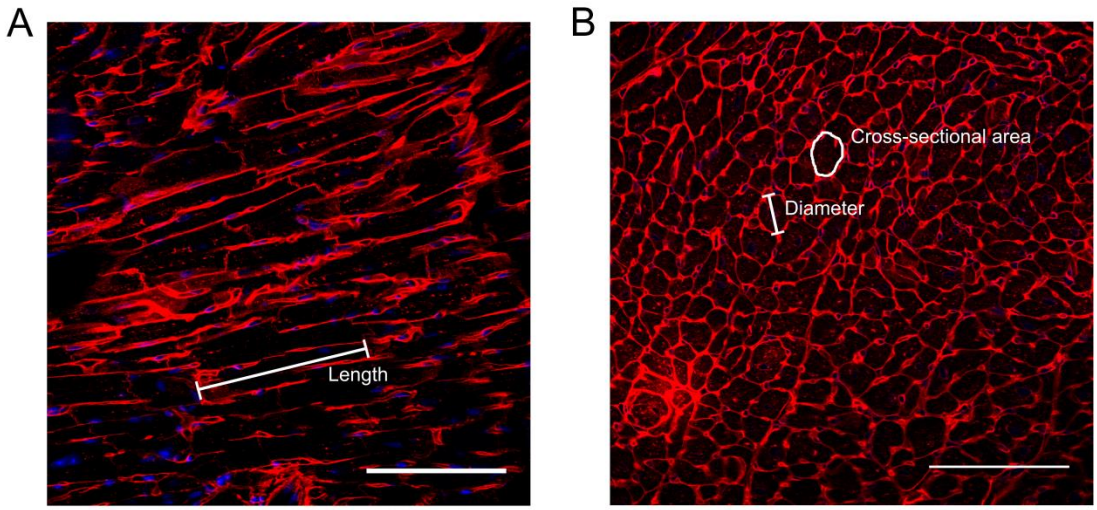

Figure 2-6. Measurements of cardiomyocyte size.
Cardiac sections were stained with wheat germ agglutinin and images were taken from longitudinal and cross-sectional cardiomyocytes and analyised using ImageJ. (A) Cell length was measured by measuring the longest part of the cell from intercalated disk to intercalated disk of adjacent cardiomyocytes (indicated by white line). (B) Cell cross-sectional area was measured by tracing the perimeter of individual cardiomyocytes (indicated by white line) and measuring cell area. Cell diameter was measured across the widest point of a cardiomyocyte cross-section (indicated by white line). Scale bar: 100 μm.

2.8 Gene expression analysis

Gene expression is the process by which the information on a gene is transcribed for the synthesis of proteins. In scientific investigations it is usually employed to assess increases or decreases in the expression of certain genes associated with specific treatment conditions or to verify the active expression of certain genes in a sample. The analysis of the mRNA profile in a sample is a multistep process which involves RNA purification and quantification before its reverse transcription to cDNA and subsequent analysis by quantitative polymerase chain reaction (qPCR).

2.8.1 RNA purification

High quality RNA extracts without genomic DNA contamination are needed for downstream applications such as qPCR and microarray analysis and may not be achieved by standard RNA extraction protocols. The miRNeasy Mini Kit (Qiagen,Manchester, UK) combines QIAzol based lysis with membrane based RNA purification to yield molecular biology grade RNA ranging from 18 nucleotides upward for downstream analysis.

2.8.1.1 Cell/Tissue lysis

QIAzol is a phenol/guanidine thiocyanate based lysis reagent that is optimised for lysis of fatty tissues and inhibits RNases to stabilise the RNA product. Organic extraction with QIAzol efficiently removes genomic DNA contamination.

Cells cultured as described in Section 2.2 were washed in PBS twice before addition of 700 µL QIAzol to each well for lysis. Cells were scraped with the rubber bung of a 1 mL syringe for optimal lysis and the solution was transferred to 1.5 mL RNase free tubes (Thermo Scientific, Paisley, UK). Samples were vortexed briefly for complete homogenisation. Samples were then processed as described in Section 2.8.1.2 or stored at -80 ºC for later analysis.

For RNA extraction from tissue, 10-30 mg of tissue sample (heart) was weighed out into 2 mL RNase free tubes on dry ice followed by the addition of 700 µL QIAzol and a 5 mm stainless steel bead (QIAgen, Manchester, UK). The tissue was then lysed in a tissue lyser (Qiagen, Manchester, UK) at 25 Hz for 4x 30 s for

complete homogenisation of the tissue. The homogenate was immediately processed and RNA extracted as outlined in Section 2.8.1.2.

2.8.1.2 Extraction

RNA extraction from QIAzol lysed cell or tissue samples was performed using the miRNeasy mini kit (QIAgen, Manchester, UK) according to the manufacturer's instructions.

Following lysis the homogenate was placed on the benchtop for 5 min at room temperature to promote dissociation of nucleoprotein complexes. This was followed by the addition of 140 µL chloroform and samples were shook vigorously for 15 s for complete mixing of the suspension. The samples were then incubated on the benchtop at room temperature for 3 min and then spun at 12,000 x g at 4 ºC for 15 min. This organic extraction step efficiently removes genomic DNA and protein from the sample by separating the solution into three phases: a lower red organic phase which contains protein; a white interphase consisting of genomic DNA and the upper colourless aqueous phase which contains RNA. The aqueous phase (usually 200 µL) was transferred to a new tube and 525 µL 100 % ethanol was added. The sample was then pipetted into a spin column and centrifuged at 8000 x g for 15 s to bind the RNA to the silica membrane in the spin column. At this step, on-column DNase digestion was performed to remove any residual contaminating genomic DNA.

Briefly, the column was washed with 350 µL of the ethanol based wash buffer RWT. A stock of DNase I was prepared as per the manufacturer's instructions (Qiagen, Manchester, UK) where per tube 10 µL of DNase I was mixed with 70 µL RDD buffer. 80 µL of prepared DNase I was added directly onto the column membrane and incubated at room temperature for 15 or 30 min for cell and tissue lysates, respectively. The DNase was removed by washing the column with 350 µL RWT buffer.

Following DNase I digestion, the column was washed twice with 500 µL of the ethanol based wash buffer RPE for 15 s and 2 min, respectively. The column was then placed in a new 2 mL collection tube and subjected to centrifugation at 16,100 g for 2 min to dry the membrane and remove carryover of RPE buffer.

The RNA was then eluted from the column by the addition of 30-50 µL of RNase free water directly on the membrane and spinning at 8000 g for 1 min. To increase RNA yield and concentration, the elute was passed through the column again. RNA concentration and quality was then assessed by nanodrop as described in Section 2.8.1.3.

2.8.1.3 RNA quantification

Purified RNA was quantified using the Nanodrop 1000 Spectrophotometer (Thermo Scientific, Paisley, UK). The Nanodrop allows the measurement of nucleic acid as well as protein concentration in a sample volume as small as 1 µL by using a novel sample retention system. It works by applying 1-2 µL of sample to a pedestal which will form a liquid column once the upper arm is lowered on the sample. A xenon light will pulse a light near 260 nm through the specimen, the absorption of which is measured by the CCD detector in the bottom and from which the concentration is calculated with a modification of the Beer-Lambert equation:

$$C = \frac{(A \times \varepsilon)}{b}$$

where C is the concentration of the sample in ng/µL, A the absorbance measured at 260 nm, ε the wavelength dependent extinction coefficient (for RNA 40 ng-cm/µL) and b the path length in cm (for the Nanodrop 1000 this is 0.2 and 1 mm) (Gallagher and Desjardins, 2006). Since ssDNA, dsDNA and RNA all absorb at 260 nm their purification is therefore essential prior to spectrophotometric quantification.

Since RNA absorbs at 260 nm but not 280 nm, the 260/280 absorbance ratio was used to determine the purity of RNA and an absorbance ratio from 1.8– 2.2 was considered as pure. Lower absorbance ratios indicate a contamination of protein or phenol or other substance that absorb at 280 nm.

2.8.2 Real time quantitative reverse transcription PCR

Real time qPCR is a method by which expression of specific genes of interest can be measured in a complex sample. It is one of the most sensitive methods for

gene expression analysis and measures the PCR reaction as it occurs which allows later quantification of the starting concentration and copy number. This is in contrast to less sensitive endpoint methods (such as Northern blots or standard PCR) where gene quantification is not possible (Schmittgen *et al.*, 2000). Real time qPCR is based on the use of fluorescent reporters that allow monitoring of the amplification reaction as it occurs. Two chemistries have been developed for use in real time qPCR: TaqMan and SYBR Green I dye. TaqMan chemistry is based on the use of Taq DNA polymerase which has intrinsic 5' nuclease activity and dual labelled hydrolysis probes. Such probes have a fluorescent reporter (FAM) located at the 5' end and a quencher (MGB) in the minor groove at the 3' end. The proximity of the MGB moiety in the intact probe significantly reduces the fluorescence of the reporter (Figure 2-7 A). When combined with cDNA product, the probe will anneal to its target sequence and as Taq polymerase extends the strand, it cleaves the probe at the 5' end and thereby separates the fluorescent reporter from the probe and significantly increases the fluorescent signal. Additionally, the probe will now be removed from the target strand and allows complete target strand extension (Figure 2-7 A). As the reaction progresses, more probe will be cleaved and the increase in fluorescent signal is directly proportional to the amount of amplicon (Heid *et al.*, 1996). In contast, SYBR Green I dye is based on its ability to bind double stranded (ds) DNA. When bound to dsDNA, SYBR Green emits fluorescence and hence, the more the target sequence is amplified, the higher the fluorescence emitted by the dye (Figure 2-7 B). However, since SYBR Green binds all dsDNA, it bears the risk of amplifying non-specific targets and protocols are lengthened by the analysis of melt curves to assess for primer-dimers in the reaction.

A PCR reaction consists of 3 phases: The exponential phase where there is exact doubling of PCR product due to high abundance of reagents; the linear phase where exact doubling of product no longer occurs due to depletion of reagents; and the plateau phase where the reaction is stopped as all reagents have been used up. This is usually measured in end-point assays of gene expression. In real time qPCR the threshold, the intensity of fluorescence above background, is set when the reaction enters its exponential phase and where variability is the lowest. The cycle at which a sample crosses this threshold is defined as the Ct and used for later quantitative analysis. Real time qPCR reactions can be

performed in one step where the reverse transcription and the PCR are performed in one system or as a two-step procedure where reverse transcription is carried out separately from the PCR reaction as outlined below.

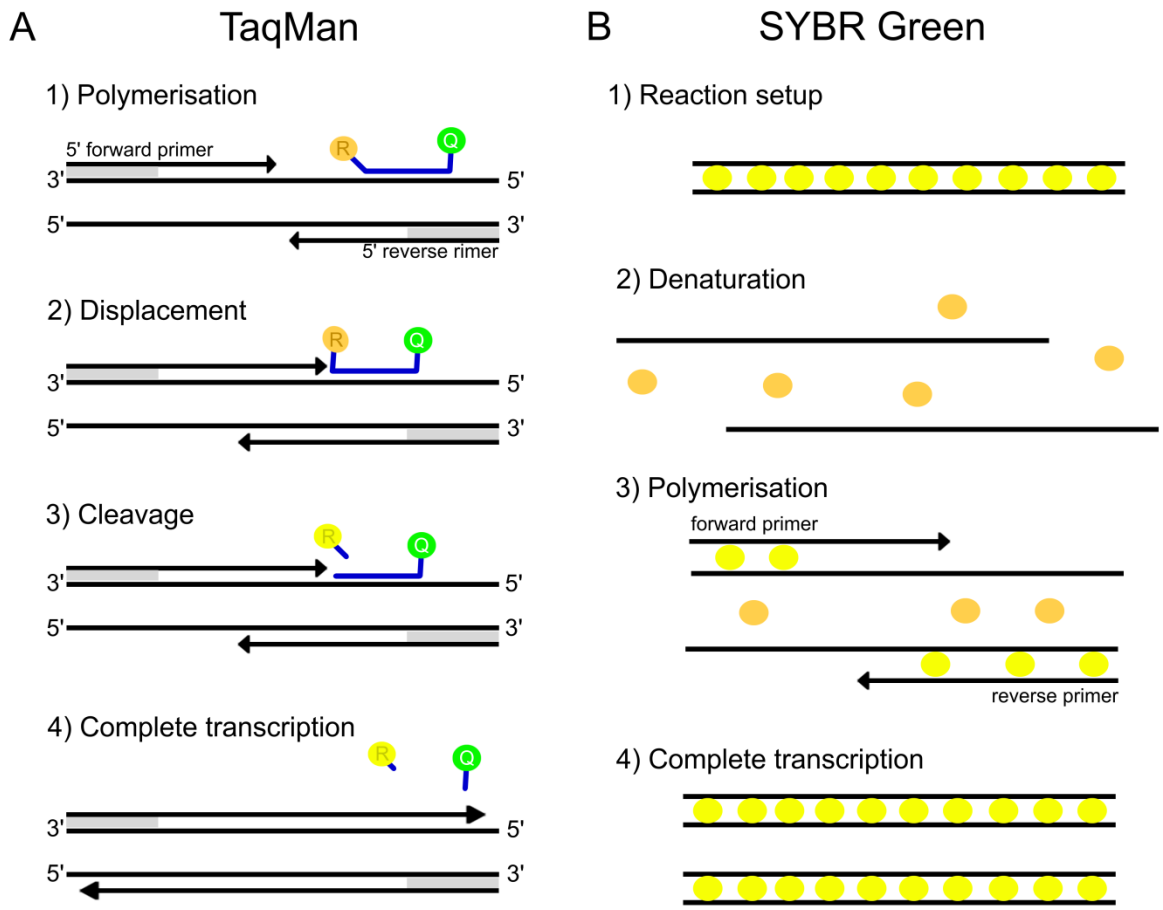

Figure 2-7. Working principle of TaqMan and SYBR Green gene expression analysis. (A) The close proximity of the Quencher (Q) to the reporter dye (R) in the TaqMan probe quenches baseline fluorescence. Upon transcription and elongation of the DNA strand by Taq polymerase, the reporter is cleaved from the quencher which now exhibits bright fluorescence. (B) SYBR green probes exhibit strong fluorescence when bound to double-stranded DNA. Upon depolymerisation, there is a net decrease in fluorescence. As new strands are extended, fluorescence increases and once polymerisation is complete there is a net increase in fluorescence. Adapted from Applied Biosystems (2010).

2.8.2.1 Reverse transcription

Reverse transcription was performed using Taqman reverse transcription reagents (Thermo Fisher, Paisley, UK) according to the manufacturer's instructions. The reactions were prepared in a 96-well PCR plate (Starlab, Milton Keynes, UK). In brief, for a 20 µL reaction, reagents were prepared as follows: 2 µL 10 x RT buffer, 4.4 µL 25mM $MgCl_2$, 4 µL 10 mM dNTPs, 1 µL 50 µM random hexamers, 0.4 µL RNase Inhibitor (20 U/µL), 0.5 µL Multiscribe reverse transcriptase (50 U/µL) and 7.7 µL of RNA pre-diluted in RNase-free water. For gene expression analysis in cell culture samples, RNA was pre-diluted to the lowest concentration in the sample set (ranging between assay-dependent concentrations of 20-200 ng/µL). For tissue samples, samples were pre-diluted to 200 ng/µL and 5 µL was added to give a final amount of 1 µg RNA in the cDNA reaction. A negative reaction where only H_2O was added served as negative control for specific amplification. The plate was sealed with an adhesive sheet and briefly centrifuged to mix the components in the bottom of the plate. The plate was placed on a PCR block set up for the cycling conditions indicated (Table 2.12). Samples were stored at -20ºC until required.

Table 2.12 Cycling conditions for reverse transcription

Step	Temperature (°C)	Time (min)
1	25	10
2	48	30
3	95	5
4	4	infinite

2.8.2.2 Quantitative PCR

qPCR was performed in 384-well MicroAmp optical PCR plates (Thermo Fisher, Paisley, UK) with a total reaction volume of 10 µL. For 1 reaction, 5 µL of TaqMan master mix II (Thermo Scientific, Paisley, UK) containing AmpliTaq Gold DNA polymerase, dNTPs, ROX passive reference and buffer was combined with 0.5 µL of the appropriate TaqMan assay containing the specific primer components (Table 2.13, Table 2.14, Table 2.15), 1.5 µL of the RT product and made up with RNase free H_2O to 10 µL. In certain circumstances where expression of the target gene was low, the volume of RT product was increased to load a maximum of 100 ng cDNA in the reaction. Reactions were performed in duplicate and the cDNA negative and H_2O served as negative controls. The plate was sealed with an optical adhesive sheet and centrifuged to mix the components and remove any air bubbles in the sample. qPCR was performed either on a 7900HT Fast or a Quantstudio 12K Flex Real Time PCR System with the accompanying software (Thermo Fisher, Paisley, UK). To reduce variability, the PCR system used was kept consistent for related data sets. The cycling conditions used are shown (Table 2.16). Cycle threshold (Ct) was determined as the cycle where the reaction entered the exponential phase. Data were expressed as relative quantity (RQ) according to the $2^{-\Delta\Delta Ct}$ method (Schmittgen and Livak, 2008) where

$$\Delta\Delta Ct = \left(Ct \text{ gene of interest}(A) - Ct \text{ internal control}(A)\right) - \left(Ct \text{ gene of interest}(B) - Ct \text{ internal control}(B)\right)$$

with A = sample of interest and B = reference sample (i.e. control).

In tissue samples, Ppib (Peptidylprolyl Isomerase B), a cyclosporine-binding protein involved in the celluar secretory pathways, was selected as housekeeping gene as it has been verified to be stable across all treatment groups in previous investigations using an endogenous control assay. For cell culture samples, GAPDH was verified as stable housekeeping gene.

Table 2.13 Mouse TaqMan probes

Gene	Assay ID	Reference Sequence	Label
ACE	Mm00802048_m1	NM_001281819.1	FAM/MGB
ACE2	Mm01159003_m1	NM_001130513.1	FAM/MGB
ACTA2	Mm00725412_s1	NM_007392.3	FAM/MGB
Agtr1a	Mm00616371_m1	NM_177322.3	FAM/MGB
Agtr2	Mm01341373_m1	NM_007429.5	FAM/MGB
Col1a1	Mm00801666_g1	NM_007742.3	FAM/MGB
Col3a1	Mm01254476_m1	NM_009930.2	FAM/MGB
MYH7	Mm01319006_g1	NM_080728.2	FAM/MGB
Nppa	Mm01255747_g1	NM_008725.2	FAM/MGB
Nppb	Mm01255770_g1	NM_001287348.1	FAM/MGB
Ppib	Mm00478295_m1	NM_011149.2	FAM/MGB
S100A4	Mm00803372_g1	NM_011311.2	FAM/MGB
TGFß1	Mm01178820_m1	NM_011577.1	FAM/MGB

Table 2.14 Human TaqMan probes

Gene	Assay ID	Reference Sequence	Label
ACTA2	Hs00426835_g1	NM_001141945.1	FAM/MGB
Cdh5	Hs00901463_m1	NM_001795.3	FAM/MGB
CNN1	Hs00154543_m1	NM_001299.4	FAM/MGB
Col1a1	Hs00164004_m1	NM_000088.3	FAM/MGB
GAPDH	4326317E	NM_002046.3	VIC/MGB
PECAM1	Hs00169777_m1	NM_000442.4	FAM/MGB
S100A4	Hs00243202_m1	NM_002961.2	FAM/MGB
Smad4	Hs00929647_m1	NM_005359.5	FAM/MGB
Smad7	Hs00998193_m1	NM_001190821.1	FAM/MGB
SNAI1	Hs00195591_m1	NM_005985.3	FAM/MGB
SNAI2	Hs00950344_m1	NM_003068.4	FAM/MGB
TAGLN	Hs01038777_g1	NM_001001522.1	FAM/MGB
TGFß	Hs00998133_m1	NM_000660.4	FAM/MGB

Table 2.15 Rat TaqMan probes

Gene	Assay ID	Reference Sequence	Label
ACE	Rn00561094_m1	NM_012544.1	FAM/MGB
ACE2	Rn01416293_m1	NM_001012006.1	FAM/MGB
Agtr1a	Rn02758772_s1	NM_030985.4	FAM/MGB
Agtr2	Rn00560677_s1	NM_012494.3	FAM/MGB
CTGF	Rn01537279_g1	NM_022266.2	FAM/MGB
Mas	Rn00562673_s1	NM_012757.2	FAM/MGB
Nppa	Rn00664637_g1	NM_012612.2	FAM/MGB
Nppb	Rn00676450_g1	NM_031545.1	FAM/MGB
Ppib	Rn00574762_m1	NM_022536.2	FAM/MGB

Table 2.16 Cycling conditions for qPCR

Step	Temperature (°C)	Time	
1	95	10 min	
2	95	15 s	Repeat 40x
3	60	1 min	

2.9 Protein expression analysis

2.9.1 Protein extraction

Protein extraction is the process by which individual cellular proteins are isolated from the intact cells and tissue. Cell lysis is the first step in the process of protein extraction and is normally achieved by the physical disruption of cell in conjunction with detergent-based lysis buffers. Such lysis buffer are physiological buffers containing detergents (e.g. Triton-X, sodium dodecyl sulphate) for membrane disruption, protease inhibitors (e.g. PMSF, EDTA, EGTA) to stabilise the cellular proteins and protect them from degradation by activated endogenous proteases as well as inhibitors of phosphatases (e.g. NaF, Na_3VO_4) to maintain the protein in its current state and prevent de-phosphorylation.

Cells cultured in 6-well plates and treated according to the experimental outline, were washed twice with cold PBS before the addition of 100 µL Western lysis buffer. Cells were disrupted with a cell scraper and the cell lysate transferred to an Eppendorff tube. The lysate was then freeze-thawed on dry ice to increase cell lysis. The sample was then sonicated at 20 Hz for 5 s using a Sonic Dismembrator (Fisher Scientific, Loughborough, UK) before centrifugation at 16,100 g for 10 min at 4 ºC to remove any cellular debris. The supernatant was then transferred to a fresh tube, protein concentration determined by BCA assay (Section 2.9.2) and the sample stored at -20 ºC until use.

For tissue, 10-30 mg of tissue sample (heart) was weighed out into 2 mL Eppendorffs containing 5 mm stainless steel beads on dry ice followed by the addition of 10x volume of lysis buffer (i.e. for 20 mg, 200 µL lysis buffer was added). The tissue was then lysed in a tissue lyser (Qiagen, Manchester, UK) at 25 Hz for 4x 30 s for complete homogenisation of the tissue and subsequently processed as described above for cell lysate.

2.9.2 The bicinchoninic acid assay

The bicinchoninic acid (BCA) assay is a colorimetric assay for the detection and quantification of total protein in a sample. It is based on the biuret reaction where Cu^{2+} is reduced to Cu^{1+} by protein in an alkaline medium to develop a purple colour on reaction with BCA which exhibits a strong absorbance at

562 nm. The colour development is highly proportional to the concentration of protein in the assay and using standards of common proteins such as BSA with known concentration allows the construction of a standard curve from which unknown protein concentration can be determined. The BCA assay has the advantage that unlike other protein assay formulations it is compatible with a wide variety of detergents and denaturing reagents found in common protein lysis buffers (Walker, 1994).

The BCA assay was performed using the Pierce BCA Protein Assay Kit (Thermo Scientific, Paisley, UK) according to manufacturer's instructions for the micro-well procedure. The assay was performed in a clear 96-well flat bottom plate. Briefly, 9 standard dilutions of known concentration were prepared using the provided BSA stock solution as outlined (Table 2.17) and 25 µL of prepared standards were pipetted in duplicate into the micro-well plate. Protein sample was diluted 1:5 or 1:2.5 by adding 20 µL or 15 µL of PBS to each well and adding 5 µL or 10 µL of sample, respectively. Samples were prepared in duplicate unless starting sample volume was low. The BCA working reagent was then prepared by mixing the required volume of Reagent A with 50 parts of Reagent B and 200 µL of the resulting green mixture was added to each well. The plate was mixed briefly and then incubated at 37ºC for 30 min. Following incubation, absorbance was then read at 562 nm using a SpectraMax Spectrophotometer and the accompanying software. Using Microsoft Excel, a standard curve was then prepared by blotting the mean absorbance of each standard on the X-axis and the corresponding amount of BSA in each well on the Y-axis. A best fit linear trendline was added and linearity was verified by an $R^2 \geq 0.98$. Using the provided linear equation, the amount of protein in the sample was calculated by solving the equation for Y using the determined absorbance values. Protein concentration was then calculated:

$$\text{Protein concentration } \left(\frac{\mu g}{\mu L}\right) = \frac{\text{Amount of protein } (\mu g)}{\text{Volume of protein sample added into reaction } (\mu L)}$$

Table 2.17 BSA protein standards for the BCA assay

Standard	BSA concentration (μg/mL)	Amount of BSA in a well (μg)
A	2000	50
B	1500	37.5
C	1000	25
D	750	18.75
E	500	12.5
F	250	6.25
G	125	3.125
H	25	0.625
I	0	0

2.9.3 Western blotting

2.9.3.1 SDS-Page

Protein samples prepared as outlined previously (Section 2.9.1 and 2.9.2) were diluted to an equal amount of 15-20 µg in a total volume of 11.25 µL PBS with 3.75 µL of 4x NuPAGE LDS sample buffer (Thermo Scientific, Paisley, UK) to make up the volume to 15 µL. This sample buffer contains lithium dodecyl sulphate at pH 8.4 which allows for optimal denaturing and reducing conditions needed for protein preparation for electrophoresis. The added coomassie dye furthermore allows for the visualisation of the progress of the electrophoresis along the gel. Prepared samples were heated to 70ºC for 10 min on a heat block to denature the protein. In the meantime, 1 L of 1x MES SDS running buffer (Thermo Scientific, Paisley, UK) was prepared. Pre-cast NuPAGE Novex Bis-Tris gels with a polyacrylamide gradient of 4-12 % (Thermo Scientific, Paisley, UK) and the appropriate number of wells were set up in a XCell SureLock Mini gel tank (Thermo Scientific, Paisley, UK) and the combs removed. These gels are made up of a low acrylamide (4 %) density stacker gel and a running gel with an acrylamide gradient (4-12%). Due to the low density of acrylamide and the resulting large pores, the stacking gel does not separate the protein but allows its concentration into a thin band (Mahmood and Yang, 2012). In the running gel, the increasing concentration of acrylamide separates the proteins by size with smaller proteins migrating faster than larger ones. Running buffer was added to the gel tank to cover the electrodes and the system was checked for leaks. Next, the heated protein samples were loaded in the wells and note was taken of the order of loading. A pre-stained molecular weight marker (Amersham ECL Rainbow Molecular Marker, GE Healthcare Life Sciences, Little Chalfont, UK) was loaded into one well for reference. The electrophoresis was run on ice for 45-60 min at 200 V until the loading dye reached the end of the gel for maximum protein separation.

2.9.3.2 Transfer

Following electrophoresis as described (Section 2.9.3.1), the gel was transferred onto a membrane to allow the detection of protein with antibodies. During electrophoresis, transfer buffer was prepared by diluting 10x Western running buffer in 20 % (v/v) methanol in distilled H_2O. The pre-cut 0.2 µm pore size

nitrocellulose membrane (GE Healthcare Life Sciences, Little Chalfont, UK) was wetted in distilled H_2O before being soaked in transfer buffer for at least 10 min. Similarly, 6 pre-cut filter papers were soaked in transfer buffer. After electrophoresis, the gel was carefully removed from the cassette and placed on top of a pre-wetted sponge and 3 pieces of filter paper. The nitrocellulose membrane was carefully placed on top of the gel, followed by 3 pieces of filter paper and a sponge. A blotting roller was used to ensure no air bubbles were trapped in this sandwich. The blotting cassette was then transferred into the transfer tank and filled with transfer buffer. Care was taken to ensure that the membrane was facing the anode to allow protein to migrate out of the gel and onto the membrane. Current was applied at 100 V and run for 90 min at 4 ºC.

2.9.3.3 Detection

Following transfer, the membrane was removed from the transfer cassette and washed with PBS for 5 min. Successful transfer was verified by the transfer of the pre-stained protein ladder. The membrane was then blocked in 30 % Sea Block (Thermo Scientific, Paisley, UK) in TBST for 1 h at room temperature. Sea block contains steelhead salmon serum in PBS and provides an alternative to milk and BSA as blocking reagents. It is especially useful in detection that involves mammalian samples as it has less specific binding interactions with antibodies and other proteins that usually occur with standard blocking reagents, thereby significantly reducing background. Following blocking, the membrane was incubated with the appropriate primary antibody (Table 2.18) made up in blocking buffer at 4 ºC overnight. As fluorescent detection was used, antibodies were multiplexed when possible. The following day, the antibody was removed and frozen at -20 ºC for re-use. The membrane was washed 3x 10 min in TBST before incubation in the appropriate secondary antibody (Table 2.19) made up in blocking buffer. As fluorescent antibodies were used, all further steps were performed in the dark. The secondary antibody was removed and frozen at -20 ºC for re-use and the membrane was washed 3x 10 min in TBST. The membrane was then placed in PBS until being scanned on an Odyssey Sa Infrared Imaging System (Licor, Cambridge, UK) and the accompanying Odyssey Sa software.

For quantification, scans were imported into Image Studio Lite version 5.2.5 (Licor, Cambridge, UK) and using the analysis tool, rectangles were placed automatically around each individual band. The background method was set to median with a border width of 3. The abundance of the protein of interest was then expressed relative to the housekeeper GAPDH:

$$\text{relative abundance} = \frac{\text{signal intensity of protein of interest}}{\text{signal intensity of GAPDH}}$$

In the case of phospho-proteins, abundance was expressed relative to the total abundance of the protein.

For the analysis of several proteins on the same membrane when antibodies cannot be multiplexed, it is necessary to strip and reprobe the membrane. Stripping removes bound primary antibody but carries the risk of releasing protein from the membrane and decreasing sensitivity. Several different stripping options exist with harsh buffers using heat and detergent and milder approaches using low or high pH. Here, membranes were stripped using high pH and agitated in 0.2 M NaOH for 15 min. Residual NaOH was then washed off with TBST for 10 min. The membrane was then re-blocked and protein detection was performed as described above.

Table 2.18 Primary antibodies for Western blotting

Antigen	Manufacturer	Host Species	Concentration	Dilution
GAPDH	Abcam (6C5)	Mouse	2 mg/mL	1:5000
GAPDH	Cell Signalling (14C10)	Rabbit	n/a	1:1000
Phospho-PKA C (Thr 197)	Cell Signalling (D45D3)	Rabbit	n/a	1:500
PKA C alpha	Cell Signalling (#4782)	Rabbit	n/a	1:1000
Phospho-Smad2 (Ser 465/467)	Cell Signalling (138D4)	Rabbit	n/a	1:500
Smad2	Cell Signalling (D43B4)	Rabbit	n/a	1:500
Phospho-p44/42 MAPK (Erk1/2) (Thr202/Tyr204)	Cell Signalling (#9109)	Rabbit	n/a	1:1000
p44/42 MAPK (Erk1/2)	Cell Signalling (#9102)	Rabbit	n/a	1:1000
Human CD31	DAKO (JC70A)	Mouse	515 mg/mL	1:500
αSMA	Abcam (ab5694)	Rabbit	0.2 mg/mL	1:500

Table 2.19 Secondary antibodies for Western blotting

Secondary antibody	Manufacturer	Concentration	Dilution
Donkey anti-mouse IRDye 680RD	Licor (926-68072)	1 mg/mL	1:15000
Goat anti-mouse IgG Alexa Fluor 700	Thermo Scientific (A21036)	2 mg/mL	1:15000
Goat anti-rabbit IgG Alexa Fluor 790	Thermo Scientific (A11367)	2 mg/mL	1:15000

2.10 Adult mouse cardiomyocyte isolation

Mouse ventricular cardiomyocytes were isolated from adult C57BL/6 mice by Langendorff perfusion with collagenase enzyme.

Mice were killed by cervical dislocation and the heart was rapidly removed and cannulated (Section 2.11.1). The heart was then perfused at a constant flow rate of 4 mL/min with Krebs-Henseleit (KH) solution to clear the heart of residual blood. Once the perfusate was clear, collagenase type I (Worthington Chemicals, USA) and protease XIV (Sigma, Dorset, UK) were added to the perfusion solution at a final concentration of 0.7 mg/mL and 0.06 mg/mL, respectively. The heart was digested for 6 min 15 s prior to perfusion with 0.5 % BSA in KH buffer for a further 4 min to de-activate the enzyme. The heart was then removed from the cannula, the RV removed and the LV was cut into small pieces which were transferred into a 15 mL falcon tube with fresh 10 mL BSA-KH buffer. The heart pieces were agitated with a flame-blunted Pasteur pipette to release cells from the tissue. Once the solution appeared cloudy, the remaining heart pieces were allowed to settle and 5 mL supernatant was transferred into a fresh tube. Fresh BSA-KH was added and the process repeated for a further 2-3 times. Visual inspection confirmed the presence of viable rod-shaped cardiomyocytes. Next, the calcium concentration of the cell suspension was gradually increased to 1 mM by incremental addition of 1 µL of 100 mM $CaCl_2$ *per* 1 mL cell suspension every 5 min. This limits rapid Ca^{2+} influx and hypercontraction of cardiomyocytes.

2.10.1 Cardiomyocyte stimulation

The cardiomyocytes were pelleted using a hand-operated centrifuge and re-suspended in 8 mL KH buffer containing 1.8 mM Ca^{2+}. The cell solution was distributed into 8 individual falcon tubes and cells were stimulated with 1 µM Ang-(1-9), 1 µM Ang-(1-7) (Phoenix Pharmaceuticals, Karlsruhe, Germany) or 1 µM forskolin in duplicate for 15 min. Untreated cell served as time matched control. The cells were then pelleted and lysed in protein lysis buffer for Western blotting of (phospho-)PKA as described in Section 2.9.

2.11 *Ex vivo* Langendorff perfusion

Ex vivo Langendorff perfusion of rat hearts was carried out by perfusion of the heart with Tyrode's solution at a constant flow of 10 mL/min which was found to be optimal in this experimental system (Figure 2-8 A).

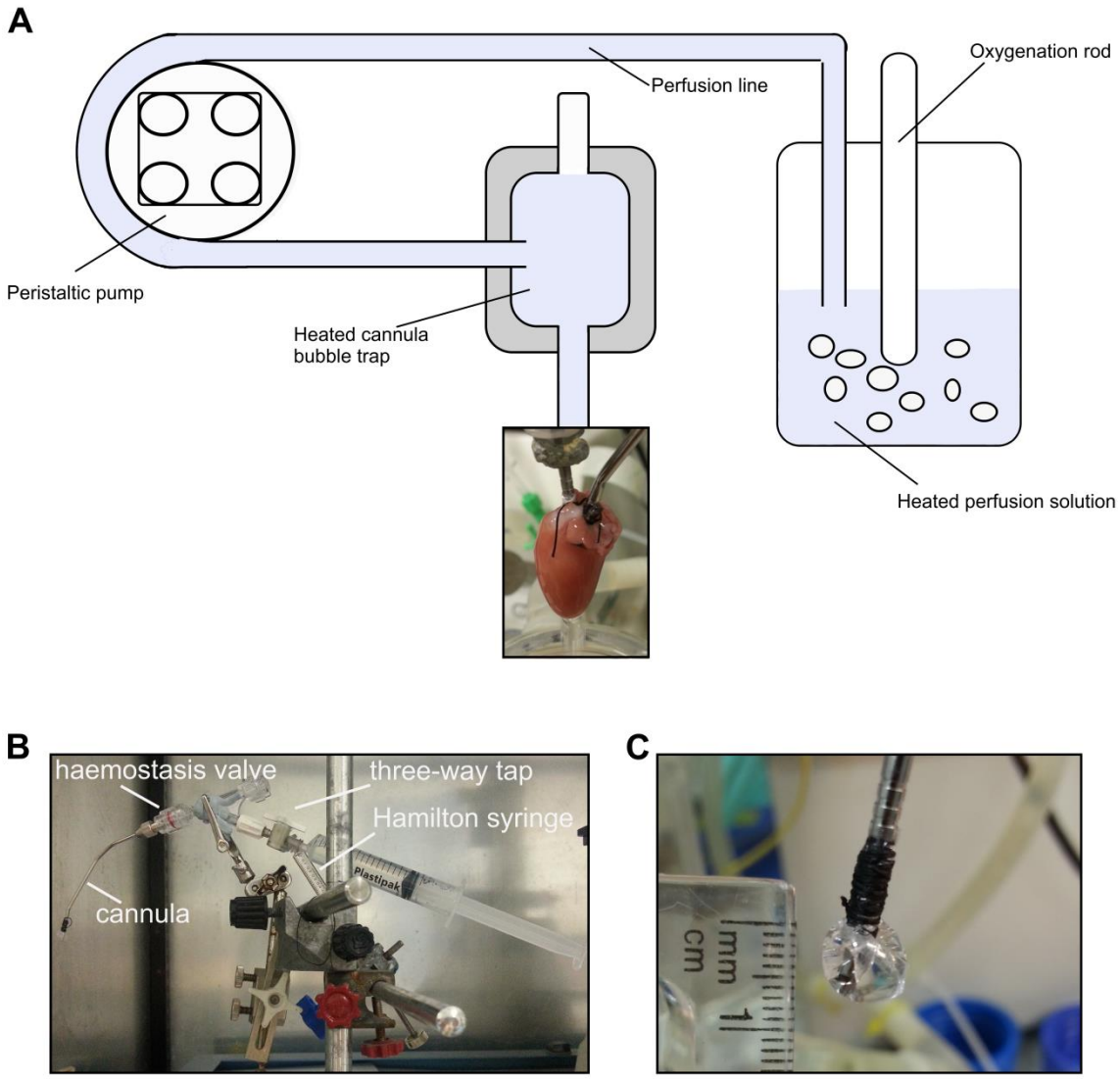

Figure 2-8. Constant flow Langendorff perfusion.
(A) Schematic of the Langendorff perfusion system with constant flow. (B - C) Cannula setup for measurement of LVP with the attached balloon prepared out of clingfilm.

2.11.1 Harvesting and cannulating the heart

Adult Wistar rats (Envigo, UK) weighing between 200–250 g were killed by concussion with subsequent cervical dislocation. The skin was incised at the xyphoid-sternum and the incision continued left and right through the ribs to expose the heart. Using blunt forceps and fine curved scissors the heart was excised by cutting the ascending aorta at the thymus level. The excised heart was immediately transferred to ice cold Ca^{2+}-free Tyrode solution, gently squeezed to expel residual blood and transferred into fresh ice cold Tyrode solution. Extra-cardiac tissue was quickly removed to dissect the aorta. Next, the heart was transferred onto the cannula while perfusate was dripping from the cannula to minimise the transfer of air emboli and was secured in place with a bulldog clip and then two secure sutures. Care was taken to not insert the cannula too deep into the aorta resulting in occlusion of coronary arteries or damage of the aortic valves leading to inadequate cardiac perfusion. To allow drainage of the perfusate, a small incision was made into the pulmonary artery. After successful cannulation, the heart will start beating within seconds, however, it may take up to 20 min for normal steady-state contractile function to be re-established. For successful and reliable measurements of cardiac function, the time from removal of the heart to cannulation and perfusion must be kept as short as possible and should not exceed 5 min.

2.11.2 Instrumentation of the heart

To measure LV pressure, a fluid-filled balloon connected to a pressure transducer is inserted into the LV. This allows the measurement of force development within the whole LV and derivation of indices of systolic and diastolic function in the heart preparation. The ideal balloon should be infinitely thin, flexible and non-elastic while being compatible with biological tissues (Skrzypiec-Spring *et al.*, 2007). Commercially available latex balloons do not meet all of these criteria and a previous investigation (unpublished) has identified that the use of latex balloons resulted in unstable readings of LVEDP and LV end systolic pressure (LVESP) over the course of a perfusion protocol. This was attributed to the high compliance of the latex balloon which may lead to slower relaxation and contraction than the myocardium itself. In contrast, balloons prepared out of cling film resulted in stable measurements of LVEDP

and LVESP with measurements close to reported values of cardiac function *in vivo*.

A balloon was prepared out of ordinary cling film (Figure 2-8 C). The LV end diastolic volume in rats is approximately 200 µL and the ideal balloon should have an approximate volume of 100 µL giving an optimal size for the measurement of LV pressure (LVP). The balloon was attached on a 1.5 mm metal cannula connected to a haemostasis valve connected to a Hamilton syringe (Figure 2-8 B-C). The system was primed with double distilled H_2O and all air bubbles were eliminated. This is important as air is compressible and would falsify pressure measurements. The balloon was then deflated and inserted into the LV by removal of the left atrial appendage to visualise the entry into the LV. Once positioned correctly, a solid state pressure transducer (Scisense, London, Canada) was inserted into the balloon. The balloon was then slowly inflated using the Hamilton syringe to give an LVEDP of approximately 3 mmHg which was found to be optimal in this preparation. When pacing was required, 2 electrodes were attached to the RA connected to a voltage stimulator with delay generator (Digitimer Ltd., Welwyn Garden City, UK). The heart was then stimulated at 5.3 Hz (320 bpm) with 2 ms duration and voltage approximately 1.5x above threshold.

2.11.3 Perfusion Protocols

Once the heart was cannulated and instrumented, it was allowed to reach a steady pressure before pacing (if required) was initiated. The perfusion solution was then switched over to a bottle with a fixed volume of perfusion solution to start the experiment according to the perfusion protocols for spontaneously beating and paced hearts (Figure 2-9). In all cases, the heart was allowed to reach a steady state for 10 min. One set of time-matched control hearts where equal volumes of Tyrode's were added at 0 and 10 min was used for comparison of all treatments (Figure 2-9 A-B).

At the end of the perfusion protocol, hearts were rapidly removed from the perfusion system and frozen at -80ºC for further analysis.

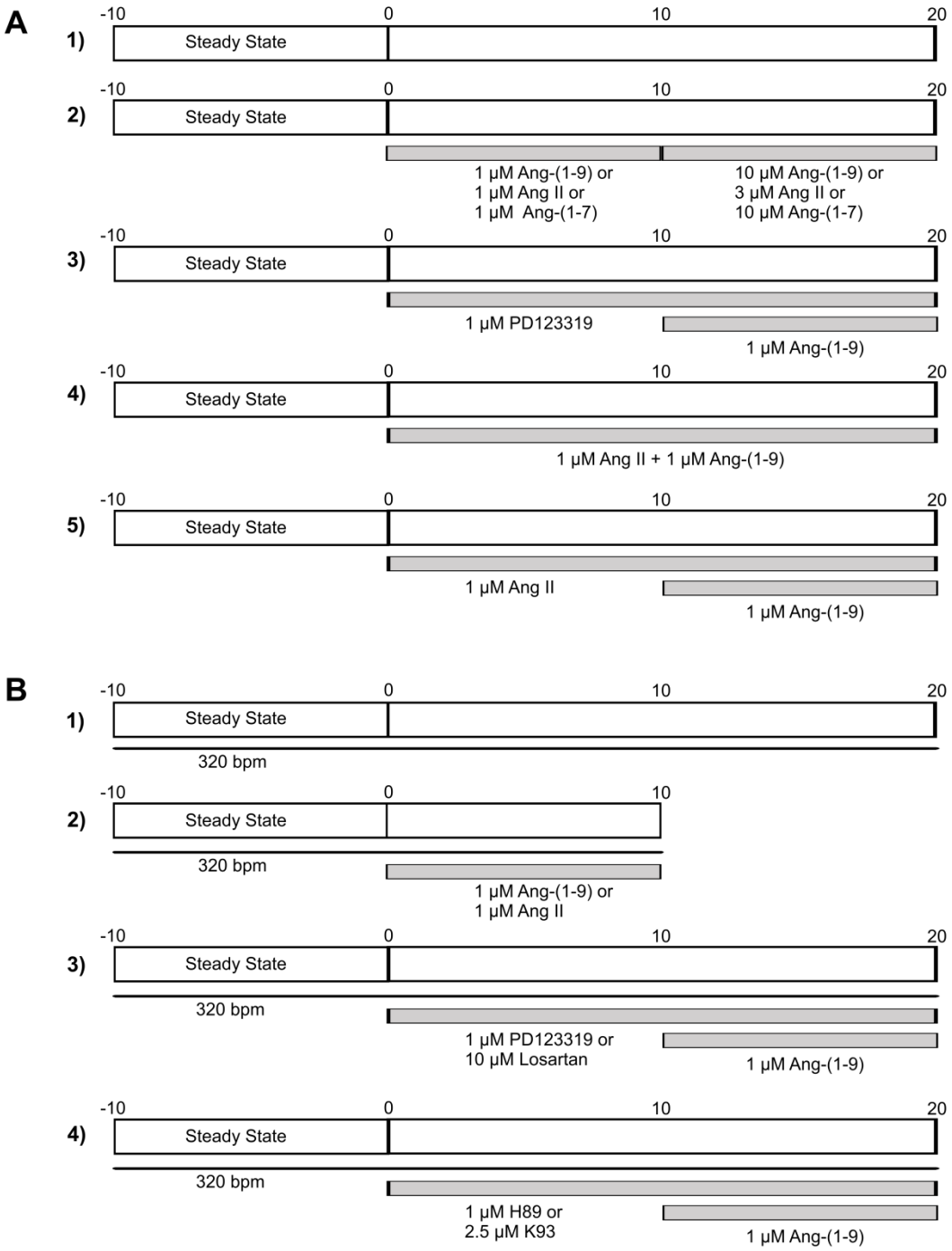

Figure 2-9. Langendorff perfusion protocols.
Hearts were allowed to reach a steady pressure before the beginning of the perfusion protocol. (A) Perfusion protocols in spontaneously beating hearts. Hearts were perfused for 10 min to reach a steady state before being perfused for 20 min 1) as control hearts with the addition of Tyrode's solution; 2) with increasing doses of Ang II (1 µM, 3 µM), Ang(1-9) or Ang-(1-7) (1 µM, 10 µM); 3) pre-perfusion with 1 µM PD123319 for 10 min prior to the addition of 1 µM Ang-(1-9); 4) a combination of Ang II and Ang-(1-9) (both 1 µM); or 5) pre-perfusion with 1 µM Ang II for 10 min prior to the addition of 1 µM Ang-(1-9) (B) Perfusion protocols in hearts paced at 320 bpm. Hearts were paced at 320 bpm and allowed to reach a steady state for 10 min before being 1) perfused as control hearts with the addition of tyrodes solution for 20 min; 2) perfused with 1 µM Ang II or Ang-(1-9) for 10 min; 3) pre-perfused with 1 µM PD123319 or 10 µM Losartan for 10 min prior to the addition of 1 µM Ang-(1-9) for a further 10 min; 4) pre-perfused with 1 µM H89 or 2.5 µM K93 for 10 min prior to the addition of 1 µM Ang-(1-9) for a further 10 min.

2.11.4 Data acquisition and analysis

The pressure transducer was connected to a Millar MPVS-400 pressure-volume loop system (Millar, Houston, Texas) and the LVP trace was recorded using LabChart 7.0 (ADInstruments, Oxford, UK). Using the in-built blood pressure module, LVESP, LVEDP, LV developed pressure (LVDP), the first derivative of LV developed pressure (dP/dt_{max} and dP/dt_{min}) and the exponential decay of LV pressure (tau) were fitted and calculated (Figure 2-10). Tau was calculated by fitting a mono-exponential decay to an asymptote pressure to the decaying portion of the pressure curve using the formula

$$P(t)=A\ e^{(-t/tau)}+B$$

where P is the pressure, t is the time in seconds from the start of the fitted region and A, B and tau are fitted parameters. The fitting range was set to start at the steepest negative slope (dP/dt_{min}) and end after 5 mmHg change from the LVEDP.

To determine baseline steady state parameters, LV function parameters were averaged across 2 min prior to the perfusion with peptide or inhibitors. Subsequently, LV parameters were sampled by averaging 10 s in 2 min intervals. In case of an arrhythmia at a sampling point that distorts the measurements, the sampling point was shifted maximally by 30 s prior or after the arrhythmia.

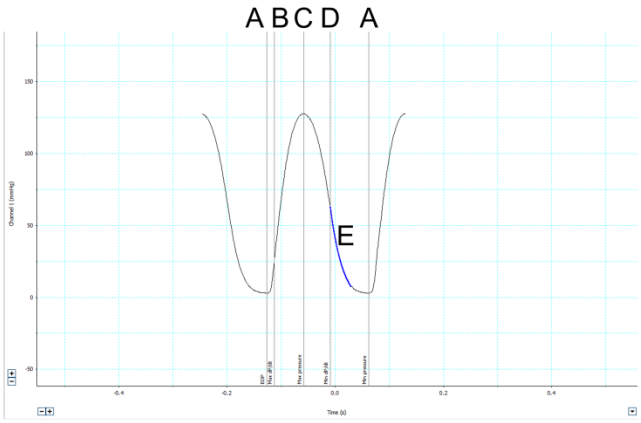

Figure 2-10. Cyclic measurements of LVP.
A = End diastolic pressure/ minimum pressure (LVEDP), B = d*P*/dt_{max}, C = end systolic pressure/ maximum pressure (LVESP), D = d*P*/dt_{min}, E = tau.

2.12 The mouse model of Ang II infusion

All surgical procedures were performed in accordance with the Animals Scientific Procedures Act (1986) and were approved by the University of Glasgow Ethical Review Panel and the UK Home Office. Male C57BL/6 mice were obtained from Envigo (UK) at 11 weeks of age and housed under controlled environmental conditions (12 hr light/dark cycle at ambient temperature and humidity) and maintained on a standard chow diet. Animals were allowed one week acclimatisation period before being used for procedure at 12 weeks of age.

2.12.1 Osmotic minipump preparation

To deliver Ang II and Ang-(1-9), subcutaneously implanted osmotic minipumps (Alzet, CA, USA) of the models 1002, 1004 or 2006 were used. Osmotic minipumps operate on the basis of an osmotic pressure difference between the pump compartment and the tissue environment. The pump consists of fluid reservoir which is encapsulated by an osmotic layer surrounded by a semi-permeable membrane (Figure 2-11). The high osmolality in the osmotic layer results in water influx from the surrounding tissue. This leads to compression of the reservoir chamber within the pump and the graded continuous delivery of the solution at a predetermined rate that is specific to each pump model (Theeuwes and Yum, 1976) (Figure 2-11).

Minipumps were prepared to deliver Ang II (Sigma, Dorset, UK) and/ or Ang-(1-9) (Phoenix Pharmaceuticals, Karlsruhe, Germany) at the predetermined rates shown in Table 2-20. To determine the concentration C_d required for delivery of the required dose, the following formula was used:

$k_o = Q \times C_d$

Where Q is the flow rate of the pump (µL/hr) (Table 2-21), C_d is the concentration of the drug solution (µg/µL) and k_o is the mass delivery rate (µg/hr) determined for a mouse weighing 28.2 g which is the average weight of a C57BL/6 mouse at 12 weeks by using the following equation:

$$\text{mass delivery rate } \left(\frac{\mu g}{hr}\right) = \text{dosage } \left(\frac{\frac{\mu g}{kg}}{hr}\right) \times 0.0282 \text{ kg.}$$

All drugs were prepared 2x concentrated in sterile dH_2O and diluted 1:2 upon filling of the pump. This allowed the combination of several drugs in one pump.

The pump was filled using the provided filling unit equivalent to a 25 gauge needle and a 1 mL syringe. Care was taken to prevent any air bubbles in the filling reservoir that may impede drug release.

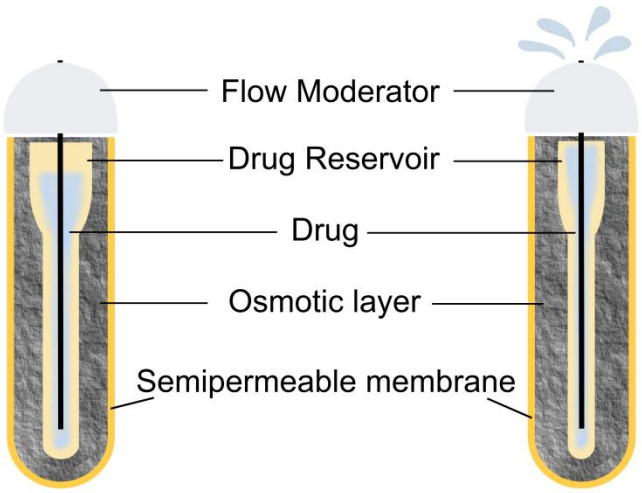

Figure 2-11. Design and working principle of osmotic minipumps.
The osmotic minipump consists of a drug reservoir which is encapsulated by an osmotic layer within a semipermeable membrane. Diffusion of water from the surrounding tissue through the semipermeable membrane expands the osmotic layer. This compresses the drug reservoir and leads to release of the drug at a predefined constant rate. The flow moderator prevents interference of air bubbles and leakage of drug.

Table 2-20. Doses of Ang II and Ang-(1-9) used in *in vivo* studies

Drug	Dose (µg/kg/hr)
Ang II	24
Ang II	48
Ang-(1-9)	48

Table 2-21. Osmotic minipump specifications

Pump model	Flow rate (µL/hr)	Pump volume (µL)
1002	0.25	100
1004	0.11	100
2006	0.15	200

2.12.2 Minipump implantation

Subcutaneous implantation of minipumps was performed under sterile technique. Prior to surgery, each animal received a subcutaneous injection of 0.125 mg carprofen (Rimadyl) in 250 µL 5 % sterile saline.

To anaesthetise the animal, the induction box was filled with 5 % isoflurane in oxygen at a flow rate of 1 mL/min and the animal was placed into the box. Once induction was confirmed, the animal was placed on a face mask delivering 3 % isoflurane in oxygen (flow rate 1 mL/min) and the hair was removed from the neck and between the shoulder blades with a hair trimmer. Residual hair was removed diligently by the use of Vetasept chlorhexidine surgical disinfectant. Using sharp surgical scissors a small horizontal incision was made in the neck anterior to the scapulae (Figure 2-12 A). Using blunt, straight dissection forceps a pocket was created under the skin for the placement of the minipump (Figure 2-12 B). Next the minipump was inserted into the subcutaneous pocket with the flow regulator pointing away from the incision site (Figure 2-12 C). The incision was closed using 6-0 Vicryl suture (Ethicon, Norderstedt, Germany) and sterilised with Vetasept (Figure 2-12 D). Isoflurane levels were reduced to 0 % and the animal was monitored until signs of recovery became visible. The animal was placed into a pre-heated cage with soft food readily available. Following surgery, the animal was checked and weighed twice daily for 1 week and was then checked once a day thereafter.

Overall mortality following minipump implantation and infusion was 12.7 %. This was solely due to adverse effects caused by Ang II infusion (irrespective of dosage or addition of Ang-(1-9)) where mortality amounted to 19.2 % (Figure 2-12 E). A thoracic or abdominal haemorrhage was present in 70 % of cases and was attributed to the rupture of an aortic aneurysm (Figure 2-12 F). Other causes of death included post-operative complications and other unknown causes.

Ang II infusion in mice results in the development of hypertension as measured by telemetry (Flores-Munoz and Nicklin, unpublished) and tail cuff plethysmography (Figure 2-12 G-H). The time period over which hypertension developed varied between low (24 µg/kg/hr) and high (48 µg/kg/hr) doses with

the low dose causing a gradual rise in BP by 14 % to 142 mmHg at one week which further increased to 147 mmHg after 2 weeks (Figure 2-12 G) while high dose Ang II caused a rapid increased in BP by 35 % to 152 mmHg after one week before levelling off (Figure 2-12 H), in agreement with previous observations (Kawada *et al.*, 2002).

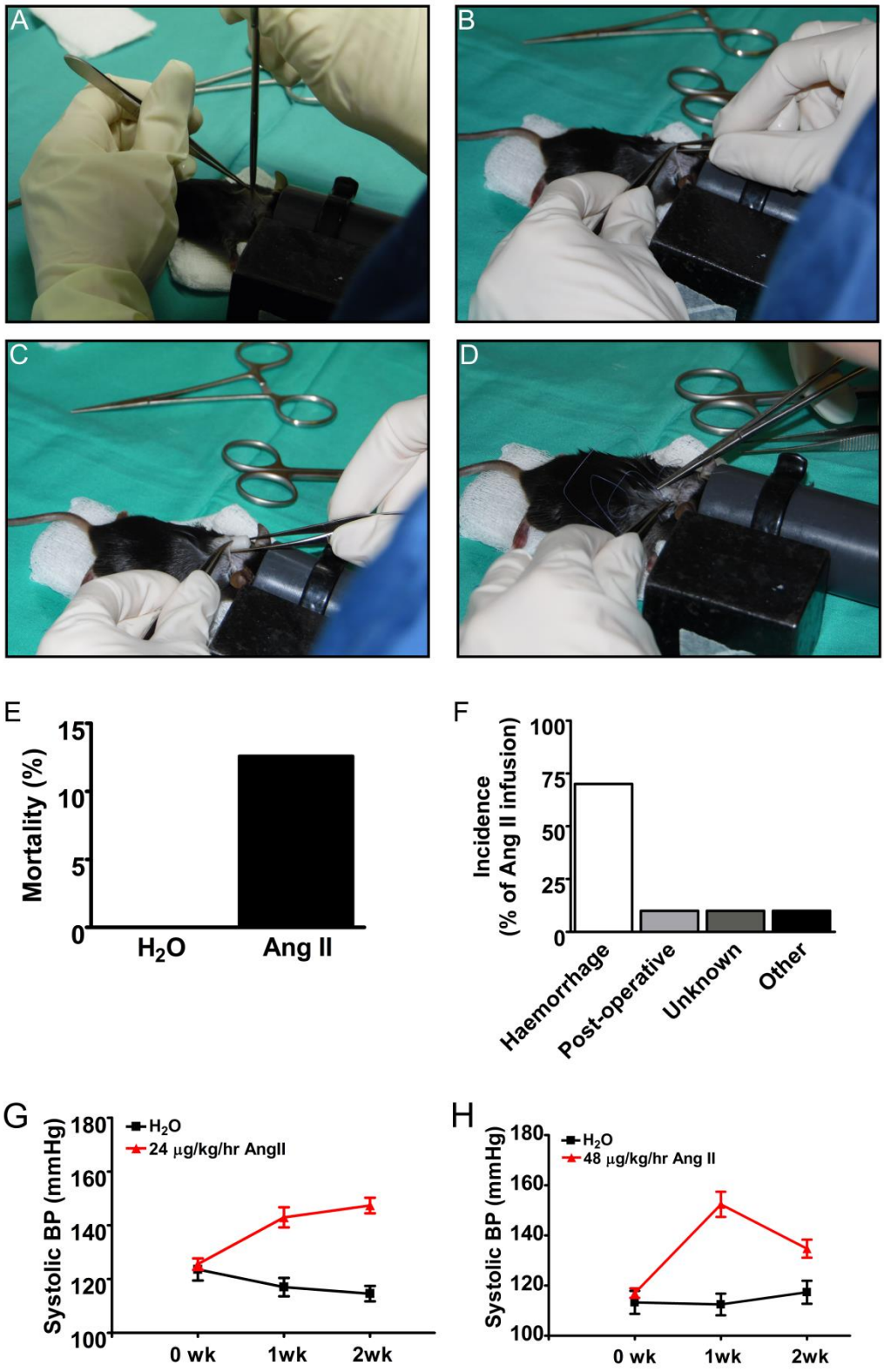

Figure 2-12. Implantation of subcutaneous osmotic minipumps for infusion of Ang II. (A-D) A midline incision was made near the scapulae and a subcutaneous pocket was formed. The minipump was placed into the pocket with the flow regulator facing away from the incision. The incision was closed using 6-0 Vicryl suture and the animal was allowed to recover. (E) Mortality for animals receiving either H_2O or Ang II irrespective of dose or Ang-(1-9) addition. (F) Percentage incidence for causes of death in Ang II-infused mice. (G) Blood pressure was measured in mice receiving either H_2O or 24 µg/kg/hr Ang II over 2 weeks by radiotelemetry. n= 6. Data generated by and used with permission of Dr Monica Flores-Munoz. (H) Blood pressure was measured in mice receiving either H_2O or 48 µg/kg/hr Ang II by tail cuff plethysmography. n= 6 for control and n= 10 for Ang II.

2.12.3 Minipump replacement

For the replacement of the minipump as required in the reversal study, animals were prepared and anesthetised as outlined (Section 2.12.2). A horizontal incision was made at the original incision site which will have formed a collagenous scar. The existing minipump was removed from the subcutaneous pocket and the new minipump was inserted. To facilitate healing of the remodelled scar, the wound edges were refreshed by scraping off connective tissue with a sharp scalpel blade until a light capillary bleed was apparent. The incision was then closed with 6-0 Vicryl suture. As previously described, the animals were recovered in a pre-heated cage with soft food and monitored twice daily for 1 week and then once daily thereafter.

2.12.4 Sacrifice & tissue collection

Mice were anaesthetised in an induction box with 5 % isoflurane in oxygen at a flow of 1 mL/min. Following induction, the animal was placed on a face mask delivering 3 % isoflurane in oxygen (flow 1 mL/min). A midline incision was made along the abdomen and chest to visualise the ribcage and heart. Animals were then euthanized by exsanguination *via* cardiac puncture. Death was confirmed by cessation of the circulation. Using a fine needle, PBS was then circulated *via* the apex of the heart to flush out residual blood from the organs. The liver, kidneys, lungs, spleen, heart and aorta were removed, placed into PBS, weighed and then trimmed for sampling. The heart was cut longitudinally at the angle of the RV. One half was snap frozen in liquid nitrogen and then stored at -80ºC until further use. The other half was placed into 10 % neutral buffered formalin (Cellstor, CellPath, Newton, UK) for fixation for at least 24 h and was then processed for histological staining as outlined previously (Section 2.7).

The collected blood was transferred into a 1.3 mL serum microtube (Sarstedt, Nümbrecht, Germany) and allowed to clot at room temperature for several hours. The serum was then purified by centrifugation at 16,000 x g for 10 min, aliquoted and sorted at -80ºC until further use.

2.13 Echocardiography

Echocardiography is useful tool for the investigation of cardiovascular structure and function and is the gold standard for the assessment of cardiac morphology in humans. The main benefits of echocardiography are its portability, the facility for real-time imaging, non-invasiveness and the possibility to carry out serial measurements over time (Ram *et al.*, 2011).

For echocardiography, the animals were placed into an induction box and anesthetised at 5 % isoflurane in oxygen with a flow of 1 mL/min. Once induction was complete, the animals were placed on a face mask delivering the same isoflurane combination and isoflurane content was gradually reduced to 1.5 %. Throughout the procedure temperature was controlled by placing the animals on a heat mat and monitoring body temperature with a rectal thermometer (Harvard Apparatus, Kent, UK). To remove interference, the chest was shaven and hair removed with Vetasept. Echocardiographic images were acquired with a Siemens Acuson Sequoia 512 ultrasound machine and a 15L8 probe set to a frequency of 14 MHz. For imaging, ultrasound gel was applied on the probe which was placed at the correct angle on the animal's chest to capture images in the longitudinal and transverse axis (Figure 2-13 A). M-mode images were captured at the same region in all animals with measurements taken just above the papillary muscle. For Doppler flow measurements, a four chamber view was achieved by placing the probe at a 45° angle below the animal's diaphragm. Mitral valve inflow was located by colour-flow mapping and a series of images were taken. Accompanying 2-lead electrocardiographic (ECG) measurements were made *via* placement of subdermal electrodes at each front paw and the corresponding earthing electrode into the right hind leg.

Analysis was performed in ImageJ. Mean data of echocardiographic indices was determined by analysing a maximum of 4 images *per* animal with three consecutive beats being analysed *per* image. Images were chosen on the basis of pre-determined criteria that 1) measurements were taken immediately above the papillary muscle; 2) the walls have to be clearly distinguishable; 3) wall contraction was synchronous. Consecutive beats were measured in-between breaths where wall movement was in steady-state. The scale was manually set using the scale provided on the image. Measurements of LV dimensions,

including LV end diastolic and end systolic dimensions (LVEDD, LVESD), LV free wall thickness during diastole and systole (LVFWd, LVFWs) and interventricular septum thickness during diastole and systole (IVSd, IVSs), were made as shown (Figure 2-13 B). HR was estimated by counting the QRS complexes in one sweep of the accompanying ECG. Fractional shortening (FS) was calculated as

$$FS\ (\%) = \left(\frac{LVEDD - LVESD}{LVEDD}\right) x\ 100$$

where LVEDD= LV end diastolic dimension and LVESD= LV end systolic dimension.

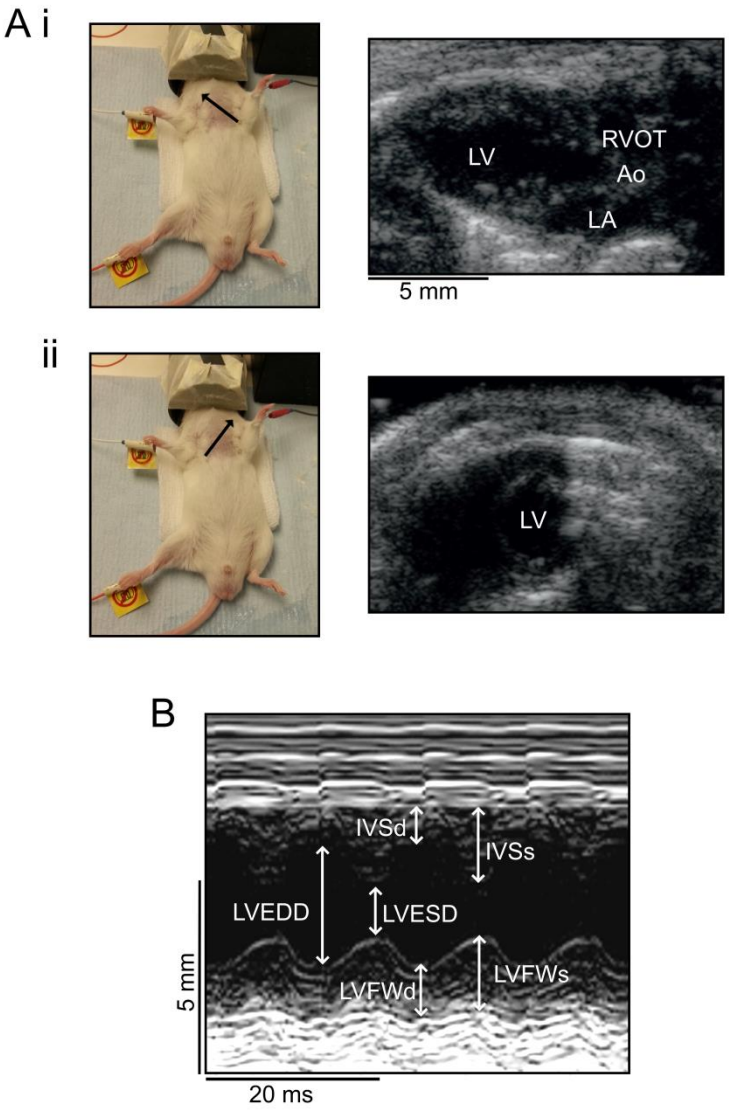

Figure 2-13. Echocardiography B-mode and M-mode analysis.
(A) Example diagram for the positioning of the probe (indicated by arrow) to obtain (i) long-axis view and (ii) short-axis view. LV= Left ventricle, LA= Left atrium, Ao= Aorta, RVOT= Right ventricular outflow tract. (B) Example M-mode image taken at baseline demonstrating the measurements of cardiac morphology performed for each image. LVEDD= Left ventricular end-diastolic dimension, LVESD= Left ventricular systolic dimension, IVSd= Interventricular septum diastole, IVSs= Interventricular septum systole, LVFWd= Left ventricular free wall diastole, LVFWs= Left ventricular free wall systole.

2.14 Tail cuff plethysmography

Tail cuff plethysmography is the most commonly employed non-invasive approach for the determination of BP in conscious experimental animals. It works on the same basis as the sphygmomanometer in humans and utilises a tail cuff placed around the proximal portion of the tail to occlude blood flow. During controlled deflation of the cuff a distal BP sensor will measure pulse, the systolic and diastolic BP. There are three types of BP sensors: photoplethysmography, piezoplethysmography and volume pressure plethysmography.

Tail cuff plethysmography was carried out with a Visitech BP-2000 Series II BP analysis system (Figure 2-14 A). This system uses transmission photoplethysmography where the variation of transmitted light through vasodilation and constriction in response to every heart beat is measured through the tail and used as signal for the determination of BP. This approach has previously shown to correlate well with direct intra-arterial BP measurements (Krege *et al.*, 1995). Upon inflation of the cuff, the diastolic pressure is determined as the point where the pulse rate waveform decreases and the systolic pressure as the point where the waveform has reached a steady state. Prior to measurements, the system was pre-heated to 37 °C and assessed for leaks in the pressure cuffs.

Prior to the start of the experimental protocol animals were trained for tail cuff plethysmography to improve result reproducibility. During the experimental period, measurements were carried out once a week at the same time of the day to remove circadian variation. The animals were placed into a restraining chamber onto a pre-heated surface to maintain body temperature. The tail was fed through the cuff which was positioned at the proximal end. The distal end was placed into the V-shaped sensor groove (Figure 2-14 B). Six animals were measured in parallel. The system was configured to carry out 5 preliminary recordings with subsequent 20 recordings for averaging. The standard time between measurements was 2.5 s and the upper pressure limit was set to 250 mmHg. In-built statistical analysis allowed the removal of outliers due to excess movement and other confounding factors.

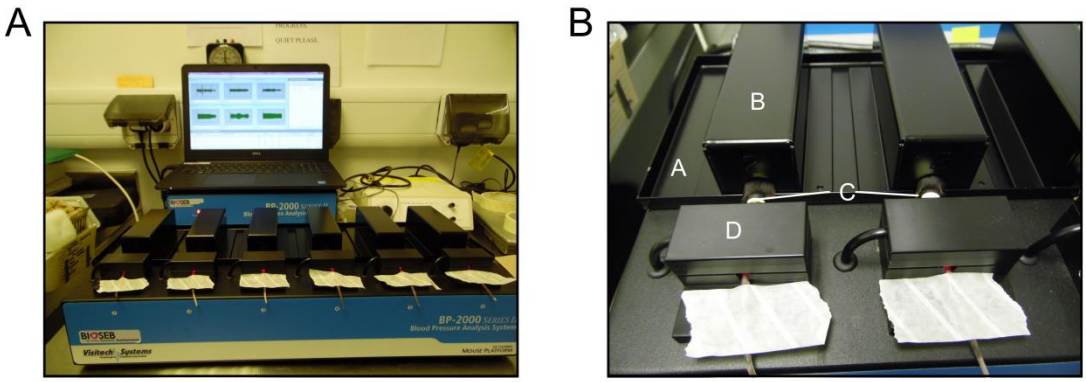

Figure 2-14. Tail cuff plethysmography setup.
(A) Setup of the BP-2000 system with blood pressure measurements made in parallel in 6 animals. (B) Magnification of the individual components of the tail cuff plethysmography system. A= heated undercover, B= Restraining chamber, C= Tail cuff, D= Sensor chamber.

2.15 Statistical Analysis

Data are expressed as mean± standard error of the mean (SEM) unless otherwise stated. Statistical analysis was performed using GraphPad Prism Version 4. Unpaired Student's t-test was performed when comparing two samples of a data set and a one-way ANOVA with Tukey's or Dunnett's post-hoc correction was employed for multiple comparisons as indicated. For traces of LV functional parameters and echocardiography, a Students's t-test was used to determine statistical significance between individual data points of one time-point when comparing two traces and a one-way ANOVA with Tukey's or Dunnett's post-hoc correction was employed as indicated when several traces were compared. Equal variance was confirmed by Brown-Forsythe test. In the case of unequal variance, the Welch's correction was applied for Student's t-test while for one-way ANOVA, data was logged prior to analysis. A p-value <0.05 was termed statistically significant.

Chapter 3 – Characterisation of a mouse model of chronic Ang II infusion and assessment of the effects of Ang-(1-9) on Ang II-induced cardiac pathology

3.1 Introduction

3.1.1 The Ang II-infusion model

Chronic Ang II infusion is a well-recognised experimental model of hypertension and cardiac remodelling in HHD (Simon *et al.*, 1995). The dosage of Ang II during chronic infusion determines the rate at which BP and subsequent cardiac remodelling increase.

High dose Ang II infusion (≥ 24 µg/kg/hr in mouse) has a pressor effect and triggers an acute increase in BP within minutes/ hours of infusion (Kawada *et al.*, 2002, Suo *et al.*, 2002, Broomé *et al.*, 2001). The acute increase in Ang II causes hypersecretion of aldosterone, ANP and vasopressin which remain elevated while plasma Ang II levels are elevated (Simon *et al.*, 1995). This is accompanied by a significant degree of salt and water retention and expansion of the extracellular fluid with a shift of the pressure-natriuresis curve to higher pressures (Simon *et al.*, 1995). Additionally, baroreceptors are reset to higher pressures which results in an increase in sympathetic output at inappropriately high arterial pressures (Brooks *et al.*, 1993). During acute infusion of high doses of Ang II, plasma Ang II levels may acutely increase up to 171-fold and chronically remain elevated during the perfusion period (Broomé *et al.*, 2001)

Infusion of low doses of Ang II (≤ 24 µg/kg/hr in mouse) have no acute effect on BP and lead to a slow pressor response with a gradual rise in BP over 7 days peaking at around 2 weeks (Von Thun *et al.*, 1994, Kawada *et al.*, 2002). Hypertension in response to low dose Ang II infusion occurs in the absence of renal dysfunction or significant sodium and water retention (Kawada *et al.*, 2002, Von Thun *et al.*, 1994, Brown *et al.*, 1981). Similarly, plasma aldosterone levels remain largely unchanged (Kisch *et al.*, 1976). Despite the slow onset hypertension, cardiac hypertrophy and phenotypic modulation is evident 3 days after low dose Ang II infusion (Kim *et al.*, 1995). The mechanisms contributing to the slow onset hypertension by low dose Ang II infusion are not fully understood. A role for vasoconstriction, oxidative stress, and activation of the central RAS has been suggested (Hood *et al.*, 2007, Ortiz *et al.*, 2001, Baltatu *et al.*, 2000). During chronic low dose Ang II infusion, plasma Ang II levels may be elevated 2-

5-fold and significant intrarenal Ang II accumulation has been observed (Von Thun *et al.*, 1994, Ocaranza *et al.*, 2014).

3.1.1.1 Cardiac remodelling in the Ang II infusion model

Despite the different phenotypes in hypertension development with low or high dose Ang II infusion, cardiac remodelling in Ang II-infused mice proceeds in a similar manner irrespective of dosage. Ang II mediates a direct pro-hypertrophic effect in cardiomyocytes by activating complex signalling cascades (Section 1.4.1.2). The development of cardiac hypertrophy with an increase in cardiac mass is evident as early as 3-7 days following Ang II infusion while the gene expression of markers of hypertrophy such as ANP and βMHC may already increase within 24 h of Ang II infusion (Kim *et al.*, 1995, Sopel *et al.*, 2011). Although no time-course studies of cardiac hypertrophy in Ang II-infused mice beyond one week have been carried out, the degree of cardiac hypertrophy reported in mice infused with Ang II for 2-6 weeks was comparable (Kurisu *et al.*, 2003, Matsui *et al.*, 2004, Tsukamoto *et al.*, 2013), suggesting that cardiac hypertrophy in response to Ang II infusion plateaus early during progression of cardiac remodelling. Maladaptive remodelling and exhaustion of the hypertrophic reserve is a major contributor to cardiac contractile dysfunction during Ang II infusion (Hermans *et al.*, 2014, Domenighetti *et al.*, 2005). Although cardiac hypertrophy is primarily described as an adaptive response to normalise wall stress in settings of increased BP (Heineke and Molkentin, 2006), the early hypertrophic response to Ang II infusion was demonstrated to be BP independent and could not be inhibited by administration of hydralazine (Kim *et al.*, 1995). This is further supported by the observation that transgenic mice with cardiac-specific elevation of Ang II production develop cardiac hypertrophy and cardiac contractile dysfunction (Domenighetti *et al.*, 2005).

Infusion of Ang II causes early cardiomyocyte apoptosis and in rats and rabbits infused acutely with high doses of Ang II intravenously, multifocal lesions are evident as early as 4 hours (Gavras *et al.*, 1971, Gavras *et al.*, 1975, Giacomelli *et al.*, 1976). Whereas this was initially attributed to the hypertension caused by Ang II infusion, low dose infusion of Ang II has demonstrated that cardiomyocyte necrosis in response to Ang II occurs independent of a hypertensive response. In this model, antimyosin labelling of cardiomyocytes (an indicator of abnormal

sarcolemmal permeability) is visible as early as 24 h of low dose Ang II infusion while myocytolysis is clearly evident microscopically after 2 days (Tan *et al.*, 1991).Furthermore, regulation of BP with hydralazine does not abrogate fibrotic remodelling in Ang II-infused rats (Kim *et al.*, 1995). Interestingly, mice with cardiac specific elevation of Ang II production do not present cardiomyocyte necrosis and do not develop cardiac fibrosis despite significant cardiac hypertrophy and contractile dysfunction (Domenighetti *et al.*, 2005), suggesting that cardiomyocyte necrosis is a driving factor of Ang II-induced fibrotic remodelling. Myocyte necrosis triggers reparative fibrosis and this corresponds with the infiltration of immune cells (macrophages, lymphocytes and neutrophils) and the occurrence of myofibroblasts within 2 days of Ang II infusion (Campbell *et al.*, 1995). The temporal development of histological fibrotic lesions in Ang II-infused mice has been well characterised and demonstrate that fibrotic lesions develop early during Ang II infusion (Campbell *et al.*, 1995) (Figure 3-1). Within 4 days early focal and perivascular scarring is visible in hearts of Ang II-infused rats which develops into extensive interstitial and perivascular fibrosis within 2 weeks of infusion before plateauing at 4-6 weeks after which fibrosis may worsen with disease progression (Campbell *et al.*, 1995). Myocardial fibrotic lesion in response to Ang II infusion are predominantly formed by the deposition of collagen I and collagen III, the expression of which increases within 3 days of Ang II infusion and is preceded by increases in $TGF\beta_1$ and CTGF (Kim *et al.*, 1995, Sopel *et al.*, 2011, Haudek *et al.*, 2006). The fibrotic remodelling in response to Ang II infusion is caused by the activation of complex signalling cascades by Ang II in fibroblasts in which it directly increases proliferation and myofibroblast transition (Section 1.4.2.3).

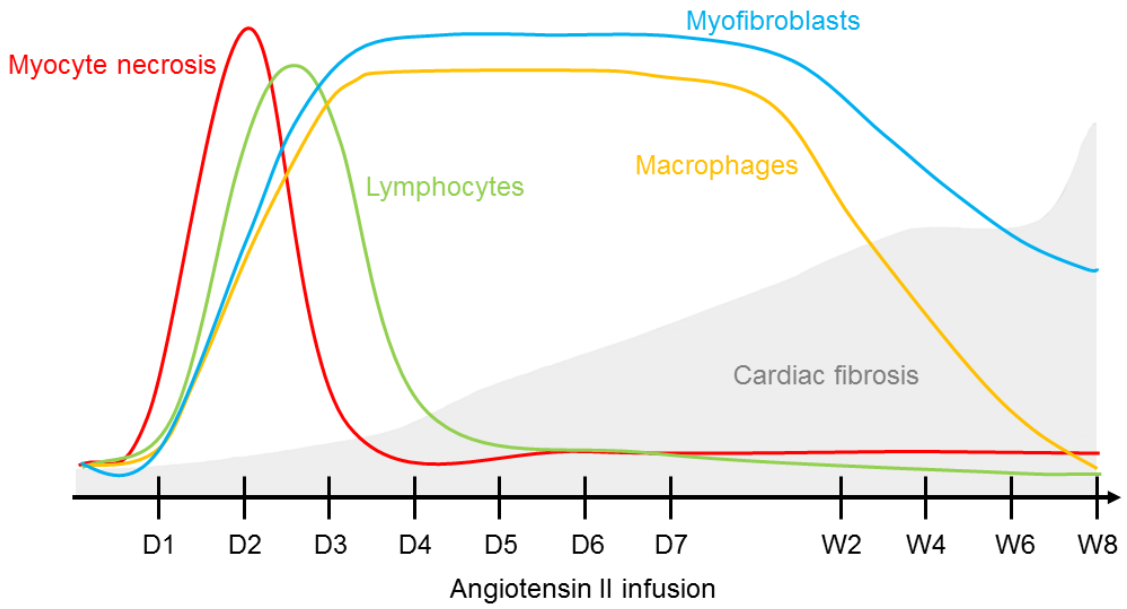

Figure 3-1. Histological changes in the development of cardiac fibrosis with Angiotensin II infusion.
Cardiomyocyte necrosis in response to Ang II infusion occurs rapidly within one day of infusion and subsides after three days. This triggers the transient infiltration of lymphocytes (1-5 days) and the more prolonged infiltration of activated macrophages (up to 2 weeks) to the site of necrosis. The immune response leads to the activation of fibroblasts to myofibroblasts and the gradual deposition of collagen fibres leading to increased cardiac fibrosis.

3.2 Aims

1) Establish and characterise a chronic model of Ang II-induced cardiac remodelling and dysfunction using low and high doses.

2) Determine the cardiac effects of Ang-(1-9) infusion in healthy normotensive mice.

3) Investigate the potential of Ang-(1-9) to reverse established Ang II-induced cardiac dysfunction and remodelling.

3.3 Results

3.3.1 Model characterisation

In order to assess the effects of Ang-(1-9) on chronic cardiac disease, a chronic model of Ang II infusion was developed and characterised. Mice were implanted with osmotic minipumps delivering either a low (24 µg/kg/hr) or high (48 µg/kg/hr) dose of Ang II and cardiac function and remodelling was assessed at 6 weeks. Animals implanted with minipumps releasing H_2O served as control. Cardiac function was measured every fortnight by echocardiography and cardiac fibrosis and hypertrophy were quantified post-mortem by immunohistochemistry.

3.3.1.1 Cardiac function

At baseline, echocardiography indices of cardiac structure and function did not significantly differ between treatment groups (Table 3-1). FS remained unchanged in control infused mice over the 6 week period, however, infusion of 24 and 48 µg/kg/hr Ang II was associated with chronic (24 µg/kg/hr) and acute (48 µg/kg/hr) reduction in FS. At 2 weeks Ang II infusion there was a significant 30 % drop ($p<0.05$) in FS from 47.2 ± 2.2 % in control mice to 33.1 ± 3.2 % in mice infused with 48 µg/kg/hr Ang II but not 24 µg/kg/hr Ang II (44.4 ± 2.6 %) (Figure 3-2 A-B). The significant reduction in FS with 48 µg/kg/hr Ang II was maintained at 4 weeks and similarly FS was significantly reduced in animals receiving 24 µg/kg/hr Ang II (control 49.3 ± 2.5 %, 24 µg/kg/hr Ang II 36.5 ± 2.5 %, 48 µg/kg/hr Ang II 34.1 ± 3.9 %, n= 3-11, $p<0.05$). After 6 weeks, the reduction in FS was maintained in both groups resulting in a FS of 31.0 ± 2.1 % ($p<0.05$) and

36.6 ± 4.2 ($p>0.05$) in mice receiving 24 and 48 µg/kg/hr Ang II, respectively (Figure 3-2 B). The decrease in FS with Ang II infusion at either dose was associated with a gradual increase in LVESD but not LVEDD (Figure 3-2 C-D). In control animals, LVEDD and LVESD were not significantly different at any time-point (Figure 3-2 D). Only small changes in LVFWd and LVFWs thickness could be observed with Ang II infusion and LVFWd and LVFWs were significantly increased by 31 % and 14 % ($p<0.05$), respectively at 2 weeks with 24 µg/kg/hr Ang II (Figure 3-2 E-F).

Table 3-1. Echocardiography parameters in mice at baseline and 6 weeks.

	Baseline			6 weeks		
	Control	24 µg/kg/hr Ang II	48 µg/kg/hr Ang II	Control	24 µg/kg/hr Ang II	48 µg/kg/hr Ang II
Body weight (g)	28.96 ± 0.46	28.35 ± 0.37	29.12 ± 0.20	30.96 ± 0.36	30.51 ± 0.64	29.80 ± 0.33
Heart rate (bpm)	496 ± 8	496 ± 9	480 ± 23	476 ± 13	472 ± 14	470 ± 10
FS (%)	48.4 ± 1.8	51.2 ± 2.3	45.9 ± 1.0	45.5 ± 1.8	31.0 ± 2.1*	36.6 ± 4.2
LVEDD (mm)	3.31 ± 0.09	3.10 ± 0.13	3.48 ± 0.12	3.60 ± 0.08	3.56 ± 0.17	3.53 ± 0.13
LVESD (mm)	1.72 ± 0.09	1.53 ± 0.12	1.89 ± 0.10	1.67 ± 0.23	2.48 ± 0.18*	2.25 ± 0.41
LVFWd (mm)	1.10 ± 0.04	1.05 ± 0.05	1.03 ± 0.05	1.16 ± 0.07	1.42 ± 0.09	1.25 ± 0.05
LVFWs (mm)	1.58 ± 0.05	1.53 ± 0.03	1.71 ± 0.04	1.57 ± 0.05	1.71 ± 0.11	1.61 ± 0.02

*p<0.05 *vs.* Control; FS= Fractional shortening; LVEDD= Left ventricular end-diastolic dimension; LVESD= Left ventricular systolic dimension; LVFWd/LVFWs= Left ventricular free wall thickness during diastole and systole

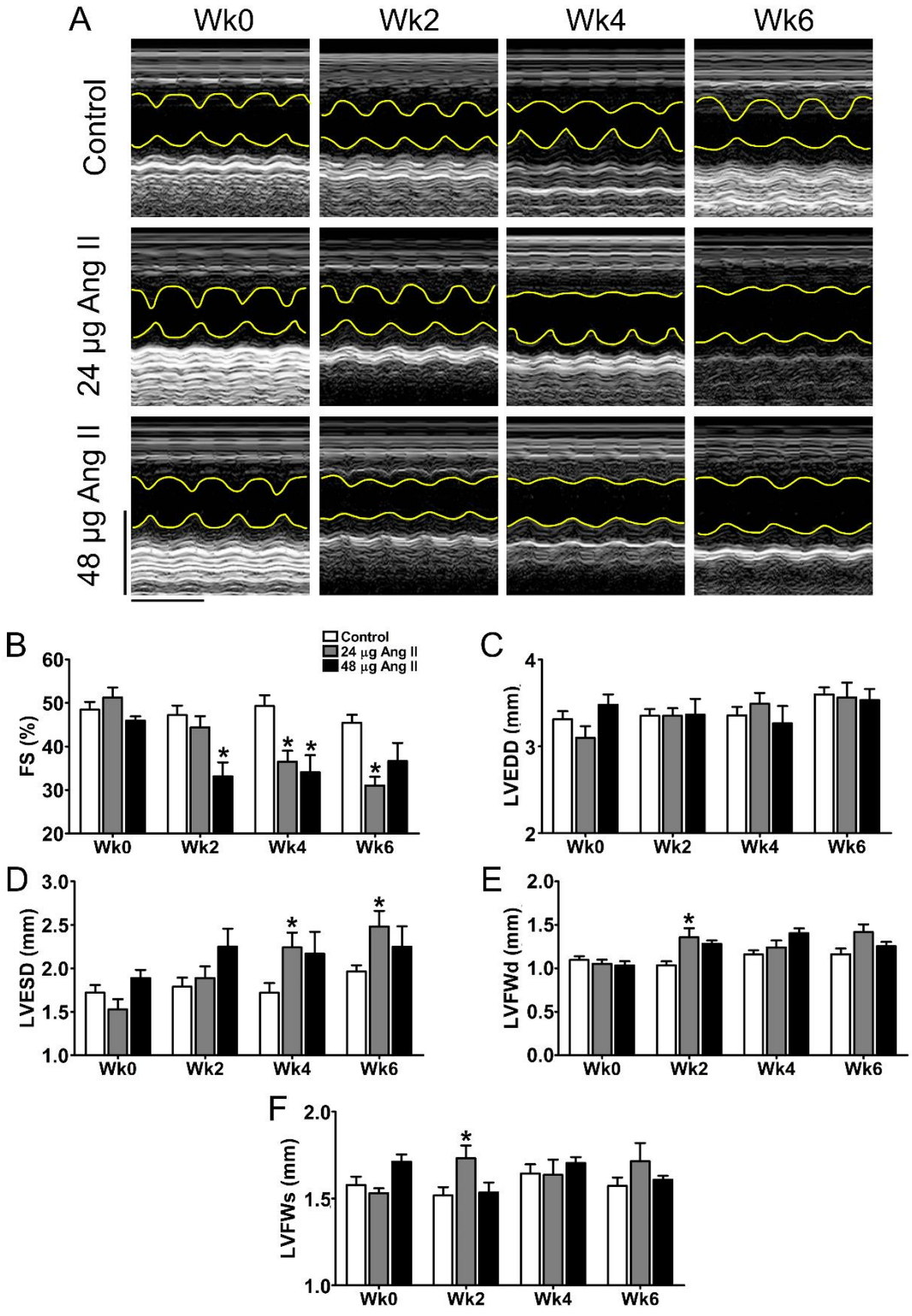

Figure 3-2. Cardiac function in Ang II-infused mice.
(A) Example M-mode images for mice receiving H_2O (control) (n= 11), 24 µg/kg/hr (24 µg Ang II, n= 10) or 48 µg/kg/hr (48 µg Ang II, n= 3) Ang II at week 0, 2, 4 and 6 weeks. Scale= 5 mm and 200 ms. Serial measurements of (B) FS, (C) LVEDD, (D) LVESD, (E) LVFWd and (F) LVFWs from longitudinal M-mode images for each treatment group over 6 weeks. Data are presented as mean ± SEM. FS= Fractional shortening; LVEDD= Left ventricular end-diastolic dimension; LVESD= Left ventricular systolic dimension; LVFWd/LVFWs= Left ventricular free wall thickness during diastole and systole *p<0.05 *vs.* control (ANOVA with Tukey post-hoc analysis).

3.3.1.2 Hypertrophy

There was a significant increase in heart weight/ tibia length (HW/TL) in animals which received 24 and 48 µg/kg/hr Ang II (control 10.01 ± 0.29 mg/mm, 24 µg/kg/hr Ang II 11.39 ± 0.42 mg/mm, 48 µg/kg/hr Ang II 12.24 ± 0.31 mg/mm, n= 3-11, $p<0.05$) (Figure 3-3 A i-ii). To determine cardiomyocyte hypertrophy, WGA staining was used to determine cardiomyocyte cross-sectional area, diameter and length (Figure 3-3 B-C). Cardiomyocyte cross-sectional area was significantly increased in the 24 µg/kg/hr Ang II group compared to control and similarly, cross-sectional area tended to be increased with 48 µg/kg/hr Ang II, despite non-significant (control 268.88 ± 7.23 μm^2, 24 µg/kg/hr Ang II 373.34 ± 17.77 μm^2, 48 µg/kg/hr Ang II 321.85 ± 23.17 μm^2, n= 3-11, $p<0.05$) (Figure 3-3 B i-ii). Similarly, cardiomyocyte diameter was significantly increased by 15 % and 19 % ($p<0.05$) with 24 and 48 µg/kg/hr Ang II compared to control (Figure 3-3 B iii). Cell length was not significantly different with Ang II infusion, however, in the 24 µg/kg/hr Ang II group cardiomyocyte length tended to be increased by 11 % ($p>0.05$) (Figure 3-3 C i-ii).

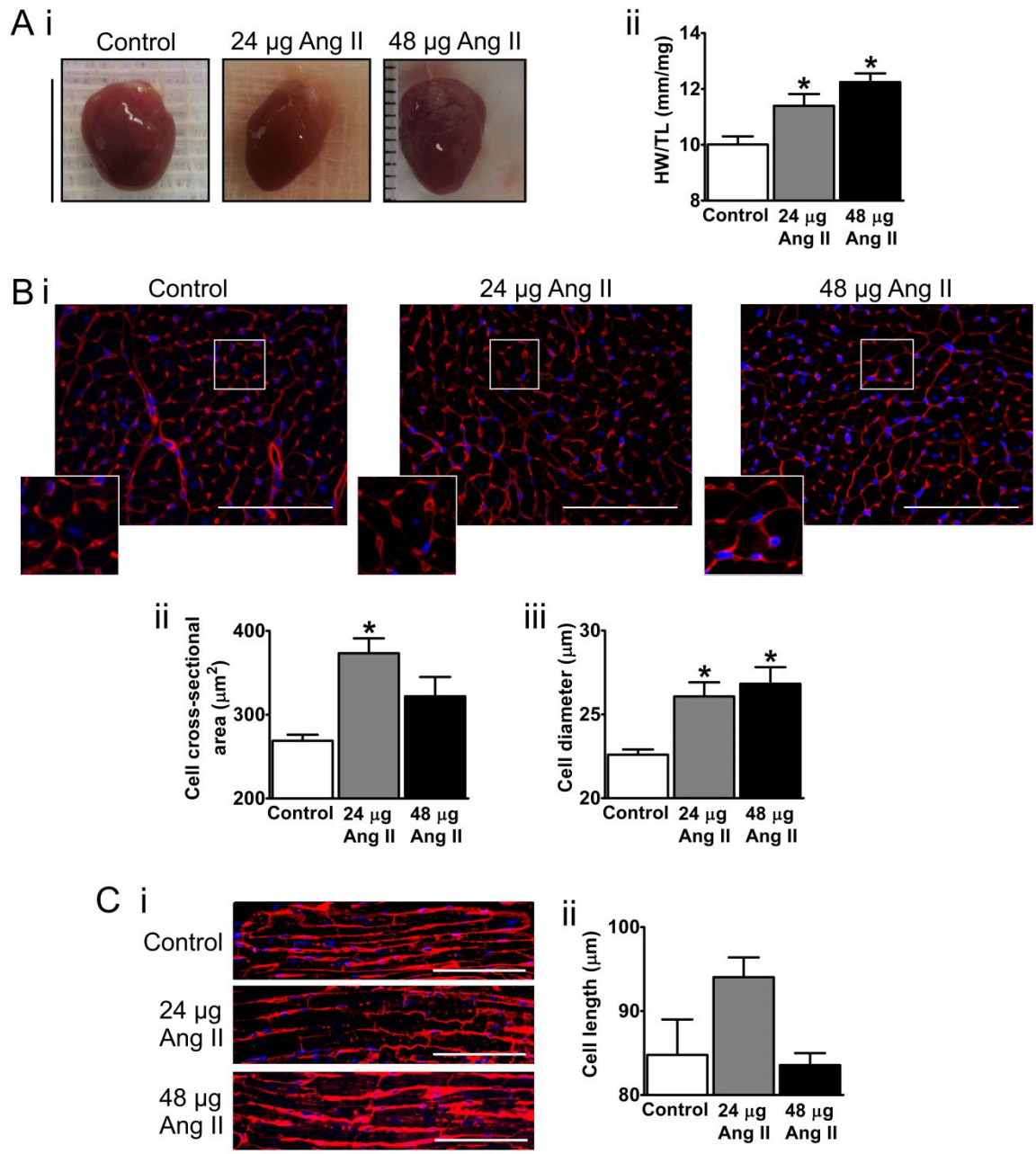

Figure 3-3. Effects of chronic Ang II infusion on cardiac hypertrophy.
(A i) Example images of hearts from animals receiving H_2O (control), 24 µg/kg/hr (24 µg Ang II) or 48 µg/kg/hr (48 µg Ang II) Ang II at 6 weeks. Scale= 10 mm. (ii) Heart weight/ tibia length (HW/TL) for control (n= 11), 24 and 48 µg Ang II (n= 10 and 3, respectively) after 6 weeks. Heart sections were stained with wheat germ agglutinin to visualise both, transverse (B i) and longitudinal (C i) sections of cardiomyocytes. The cardiomyocyte membrane is stained red and nuclei blue. The inset represents a magnification of the area within the white square. Scale= 100 µm. (B ii) Cell cross-sectional area, (B iii) cell diameter and (C ii) cell length were determined in control (n= 11), 24 and 48 µg Ang II (n= 10 and 3, respectively). Data are presented as mean ± SEM. *p<0.05 *vs.* control (ANOVA with Tukey post-hoc anlysis).

3.3.1.3 Fibrosis

Total fibrosis measured by picrosirius red staining was significantly increased in Ang II-infused animals compared to control (Figure 3-4 A i, B i). Infusion of 48 µg/kg/hr Ang II significantly exacerbated total fibrosis compared to 24 µg/kg/hr Ang II (control 2.35 ± 0.54 %, 24 µg/kg/hr Ang II 5.34 ± 0.36 %, 48 µg/kg/hr Ang II 12.05 ± 1.61 %, n= 3-11, $p<0.05$). The increase in fibrosis was due to the deposition of collagen I and collagen III which were both significantly increased by 75 % and 81 % ($p<0.05$), respectively in animals receiving 24 µg/kg/hr Ang II (Figure 3-4 A ii-iii, B ii-iii). In animals receiving 48 µg/kg/hr Ang II, collagen I was increased by 56 % while collagen III increased by 136 % compared to control ($p<0.05$) (Figure 3-4 A ii-iii, B ii-iii). The collagen I/ collagen III ratio was 1.95 ± 0.29 in control animals and this was not significantly changed by Ang II infusion (Figure 3-4 B iv).

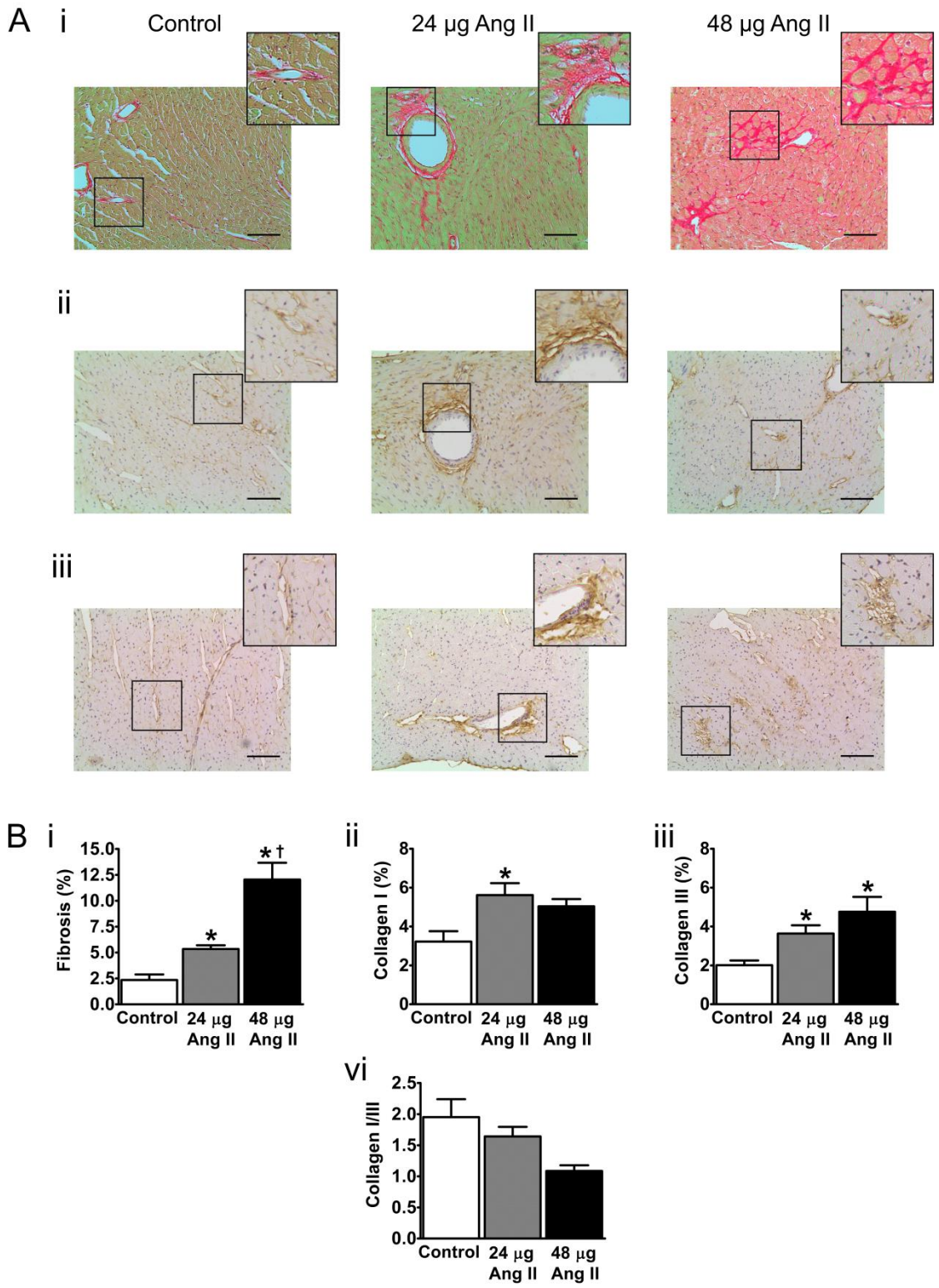

Figure 3-4. Effects of chronic Ang II infusion on cardiac fibrosis.
(A) Heart sections of animals receiving H_2O (control), 24 µg/kg/hr (24 µg Ang II) or 48 µg/kg/hr (48 µg Ang II) Ang II for 6 weeks were stained with (i) picrosirius red, (ii) collagen I and (iii) collagen III. The inset represents a magnification of the area within the black square. Scale= 100 µm. (B i) Total cardiac fibrosis, (ii) the collagen I and (iii) collagen III fractions as well as the (iv) collagen I/ collagen III ratio were determined for control (n= 11), 24 and 48 µg Ang II (n= 10 and 3, respectively). Data are presented as mean ± SEM. *p<0.05 *vs.* control. † p<0.05 *vs.* 24 µg Ang II (ANOVA with Tukey post-hoc analysis).

3.3.1.4 Gene expression analysis

qRT-PCR analysis was performed to investigate the expression of components of the RAS as well as markers of fibrosis and hypertrophy. Expression of the RAS components Agtr1a (AT_1R), Agtr2 (AT_2R), Mas1, Ace and Ace2 were not significantly altered between Ang II infusion and control (Figure 3-5 A i-v). Col1A1, Col3A1 and ACTA2 (αSMA) gene expression were significantly increased with 48 µg/kg/hr Ang II compared to control and 24 µg/kg/hr Ang II (RQ: 1.50 ± 0.21, 1.52 ± 0.17 and 2.48 ± 0.71, respectively, $p<0.05$) (Figure 3-5 B i-ii, vi). Expression of $TGFß_1$, Ctgf and S100A4 were unchanged across all treatment groups (Figure 3-5 B iii-v). Gene expression of the hypertrophy markers Nppa (ANP) and Nppb (BNP) were not significantly altered across any group (Figure 3-5 C i-ii). However, expression of Myh7 (ßMHC) was significantly increased with 48 µg/kg/hr Ang II compared to control (RQ: control 1.0 ± 0.31, 24 µg/kg/hr Ang II 1.01 ± 0.59, 48 µg/kg/hr Ang II 4.09 ± 1.21, n= 3-6, $p<0.05$) (Figure 3-5 C iii).

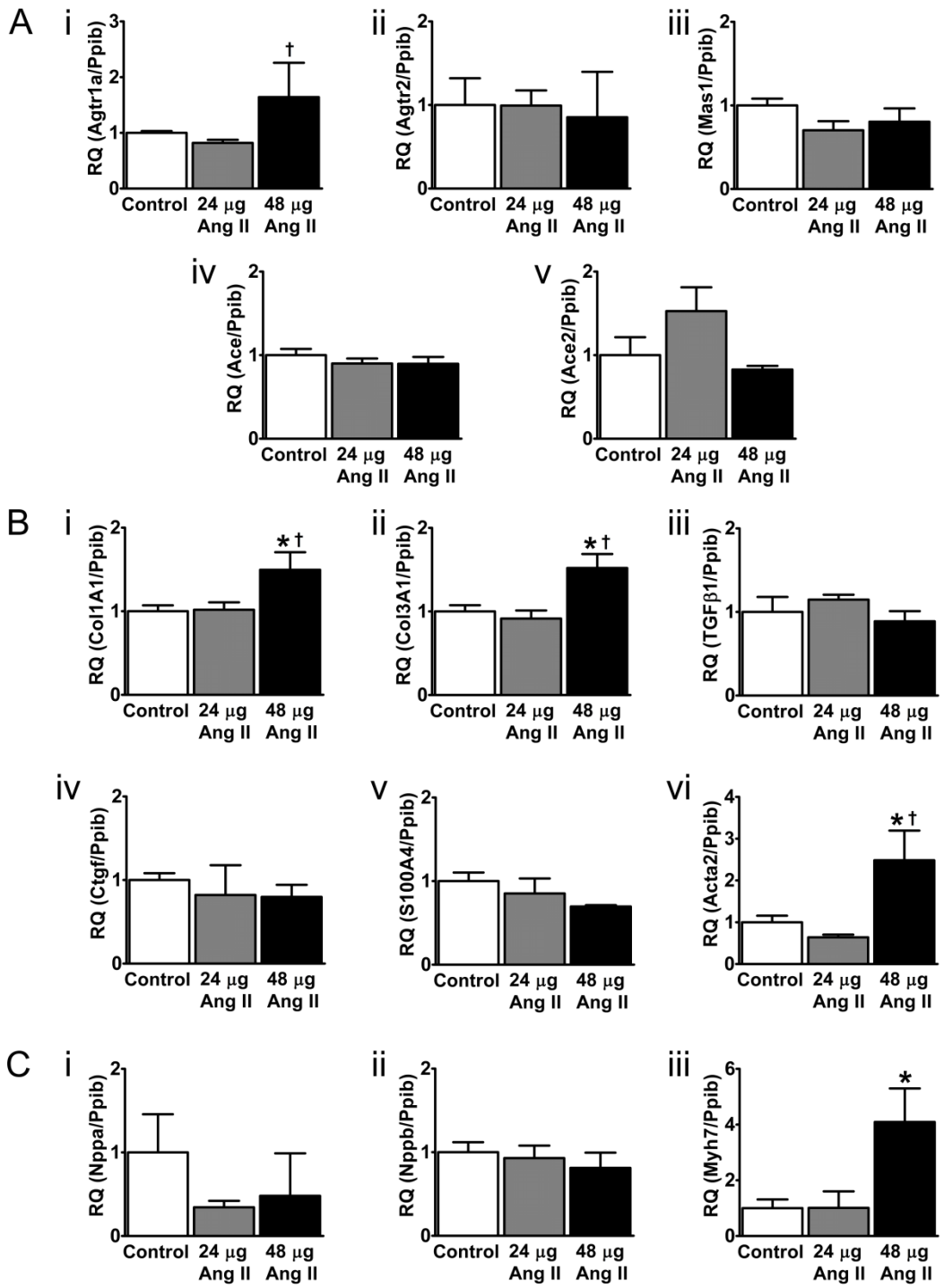

Figure 3-5. Effects of Ang II infusion on the gene expression of RAS components, hypertrophic and fibrotic markers.
Gene expression analysis was carried out in cardiac homogenates of mice receiving H_2O (control), 24 μg/kg/hr (24 μg Ang II) or 48 μg/kg/hr (48 μg Ang II) Ang II for 6 weeks for (A) the RAS components (i) Agtr1a, (ii) Agtr2, (iii) Mas1, (vi) Ace and (v) ACE2; (B) fibrosis makers (i) Col1A1, (ii) Col3A1, (iii) TGFβ1, (vi) Ctgf, (v) S100A4, (vi) Acta2; and (C) hypertrophy markers (i) Nppa, (ii) Nppb and (iii) Myh7. Gene expression was normalised to the housekeeper Ppib and expressed as the relative quantity (RQ) ± rqmax of control which was set as RQ= 1. n= 6, 4 and 3 for control, 24 and 48 μg Ang II, respectively. *P<0.05 *vs.* control. † p<0.05 *vs.* 24 μg Ang II (ANOVA with Tukey's post-hoc analysis).

3.3.2 Effects of Ang-(1-9) on cardiac structure and function

Next the cardiac effects of chronic Ang-(1-9) infusion in healthy normotensive mice were assessed. Mice were implanted with minipumps delivering 48 µg/kg/hr Ang-(1-9) for 6 weeks and cardiac function was assessed by echocardiography at fortnightly intervals. The effects of Ang-(1-9) were compared to control mice infused with H_2O (Section 3.3.1).

Example M-mode images from Ang-(1-9)-infused mice at all time-points are shown in Figure 3-6 A. Infusion of Ang-(1-9) had no effect on any echocardiographic indices of cardiac function (FS) and morphology (LVEDD, LVESD, LVFWd, LVFWs) at all time-points (Figure 3-6 B-F).

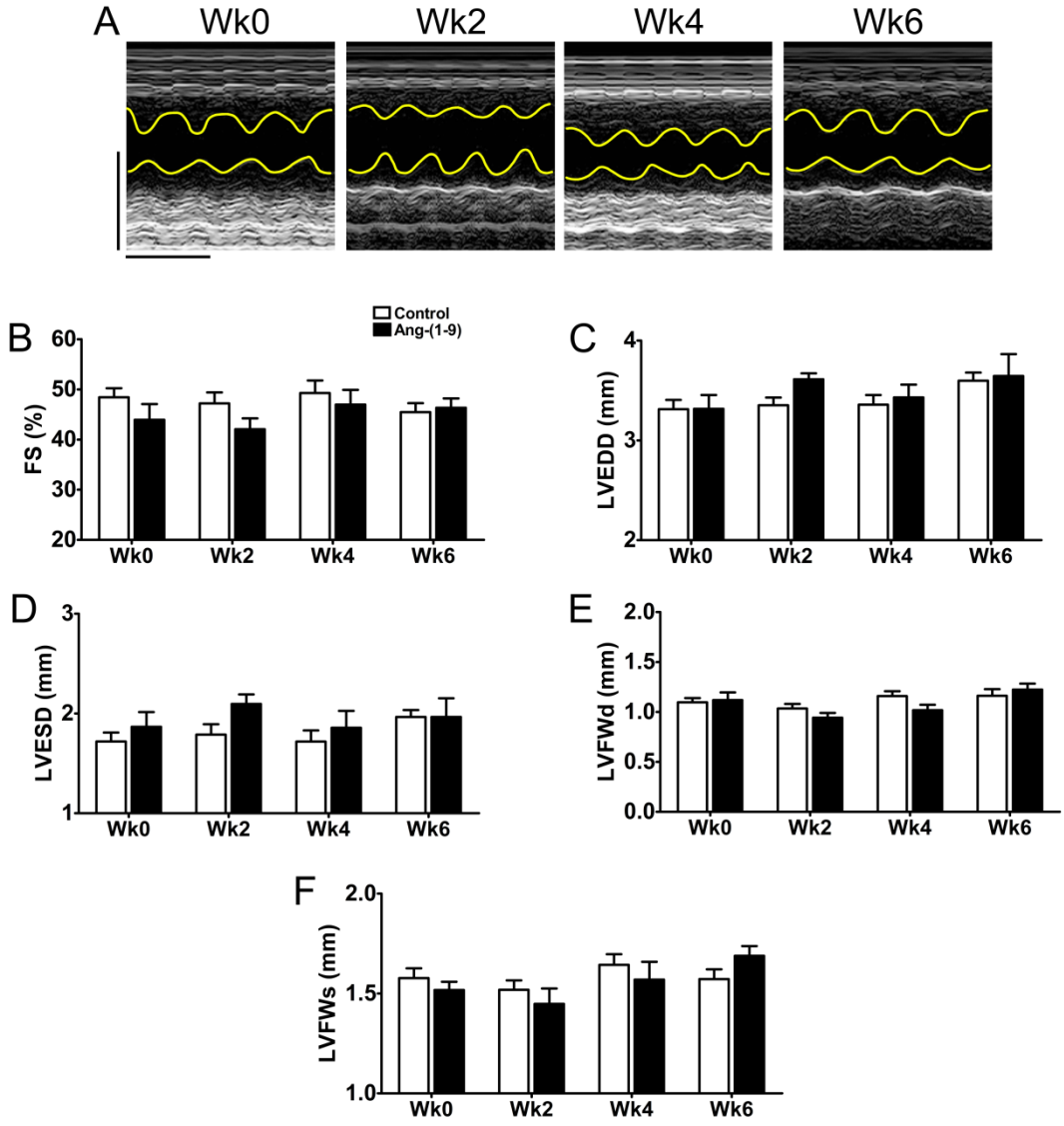

Figure 3-6. Effects of Ang-(1-9) on cardiac function.
(A) Example M-mode images for mice receiving 48 µg/kg/hr Ang-(1-9) (n= 4) at week 0, 2, 4 and 6. Scale= 5 mm and 200 ms. Serial measurements of (B) FS, (C) LVEDD, (D) LVESD, (E) LVFWd and (F) LVFWs from longitudinal M-mode images over 6 weeks for animals receiving Ang-(1-9) compared to control (n= 11) previously presented in Figure 3-2. Data are presented as mean ± SEM. FS= Fractional shortening; LVEDD= Left ventricular end-diastolic dimension; LVESD= Left ventricular systolic dimension; LVFWd/LVFWs= Left ventricular free wall thickness during diastole and systole *p<0.05 *vs.* control (Student's t-test).

At necropsy, HW/TL of mice infused with Ang-(1-9) was not significantly different to control hearts ($p>0.05$) (Figure 3-7 A i-ii). A lack of an effect on cardiomyocyte hypertrophy was confirmed by WGA staining (Figure 3-7 B-C). Total fibrosis as measured by picrosirius red, collagen I and collagen III staining as well as the collagen I/ collagen III ratio was not significantly different between Ang-(1-9)- and control-infused mice (Figure 3-7 D-E).

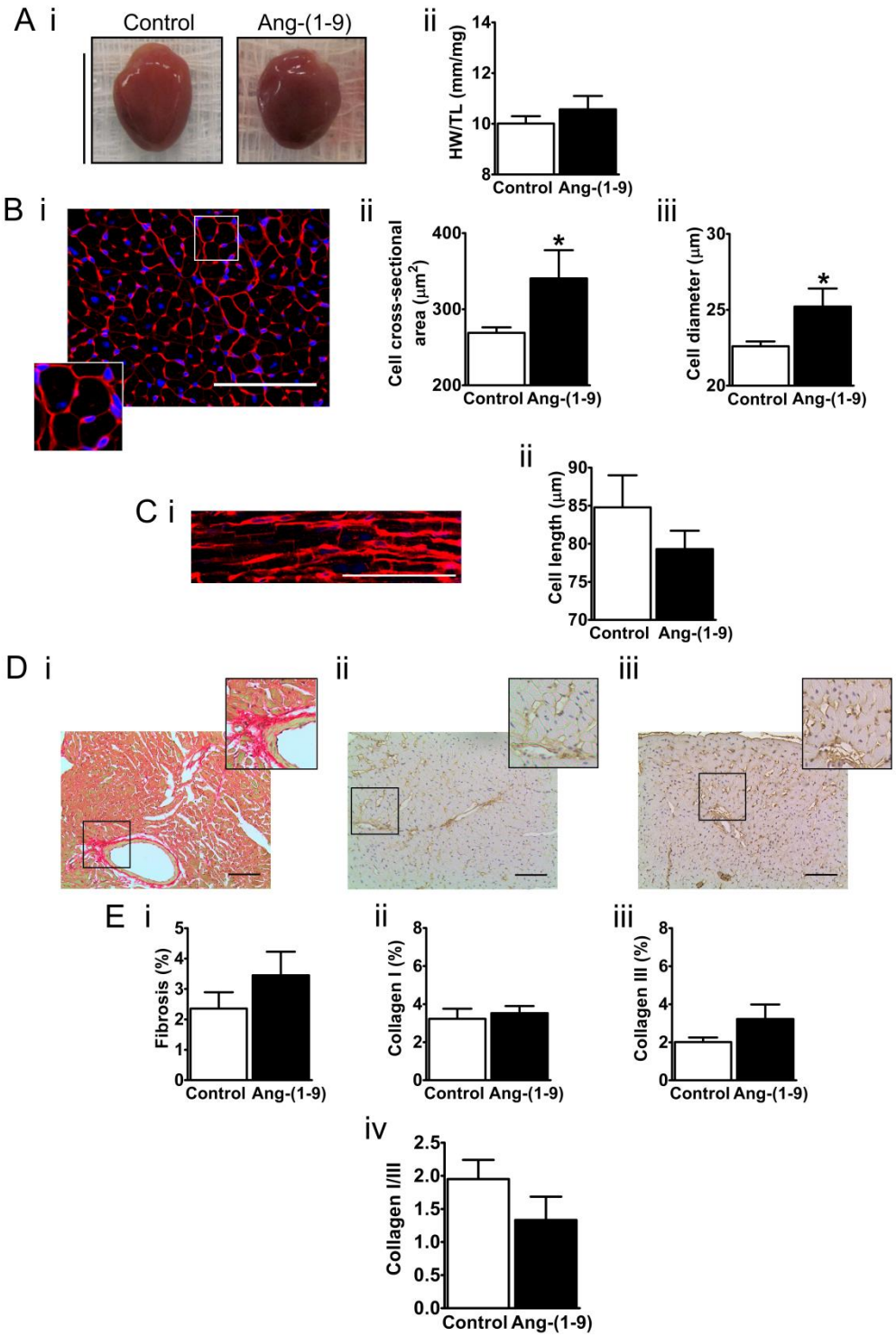

Figure 3-7. Effects of Ang-(1-9) infusion on cardiac hypertrophy and fibrosis.
(A i) Example image of a heart from a mouse receiving H_2O (control) or 48 μg/kg/hr Ang-(1-9). Scale= 10 mm. (ii) Heart weight/tibia length (HW/TL) at 6 weeks for Ang-(1-9) (n= 4) compared to control (n= 11) previously presented in Figure 3-3. Example images of wheat germ agglutinin staining in both, (B i) transverse and (C i) longitudinal sections of cardiomyocytes in Ang-(1-9)-infused mice. The cardiomyocyte membrane is stained red and nuclei blue. The inset represents a magnification of the area within the white square. Scale= 100 μm. (B ii) Cell cross-sectional area, (B iii) cell diameter and (C ii) cell length were determined in the Ang-(1-9) group (n= 4) and compared to control (n= 11). (D) Example images of (i) picrosirius red, (ii) collagen I and (iii) collagen III staining in hearts of Ang-(1-9)-infused mice. The inset represents a magnification of the area within the black square. Scale= 100 μm. (E i) Total cardiac fibrosis, (ii) the collagen I and (iii) collagen III fractions and the (iv) collagen I/ III ratio were determined for Ang-(1-9)-infused mice (n= 4) and compared to control (n= 11). Data are presented as mean ± SEM. *p<0.05 *vs.* control (Student's t-test with Welch's correction for cardiomyocyte cross-sectional area and cell diameter).

3.3.3 Assessment of reversal of Ang II-induced cardiac disease by Ang-(1-9)

To assess whether Ang-(1-9) can reverse established Ang II-induced cardiac remodelling and contractile dysfunction a reversal model was developed (Figure 3-8). At 12 weeks of age, mice were implanted with osmotic minipumps delivering either H_2O as control or 48 µg/kg/hr Ang II for 2 weeks to induce cardiac contractile dysfunction. Minipumps were then replaced and animals were either maintained on H_2O and 48 µg/kg/hr Ang II or received a combination of 48 µg/kg/hr Ang II and 48 µg/kg/hr Ang-(1-9) for a further 2 or 4 weeks (i.e. 4 and 6 weeks in total, respectively). BP and cardiac function were assessed by tail cuff plethysmography and echocardiography, respectively.

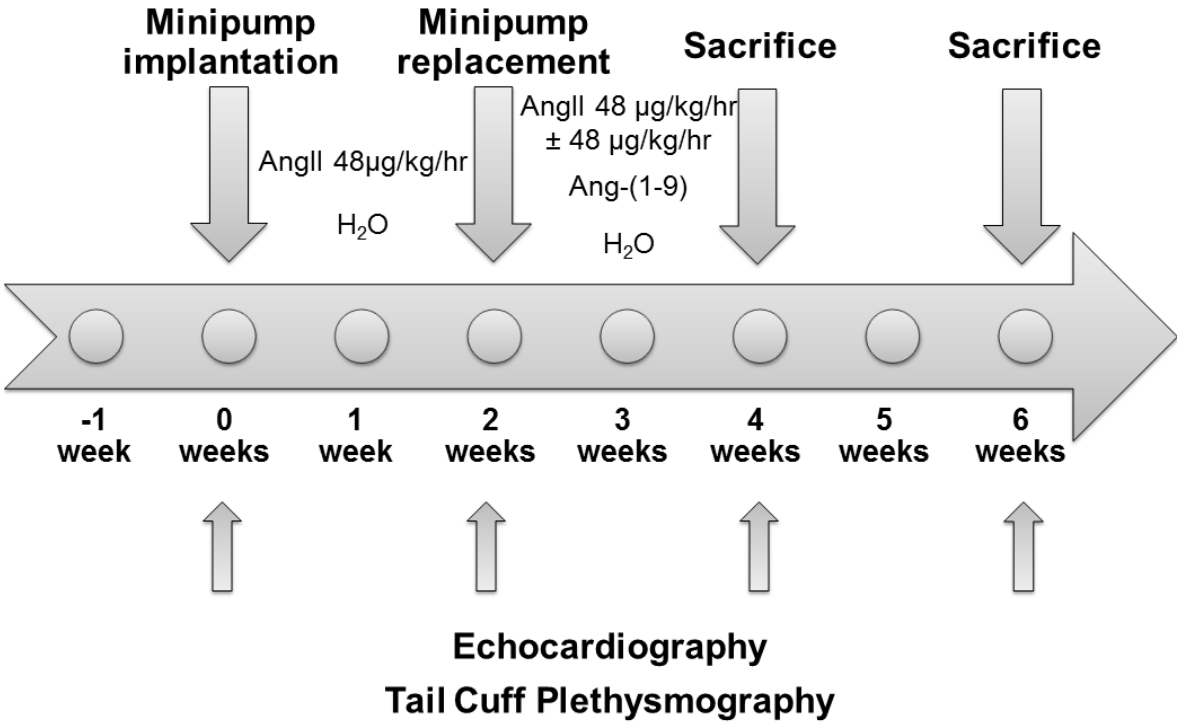

Figure 3-8. Study outline for the assessment of the role of Ang-(1-9) in established Ang II-induced cardiac pathology.
Minipumps were implanted in male C57BL/6J mice at 12 weeks of age (week O) to deliver either H_2O (control) or 48 µg/kg/hr Ang II for 2 weeks. Minipumps were then replaced and Ang II-infused animals were randomised to either be maintained on 48 µg/kg/hr Ang II alone or receive a coinfusion of 48 µg/kg/hr Ang II with 48 µg/kg/hr Ang-(1-9) for a further 2-4 weeks. Control animals received a further infusion of H_2O. Cardiac function and blood pressure were assessed by echocardiography and tail cuff plethysmography in fortnightly intervals.

3.3.3.1 Blood pressure

BP was assessed by tail cuff plethysmography. Baseline measurements of BP were not significantly different between animal groups (Table 3-2). Systolic and diastolic BP were increased by 15 % and 33 % in the Ang II group at 2 weeks ($p<0.05$) and this was maintained over the course of the infusion peaking at 6 weeks with 153 ± 6 mmHg and 81 ± 9 mmHg for systolic and diastolic BP, respectively ($p<0.05$) (Figure 3-9 A-B). Infusion of Ang-(1-9) did not alter Ang II-induced increases in systolic and diastolic BP (Figure 3-9 A-B). Similarly, mean BP was significantly increased with Ang II at 2 weeks (control 74 ± 2 mmHg *vs.* Ang II 91 ± 3 mmHg, n= 6-10, $p<0.05$) which was maintained at 4 and 6 weeks (Figure 3-9 C). Ang-(1-9) did not alter Ang II-induced increases in mean BP (Figure 3-9 C). At 2 weeks, the pulse rate was significantly decreased by Ang II (control 594 ± 17 bpm *vs.* Ang II 492 ± 14 bpm, n= 6-10, $p<0.05$) (Figure 3-9 D). This returned to control values by 4 weeks and was not altered by Ang-(1-9) (Figure 3-9 D).

Table 3-2. Functional indices measured by tail cuff plethysmography and echocardiography.

	Baseline		2 weeks		4 weeks			6 weeks		
	Control	Ang II	Control	Ang II	Control	Ang II	Ang II+ Ang-(1-9)	Control	Ang II	Ang II+ Ang-(1-9)
MAP (mmHg)	75 ± 3	76 ± 2	74 ± 2	90 ± 3*	78 ± 3	92 ± 7	100 ± 5	70 ± 2	105 ± 7*	91 ± 9
SBP (mmHg)	113 ± 5	117 ± 2	117 ± 5	135 ± 4*	118 ± 4	139 ± 9	156 ± 6	108 ± 3	153 ± 6*	142 ± 10
DBP (mmHg)	55 ± 3	55 ± 2	51 ± 3	68 ± 4*	55 ± 3	69 ± 7	71 ± 6	51 ± 2	81 ± 9*	66 ± 9
Pulse (bpm)	636 ± 15	619 ± 13	594 ± 17	492 ± 14*	635 ± 15	625 ± 27	630 ± 37	627 ± 15	565 ± 39	562 ± 20
FS (%)	52.26 ± 2.03	51.30 ± 1.09	54.82 ± 3.00	35.47 ± 1.87*	50.48 ± 2.17	33.56 ± 1.88*	43.98 ± 3.54†	49.28 ± 5.24	35.02 ± 1.60	33.17 ± 0.55
LVEDD (mm)	3.41 ± 0.15	3.43 ± 0.08	3.39 ± 0.12	3.34 ± 0.09	3.56 ± 0.10	3.25 ± 0.21	3.39 ± 0.15	3.64 ± 0.28	3.54 ± 0.26	3.17 ± 0.12
LVESD (mm)	1.63 ± 0.14	1.67 ± 0.07	1.56 ± 0.16	2.16 ± 0.11*	1.78 ± 0.11	2.17 ± 0.18	1.93 ± 0.19	1.88 ± 0.33	2.28 ± 0.13	2.12 ± 0.10
LVFWd (mm)	0.84 ± 0.04	0.87 ± 0.03	0.84 ± 0.05	1.40 ± 0.07*	0.90 ± 0.05	1.16 ± 0.09	1.29 ± 0.10	0.85 ± 0.15	1.02 ± 0.07	1.69 ± 0.19 †
LVFWs (mm)	1.45 ± 0.03	1.43 ± 0.03	1.44 ± 0.01	1.79 ± 0.06*	1.37 ± 0.07	1.50 ± 0.08	1.75 ± 0.11	1.49 ± 0.13	1.57 ± 0.14	2.00 ± 0.20

*p<0.05 *vs.* Control, † p<0.05 *vs.* Ang II. DBP= diastolic blood pressure; FS= Fractional shortening; MAP= Mean arterial pressure; SBP= Systolic blood pressure; LVEDD= Left ventricular end-diastolic dimension; LVESD= Left ventricular systolic dimension; LVFWd/LVFWs= Left ventricular free wall thickness during diastole and systole

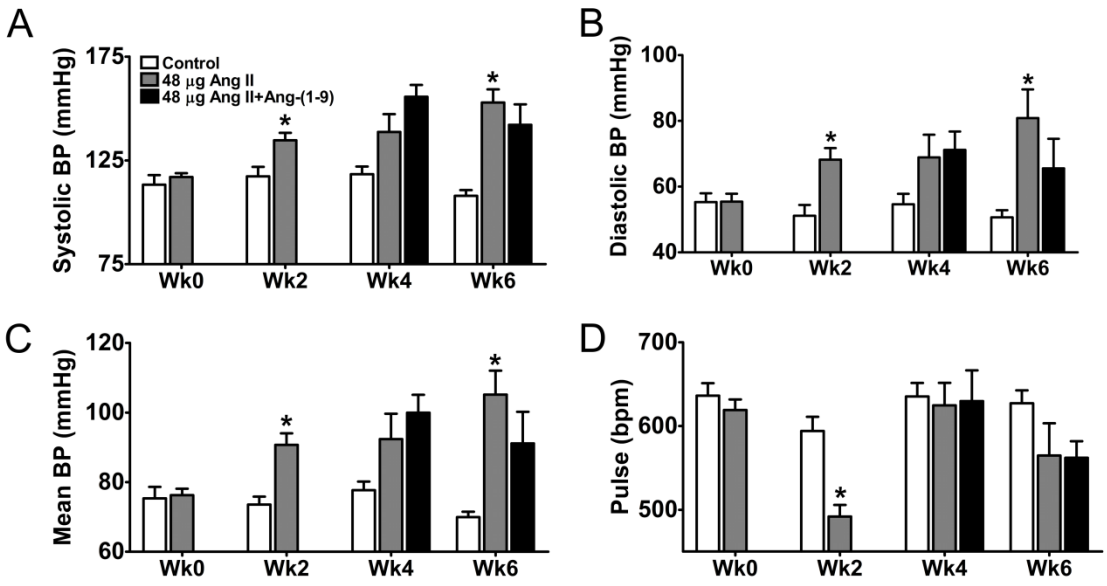

Figure 3-9. Effects of Ang-(1-9) on Ang II-induced hypertension.
Mice were infused with H_2O (control) or 48 μg/kg/hr Ang II (48 μg Ang II) for 2 weeks and minipumps were replaced to deliver H2O, 48 μg/kg/hr Ang II or 48 μg/kg/hr Ang II+48 μg/kg/hr Ang-(1-9) for a further 4 weeks. (A) Systolic BP, (B) diastolic BP, (C) mean BP and (D) pulse rate were determined by tail cuff plethysmography. n= 6 and 10 for control and 48 μg Ang II, respectively at week 0 and 2 and n= 6, 5, and 5 for control, 48 μg Ang II and 48 μg Ang II+Ang-(1-9), respectively at week 4 and 6. Data are presented as mean ± SEM. *p<0.05 *vs.* control (ANOVA with Dunnett's post-hoc analysis).

3.3.3.2 Cardiac function

At baseline, measurements of cardiac structure and function did not significantly differ between groups (Table 3-2). After 2 weeks Ang II infusion, FS was significantly decreased from 54.82 ± 3.00 % in control animals to 35.47 ± 1.87 % ($p<0.05$) (Figure 3-10 A-B). This was maintained at 4 and 6 weeks where FS measured 33.56 ± 1.88 % and 35.02 ± 1.60 %, respectively (Figure 3-10 B). Infusion of Ang-(1-9) for 2 weeks (i.e. at week 4), significantly improved FS compared to Ang II (Ang II 33.56 ± 1.88 % *vs.* Ang II+Ang-(1-9) 43.98 ± 3.54 %, n= 6-8, $p<0.05$) (Figure 3-10 B). However, after 4 weeks of Ang-(1-9) addition (i.e. at 6 weeks) FS was not significantly different compared to Ang II ($p>0.05$) (Figure 3-10 B). LVEDD remained unchanged in all treatment groups at all timepoints (Figure 3-10 C). However, the reduction in FS with Ang II infusion was associated with a significant increase in LVESD. Infusion of Ang-(1-9) at 4 and 6 weeks did not significantly alter Ang II-induced changes in LVESD (Figure 3-10 D). At 2 weeks, LVFWd and LVFWs were significantly increased by 67 % and 24 %, respectively with Ang II compared to control ($p<0.05$) (Figure 3-10 E-F). Ang-(1-9) significantly increased LVFWd after 4 weeks of co-infusion with Ang II compared to Ang II alone ($p<0.05$) but did not affect LVFWs (Figure 3-10 E-F).

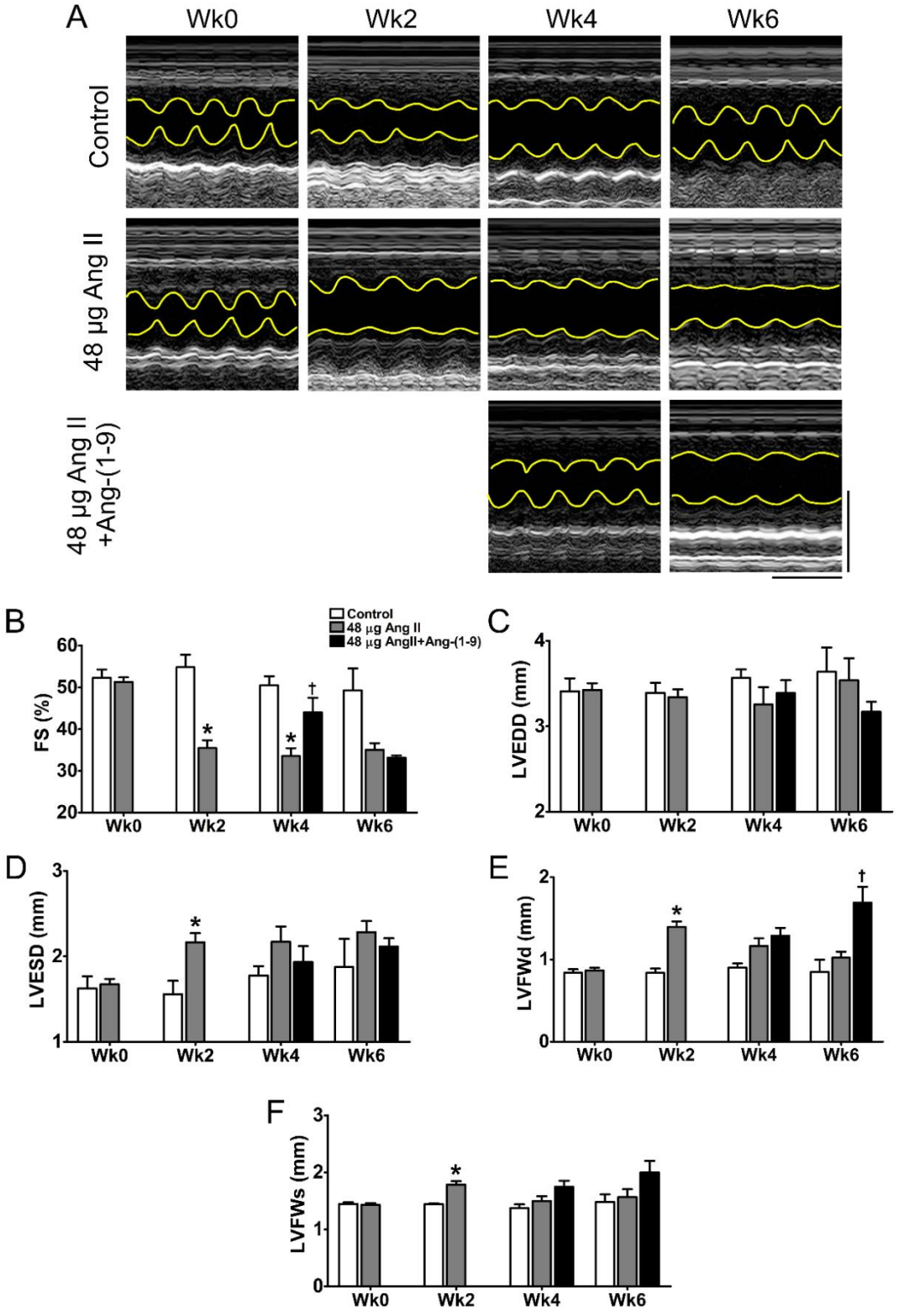

Figure 3-10. Effects of Ang-(1-9) on established Ang II-induced cardiac dysfunction. (A) Example M-mode images for mice receiving H_2O (control), 48 µg/kg/hr Ang II (48 µg Ang II) or 48 µg/kg/hr Ang II+48 µg/kg/hr Ang-(1-9) at week 0, 2, 4 and 6 weeks. Scale= 5 mm and 200 ms. Serial measurements of (B) FS, (C) LVEDD, (D) LVESD, (E) LVFWd and (F) LVFWs from longitudinal M-mode images for each treatment group over 6 weeks. n= 8 and 14 for control and 48 µg Ang II, respectively at 0 and 2 weeks. n= 8, 6 and 8 for control, 48 µg Ang II and 48 µg Ang II+Ang-(1-9), respectively at 4 weeks. n= 4, 3 and 3 for control, 48 µg Ang II and 48 µg Ang II+Ang-(1-9), respectively at 6 weeks (data produced by Lauren Wills). FS= Fractional shortening; LVEDD= Left ventricular end-diastolic dimension; LVESD= Left ventricular systolic dimension; LVFWd/LVFWs= Left ventricular free wall thickness during diastole and systoleData are presented as mean ± SEM. *p<0.05 *vs.* control. † p<0.05 *vs.* 48 µg Ang II (ANOVA with Dunnett's post-hoc analysis).

3.3.3.3 Hypertrophy

Hearts dissected from mice after 4 and 6 weeks infusion of Ang II irrespective of Ang-(1-9) treatment were visibly larger than hearts from control animals (Figure 3-11 A). At 4 weeks, despite being non-significant, HW/TL tended to be increased with Ang II. Infusion of Ang-(1-9) in the last 2 weeks did not significantly alter Ang II-induced hypertrophy (control 10.36 ± 0.30 mg/mm, Ang II 11.75 ± 0.36 mg/mm, Ang II+Ang-(1-9) 12.90 ± 0.60 mg/mm, n= 6, $p>0.05$) (Figure 3-11 B). At 6 weeks, HW/TL was significantly increased by Ang II from 10.86 ± 0.38 mg/mm in control animals to 13.34 ± 0.60 mg/mm with Ang II infusion ($p<0.05$) (Figure 3-11 B). The addition of Ang-(1-9) to Ang II infusion in the last four weeks did not alter the Ang II induced increase in HW/TL (13.49 ± 0.74, $p>0.05$) (Figure 3-11 B).

Cardiomyocyte size was assessed by WGA staining in heart tissue sections (Figure 3-12 A i-B i). Cardiomyocyte cross-sectional area was significantly increased by 40 % and 28 % ($p<0.05$) in Ang II-infused mice at 4 and 6 weeks, respectively and this was not reversed by the infusion of Ang-(1-9) (Figure 3-12 A ii). Cell diameter was significantly increased by 13 % and 19 % in the Ang II group at 4 and 6 weeks, respectively ($p<0.05$) (Figure 3-12 A iii). The addition of Ang-(1-9) after 2 weeks of Ang II-infusion did not reverse Ang II-induced increases in cell diameter ($p>0.05$) (Figure 3-12 A iii). Measurements of cell length revealed no significant difference in cell length between control, Ang II and Ang II+Ang-(1-9) at 4 weeks ($p>0.05$) (Figure 3-12 B ii). At 6 weeks, cell length was significantly increased by 16 % with Ang II ($p<0.05$), however, Ang-(1-9) did not alter the Ang II-induced increase in cell length ($p>0.05$) (Figure 3-12 B ii).

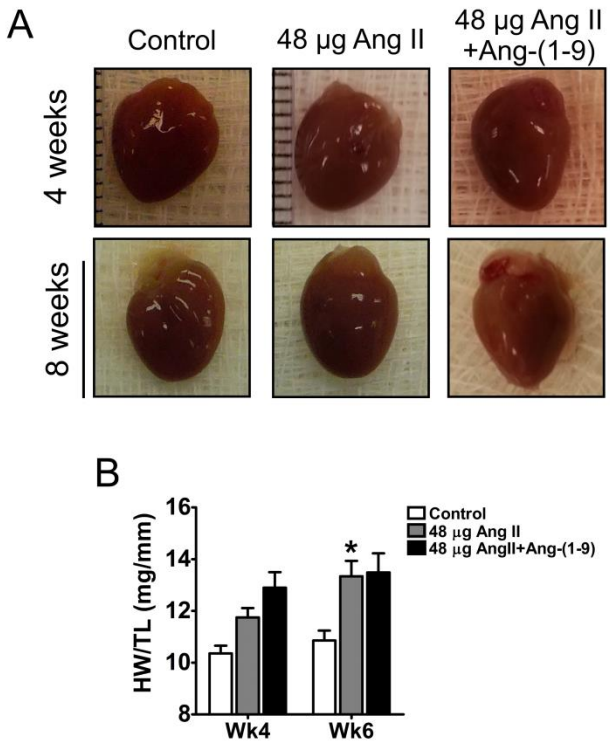

Figure 3-11. Effects of Ang-(1-9) on established Ang II-induced cardiac hypertrophy. Mice were infused with either H_2O (control) or 48 µg /kg/hr Ang II (48 µg Ang II) for 2 weeks when minipumps were replaced and animals were infused with H_2O, 48 µg /kg/hr Ang II or 48 µg /kg/hr Ang II+48 µg /kg/hr Ang-(1-9) for a further 2-4 weeks. (A) Example images of hearts from control, 48 µg Ang II and 48 µg Ang II+Ang-(1-9) after 4 and 6 weeks. Scale= 10 mm. (B) Heart weight/tibia length (HW/TL) for control, 48 µg Ang II and 48 µg Ang II+Ang-(1-9) after 4 and 6 weeks. n= 6 for all groups at 4 weeks and n= 10, 8 and 8 for control, 48 µg Ang II and 48 µg Ang II+Ang-(1-9), respectively at 6 weeks (n= 4 and 3 for control and 48 µg Ang II±Ang-(1-9) at 6 weeks, respectively produced by Lauren Wills). Data are presented as mean ± SEM. *$p<0.05$ *vs.* control (ANOVA with Dunnett's post-hoc analysis).

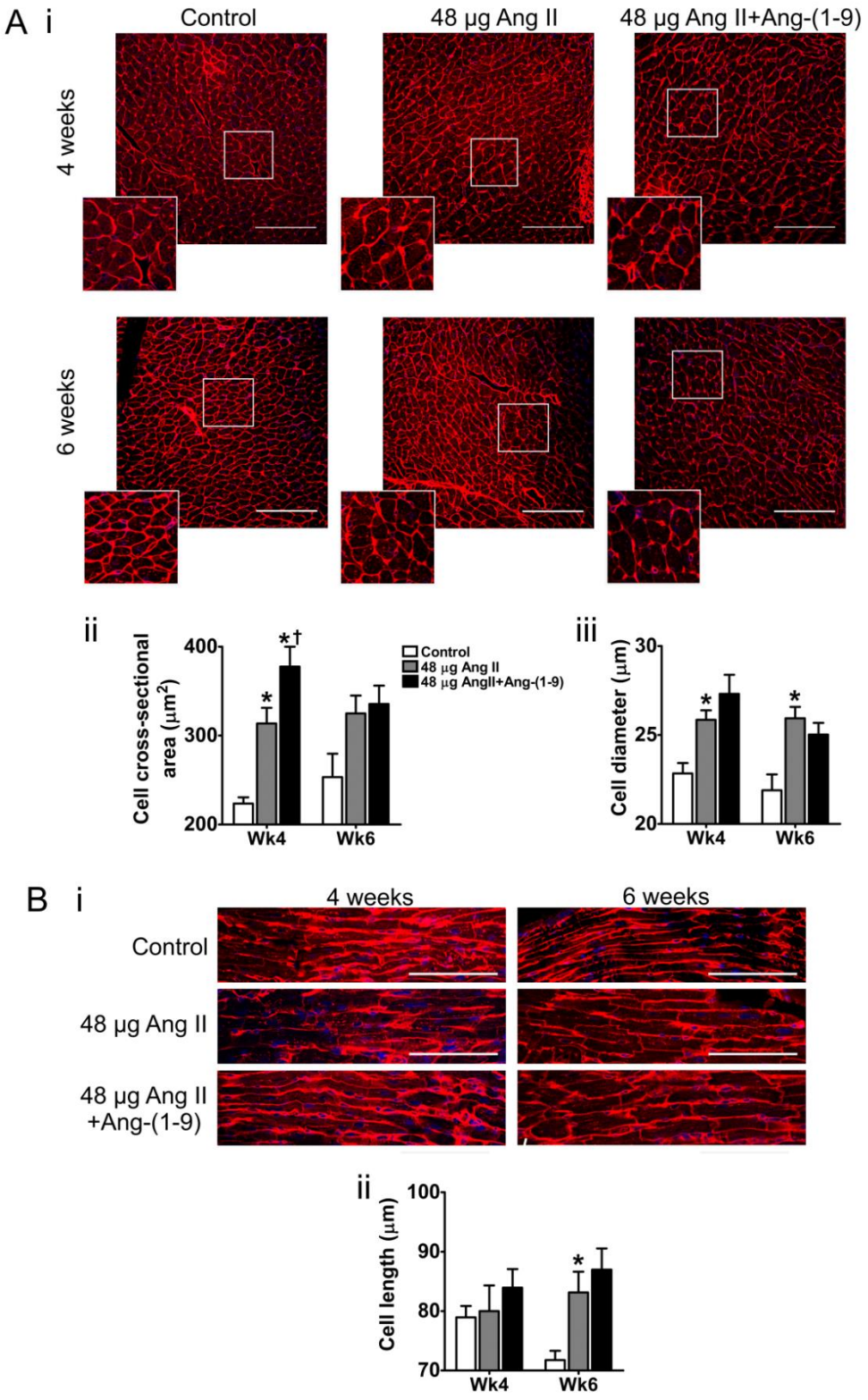

Figure 3-12. Effects of Ang-(1-9) on established Ang II-induced cardiomyocyte hypertrophy. Example images of wheat germ agglutinin staining in both, (A i) transverse and (B i) longitudinal sections of hearts from mice infused with H_2O (control), 48 µg/kg/hr Ang II (48 µg Ang II) and 48 µg/kg/hr Ang II+48 µg/kg/hr Ang-(1-9) for 4 and 6 weeks. The cardiomyocyte membrane is stained red and nuclei blue. The inset represents a magnification of the area within the white square. Scale= 100 µm. (A ii) Cell cross-sectional area, (A iii) cell diameter and (B ii) cell length were determined in control, 48 µg Ang II and 48 µg Ang II+Ang-(1-9) at 4 and 6 weeks. n= 6 for all groups at 4 weeks and n= 10, 8 and 8 for control, 48 µg Ang II and 48 µg Ang II+Ang-(1-9), respectively at 6 weeks (n= 4 and 3 for control and 48 µg Ang II±Ang-(1-9) at 6 weeks, respectively produced by Lauren Wills). Data are presented as mean ± SEM. *p<0.05 *vs.* control, † p<0.05 *vs.* 48 µg Ang II (ANOVA with Dunnett's post-hoc analysis).

3.3.3.4 Fibrosis

Total cardiac fibrosis as assessed by picrosirius red staining (Figure 3-13 A) revealed a significant increase in cardiac fibrosis with Ang II compared to control at 4 weeks (control 0.94 ± 0.16 % *vs.* Ang II 9.26 ± 2.05 %, n= 6, $p<0.05$) (Figure 3-13 B). Infusion of Ang-(1-9) did not significantly change Ang II-induced cardiac fibrosis ($p>0.05$) (9.07 ± 1.89 %, n=6). Similarly, at 6 weeks, cardiac fibrosis was significantly increased by 285 % in the Ang II group compared to control ($p<0.05$) and infusion of Ang-(1-9) for the last 4 weeks did not affect Ang II-induced cardiac fibrosis ($p>0.05$) (Figure 3-13 B).

Collagen I deposition revealed a significant increase in cardiac collagen I content with Ang II by 124 % and 50 % at 4 and 6 weeks, respectively ($p<0.05$) and infusion of Ang-(1-9) for 2 or 4 weeks did not reduce Ang II-induced collagen I deposition ($p>0.05$) (Figure 3-14 A-B).

At 4 weeks, cardiac collagen III content was significantly increased by Ang II and this was not altered by the addition of Ang-(1-9) (control 1.94 ± 0.22 %, Ang II 4.07 ± 0.38 %, Ang II + Ang-(1-9) 3.01 ± 0.92 %, n= 6, $p<0.05$) (Figure 3-15 A-B). At 6 weeks, collagen III content was increased by 87 % with Ang II infusion compared to control ($p<0.05$) (Figure 3-15 B). Infusion of Ang-(1-9) for the last 4 weeks did not significantly alter Ang II-induced collagen III deposition ($p>0.05$) (Figure 3-15 B). Infusion of Ang II in the presence of absence of Ang-(1-9) for 4 to 6 weeks did not significantly alter the collagen I/ III ratio (Figure 3-15 C).

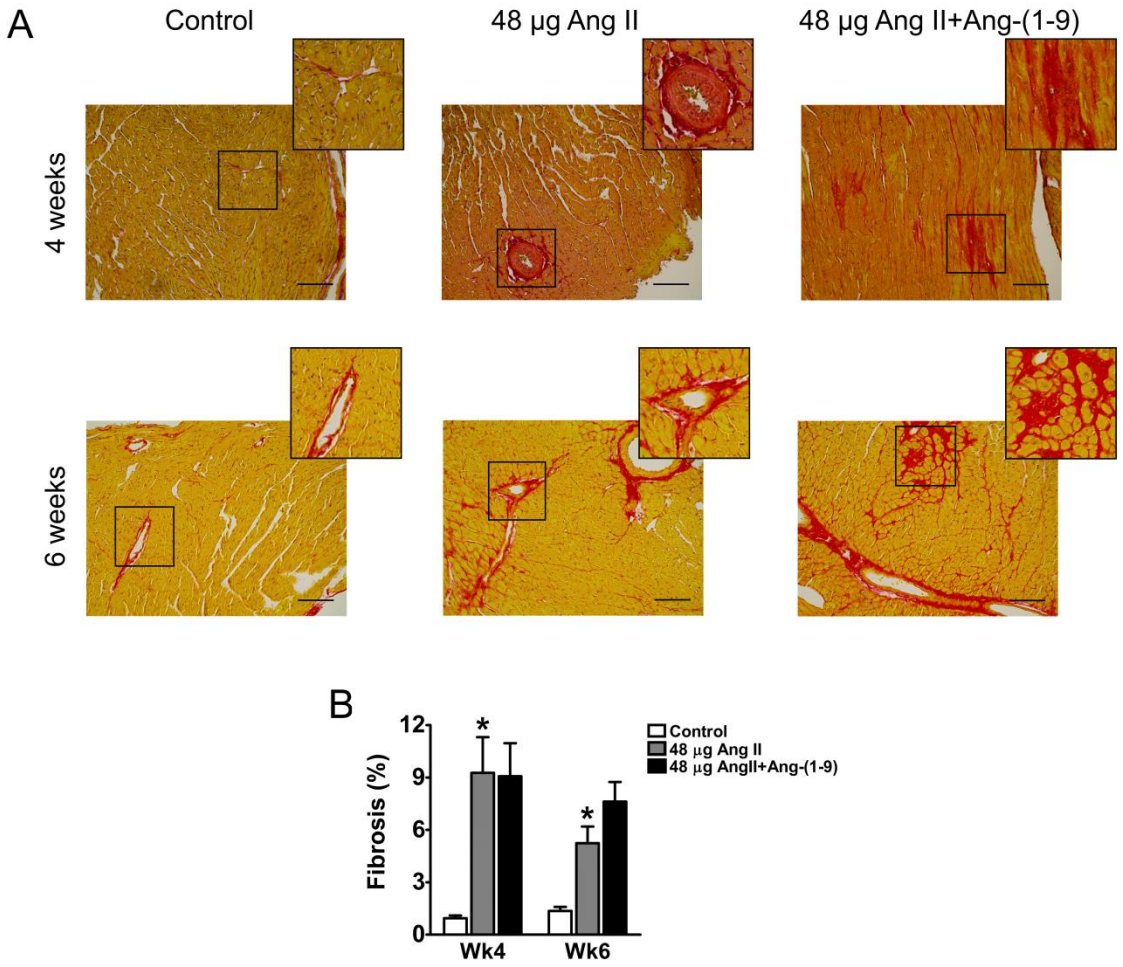

Figure 3-13. Effects of Ang-(1-9) on established Ang II-induced cardiac fibrosis.
(A) Cardiac section from mice infused with H_2O (control), 48 µg/kg/hr Ang II (48 µg Ang II) or 48 µg/kg/hr Ang II+48 µg/kg/hr Ang-(1-9) for 4 or 6 weeks were stained with picrosirius red. The inset represents a magnification of the area within the black square. Scale= 100 µm. (B) Total cardiac fibrosis was determined. n= 6 for all groups at 4 weeks and n= 10, 8 and 8 for control, 48 µg Ang II and 48 µg Ang II+Ang-(1-9), respectively at 6 weeks (n= 4 and 3 for control and 48 µg Ang II±Ang-(1-9) at 6 weeks, respectively produced by Lauren Wills). Data are presented as mean ± SEM. *p<0.05 *vs.* control (ANOVA with Dunnett's post-hoc analysis).

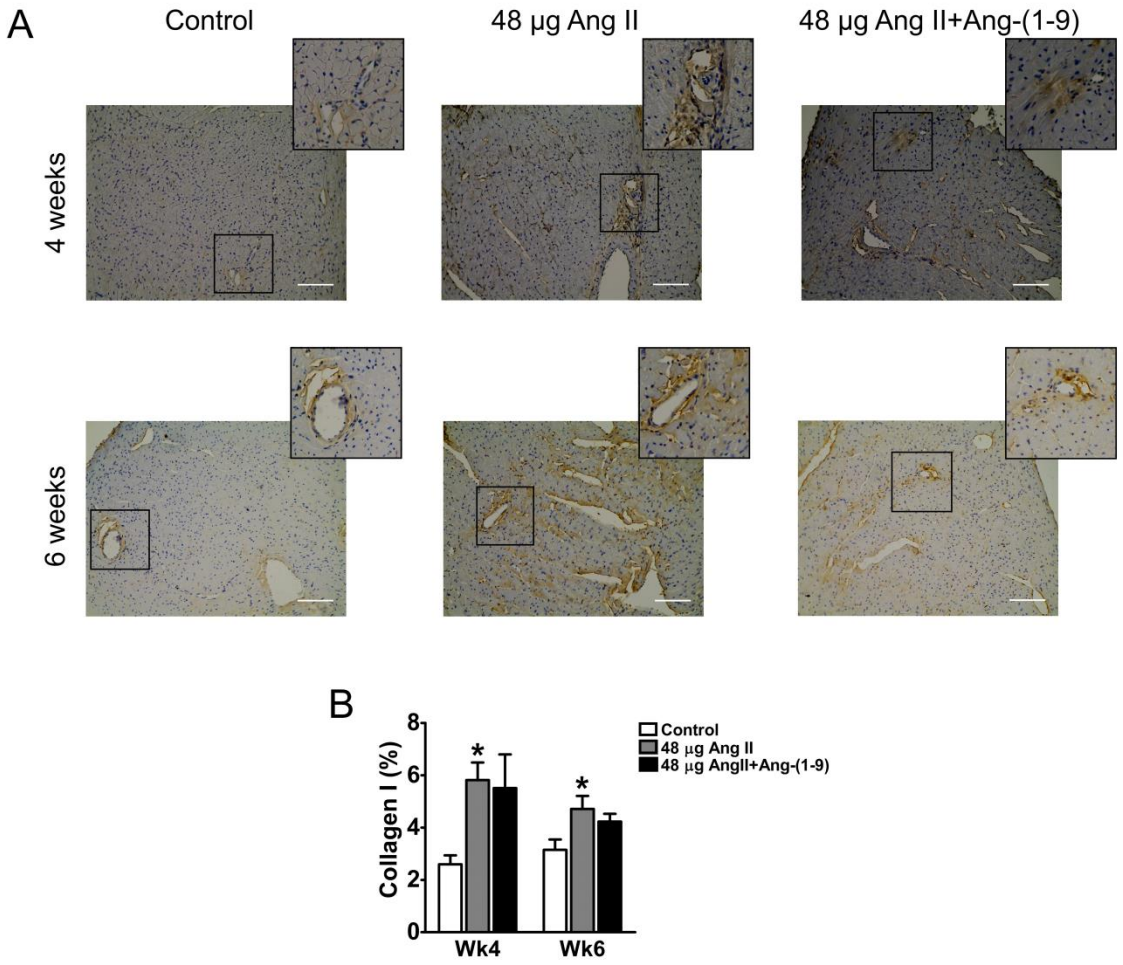

Figure 3-14. Effects of Ang-(1-9) on established Ang II-induced collagen I deposition.
(A) Cardiac section from mice infused with H_2O (control), 48 µg/kg/hr Ang II (48 µg Ang II) or 48 µg/kg/hr Ang II+48 µg/kg/hr Ang-(1-9) for 4 or 6 weeks were stained for collagen I. The inset represents a magnification of the area within the black square. Scale= 100 µm. (B) Mean collagen I content was determined. n= 6 for all groups at 4 weeks and n= 10, 7 and 8 for control, 48 µg Ang II and 48 µg Ang II+Ang-(1-9), respectively at 6 weeks (n= 4 and 3 for control and 48 µg Ang II±Ang-(1-9) at 6 weeks, respectively produced by Lauren Wills). Data are presented as mean ± SEM. *p<0.05 *vs.* control (ANOVA with Dunnett's post-hoc analysis).

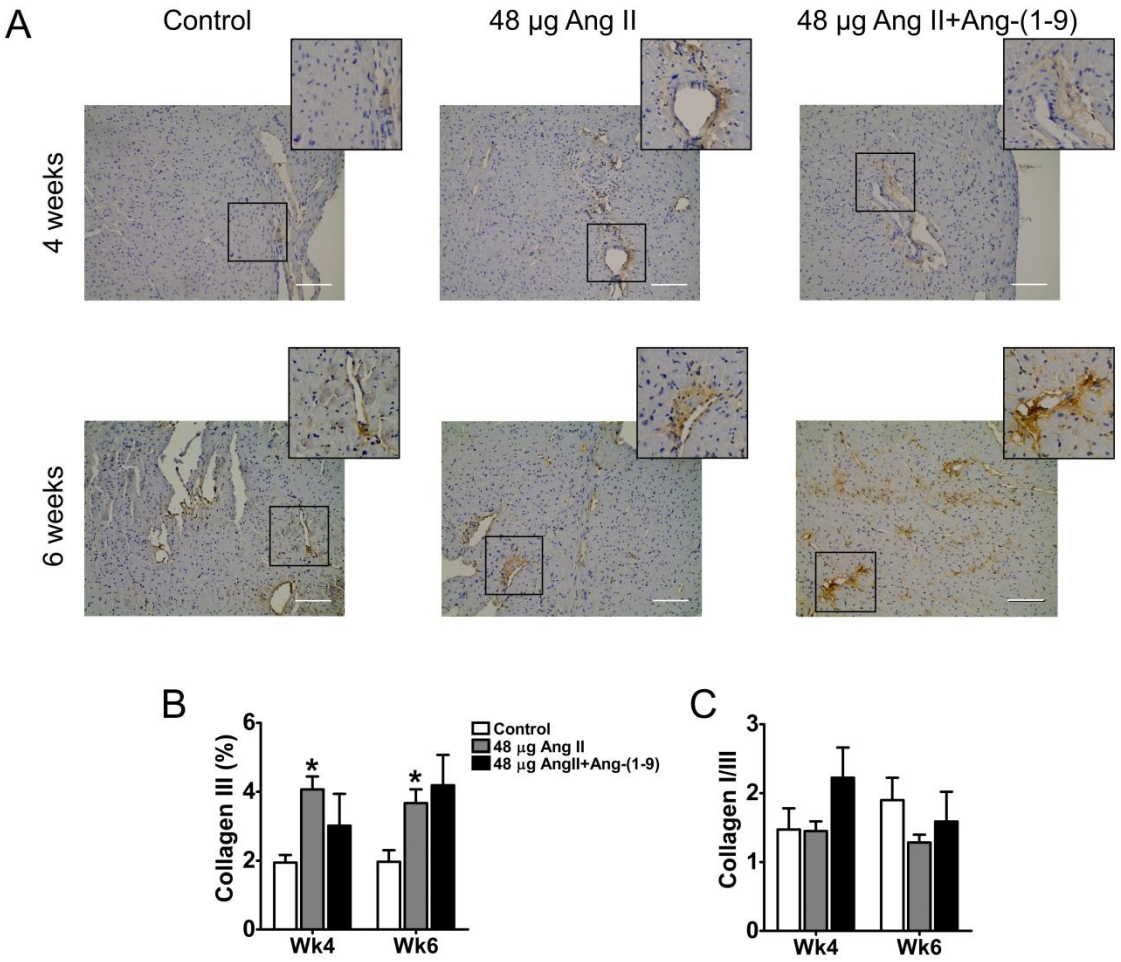

Figure 3-15. Effects of Ang-(1-9) on established Ang II-induced collagen III deposition. (A) Cardiac section from mice infused with H_2O (control), 48 µg/kg/hr Ang II (48 µg Ang II) or 48 µg/kg/hr Ang II+48 µg/kg/hr Ang-(1-9) for 4 or 6 weeks were stained for collagen III. The inset represents a magnification of the area within the black square. Scale= 100 µm. (B) Mean collagen III content and (C) the collagen I/ III ratio was determined. n= 6 for all groups at 4 weeks and n= 10, 8 and 8 for control, 48 µg Ang II and 48 µg Ang II+Ang-(1-9), respectively at 6 weeks (n= 4 and 3 for control and 48 µg Ang II±Ang-(1-9) at 6 weeks, respectively produced by Lauren Wills). Data are presented as mean ± SEM. *p<0.05 *vs.* control (ANOVA with Dunnett's post-hoc analysis).

3.3.3.5 Gene expression analysis

qRT-PCR analysis of RAS components and markers of fibrosis and hypertrophy revealed no significant changes in the expression of Agtr1a, Agtr2, Mas1, Ace2, Col1A1, Col3A1, S100A4, ACTA2 and Nppa between control, Ang II and Ang II+Ang-(1-9) at either 4 or 6 weeks ($p>0.05$) (Figure 3-16 A-C). Ang II infusion significantly increased the expression of CTGF (RQ: 2.03 ± 0.54, $p<0.05$), Nppb (RQ: 2.80 ± 0.51, $p<0.05$) and Myh7 (RQ: 3.11 + 0.87, $p<0.05$) at 4 and 6 weeks, respectively (Figure 3-16 B-C). This was not altered by co-infusion of Ang-(1-9). In contrast, Ang-(1-9) co-infusion with Ang II for 2-4 weeks induced the gene expression of ACE (RQ: 2.47 ± 0.41, $p<0.05$), TGFβ1 (RQ: 1.83 ± 0.16, $p<0.05$) and Ctgf (RQ: 4.81 ± 1.30, $p<0.05$), respectively which remained unchanged with Ang II alone (Figure 3-16 A-B).

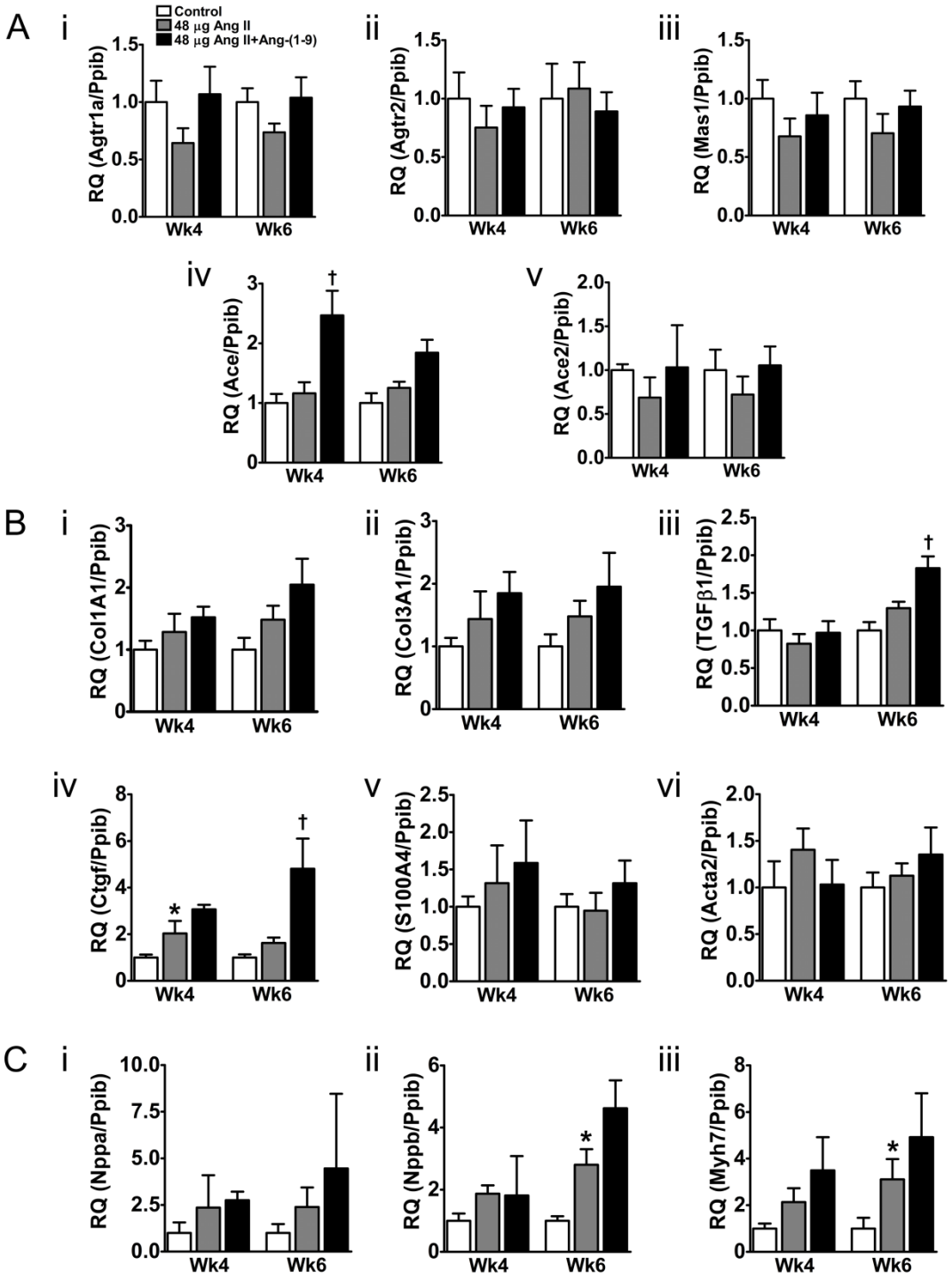

Figure 3-16. Effects of Ang-(1-9) on Ang II-induced gene expression of RAS components, fibrotic and hypertrophic markers.
Gene expression analysis was performed in the cardiac homogenates of mice infused with H_2O (control), 48 μg/kg/hr Ang II (48 μg Ang II) or 48 μg/kg/hr Ang II+48 μg/kg/hr Ang-(1-9) for 4 to 6 weeks for (A) the RAS components (i) Agtr1a, (ii) Agtr2, (iii) Mas1, (vi) Ace and (v) ACE2; (B) fibrosis makers (i) Col1A1, (ii) Col3A1, (iii) TGFβ1, (vi) Ctgf, (v) S100A4, (vi) Acta2; and (C) hypertrophy markers (i) Nppa, (ii) Nppb and (iii) Myh7. Gene expression was normalised to the housekeeper Ppib and expressed as the relative quantity (RQ) ± rqmax of the time-matched control which was set as RQ= 1. n= 6 for all groups. *p<0.05 *vs.* control. † p<0.05 *vs* 48 μg Ang II (ANOVA with Dunnett's post-hoc analysis).

3.4 Discussion

Here, a chronic model of Ang II infusion using either high or low doses of Ang II was characterised for both, its functional effects and its effects on cardiac remodelling to allow assessment of the role of Ang-(1-9) in the context of Ang II-induced cardiac remodelling. The main findings of this study are summarised in Table 3-3. The data shows that Ang II infusion leads to adverse changes in cardiac function with associated cardiac remodelling while Ang-(1-9) infusion alone has no effect on cardiac function and remodelling.

Table 3-3. Summary of pathological changes observed in Ang II and Ang-(1-9)-infused mice.

Treatment	Contractile Function	Hypertrophy	Fibrosis	
			Collagen I	Collagen III
24 µg/kg/hr Ang II	Gradual decline, dysfunction at 6 weeks	+	+	+
48 µg/kg/hr Ang II	Acute dysfunction at 2 weeks	+	+	+
Ang-(1-9)	—	—	—	—

It has previously been demonstrated that the infusion of 24 µg/kg/hr Ang II leads to the development of hypertension within 2 weeks (Flores-Munoz *et al.*, 2013). Here, it was demonstrated that a high dose of Ang II (48 µg/kg/hr) leads to the development of sustained hypertension within 1 week of infusion as previously described (Suo *et al.*, 2002, Lakó-Futó *et al.*, 2003). Interestingly, Ang II infusion leads to a significant decrease in HR in the first two weeks of infusion. This is in contrast to the positive chronotropic actions that have been described for Ang II in isolated hearts and cardiomyocytes (Masaki *et al.*, 1998, Lambert, 1995). Similar observations on a reduction in HR have previously been made with Ang II infusion (Suo *et al.*, 2002, Lakó-Futó *et al.*, 2003, Földes *et al.*, 2001). However, these effects occurred acutely only over the first 3 days of Ang II infusion before HR normalised or increased (Suo *et al.*, 2002, Lakó-Futó *et al.*, 2003, Földes *et al.*, 2001). This response has been attributed to the inhibition of sympathetic outflow and parasympathetic activation by the baroreceptors in response to the sudden increase in BP (Suo *et al.*, 2002). With a gradual loss in baroreceptor sensitivity the release of norepinephrine from cardiac nerve terminals is facilitated and HR begins to normalise (Suo *et al.*, 2002).

Echocardiography was used to assess the functional consequences of chronic Ang II infusion on the heart. Baseline echocardiographic measurements of cardiac function and morphology were in the range previously reported for C57BL/6 mice (Ram *et al.*, 2011, Rottman *et al.*, 2007). The infusion of a low dose of Ang II in mice over 6 weeks led to a gradual reduction in FS with a depression clearly visible at 4 weeks. In contrast, infusion of a high dose Ang II resulted in severe depression in FS within 2 weeks indicating distinct dose-dependent response profiles to Ang II infusion (Simon *et al.*, 1995). FS is a measure of LV systolic function and together with indices of LV dimension, LVEDD and LVESD, allows the determination of overall LV structure and function (Ram *et al.*, 2011). LVESD, a measure of systolic function where an increase indicates impaired contractile function, followed the trend observed in FS further indicating that LV systolic function is impaired in Ang II-infused mice. LVEDD, a measure of LV chamber size at diastole and an indicator of diastolic function, in contrast, remained unchanged suggesting that no chamber dilation was evident. Cardiac fibrosis and hypertrophy occur within one week of Ang II infusion at similar doses employed here (Wang *et al.*, 2014, Kim *et al.*, 1995, Sopel *et al.*, 2011) and

evidence from our lab has also shown the presence of cardiac fibrosis and hypertrophy with 24 µg/kg/hr Ang II after 2 weeks (Flores-Munoz *et al.*, 2013). Since cardiac remodelling is well established at 2 weeks of 24 µg/kg/hr Ang II but FS remains normal, this indicates that the heart is in an adaptive and compensated stage of cardiac remodelling where cardiac contractile function and output are maintained by the adaptive thickening and stiffening of the heart to withstand the increase in BP and maintain cardiac output (Legault *et al.*, 1990). After 4 weeks, FS is significantly reduced, indicating systolic dysfunction. This suggests that the heart may be in the decompensated maladaptive phase of cardiac remodelling where excessive cardiac hypertrophy and fibrosis impede normal cardiac contraction (Diwan and Dorn, 2007). In contrast, animals receiving 48 µg/kg/hr Ang II entered the decompensated phase as early as 2 weeks. This may be due to the significant extracardiac effects of high doses of Ang II resulting in additional volume overload and an exaggerated process of cardiac remodelling (Simon *et al.*, 1995). The significant decrease in cardiac contractile function with either dose of Ang II is in contrast to previous studies using similar experimental protocols: Previously, the infusion of low and high doses of Ang II for 2-6 weeks in mice and rats either led to no change or an increase in FS while LVFW thickening was clearly evident (Izumiya *et al.*, 2003, Ocaranza *et al.*, 2014, Kawano *et al.*, 2005b, Hermans *et al.*, 2014, Suo *et al.*, 2002, Matsui *et al.*, 2004, Tsukamoto *et al.*, 2013, Peng *et al.*, 2011). The discrepancies of these studies to the results presented here are unclear. It has previously been demonstrated that the genetic background of various mouse strains can significantly impact basal cardiovascular function and the cardiovascular phenotypes developed by Ang II infusion and chronic pressure overload (Peng *et al.*, 2011, Gao *et al.*, 2011, Shah *et al.*, 2010, Barnabei *et al.*, 2010, Garcia-Menendez *et al.*, 2013). This may be one factor contributing to the different observations made. However, so far no other study has characterised in detail and directly compared the acute and chronic cardiac effects of a low and high dose of Ang II and this is the first study to present the distinct temporal effects of two doses of Ang II infusion on cardiac function.

Development of cardiac hypertrophy is one of the major phenotypes that occur early during Ang II infusion (Kim *et al.*, 1995). The extend of cardiac hypertrophy was not significantly different between infusion of a low or high dose of Ang II

although dose-dependent effects of Ang II on cardiac hypertrophy have been reported at lower doses of Ang II where a BP response was absent (Kawano *et al.*, 2005b). Cardiac hypertrophy was found to be already fully developed after 4 weeks of Ang II infusion and previous studies have demonstrated a similar degree of cardiac hypertrophy after 1 week of high dose Ang II infusion (Wang *et al.*, 2014). This suggests that cardiac hypertrophy plateaus early during cardiac remodelling before the heart gradually decompensates correlating with a decrease in FS (Legault *et al.*, 1990). Sizing of cardiomyocytes revealed that cardiomyocyte hypertrophy induced by a low dose of Ang II was largely due to concentric hypertrophy associated with the thickening of cardiomyocytes and to a lesser extent eccentric hypertrophy and lengthening of cardiomyocytes. In contrast, utilising a high dose of Ang II infusion, additional lengthening of cardiomyocytes could be observed. Concentric hypertrophy is usually observed in models of chronic pressure overload, including the Ang II-infusion model (Hermans *et al.*, 2014, Heineke and Molkentin, 2006). This form of hypertrophy is typically associated with the functionally compensated phase of cardiac remodelling while progression to an eccentric phenotype is linked to decompensation and increased mortality (Domenighetti *et al.*, 2005). Interestingly, more recently, it has been demonstrated that the delivery of a high dose of Ang II for 4 weeks in mice induced a mixed cardiac phenotype with concentric or eccentric hypertrophy involving aortic valve insufficiency and chronic volume overload (Hermans *et al.*, 2014). A similar phenotype has been observed in transgenic mice with elevated cardiac Ang II (Domenighetti *et al.*, 2007). This correlates with the observation of an increase in cell length after chronic high dose Ang II infusion in mice which enter the decompensated phase within 2 weeks of infusion while at a low dose, decompensation only occurs within 4-6 weeks and eccentric remodelling may not yet be evident.

Despite the obvious development of cardiac hypertrophy in mice receiving Ang II infusion, gene expression of the hypertrophy markers ANP and BNP were unchanged with Ang II infusion. Previous studies using comparable doses of Ang II have demonstrated increases in the mRNA and protein levels of ANP and BNP after 1-4 weeks of Ang II infusion (Izumiya *et al.*, 2003, Yang *et al.*, 2013b) while no change in ANP and BNP was detected after a 6 week high dose of Ang II (Tsukamoto *et al.*, 2013) correlating with observations made here. Discrepancies

in ANP and BNP gene expression were previously demonstrated in other models of chronic pressure overload where ANP and BNP either remained unchanged or increased (Suo *et al.*, 2002, Marttila *et al.*, 1996, Yokota *et al.*, 1995). In a study of Ang II infusion in rats over 2 weeks, Suo *et al.* (2002) demonstrated that BNP mRNA is dynamically regulated and increases within 2 h of Ang II infusion, peaking within 12 h before it gradually decreases to baseline levels after 1 week while plasma BNP levels remain elevated (Suo *et al.*, 2002). Similarly, in transgenic rats overexpressing human renin, BNP mRNA levels remained unchanged despite established hypertension and cardiac hypertrophy (Marttila *et al.*, 1996). In a mouse model of Ang II infusion, ANP similarly tended to be increased after 2 days but returned to basal levels after 2 weeks (Cardin *et al.*, 2014). Additionally, increases in ANP and BNP tended to initially occur in the atria which were not assessed here (Marttila *et al.*, 1996, Luchner *et al.*, 1998). Overall, this suggests a mismatch between ANP and BNP protein and gene expression which was suggested to be due to post-translation regulation (Suo *et al.*, 2002). This may in part explain the current observation on ANP and BNP gene expression, however, ANP and BNP protein levels were not assessed here to confirm this hypothesis.

The re-expression of the foetal isoform of myosin heavy chain, βMHC, is defined as a classical marker for pathological hypertrophy. In isolated cardiomyocytes, Ang II directly induces an increase in βMHC without affecting αMHC (Shalitin *et al.*, 1996), however, here, βMHC was only found to be elevated after administration of a high dose but not a low dose of Ang II. This has previously been observed by others suggesting that βMHC is not exclusively coupled to cardiac hypertrophy (Schultz *et al.*, 2002, Matsumoto *et al.*, 2013). Recent evidence has demonstrated that βMHC expression is not uniform across the heart but rather tends to be localised in perivascular and fibrotic regions and is not always associated with cardiac hypertrophy (Pandya *et al.*, 2006, Schiaffino *et al.*, 1989, López *et al.*, 2011). Hence, it has been suggested that βMHC is instead a marker of cardiac fibrosis (Pandya *et al.*, 2006) and this correlates with the exacerbated degree of cardiac fibrosis induced by a high dose compared to a low dose of Ang II observed here.

The significant cardiac dysfunction induced by Ang II infusion after 4 and 6 weeks was associated with a significant increase in cardiac fibrosis

predominantly characterised by the increased deposition of collagen I and collagen III. Collagen I and collagen III are the main collagens in the heart with abundance of 85 and 10-15 % respectively (Weber *et al.*, 2013) and in line with this, LV collagen I content was always higher than collagen III. Basal collagen content in the adult myocardium is estimated to be between 1-4 % and basal values of collagen content reported here in control mice are in line with these observations (Brower *et al.*, 2006, Izumiya *et al.*, 2003, Peng *et al.*, 2011, Ichihara *et al.*, 2001).

Cardiac ECM content has been shown to directly impact cardiac contractile function with a strong relationship between the cardiac collagen fraction and diastolic and systolic function and overall chamber stiffness (Kitamura *et al.*, 2001, Doering *et al.*, 1988, Jalil *et al.*, 1989, Brower *et al.*, 2006, Weber *et al.*, 1988, Badenhorst *et al.*, 2003). This link persisted irrespective of cardiac hypertrophy, strengthening the notion of a direct influence of the ECM on cardiac contractile properties (Brower *et al.*, 2006). Here, after chronic Ang II infusion for 4-6 weeks, both, collagen I and collagen III fractions were significantly increased while collagen I content was higher than collagen III. An increase in ECM deposition, especially collagen I, is part of the initial adaptive response to hypertension to account for changes in ventricular filling and maintain cardiac contractile function (reactive fibrosis) (Brower *et al.*, 2006, Weber *et al.*, 1989) and interference with collagen deposition during pressure overload reduces cardiac function (Baicu *et al.*, 2003). Collagen I forms thick collagen fibres and provides rigidity to tissues such as ligaments, tendons and scars (Burgess *et al.*, 1996). It has a high elastic recoil and therefore a greater ability to resist stretch which is advantageous in situations with increased afterload such as hypertension (Collier *et al.*, 2012). Previous evidence from our lab has shown that collagen I deposition in hearts of Ang II-infused mice precedes collagen III at 2 weeks (Flores-Munoz *et al.*, 2013) correlating with the compensated phase and maintenance of cardiac contractile function. However the excessive deposition of collagen I has been associated with myocardial stiffness (Jalil *et al.*, 1989, Doering *et al.*, 1988, Díez *et al.*, 2002) eventually resulting in impaired diastolic and systolic function that developed over longer Ang II perfusion times. Collagen III forms thin fibres and provides compliance to tissues such as the skin. It is less stiff and has a lower elastic recoil and is

increased in situations of increased strain which occur in the decompensated phase of hypertensive cardiac remodelling (Collier *et al.*, 2012, Vanderheyden *et al.*, 2004). Due to its high compliance, the excessive deposition of collagen III predisposes the heart to chamber dilation and worsens outlook (Kitamura *et al.*, 2001). The ratio of type I collagen to type III collagen (or *vice versa*) is thought to be an important determinant of the stiffness/ elasticity of the heart and has been reported to be increased in experimental hypertension and dilated cardiomyopathy correlating with a decrease in cardiac function (Burgess *et al.*, 1996, Mukherjee and Sen, 1993, Marijianowski *et al.*, 1995). Here, the collagen I/ collagen III ratio was unchanged following a low dose of Ang II infusion, but the collagen I/collagen III ratio tended to be decreased by 48 μg/kg/hr Ang II after 6 weeks. This was likely due to a decrease in collagen I rather than an increase in collagen III. The relative increase in collagen III may therefore contribute to cardiac dysfunction in the decompensated phase and together with the eccentric remodelling of cardiomyocytes participate in the progression from a concentric to an eccentric phenotype.

While collagen I and collagen III deposition was clearly visible on histological assessment, gene expression analysis of collagen I and collagen III revealed an up-regulation only at 6 weeks in the 48 μg/kg/hr Ang II group. This mismatch in protein and gene expression may be explained by the dynamic nature of collagen synthesis in the heart. Cardiac collagen deposition occurs early during Ang II infusion and this is correlated with an increase in collagen I and collagen III mRNA (Kim *et al.*, 1995, Sopel *et al.*, 2011, Izumiya *et al.*, 2003). However, as fibrosis becomes established and reaches a plateau, a new steady state may be reached where *de novo* collagen synthesis decreases and ECM content is maintained by the actions of MMPs and TIMPs (López *et al.*, 2006). The continued elevation in collagen I and collagen III mRNA with 48 μg/kg/hr Ang II is also seen in other studies using chronic high dose Ang II infusion (Matsui *et al.*, 2004, Tsukamoto *et al.*, 2013) and suggests that *de novo* collagen synthesis is still ongoing and this may be the result of excessive cardiomyocyte necrosis occurring in the decompensated phase of cardiac remodelling. CTGF has been postulated as a downstream mediator of the pro-fibrotic actions of $TGF\beta_1$ and more recently also Ang II (Iwanciw *et al.*, 2003, Finckenberg *et al.*, 2003, Che *et al.*, 2008). Here $TGF\beta_1$ remained unchanged with either dose of AngII and this

correlates with reports that TGFß$_1$ and CTGF mRNA increase within 24 h of Ang II infusion (Kim *et al.*, 1995, Sopel *et al.*, 2011) but decrease thereafter and no changes can be detected after 2-6 weeks following Ang II infusion (Sopel *et al.*, 2011, Tsukamoto *et al.*, 2013, Cardin *et al.*, 2014). CTGF was found to be increased with 48 µg/kg/hr Ang II after 4 weeks correlating with the persistent increase in collagen I and collagen III which is in line with the role of CTGF in Ang II-mediated collagen deposition. S100A4 and αSMA are commonly used markers of fibroblasts and myofibroblasts, respectively and an increase in their expression may suggest an increase in the fibroblast population as a result of fibrotic signalling (Swaney *et al.*, 2005, Zeisberg *et al.*, 2007b, Strutz *et al.*, 1995). Here, S100A4 was unchanged by treatment with either dose of Ang II over 4-6 weeks. While this may suggest the absence of an S100A4-positive fibroblast population in the heart, it however also coincides with the relative decrease in the fibroblast number reported in Ang II-infused rats at such time points (Campbell *et al.*, 1995). However, this was not investigated further in this study. αSMA mRNA was found to be increased after 6 weeks infusion of Ang II at a high dose. This may suggest an increase in the myofibroblast population in the heart either through the activation of resident fibroblasts or EndMT which has been shown to occur in the hearts of Ang II-infused mice (Section 5). Additionally, it has been shown that the *Acta2* gene can be re-activated as part of the foetal gene programme strongly correlating with the development of cardiac hypertrophy (Black *et al.*, 1991) and it cannot be excluded that the increase in Acta2 mRNA is of cardiomyocyte origin. This would be of interest for further investigations.

Expression of RAS components has been shown to be dynamically regulated in the development of cardiac hypertrophy and the transition to HF: The AT_1R was shown to be upregulated during the development of cardiac hypertrophy in the SHR and 2K1C hypertension with increased Ang II levels (Suzuki *et al.*, 1993). Similarly, AT_1R expression tended to be increased in a model of pressure overload while no change was detected following chronic volume overload (Wolf *et al.*, 1996, Iwai *et al.*, 1995). In patients with HF, ventricular AT_1R levels were significantly lower compared to non-failing hearts suggesting the dynamic expression of AT_1R with disease progression (Haywood *et al.*, 1997). Here, Agtr1a expression following chronic Ang II infusion was similar to control animals and

differs from observations made in other models of chronic cardiac hypertrophy described above. This is most likely due to regulation of AT_1R by Ang II as it has previously been demonstrated that in a mouse model of low dose Ang II infusion AT_1R mRNA transiently increased after 3 days before it decreased to baseline within 7 days possibly due to a negative feedback loop (Ichihara *et al.*, 2001).

The tissue expression of Agtr2 is very low in the adult heart but increases in pathophysiological conditions as part of the foetal gene program (Dinh *et al.*, 2001). As such, a significant upregulation of Agtr2 mRNA has been demonstrated post-MI and in 2K1C rats (Nio *et al.*, 1995, Suzuki *et al.*, 1993). Here, Agtr2 expression was unchanged by chronic Ang II infusion. Although this contrasts with the reports that the AT_2R increases during cardiac pathology, Agtr2 expression has previously been demonstrated to remain unchanged in pressure overloaded rats and in patients with HF despite significant expression of ßMHC and ANP, indicating foetal gene expression (Wolf *et al.*, 1996, Haywood *et al.*, 1997). Furthermore, Ang II has been demonstrated to downregulate Agtr2 expression (Ouali *et al.*, 1997). Decreased Agtr2 is observed in cardiomyocytes from patients with HF while cardiac fibroblasts from patients with interstitial fibrosis selectively re-express the AT_2R (Tsutsumi *et al.*, 1998, Matsumoto *et al.*, 2000). Thus, it cannot be excluded that any cell-specific changes in Agtr2 expression were diluted in the gene expression analysis of total ventricular tissue.

ACE and ACE2 are found up-regulated in human heart disease and experimental models of HF (Iwai *et al.*, 1995, Weinberg *et al.*, 1997, Studer *et al.*, 1994, Serneri *et al.*, 2001, Goulter *et al.*, 2004) and ACE expression has been demonstrated to correlate with the extent of cardiac hypertrophy (Weinberg *et al.*, 1997, Iwai *et al.*, 1995). Here, neither dose of Ang II induced significant changes in ACE and ACE2 expression. This discrepancy may result from a differential regulation of the RAS in the Ang II infusion model compared to models of chronic pressure and volume overload (Brilla *et al.*, 1990, Ruzicka *et al.*, 1995). In the rat Ang II-infusion model, it was demonstrated that Ang II increases cardiac ACE activity, however, ACE mRNA levels were not measured (Ocaranza *et al.*, 2014).

Here, two protocols were employed to assess the cardiac effects of Ang-(1-9) in the healthy and diseased heart. The main findings are 1) chronic Ang-(1-9)

infusion into healthy normotensive mice has no effect on cardiac contractile function, fibrosis or hypertrophy; 2) the co-infusion of Ang-(1-9) after the induction of cardiac contractile dysfunction with a high dose of Ang II for 2 weeks (reversal study) transiently reversed systolic dysfunction after 4 weeks independent of any anti-hypertensive, anti-hypertrophic and anti-fibrotic effects. These results highlight the complexity of Ang-(1-9) signalling in the heart.

So far only one other study has presented data on the cardiac effects of Ang-(1-9) infusion in the healthy heart (Zheng *et al.*, 2015). In this study, rats were infused with Ang-(1-9) for 4 weeks and no significant changes were detected in measures of cardiac contractile function and remodelling (Zheng *et al.*, 2015). This correlates with data presented here where it was demonstrated that Ang-(1-9) does not significantly modulate cardiac systolic and diastolic function or cardiac remodelling. However, when Ang-(1-9) was co-infused with Ang II into mice with established Ang II-induced cardiac dysfunction, Ang-(1-9) transiently improved cardiac systolic function after 4 weeks before it declined to levels similar to Ang II infusion at 6 weeks. This may suggest that Ang-(1-9) has a direct effect on cardiac contraction (investigated in Section 4). The functional recovery was independent of any anti-hypertensive or anti-fibrotic actions by Ang-(1-9) and in fact Ang-(1-9) may exacerbate Ang II-induced cardiac hypertrophy at this stage. Cardiomyocytes possess an intrinsic hypertrophic reserve which was demonstrated to differ between males and females (Tamura *et al.*, 1999, Brower *et al.*, 2006). Whether Ang-(1-9) may trigger an additionally hypertrophic reserve or whether the exacerbation of Ang II-induced hypertrophy by Ang-(1-9) is secondary to effects on contraction induced by Ang-(1-9) is unknown. At 6 weeks, cardiac function declined to levels seen in Ang II-infused mice and the hearts began to transition from a concentric to an eccentric phenotype as evidenced by the increase in cell length. This remodelling process corresponded with the significant increase in the gene expression of collagen I, TGFß$_1$, CTGF, BNP and ßMHC. It can be hypothesised that the rapid decompensation after functional recovery is partially due to the uncontrolled hypertension and cardiac remodelling which results in an already structurally remodelled and stiffer heart having to work against an increased afterload which over long term becomes unsustainable and the heart begins to fail. Using a similar study design, Ocaranza

et al. (2014) recently demonstrated that Ang-(1-9) reverses established Ang II-induced cardiac pathology in rats by decreasing BP and reversing established cardiac remodelling (Ocaranza *et al.*, 2014). This is in contrast to the results presented here where Ang-(1-9) normalised cardiac function independent of an effect on BP and cardiac remodelling. The anti-hypertensive effects of Ang-(1-9) observed in the published report may in part contribute to the regression of cardiac remodelling (Ocaranza *et al.*, 2014). However, the dose of Ang II was half that employed here with a 1.5:1 ratio of Ang-(1-9) to Ang II compared to the 1:1 ratio employed here. Since it has been identified that there are dose-dependent differences in the cardiac phenotype of Ang II-infused mice, it cannot be excluded that dosage-specific differences as well as species-specific differences contribute to the contrasting results.

Here, Ang-(1-9) did not alter Ang II-induced hypertension and this supports previous findings in the SHRSP (Flores-Munoz *et al.*, 2012) and Ang II-infused mice (Flores-Munoz *et al.*, 2013). Conversely, the data presented here do not suggest any effect on cardiac fibrosis and hypertrophy presented in other studies. Flores-Munoz *et al.* (2012) demonstrated that Ang-(1-9) prevents the development of cardiac fibrosis in the SHRSP (Flores-Munoz *et al.*, 2012) and inhibits cardiomyocyte hypertrophy *in vitro* (Flores-Muñoz *et al.*, 2011). Similar observations were made in a rat model of streptozotocin-induced diabetes where Ang-(1-9) reversed cardiac remodelling and improved cardiac contractile function (Zheng *et al.*, 2015). Additionally, in a rat model of MI, Ang-(1-9) prevented chamber dilatation and wall thinning and was highly correlated to the regression of LV hypertrophy (Ocaranza *et al.*, 2010). However, these studies investigated the effects of Ang-(1-9) acutely at 2 weeks or in models that lack chronic hypertension. Hence, it cannot be excluded that Ang-(1-9) may acutely alter cardiac hypertrophy and fibrosis during acute hypertension which disappear when BP is chronically increased.

To-date, no other studies have directly associated Ang-(1-9) with improved cardiac function in the absence of an anti-remodelling effect. *In vitro* and *in vivo* evidence suggests that Ang-(1-9) signals *via* the AT_2R to mediate its beneficial effects in the heart and activation of the AT_2R has been linked to improved cardiac contractile function (Flores-Muñoz *et al.*, 2011, Flores-Munoz *et al.*, 2012, Lauer *et al.*, 2014). Although Ang-(1-9) has so far not been

implicated in the modulation of cardiac contractility prior evidence has shown that Ang-(1-7) can improve cardiac function in animal models of HF by direct actions on cardiomyocyte calcium handling (Zhou *et al.*, 2015, de Almeida *et al.*, 2015). Similarly, ACE2 has been implicated in the modulation of cardiac contractility and ACE2 deficient mice suffer from serve cardiac contractile dysfunction in the absence of cardiac remodelling (Crackower *et al.*, 2002). Overall this suggests a role for the counter-regulatory RAS in the direct modulation of cardiac contractile function. Although Ang-(1-9) has been demonstrated to mediate biological effects independent of its conversion to Ang-(1-7), given their overlapping biological actions, effects on cardiac contractility may be mediated by similar mechanisms.

3.5 Summary

In summary, these data demonstrate that the chronic Ang II infusion model is a valid model of Ang II induced cardiac remodelling which presented with measurable changes in LV contractile function, hypertrophy and fibrosis comparable to previously reported studies. Additionally, these data confirm the previously reported temporal and pathophysiological differences in disease development reported with the infusion of low and high doses of Ang II.

Furthermore, the results demonstrate the complex nature of the cardiovascular effects of Ang-(1-9) and it can be hypothesised that the state of the heart, time of administration, disease model and stimulus largely determine the cardiac response to Ang-(1-9). While systemic delivery of Ang-(1-9) alone had no significant effect on cardiac function and remodelling in the healthy heart, it was demonstrated that the administration of Ang-(1-9) to animals with established Ang II-induced cardiac pathology transiently improved cardiac contractile function independently of an effect on BP or cardiac remodelling. These data suggest that Ang-(1-9) may have beneficial effects in improving cardiac contractile function in the diseased heart with adequate BP control.

Chapter 4 – Assessment of the direct cardiac effects of Ang-(1-9) in the isolated rat heart

4.1 Introduction

4.1.1 Cardiomyocyte excitation-contraction-coupling

Cardiomyocytes are the contractile cells of the heart and perform two major functions: initiation and conduction of an electrical impulse and contraction. Cardiac EC coupling is the process by which the electrical stimulation of the cardiac muscle by an action potential is converted into contraction of the myofibrils of the cardiac muscle resulting in the expulsion of blood into the circulation. As a direct activator of myofilament crosslinking and contraction, the second messenger Ca^{2+} is the essential mediator of cardiac EC coupling and alterations in Ca^{2+} handling forms the basis of many CVDs with cardiac contractile dysfunction (Bers, 2002).

Cardiac EC coupling is initiated by the cardiac action potential which is distinct from fast action potentials observed in neurons and is characterised by a plateau phase mediated by influx of Ca^{2+} through the L-type Ca^{2+} channels (Figure 4-1 A). The resting membrane potential in atrial and ventricular cardiomyocytes is governed by a small potassium current I_{k1} (the inward rectifier) and lies at approximately -90 mV. The arrival of an action potential from nearby cells or the sinoatrial node which increases membrane potential above the -70 mV threshold triggers the opening of voltage gated, fast sodium channels (I_{Na}) that rapidly inactivate giving rise to a sharp increase in membrane potential to just above 0 mV. Opening of transient outward rectifier potassium channels (I_{to}) partially repolarise the membrane. This is followed by a plateau phase mediated by influx of Ca^{2+} through the L-type Ca^{2+} channels. This plateau phase is unique to cardiomyocytes and is an important determinant of cardiac contraction by directly influencing the strength of contraction and preventing early re-activation of cardiomyocytes by another action potential. The slow de-activation of the L-type Ca^{2+} current leads to the opening of a delayed rectifier potassium current (I_{Ks}, I_{Kr}, I_{K1}) which repolarises the membrane This plateau phase prevents early re-activation of cardiomyocytes by another action potential and allows for adequate cardiac contraction and relaxation. (Camm and Bunce, 2009)

A schematic of cardiac EC-coupling is shown in Figure 4-1 B. During systole, the cardiac action potential leads to the opening of T-tubular L-type Ca^{2+} channels

and influx of Ca^{2+} into the sarcoplasm. The increase in $[Ca^{2+}]_i$ which can rise up to 50 µM locally leads to the opening of the sarcoplasmic reticulum Ca^{2+} release channel, the ryanodine receptor (RyR), to mediate Ca^{2+} induced Ca^{2+} release (CICR) (Bers, 2002). The global increase in Ca^{2+} allows the binding of Ca^{2+} to the regulatory myofilament protein troponin C allowing crossbridge formation between actin and myosin resulting in contraction. Cardiac contractile force is a function of $[Ca^{2+}]_i$ and a rise of $[Ca^{2+}]_i$ from 150 nM to approximately 600 nM is required for half-maximal activation of contractile force (Bers, 2000).

For relaxation to occur, $[Ca^{2+}]_i$ must decrease to basal levels to allow dissociation of Ca^{2+} from the contractile apparatus (Figure 4-1 B right). Extrusion of Ca^{2+} from the cytosol occurs *via* four different mechanisms: SERCA, the sarcolemmal sodium-calcium exchanger (NCX), the sarcolemmal Ca^{2+}-ATPase and the mitochondrial Ca^{2+} uniporter. The contribution of each system to the removal of cytosolic Ca^{2+} varies between species. Thus, for example, in rabbit, 70 % of Ca^{2+} is extruded by SERCA, 28 % *via* NCX and 1 % by other mechanisms such as the Ca^{2+} ATPase in the sarcolemma and the mitochondrial Ca^{2+} uniporter. In contrast, in rats, SERCA accounts for 92 % of Ca^{2+} removal while NCX contributes 7 % and other systems 1 % (Bers, 2000). Ca^{2+} handling in mice is similar to rat whereas in humans Ca^{2+} fluxes are more similar to the rabbit (Bers, 2002).

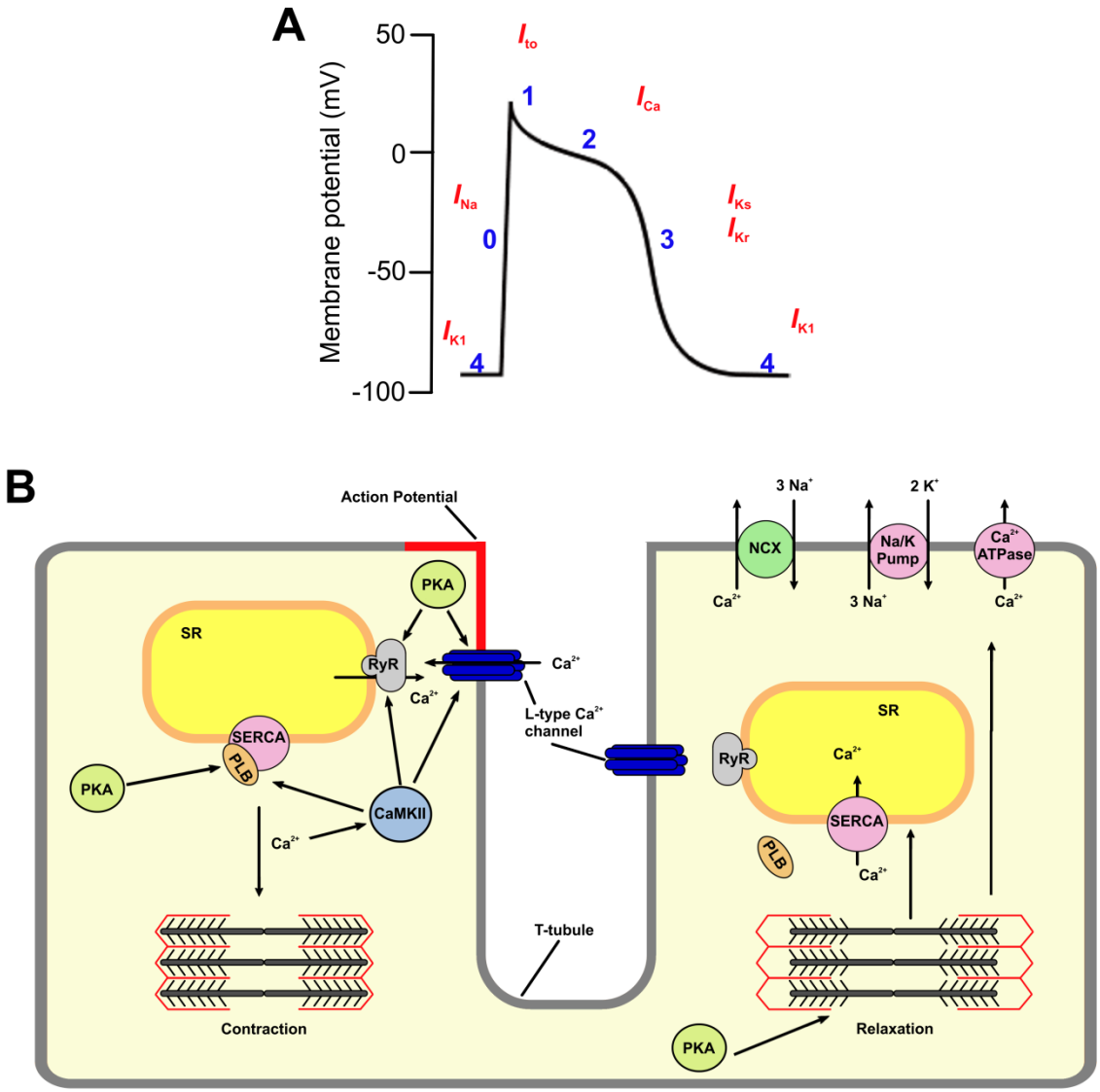

Figure 4-1. The cardiac action potential and excitation-contraction coupling.
(A) The cardiac action potential with the associated currents. I_{K1}= inward rectifier K^+ current, I_{to}= transient outward K^+ current, I_{Na}= rapid Na^+ current, I_{Ca}= L-type Ca^{2+} current, I_{Ks}= slow delayed rectifier K^+ current, I_{Kr}= rapid delayed rectifier K^+ current. (B) Schematic of EC coupling in cardiomyocytes. The arrival of an action potential triggers the opening of the L-type Ca^{2+} channel. The increase in intracellular Ca^{2+} results in the opening of the RyR and Ca^{2+}-induced Ca^{2+} release. The free Ca^{2+} interacts with troponin C and allows cardiomyocyte contraction to occur. For relaxation to occur during diastole, the intracellular Ca^{2+} concentration is decreased by the actions of SERCA, NCX and the sarcolemmal Ca^{2+} ATPase. Cardiac excitation-contraction coupling is regulated by the two kinases PKA and CaMKII both of which can phosphorylate the L-type Ca^{2+} channel and increase Ca^{2+} flux, the RyR to increase opening probability and phosphlamban to disinhibit SERCA. Additionally, PKA phosphorylates troponin C and thereby increases Ca^{2+} dissociaton for relaxation to occur. CaMKII= Calcium Calmodulin Kinase II, NCX= Sodium-calcium exchanger, PKA= Protein Kinase A, PLB= Phospholamban, RyR= Ryanodine receptor, SR= Sarcoplasmic reticulum, SERCA= sarcoplasmic reticulum Ca^{2+} ATPase.

4.1.2 RAS and EC coupling

Activation of the RAS has also been linked to the modulation of EC coupling affecting various components of the Ca^{2+} handling mechanisms in the cell. *In vivo* modulation of EC coupling by Ang II has been assessed in detail in the TG1306/1R transgenic mice which express several copies of the rat angiotensinogen gene under the αMHC promoter resulting in increased cardiac Ang II levels without systemic increases in BP (Domenighetti *et al.*, 2005, Gusev *et al.*, 2009). These mice progressively develop cardiac dysfunction and cardiac remodelling with concentric and dilated hypertrophy associated with dysregulation of Ca^{2+} handling proteins (Domenighetti *et al.*, 2005, Gusev *et al.*, 2009). In the initial adaptive phase, an increase in NCX and I_{NCX} was observed which is thought to be a compensatory mechanism to cellular hypertrophy, a reduction in Ca^{2+} transient amplitude and SERCA2 expression. Progression to decompensated cardiac remodelling resulted in a decrease in NCX current which was suggested to protect the reduced sarcoplasmic reticulum (SR) $[Ca^{2+}]$ and hypersensitivity of CICR resulting in cardiac contractile dysfunction (Domenighetti *et al.*, 2005, Gusev *et al.*, 2009). Similarly, in mice overexpressing the AT1R, expression of SERCA2 and NCX were significantly reduced resulting in an increase in the Ca^{2+} decay rate, prolonging relaxation (Rivard *et al.*, 2011).

Increased cardiac Ang II levels result in QT prolongation due to the lengthening of action potential duration and thereby increased susceptibly for fatal arrhythmias (Domenighetti *et al.*, 2007). This was demonstrated to be a result of a decrease in the expression of Kir2.1 and Kir2.2 which encode subunits for the I_{k1}-related potassium channel. Similarly, in mice with cardiomyocyte specific overexpression of the AT_1R which develop cardiac dysfunction at an early age independent of cardiac hypertrophy, action potential duration was nearly doubled at a young age compared to wild type littermates (Rivard *et al.*, 2008). This was due to a significant decrease in the total potassium current of the action potential and includes a decrease in I_{to}, I_{kur} and I_{k1} whose channels were significantly downregulated. Furthermore, cell shortening was significantly reduced as a result of a decrease in the L-type Ca^{2+} channel current and Ca^{2+} transient amplitude (Rivard *et al.*, 2011).

In vitro positive inotropic actions of Ang II have been associated with an increase in L-type Ca^{2+} channel current which is thought to be due to PKC-dependent modulation of the channel gating properties (Aiello and Cingolani, 2001, Salas *et al.*, 2001, Liang *et al.*, 2010). However, in rat and mouse cardiomyocytes it has also been demonstrated that Ang II modulates the L-type Ca^{2+} channel as well as I_{Na} in a Nox2 and PKA-sensitive manner (Wagner *et al.*, 2014). In chick ventricular cardiomyocytes, Ang II increased nuclear and cytosolic Ca^{2+} wave frequency and this was due to activation of the AT_1R and AT_2R (Bkaily *et al.*, 2005). In rabbit cardiomyocytes, Ang II signalling led to a biphasic change in the Ca^{2+}-dependent Cl^- current which was decreased acutely but increased following prolonged incubation coinciding with an increase in action potential duration (Morita *et al.*, 1995). An increase in action potential duration has also been associated with Ang II-mediated inhibition of I_{to}. Interestingly, in rat myocytes, I_{to} inhibition was due to an AT_2R mediated activation of PP2A (Caballero *et al.*, 2004). In contrast, in endocardial canine cardiomyocytes, AngII modulated I_{to} in an AT_1R-dependent manner to reduce density and slow recovery from inactivation thereby prolonging action potential duration. Treatment of epicardial cardiomyocytes which have high I_{to} density, with losartan transformed I_{to} characteristics and action potential wave form to those of endocardial cells, suggesting differential modulation of the RAS in cardiomyocytes across different regions of the heart (Yu *et al.*, 2000). In contrast, in guinea pig atrial cardiomyocytes, Ang II-AT_1R signalling increased I_{Ks} *via* PKC thereby shortening action potential duration (Zankov *et al.*, 2006).

Overall, these studies highlight the complex role of the classical RAS in the regulation of various components of the cardiac contractile machinery and how the RAS can influence cardiac contractile function acutely and chronically to mediate cardiac contractile dysfunction. However, few studies so far have investigated the counter-regulatory RAS in the modulation of EC coupling and cardiac contractility (De Mello, 2004, Zhou *et al.*, 2015, de Almeida *et al.*, 2015). In a model of ischaemia-reperfusion injury in rat hearts it was demonstrated that administration of Ang-(1-7) to RV muscle sections following ischaemia hyperpolarises the muscle thereby restoring impulse conduction (De Mello, 2004). This was found to be due to stimulation of the Na^+/K^+ ATPase by Ang-(1-7) (De Mello, 2004). More recently, it was reported that Ang-(1-7)

increased L-type Ca^{2+} currents in isolated cardiomyocytes from rats with HF but not control rats *via* a mechanism involving the NO/bradykinin pathway (Zhou *et al.*, 2015). Additionally, Ang-(1-7) increased Ca^{2+} transient amplitude by preventing the downregulation of SERCA and PLB dephosphorylation in cardiomyocytes from DOCA-salt loaded rats (de Almeida *et al.*, 2015). The stimulation of Ca^{2+} fluxes by Ang-(1-7) may be due to the activation of PKA that has been demonstrated by the intracellular application of Ang-(1-7) in isolated rat cardiomyocytes (De Mello, 2015). This demonstrates that the counter-regulatory RAS may beneficially modulate cardiomyocyte EC coupling in CVD, however, so far, no studies have investigated whether Ang-(1-9) can modulate EC coupling and cardiac contractility.

4.1.3 The RAS in the isolated Langendorff heart

Studies in the isolated Langendorff-perfused heart have contributed significantly to the understanding of the cardiac actions of Ang II and the cardiac RAS as a whole. Using a modulation of the Langendorff-perfused rat heart de Lannoy *et al.* (1997) and Müller *et al.* (1998) demonstrated the presence of Ang I and Ang II in the coronary effluent of renin-perfused rat hearts confirming the production of Ang I and Ang II from local angiotensinogen and strengthening the notion of a tissue RAS (de Lannoy *et al.*, 1997, Müller *et al.*, 1998). While renin has been shown to be present in cardiac tissue it was largely unclear whether this was due to expression of renin in the heart. In the absence of perfusion with renin however, little angiotensinogen was converted to Ang I (de Lannoy *et al.*, 1997) confirming that cardiac renin is largely derived from exogenous diffusion of plasma renin into the tissue, while ACE is present locally to mediate the formation of Ang II (Müller *et al.*, 1998, de Lannoy *et al.*, 2001). Perfusion of Ang II in isolated heart preparations mediates dose- and time-dependent chronotropic and inotropic effects within minutes of perfusion which is largely dependent on activation of the AT_1R (Aplin *et al.*, 2007, van Esch *et al.*, 2010, Masaki *et al.*, 1998). However, using [^{3}H] phenylalanine, it was shown that within 60 min of perfusion, Ang II can also mediate a 3.9-fold increase in protein synthesis independent of induction of the proto-oncogenes *c-fos* and *c-jun* and demonstrating the direct actions of Ang II on cardiomyocyte growth independent of systemic changes in cardiac loading (Schunkert *et al.*, 1995).

Perfusion of Ang II in the mouse and rat heart results in coronary vasoconstriction, decreasing coronary flow and increasing perfusion pressure that are manifested in a reduction in cardiac contractile performance (van Esch *et al.*, 2010). Using mice with genetic deletions of the $AT_{1a}R$, $AT_{1b}R$ and AT_2R, van Esch *et al.* (2010) demonstrated that this effect is solely due to the activation of $AT_{1a}R$ in the coronary vasculature (van Esch *et al.*, 2010). Perfusion of hearts with losartan in the absence of Ang II increases coronary flow and improves cardiac contractile function suggesting a tonic constrictor response *via* the AT_1R in coronary vessels (Paz *et al.*, 1998). In contrast, Ang-(1-7) was demonstrated to mediate coronary vasodilation and potentiate bradykinin-mediated vasorelaxation (Almeida *et al.*, 2000) while vessel resistance was increased in mice with genetic deletion of the Mas receptor (Santos *et al.*, 2006).

Using the Langendorff model of global ischaemia-reperfusion, the AT_1R was demonstrated to be acutely upregulated in the rat LV after 40 min ischaemia and 30 min reperfusion correlating with the development of post-ischaemic cardiac dysfunction that could be abolished by losartan (Yang *et al.*, 1997). More widely investigated however is the effect of reducing Ang II in ischaemia reperfusion injury using ARBs and ACE-Is. Perfusion of an ACE-I, ARB or renin inhibitor prior to ischaemia reduced the incidence of reperfusion arrhythmias and improved post-ischaemic recovery of cardiac contractile function (Fleetwood *et al.*, 1991, Chen *et al.*, 2001, Paz *et al.*, 1998) suggesting that local production of Ang II by renin and ACE participates in the development of potentially fatal reperfusion arrhythmias and impaired recovery of post-ischaemic cardiac contractile function. In this regard, administration of the Ang-(1-7) during reperfusion period mediated an anti-arrhythmic effect compared to the pro-arrhythmic actions of Ang II (Ferreira *et al.*, 2001). Furthermore, perfusion of Ang-(1-7) preserved systolic and diastolic tension and the rate of contractility and relaxation post-ischaemia and this was absent in mice lacking Mas or mice treated with A779 or indomethacin suggesting a role for prostaglandins (Castro *et al.*, 2006, Ferreira *et al.*, 2002). However, the underlying mechanism remains elusive and whether Ang-(1-9) mediates similar effects in ischaemia-reperfusion injury has so far not been investigated.

4.2 Aims

4) Establish the effects of Ang-(1-9) and Ang II on cardiac contractile function in the isolated Langendorff-perfused rat heart

5) Determine the role of angiotensin receptors in the cardiac response to Ang-(1-9) perfusion

6) Investigate downstream signalling pathways activated by Ang-(1-9).

4.3 Results

4.3.1 Spontaneously beating hearts

4.3.1.1 Ang II perfusion

Ang II has previously been shown to modulate cardiac contractility in the isolated Langendorff perfused mouse and rat heart. Additionally, it has been demonstrated that chronic Ang II infusion in mice *in vivo* results in cardiac contractile dysfunction (Section 3). Therefore, to determine the effects of Ang II on cardiac contractility in the present model of rat Langendorff perfusion, rat hearts were perfused with increasing doses of Ang II as outlined in protocol 2 (Figure 2-9 A) and LV contractile parameters measured (Figure 4-2). Addition of an equal volume of Tyrodes to the perfusion solution served as control in time-matched perfused hearts.

An example trace of Ang II perfusion in the isolated rat heart is shown (Figure 4-2 A). Baseline parameters of Ang II-infused hearts were not significantly different from control-perfused hearts (Table 4-1). HR significantly increased within 2 min of perfusion with 1 μM Ang II and peaked after 6 min with 106.70 ± 2.14 % ($p<0.05$) (Figure 4-2 B). Increasing concentration to 3 μM had no further effect on HR (Figure 4-2 B). Perfusion of rat hearts with Ang II at either 1 or 3 μM did not alter LVDP (Figure 4-2 C). Similarly, 1 μM Ang II did not affect the maximal rate of pressure change dP/dt_{max} (Figure 4-2 D). However, increasing Ang II concentration to 3 μM significantly increased dP/dt_{max} after 6 min of perfusion (control 97.18 ± 1.51 % *vs.* Ang II 103.35 ± 1.68 %, n= 7, $p<0.05$) and remained elevated over the length of the perfusion protocol (Figure 4-2 D).

Perfusion with 1 μM Ang II caused a significant peak in dP/dt_{min} at 4 min of perfusion (control 98.40 ± 1.02 % *vs.* Ang II 102.00 ± 1.12 %, n= 7, $p<0.05$) before decreasing to control levels (Figure 4-2 E). Similar to dP/dt_{max}, 3 μM Ang II significantly elevated dP/dt_{min} after 8 min of perfusion (control 90.00 ± 2.88 % *vs.* Ang II 99.34 ± 1.83 %, n= 7, $p<0.05$) which remained elevated for the remainder of the protocol (Figure 4-2 E). Tau was significantly decreased 6 min after the addition of 1 μM Ang II (control 101.23 ± 2.41 % *vs.* Ang II 93.67 ± 1.88 %, n= 7, $p<0.05$) (Figure 4-2 F). This effect was maintained after increasing Ang II concentration to 3 μM with a maximum decrease to 89.68 ± 2.48 % at 18 min. (Figure 4-2 F).

Table 4-1. Baseline steady state parameters in spontaneously beating Langendorff-perfused rat hearts.

	n	LVDP (mmHg)	d*P*/dt_{max} (mmHg/s)	d*P*/dt_{min} (mmHg/s)	Tau (ms)	Heart rate (bpm)
Control	7	124.98 ± 10.48	3429.10 ± 250.61	-2352.30 ± 168.59	30.69 ± 2.24	251.20 ± 12.89
Ang-(1-9)	6	117.28 ± 7.77	3249.20 ± 206.42	-2291.96 ± 138.31	28.46 ± 0.78	260.44 ± 11.47
PD123319 + Ang-(1-9)	7	131.30 ± 4.89	3702.14 ± 98.50	-2529.21 ± 93.33	29.34 ±1.39	261.50 ± 5.28
Ang II	7	129.71 ± 6.09	3537.58 ± 147.59	-2721.90 ± 137.14	26.87 ± 1.56	278.58 ± 11.82
Ang II + Ang-(1-9) (co-infusion)	6	137.01 ± 3.70	3883.66 ± 95.70	-2689.07 ± 136.85	29.06 ± 1.14	273.08 ± 9.94
Ang II + Ang-(1-9) (pre-infusion)	3	137.64 ± 3.05	3907.35 ± 207.42	-2673.51 ± 88.09	27.29 ± 2.13	278.62 ± 10.58
Ang-(1-7)	7	130.73 ± 4.36	3718.07 ± 123.39	-2612.91 ± 112.34	29.17 ± 2.39	277.41 ± 12.19

LVDP= Left ventricular developed pressure; d*P*/d$t_{max/min}$= rat of left ventruclar pressure rise and fall; Tau= exponential decay of left ventricular pressure fall

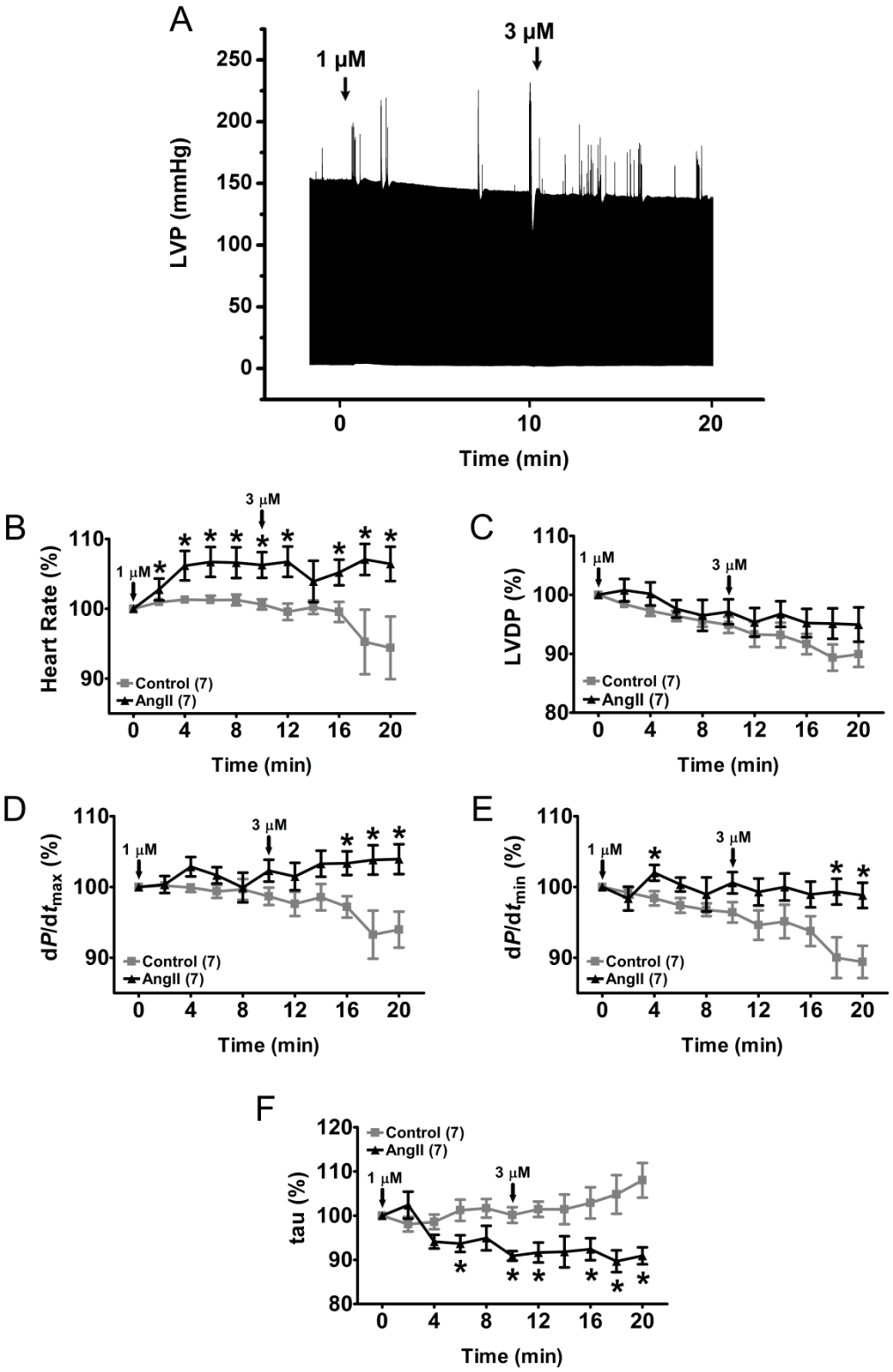

Figure 4-2. Ang II perfusion in spontaneously beating hearts.
Rat hearts were perfused according to the Langendorff method. After reaching maximal pressure, the heart was allowed to reach a steady state for 10 min prior to the perfusion with 1 µM Ang II for 10 min. The concentration was then increased to 3 µM Ang II for a further 10 min. Time-matched perfused hearts served as control. (A) Example left ventricular pressure (LVP) trace of Ang II perfusion in the isolated rat heart. (B) Heart rate, (C) left ventricular developed pressure (LVDP), (D) dP/dt_{max}, (E) dP/dt_{min} and (F) tau were measured using a fluid filled balloon connected to a pressure transducer and changes were expressed as percent-change compared to steady state. Data are presented as mean ± SEM. n= 7. $p<0.05$ *vs.* control (Student's t-test).

4.3.1.2 Ang-(1-9) perfusion

To investigate the effects of Ang-(1-9) on cardiac contractility in spontaneously beating hearts, rat hearts were perfused with increasing doses of Ang-(1-9) as outlined in protocol 2 in Figure 2-9 A. LVDP and contractile parameters calculated in 2 minute intervals were expressed as percent-change from steady state prior to the addition of Ang-(1-9) (Figure 4-3). Time-matched perfused hearts with the addition of Tyrodes solution as shown in Figure 4-2 served as control.

An example LVP trace of Ang-(1-9) perfusion in the isolated rat heart is shown in Figure 4-3 A. Baseline steady state parameters of cardiac function were not significantly different between control and Ang-(1-9)-perfused rat hearts (Table 4-1). HR significantly decreased within 2 min of 1 µM Ang-(1-9) perfusion (control 100.94 ± 0.23 % *vs.* Ang-(1-9) 98.36 ± 1.20 %, n= 6-7, $p<0.05$) before increasing above control levels, despite being non-significant (Figure 4-3 B). Increasing Ang-(1-9) concentration to 10 µM significantly increased HR within 4 min to 104.25 ± 1.61 % ($p<0.05$) and remained elevated for the length of the perfusion protocol (Figure 4-3 B). Perfusion of 1 µM Ang-(1-9) caused a significant increase in LVDP within 2 min of perfusion and peaked after 4 min at 105.03 ± 1.99 % ($p<0.05$) (Figure 4-3 C). This effect was transient and LVDP returned to control level after 8 min of perfusion. Increasing Ang-(1-9) concentration to 10 µM had no further effect on LVDP (Figure 4-3 C). In a similar manner, dP/dt_{max} and dP/dt_{min} transiently increased within the first 6 min of perfusion of 1 µM Ang-(1-9) and peaked at 4 min (dP/dt_{max}: control 99.92 ± 0.63 % *vs.* Ang-(1-9) 106.61 ± 1.77; dP/dt_{min}: control 98.40 ± 1.02 % *vs.* Ang-(1-9) 104.26 ± 2.03 %; n= 6-7, $p<0.05$) (Figure 4-3 D,-E). While dP/dt_{max} tended to stay elevated compared to control, dP/dt_{min} returned to control values and 10 µM Ang-(1-9) did not significantly alter dP/dt_{max} and dP/dt_{min}, In contrast, the isovolumic relaxation constant tau remained unchanged during perfusion with either dose Ang-(1-9) (Figure 4-3 F). Overall, this data suggests that Ang-(1-9) is acting as a positive inotrope.

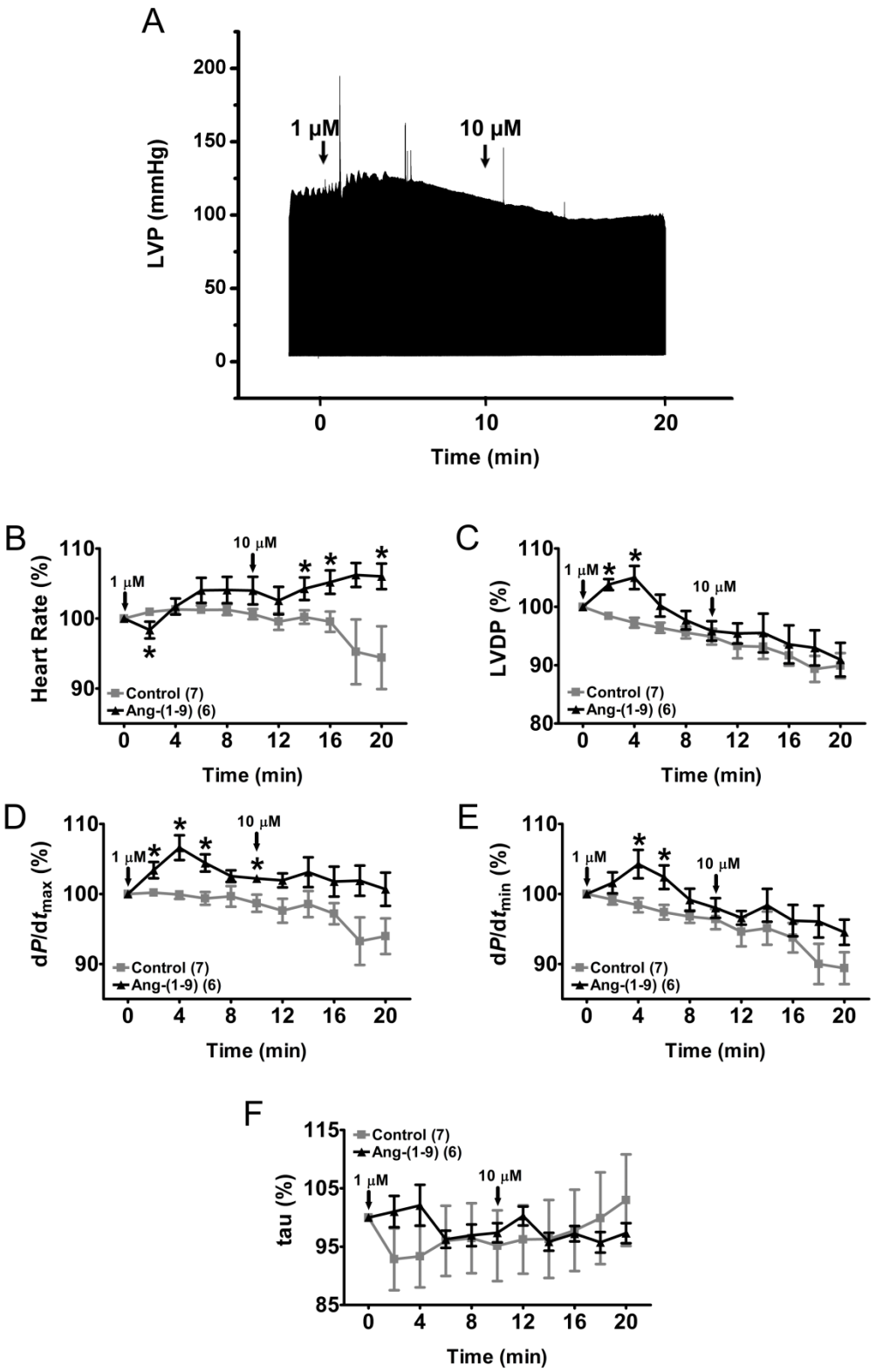

Figure 4-3. Ang-(1-9) perfusion in spontaneously beating hearts.
Rat hearts were perfused according to the Langendorff method. After reaching maximal pressure, the heart was allowed to reach a steady state for 10 min prior to the perfusion with 1 µM Ang-(1-9) for 10 min. The concentration was then increased to 10 µM Ang-(1-9) for a further 10 min. Time-matched perfused hearts presented in Figure 4-2 served as control. (A) Example left ventricular pressure (LVP) trace of Ang-(1-9) perfusion in the isolated rat heart. (B) Heart rate, (C) left ventricular developed pressure (LVDP), (D) dP/dt_{max}, (E) dP/dt_{min} and (F) tau were measured using a fluid filled balloon connected to a pressure transducer and changes were expressed as percent-change compared to steady state. Data are presented as mean ± sem. n= 7 for control and n= 6 for Ang-(1-9). Data are presented as mean ± SEM. *p<0.05 *vs.* control (Student's t-test).

Ang-(1-9) has been shown to mediate its anti-hypertrophic effects in cardiomyocytes by binding the AT_2R (Flores-Muñoz *et al.*, 2011). To investigate the role of the AT_2R in the transient inotropic effect observed by perfusion with Ang-(1-9), rat hearts were perfused with 1 μM of the AT_2R antagonist PD123319 for 10 min prior to the addition of 1 μM Ang-(1-9) for a further 10 min (Protocol 3, Figure 2-9 A) (Figure 4-4).

Perfusion with PD123319 did not alter cardiac contractile function compared to control (Table 4-1). In the presence of PD123319, Ang-(1-9) induced a significant increase in HR as early as 2 min (control 98.79 ± 0.94 % *vs.* PD123319+Ang-(1-9) 102.48 ± 1.41 %, n= 7, $p<0.05$) and this remained elevated throughout the perfusion protocol, peaking at 107.13 ± 2.34 % ($p<0.05$) (Figure 4-4 A). The presence of PD123319 however seemed to completely abolish the increase in LVDP, dP/dt_{max} and dP/dt_{min} observed with Ang-(1-9) while tau remained unchanged (Figure 4-4 B-E).

To further elucidate the effect of PD123319 in the inotropic response to Ang-(1-9), HR, LVDP, dP/dt_{max} and dP/dt_{min} measured at 4 min of perfusion with Ang-(1-9) (where the increase in LVDP with Ang-(1-9) perfusion was maximal) in the presence and absence of PD123319 were directly plotted against each other with their time-matched control and analysed by one-way ANOVA (Figure 4-5). At 4 min, Ang-(1-9) had no effect on HR but this tended to be increased in the presence of PD123319 (control 1 101.30 ± 0.38 %, control 2 99.46 ± 0.93 %, Ang-(1-9) 101.72 ± 1.14 %, PD123319+Ang-(1-9) 104.69 ± 2.44 %, n= 6-7, $p>0.05$) (Figure 4-5 A). Ang-(1-9) significantly increased LVDP to 105.03 ± 1.99 % and despite being a non-significant change, this tended to be decreased in the presence of PD123319 (99.31 ± 1.95 %) (Figure 4-5 B). Similarly, dP/dt_{max} was significantly increased by Ang-(1-9) and this was abolished by PD123319 (control 1 99.92 ± 0.63 %, control 2 98.86 ± 0.76 %, Ang-(1-9) 106.61 ± 1.77 %, PD123319+Ang-(1-9) 100.44 ± 1.83 %, n= 6-7, $p<0.05$) (Figure 4-5 C). dP/dt_{min} was elevated to 104.26 ± 2.03 % with Ang-(1-9) perfusion and PD123319 reduced this to 98.55 ± 1.71 % ($p>0.05$) (Figure 4-5 D). Overall, these results demonstrate an inhibitory effect of PD123319 on the positive inotropic effect induced by Ang-(1-9).

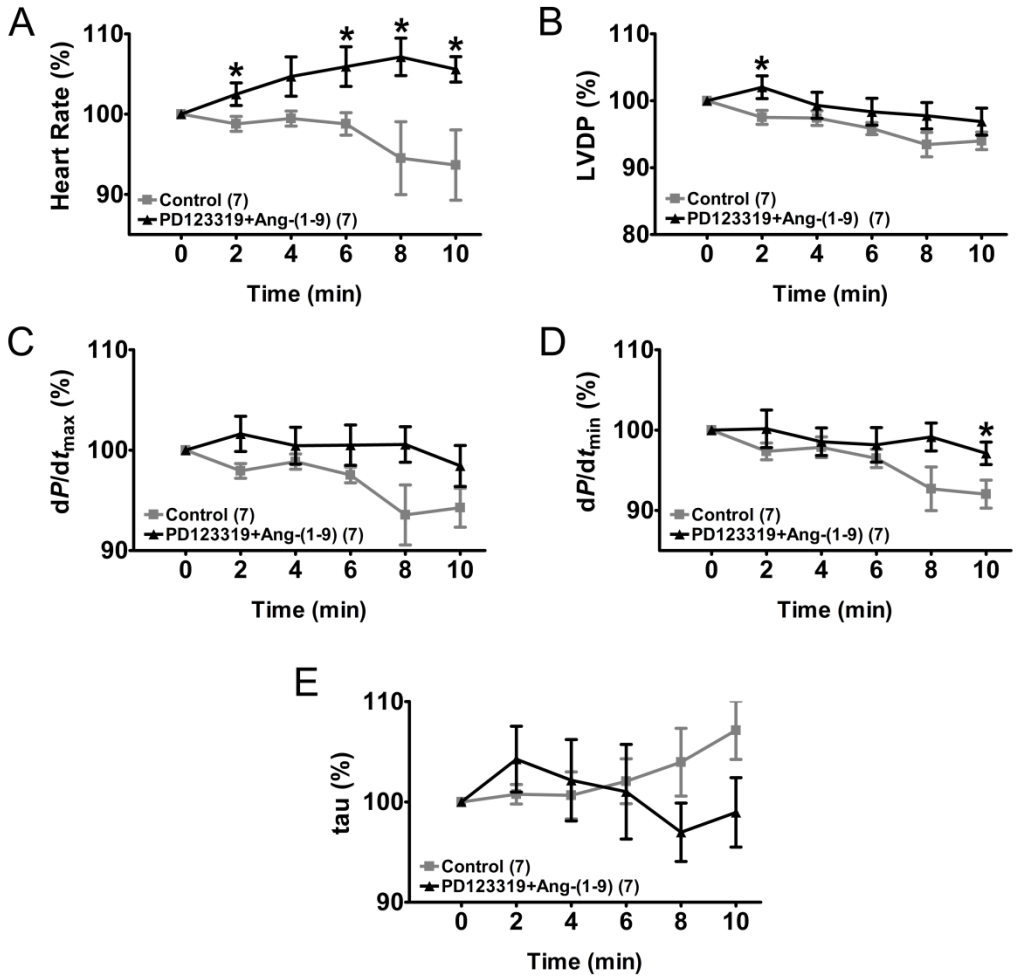

Figure 4-4. Role of the AT_2R in Ang-(1-9)-induced positive inotropy.
Rat hearts were perfused according to the Langendorff method. After reaching maximal pressure, the heart was allowed to reach a steady state for 10 min prior to the perfusion with 1 μM PD123319 for 10 min at which point 1 μM Ang-(1-9) was added to the perfusate for a further 10 min. Time-matched control hearts presented in Figure 4-2 served as control. (A) Heart rate, (B) left ventricular developed pressure (LVDP), (C) dP/dt_{max}, (D) dP/dt_{min} and (E) tau were measured using a fluid filled balloon connected to a pressure transducer and changes were expressed as percent-change compared to steady state prior to the addition of Ang-(1-9). Data are presented as mean ± SEM. n= 7. *p<0.05 *vs.* control (Student's t-test).

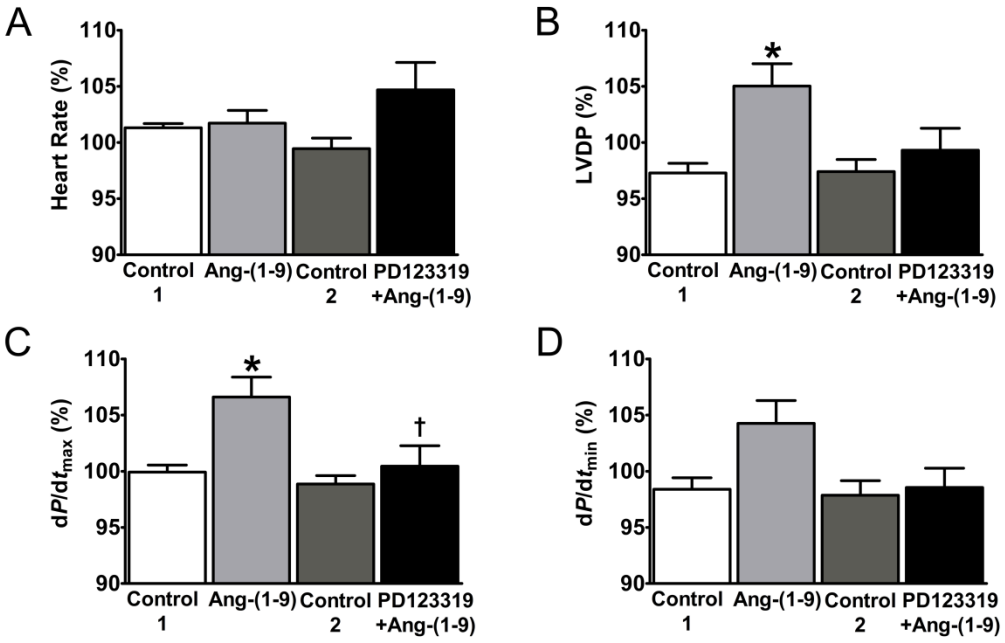

Figure 4-5. PD123319 in Ang-(1-9)-induced inotropy.
(A) Heart rate, (B) left ventricular developed pressure (LVDP), (C) d*P*/dt_{max} and (D) d*P*/dt_{min} at 4 min perfusion with 1 μM Ang-(1-9) in the presence or absence of 1 μM PD123319. Time-matched control hearts presented in Figure 4-2 served as control. Data are presented as mean ± SEM. n= 6 for Ang-(1-9) and n= 7 for control and PD123319+Ang1-9. *p<0.05 *vs.* control. † p<0.05 *vs* Ang-(1-9) (ANOVA with Tukey's post-hoc analysis).

4.3.1.3 Crosstalk between Ang-(1-9) and Ang II

Since it has been observed that Ang-(1-9) can reverse Ang II-induced cardiac contractile dysfunction *in vivo* (Section 3.3.3) and that Ang-(1-9) acts as a positive inotrope in the isolated rat heart (Section 4.3.1.2), next it was assessed whether Ang-(1-9) modulates the actions of Ang II on cardiac contractile function. Mimicking *in vivo* protocols, rat hearts were either perfused with a combination of Ang II and Ang-(1-9) (Figure 4-6) or pre-perfused with Ang II prior to the addition of Ang-(1-9) (Figure 4-7) as outlined in protocols 3 and 4 (Figure 2-9 A). Control data presented previously served as control (Figure 4-2).

Baseline parameters between control and Ang II+Ang-(1-9)-perfused hearts were not significantly different (Table 4-1). HR was significantly increased within 2 min of perfusion of Ang II+Ang-(1-9) and peaked with 107.62 ± 1.90 % at 16 min similar to Ang II alone (Figure 4-6 A). Co-perfusion with Ang II and Ang-(1-9) over 20 min did not alter LVDP and the inotropic effect observed with Ang-(1-9) alone at 2 and 4 min of perfusion was absent (Figure 4-6 B). Similarly, dP/dt_{max}, dP/dt_{min} were unaffected by Ang II+Ang-(1-9) co-infusion and the increases in dP/dt_{max} and dP/dt_{min} with Ang-(1-9) were absent (Figure 4-6 C-D). Similar to perfusion with Ang II alone, tau was significantly decreased to 91.70 ± 2.01 % ($p<0.05$) at 8 min and this was maintained throughout the perfusion protocol (Figure 4-6 E).

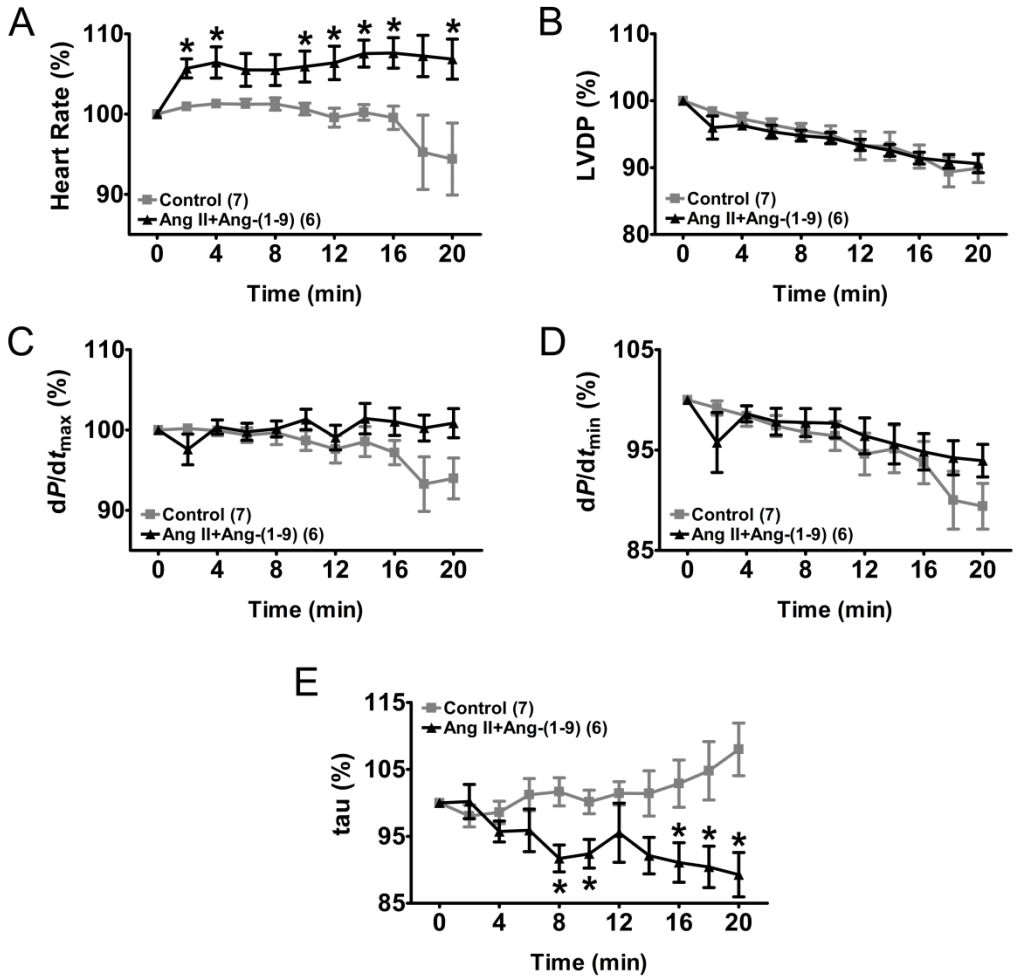

Figure 4-6. Ang II and Ang-(1-9) co-infusion in spontaneously beating hearts.
Rat hearts were perfused according to the Langendorff method. After reaching maximal pressure, the heart was allowed to reach a steady state for 10 min prior to the co-perfusion with 1 µM Ang II and 1µM Ang-(1-9) for 20 min. Time-matched perfused hearts presented in Figure 4-2 served as control. (A) Heart rate, (B) left ventricular developed pressure (LVDP), (C) dP/dt_{max}, (D) dP/dt_{min} and (E) tau were measured using a fluid filled balloon connected to a pressure transducer and changes were expressed as percent-change compared to steady state. Data are presented as mean ± SEM. n= 7 for control and n= 6 for Ang II+Ang-(1-9). *p<0.05 *vs.* control (Student's t-test).

When Ang II was pre-perfused for 10 min, as previously observed, Ang II induced a significant increase in HR with a maximum increase of 107.20 ± 2.36 % ($p<0.05$) and this was unaffected by addition of Ang-(1-9) (Figure 4-7 A). Addition of Ang-(1-9) to the perfusate after 10 min pre-perfusion of Ang II did not alter LVDP and Ang-(1-9) failed to induce an inotropic response (Figure 4-7 B). In a similar manner, addition of Ang-(1-9) failed to induce an increase in dP/dt_{max} and dP/dt_{min} in the presence of Ang II (Figure 4-7 C-D). Ang II induced a transient increase in tau at 2 min to 105.52 ± 1.88 % ($p<0.05$) which returned to control values (Figure 4-7 F). Addition of Ang-(1-9) did not significantly alter tau but tau was significantly decreased at the end of the perfusion protocol (control 108.00 ± 3.93 *vs.* Ang II+Ang-(1-9) 92.87 ± 1.81 %, n= 3-7, $p<0.05$) (Figure 4-7 F).

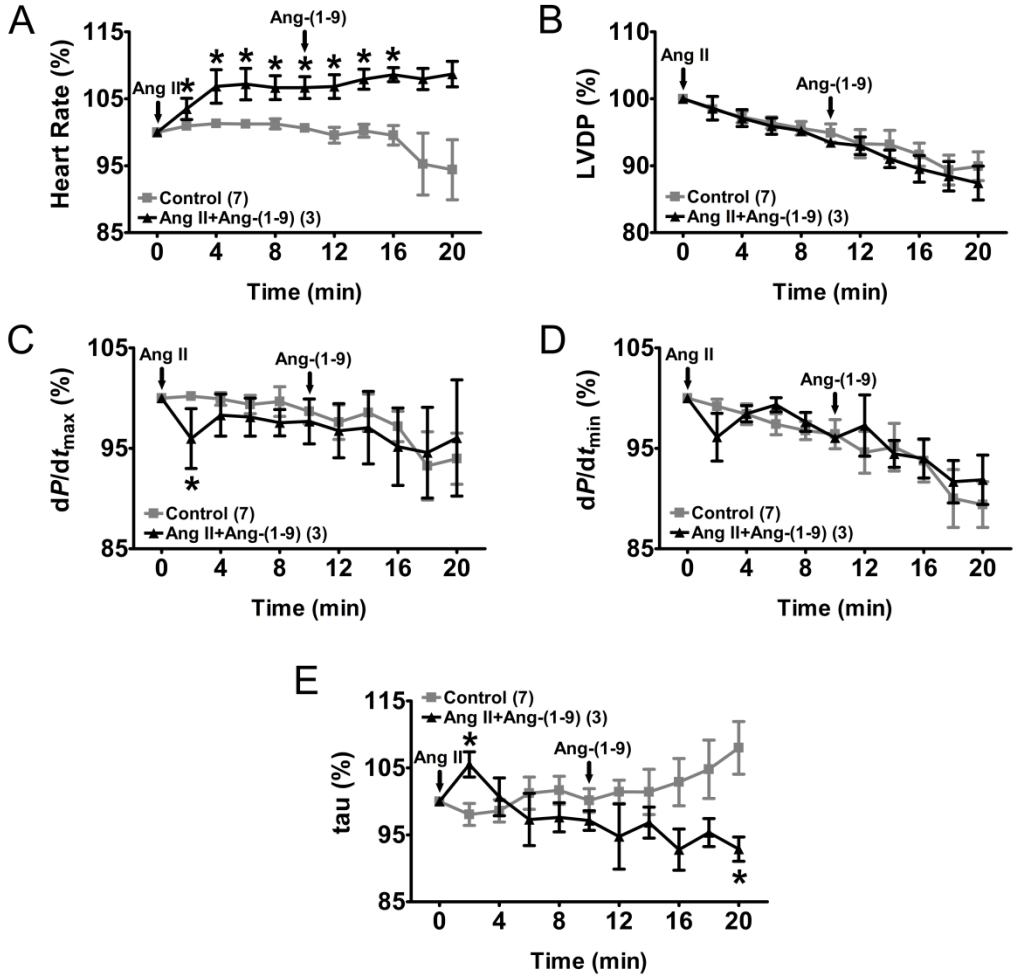

Figure 4-7. Effects of Ang-(1-9) in Ang II-perfused spontaneously beating hearts.
Rat hearts were perfused according to the Langendorff method. After reaching maximal pressure, the heart was allowed to reach a steady state for 10 min prior to the perfusion with 1 µM Ang II for 10 min. 1 µM Ang-(1-9) was then added for a further 10 min. Time-matched perfused hearts presented in Figure 4-2 served as control. (A) Heart rate, (B) left ventricular developed pressure (LVDP), (C) dP/dt_{max}, (D) dP/dt_{min} and (E) tau were measured using a fluid filled balloon connected to a pressure transducer and changes were expressed as percent-change compared to steady state. Data are presented as mean ± SEM. n= 7 for control and n= 3 for Ang II+Ang-(1-9). *p<0.05 *vs.* control (Student's t-test).

4.3.1.4 Ang-(1-7) perfusion

Ang-(1-9) can be broken down to Ang-(1-7) by ACE and Ang-(1-7) has previously been shown to improve cardiac contractile function in models of cardiac disease (Zhou *et al.*, 2015, de Almeida *et al.*, 2015). Therefore, to determine whether the actions of Ang-(1-9) may be through breakdown to Ang-(1-7), rat hearts were perfused with increasing doses of Ang-(1-7) as *per* protocol 2 (Figure 2-9 A) and its effects on cardiac function were assessed (Figure 4-8). Time-matched controls served as control (Figure 4-2).

Baseline steady state parameters of cardiac contractile function were not significantly different between control and Ang-(1-7)-perfused hearts (Table 4-1). An example LVP of Ang-(1-7) perfusion in the isolated rat heart is shown (Figure 4-8 A). Perfusion with either 1 or 10 μM Ang-(1-7) had no effect on HR, LVDP, dP/dt_{max} or dP/dt_{min} (Figure 4-8 B-E). Tau was significantly decreased after 10 min of perfusion with either 1 μM or 3 μM Ang-(1-7) to 94.40 ± 1.54 % and 95.62 ± 3.29 % ($p<0.05$), respectively (Figure 4-8 F). Overall, this suggests that Ang-(1-9) is not broken down to Ang-(1-7).

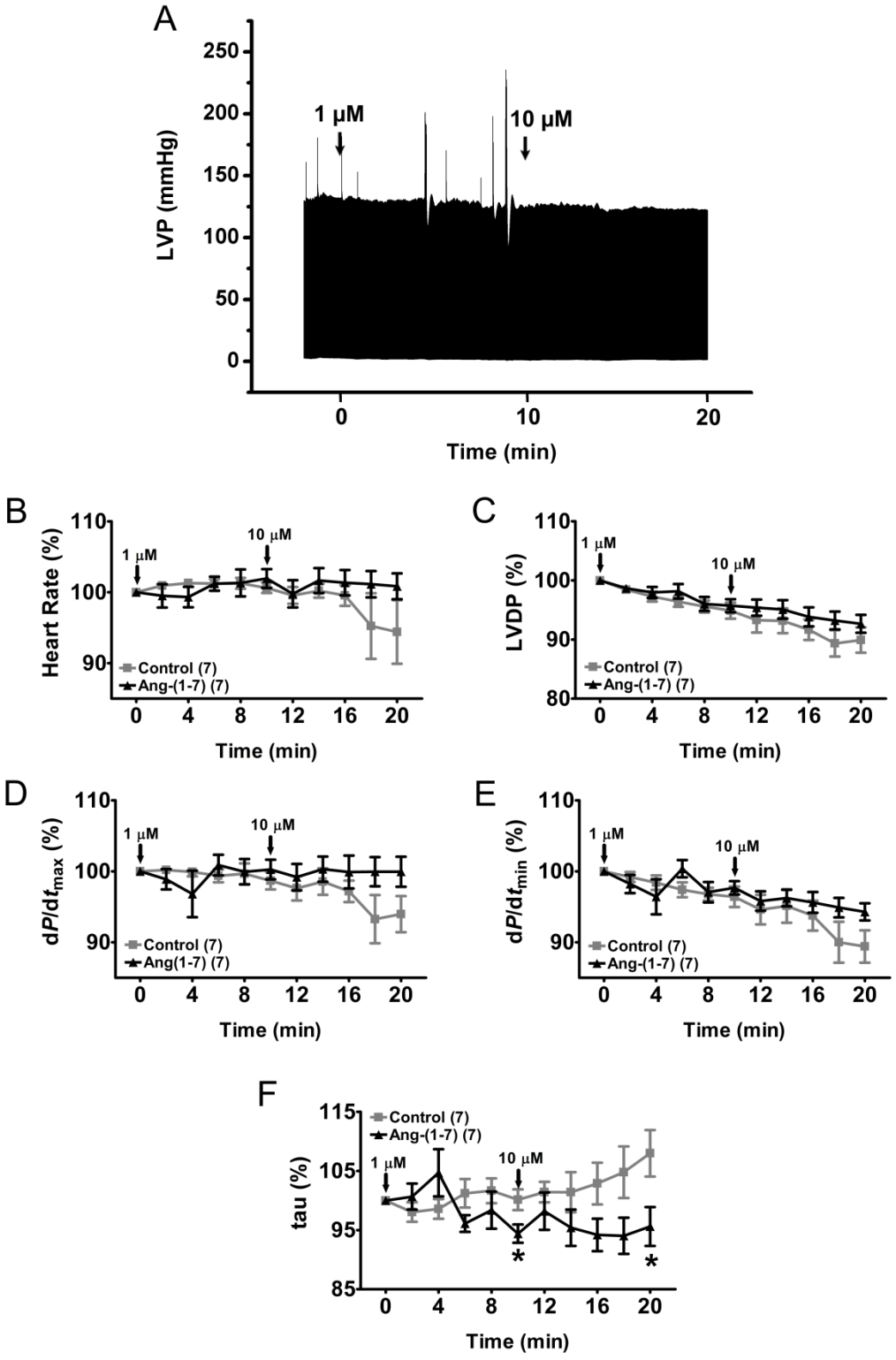

Figure 4-8. Ang-(1-7) in spontaneously beating hearts.
Rat hearts were perfused according to the Langendorff method. After reaching maximal pressure, the heart was allowed to reach a steady state for 10 min prior to the perfusion with 1 µM Ang-(1-7). After 10 min, the concentration was increased to 10 µM and the hearts perfused for a further 10 min. Time-matched perfused hearts presented in Figure 4-2 served as control. (A) Example left ventricular pressure (LVP) trace from an Ang-(1-7) perfused rat heart. (B) Heart rate, (C) left ventricular developed pressure (LVDP), (D) dP/dt_{max}, (E) dP/dt_{min} and (F) tau were measured using a fluid filled balloon connected to a pressure transducer and changes were expressed as percent-change compared to steady state. Data are presented as mean ± SEM. n= 7. *p<0.05 *vs.* control (Student's t-test).

4.3.2 Paced Hearts

Since investigations of Ang-(1-9) and Ang II in unpaced, spontaneously beating hearts revealed significant effects on HR and HR has previously been shown to mask changes in other cardiac function parameters (Derumeaux *et al.*, 2008), the effects of Ang-(1-9) and Ang II were also assessed in paced Langendorff-perfused rat hearts. Hearts were paced at 320 bpm which was approximately 20 bpm above the maximum increase in HR measured by 1 µM Ang II (296.53 ± 10.88 bpm). This was determined to be optimal to prevent the occurrence of arrhythmias in response to the chronotropic effects of Ang II. A set of hearts perfused over 20 min with the addition of equal volumes of Tyrodes solution served as time-matched controls for the data presented below (Protocol 1, Figure 2-9 B).

4.3.2.1 Ang II perfusion

Paced rat hearts were perfused with 1 µM Ang II for 10 min as outlined (protocol 2, Figure 2-9 B). Baseline steady-state parameters of cardiac function did not differ between control and Ang II-perfused hearts (Table 4-2). Over 10 min of perfusion, LVDP pressure loss in control hearts was approximately 3 % (Figure 4-9 B). Ang II caused a transient significant increase in LVDP at 4 min of perfusion (control 98.71 ± 0.46 *vs.* Ang II 100.55 ± 0.41, n= 5-6, $p<0.05$) which subsequently returned to control levels. dP/dt_{max} and dP/dt_{min} were unaffected by Ang II perfusion, even though an initial drop could be observed at 2 min although this did not reach significance (Figure 4-9 C-D). Similarly, Ang II perfusion did not alter tau, despite an initial increase observed at 2 min perfusion (Figure 4-9 E).

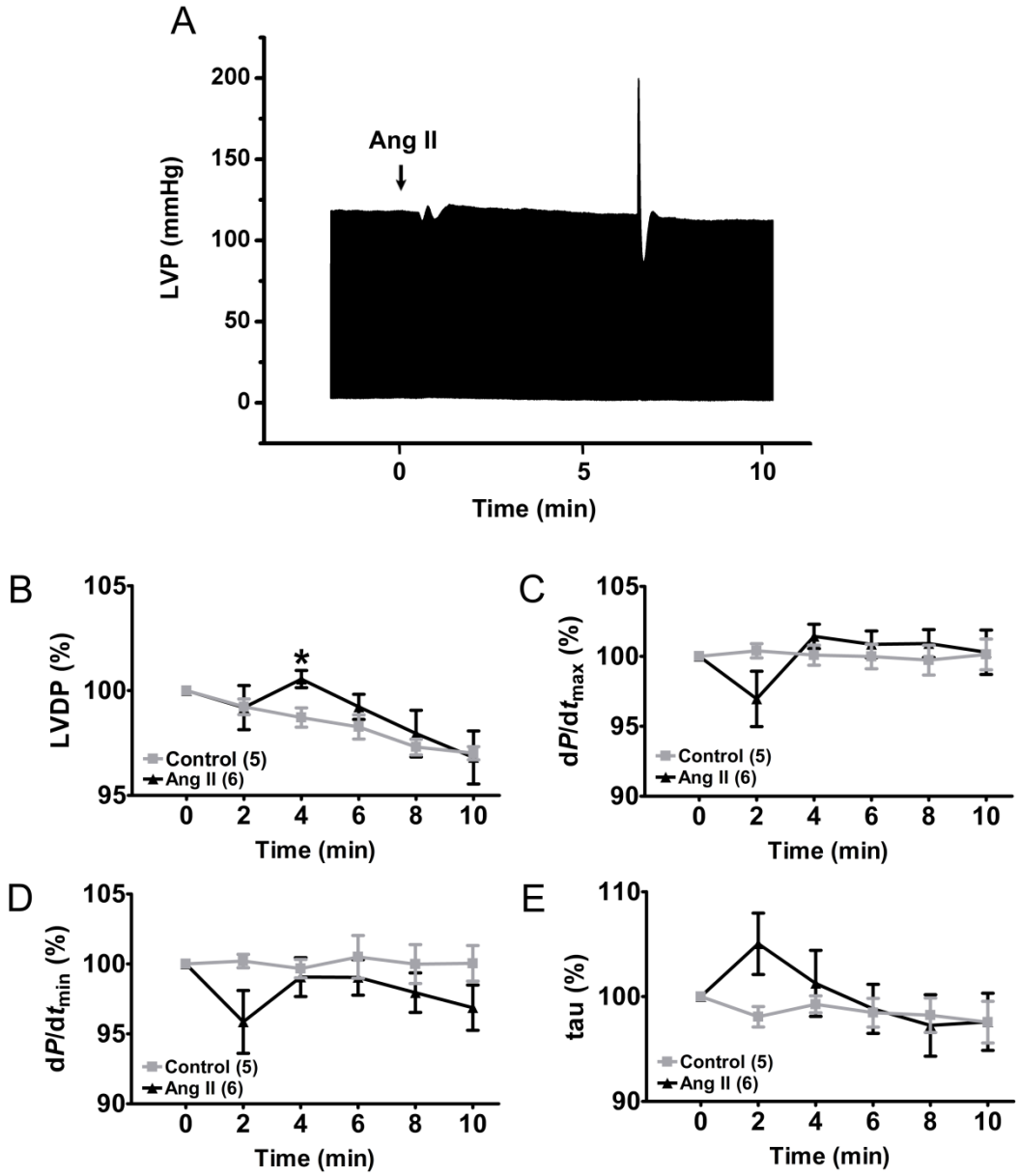

Figure 4-9. Ang II in paced Langendorff-perfused rat hearts.
Rat hearts were perfused according to the Langendorff method. After reaching maximal pressure, hearts were paced at 320 bpm and allowed to reach a steady state for 10 min prior to the perfusion with 1 μM Ang II for 10 min. Time-matched perfused hearts served as control. (A) Example left ventricular pressure (LVP) trace of Ang II perfusion in a paced rat heart. (B) left ventricular developed pressure (LVDP), (C) d*P*/dt_{max}, (D) d*P*/dt_{min} and (E) tau were measured using a fluid filled balloon connected to a pressure transducer and changes were expressed as percent-change compared to steady state. n= 5 for control and n= 6 for Ang II. Data are presented as mean ± SEM. *p<0.05 *vs.* control (Student's t-test).

Table 4-2. Baseline cardiac function parameters in paced rat hearts.

	n	LVDP (mmHg)	d*P*/dt_{max} (mmHg/s)	d*P*/dt_{min} (mmHg/s)	Tau (ms)
Control	5	138.84 ± 2.12	3811.10 ± 106.67	-2654.61 ± 102.23	26.67 ± 1.05
Ang-(1-9)	6	125.64 ± 3.20	3756.27 ± 107.14	-2599.57 ± 107.20	26.67 ± 1.12
Ang II	6	128.01 ± 3.25	3759.65 ± 102.27	-2760.33 ± 130.48	24.79 ± 1.53

4.3.2.2 Ang-(1-9) perfusion

Next, the effect of Ang-(1-9) on cardiac contractile function was assessed in paced Langendorff-perfused rat hearts (Figure 4-10). Time-matched control perfused hearts presented in Section 4.3.2.1 served as control.

Steady state characteristic of cardiac function did not differ between control and Ang-(1-9)-perfused hearts (Table 4-2). Perfusion with 1 μM Ang-(1-9) induced a sustained increase in LVDP within 2 min of perfusion which reached statistical significance at 4 min (control 98.71 ± 0.46 % *vs.* Ang-(1-9) 103.20 ± 1.46 %, n= 5-6, $p<0.05$) and this was maintained throughout the perfusion period (Figure 4-10 A-B). dP/dt_{max} remained stable in control perfused hearts and perfusion with Ang-(1-9) induced an elevation of dP/dt_{max} which was significant at 6 min of perfusion (control 99.99 ± 0.87 % *vs.* Ang-(1-9) 104.02 ± 1.07 %, n= 5-6, $p<0.05$) (Figure 4-10 C). In contrast, dP/dt_{min} was unaffected by perfusion with Ang-(1-9) (Figure 4-10 D). However, Ang-(1-9) induced a significant and sustained increase in tau within 2 minutes of perfusion which peaked at 6 min at 114.08 ± 2.58 % ($p<0.05$) (Figure 4-10 E), contrary to observations in spontaneously beating hearts (Section 4.3.1.2). This data confirms that Ang-(1-9) is a positive inotrope but also a negative lusitrope in paced Langendorff-perfused rat hearts.

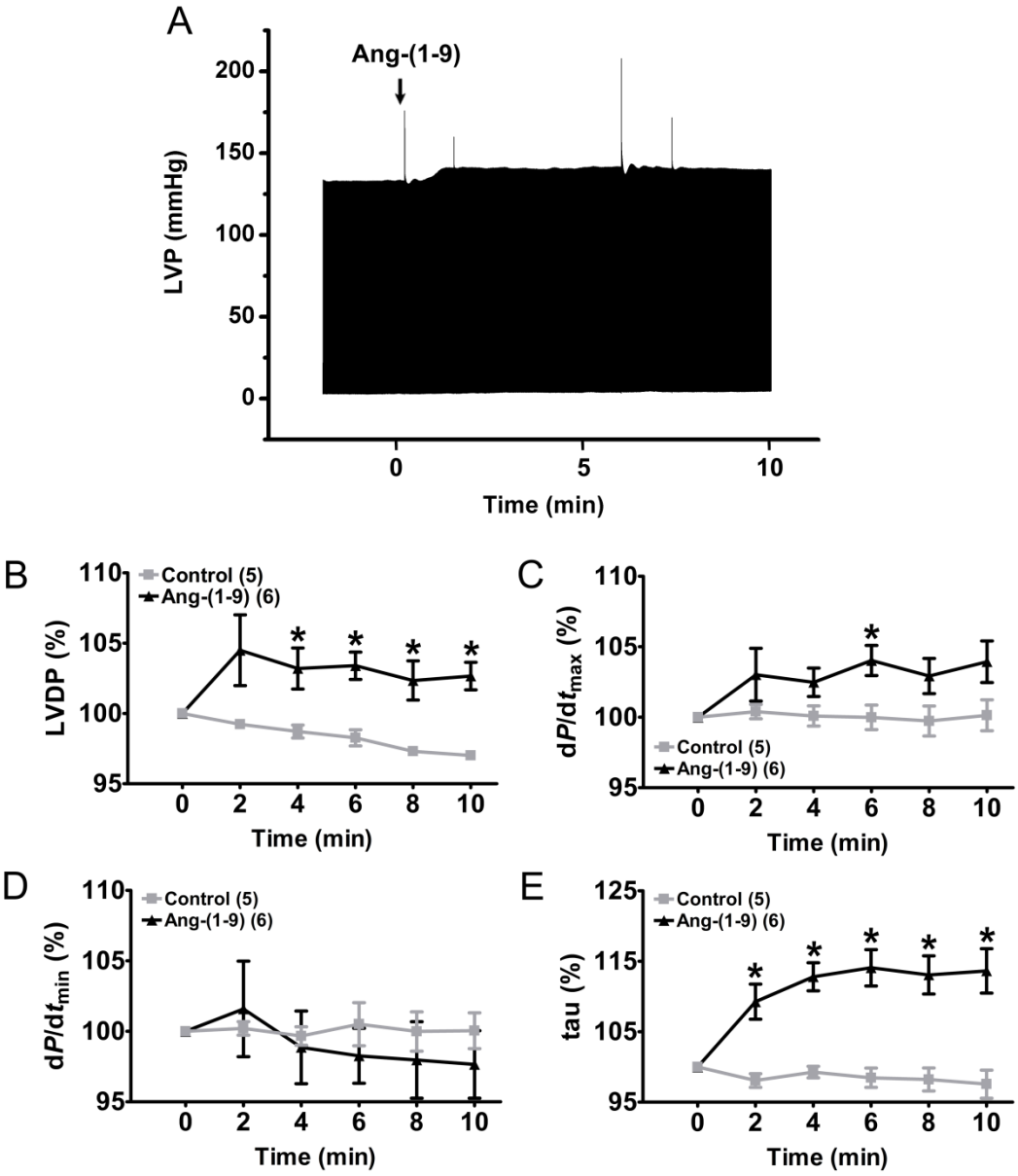

Figure 4-10. Ang-(1-9) in paced Langendorff-perfused rat hearts.
Rat hearts were perfused according to the Langendorff method. After reaching maximal pressure, hearts were paced at 320 bpm and allowed to reach a steady state for 10 min prior to the perfusion with 1 μM Ang-(1-9) for 10 min. Time-matched perfused hearts presented in Figure 4-9 served as control. (A) Example left ventricular pressure (LVP) trace of Ang-(1-9) perfusion in a paced rat heart. (B) left ventricular developed pressure (LVDP), (C) d*P*/dt_{max}, (D) d*P*/dt_{min} and (E) tau were measured using a fluid filled balloon connected to a pressure transducer and changes were expressed as percent-change compared to steady state. Data are presented as mean ± SEM. n= 5 for control and n= 6 for Ang-(1-9). *p<0.05 *vs.* control (Student's t-test).

To assess the role of the AT_1R and AT_2R in this process, rat hearts were pre-perfused with 10 µM of the AT_1R antagonist losartan or 1 µM of the AT_2R antagonist PD123319 as outlined in protocol 3 in Figure 2-9 B (Figure 4-11).

Pre-perfusion with PD123319 significantly reduced LVDP and dP/dt_{min} compared to control but dP/dt_{max} and tau were unaffected (Table 4-3). In the presence of PD123319, Ang-(1-9) induced a significant increase in LVDP within 2 min of perfusion (control 99.64 ± 0.45 % *vs.* PD123319+Ang-(1-9) 107.04 ± 0.63 %, n= 5, $p<0.05$) which was sustained throughout the perfusion period (Figure 4-11 A), similar to what has been observed with Ang-(1-9) alone (Figure 4-10 A). In a similar manner, dP/dt_{max} was significantly increased within 2 min of Ang-(1-9) perfusion (control 100.03 ± 0.64 % *vs.* PD123319+Ang-(1-9) 105.96 ± 0.75 %, n= 5, $p<0.05$) and remained elevated for the remaining perfusion period (Figure 4-11 B). In contrast, dP/dt_{min} and tau were unaffected by perfusion with Ang-(1-9) in the presence of PD123319 (Figure 4-11 C-D).

Pre-perfusion with losartan significantly reduced tau but LVDP, dP/dt_{max} and dP/dt_{min} were unaffected (Table 4-3). In the presence of losartan, Ang-(1-9) did not induce significant changes in LVDP, dP/dt_{max} and tau while dP/dt_{min} was significantly decreased to 96.97 ± 0.95 % and 96.31 ± 1.03 % after 4 and 6 min of perfusion, respectively ($p<0.05$) (Figure 4-11 A-D).

To further elucidate the effect of losartan and PD123319 in Ang-(1-9)-induced inotropy, LVDP, dP/dt_{max} and tau measured after 6 min of perfusion (where most significant changes occurred with Ang-(1-9)) were directly plotted against Ang-(1-9) and their respective controls and assessed by one-way ANOVA (Figure 4-11 E–G). Ang-(1-9) significantly increased LVDP to 103.40 ± 0.97 % ($p<0.05$) and this was unaffected by PD123319. However, losartan fully blocked the increase in LVDP by Ang-(1-9) ($p<0.05$) (Figure 4-11 E). In a similar manner, dP/dt_{max} was increased by Ang-(1-9) and while this was unaffected by PD123319, losartan blocked the Ang-(1-9) induced increase in dP/dt_{max} (Ang-(1-9) 104.02 ± 1.07 %, PD1233319+Ang-(1-9) 102.63 ± 1.40 %, Losartan+Ang-(1-9) 99.22 ± 1.24 %, n= 5–6, $p<0.05$) (Figure 4-11 F). Tau was significantly increased to 114.08 ± 2.58 % by Ang-(1-9) and this was abolished equally by both PD123319 and losartan ($p<0.05$) (Figure 4-11 G).

Table 4-3. Baseline parameters of inhibitor treated paced rat hearts prior to perfusion with Ang-(1-9).

	n	LVDP (mmHg)	d*P*/dt_{max} (mmHg/s)	d*P*/dt_{min} (mmHg/s)	Tau (ms)
Control	5	127.17 ± 2.02	3812.20 ± 117.94	-2653.23 ± 121.55	26.05 ± 0.81
PD123319	5	102.97 ± 4.78*****	3557.98 ± 191.40	-2208.50 ± 113.26*****	26.95 ± 1.39
Losartan	5	119.09 ± 5.81	4046.77 ± 262.62	-2840.65 ± 167.14	21.68 ± 1.23*****
H89	5	118.30 ± 2.98*****	3734.58 ± 57.16	-2436.91 ± 95.29	25.74 ± 0.67
K93	5	119.39 ± 3.91	4056.90 ± 92.32	-2613.40 ± 144.28	22.95 ± 1.18

*p<0.05 *vs.* control; LVDP= Left ventricular developed pressure; d*P*/d$t_{max/min}$= rat of left ventruclar pressure rise and fall; Tau= exponential decay of left ventricular pressure fall

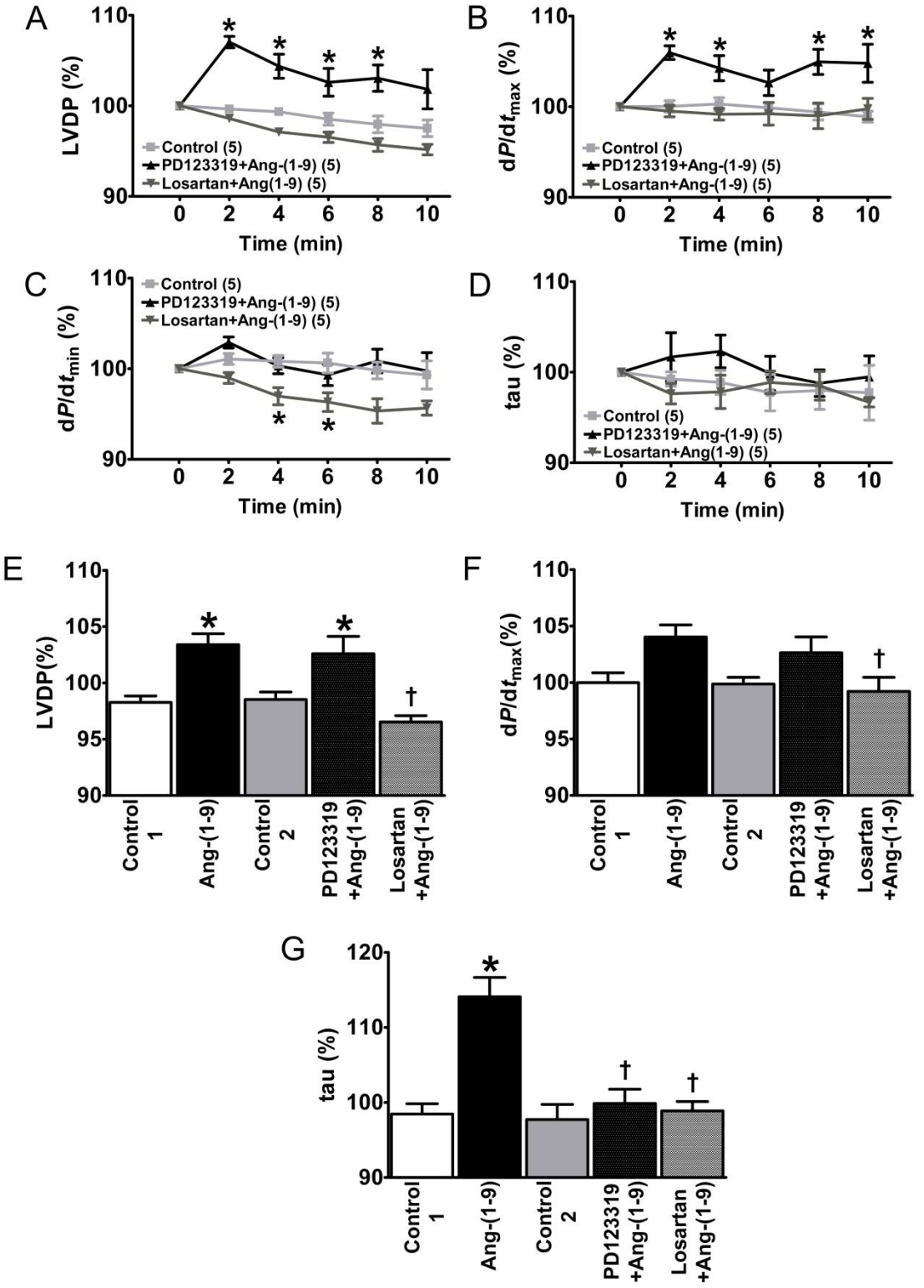

Figure 4-11. Role of Angiotensin receptors in paced Ang-(1-9)-perfused rat hearts
Rat hearts were perfused according to the Langendorff method. After reaching maximal pressure, hearts were paced at 320 bpm and allowed to reach a steady state for 10 min and pre-perfused with 10 µM losartan or 1 µM PD123319 for 10 min prior to the addition of 1 µM Ang-(1-9). Time-matched perfused hearts presented in Figure 4-9 served as control. (A) left ventricular developed pressure (LVDP), (B) d*P*/dt_{max}, (C) d*P*/dt_{min} and (D) tau were measured using a fluid filled balloon connected to a pressure transducer and changes were expressed as percent-change compared to steady state. (E) LVDP, (F) d*P*/dt_{max} and (G) tau measured after 6 min of perfusion were directly plotted against Ang-(1-9) and their time-matched control (control 1 for Ang-(1-9), control 2 for PD123319 and losartan). Data are presented as mean ± SEM. n= 6 for Ang-(1-9) and n= 5 for control, PD123319+Ang-(1-9) and losartan+Ang1-9. *p<0.05 *vs.* control. † p<0.05 *vs.* Ang-(1-9) (ANOVA with Tukey's post-hoc analysis).

4.3.2.3 Role of CaMKII and PKA in Ang-(1-9)-perfused hearts

Next to assess the downstream pathways that may play a role in the inotropic response induced by Ang-(1-9), the role of CaMKII and PKA were assessed due to their role in the regulation of EC coupling and previous evidence demonstrating CaMKII and PKA activation by Ang II (Wagner *et al.*, 2014) (Figure 4-12). Rat hearts were perfused with 1 µM H89 or 2.5 µM K93 for 10 min prior to the addition of Ang-(1-9) to inhibit PKA, and CaMKII, respectively (protocol 4, Figure 2-9 B). These doses have previously been found to be effective in inhibiting the activity of these kinases (Salas *et al.*, 2010, Gonano *et al.*, 2011, García-Villalón *et al.*, 2011, Robinet *et al.*, 2005).

Pre-perfusion with H89 significantly reduced LVDP while all other parameters were unaffected (Table 4-3). K93 did not alter cardiac contractile parameters (Table 4-3). In the presence of K93, Ang-(1-9)-induced a significant increase in LVDP peaking at 4 min with 104.23 ± 1.13 % ($p<0.05$) (Figure 4-12 A). Similarly, dP/dt_{max} was significantly increased within 2 min peaking at 8 min with 104.09 ± 1.24 % (Figure 4-12 B). dP/dt_{min} and tau were unaffected by perfusion with Ang-(1-9) in the presence of K93 (Figure 4-12 C-D). In contrast, in the presence of H89 Ang-(1-9)-did not modulate LVDP and, in contrast, LVDP was significantly reduced after 10 min (control 97.51 ± 0.92 % *vs.* H89+Ang-(1-9) 92.54 ± 0.83 %, n= 5, $p<0.05$) (Figure 4-12 A). Similarly, Ang-(1-9)-did not alter dP/dt_{max} or tau in the presence of H89 (Figure 4-12 B-D). However, dP/dt_{min} was significantly reduced after 6 min of perfusion with a maximum reduction of 6.94 % ($p<0.05$) (Figure 4-12 C).

To further elucidate the above observations with H89 and K93, LVDP, dP/dt_{max} and tau measured at 6 min perfusion were plotted directly against Ang-(1-9) and assessed by one-way ANOVA (Figure 4-12 E–G). K93 did not significantly alter the significant increase in LVDP induced by Ang-(1-9). However, this was completely abolished in the presence of H89 (Ang-(1-9) 103.40 ± 0.97 % *vs.* H89+Ang-(1-9) 95.38 ± 1.00 %, n= 5-6, $p<0.05$) (Figure 4-12 E). Similarly, H89 blocked the Ang-(1-9)-induced increase in dP/dt_{max} while K93 had no effect (Ang-(1-9) 104.02 ± 1.07, H89+Ang-(1-9) 97.22 ± 1.47 %, K93+Ang-(1-9) 103.09 ± 0.96 %, n= 5–6, $p<0.05$) (Figure 4-12 F). Both, H89 and K93 blocked the Ang-(1-9)-induced increase in tau (Ang-(1-9) 114.08 ± 2.58, H89+Ang-(1-9) 102.89 ± 2.09 %,

K93+Ang-(1-9) 100.81 ± 1.25 %, n= 5–6, $p<0.05$) (Figure 4-12 G). Overall, this data suggests that PKA and to a lesser extent CaMKII may play a role in mediating Ang-(1-9)-induced positive inotropy and negative lusitropy.

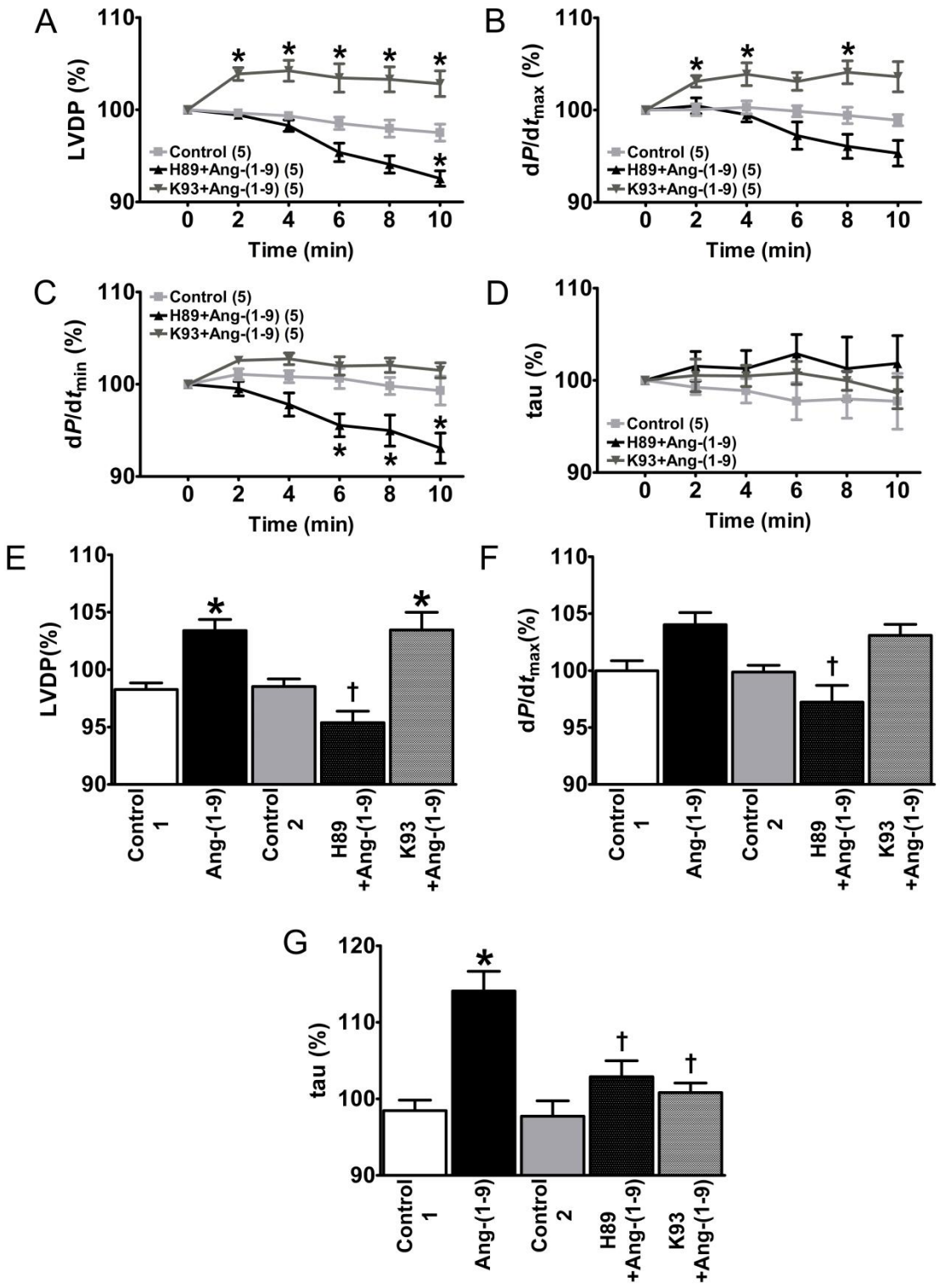

Figure 4-12. Role of CaMKII and PKA in Ang-(1-9) perfused rat hearts.
Rat hearts were perfused according to the Langendorff method. After reaching maximal pressure, hearts were paced at 320 bpm and allowed to reach a steady state for 10 min and pre-perfused with 1 μM H89 (for PKA) or 2.5 μM K93 (for CaMKII) for 10 min prior to the addition of 1 μM Ang-(1-9). Time-matched perfused hearts presented in Figure 4-9 served as control. (A) left ventricular developed pressure (LVDP), (B) dP/dt_{max}, (C) dP/dt_{min} and (D) tau were measured using a fluid filled balloon connected to a pressure transducer and changes were expressed as percent-change compared to steady state. (E) LVDP, (F) dP/dt_{max} and (G) tau measured after 6 min of perfusion were directly plotted against Ang-(1-9) and their time-matched control. n= 6 for Ang-(1-9) and n= 5 for control, H89+Ang-(1-9) and K93+Ang-(1-9). Data are presented as mean ± SEM. *p<0.05 *vs.* control. † p<0.05 *vs.* Ang-(1-9) (ANOVA with Tukey's post-hoc analysis).

4.3.3 PKA activity in rat hearts and adult mouse cardiomyocytes

PKA is activated by increases in cyclic AMP (cAMP) formed by adenylate cyclase. Two cAMP molecules bind to each of the two regulatory subunits of PKA inducing their dissociation and thereby activating PKA catalytic activity (Dulin *et al.*, 2001). However, PKA has also been shown to be activated in a cAMP-independent pathway by Thr-197 phosphorylation of the catalytic subunit (Adams *et al.*, 1995, Dulin *et al.*, 2001). Therefore, phosphorylation of PKA in response to Ang-(1-9) was assessed by Western immunoblot in Langendorff-perfused rat hearts with Ang-(1-9) or PD123319+Ang-(1-9) (Figure 4-13).

Compared to control hearts, PKA phosphorylation was 89.94 ± 8.77 % and 87.21 ± 6.59 % in Ang-(1-9) and PD123319+Ang-(1-9)-perfused hearts, respectively and not significantly different from baseline PKA phosphorylation (Figure 4-13 A-B). Additionally, PKA phosphorylation was assessed in isolated adult mouse cardiomyocytes where it has previously been shown that Ang-(1-9) increases Ca^{2+} transients *via* the L-type Ca^{2+} channel (Fattah *et al.*, unpublished) (Figure 4-13 C-D). Mouse cardiomyocytes were treated with 1 μM Ang-(1-7) and Ang-(1-9) for 20 min with Forskolin (which activates adenylate cyclase and leads to cAMP generation) serving as control and phosphorylation of PKA measured by Western immunoblot (Figure 4-13 C). Ang-(1-9) tended to increase phosphorylation of PKA to 104.22 % compared to control, however, this did not reach significance. In contrast, Ang-(1-7) had no effect on PKA phosphorylation while forskolin tended to decrease phosphorylated PKA to 90.48 % (Figure 4-13 D).

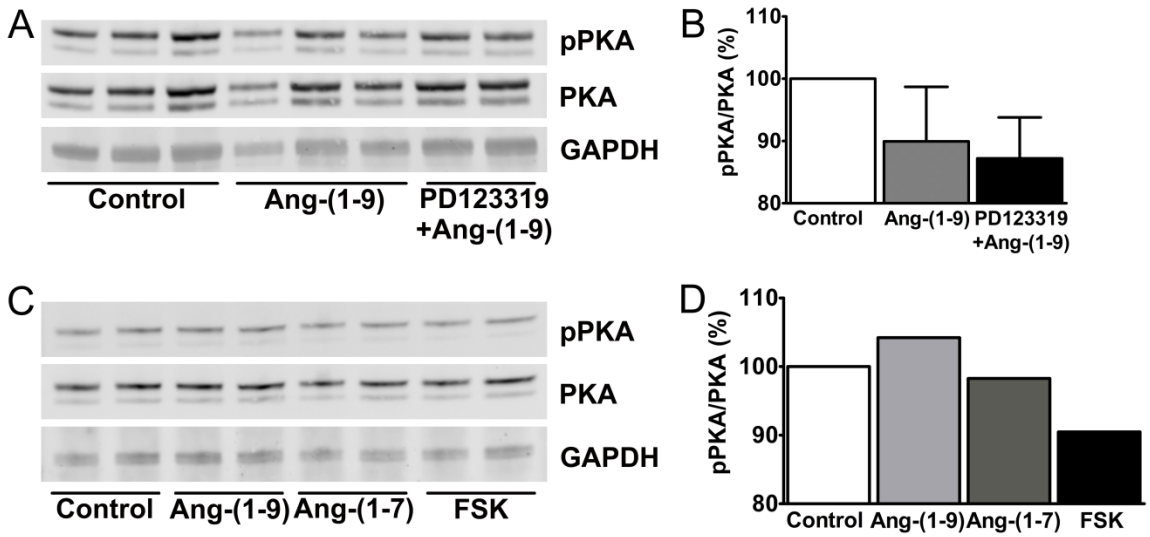

Figure 4-13. PKA phosphorylation in rat hearts and mouse cardiomyocytes.
(A) Representative Western blot of phosphorylated PKA (pPKA) in homogenates of Langendorff-perfused rat hearts treated with 1 µM Ang-(1-9) (n= 6), 1 µM PD123319+Ang-(1-9) (n= 5) or a solvent control (n= 6). (B) PKA phosphorylation was expressed as a ratio to total PKA and normalised to control. GAPDH served as loading control. (C) Adult mouse cardiomyocytes were stimulated with 1 µM Ang-(1-7) or Ang-(1-9) for 20 min and pPKA was assessed by Western blot. Forskolin served as control. Representative Western blot of pPKA in adult mouse cardiomyocytes. (D) pPKA was expressed as a ratio of total PKA and normalised to control. GAPDH served as loading control. Results were confirmed in three independent experiments.

4.3.4 Angiotensin receptor expression

The expression of the angiotensin receptors AT_1R, AT_2R and Mas were determined by qPCR in control-perfused rat hearts. Expression was normalised to expression of the stable housekeeper Ppib and are reported as ΔCt (Figure 4-14).

Expression of all receptors could be detected in rat hearts. The AT_1R and Mas were expressed at similar levels (AT_1R: 6.52 ± 0.13; Mas: 6.64 ± 0.25) while expression of the AT_2R was substantially lower with a ΔCt of 10.85 ± 0.55 (Figure 4-14).

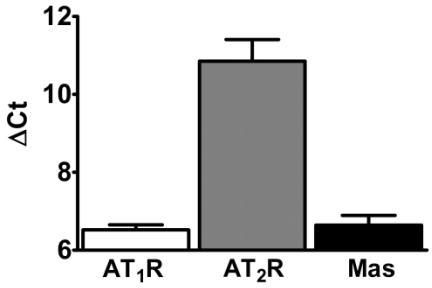

Figure 4-14. Angiotensin receptor expression in rat hearts.
RNA was extracted from control-perfused rat hearts and gene expression of AT_1R, AT_2R and Mas was assessed by qPCR and normalised to expression of the stable housekeeper Ppib as ΔCt. n= 4 for AT_2R and n= 6 for AT_1R and Mas.

4.4 Discussion

Here, the effects of Ang-(1-9) and Ang II on the isolated spontaneously beating and paced Langendorff-perfused rat heart were investigated. The results demonstrated that Ang II mediated little direct effects on cardiac contractility whereas Ang-(1-9) mediated a positive inotropic effect by increasing LVDP, dP/dt_{max} and dP/dt_{min}. The positive inotropic effect by Ang-(1-9) was attenuated by the AT_2R antagonist PD123319 and abolished by the AT_1R antagonist losartan. Furthermore, inhibition of PKA abolished the positive inotropic effects of Ang-(1-9) in the isolated rat heart. The results are summarised in Table 4-4.

Table 4-4. Summary of effects of Ang II and Ang-(1-9) in Langendorff-perfused rat hearts.

	Spontaneously beating					Paced			
	HR	LVDP	dP/dt_{max}	dP/dt_{min}	tau	LVDP	dP/dt_{max}	dP/dt_{min}	tau
1 µM Ang II	↑	–	–	↗	↓	↗	–	–	–
1 µM Ang-(1-9)	↘	↗	↗	↗	–	↑	↑	–	↑
PD123319 + Ang-(1-9)	↑	↗	–	–	–	↑	↑	–	–
Losartan + Ang-(1-9)	Not investigated					–	–	↓	–
H89 + Ang-(1-9)						↘	–	↓	–
K93 + Ang-(1-9)						↑	↑	–	–

↑/↓= sustained increase/decrease; ↗/↘= transient increase/decrease.

Here, it was identified that the contractile response of isolated rat hearts to Ang II and Ang-(1-9) infusion was partially influenced by whether the hearts was paced or allowed to beat spontaneously. Experimental design usually dictates whether hearts will need to be paced or are allowed to follow their natural rhythm during Langendorff perfusion. When the heart is allowed to beat spontaneously, it usually adopts a HR lower than observed *in vivo* due to the loss of nervous input (Bell *et al.*, 2011). Slowing of the HR intrinsically alters cardiac contractile function as described in the force-frequency relationship (FFR), also called Bowditch staircase and may complicate interpretation of results regarding

their relevance *in vivo* (Ross *et al.*, 1995). The FFR is an intrinsic mechanism of cardiac reserve during physiological stress and dictates that increases in frequency lead to an increase in contractile force (Ross *et al.*, 1995). This effect is due to an increased Ca^{2+} loading of the SR due to the high frequency of Ca^{2+} influx and a shorter time for Ca^{2+} extrusion by NCX (Bers, 2000). In large mammals, this relationship is biphasic with peak contractility at physiological frequencies before contractility declines at supraphysiological rates (Taylor *et al.*, 2004). A drug with chronotropic actions may alter cardiac function through the FFR and at high heart rates this can mask direct effects of the drug on cardiomyocyte contractility (Derumeaux *et al.*, 2008). In contrast, allowing the hearts to beat spontaneously may uncover unknown effects of a given drug on HR. For example, Masaki *et al.* (1998) demonstrated that Ang II increases HR in isolated Langendorff-perfused mouse hearts but this effect was absent *in vivo* (Masaki *et al.*, 1998). Removing HR as a variable through pacing is beneficial when assessing drugs with known chronotropic actions to uncover direct drug effects on the myocardium. Additionally, this allows a physiological preparation mimicking *in vivo* heart rates which does not suffer deterioration of HR over lengthy perfusion protocols.

In this study it was observed that Ang II mediates contrasting responses in spontaneously beating hearts and hearts maintained at a constant HR. In spontaneously beating hearts, Ang II mediated a positive chronotropic effect accompanied by a transient increase in dP/dt_{max}, dP/dt_{min} and a decrease in tau. This suggests an increase in inotropy and lusitropy while LVDP remained relatively unaffected. In contrast, in paced hearts, Ang II transiently increased LVDP but this was preceded by a decrease in dP/dt_{max}, dP/dt_{min} and an increase in tau collectively indicating a negative inotropic effect.

How Ang II mediates its positive chronotropic actions is still controversial. In the pithed rat the positive chronotropic actions of Ang II were similar to those observed in animals with intact autonomic control (Li *et al.*, 1996) confirming that the positive chronotropic actions of Ang II are largely independent of central actions. However, it is yet unclear whether Ang II predominantly mediates its chronotropic effect by altering Ca^{2+} and other ionic fluxes in ventricular cardiomyocytes or sinoatrial pacemaker cells. In isolated ventricular cardiomyocytes, Ang II has been shown to increase the frequency of spontaneous

contractions and L-type Ca^{2+} channel current in the mouse (Liang *et al.*, 2010, Masaki *et al.*, 1998), rat (Allen *et al.*, 1988, Touyz *et al.*, 1996b), chicken (Bkaily *et al.*, 2005) and cat (Aiello and Cingolani, 2001, Salas *et al.*, 2001) in an AT_1R-dependent manner. Similarly, in rat and mouse right atrial preparations, the location of the SA node, Ang II mediated positive chronotropy by binding the AT_1R receptor (Mori and Hashimoto, 2006, Li *et al.*, 1996) and direct injection of Ang II into the canine sinus node artery increased HR in a manner involving the AT_1R and L-type Ca^{2+} channels (Lambert, 1995). In contrast, however, in guinea pig and rabbit SA pacemaker cells, Ang II was reported to decrease spontaneous firing by inhibiting the L-type Ca^{2+} channel current suggesting that species-specific differences exist (Habuchi *et al.*, 1995, Sheng *et al.*, 2011). Since in Langendorff perfusion, both, the SA node and ventricular cardiomyocytes are equally exposed to Ang II in the perfusate and the organ bath, it is likely that Ang II activates both SA node cells and cardiomyocytes which may contribute to the positive chronotropic and ultimately pro-arrhythmic effects of Ang II (Wagner *et al.*, 2014).

Previous studies of Ang II have presented controversial data on the inotropism of Ang II in various heart preparations. While it has been suggested that Ang II is a positive inotrope in rabbits and pigs *via* a mechanism that involves the AT_1R and phosphoinositide hydrolysis (Ishihata and Endoh, 1995, Broomé *et al.*, 2001), others have shown that, for example in mice and humans, Ang II acts as a negative inotrope or has no effect at all (Holubarsch *et al.*, 1993, Sekine *et al.*, 1999, Sakurai *et al.*, 2002). The contrasting observations are most likely due to species specificity and experimental differences and therefore make direct comparisons difficult. Ishihata & Endoh (1995) previously demonstrated that in ventricular muscle preparations from dogs, rats and ferrets but not rabbit, Ang II failed to induce an inotropic effect despite its ability to mediate phosphoinositide hydrolysis which is linked to PKC activation and stimulation of Ca^{2+} transients *via* the L-type Ca^{2+} channel (Ishihata and Endoh, 1995, Kamp and Hell, 2000, Aiello and Cingolani, 2001, Salas *et al.*, 2001). Similar observations have also been made in human atrial and ventricular preparations (Holubarsch *et al.*, 1993). Interestingly, it was previously demonstrated that the inotropic response to Ang II switches during development and while Ang II significantly increased cardiac contractile force in right ventricular heart strips from neonatal

mice it decreased in the adult (Sekine *et al.*, 1999). In contrast to neonatal cardiomyocytes stimulated with endothelin-1, in adult rat cardiomyocytes no changes in intracellular Ca^{2+} were observed with Ang II stimulation and this was concomitant with observations on cell shortening which remained unaltered with Ang II stimulation (Lefroy *et al.*, 1996, Touyz *et al.*, 1996a).

The positive chronotropic and vasoconstrictive actions of Ang II in organ preparations are well established and given the evidence on a lack of positive inotropic actions of Ang II in the rat demonstrated here and by others (Ishihata and Endoh, 1995), it can be hypothesised that Ang II mediates very few direct effects on the rat myocardium and the majority of contractile effects by Ang II are due to its effects on HR and coronary vascular dynamics. Therefore, in the spontaneously beating heart, evidence suggests that while HR may drive an increase in cardiac contractile function, this is offset by the vasoconstrictive effects of Ang II. As discussed previously, in isolated heart and ventricular preparations, increases in stimulation frequency lead to an increase in contractile force, the FFR. In rats and mice whose HR is intrinsically high and whose contractile force is primarily governed by Ca^{2+} release from the SR (Monasky and Janssen, 2009), negative FFR has been observed (Narayan *et al.*, 1995, Morii *et al.*, 1996) but a positive or unchanged FFR is evident in physiological preparations (Layland and Kentish, 1999, Taylor *et al.*, 2004, Georgakopoulos and Kass, 2001). The mean intrinsic rate of rat hearts in this study corresponds to a frequency of 4.6 Hz which increases to approximately 5 Hz upon Ang II perfusion and these frequencies are on the positive staircase of the rat FFR (Layland and Kentish, 1999, Joulin *et al.*, 2009). Increases in HR with Ang II perfusion in spontaneously beating hearts occur within 2 min before reaching steady state at 4 min at which point cardiac contractility and relaxation, measured by dP/dt_{max}, dP/dt_{min} and tau, respectively, is increased. Contractile changes in response to HR may take up to 3 min to reach steady state (Layland and Kentish, 1999) and it therefore can be assumed that the rise in cardiac contractility and lusitropy at 1 μM Ang II may be direct function of Ang II-induced increases in HR. The transient nature of this observation may be explained by the effects of Ang II on the coronary vasculature which offset the effects of HR and the FFR: Ang II is a potent vasoconstrictor and when applied to the isolated heart mediates a significant reduction in coronary flow peaking at

Ang II concentrations of 1 μM (Liang *et al.*, 2010, van Esch *et al.*, 2006, van Esch *et al.*, 2010, Aplin *et al.*, 2007). While HR usually increases coronary flow to increase oxygen and nutrient delivery (Heusch, 2008), vasoconstriction and the resulting decrease in blood flow decrease cardiac contractile function. As such, in Langendorff-perfused spontaneously beating mouse hearts, Ang II was observed to induce a significant reduction in coronary flow despite a peak increase in heart rate by 71 bpm (Liang *et al.*, 2010). Since LVDP and cardiac contractile function are in part governed by coronary flow (Opie, 1965), Ang II mediated vasoconstriction may therefore counteract the FFR by reducing cardiac contractile performance before reaching a new steady state of vasodilation after longer perfusion periods induced by the release of vasodilators and Ang II receptor desensitisation (Pörsti *et al.*, 1993).

In line with this hypothesis, in hearts maintained at a constant HR, Ang II-mediated changes in cardiac chronotropy are prevented and therefore, force-frequency mediated changes in cardiac contractility are removed. This would suggest that in paced hearts, Ang II-mediated changes in cardiac contractility are largely dependent on coronary vascular dynamics. Although vascular autoregulation is overridden in constant flow Langendorff preparations and therefore does not allow flow adaptations to changes in workload and ischaemia, the coronary vascular dynamics in response to vasoactive drugs such as Ang II can be assessed by measuring coronary perfusion pressure (Bell *et al.*, 2011). In isolated constant-flow perfused rabbit hearts, Ang II mediates a biphasic response in cardiac contractility with an initial decrease in LVDP that is concomitant with an increase in coronary perfusion pressure (i.e. a reduction in coronary flow) followed by a period of vasodilation and increase in LVDP that returned to near basal levels after 9 min of perfusion (Pörsti *et al.*, 1993). This response shares some similarity with the response observed here in paced rat hearts where a transient increase in LVDP was preceded by a significant reduction in cardiac contractility and relaxation although a decrease in LVDP was not observed. A similar response to Ang II has also been observed in spontaneously beating mouse hearts albeit over a different time-course (Liang *et al.*, 2010) and therefore, it can be assumed that the vascular effects of Ang II contribute significantly to the response observed in paced rat hearts. Coronary dynamics have not been assessed in this study by measuring perfusion pressure

and therefore it cannot be directly verified that in the rat, Ang II modulates the coronary microvasculature in a similar manner to the rabbit and this would be of interest for future studies.

In hearts perfused with Ang-(1-9) a positive inotropic response was observed and the nature of this response was dependent on HR. In spontaneously beating hearts, perfusion with Ang-(1-9) induced a transient positive inotropic effect peaking at 4 min of perfusion. This effect was partially inhibited by the AT_2R antagonist PD123319 but this led to a significant increase in HR. In contrast, in hearts maintained at a constant HR, Ang-(1-9) induced a sustained inotropic effect that was resistant to AT_2R inhibition by PD123319 but could be blocked by the AT_1R antagonist losartan. These contrasting observations suggest a complex interaction between Ang-(1-9) and the AT_1R and AT_2R.

As previously discussed, investigations in spontaneously beating hearts are often complicated and confounded by drug effects on HR. While Ang-(1-9) itself induced a transient decrease in HR and only increased HR after longer perfusion times, in the presence of PD123319, Ang-(1-9) significantly increased HR within 2 min. This suggests that in the presence of an AT_2R antagonist, Ang-(1-9) may bind to the AT_1R to mediate positive chronotropic effects similar to Ang II. As HR can significantly alter cardiac contractile parameters and high HRs have been shown to confound changes in cardiac contractility (Derumeaux *et al.*, 2008, Taylor *et al.*, 2004), the modulation in HR by Ang-(1-9) in the presence of PD123319 may result in the contrasting observation of AT_2R blockade in paced and spontaneously beating hearts.

On a molecular level, two possibilities exist for modulation of EC coupling by angiotensin receptors: Alterations in intracellular Ca^{2+} haemodynamics or modulation of myofilament proteins. The former include modulations of ion channels and receptors involved in intracellular Ca^{2+} homeostasis and include the L-type Ca^{2+} channel, the RyR, SERCA and phospholamban. The latter includes modulation of cross-link formation and the Ca^{2+} sensitivity of myofilaments targeting troponin I and myosin light chain. While the AT_1R can modulate cardiac contractility by activation of PKC, as previously discussed, little is known about the role of the AT_2R in cardiac contractility. The AT_2R is an atypical GPCR and is not linked to activation of any G-protein but rather mediates activation of cGMP,

NO and protein phosphatases such as PP2A and SHP1. PP2A, like PP1, is a major phosphatases regulating EC-coupling and its targets include the L-type Ca^{2+} channel, RyR, NCX and cardiac troponin I (Lei *et al.*, 2015). PP2A activity is usually associated with a decrease in inotropy and lusitropy exemplified by the attenuation of ß-adrenergic signalling *via* dephosphorylation of the L-type Ca^{2+} channel as well as the myofilament proteins troponin I, myosin-binding protein C and myosin light chain 2 (Kirchhefer *et al.*, 2014, Davare *et al.*, 2000). The net effect is a decrease in Ca^{2+} transients alongside an increase in myofilament Ca^{2+} sensitivity, decreasing contraction and relaxation (Kirchhefer *et al.*, 2014, Davare *et al.*, 2000). Additionally, dephosphorylation of the RyR by PP2A stimulates Ca^{2+} release and decreases SR Ca^{2+} content (Terentyev *et al.*, 2003). In contrast, the effects of cGMP and NO in the heart are complex (Massion *et al.*, 2003). While NO may increase cardiac contractility indirectly by increasing coronary flow, endogenous and exogenous NO in cardiomyocytes exhibits a bimodal effect on cardiac contractility (Mohan *et al.*, 1996, Pellegrino *et al.*, 2009) . At physiological concentrations, NO acts as a positive inotrope possibly by increasing cardiac Ca^{2+} transients *via* cGMP-dependent inhibition of cAMP phosphodiesterases, while at high concentrations, NO is a negative inotrope by shortening twitch duration and contractile force *via* cGMP-PKG pathways (Mohan *et al.*, 1996, Pellegrino *et al.*, 2009). Barouch *et al.* (2002) demonstrated that in cardiomyocytes, NOS1 selectively associates with the RyR to facilitate SR Ca^{2+} release (Barouch *et al.*, 2002). In contrast, NOS3 is associated with the L-type Ca^{2+} channel where it negatively regulates ß-adrenergic inotropy suggesting that NO signals in microdomains and the final outcome is dependent on selective activation of NOS isoforms (Barouch *et al.*, 2002). cGMP has largely been associated with negative inotropic effects (Layland *et al.*, 2002, Flesch *et al.*, 1997) and an increase in cellular cGMP decreases spontaneous contractile frequency in isolated cardiomyocytes (Balligand *et al.*, 1993), in similarity to the transient fall in HR observed here with Ang-(1-9). While this may suggest an involvement of AT_2R mediated signalling pathways in the inotropic response of Ang-(1-9), given the complex nature of the data and observations that 1) AT_2R activation was demonstrated to counteract Ang II-induced inotropy (Masaki *et al.*, 1998, Castro-Chaves *et al.*, 2008) and 2) the AT_1R and AT_2R can heterodimerize to form a signalling network (AbdAlla *et al.*, 2001, van Esch *et al.*, 2006), further experiments, including dual blockade of the AT_1R and AT_2R,

and assessment of EC coupling in isolated cardiomyocytes are needed to definitively elucidate the receptors and signalling pathways mediating the positive inotropic actions of Ang-(1-9).

In paced hearts, it was identified that Ang-(1-9) mediates its positive inotropic actions by interacting with the AT_1R. Ang-(1-9) can bind the AT_1R and AT_2R with equal affinities but its affinity for the AT_1R is 100-fold lower than Ang II (Flores-Muñoz *et al.*, 2011). The data here shows that in rat hearts, the expression of the AT_1R is nearly 2-fold higher than the AT_2R corresponding with the low expression of the AT_2R in the adult. In support of the observation that Ang-(1-9) is acting through the AT_1R is the observation that in the presence of Ang II, Ang-(1-9) failed to elicit an increase in inotropy seen during Ang-(1-9) application alone in spontaneously beating hearts suggesting that Ang-(1-9) is competing with Ang II for receptor occupation and Ang II in this instance may be acting as a competitive inhibitor. If Ang-(1-9) is acting through the AT_1R, this raises the question as to why, despite engaging the same receptor, Ang II and Ang-(1-9) mediate contrasting effects on cardiac contractility. There are two possibilities that stand to reason: biased agonist activity/ functional selectivity or receptor modulation and dimerization. The potential of ligands to stabilise a given receptor in certain conformations eliciting distinct signalling pathways, called biased agonism or functional selectivity, has been explored increasingly (Rajagopal *et al.*, 2010). As discussed previously in Section 1.3.5 biased agonism at the AT_1R has also been characterised. Full activation of the AT_1R by Ang II is particularly governed by interactions of Asp1, Tyr4 and Phe8 with the receptor and modifications of these amino acids to Sar1, Ile4, Ile8 (SII) prevents G-protein and Ca^{2+} mobilisation by the AT_1R while selectively engaging ß-arrestin signalling (Miura and Karnik, 1999). Selectively engaging the AT_1R with SII increases inotropy and lusitropy in isolated mouse cardiomyocytes distinct from Ang II and independent of Ca^{2+} mobilisation and PKC activation (Rajagopal *et al.*, 2006). In a similar manner, the synthetic peroxisome proliferator-activated receptor γ agonist troglitazone has been characterised as a biased agonist at the AT_1R, mediating an increase in FS in isolated mouse cardiomyocytes in a ß-arrestin2-depedent and G_q-independent pathway (Tilley *et al.*, 2010). This has been extrapolated to *in vivo* observations where the two synthetic peptides TRV120023 and TRV120027 increased cardiac contractility while simultaneously

decreasing BP, contrasting normal ARBs which negatively affected cardiac contractile function (Violin *et al.*, 2010). Specifically, the positive inotropic actions of TRV120023 in a model of dilated cardiomyopathy were due to an increase in the phosphorylation of myosin light chain 2 increasing cardiac output and stroke work despite no change in LVDP (Tarigopula *et al.*, 2015). These observations suggest the potential of Ang-(1-9) to show functional selectivity at the AT_1R. The possibilities of selective modulation of a receptor range from allosteric modulation to function as a dualsteric ligand (Smith *et al.*, 2011). One example of allosteric modulation by Ang-(1-9) is the re-sensitisation of the bradykinin receptor by allosteric modulation of the ACE active domains interacting with the B_2 receptor (Deddish *et al.*, 1998, Marcic *et al.*, 1999, Chen *et al.*, 2005). Ang-(1-9) is an inhibitor of ACE (Kokkonen *et al.*, 1997) and in a similar manner to the B_2 receptor may allosterically modulate the AT_1R *via* an interaction with ACE stabilising the AT_1R at the plasma membrane and preventing de-sensitisation (Chen *et al.*, 2005). Interestingly, the AT_2R has previously been shown to inhibit cardiac fibrosis by stimulation of bradykinin release while bradykinin itself can act as a positive inotrope (Munch and Longhurst, 1991). Both, the AT_2R and AT_1R form heterodimers with the B_2 receptor and especially AT_1R-B_2 dimerisation has been shown to significantly enhance AT_1R signal transduction (Abadir *et al.*, 2006, AbdAlla *et al.*, 2000). Whether such interactions also occur in the heart needs to be established and their potential in modulating the cardiac effects of Ang II and Ang-(1-9) investigated. Overall, this evidence highlights the complexity in the signalling of angiotensin peptides which make direct assessments of RAS signalling in isolation using specific receptor antagonists difficult. Future studies are needed to assess the potential of Ang-(1-9) to act as a biased agonist on the AT_1R by assessment of activated signalling pathways, G-protein and ß-arrestin dependency and tracing of ligand-receptor interactions. Furthermore, the contributions of bradykinin, and receptor interactions by formation of homo- and heterodimers in this process should be investigated.

Using perfusion with H89, it was shown that the positive inotropic effects by Ang-(1-9) are due to PKA-mediated changes in EC-coupling. PKA is a holoenzyme consisting of two catalytic subunits bound by 2 regulatory subunits that inhibit PKA enzymatic activity. The canonical pathway of PKA activation involves the

activation of the stimulatory G protein G_s which stimulates adenylate cyclase to increase production in cAMP. The binding of cAMP to the regulatory subunits of PKA leads to their dissociation and subsequent activation of PKA (Dulin *et al.*, 2001). This PKA pathway is classically activated by $ß_1$-adrenergic stimulation in cardiomyocytes mediating positive inotropic and lusitropic actions (Kamp and Hell, 2000). Here, Ang-(1-9) was shown to mediate its positive inotropic actions *via* a pathway involving the AT_1R and PKA but not its proposed receptor the AT_2R. The AT_2R is an atypical GPCR linked to the activation of phosphatases such as PP2A, NO release as well as cGMP formation and PKG activation, all of which have been shown to counteract target activation by PKA (Nouet and Nahmias, 2000, Kamp and Hell, 2000), confirming that it is unlikely the mediator of PKA activation in cardiomyocytes. The AT_1R classically has been shown to couple to the G proteins $G_{q/11}$, G_i and $G_{12/13}$ but not G_s and hence would be unable to activate PKA *via* the canonical pathway but instead has the ability to inhibit adenylate cyclase and cAMP formation (Higuchi *et al.*, 2007). In line with this, ample evidence suggests that in cardiomyocytes, activation of the AT_1R is linked to the G-protein G_q activating PKC which mediates the inotropic effects in response to Ang II binding (Kamp and Hell, 2000, Salas *et al.*, 2001, Liang *et al.*, 2010). However, it has been shown that PKA can be activated in G_s and cAMP-independent pathways involving G_{13} and AKAP110 or Nox2 (Niu *et al.*, 2001, Wagner *et al.*, 2014). Additionally, it has been shown that vasoactive peptides such as Ang II and ET-1 can activate PKA in a cAMP-independent mechanism involving degradation of IκB in VSMC (Dulin *et al.*, 2001) suggesting that the AT_1R has the potential of activating PKA in cAMP independent pathways. In cardiomyocytes, the phosphorylation targets of PKA include the L-type Ca^{2+} channel, RyR, phospholamban and troponin I, all of which collectively mediate an increase in Ca^{2+} transient amplitude and extrusion resulting in positive inotropy and lusitropy. Ang-(1-9) stimulation mediated positive inotropy as seen by an increase in LVDP and dP/dt_{max}, however, the rate of relaxation was less affected and indeed, isovolumetric relaxation time, tau, tended to increase suggesting impaired relaxation. This corresponds to observations made with $ß_2$-adrenergic stimulation where PKA–mediated phosphorylation of phospholamban and troponin I cannot be observed resulting in slower relaxation time (Xiao and Lakatta, 1993, Kuschel *et al.*, 1999). A J-shaped relationship between changes in LVP (due to increased afterload) and tau have previously been observed in the

dog and mouse where tau begins to exponentially increase after reaching an inflection point of LVP increase while contraction time tended to increase (Leite-Moreira and Gillebert, 1994, Yang *et al.*, 2013a). This corresponds to observations made here where tau increased concomitant with LVDP in response to Ang-(1-9). An increase in isovolumetric relaxation time suggests a decrease in the mechanism of Ca^{2+} extrusion including SR Ca^{2+}-reuptake by SERCA and sarcoplasmic Ca^{2+} extrusion by NCX (Bers, 2002). In cat myocytes Salas *et al.* (2001) previously demonstrated that Ang II *via* the AT_1R mediates negative lusitropy by elongation of the action potential and a decreased extrusion of Ca^{2+} by NCX. The increase in tau was equally blocked by PD123319, losartan, K93 and H89 suggesting a complex interplay between the AT_1R, AT_2R, CaMKII and PKA. The AT_1R and AT_2R have previously been shown to form dimers and can also signal in a complex with the Mas receptor (Castro *et al.*, 2005). Indeed, interplay of the AT_1R, PKA and CaMKII mediating Ang II-induced arrhythmias has recently been demonstrated (Wagner *et al.*, 2014). In this study, Ang II mediated the cAMP-independent activation of PKA and CaMKII *via* Nox2 resulting in an increase in the Ca^{2+} and Na^{+} current and RyR-dependent diastolic Ca^{2+} leak, respectively which may also collectively lead to a decrease in Ca^{2+} extrusion and slower relaxation time (Wagner *et al.*, 2014).

Recent data from our group suggests that in isolated mouse cardiomyocytes, Ang-(1-9) increases Ca^{2+} transient amplitude *via* an increase in L-type Ca^{2+} current (Fattah et al, unpublished). In line with this, the L-type Ca^{2+} channel has been shown to be phosphorylated by PKA on its α_{1c} (Ser1928) and $ß_{2a}$ (Ser459, Ser 478, Ser479) subunit which increase the available fraction and opening probability of channels during depolarisation (Kamp and Hell, 2000, Bünemann *et al.*, 1999). Ang II has already been shown to increase L-type Ca^{2+} current in various animal models mainly by the activation of PKC (Salas *et al.*, 2001, Aiello and Cingolani, 2001, Liang *et al.*, 2010). Furthermore, enhanced coupling of the AT_1R with L-type Ca^{2+} channels has been reported in the aortas of diabetic rats (Arun *et al.*, 2005) confirming a functional link. More recently, Ang-(1-7) was also shown to activate the L-type Ca^{2+} current in a PKA-dependent manner when applied intracellularly in rat ventricular cardiomyocytes (De Mello, 2015) and in cardiomyocytes from rats with HF (Zhou *et al.*, 2015). This suggests that the

activation of the L-type Ca^{2+} channel and PKA may be a mechanism that is global to peptides of the RAS albeit with different outcomes on cell behaviour.

Thr-197 phosphorylation is required for optimal PKA enzyme activity (Adams *et al.*, 1995). However, here no significant difference was found in Thr-197 phosphorylation of PKA in cardiomyocytes stimulated with Ang-(1-9) and similarly, forskolin did not alter PKA phosphorylation. PKA is a unique enzyme as it is assembled as an active enzyme with a fully phosphorylated activation loop and is regulated by holoenzyme formation dependent on cAMP. The catalytic subunit is always found fully phosphorylated when purified from mammalian tissue and hence suggests that although no changes in PKA phosphorylation were detectable, this is not a direct measure of PKA activation (Moore *et al.*, 2002). PKA activity can be assessed by PKA substrate antibodies or specifically by the phosphorylation of vasodilator-stimulated phosphoprotein (VASP) in an electrophoretic mobility shift assay (Dulin *et al.*, 2001) and this would be of interest to verify PKA activity in response to Ang-(1-9).

4.5 Summary

Ex vivo Langendorff perfusion is the gold standard for the assessment of cardiac contractile function in the absence of systemic effects. Perfusion of isolated rat hearts with Ang-(1-9) conveyed positive inotropy with an increase in LVDP, dP/dt_{max} and dP/dt_{min}. This effect was mediated by both, the AT_1R and AT_2R with activation of PKA. In contrast, Ang II and Ang-(1-7) had little effect on cardiac contractility. These results suggest a direct effect of Ang-(1-9) on the heart distinct from the related peptides Ang II and Ang-(1-7) which may contribute to the beneficial effects of Ang-(1-9) in the heart.

Chapter 5 – Characterisation of EndMT in Ang II-induced cardiac remodelling *in vivo* and its role in TGFβ-induced EndMT *in vitro*

5.1 Introduction

5.1.1 Endothelial-to-mesenchymal transition

ECs form the inner lining of blood vessels separating the blood from the underlying VSMCs and therefore have an important gate-keeping function. ECs are characterised by the expression of cluster of differentiation (CD) 31 [also known as platelet endothelial adhesion molecule-1 (PECAM-1)] and vascular endothelial (VE)-cadherin both of which are crucial for the transduction of changes in blood flow to the endothelial cytoskeleton to mediate endothelial alignment with the flow of blood (Tzima *et al.*, 2005). Endothelial plasticity is important for the maintenance of normal vascular function to facilitate changes in blood flow. One extreme form of endothelial plasticity is EndMT which has been demonstrated to play a crucial role in cardiac development and disease.

EndMT describes the process during which ECs transdifferentiate into mesenchymal cells such as fibroblasts and VSMCs (Garside *et al.*, 2013). During this process, ECs delaminate from the layer of ECs and infiltrate the underlying tissue. This is accompanied by a loss in cell-cell junctions, cell polarity and changes in cytoskeletal dynamics eliciting increased motility (Yoshimatsu and Watabe, 2011). On a molecular level, cells lose expression of EC-specific markers such as CD31 and VE-cadherin (Frid *et al.*, 2002). Parallel to these changes, cells also gain expression of mesenchymal markers such as FSP1, αSMA, calponin and smooth muscle (SM)22-α (also known as transgelin) which are part of the contractile apparatus of smooth muscle and other mesenchymal cells. This process is predominantly governed by TGFß signalling (Goumans *et al.*, 2008). EndMT is a specific form of epithelial-to-mesenchymal transition (EMT) which has been extensively studied both on a molecular level and in physiological and pathological settings (Lamouille *et al.*, 2014). Physiological EndMT is primarily involved in the formation of the cardiac valves and the interventricular septum during cardiogenesis (Garside *et al.*, 2013). Pathological EndMT has been demonstrated in various fibrotic diseases including renal and hepatic fibrosis, cancer and CVDs (Zeisberg *et al.*, 2007a, Zeisberg *et al.*, 2007c, Zeisberg *et al.*, 2008, Zeisberg *et al.*, 2007b).

5.1.2 EndMT in cardiovascular disease

In the past experimental efforts focussed on the understanding of EndMT in the embryo and it was thought that EndMT in the adult was very rare (Piera-Velazquez *et al.*, 2011). The first pioneering study demonstrating the occurrence of EndMT in adult endothelium was demonstrated by Arciniegas *et al.* in 1992 (Arciniegas *et al.*, 1992) who cultured bovine aortic ECs for up to 20 days in the presence of $TGF\beta_1$. At the end of the protocol up to 90 % of ECs were found to have irreversibly lost their EC phenotype, be αSMA positive and had differentiated into mature contractile SMC. This was further corroborated by Frid *et al.* (2002) who used fluorescence activated cell sorting to obtain a pure culture of bovine aortic EC and when maintained in culture, these cells were found to spontaneously transition to mesenchymal cells with a differentiated smooth muscle phenotype (Frid *et al.*, 2002). This phenotypic switch was found to be dependent on $TGF\beta_1$ and only occurred in cells cultured on tissue plastic but not on denatured collagen, suggesting that the matrix is inhibitory to mesenchymal transition. The phenotypic switch could however be activated by addition of $TGF\beta_1$ to the culture (Frid *et al.*, 2002). Similarly, Ishisaki *et al.* (2003) provided evidence that ECs from the venous system retain the potential to transform into smooth muscle like cells. In this study, they deprived human umbilical vein ECs of fibroblast growth factor 1 (FGF-1) which can be routinely added as a growth supplement to EC cultures. After several weeks in culture they identified that ECs switched on a mesenchymal gene expression profile with increases in calponin and SM22-α and were able to contract collagen gels when stimulated with ET-1 (Ishisaki *et al.*, 2003). This spontaneous transition was thought to be mediated by increases in activin A, a member of the TGFβ superfamily, and highlights the plasticity of ECs to adjust to changes in their environment which may also occur during disease development.

An increasing body of evidence now suggests that EndMT can also occur postnatally as a feature of various pathologies such as fibrosis and cancer (Zeisberg *et al.*, 2007a, Zeisberg *et al.*, 2008). Similar to the embryonic gene expression program activated during cardiac hypertrophy, it has been postulated that pathological EndMT in the adult, recapitulates the embryonic developmental process. As discussed in detail in Section 1.4.2 tissue fibrosis is characterised by the disordered and excessive deposition of ECM by persistently

activated fibroblasts which results in the disruption of normal tissue architecture and ultimately leads to organ dysfunction. In a hallmark study, Zeisberg *et al.* (2007b) provided evidence that EndMT significantly contributes to cardiac fibrosis in the pressure-overloaded heart (Zeisberg *et al.*, 2007b). Using endothelial lineage tracing by employing Cre-lox technology under the *Tie1* promoter which encodes for a vascular endothelium specific receptor tyrosine kinase involved in angiogenesis (Korhonen *et al.*, 1994), they identified that up to 30 % of fibroblasts positive for either FSP1 or αSMA in the fibrotic heart were derived from endothelial origin. This was found to be partially due to signalling through the TGFß$_1$-SMAD3 axis and could be prevented by administration of BMP7 (Zeisberg *et al.*, 2007b). Since then, EndMT as a source of fibroblasts has been confirmed in several other models of cardiac fibrosis. In a model of streptozotocin-induced diabetes, EndMT was found to contribute to the increase in perivascular cardiac fibrosis and a reduction in myocardial capillary density where up to 20 % of the S100A4-positive fibroblast population was found to also express CD31 (Widyantoro *et al.*, 2010). This phenotype was abolished by endothelial-specific deletion of ET-1 and could be recapitulated in human ECs cultured in high glucose conditions *in vitro* by ET-1 knockdown. This was found to be due to the reciprocal increase of ET-1 and TGFß in high glucose conditions leading to phosphorylation of SMAD3 and Akt activation which could be abolished by TGFß neutralising antibodies (Widyantoro *et al.*, 2010). Furthermore, EndMT was shown to contribute to the pathogenesis of endocardial fibroelastosis, a rare disorder usually occurring in young children characterised by the aberrant deposition of fibrous tissue in the endocardial layer leading to thickening of the ventricular wall and impairment of cardiac contractile function (Xu *et al.*, 2015). Dyssynchronous contraction of the ventricles due to contraction delay is a common phenomenon of HF. In a model of canine dyssynchronous HF, Mai *et al.* (2015) recently showed that the increases in cardiac fibrosis especially in the LV lateral wall were partially due to an increase in EndMT which could be modelled *in vitro* by exposing ECs to cyclic stretch correlating to previous reports on the role of fluid shear stress on EndMT (Egorova *et al.*, 2011, Moonen *et al.*, 2015, Mai *et al.*, 2015). Interestingly, cyclic stretch synergistically acted with TGFß$_1$ to induce EndMT and caused a greater transition than either of the factors alone (Mai *et al.*, 2015) suggesting a self-perpetuating axis of cardiac fibrosis *in vivo*. More controversially, EndMT was also present in aged mice with a genetic

deficiency of plasminogen activator inhibitor-I (Ghosh *et al.*, 2010) but its clinical relevance still needs to be determined. Interestingly, despite the widely accepted notion of a pathological role for EndMT in cardiac fibrosis, EndMT was shown to be activated during granulation tissue formation following MI (Aisagbonhi *et al.*, 2011) suggesting its involvement in neovascularisation and scar formation following the ischaemic insult. Partial EndMT with the loss of cell-cell contacts and cell polarity and the gain of a migratory phenotype is associated with neovascularisation and angiogenesis (Welch-Reardon *et al.*, 2015), suggesting that EndMT may act as a double-edged sword in cardiac remodelling.

5.1.3 The RAS in EndMT and EMT

The role of Ang II has been extensively assessed in renal EMT and its potent inductive role is well characterised. Ang II infusion in rats by osmotic minipumps leads to EMT within the renal tubules and can be replicated by *in vitro* stimulation of renal proximal tubular cells (HK2) with Ang II (Carvajal *et al.*, 2008). Ang II induces EMT in a time-and dose dependent manner and was able to downregulate E-cadherin and upregulate αSMA mRNA expression in NRK52E cells within 6 h of exposure (Yang *et al.*, 2009). This was correlated with a decrease in E-cadherin and increase in αSMA protein expression after 1 and 3 days of Ang II exposure, respectively and linked to the induction of CTGF by Ang II *via* SMAD3 (Yang *et al.*, 2010) which could be attenuated by CTGF antisense oligonucleotide (Chen *et al.*, 2006). Similarly, in an *in vitro* model of high glucose induced EMT using a renal proximal tubular epithelial cell line, exposure to high glucose for 24 or 48 h resulted in significant upregulation of components of the RAS including angiotensinogen, ACE and AT_1R which increased the secretion of Ang II into the cell culture medium (Zhou *et al.*, 2010). The AT_1R antagonist losartan blocked the phenotypic switch in the epithelial cells characterised by increases in vimentin, fibronectin and $TGFß_1$ secretion and a reduction in E-cadherin (Zhou *et al.*, 2010). Furthermore, Ang II has been demonstrated to be involved in EMT in other organs. For example, in a model of dermal fibrosis, Ang II infusion caused skin fibrosis at the site of subcutaneous infusion and co-localisation studies with VE-cadherin and FSP1 confirmed EMT was present in the skin lesions (Stawski *et al.*, 2012). This could be replicated by stimulating human dermal microvascular ECs with Ang II for 96 h (Stawski *et al.*, 2012). In cancer research,

Ang II was associated with increasing EMT in intrahepatic cholangiocarcinoma by activating the stromal cell-derived factor-1/CXCR4 signalling axis (Okamoto *et al.*, 2012) and in a recent abstract published by Oh *et al.* (2015), AT_1R overexpression in the MCF7 breast cancer cell line increased cell proliferation, migration and invasion which was accompanied with a mesenchymal cell phenotype (Oh *et al.*, 2015). Overall, these results indicate a potent role of Ang II in EMT in various diseases settings *in vitro* and *in vivo*.

In contrast, the role of Ang II in EndMT is less well understood. Recent advances in elucidating the contribution of the RAS in EndMT have been made by the use of AT_1R receptor antagonists. In human aortic ECs, high glucose conditions have been demonstrated to induce EndMT by elevating αSMA and FSP1 gene and protein expression (Tang *et al.*, 2010). This was associated with a significant increase in Ang II secretion. Inhibition of Ang II signalling with irbesartan reduced Ang II secretion and blocked mesenchymal gene expression, suggesting that Ang II mediates high glucose-induced EndMT (Tang *et al.*, 2010). This was further corroborated in an *in vivo* model of streptozotocin-induced diabetes in rats where administration of irbesartan not only reduced diabetes-induced adverse cardiac remodelling but also decreased the number of cells double-labelled for CD31 and FSP1 (Tang *et al.*, 2013). More recently, it has been demonstrated that the AT_1R antagonist losartan inhibits $TGFß_1$-induced EndMT in mitral valve ECs by inhibition of ERK phosphorylation while high concentrations of Ang II directly induced αSMA protein expression in valvular ECs which was linked to TGFß production (Wylie-Sears *et al.*, 2014). More recently, it was demonstrated that endothelial-specific overexpression of Nox2 promotes ECs to undergo EndMT in response to Ang II stimulation *in vivo* and *in vitro* thereby contributing to Ang II-induced cardiac fibrosis *in vivo* (Murdoch *et al.*, 2014). This suggests that ROS may play an important role in mediating EC transformation in various models of EMT and EndMT involving $TGFß_1$ and Ang II. Overall, these results demonstrate a role of Ang II in several models of EndMT, however, the direct effects of Ang II on mesenchymal gene expression in ECs has so far not been investigated in detail.

5.2 Aims

- Assess capillary density and EndMT in mice with Ang II-induced cardiac remodelling.

- Assess the role of the counter-regulatory RAS axis peptide Ang-(1-9) on myocardial capillary density and EndMT in Ang II-infused mice *in vivo*.

- Develop and characterise an *in vitro* model of EndMT to determine the role of Ang II in this process and identify signalling pathways that are modulated by Ang II.

5.3 Results

5.3.1 Capillary density in Angiotensin II-infused mice

Changes in the cardiac microvasculature have previously been described in patients with HHD (Mohammed *et al.*, 2015). To assess the state of the microvasculature in Ang II-dependent hypertension, cardiac capillary density was assessed in Ang II-infused mice from Section 3 by CD31 immunostaining and quantified as capillary density (capillaries/mm^2) and capillary/cardiomyocyte ratio (Figure 5-1, Table 5-1).

In control mice capillary density ranged from 2161 ± 111 capillaries/mm^2 at 4 weeks to 2894 ± 119 capillaries/mm^2 at 6 weeks with an estimated capillary/cardiomyocyte ratio between 1.1 ± 0.1 to 0.8 ± 0.1. Infusion of 24 µg/kg/hr Ang II for 2 weeks tended to reduce capillary density (control 2518 ± 209 *vs.* 24 µg/kg/hr Ang II 1775.0 ± 364, n= 6, p= 0.11) and capillary/cardiomyocyte ratio (control 1.1 ± 0.1 *vs.* 24 µg/kg/hr Ang II 0.7 ± 0.2, n= 6, p= 0.06) (Figure 5-1 B-C). After 4 weeks, microvascular rarefaction was apparent as a significant reduction in myocardial capillary density (control 2161 ± 111 *vs.* 24 µg/kg/hr Ang II 835.0 ± 132, n= 4, $p<0.05$) and capillary/cardiomyocyte ratio (Control 0.8 ± 0.1 vs 24 µg/kg/hr Ang II 0.3 ± 0.1, n= 4, $p<0.05$) and this was maintained until week 6. Infusion of 48 µg/kg/hr Ang II for 6 weeks tended to exacerbate microvascular rarefaction compared to the low dose of 24 µg/kg/hr Ang II (Table 5-1, Figure 5-1 B-C). At 2 weeks, capillary density tended to correlate with cardiac hypertrophy measured as

HW/TL (R^2= 0.24, p= 0.11) and at 4 weeks, there was a strong correlation between capillary density and cardiac hypertrophy with an overall R^2= 0.91 ($p<0.05$). This correlation was lost after 6 weeks with an R^2= 0.02 ($p>0.05$).

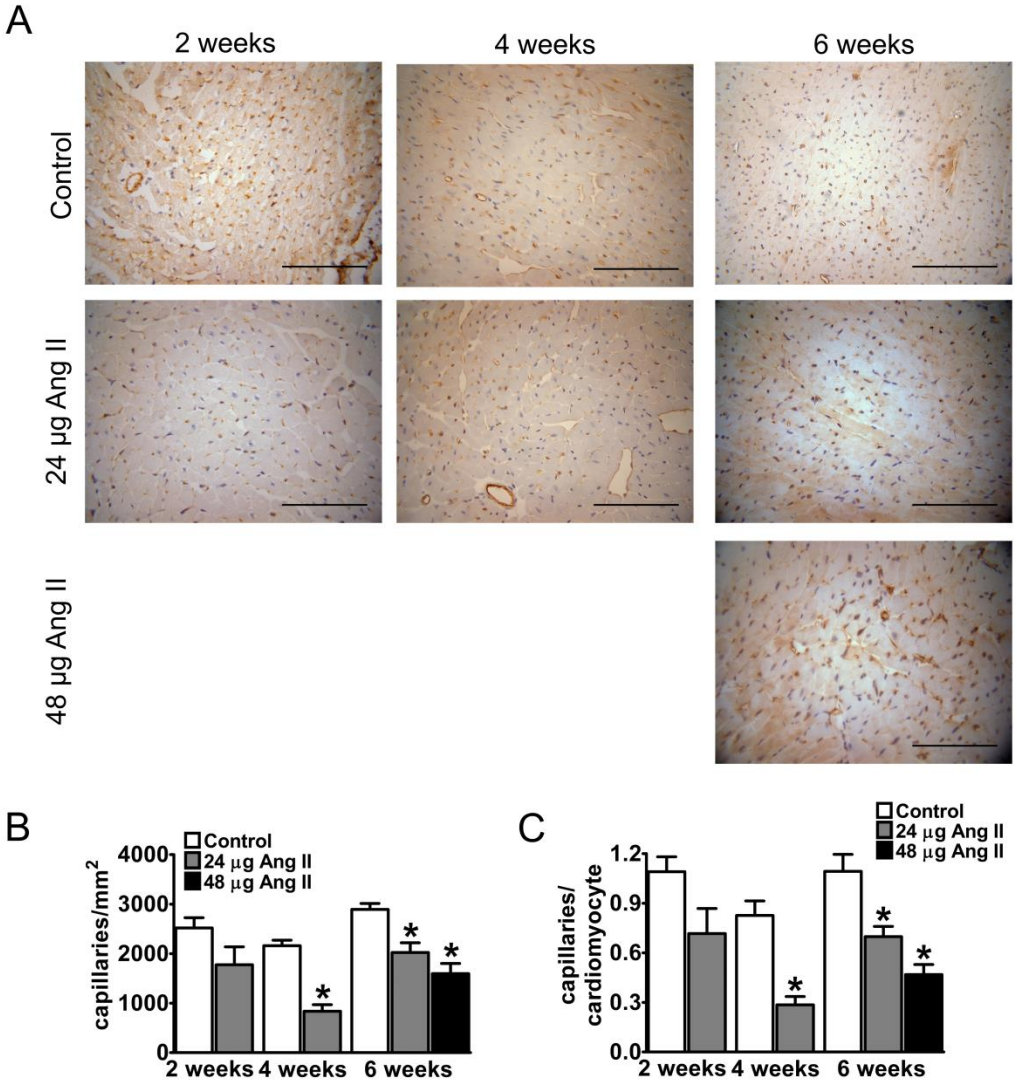

Figure 5-1. Capillary density in Ang II-infused mice.
(A) Capillary density was assessed by CD31 immunohistochemistry in mice infused with H_2O (control), 24 µg/kg/hr Ang II (24 µg Ang II) or 48 µg/kg/hr Ang II (48 µg Ang II) for 2–6 weeks. Capillaries were counted and expressed as (B) capillaries/mm^2 and (C) capillaries/cardiomyocyte. n= 6 and 4 at 2 and 4 weeks, respectively and n= 11, 10, 3 for control, 24 µg/kg/hr and 48 µg/kg/hr Ang II, respectively at 6 weeks. Histological sections for animals at 2 weeks were provided by Dr Monica Flores-Munoz. Data are presented as mean ± SEM.Scale bar: 100 µm. *<0.05 vs. time-matched control (Student's t-test and ANOVA with Tukey's post-hoc analysis).

Table 5-1. Microvascular characteristics in hearts of Ang II-infused mice after 6 weeks

	Capillaries/mm^2				Capillaries/cardiomyocyte			
	MEAN	SEM	n	p-value	MEAN	SEM	n	p-value
Control	2894	119	11		1.09	0.10	11	
24 µg/kg/hr Ang II	2023	197	10	<0.01	0.70	0.06	10	<0.01
48 µg/kg/hr Ang II	1597	206	3	<0.01	0.47	0.06	3	<0.01

p-value *vs*. control

5.3.2 Endothelial-to-mesenchymal transition in mouse hearts

To investigate the occurrence of EndMT in the hearts of Ang II-infused mice which may contribute to the loss in capillary density, cardiac sections from a subset of Ang II-infused mice from Section 3 were stained for the EC marker CD31 and the fibroblast markers S100A4 (FSP1) or αSMA (Figure 5-2). Co-localisation was assessed using Pearson's coefficient R and Mander's coefficients M1 and M2 which provide a measure of the linearity and ratio of overlap of the two channels, respectively (Table 5-2, Table 5-3).

At 4 weeks, co-expression of CD31 and S100A4 was apparent in the hearts of Ang II-infused mice (Figure 5-2 A) and this was reflected in a significant increase of Pearson's coefficient R which significantly correlated with the decrease in capillary density during Ang II infusion (R^2= 0.59, $p<0.05$). Similarly, Mander's M1 and M2 ratios of co-localisation between CD31 and S100A4 were significantly increased ($p<0.05$) (Table 5-2). In contrast, αSMA only partially co-localised with CD31 and no significant increase in Pearson's and Mander's coefficients of co-localisation was detected (Figure 5-2 A, Table 5-2). Following 6 weeks of Ang II infusion, co-expression of CD31 and S100A4 was still apparent (Figure 5-2 B) and reflected in an increase in the coefficients of co-localisation (Table 5-3). Infusion with a high dose of Ang II (48 µg/kg/hr) significantly increased the co-expression of CD31 and S100A4 or αSMA as measured by Pearson's R (Table 5-3). However, 24 µg/kg/hr AngII infusion did not induce significant co-expression of CD31 with either S100A4 or αSMA after 6 weeks (Table 5-3).

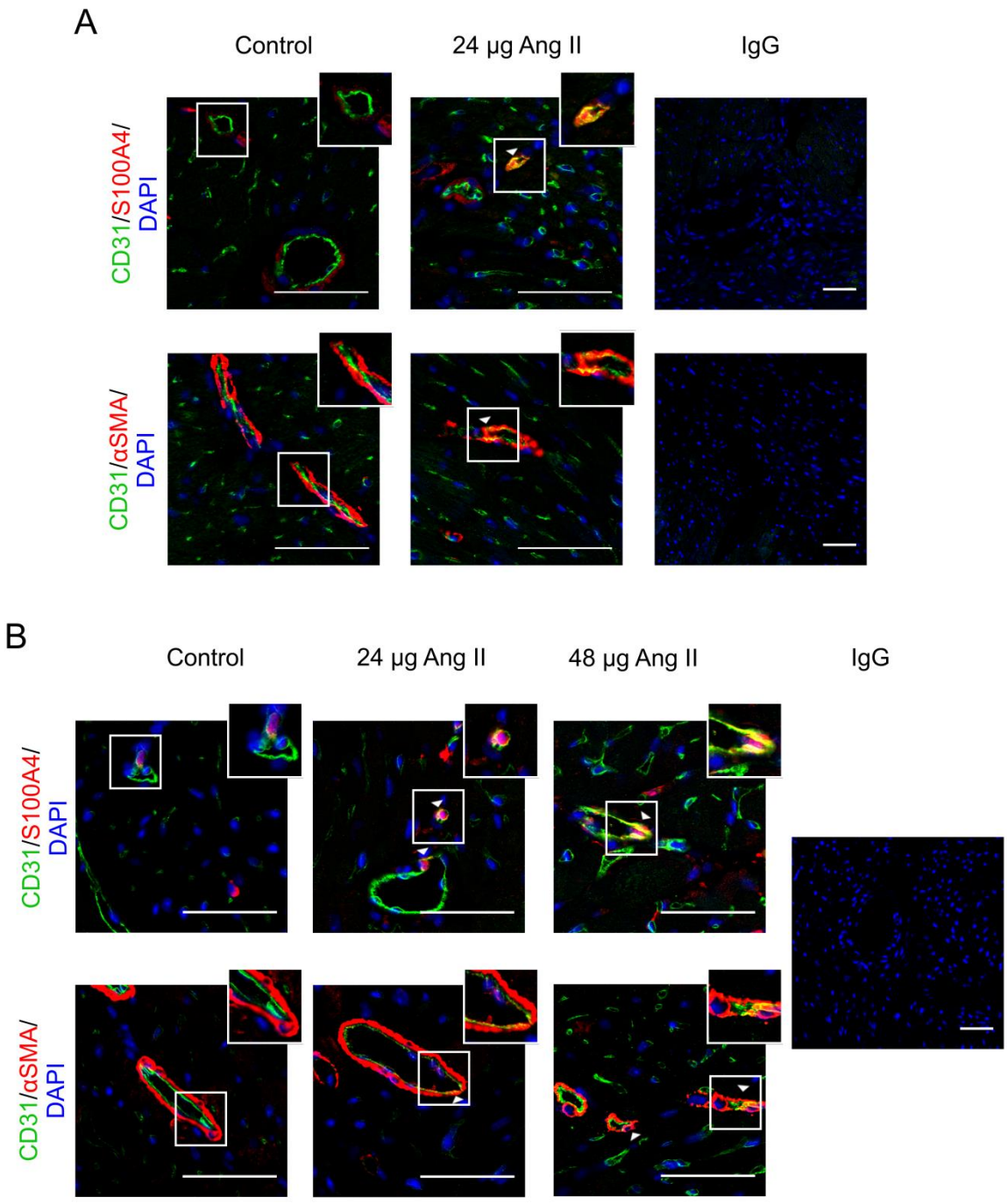

Figure 5-2. EndMT in hearts of Ang II-infused mice
Cardiac sections of mice infused with H_2O (control), 24 µg/kg/hr Ang II (24 µg Ang II) or 48 µg/kg/hr (48 µg Ang II)for (A) 4 or (B) 6 weeks were dual stained for CD31 (green) and S100A4 or αSMA (red) and co-localisation was assessed. Nuclei were counterstained with DAPI. Arrowheads indicate co-localisation. The inset represents a magnification of the area within the white square. Magnification: 40x. Scale bar 50 µm.

Table 5-2. Co-localisation analysis of CD31 with S100A4 and αSMA in hearts of Ang II-infused mice after 4 weeks

		Pearson's coefficient R				Mander's coefficient M1				Mander's coefficient M2			
		MEAN	SEM	n	p-value	MEAN	SEM	n	p-value	MEAN	SEM	n	p-value
CD31 & S100A4	Control	0.029	0.015	4		0.023	0.005	4		0.062	0.010	4	
	24 µg/kg/hr Ang II	0.199	0.044	4	0.011	0.126	0.030	4	0.015	0.305	0.058	4	0.006
CD31 & αSMA	Control	0.104	0.020	4		0.148	0.014	4		0.157	0.016	4	
	24 µg/kg/hr Ang II	0.121	0.014	4	0.518	0.157	0.035	4	0.816	0.175	0.020	4	0.504

p-value *vs*. control (Student's t-test).

Table 5-3. Co-localisation analysis of CD31 with S100A4 and αSMA in hearts of Ang II-infused mice after 6 weeks

		Pearson's coefficient R				Mander's coefficient M1				Mander's coefficient M2			
		MEAN	SEM	n	p-value	MEAN	SEM	n	p-value	MEAN	SEM	n	p-value
CD31 & S100A4	Control	0.132	0.031	4		0.104	0.038	4		0.203	0.055	4	
	24 µg/kg/hr Ang II	0.227	0.033	4	>0.05	0.139	0.036	4	>0.05	0.335	0.071	4	>0.05
	48 µg/kg/hr Ang II	0.291	0.022	2	n.a.	0.192	0.046	2	n.a.	0.409	0.012	2	n.a.
CD31 & αSMA	Control	0.103	0.018	4		0.209	0.033	4		0.075	0.011	4	
	24 µg/kg/hr Ang II	0.134	0.015	4	>0.05	0.190	0.035	4	>0.05	0.118	0.023	4	>0.05
	48 µg/kg/hr Ang II	0.192	0.028	3	<0.05	0.205	0.003	3	>0.05	0.182	0.075	3	>0.05

p-value *vs*. control (ANOVA with Tukey's post-hoc analysis).

5.3.3 Ang-(1-9) in Ang II-induced microvascular rarefaction and EndMT *in vivo*

Ang-(1-7) and Ang-(1-9) have previously been shown to counteract the actions of Ang II (Flores-Munoz *et al.*, 2012). To assess whether Ang-(1-9) can also counteract the actions of Ang II on the microvasculature *in vivo*, capillary density and EndMT was assessed in the Ang-(1-9) infusion models outlined in Section 3.3.2 & 3.3.3.

Ang-(1-9) infusion over 6 weeks did not significantly affect capillary density and the co-localisation of CD31 with either S100A4 or αSMA (Table 5-4). Similarly, when Ang-(1-9) was infused for 2–4 weeks following an initial 2 week infusion of 48 μg/kg/hr Ang II (Section 3.3.3), Ang-(1-9) did not affect the Ang II-induced reduction in capillary density (Figure 5-3 A-B) and co-localisation of S100A4 and αSMA with CD31 (Figure 5-3 C-D, Table 5-5, Table 5-6).

Table 5-4. Capillary density and co-localisation analysis of CD31 with S100A4 and αSMA in hearts of Ang-(1-9)-infused mice.

	Capillaries/mm^2				Capillaries/cardiomyocyte			
	MEAN	SEM	n	p-value	MEAN	SEM	n	p-value
	3296	216	4	0.11	1.03	0.04	4	0.57

	Pearson's coefficient R				Mander's coefficient M1				Mander's coefficient M2			
	MEAN	SEM	n	p-value	MEAN	SEM	n	p-value	MEAN	SEM	n	p-value
CD31 & S100A4	0.148	0.034	4	0.73	0.050	0.018	4	0.25	0.322	0.034	4	0.11
CD31 & αSMA	0.152	0.041	4	0.32	0.228	0.063	4	0.80	0.126	0.018	4	0.05

p-value *vs*. control (presented in Table 5-3) (Student's t-test)

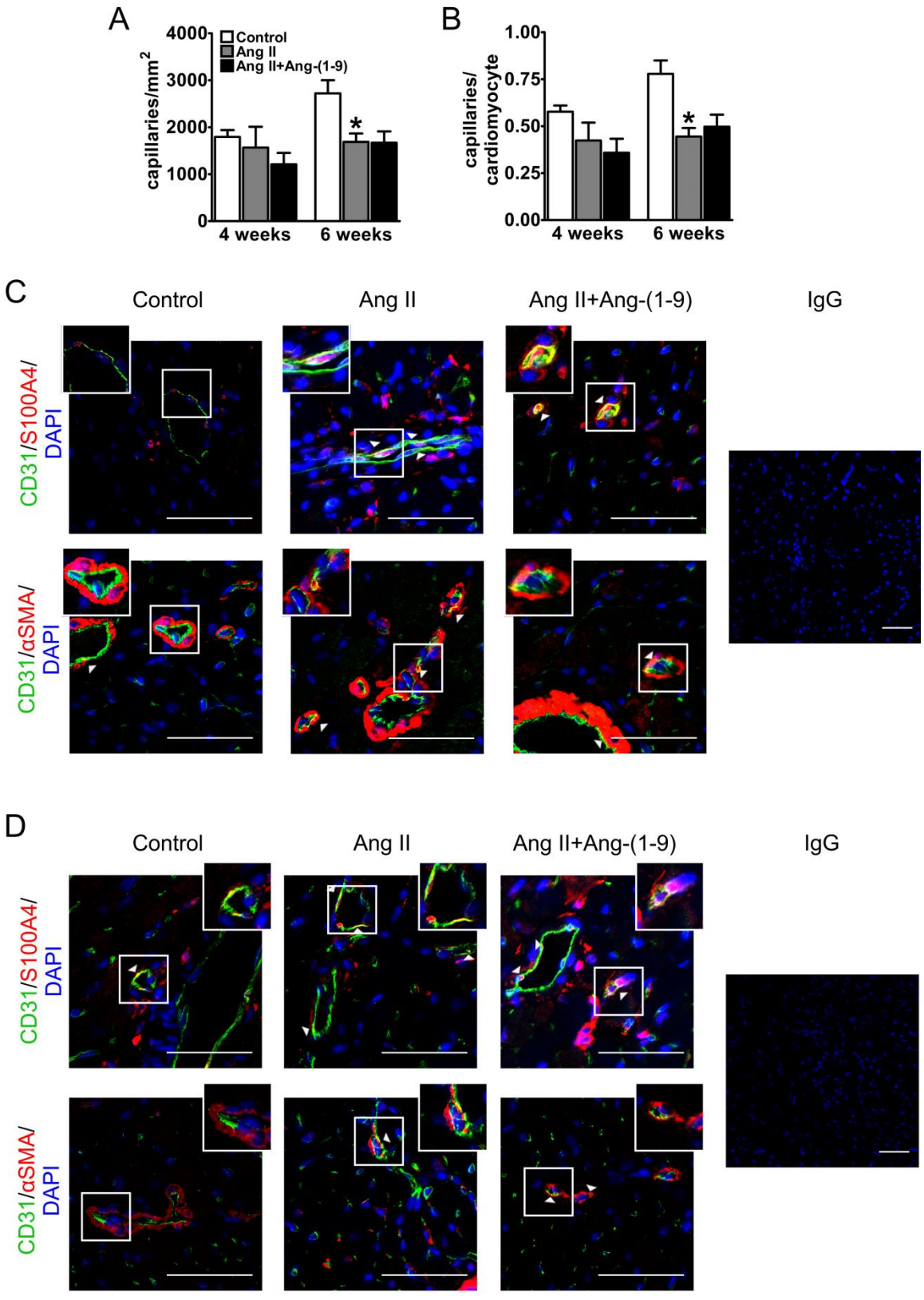

Figure 5-3. EndMT in Ang II-infused mice after reversal with Ang-(1-9)
Cardiac sections of mice infused with H_2O (control), 48 µg/kg/hr Ang II or 48 µg/kg/hr+Ang-(1-9) for (A) 4 or (B) 6 weeks were stained for CD31 and (A) capillaries/mm^2 and (B) capillaries/ cardiomyocyte determined. n= 6 and 8 for 4 and 6 weeks, respectively. Data are presented as mean ± SEM. *p<0.05 *vs.* control (ANOVA with Dunnett's post-hoc analysis). Cardiac section of mice infused for (C) 4 and (D) 6 weeks were dual stained for CD31 (green) and S100A4 or αSMA (red). Nuclei were counterstained with DAPI (blue). Arrowheads indicate co-localisation. The inset represents a magnification of the area within the white square. Magnification: 40x. Scale bar 50 µm.

Table 5-5. Co-localisation analysis of CD31 with S100A4 and αSMA after 2 weeks reversal with Ang-(1-9)

		Pearson's coefficient R				Mander's coefficient M1				Mander's coefficient M2			
		MEAN	SEM	n	p-value	MEAN	SEM	n	p-value	MEAN	SEM	n	p-value
CD31 & S100A4	Control	0.144	0.029	5		0.106	0.034	5		0.084	0.040	5	
	Ang II	0.255	0.040	3	>0.05	0.432	0.106	3	<0.05	0.165	0.045	3	>0.05
	Ang II+Ang-(1-9)	0.315	0.070	4	>0.05	0.305	0.083	4	>0.05	0.246	0.085	4	>0.05
CD31 & αSMA	Control	0.018	0.015	5		0.086	0.020	5		0.028	0.010	5	
	Ang II	0.163	0.011	3	<0.05	0.335	0.101	3	<0.05	0.138	0.036	3	>0.05
	Ang II+Ang-(1-9)	0.149	0.051	4	>0.05	0.184	0.069	4	>0.05	0.134	0.048	4	>0.05

p-value Ang II *vs*. control, Ang II+Ang-(1-9) *vs*. Ang II (ANOVA with Dunnett's post-hoc analysis)

Table 5-6. Co-localisation analysis of CD31 with S100A4 and αSMA after 4 weeks reversal with Ang-(1-9)

		Pearson's coefficient R				Mander's coefficient M1				Mander's coefficient M2			
		MEAN	SEM	n	p-value	MEAN	SEM	n	p-value	MEAN	SEM	n	p-value
CD31 & S100A4	Control	0.090	0.077	5		0.064	0.055	5		0.119	0.096	5	
	Ang II	0.283	0.032	4	>0.05	0.251	0.074	4	>0.05	0.281	0.044	4	>0.05
	Ang II+Ang-(1-9)	0.308	0.035	5	>0.05	0.216	0.041	5	>0.05	0.270	0.060	5	>0.05
CD31 & αSMA	Control	0.042	0.022	5		0.098	0.030	5		0.052	0.030	5	
	Ang II	0.108	0.042	3	>0.05	0.159	0.030	3	>0.05	0.144	0.066	3	>0.05
	Ang II+Ang-(1-9)	0.159	0.037	4	>0.05	0.085	0.045	4	>0.05	0.113	0.050	4	>0.05

p-value Ang II *vs*. control, Ang II+Ang-(1-9) *vs*. Ang II (ANOVA with Dunnett's post-hoc analysis)

5.3.4 *In vitro* model of EndMT

The potential of TGFß$_1$ and TGFß$_2$ to induce EndMT in ECs has already been well established (Maleszewska *et al.*, 2013, Arciniegas *et al.*, 1992, Frid *et al.*, 2002). To assess whether Ang II can induce mesenchymal marker expression in ECs, Ang II was assessed in an *in vitro* model of EndMT based on previous protocols (Maleszewska *et al.*, 2013) where HCAEC were stimulated with 1 µM Ang II for 5-15 days (Figure 5-4). TGFß$_1$ and TGFß$_2$ served as positive controls. Gene expression of mesenchymal markers (ACTA2, S100A4, Col1A1, CNN1, TAGLN) was assessed by qRT-PCR, normalised to the housekeeper GAPDH and expressed as relative quantity (RQ) compared to time-matched control cells.

After 5 days of stimulation, TGFß$_1$ and TGFß$_2$ significantly increased expression of ACTA2 whereas Ang II had no effect (RQ: TGFß$_1$ 5.33 ± 1.10, TGFß$_2$ 10.99 ± 0.28, Ang II 1.77 ± 0.28, n= 3, $p<0.05$) (Figure 5-4 A). S100A4 remained unchanged with TGFß$_1$ and TGFß$_2$ whereas Ang II significantly down-regulated S100A4 mRNA (RQ: TGFß$_1$ 0.74 ± 0.07, TGFß$_2$ 0.82 ± 0.21, Ang II 0.36 ± 0.04, n= 3, $p<0.05$) (Figure 5-4 B). After 15 days, ACTA2 expression was significantly increased by TGFß$_2$ (RQ: 2.11 + 0.62, $p<0.05$) and trended to be increased with TGFß$_1$ (RQ: 1.50 + 0.15) and Ang II (RQ: 1.48 + 0.37) but did not reach statistical significance (Figure 5-4 C). In contrast, Col1A1 was significantly elevated by TGFß$_1$ and TGFß$_2$ whereas Ang II had no significant effect (RQ: TGFß$_1$ 4.94 ± 0.82, TGFß$_2$ 14.97 ± 4.52, Ang II 2.01 ± 0.35, n= 4, $p<0.05$) (Figure 5-4 D). Similarly to 5 days, S100A4 expression remained unchanged by TGFß$_1$ and TGFß$_2$ but AngII significantly reduced S100A4 expression (RQ: TGFß$_1$ 0.89 ± 0.26, TGFß$_2$ 0.76 ± 0.05, Ang II 0.33 ± 0.12, n= 4, $p<0.05$) (Figure 5-4 E). This was in contrast to protein expression assessed by dual-immunofluorescence for CD31 and S100A4. S100A4 was undetectable in control cells, but expression was visibly increased by TGFß$_1$, TGFß$_2$ and Ang II (Figure 5-4 F), suggesting a mismatch between gene and protein expression. When cell morphology was assessed microscopically, control cells appeared with a characteristic cobblestone shape whereas cells treated with TGFß$_1$, TGFß$_2$ and Ang II presented with a loss of cell-cell contacts and elongated cell shape characteristic of fibroblasts and SMCs (Figure 5-4 F). Overall these results indicate that both, TGFß$_1$ and TGFß$_2$ induce EndMT in HCAEC with TGFß$_2$ being more potent. Even after 15 days exposure,

Ang II alone had only mild effects on mesenchymal gene expression, affecting a subset of genes induced by TGFß$_1$ and TGFß$_2$.

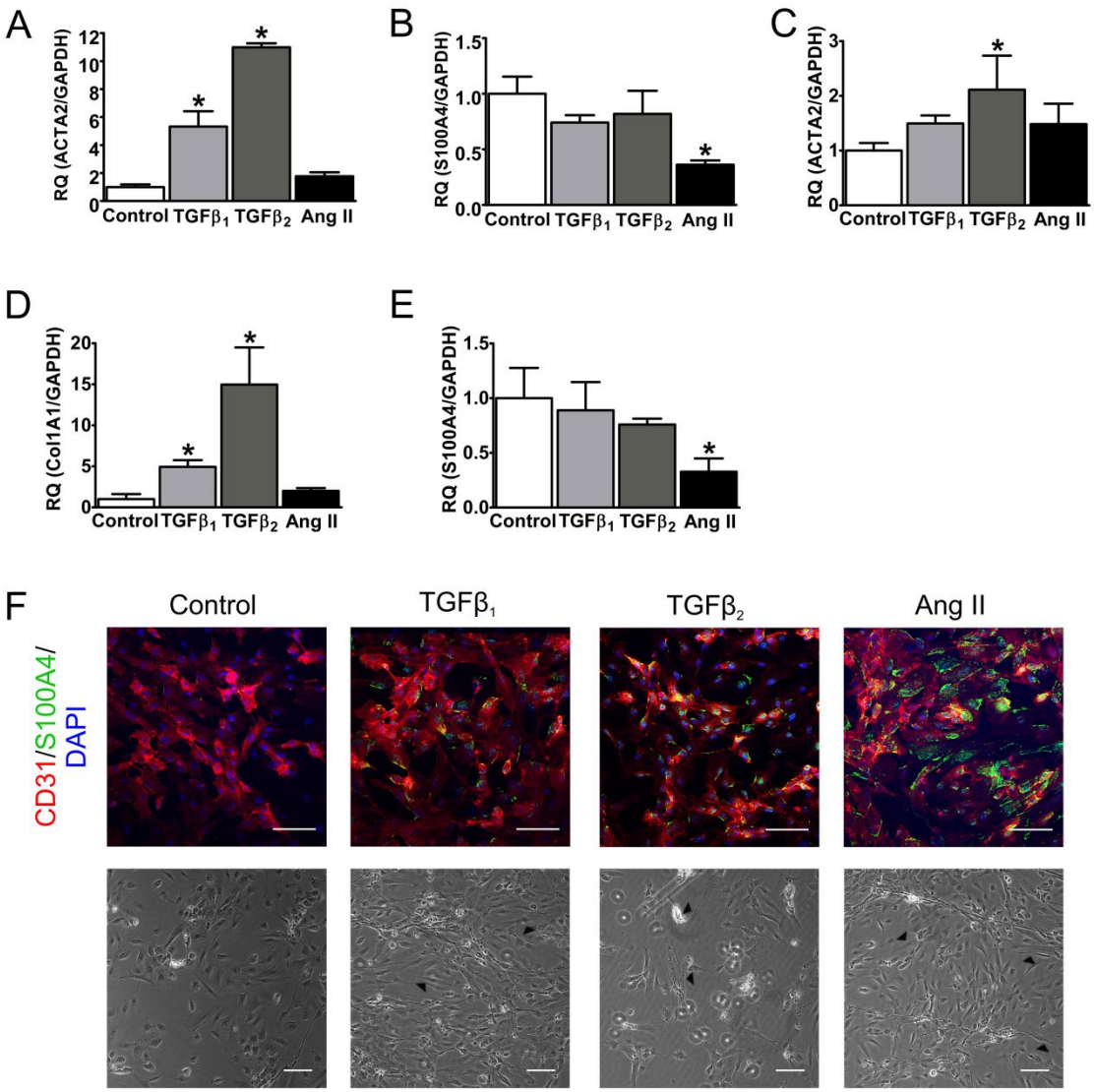

Figure 5-4. Effects of Ang II on mesenchymal gene expression in HCAEC
HCAEC were stimulated with 10 ng/mL TGFβ$_1$ or TGFβ$_2$ or 1 μM Ang II and gene expression for ACTA2, S100A4 and Col1A1 was assessed following (A, B) 5 and (C, D, E) 15 days. Gene expression was normalised to the housekeeper GAPDH and expressed as relative quantity (RQ) to time-matched controls cells which were set at RQ= 1. Data are presented as RQ+ rqmax. n= 3 and 4 individual biological repeats *per* group for 5 and 15 days, respectively. Experiments were repeated on two independent occasions. *p<0.05 *vs.* control (ANOVA with Dunnett's post-hoc analysis). (F) After 15 days of stimulation, HCAEC morphology was assessed by light microscopy and were then fixed and dual stained for CD31 (red) and S100A4 (green). Black arrowheads indicate changes in EC morphology. Magnification: 25x (immunofluorescence), 10x (light microscope), Scale bar: 100 μm.

5.3.5 Assessing the role of angiotensin II in TGFβ$_1$-induced EndMT

Various molecules have previously been reported to act synergistically with TGFß to induce EndMT in ECs from various origins (Maleszewska *et al.*, 2013, Rieder *et al.*, 2011). Since Ang II alone only had mild effects on mesenchymal markers in ECs and Ang II and TGFß$_1$ have previously been reported to act in a signalling network *in vivo* (Rosenkranz, 2004), the role of AngII in TGFß-induced EndMT was assessed. EndMT was established in HCAEC as described in Section 2.3 by stimulation with 10 ng/mL TGFß$_1$ in the presence or absence of AngII (100 nM or 1 µM). Gene and protein expression were assessed after 3 (Figure 5-5) and 10 days (Figure 5-6) to capture acute and chronic changes in gene expression.

5.3.5.1 Day 3

After 3 days of stimulation, gene expression of the EC markers PECAM1 (CD31) and CDH5 (VE-cadherin) were not significantly altered by any treatment compared to the time-matched control (Figure 5-5 A-B). However, compared to TGFß$_1$, the co-addition of AngII significantly increased CDH5 and PECAM1 gene expression. Whereas TGFß$_1$ alone did not significantly alter ACTA2 gene expression, the co-addition of Ang II dose-dependently increased ACTA2 mRNA compared to control and TGFß$_1$ (RQ: TGFß$_1$ 1.29 ± 0.13, 100 nM Ang II 1.75 ± 0.06, 1 µM Ang II 1.96 ± 0.17, n= 4, $p<0.05$) (Figure 5-5 C). Similarly, Ang II dose-dependently exacerbated Col1a1 gene expression by 6.69 ± 0.81 and 10.61 ± 1.44-fold, respectively ($p<0.05$) (Figure 5-5 D). In contrast, gene expression of S100A4 trended to be decreased by TGFß1 which was further decreased by addition of AngII in a dose-dependent manner with a significant 0.39 ± 0.03-fold reduction with 1 µM AngII (Figure 5-5 E). Further gene expression analysis of CNN1 (calponin) and TAGLN (transgelin, SM22α), mesenchymal markers that have been shown to be expressed early during mesenchymal transition and associated with immature SMCs, revealed no significant up-regulation with TGFß$_1$ alone but the addition of Ang II significantly up-regulated CNN1 (RQ: TGFß$_1$ 1.12 ± 0.15, 1 µM Ang II 1.89 ± 0.13, n= 4, $p<0.05$), whereas TAGLN remained unchanged (Figure 5-5 F-G). Similar to its gene expression data, protein expression of CD31 was not significantly changed by any treatment compared to control (Figure 5-5 H-I). Unlike the increase in the αSMA gene expression, αSMA protein expression

could not be detected with any treatment and was only expressed in a human fibroblast control suggesting a mismatch between gene and protein expression during the early stages of EndMT.

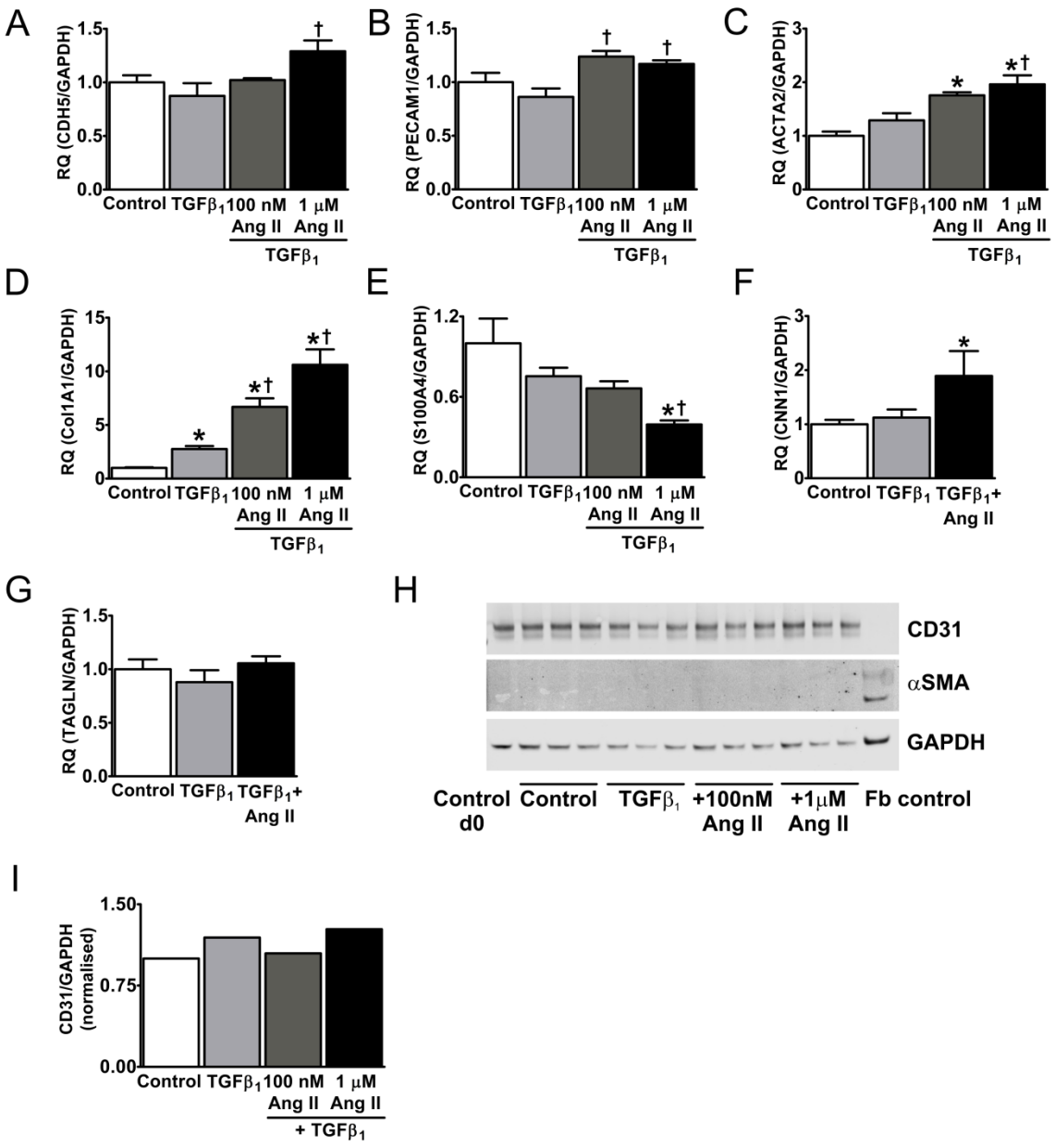

Figure 5-5. Role of Ang II in acute TGFβ$_1$-induced EndMT
Plated and quiesced HCAEC were stimulated with 10 ng/mL TGFβ$_1$ in the presence or absence of 100 nM or 1 μM Ang II for 3 days. qPCR gene expression analysis for (A) CDH5, (B) PECAM1, (C) ACTA2, (D) Col1a1, (E) S100A4, (F) CNN1 and (G) TAGLN was normalised to the housekeeper GAPDH and expressed as relative quantity (RQ) to time-matched controls cells which were set at RQ= 1. Data are presented as RQ+ rqmax. (H) Protein expression analysis of CD31 and αSMA after 3 days by Western blot was normalised to the housekeeper GAPDH. Normalised protein expression was expressed as fold change in (I) CD31 compared to time-matched control cells. Experiments were performed with n= 4 individual biological repeats (for gene expression) and n= 3 individual biological repeats (for protein expression) *per* group and confirmed in three independent repeats *p<0.05 *vs*. control, † p<0.05 *vs.* TGFβ$_1$ (ANOVA with Tukey's post-hoc analysis).

5.3.5.2 Day 10

After 10 days of stimulation, gene expression of CDH5 and PECAM1 was not significantly altered by any treatment (Figure 5-6 A-B). Expression of ACTA2 and Col1A1 were significantly up-regulated 1.76 ± 0.11 and 9.16 ± 1.45-fold by $TGF\beta_1$ alone, respectively (Figure 5-6 C-D). Addition of AngII significantly increased ACTA2 (RQ: 100 nM AngII 3.04 ± 0.69, 1 µM AngII 4.31 ± 0.26, n= 4, $p<0.05$) and Col1a1 (RQ: 100 nM Ang II 19.58 ± 3.49, 1 µM Ang II 30.17 ± 3.34, n= 4, $p<0.05$) gene expression compared to control cells and $TGF\beta_1$ alone in a dose dependent manner. Similar to its expression at day 3, S100A4 was reduced by co-stimulation with $TGF\beta_1$ and AngII despite not being significant (RQ: $TGF\beta_1$ 0.77 ± 0.18, 100 nM AngII 0.50 ± 0.20, 1 µM AngII 0.48 ± 0.06, n= 4, $p>0.05$) (Figure 5-6 E). CNN1 was significantly up-regulated 2.25 ± 0.22-fold by $TGF\beta_1$ alone and this was significantly exacerbated to 6.09 ± 0.74-fold by 1 µM AngII (Figure 5-6 F). In contrast, TAGLN was not modulated by $TGF\beta_1$ alone but addition of AngII significantly up-regulated TAGLN 1.89 ± 0.23-fold (Figure 5-6 G). Protein expression analysis of CD31 showed a trend to decrease with the combination of $TGF\beta_1$+Ang II reducing CD31 levels to 0.69-fold compared to time-matched control cells (Figure 5-6 H-I). αSMA expression was detected in cells that had been treated with $TGF\beta_1$+AngII whereas expression in cells treated with TGFβ1 alone was negligible (Fold: $TGF\beta_1$ 1.81, 100 nM AngII 2.84, 1 µM AngII 8.40, $p<0.05$). αSMA was not detected in time-matched control cells and cells harvested at the beginning of the protocol (Figure 5-6 J-H)

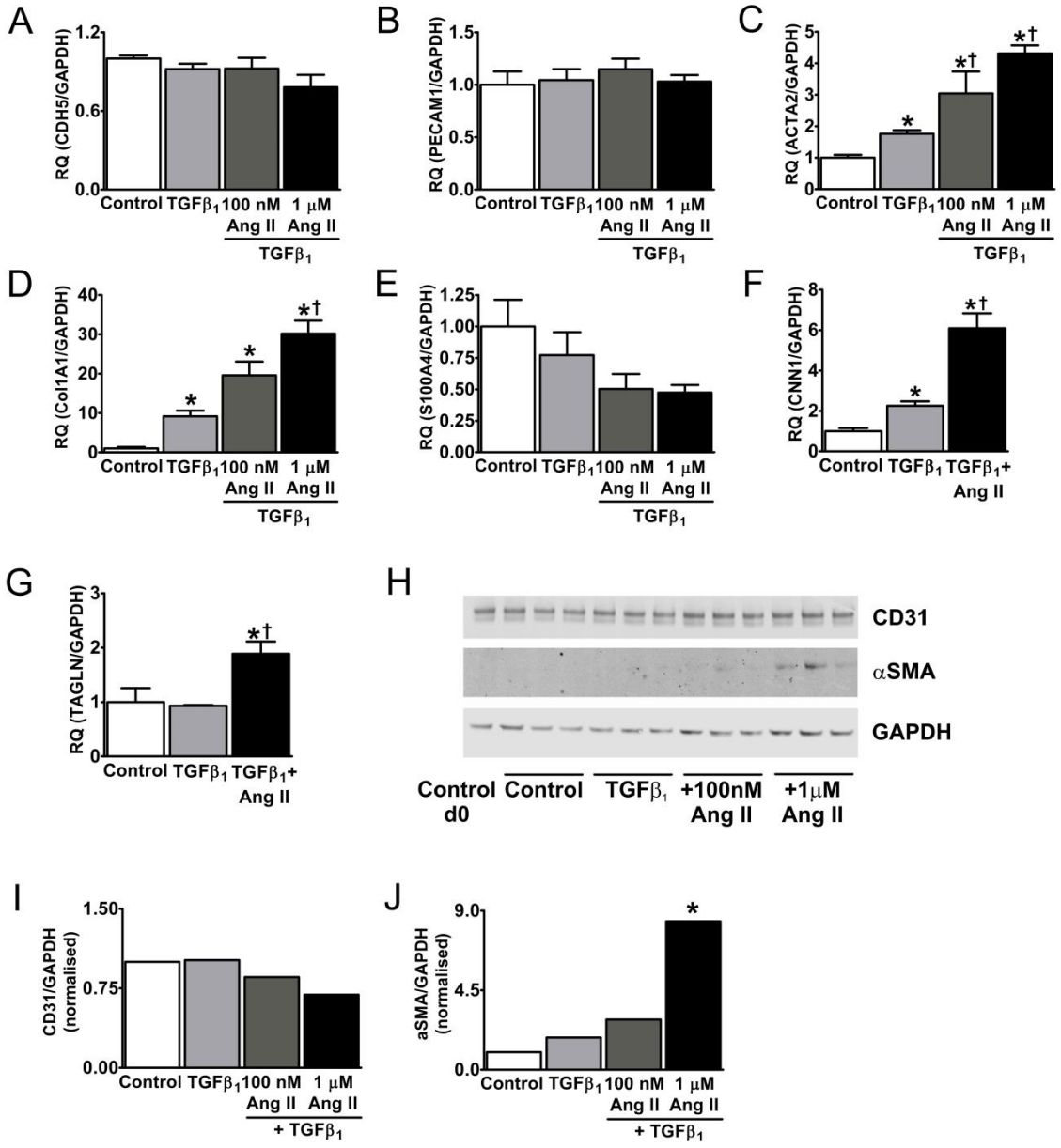

Figure 5-6. Role of Ang II in chronic TGFβ1-induced EndMT
Plated and quiesced HCAEC were stimulated with 10 ng/mL TGFβ1 in the presence or absence of 100 nM or 1 μM Ang II for 10 days. qPCR gene expression analysis (A) CDH5, (B) PECAM1, (C) ACTA2, (D) Col1a1, (E) S100A4, (F) CNN1 and (G) TAGLN was normalised to the housekeeper GAPDH and expressed relative quantity (RQ) to time-matched controls cells which were set at RQ= 1. Data are presented as RQ+ rqmax. (H) Protein expression analysis of CD31 and αSMA by Western blot after 10 days was normalised to the housekeeper GAPDH. Normalised protein expression was expressed as fold change in (I) CD31 and (J) αSMA compared to time-matched control cells. Experiments were performed with n=4 individual biological repeats (for gene expression) and n=3 individual biological repeats *per* group (for protein expression) and confirmed in three independent repeats *p<0.05 *vs*. control, † p<0.05 *vs.* TGFβ1 (ANOVA with Tukey's post-hoc analysis).

5.3.5.3 Role of AT_1R and AT_2R

To investigate the receptor by which Ang II mediates the observed exacerbation of $TGF\beta_1$-induced EndMT, losartan and PD123319 were used to block the AT_1R and AT_2R, respectively.

Preliminary data shows that following 10 days of stimulation, inhibition of either AT_1R or AT_2R significantly exacerbated the expression of ACTA2, Col1A1, CNN1 and TAGLN compared to $TGF\beta_1$+Ang II (Figure 5-7 A-D). This suggests that Ang II mediated effects are independent of the AT_1R and AT_2R.

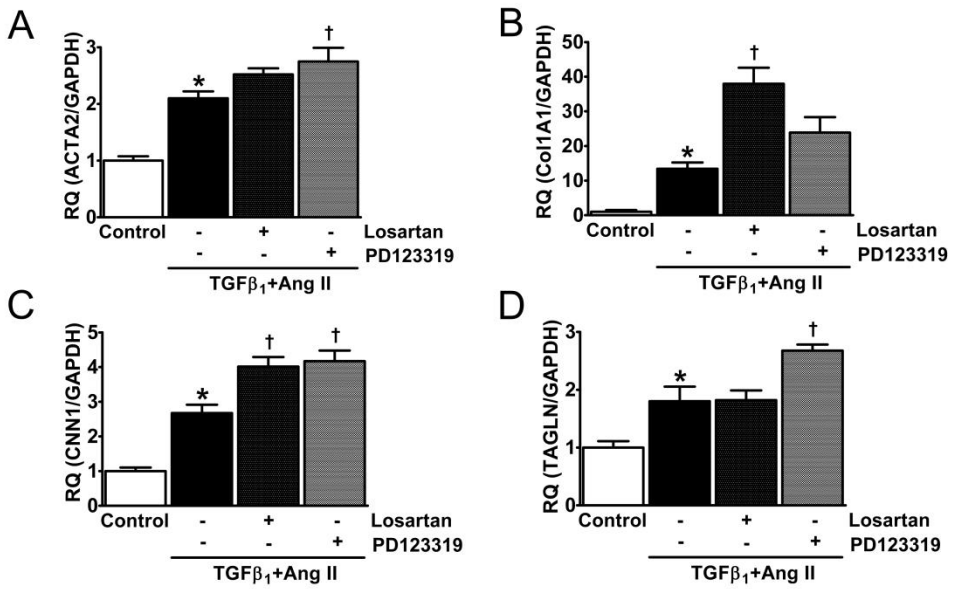

Figure 5-7. Role of AT_1R and AT_2R in Ang II-induced EndMT
Plated and quiesced HCAEC were treated with 1 μM losartan and 500 nM PD123319 15 min prior to stimulation with 10 ng/mL $TGF\beta_1$ and 1 μM Ang II. Mesenchymal gene expression of (A) ACTA2, (B) Col1a1, (C) CNN1 and (D) TAGLN was assessed by q-PCR normalised to the internal housekeeper GAPDH and expressed as relative quantity (RQ) to time-matched control cells. Data are presented as RQ + rqmax. Experiments were performed once with n=4 individual biological repeats *per* group. *p<0.05 *vs.* control, † p<0.05 *vs.* $TGF\beta_1$+Ang II (ANOVA with Dunnett's post-hoc analysis).

5.3.6 Signalling pathways activated during EndMT

TGFß$_1$-induced SMAD2/3 signalling is indispensable for EndMT (Cooley *et al.*, 2014). To assess the role of the SMAD pathway in mediating TGFß$_1$ and Ang II-induced EndMT, HCAEC were treated with the ALK5 (TGFßRI) inhibitor SB525334 which specifically blocks the activation of SMAD2/3.

HCAEC treated with the ALK5-inhibitor in addition to TGFß$_1$ and Ang II over 10 days visibly retained their EC morphology whereas TGFß$_1$ alone or in combination with Ang II induced a fibroblast phenotype (Figure 5-8 A). Further, gene expression analysis showed that SB525334 prevented the induction of gene expression for Col1a1, CNN1 and TAGLN (Figure 5-8 B-D).

To assess whether the expression of components of the SMAD signalling pathway are altered during EndMT, gene expression of the SMAD-induced transcription factors SNAI1 (Snail) and SNAI2 (Slug), the SMAD2/3 co-factor SMAD4 and the inhibitory SMAD7 were assessed. TGFß$_1$ reduced expression of SNAI1 which was reversed by the addition of Ang II (RQ: TGFß$_1$ 0.82 ± 0.04 vs. TGFß$_1$+Ang II 1.11 ± 0.06; $p<0.05$) (Figure 5-8 E). In contrast, expression of SNAI2, SMAD4 and SMAD7 were unaltered over the course of EndMT in HCAEC (Figure 5-8 F-H).

To assess whether AngII differentially regulates SMAD2 phosphorylation compared to TGFß$_1$ alone or in combination, pSMAD2 was assessed over a time-course of 60 min by Western blotting. Phosphorylation was expressed as a ratio of phosphorylated SMAD2 to total SMAD2 and then normalised to unstimulated control cells. Stimulation with TGFß$_1$ induced phosphorylation of SMAD2 in a time-dependent manner with an initial 2.16 ± 0.18-fold increase observed at 15 min that increased to 3.23 ± 0.50-fold at 30 min and peaked at 5.25 ± 1.43-fold after 60 min (Figure 5-9 A-B). In contrast, Ang II did not induce any significant SMAD2 phosphorylation with a maximum increase in pSMAD2 of 1.79 ± 0.57-fold at 60 min. Co-stimulation with TGFß$_1$+Ang II did not alter TGFß$_1$-induced SMAD2 phosphorylation (Figure 5-9 A-B).

ERK1/2 has previously been shown to mediate EndMT in bovine valvular ECs (Wylie-Sears *et al.*, 2014). Given that Ang II did not affect TGFß$_1$-induced SMAD2 phosphorylation, the role of ERK1/2 was assessed. TGFß$_1$ and Ang II alone

induced phosphorylation of ERK1/2 in a time-dependent manner which peaked at 30 min with a 1.80 ± 0.01- and 1.98 ± 0.03- fold increase, respectively, and was not significantly different between the two treatments (Figure 5-9 C-D). The combination of TGFß$_1$+Ang II did not significantly alter ERK1/2 phosphorylation. However, there was a trend towards an increase in pERK1/2 at 30 min that was reproducible in independent repeats.

Overall, these results show that inhibition of the SMAD2/3 pathway can block TGFß$_1$ and Ang II induced EndMT. However, Ang II neither modulates gene expression of members of the SMAD signalling pathway nor does it alter TGFß$_1$-induced activation of SMAD2 and ERK1/2.

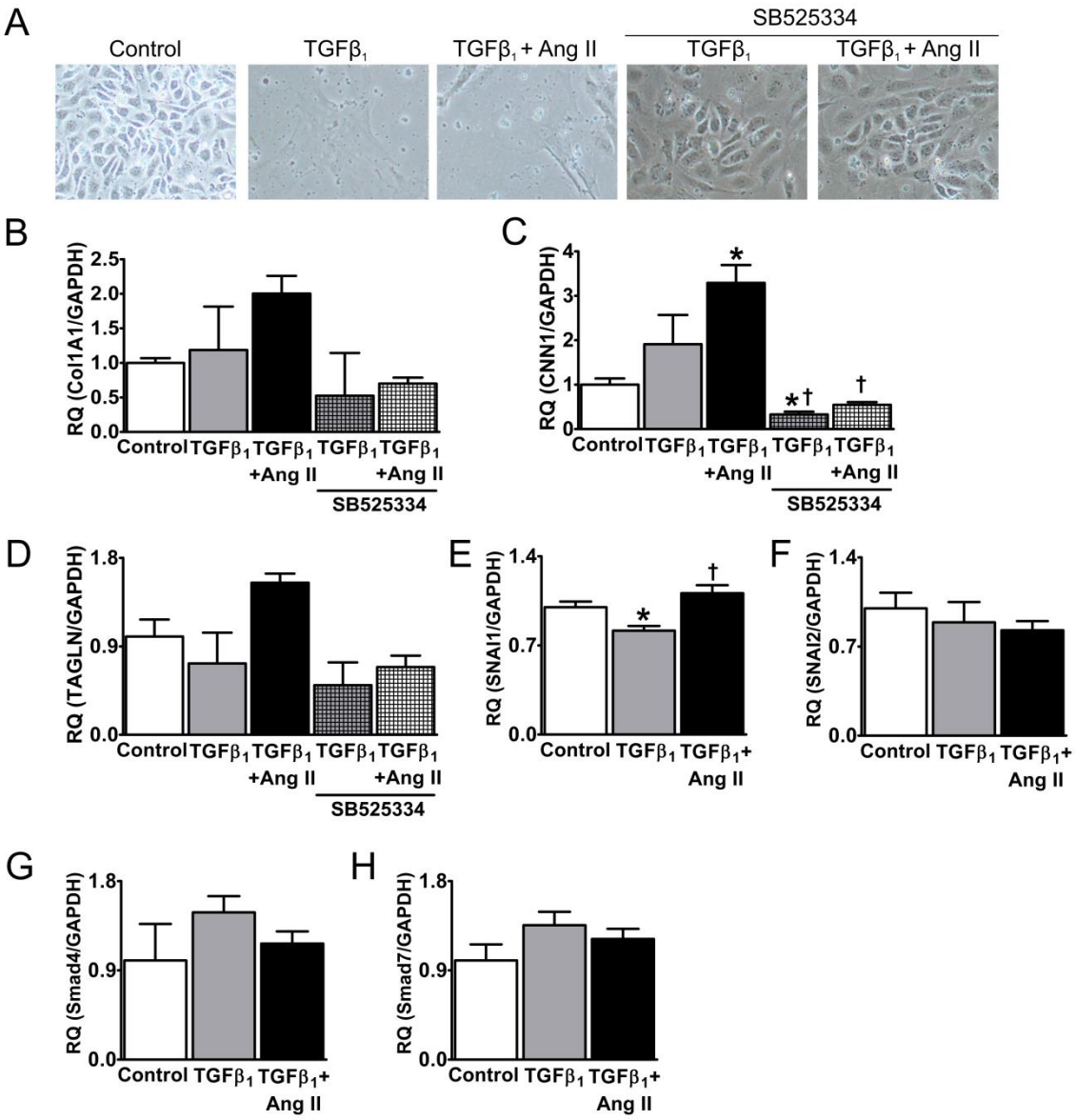

Figure 5-8. Role of SMAD pathway in Ang II-induced EndMT
Plated and quiesced HCAEC were stimulated with 10 ng/mL TGFβ$_1$ in the presence or absence of 1 μM Ang II for 10 days. For inhibition of SMAD2/3, HCAEC were pre-treated with 1 μM SB525334 for 30 min. (A) Light microscopy images of HCAEC phenotype after 10 days of stimulation with TGFβ$_1$±Ang II in the presence or absence of SB525334. TGFβ$_1$ and TGFβ$_1$+Ang II-treated HCAEC are visibly larger and have lost their cobblestone morphology. Mesenchymal gene expression of (B) Col1A1, (C) CNN1 and (D) TAGLN was assessed by qPCR normalised to the internal housekeeper GAPDH and expressed as relative quantity (RQ) to time-matched control cells. *p<0.05 *vs.* control, † p<0.05 *vs.* matched treatment (ANOVA with Tukey's post-hoc analysis). In a different set of cells, (E) SNAI1, (F) SNAI2, (G) SMAD4 and (H) SMAD7 gene expression was determined. *p<0.05 *vs*. control, † p<0.05 *vs*. TGFβ$_1$ (ANOVA with Tukey's post-hoc analysis). Data are presented as RQ+ rqmax. Experiments were performed once with n= 4 individual biological repeats *per* group.

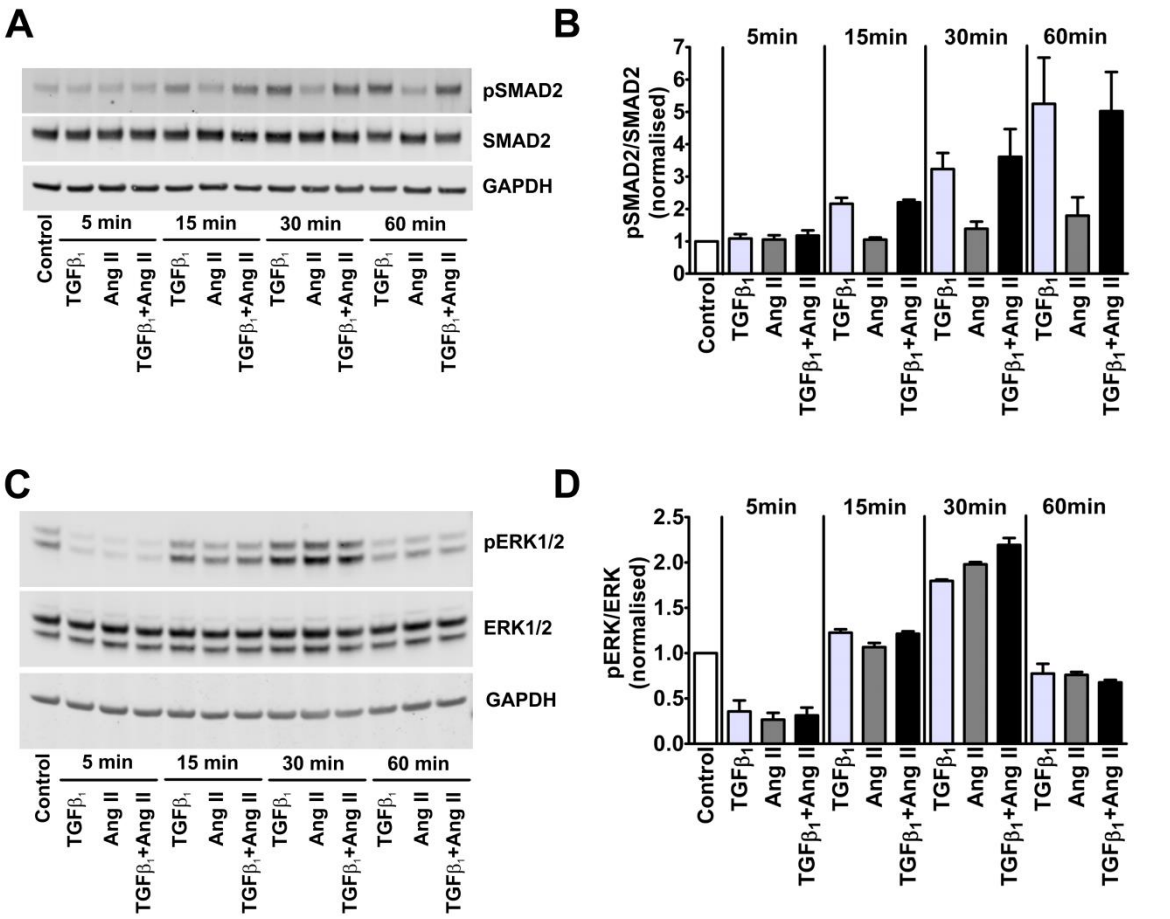

Figure 5-9 Effects of AngII on cellular signalling pathways during EndMT
Plated and quiesced HCAEC were stimulated with 10 ng/mL TGFβ$_1$, 1 μM Ang II or in combination for 5–60 min, lysed and assessed for (A, B) pSMAD2 and (C,D) pERK1/2 by Western blotting. Phosphorylation was expressed as ratio of phospho-protein against total protein and normalised to unstimulated control cells. Data are presented as mean ± SEM. Experiments were performed with n= 2 individual biological repeats and confirmed in three independent repeats.

5.3.7 The role of ROS in Ang II-induced EndMT

ROS were previously demonstrated to contribute to TGFß-induced EndMT (Montorfano *et al.*, 2014, Boudreau *et al.*, 2012, Rhyu *et al.*, 2005). Ang II has previously been associated with the activation of Noxs in ECs which has been linked to its pathological actions mediating EC dysfunction (Li *et al.*, 2004, Landmesser *et al.*, 2002). To assess whether Ang II may exacerbate $TGFß_1$-induced EndMT through the activation of Noxs and generation of ROS, quiesced HCAEC were stimulated with $TGFß_1$, Ang II or their combination for 1–30 min and O_2^- production was measured by lucigenin assay (Section 2.3.2). Mean absorbance was normalised to protein content and O_2^- generation was expressed as fold-increase compared to unstimulated HCAEC.

$TGFß_1$ did not induce significant O_2^- production in HCAEC and peaked with a 1.33 ± 0.24-fold increase after 30 min (Figure 5-10 A). In contrast, Ang II induced a rapid 1.49 ± 0.26-fold increase in O_2^- following 1 min which decreased to control levels within 5 min. Co-stimulation with $TGFß_1$ and Ang II only induced a small 1.17 ± 0.15-fold increase after 1 min. $TGFß_1$ was previously shown to only activate Nox4 mediating H_2O_2 production (Dikalov *et al.*, 2008). Therefore, to assess which Nox is responsible for the rapid Ang II-induced increase in O_2^-, HCAEC were pre-treated with the Rac1/2 inhibitor EHT1864 (which inhibits, Rac1/2-dependent Nox1 and Nox2) (Shutes *et al.*, 2007), the Nox1 inhibitor ML171 (Gianni *et al.*, 2010) and the dual Nox1/4 inhibitor GKT137831 (Aoyama *et al.*, 2012) (Figure 5-10 B). All inhibitors tended to decrease Ang II-induced O_2^- production to below basal levels with ML171 and GKT137831 being the most effective (Fold: Ang II 1.49 ± 0.26, EHT1864 0.96 ± 0.12, ML171 0.78 ± 0.08, GKT137831 0.76 ± 0.10, $p<0.05$). Given that Rac1/2 inhibition prevents Nox1/2 activation and that ML171 and GKT137831 specifically target the O_2^- generating Nox1, this suggests that Nox1 is the major source of O_2^- in Ang II-stimulated HCAEC.

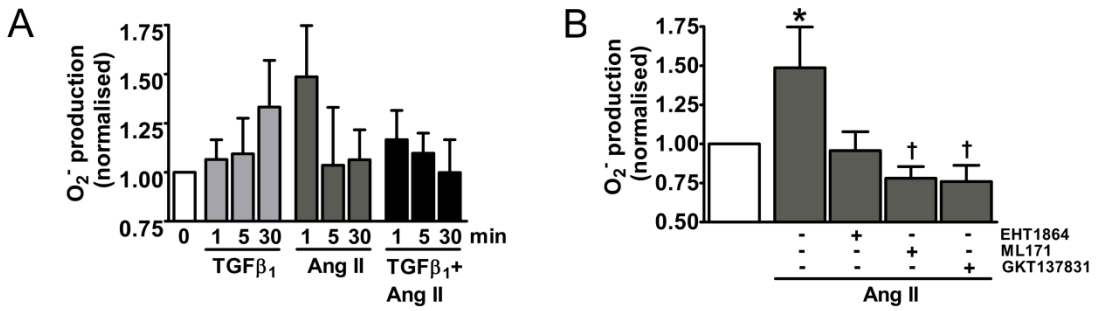

Figure 5-10. Ang II-induced oxidative stress in HCAEC
Plated and quiesced HCAEC were stimulated with 10 ng/mL TGFβ$_1$, 1 μM Ang II or their combination for 1–30 min, lysed and assayed for O_2^- production using the lucigenin assay. O_2^- production was normalised to protein content and expressed as fold-increase compared to unstimulated control cells. (A) Time-course of O_2^- production with TGFβ$_1$, Ang II and TGFβ$_1$+Ang II over 30 min (n= 8 for control, 7 for 1 min, 4 for 5 min, 5 for 30 min). (B) HCAEC were pre-incubated with 10 μM EHT1864 (n= 3), 1 μM ML171 (n= 3) or 1 μM GKT137831 (n= 3) for 30 min prior to stimulation with 1 μM Ang II for 1 min (n= 8 from A) and O_2^- was measured. Data are presented as mean ± SEM. *p<0.05 *vs.* control, † p<0.05 *vs*. Ang II (ANOVA with Dunnett's post-hoc analysis).

5.4 Discussion

Here, it was shown that following Ang II infusion over 2–6 weeks, myocardial capillary density progressively decreased leading to significant microvascular rarefaction. This coincided with the presence of EndMT in the hearts of Ang II-infused mice which may contribute to the loss in myocardial capillaries. In contrast, co-infusion of Ang-(1-9) did not reverse Ang II-induced loss in capillary density or EndMT. This highlights that microvascular rarefaction and EndMT are Ang II-driven processes to which Ang-(1-9) does not contribute either when infused alone or in established Ang II-induced cardiac remodelling.

In the heart, EC: cardiomyocyte interactions are important for the maintenance of normal cardiac function which demands a constant supply of oxygen and nutrients in order to maintain cardiac contractile output (Brutsaert, 2003). Adequate delivery of oxygen and nutrients is crucially dependent on cardiomyocyte/capillary ratio and intercapillary distance and is facilitated by a high density of capillaries in the myocardium (Brutsaert, 2003). Capillary density in the adult mammalian heart is estimated between 2000–5000 capillaries/mm^2 (Shiojima *et al.*, 2005, Banerjee *et al.*, 2009, Zentilin *et al.*, 2010, Ikeda *et al.*, 2009) with capillary/cardiomyocyte ratios usually ranging from 0.9–1.12 but ratios as high as 1.8 have been reported (Messaoudi *et al.*, 2009). With an overall mean capillary density of 2647 ± 106 capillaries/mm^2 and a capillary/cardiomyocyte ratio of 1.04 ± 0.06 in control mice, the data fits well within the range of reported capillary densities in the heart.

It is already well established that clinically, hypertension is associated with a reduction in myocardial capillary density (Mohammed *et al.*, 2015) and this is replicated in animal models of hypertension: In the SHRSP, myocardial capillary density was shown to decrease by 57 % with a 62.5 % increase in arteriolar density (Pu *et al.*, 2003). Similarly, capillaries were decreased by 60 % in rats with renovascular hypertension (Kobayashi *et al.*, 1999) and in the Goldblatt 1K1C model, capillaries were decreased by 12 % while arterioles increased by 27 % (Levy *et al.*, 2001). Here, a loss in myocardial capillary density following Ang II infusion was already apparent after 2 weeks with further reductions after 4 and 6 weeks and confirms previous studies in mice and rats where Ang II infusion led to a 16–30 % reduction in capillary density (Sabri *et al.*, 1998,

Belabbas *et al.*, 2008, Graiani *et al.*, 2005). Previously, myocardial capillary density has been shown to increase in the compensated phase of cardiac remodelling following TAC but then rapidly decline during decompensation (Sano *et al.*, 2007). A similar trend in pro-angiogenic gene expression with Ang II infusion has been observed where vascular endothelial growth factor (VEGF) and Hif-1α peak after 7 days of Ang II infusion (Zhao *et al.*, 2004) suggesting that Ang II may have a dual effect on cardiac capillary density. During the initial compensated phase of cardiac remodelling Ang II induces angiogenesis but as the heart progressively decompensates, Ang II signalling contributes to a reduction in capillary density. This dual effect is supported by the controversial observations that Ang II can promote angiogenesis through VEGF signalling either *via* the AT_1R or the AT_2R (Munk *et al.*, 2007, Tamarat *et al.*, 2002, Walther *et al.*, 2003) whereas others have reported that each receptor is anti-angiogenic (Benndorf *et al.*, 2003, Lakó-Futó *et al.*, 2003, de Boer *et al.*, 2003). Since in the data presented here, capillary density was already decreased after 2 weeks of low dose Ang II infusion which correlates with reduced pro-angiogenic gene expression observed previously (Zhao *et al.*, 2004), this suggests that the heart is beginning to decompensate with a mismatch between cardiac growth and microvascular density. In fact, in the present study, it was shown that the relationship between capillary density and cardiac hypertrophy is a dynamic process as correlation of capillary density and hypertrophy increases during the progression of capillary loss within the heart.

The mechanism by which Ang II decreases capillary density is still largely unknown. It has previously been shown that Ang II reduces the proliferation of coronary ECs following 2 week infusion of Ang II in rats (McEwan *et al.*, 1998) and EC apoptosis was evident following 4 week delivery of Ang II relating to the progressive loss of ECs *in vivo* (Graiani *et al.*, 2005). Furthermore, Ang II was shown to enhance ischaemia-induced HCAEC apoptosis *in vitro* (Li *et al.*, 1999) and to induce senescence of endothelial progenitor cells participating in angiogenesis (Kobayashi *et al.*, 2006) suggesting multifactorial effects of Ang II that collectively contribute to microvascular rarefaction. More recently, it was demonstrated that Ang II infusion in Nox2 overexpressing mice results in EndMT of myocardial ECs (Murdoch *et al.*, 2014) and for the first time demonstrated EndMT in Ang II-infused mice. Here, we extended this finding and provide

evidence that EndMT is present in wildtype mice infused with low and high doses of Ang II. The increase in EndMT may contribute to the observed net loss in capillary density. Importantly, EndMT has previously shown to contribute to up to 30 % of the myofibroblast population following TAC (Zeisberg *et al.*, 2007b) highlighting its significant contribution to myocardial collagen deposition and fibrosis.

Here, an *in vitro* model of EndMT was developed by comparing the effects of $TGF\beta_1$ and $TGF\beta_2$ on mesenchymal marker expression in HCAEC over a time-course of up to 15 days. Models of EndMT have been developed in a variety of ECs with varying protocols differing in their time of stimulation and cell culture conditions (Cooley *et al.*, 2014, Rieder *et al.*, 2011, Maleszewska *et al.*, 2013, Wylie-Sears *et al.*, 2014, Zeisberg *et al.*, 2007b). Hence, no uniform protocol for EndMT exists which makes direct comparisons difficult. In the present study, it was shown that $TGF\beta_2$ is more potent in inducing mesenchymal gene expression than $TGF\beta_1$. This corroborates a previous study of Maleszewska *et al.* (2013) who showed that $TGF\beta_2$ was twice as potent as $TGF\beta_1$ in inducing SM22α (transgelin) gene expression in human umbilical vein ECs after 96 h stimulation (Maleszewska *et al.*, 2013). Furthermore, similar to the results presented here, a study by Rieder *et al.* (2011) did not identify any changes in EC markers and phenotype in human intestinal microvascular ECs that had been stimulated with $TGF\beta_1$ for up to 30 days (Rieder *et al.*, 2011). In *in vitro* models of EMT, $TGF\beta_1$ has been shown to induce mesenchymal transformation in mammary gland and renal tubular epithelial cells (Brown *et al.*, 2004, Carvajal *et al.*, 2008, Yang *et al.*, 2010). However, a systematic review of human and murine epithelial cell lines has shown that despite responsiveness to and necessity of $TGF\beta_1$, only few cells lines actually undergo $TGF\beta_1$-induced EMT (Brown *et al.*, 2004, Scheel *et al.*, 2011) highlighting the differing potential across ECs to respond to TGFβ. Despite its minor role in EndMT and reduced potency compared to $TGF\beta_2$, $TGF\beta_1$ was chosen to assess EndMT in HCAEC to mimic myocardial capillary loss *in vivo*. This is based on observations that $TGF\beta_1$ acts in a network with Ang II (Rosenkranz, 2004) and plays a key role in the pathogenesis of CVDs and cardiac remodelling with direct effects on myofibroblast differentiation (Cucoranu *et al.*, 2005) and cardiomyocyte growth (Schultz *et al.*, 2002). Increased $TGF\beta_1$ expression has been demonstrated in CVD models such as pressure overload (Kuwahara *et al.*,

2002) and myocardial infarction (Dewald *et al.*, 2004) and similarly cardiac-specific overexpression of TGFß$_1$ directly induces cardiac fibrosis and cardiac hypertrophy (Rosenkranz *et al.*, 2002).

In the present study it was demonstrated that Ang II alone only marginally affects mesenchymal gene expression in HCAEC but that it exacerbates TGFß$_1$-induced EndMT *in vitro*. This correlates with previous observations on inflammatory cytokines which only induce EndMT in ECs when co-stimulated with TGFß$_1$ and that this exacerbated the response by TGFß$_1$ alone (Maleszewska *et al.*, 2013, Rieder *et al.*, 2011). This suggests that TGFß$_1$ is needed as an inductive signal for a mesenchymal switch in ECs before Ang II can significantly modulate mesenchymal gene expression. In this context, Ang II has previously been shown to directly alter mesenchymal gene expression in cells of mesenchymal origin. For example, in rat VSMC, Ang II increases the expression of calponin *in vivo* and *in vitro* (di Gioia *et al.*, 2000, Castoldi *et al.*, 2001) whereas in fibroblasts and mesothelial cells, Ang II stimulates the secretion of collagen, fibronectin and laminin (Kawano *et al.*, 2000, Kiribayashi *et al.*, 2005).

Previous studies have already shown that HCAEC express AT$_1$R and AT$_2$R (Li *et al.*, 2000) and other RAS components such as renin and ACE (Hokimoto *et al.*, 1996, Xiao *et al.*, 2000). Despite its well defined role in mediating organ fibrosis, the role of Ang II in EC transformation only started to be investigated very recently and in contrast to this study, has only been assessed indirectly by the use of receptor antagonists. As such, irbesartan was demonstrated to inhibit high glucose-induced EndMT *in vivo* and *in vitro* (Tang *et al.*, 2010, Tang *et al.*, 2013). Furthermore, losartan abolished TGFß$_1$-induced EndMT in bovine valve ECs while supra-physiological doses of Ang II (50 µM) directly increased expression of αSMA (Wylie-Sears *et al.*, 2014). Overall these studies suggest a role of Ang II in EndMT. However, here it was investigated whether Ang II plays a direct role in mediating EndMT and demonstrated that Ang II significantly exacerbates TGFß$_1$-induced mesenchymal transition in HCAEC. The effects of Ang II could not be blocked by inhibition of either AT$_1$R or AT$_2$R by losartan and PD123319, respectively and this is in contrast to the studies outlined above where AT$_1$R antagonism was able to prevent EndMT in high glucose conditions. However, these studies investigated Ang II as part of another pathology/mechanism rather than directly as a causative factor suggesting that

model-specific differences exist. Furthermore, in a model of EMT in renal tubular epithelial cells it has previously been demonstrated that Ang II mediates EMT through a pathway involving the ACE2/Ang-(1-7)/Mas-axis which was resistant to blockade of either the AT_1R or AT_2R (Burns *et al.*, 2010) strengthening the observation that Ang II-induced EndMT in HCAEC may be mediated *via* AT_1R and AT_2R-independent pathways. Further investigations are required to verify the role of the AT_1R, AT_2R and Mas in Ang II-induced EndMT.

An inductive role for Ang II in EMT is already well established and in cell culture models of EMT, stimulation of epithelial cells with Ang II induces a mesenchymal phenotypic switch within as little as 24 h (Carvajal *et al.*, 2008, Yang *et al.*, 2009, Yang *et al.*, 2010, Zhou *et al.*, 2010). This is in direct contrast to observations made here where similar doses of Ang II alone were not able to robustly induce a mesenchymal phenotype in ECs even after 15 days of stimulation. This may be linked to fundamental differences in cell environment and physiology. For example, kidney epithelial cells are exposed to 100 x higher Ang II concentrations than ECs (van Kats *et al.*, 2001) and due to their key role in mediating fluid balance, kidney epithelial cells may be more sensitive to Ang II stimulation activating differential signalling pathways. In this context, SMAD3 signalling and the induction of CTGF have been identified as a central pathway in Ang II-induced EMT mediating the early $TGFß_1$-independent induction of mesenchymal gene expression (Chen *et al.*, 2006, Yang *et al.*, 2009, Yang *et al.*, 2010). In contrast, here SMAD3 signalling could only be detected very weakly in HCAEC in response to Ang II stimulation.

Activation of the SMAD pathway has been shown to be essential for EndMT and EMT (Zeisberg *et al.*, 2007b, Li *et al.*, 2010, Cooley *et al.*, 2014). The present study demonstrates that $TGFß_1$ induced a time-dependent increase in SMAD2 phosphorylation which is in line with previous observations on rapid SMAD activation by TGFß which can be sustained over hours and days (Wylie-Sears *et al.*, 2014, Kim *et al.*, 2008, Yang *et al.*, 2009). In contrast, it was observed that Ang II did not induce SMAD2 phosphorylation even after 60 min. This is in contrast to previous studies which have demonstrated that Ang II induces the TGFß-independent activation of SMADs within 15-20 min in cardiac fibroblasts, VSMC and renal epithelial cells (Hao *et al.*, 2000, Rodríguez-Vita *et al.*, 2005, Carvajal *et al.*, 2008). During EMT, especially Ang II-induced SMAD3

phosphorylation has been linked to the induction of mesenchymal gene expression in epithelial cells *via* the expression of CTGF (Chen *et al.*, 2006, Yang *et al.*, 2009, Yang *et al.*, 2010). Here, SMAD3 activation in HCAEC could only be detected very weakly following stimulation with Ang II or TGFß$_1$ and suggests overall no significant role of Ang II in the early activation of the SMAD2/3 pathway during EndMT. However, preliminary results show that inhibition of SMAD2/3 abolishes most transcriptional changes induced during EndMT in HCAEC suggesting a critical role of the SMAD pathway in the long-term effects of TGFß$_1$ and Ang II. Although not investigated here, delayed phosphorylation of SMAD2 by Ang II after 2 days has been observed in the transformation of adipose mesenchymal stem cells to SMC and has been linked to MAPK-mediated TGFß secretion and activation of the TGFß–SMAD pathway (Kim *et al.*, 2008). This suggests that Ang II may enhance chronic TGFß$_1$-induced SMAD2 phosphorylation by activation of the MAPK pathway.

Investigation on the role of the ERK1/2 pathway showed that both, TGFß$_1$ and Ang II activate ERK1/2 in a time-dependent manner and that TGFß$_1$ and Ang II co-stimulation of HCAEC tends to enhance ERK1/2 activation acutely following 30 min stimulation. Rapid activation of ERK1/2 by TGFß$_1$ and Ang II is already well established (Yang *et al.*, 2009, Wylie-Sears *et al.*, 2014) and it has already been found to be indispensable for Ang II induced EMT in renal epithelial cells by activation of downstream signalling pathways involving SMAD2/3 (Carvajal *et al.*, 2008, Yang *et al.*, 2009) and RhoA (Rodrigues-Díez *et al.*, 2008). Furthermore, losartan was found to inhibit EndMT in mitral valve EC by inhibition of ERK1/2 (Wylie-Sears *et al.*, 2014). Whereas these results suggest a crucial role for the cross-activation of ERK1/2 and SMAD pathways by TGFß$_1$ and AngII in EndMT, results presented here suggest that it is unlikely that alterations in these pathways by Ang II are responsible for the exacerbated response in TGFß$_1$-induced mesenchymal gene expression by Ang II. This is supported by no detectable changes in the gene expression of members of the SMAD pathway during EndMT in HCAEC suggesting actions of Ang II independent of SMAD and ERK1/2 signalling pathways.

Here, it was shown that HCAEC significantly increase O_2^- production in response to Ang II stimulation which could be abolished by inhibition of Nox1 and Rac1 suggesting an important role for Nox1 in Ang II-induced EC dysfunction. In

agreement with this, it has previously been shown that Ang II stimulation of ECs leads to a significant increase in O_2^- production mediated *via* the AT_1R and AT_2R (Zhang *et al.*, 1999) which is due to the induction of Nox1 and Nox2 gene expression and promotion of their assembly via $p47^{phox}$ phosphorylation (Li and Shah, 2003, Higashi *et al.*, 2003, Dikalov *et al.*, 2008). Ang II-induced O_2^- was shown to peak after 1 h in human umbilical artery ECs (Zhang *et al.*, 1999) and after 10 h in human umbilical vein ECs (Rueckschloss *et al.*, 2002) whereas in HCAEC presented here O_2^- production peaked after 1 min suggesting different kinetics in O_2^- production dependent on EC origin and activated Nox isoforms. Interestingly, it has been widely noted that Ang II regulates Noxs in a dose-dependent manner with doses < 1 μM substantially increasing O_2^- formation and Nox expression whereas doses ≥ 1 μM have very little to no effect (Zhang *et al.*, 1999, Rueckschloss *et al.*, 2002) and may therefore explain the acute response in O_2^- formation observed in HCAEC in this study. Here, $TGFß_1$ stimulation did not induce any O_2^- production in HCAEC and supports previous observations that TGFβ preliminarily activates the H_2O_2 generating Nox4 which has been linked to TGFβ-induced angiogenesis (Peshavariya *et al.*, 2014) and myofibroblast differentiation (Cucoranu *et al.*, 2005).

ECs have been shown to express Nox1, Nox2, Nox4 and Nox5 which are constitutively active at low levels (Drummond and Sobey, 2014, Li and Shah, 2003). Although Nox expression in HCAEC used here was not assessed, it has already been shown previously that HCAEC express Nox1, Nox2 and Nox4 mRNA as well as mRNA for the essential subunits $p22^{phox}$, $p47^{phox}$, $p67^{phox}$ and Rac1 (Sorescu *et al.*, 2002, Yoshida and Tsunawaki, 2008). With the observation that Ang II significantly increases Nox1-dependent O_2^- production in HCAEC it can be hypothesised that Nox1 may contribute to the exacerbation of $TGFß_1$-induced EndMT by Ang II in HCAEC. This is supported by previous observations in epithelial cells and ECs where overexpression of Nox1 and Nox2 predisposed cells to undergo EMT and EndMT, respectively (Murdoch *et al.*, 2014, Liu *et al.*, 2012).

5.5 Summary

In summary, this study has shown that Ang II infusion in mice leads to the dynamic loss of capillaries that coincided with the presence of EndMT in the hearts of Ang II infused mice, an effect not blocked by co-infusion with Ang-(1-

9). Investigations of Ang II in an *in vitro* model of EndMT revealed that Ang II exacerbated TGFß$_1$-induced EndMT and that Ang II stimulation of HCAEC induces oxidative stress which may contribute to the underlying mechanism. Overall, these results present a novel pathway by which Ang II can mediate cardiac capillary loss and contribute to cardiac fibrosis *in vivo*.

Chapter 6 – Determination of Ang II in fibroblast-derived microvesicles and its role in cardiomyocyte hypertrophy

6.1 Introduction

In the last decades, the actions of cellular microvesicles (MVs), fragments of the plasma membrane shed by cells, in cellular communication has been reported as a novel method of intracellular communication within any living organism (Ibrahim and Marbán, 2015). The presence of MVs in blood has been known since 1946 when Chargaff & West (1946) explored a thromboplastic lipoprotein that sedimented at high centrifugal forces while remaining in solution at low spinning speeds (Chargaff F and West, 1946). Wolf (1967) was the first to isolate these particles and image them using electron microscopy (Wolf, 1967). The term exosomes was first used by Johnstone *et al.* (1987) to describe the MVs derived from reticulocytes during their maturation to erythrocytes *in vivo* and *in vitro* (Johnstone *et al.*, 1987). The characteristics of these vesicles were similar to the cell membrane of the reticulocytes they derived from and were enriched in acetylcholinesterase and transferrin which was lost during erythrocyte maturation (Johnstone *et al.*, 1987). While it was then thought that the secretion of MVs was part of the cells waste management, the use of proteomics and genomics identified MVs as major carriers of DNA, RNA and proteins revealing MVs as a major pathway for intracellular communication (Waldenström *et al.*, 2012, Pisitkun *et al.*, 2004). The production of MVs has been confirmed for eukaryotes ranging from amoebas, plants to animals and humans and it is now accepted that MVs function as autocrine, paracrine and endocrine signalling systems to convey cell specific messages within an organism (Ibrahim and Marbán, 2015). A single cell releases a variety of different vesicles that overlap in their size distribution, membrane profile and function (Heijnen *et al.*, 1999). These include apoptotic bodies (1–5 μm), MVs (100–1000 nm) and exosomes (20–150 nm). The role of apoptotic bodies is purely the removal of damaged cells whereas MVs and exosomes have both been shown to participate in cellular communication (Sluijter *et al.*, 2014). MVs are derived from shedding of the plasma membrane and closely reflect the plasma membrane of the cell of origin and may be enriched in cell lineage markers as well as MMPs (Lee *et al.*, 2011) (Figure 6-1). In contrast, exosomes are derived *via* the endosomal pathway and the formation of multivesicular bodies (MVB) and have been found to be enriched in tetraspanins CD63, CD9 and CD81 all of which are involved in intracellular MVB formation. However, because these markers are not mutually

exclusive over the MV populations (Ibrahim and Marbán, 2015), MVs and exosomes are largely discriminated by their intracellular origin and so far it has been difficult to attribute the mechanistic effects to either vesicle population as current isolation protocols are unable to distinguish between the two populations.

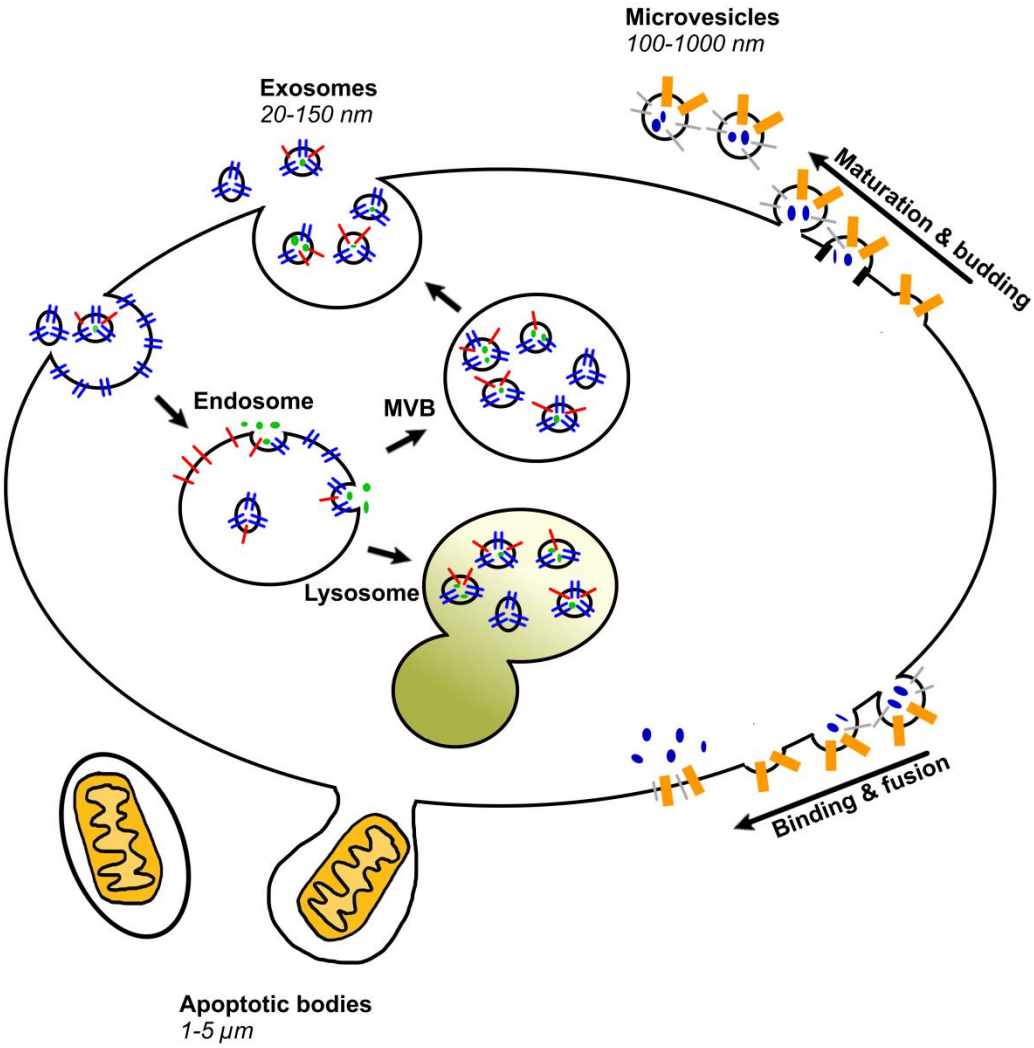

Figure 6-1. Biosynthesis of exosomes and microvesicles.
Exosomes in the extracellular space and membrane proteins are endocytosed into endosomes (left). Intraluminal vesicles bud of the endosomal membrane, incorporating ubiquitinated proteins as well as other membrane and cytoplasmic components to form multivesicular bodies (MVB). MVBs eventually fuse with the plasma membrane to release exosomes into the extracellular space. Alternatively, endosomes can fuse with lysosomes for degradation. Microvesicles (MV) are released by budding of the plasma membrane (right). This involves the clustering of the molecular cargo at the plasma membrane and subsequent maturation and budding of the MV. For re-uptake, MVs may then fuse with the plasma membrane of the cells, incorporating into the membrane and release its content into the cytoplasm (bottom right). Alternatively, MVs can be taken up by endocytosis into endosomes. Apoptotic bodies are released from cells undergoing apoptosis and contain intracellular organelles which are subsequently removed by macrophages. Schematic adapted from Cocucci and Meldolesi (2015).

6.1.1 Microvesicle Biosynthesis

Exosomes

Exosomes are MVs that are derived *via* the endosomal pathway involving the formation of MVB that fuse with the cell membrane (Figure 6-1). In the first step of exosome formation, the molecular cargo laterally segregates along the delimiting membrane of the endosome which then invaginates and pinches off releasing the vesicle into the endosome, creating MVBs (Raposo and Stoorvogel, 2013). The machinery involved in the formation of MVBs comprises the family of endosomal sorting complex responsible for transport (ESCRT) proteins 0–III (Wollert and Hurley, 2010). ESCRT complex 0 recognizes ubiquitinated proteins marked for lysosomal degradation and sequesters them to the delimiting membrane on the endosome. ESCRT complexes I and II then induce the budding of the membrane while the ESCRT complex III mediates the fission of the endosomal membrane into the endosome (Wollert and Hurley, 2010). Although the ESCRT complex has been shown to be involved in the generation of exosomes, cells with silenced ESCRT complexes are still able to form MVBs, secrete exosomes and load non-ubiquitinated proteins suggesting ESCRT independent mechanisms of MVB and exosome formation (Colombo *et al.*, 2013, Stuffers *et al.*, 2009). In this aspect, sphingomyelinase was shown to be involved in the formation of exosomes in oligodendroglial cells and this corresponds with the high content of ceramide in exosomes (Trajkovic *et al.*, 2008). Following MVB formation, endosomes are either destined for degradation in the lysosomal pathway or fusion with the cell membrane and evidence suggests that this is in part governed by the composition of MVBs. In line with this, intraluminal vesicles of MVB that were secreted as exosomes were found to be rich in cholesterol while vesicles associated with lysosomes were cholesterol-poor (Möbius *et al.*, 2002). Fusion of MVBs requires exocytosis, however, the machinery involved in the fusion of MVB with the plasma membrane is only starting to be uncovered and a role for the small GTPases Rab11, Rab27 and Rab35 as well as the classic tSNARE–vSNARE system employed in the release of synaptic vesicles has been suggested (Cocucci and Meldolesi, 2015). Exosome release usually occurs several minutes after stimulation and this is in line with the requirement of exocytosis of MVBs to release vesicles into the extracellular space (Qu *et al.*, 2009).

Microvesicles

MVs other than exosomes do not require exocytosis but rather are thought to originate from the regulated outward budding of the plasma membrane. Release of MVs can occur instantly following stimulation (Baroni *et al.*, 2007, Pizzirani *et al.*, 2007); however, the mechanisms involved in the formation of MVs are largely unknown. Recently it has been shown that post-translational modifications such as palmitoylation and myristoylation as well as binding sites for PIP_2 and PIP_3 are sufficient to anchor cytoplasmic proteins to the plasma membrane and lead to their incorporation in MVs (Shen *et al.*, 2011). While it has been shown that activation of PKC and increases in intracellular Ca^{2+} can induce and sustain the release of MVs (Pizzirani *et al.*, 2007, Stratton *et al.*, 2015), the ESCRT complex has also recently been shown to be involved in the loading of proteins into MV and the budding off the plasma membrane (Nabhan *et al.*, 2012) suggesting that despite their different spatial origins, the biogenesis of MVs and exosomes share common pathways. Interestingly, in contrast to the release of exosomes, vesicle shedding in erythrocytes was shown to be facilitated by depletion of cholesterol (Gonzalez *et al.*, 2009).

MVs and exosomes released into the extracellular space can act either as an autocrine or paracrine signal to the surrounding cells within the tissue or enter the blood stream, lymph or cerebrospinal fluid to navigate to target tissue in an endocrine fashion (Caby *et al.*, 2005, Luketic *et al.*, 2007). MVs do not arbitrarily bind with any cell but show target selectivity. For example, MHCII-positive B-cell derived exosomes show a high specificity for the MHCII negative follicular dendritic cells and bind only weakly to macrophages and plasma cells (Denzer *et al.*, 2000). Similarly, exosomes derived from a luciferase reporter expressing B16BL6 melanoma cell line were shown to preferentially bind to hepatic and splenic macrophages and pulmonary endothelial cells when administered *in vivo* (Imai *et al.*, 2015). Similar to the binding of immune cells to activated endothelial cells, MVs initially roll over the cell surface before attaching to the plasma membrane by cell surface receptors (Tian *et al.*, 2013b). The MVs can then either directly fuse with the plasma membrane to release their contents into the cytoplasm or be taken up by a form of endocytosis, including clathrin mediated endocytosis and phagocytosis (Tian *et al.*, 2013b, Denzer *et al.*, 2000, Montecalvo *et al.*, 2012). In other cases, MVs may not be internalised and

instead activate intracellular signalling pathways on their binding to the plasma membrane (Vicencio *et al.*, 2015, Lyu *et al.*, 2015) while other MVs can break upon their release thereby liberating their contents into the extracellular space which is then free to interact with receptors on nearby cells (Cocucci and Meldolesi, 2015, Pizzirani *et al.*, 2007).

6.1.2 Microvesicles in cardiovascular disease

The concept that exosomes participate in the propagation of disease has developed in recent years in particular with the identification of the crucial role of exosomes and MVs in cancer progression and metastasis. CVD is commonly associated with cardiac remodelling including cardiac hypertrophy and fibrosis and increasing evidence suggests a role of exosomes/MVs in mediating pathological signalling in the heart, giving them the name pathosomes (Ibrahim and Marbán, 2015). Cardiomyocytes have previously been shown to secrete MVs (cardiosomes) that contain DNA and RNA and modulate the transcriptome of the recipient cells (Waldenström *et al.*, 2012, Gennebäck *et al.*, 2013). Cardiomyocytes exposed to hypoxia as it occurs during myocardial ischaemia double their secretion of MVs and exosomes within 2 h of hypoxia (Gupta and Knowlton, 2007). The released vesicles are enriched in the molecular chaperone heat shock protein (Hsp) 60 which applied extracellularly has been associated with the activation of toll like receptor 4 (Tlr4) and concomitant production of TNFα and inflammatory cytokines contributing to cardiomyocyte dysfunction and death (Tian *et al.*, 2013a). In contrast, plasma derived exosomes rich in Hsp70 were shown to protect the rat myocardium against ischaemia-reperfusion injury by activation of Tlr4 and the cardioprotective Hsp27 (Vicencio *et al.*, 2015) highlighting that the source of MVs strongly affects the signals they elicit in their target cells. Cardiac fibroblasts have previously been shown to mediate cardiomyocyte hypertrophy by soluble mediators (Cartledge *et al.*, 2015). Recently, two independent groups have presented evidence that exosomes/MVs play a role in transfer of pro-hypertrophic messages from fibroblast to cardiomyocytes. Bang *et al.* (2014) showed that fibroblast derived exosomes were enriched in miR-21* and transfer of miR-21* to cardiomyocytes induced cardiomyocyte hypertrophy *via* the silencing of Sorbin And SH3 Domain Containing 2 (SORBS2) and PDZ And LIM Domain 5 (PDLIM5) in cardiomyocytes (Bang *et al.*, 2014). In particular, miR-21* was further increased in the exosomes

from fibroblasts stimulated with Ang II and in the exosomes derived from the pericardial fluid of animals following TAC suggesting a role in disease propagation (Bang *et al.*, 2014). In an independent study, Lyu *et al.* (2015) also reported pro-hypertrophic actions of cardiac fibroblast-derived exosomes on isolated cardiomyocytes *via* the activation of the cardiomyocyte RAS (Lyu *et al.*, 2015). This was dependent on the activation of intracellular signalling pathways including ERK1/2, JNK and Akt by extracellular exosomes and was independent of the activation of cardiac fibroblasts by Ang II or TGFβ (Lyu *et al.*, 2015). More recently, it has been demonstrated that following pressure overload, cardiomyocytes release exosomes enriched with functional AT_1R and by targeting cardiomyocytes, skeletal muscle and resistance vessels can modulate vascular responses thereby potentially contributing to CVD development (Pironti *et al.*, 2015).

6.2 Aims

- Assess the release of MVs from cardiac fibroblasts and characterise the MV population.

- Determine whether Ang II is present in fibroblast-derived MVs and MVs isolated from blood in animal models of hypertension and cardiac remodelling.

- Assess the effects of fibroblast-derived MVs in cardiomyocyte hypertrophy.

6.3 Results

6.3.1 Microvesicle characterisation

MVs were purified from conditioned media from untreated or Ang II-stimulated fibroblasts and characterised using NTA (Figure 6-2). Over a period of 48 h, a 90–100 % confluent monolayer of NRCF cultured in a 150 cm^2 flask released approximately 10^8–10^{10} MVs with a modal particle size between 100–200 nm (Figure 6-2 A-B). There was no difference in the number of MVs secreted by control or Ang II-stimulated fibroblasts [MV no. ($x10^8$): Control 7.46 ± 0.48 *vs.* Ang II 9.33 ± 0.78, n= 3, $p>0.05$] (Figure 6-2 C).

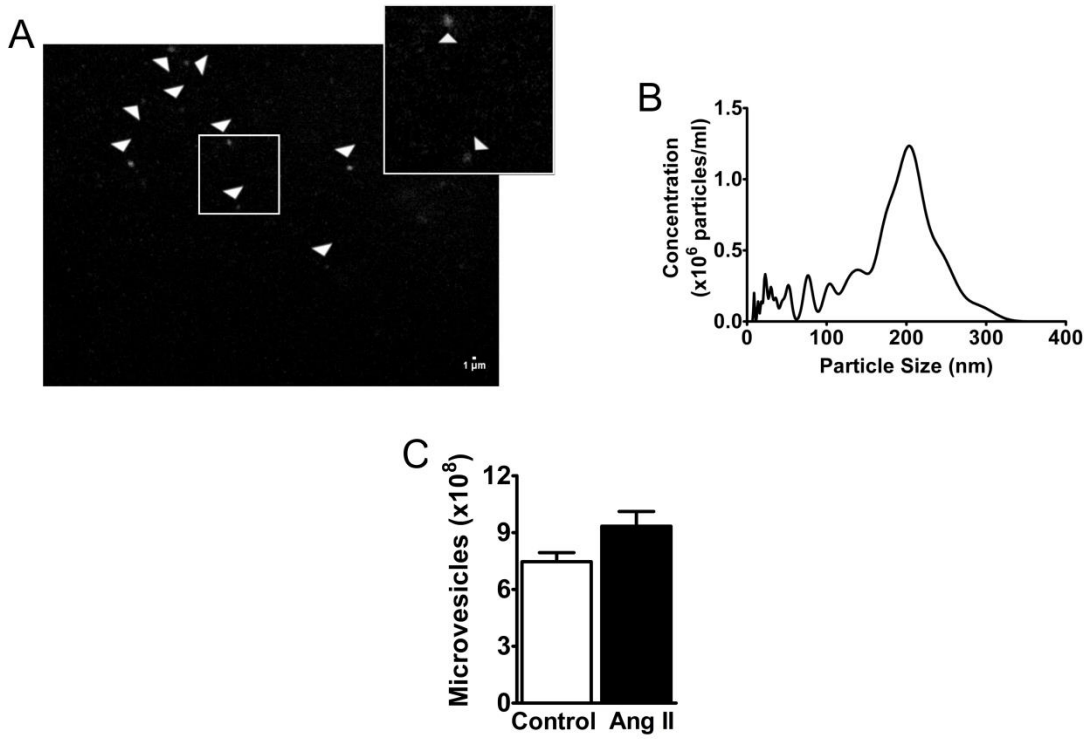

Figure 6-2. NRCF secrete microvesicles.
(A) Example image of microvesicles captured by nanoparticle tracking analysis (NTA). (B) Representative graph of microvesicle size distribution measured by NTA. (C) Representative graph of the mean number of MVs purified from a confluent monolayer of NRCF in a 150 cm^2 tissue culture flask. n= 3. Data are presented as mean ± SEM.

6.3.2 Angiotensin II in microvesicles

Since it has previously been shown that exosomes can contain ACE and ACE2 (Gonzales *et al.*, 2009, Pisitkun *et al.*, 2004), next, it was assessed whether MVs released from fibroblasts also contained Ang II. For this, MVs were purified from control NRCF or NRCF stimulated with 1 μM Ang II for 48 h. Conditioned media was prepared in triplicate from NRCF at passage 2, 3 and 4. Purified MVs were sonicated and Ang II levels were determined in MVs and MV-depleted supernatant using the Angiotensin II EIA ELISA (Section 2.4.7.1, Figure 6-3).

Ang II was present at low concentrations in the MV-depleted supernatant of control NRCF and this was significantly increased following the treatment of NRCF with 1 μM Ang II for 48 h (control 1.46 ± 0.51 pg/mL *vs.* Ang II 29.95 ± 5.31 pg/mL, n= 9, $p<0.05$) (Figure 6-3 A). Ang II was also detected at low concentrations of 3.42 ± 0.85 pg/mL in MVs isolated from control NRCF. Ang II stimulation of NRCF increased Ang II content in MV to 7.81 ± 2.05 pg/mL (p= 0.06) (Figure 6-3 A).

To further confirm the presence of Ang II in MVs, DiI-labelled NRCF were treated with FAM-labelled Ang II and the purified MVs were tracked on H9c2 cells which are a rat cardiomyoblast cell line, by confocal imaging (Figure 6-3 C). After 30 min, MVs had settled onto the H9c2 cells and were bound to the cell membrane. DiI signal could be detected in H9c2 cardiomyocytes treated with MVs from unstimulated NRCF. In contrast, in H9c2 cardiomyocytes treated with MVs from FAM-Ang II stimulated NRCF, the red DiI signal co-localised with green FAM-Ang II signal (Figure 6-3 C). This was confirmed by a corresponding significant increase in the co-localisation coefficients Pearson's R, Mander's M1 and M2 (Table 6-1) and confirms packaging of exogenous Ang II into MVs by cardiac fibroblasts.

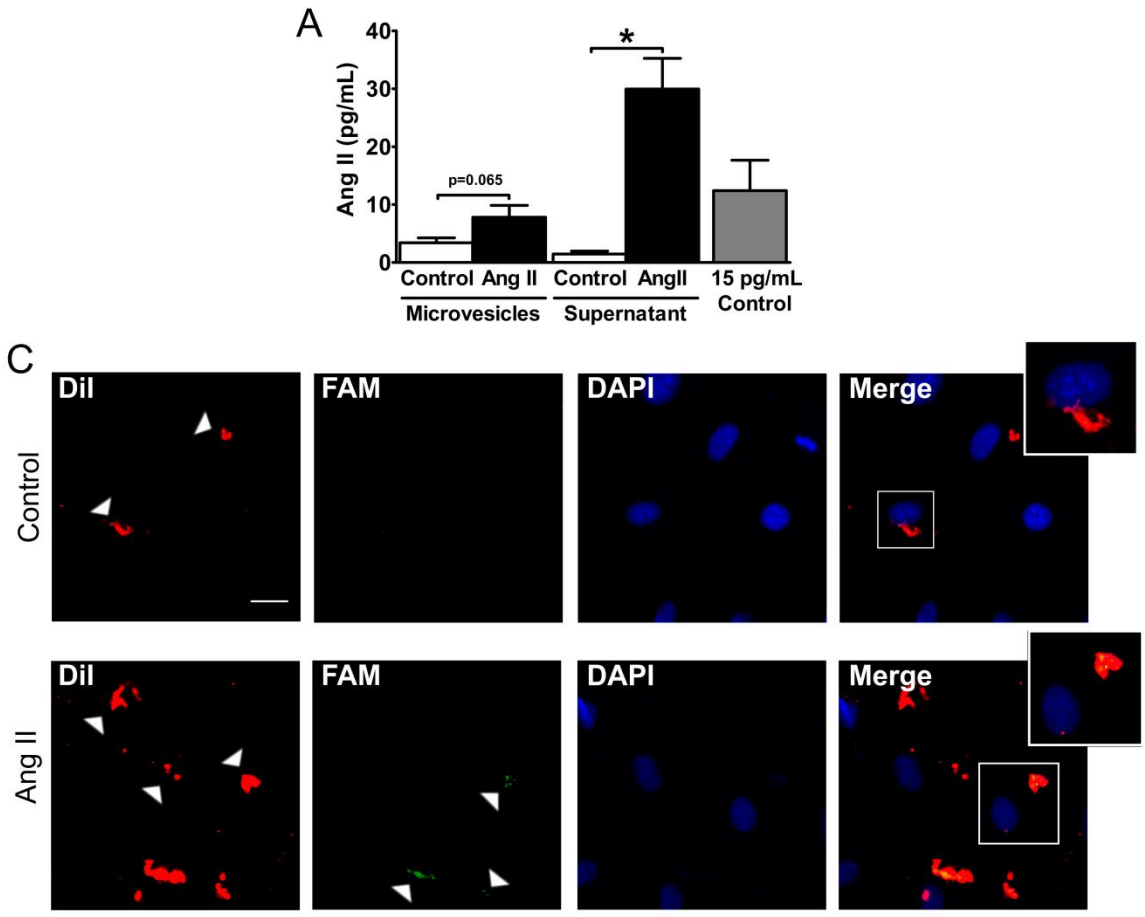

Figure 6-3. Ang II is located in microvesicles
Microvesicles were purified from conditioned medium of untreated or Ang II-stimulated neonatal rat cardiac fibroblasts (NRCF). Ang II concentration was measured in (A) microvesicles and the microvesicle-depleted supernatant. A sample of predetermined Ang II concentration (15 pg/mL) was used as positive control. n= 9 for each group. *p<0.05 *vs.* control (Student's t-test). (C) H9c2 cardiomyocytes were incubated with microvesciles from DiI labelled unstimulated or FAM-Ang II-stimulated NRCF for 30 min and microvesicles were imaged for DiI (red) and FAM-Ang II (green) using confocal microscopy. The inset represents the magnified area in the white square. Magnification: 40 x. Scale bar: 100 µm.

Table 6-1. Co-localisation coefficients of FAM-Ang II in DiI-labelled microvesicles

	Pearson's coefficient R				Mander's coefficient M1				Mander's coefficient M2			
	MEAN	SEM	n	p	MEAN	SEM	n	p	MEAN	SEM	n	p
Control	0.028	0.014	6		0.003	0.002	6		0.084	0.063	6	
Ang II	0.348	0.045	8	<0.0001	0.203	0.038	8	0.0007	0.762	0.106	8	0.0003

6.3.3 Fibroblasts and cardiomyocyte communication by MVs

It has previously been shown that fibroblasts and cardiomyocytes can exchange exosomes (Lyu *et al.*, 2015, Bang *et al.*, 2014). To verify MV exchange between NRCF and H9c2 cardiomyocytes, NRCF were labelled with DiI (Figure 6-4 A) and plated in the top chamber of a 0.4 µm transwell while H9c2 cardiomyocytes were plated in the bottom (Figure 6-4 B). DiI exchange was visualised by confocal microscopy in H9c2 cardiomyocytes after 48 and 96 h of co-culture (Figure 6-4 C) and supporting the assertion that MVs were transferred between NRCF and H9c2 cardiomyocytes.

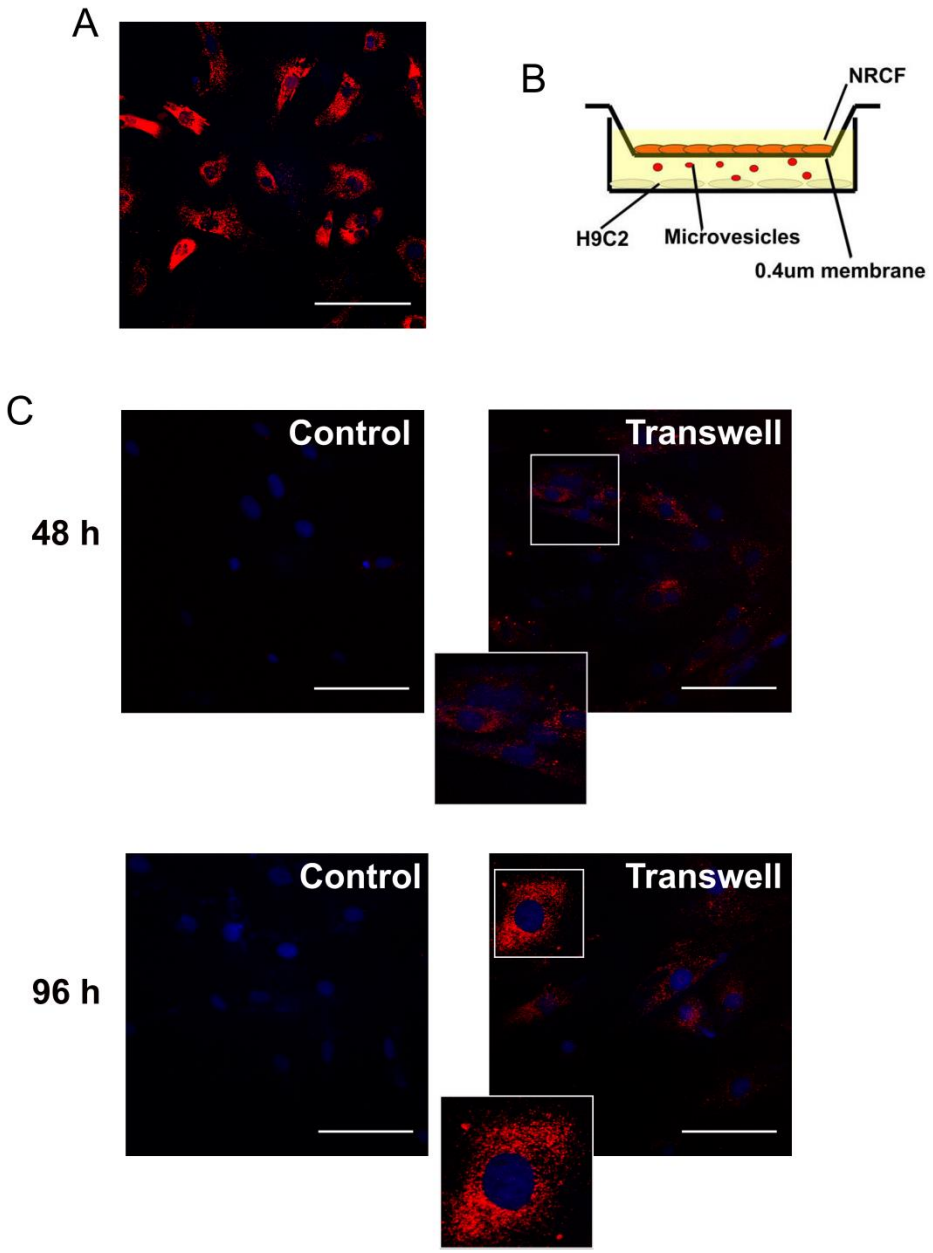

Figure 6-4. Fibroblasts and cardiomyocytes communicate via microvesicles
(A) Neonatal rat cardiac fibroblasts (NRCF) were labelled with Vybrant DiI for 30 min and plated on glass coverslips. DiI labelling of NRCF was examined by confocal microscopy after 48 h in culture. (B) DiI-labelled NRCF were plated in the top chamber of a 0.4 µm pore size transwell while H9c2 cardiomyocytes were seeded in the bottom. Microvesicle exchange was allowed for 48–96 h prior to fixation of H9c2 cardiomyocytes. DiI transfer *via* NRCF-derived microvesicles was assessed by confocal microscopy (C). The inset represents the magnified area within the white square. DiI: red, DAPI: blue. Magnification: 40x. Scale bar: 100 µm.

6.3.4 Microvesicles in cardiomyocyte hypertrophy

To assess whether the Ang II contained in the MVs is biologically active, H9c2 cardiomyocytes were incubated with MVs derived from control and 1 μM Ang II-stimulated NRCF for 96 h to induce cardiomyocyte hypertrophy. Cells were then stained with phalloidin to outline cell boundaries and their cross-sectional area measured. Stimulation with 100 nM Ang II served as a positive control (Figure 6-5)

MVs from 1 μM Ang II-stimulated NRCFs induced significant 64% ($p<0.05$) increase in H9c2 cardiomyocyte size compared to cells treated with MVs from unstimulated NRCFs (Figure 6-5 A-B). The increase in cross-sectional area was similar to hypertrophy achieved by direct stimulation with 100 nM Ang II (Control 3575.45 ± 123.77 μm^2 *vs.* AngII 6151.49 ± 281.35 μm^2, n= 109-194, $p<0.05$). This confirms that the Ang II contained in MVs from Ang II-stimulated fibroblasts is biologically active and is as potent as direct stimulation with Ang II.

To further verify that this response was not limited to H9c2 cardiomyocytes, primary NRCM were treated with MVs derived from unstimulated and 1 μM Ang II-stimulated NRCF (Figure 6-5 C-D). MVs from Ang II-stimulated fibroblasts induced a 94 % ($p<0.05$) increase in NRCM cross-sectional area. Similarly, direct stimulation with Ang II induced a 51 % ($p<0.05$) increase in NRCM size (Figure 6-5 D) confirming that the pro-hypertrophic effect of MVs derived from Ang II-stimulated fibroblasts can be observed in cell line models and primary cardiomyocytes.

Due to the different Ang II concentrations used for the stimulation of NRCF to generate MV-conditioned medium and H9c2 cardiomyocytes to induce cell hypertrophy, it was assessed whether stimulation of NRCF with 100 nM Ang II also led to loading of Ang II into MVs to transfer a pro-hypertrophic effect onto H9c2 cells (Figure 6-5 E-F). MVs from NRCF stimulated with 100 nM Ang II induced a 25 % increase in cell size ($p<0.05$) and this was significantly smaller than the 55 % increase in cell size observed with direct stimulation ($p<0.05$) (Figure 6-5 F). This suggests that loading of Ang II into MVs is dose-dependent.

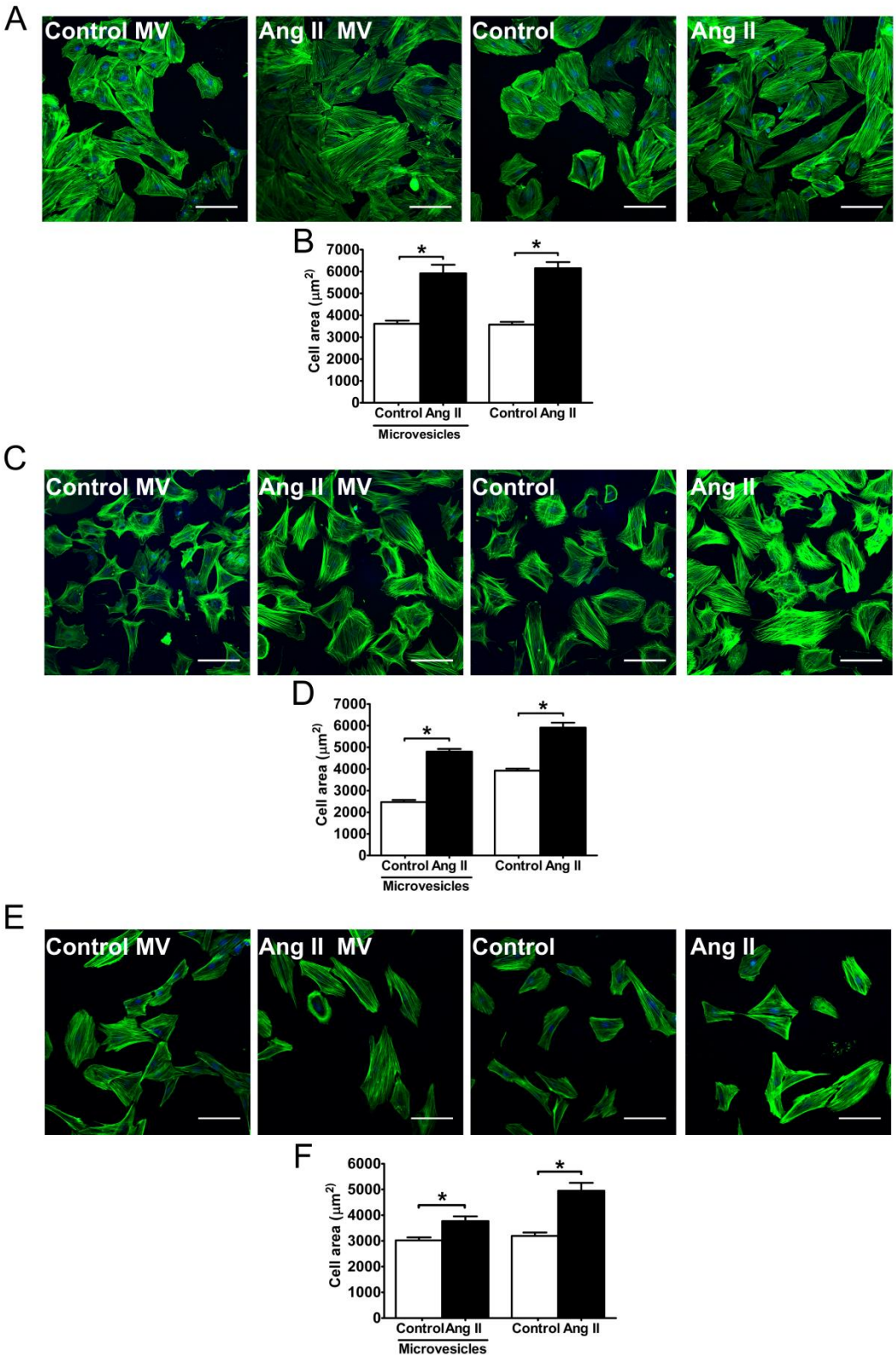

Figure 6-5. Microvesicles induce cardiomyocyte hypertrophy.
Microvesicles (MVs) were isolated from the conditioned medium of unstimulated and 1 µM Ang II-stimulated neonatal rat cardiac fibroblasts (NRCF). H9c2 cardiomyocytes were either treated with 100 nM Ang II or purified NRCF MVs for 96 h. Cells were then stained with (A) phalloidin and (B) cell area was determined (n= 109–194). (C-D) In a similar manner, NRCM were treated with MVs from control and Ang II-stimulated NRCF and cells size determined (n= 160–221). (E-F) MVs were purified from the conditioned medium of unstimulated or 100 nM Ang II-stimulated NRCF and H9c2 cardiomyocyte size was determined (n= 110–167). Data are presented as mean ± SEM. Experiments were performed in triplicate and repeated on three independent occasions. Scale bar: 100 µm. *p<0.05 (Student's t-test).

6.3.5 Effects of Brefeldin A and Proteinase K

To verify that the pro-hypertrophic effect of MVs from Ang II-stimulated fibroblasts is specific to the release of MVs and not a paracrine factor, MV release was inhibited by BFA. BFA is an inhibitor of the endosomal secretory pathway (Islam *et al.*, 2007) but due to its global effect on cellular secretion, its application is limited by its effects on cell viability and only allows stimulation for a maximum of 24 h.

BFA significantly reduced the number of MVs released from NRCF in a 24 h period by approximately 50 % ($p<0.05$) which were then incubated on H9c2 cardiomyocytes (Figure 6-6 A). While it was confirmed that even after only 24 h stimulation with Ang II, MVs derived from Ang II-stimulated NRCF induced cardiomyocyte hypertrophy, treatment of NRCF with BFA abolished the pro-hypertrophic effect of the purified MVs when added to cardiomyocytes (control 3731.66 ± 106.78 μm^2, Ang II 4993.07 ± 215.14 μm^2, Ang II BFA 3811.01 ± 105.58 μm^2, n= 153-224, $p<0.05$) (Figure 6-6 B-C).

Secondly, to verify that the pro-hypertrophic effect of NRCF-derived MVs was due to Ang II encapsulated in MVs and not a factor attached to the vesicular membrane, MVs were treated with Proteinase K (Figure 6-6 D-E). Proteinase K is a serine protease that can cleave proteins over a broad spectrum and allows the breakdown of proteins contained on the vesicular surface while leaving proteins contained in the vesicular lumen intact (Shelke *et al.*, 2014, Gupta and Knowlton, 2007). Treatment of MVs with proteinase K did not alter their pro-hypertrophic effect (control 2980.39 ± 86.01 μm^2 *vs.* Ang II 4891.256.71 µm2, n= 166-215, $p<0.05$) (Figure 6-6 D-E). This confirms that the effect of NRCF-derived MVs is specific to vesicular release and Ang II packaged within rather than attached to the outside of MVs.

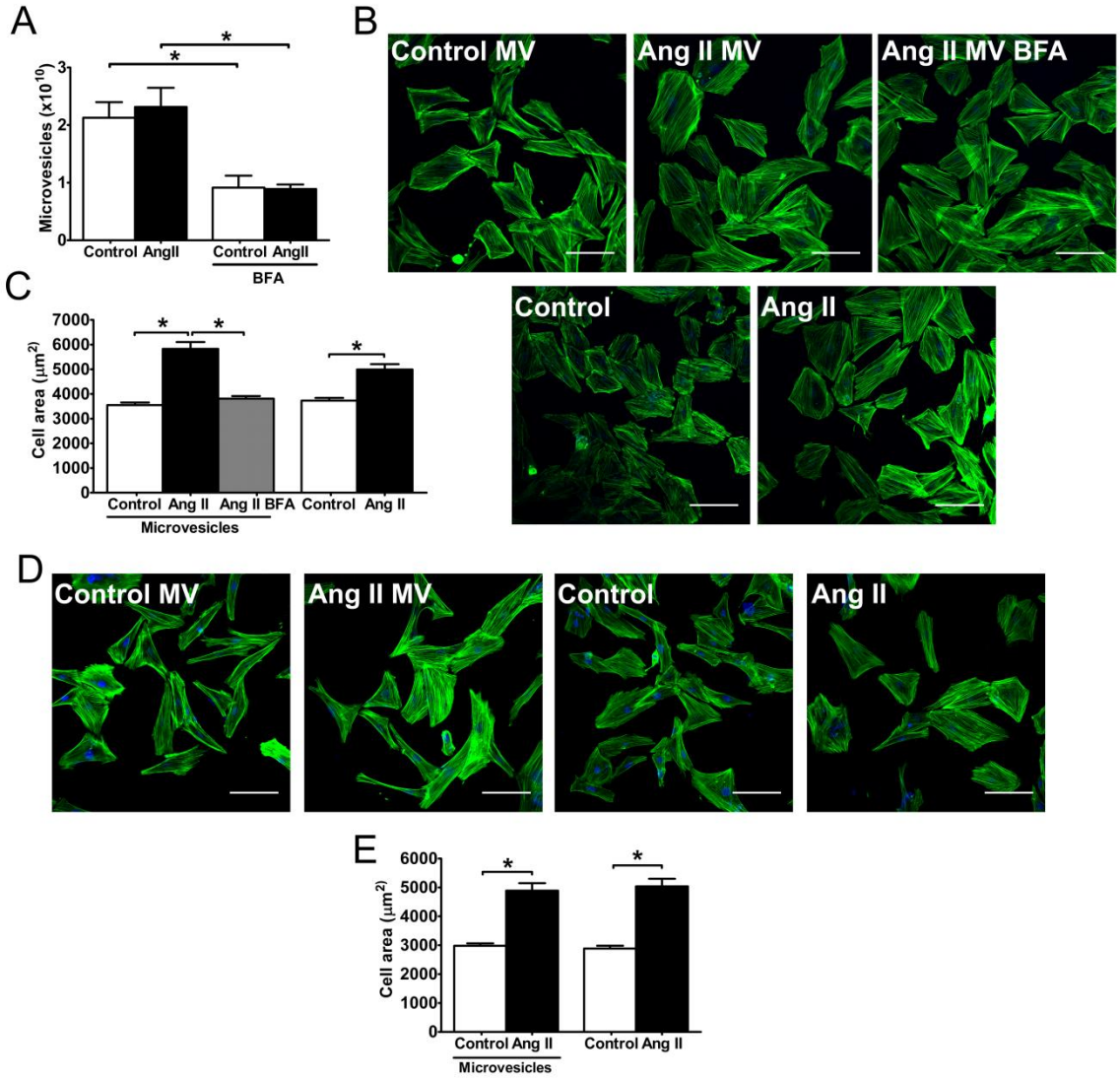

Figure 6-6. Effects of BFA and Proteinase K on microvesicle-induced hypertrophy. Neonatal rat cardiac fibroblasts (NRCF) were stimulated with 1 µM Ang II in the presence or absence of 5 µg/mL BFA for 24 h and microvesicles (MVs) were purified from the conditioned medium. (A) MV concentration was quantified by nanoparticle tracking analysis (NTA) (n= 3 for each treatment). (B) Isolated MVs were incubated on H9c2 cardiomyocytes for 96 h and stained with phalloidin and (C) mean cell size was determined (n= 153–224). (D) Example images of phalloidin stain of H9c2 cardiomyocytes treated with 100 nM Ang II or MVs from 1 µM Ang II and unstimulated NRCF that were treated with 500 µg/mL Proteinase K at 37 ºC for 1 h. (E) Mean cell size of H9c2 cardiomyocytes treated with Proteinase K treated MVs (n= 136–219). Data are presented as mean ± SEM. Experiments were performed in triplicate and repeated on three independent occasions. Scale bar: 100 µm. *p<0.05 (Student's t-test and ANOVA with Tukey's post-hoc analysis).

6.3.6 Role of angiotensin receptors

Next, to assess whether the Ang II contained in MVs is mediating pro-hypertrophic changes *via* the classical AT_1R signalling pathway, the AT_1R was blocked by the addition of losartan (Figure 6-7).

Losartan fully blocked cardiomyocyte hypertrophy induced by direct application of 100 nM Ang II ($p<0.05$) (Figure 6-7), confirming an AT_1R mediated effect. In a similar manner, Losartan prevented the increase in cell size induced by MVs from Ang II-stimulated NRCF (control 3490 ± 107.51 μm^2, Ang II 6101.65 ± 297.64 μm^2, Ang II+Losartan 3547.93 ± 112.23 μm^2, n= 134–225, $p<0.05$) (Figure 6-7). This confirms that the Ang II contained in MVs is mediating cardiomyocyte hypertrophy in an AT_1R dependent pathway similar to stimulation with free Ang II.

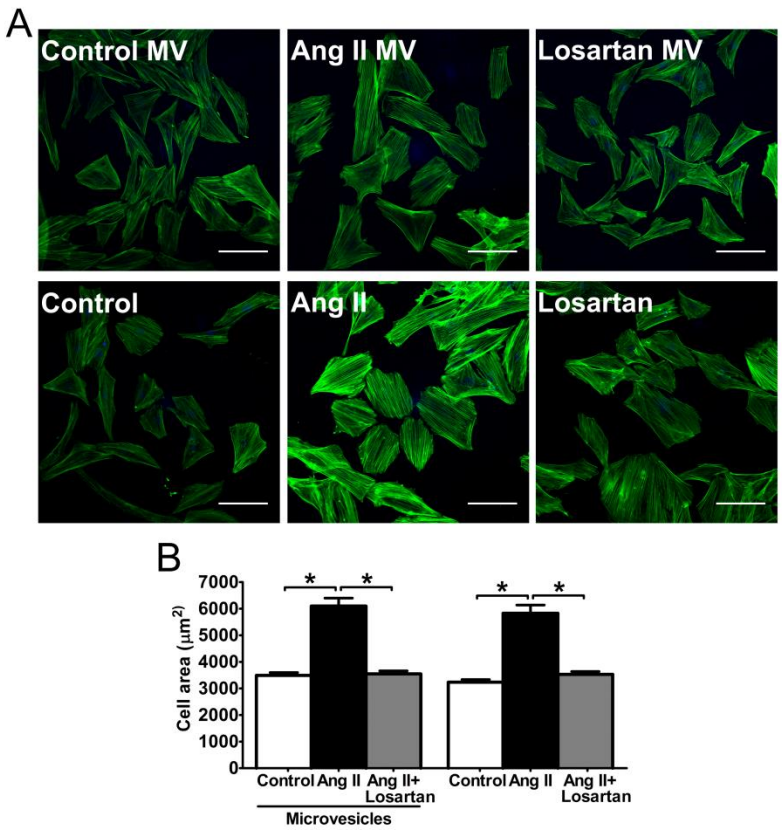

Figure 6-7. Effect of Losartan on microvesicle-induced hypertrophy.
H9c2 cardiomyocytes were treated with 100 nM Ang II or microvesicles (MVs) of untreated or Ang II-stimulated neonatal rat cardiac fibroblasts (NRCF) in the presence or absence of 1 μM Losartan. (A) Example images of phalloidin stain in the different treatment groups. (B) Mean cell size quantified by phalloidin stain (n= 134–225). Data are presented as mean ± SEM. Experiments were performed in triplicate and repeated on three independent occasions. Scale bar: 100 μm. *p<0.05 (ANOVA with Tukey's post-hoc analysis).

Since it has previously been shown that fibroblast-derived exosomes can induce cardiomyocyte hypertrophy by transfer of miR-21* (Bang *et al.*, 2014) and by activation of cardiomyocyte RAS (Lyu *et al.*, 2015), gene expression of miR-21* and RAS components was assessed by qPCR in NRCF-derived MVs and H9c2 cells treated with MVs, respectively (Figure 6-8). Expression of miR-21* in NRCF and NRCF-derived exosomes was below the detection limit of the Taqman assay. Preliminary results show that H9c2 cardiomyocytes, express mRNA for AT_1R, AT_2R, Mas and ACE. Stimulation of cardiomyocytes with exogenous Ang II did not modify mRNA levels of the AT_1R but treating cells with MVs irrespective of Ang II treatment tended to increase AT_1R expression (RQ: Ang II 1.15 ± 0.43, control MV 2.51 ± 0.45, Ang II MV 2.63 ± 3.56, $p>0.05$) (Figure 6-8 A). AT_2R gene expression in H9c2 cells was significantly increased 4-fold by treatment with control MVs compared to untreated H9c2 cardiomyocytes ($p<0.05$) (Figure 6-8 B). There was no difference in AT_2R expression between treatment with control or Ang II MVs ($p>0.05$). Expression of the Mas receptor was not changed (Figure 6-8 C). Similarly, ACE gene expression was unaffected by treatment with control MVs or Ang II MVs (Figure 6-8 D).

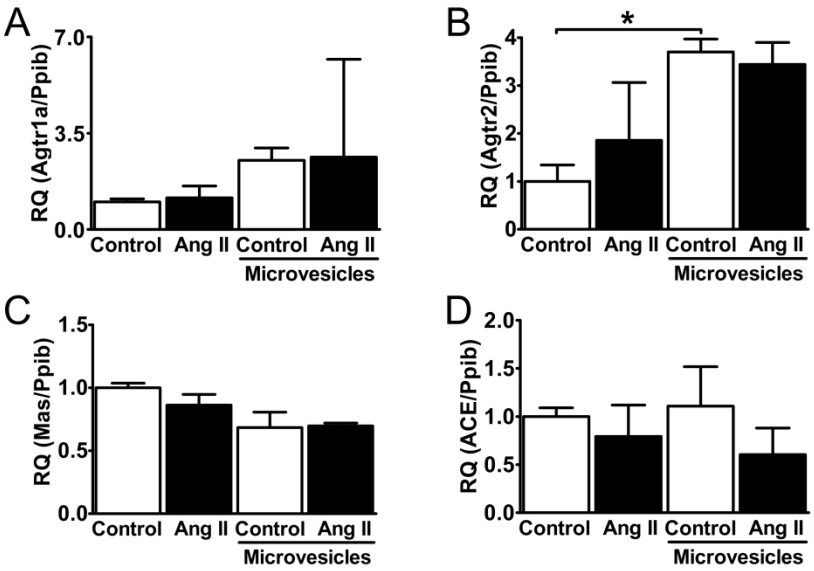

Figure 6-8. Gene expression of RAS components following MV treatment.
H9c2 cardiomyocytes were treated with 100 nM Ang II or microvesicles (MVs) purified from unstimulated or Ang II-stimulated neonatal rat cardiac fibroblasts (NRCF) for 96 h. Gene expression of (A) Agtr1a , (B) Agtr2, (C) Mas and (D) ACE was assessed by qPCR, normalised to the housekeeper Ppib and expressed as relative quantity (RQ) compared to untreated control cells which was arbitrarily set as RQ= 1. Data are presented as RQ + rqmax. n= 4 individual biological repeats for each group. *$p<0.05$ (ANOVA with Tukey's post-hoc analysis)

6.3.7 Angiotensin II in microvesicles isolated from blood

Since Ang II was localised in MVs isolated from NRCF in culture, it was determined next whether Ang II is also present in circulating blood MVs from two animal models of hypertension, a murine model of Ang II infusion hypertension (Section 3) and the SHRSP (Doggrell and Brown, 1998) (Figure 6-9). MVs were isolated from the serum of control mice and mice infused with Ang II and the plasma of 21-week old WKY and SHRSP rats (at this age hypertension is fully developed). MVs were quantified using NTA and Ang II content was measured by ELISA.

On average, there were 15.56 ± 3.95 x 10^7 MVs/µL serum in control mice (Figure 6-9 A). This was unchanged by the infusion of either 24 or 48 µg/kg/hr Ang II (x10^7 MVs/µL: 24 µg/kg/hr Ang II 9.61 ± 2.45, 48 µg/kg/hr Ang II 15.96 ± 4.36, n= 3-6, $p>0.05$) (Figure 6-9 A). Ang II was detected in the serum MVs from all treatment groups with an average of 0.36 ± 0.15 pg/mL *per* 10^9 MVs in control animals (Figure 6-9 B). This was unchanged by low dose Ang II infusion. However, the high dose of Ang II tended to increase Ang II content in MVs to 2.08 ± 1.50 pg/mL/10^9 MVs, although this did not reach significance (Figure 6-9 B). Interestingly, Ang II concentration in the MV depleted serum was decreased by Ang II infusion (control 179.20 ± 8.20 pg/mL, 24 µg/kg/hr Ang II 71.55 ± 22.60 pg/mL, 48 µg/kg/hr Ang II 93.33 ± 41.50 pg/mL, n= 3-6, $p>0.05$) (Figure 6-9 C).

In the plasma of WKY rats there were on average 1.86 ± 0.36 x 10^8 MVs/µL plasma and this was not different in the SHRSP (2.96 ± 0.32 x 10^8 MV/µL, n= 3, p= 0.08) (Figure 6-9 D). Ang II was present in the plasma MVs from both, WKY and SHRSP rats and levels were unchanged by the development of hypertension in SHRSP (pg/mL/10^{10} MVs: WKY 15.86 ± 4.59 *vs.* SHRSP 10.32 ± 2.88 , n= 3, $p>0.05$] (Figure 6-9 E).

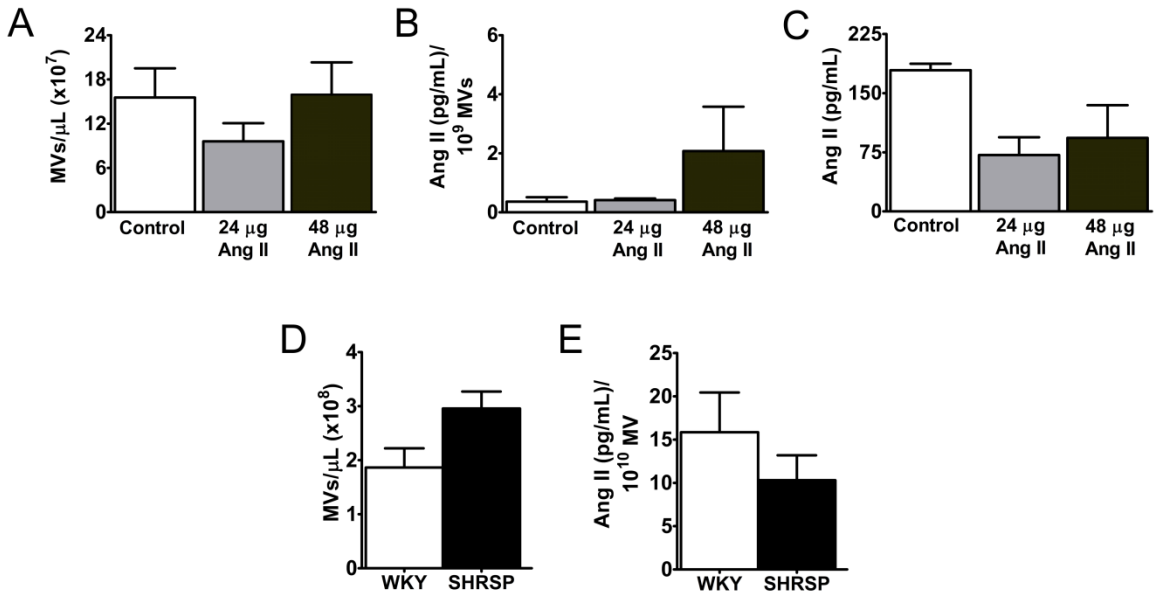

Figure 6-9. Ang II is located in blood MVs.
(A) MVs were isolated from serum of mice infused with either H_2O (control, n= 6), 24 µg/kg/hr Ang II (24 µg Ang II, n= 3) or 48 µg/kg/hr Ang II (48 µg Ang II, n= 6), quantified using nanoparticle tracking analysis and expressed as MVs/µL serum. (B) Ang II was measured in serum MVs and Ang II content per 10^9 MVs was determined. (C) Ang II concentration was measured in the MV depleted serum of Ang II infused mice. (D) MVs were isolated from the plasma of 21-week old WKY (n= 3) and SHRSP (n= 3) rats, quantified by NTA and expressed as MVs/µL. (E) Ang II was measured in the plasma MVs of WKY and SHRSP rats and expressed as Ang II per 10^{10} MVs. WKY and SHRSP serum was provided by Dr Delyth Graham. Data are presented as mean ± SEM.

6.4 Discussion

Here it was shown that fibroblasts secrete MVs and when stimulated with Ang II, Ang II localises to MVs and could be detected fluorescently and by ELISA. MVs derived from Ang II-stimulated fibroblasts stimulated cardiomyocyte hypertrophy in the H9c2 cardiomyoblast cell line which was prevented by the AT_1R specific antagonist Losartan. Inhibition of exosome biosynthesis with BFA and treatment with proteinase K confirmed that the pro-hypertrophic effect of MVs derived from Ang II-stimulated NRCF was specific to Ang II located in MVs. Additionally, Ang II was found to be present in MVs circulating in the serum and plasma of healthy mice and rats and Ang II content may increase with the development of hypertension in Ang II-infused mice.

Components of the RAS have previously been shown contained in exosomes. In a large scale proteomic analysis of urinary exosomes ACE and ACE2 were shown to be contained in the vesicles shed by the renal tubules and urinary tract (Gonzales *et al.*, 2009, Pisitkun *et al.*, 2004) and more recently, it was shown that cardiomyocytes release exosomes enriched with AT_1R during pressure overload (Pironti *et al.*, 2015). However, so far the presence of angiotensin peptides has not been explored and these results presented here demonstrate the presence of Ang II in MVs. Lyu *et al.* (2015) recently showed that cardiac fibroblast-derived exosomes can activate the cardiomyocyte RAS and thereby mediate a pro-hypertrophic effect (Lyu *et al.*, 2015). However, they did not detect Ang II in fibroblast-derived exosomes after Ang II stimulation, in direct contrast to the results presented here. However, previously only the exosome population of fibroblast-derived MVs was investigated (Lyu *et al.*, 2015) while here a fibroblast-derived MV population with a particle size between 100–200 nm was investigated which does not fit exosome criteria. This data may therefore suggest that Ang II is preferentially packaged into vesicles other than exosomes. This is indirectly supported by observations of MV secretion in platelets which differentially increase secretion of exosomes or MVs in a stimulus-dependent manner and when comparing exosome and MV content, it was observed that they only have 13 of the 267 detected proteins in common (Aatonen *et al.*, 2014). Additionally, experimental differences may account for the observations. For example, here it was shown that Ang II in MVs is present at low levels and ranges between 1–20 pg/mL out with the detection range of the ELISA employed

previously (Lyu *et al.*, 2015). Furthermore, fibroblasts were stimulated in the presence of serum and it was previously demonstrated that the presence of serum influence MV release and vesicular cargo (Li *et al.*, 2015).

The serum and plasma levels of circulating free Ang II are estimated to range between 5–15 pg/mL and 60–200 pg/mL in healthy human subjects and rodents, respectively even though levels as high as 1000 pg/mL have been reported (Roig *et al.*, 2000, Cervenka *et al.*, 1999, dos Santos *et al.*, 2014, Zou *et al.*, 2014, Yang *et al.*, 2012). Levels of Ang II determined here in MV-depleted serum from control mice fits within the range of reported values. The finding that Ang II circulates in MVs from serum and plasma may have important implications in disease development where circulating levels of Ang II are increased as shown here in the Ang II-infusion model. As shown here with proteinase K treatment, the vesicular cargo and therefore Ang II is protected against the degradation by peptidases and protease. While the half-life of free Ang II in the circulation is estimated to be approximately 30 s (van Kats *et al.*, 1997), packaging of Ang II into MVs may increase its half-life by protecting it from cleavage by ACE, ACE2 and other peptidases. Previously, MVs in lymph nodes have been shown to be stable for at least 3 days *in vivo* (Luketic *et al.*, 2007) and in isolated plasma, MVs remained intact for up to 30 days at physiological temperatures (Kalra *et al.*, 2013). This will be important to assess further in future studies to determine the pharmacological impact of packaging Ang II into MVs.

The mechanism by which Ang II is loaded into MVs still remains unclear. On binding of Ang II to the AT_1R or AT_2R, the AT_1R is subsequently internalised and recycled in a ß-arrestin dependent manner while the AT_2R remains at the plasma membrane (Hein *et al.*, 1997, Anborgh *et al.*, 2000). Recently, Pironti *et al.* (2015) showed that this pathway is involved in the enrichment of exosomes with AT_1R during osmotic stress and pressure overload in cardiomyocytes suggesting that this pathway may also play a role of Ang II loading into MVs (Pironti *et al.*, 2015). Using fluorescently-labelled Ang II, the recycling of the Ang II–AT_1R complex has been visualised in HEK293 cells revealing that the complex was trafficked into early endosomes as well as recycling endosomes which is dependent on the activation of PI 3-kinase (Hunyady *et al.*, 2002, Hein *et al.*, 1997). Inhibition of PI 3-kinase by wortmannin induced the formation of large MVB-like vesicles that contained the AT_1R and Ang II in small internal vesicles

(Hunyady *et al.*, 2002) providing a functional link between receptor recycling and MV formation. It has been demonstrated that the AT_1R but not the AT_2R is involved in the plasma clearance of Ang II and thereby contributes to the increase in intrarenal Ang II levels which can be prevented by AT_1R blockers highlighting that Ang II must be accumulated intracellularly (Zou *et al.*, 1996, Zou *et al.*, 1998). In support of this, a study by Wang *et al.* (1995) has previously shown that bovine medullary adrenal cells internalise exogenous Ang II by receptor mediated endocytosis and process it *via* the endosomal pathway prior to its renewed secretion in its intact form or as biologically active Ang II fragments (Wang *et al.*, 1995). Indeed, renal endosomes were shown to contain Ang II as well as Ang II receptors and ACE and renal endosomal Ang II was increased in rats fed on a high salt diet or receiving Ang II infusion (Imig *et al.*, 1999, Zhuo *et al.*, 2002) providing a potential link between the loading of Ang II into MV and the increases in serum MV Ang II levels seen during high dose Ang II infusion.

Whilst it was previously shown that stimulation of cardiac fibroblasts with Ang II leads to the enrichment of miR-21* in exosomes to mediate cardiomyocyte hypertrophy (Bang *et al.*, 2014), here miR-21* could not be detected in MVs derived from Ang II-stimulated fibroblasts. In contrast, recently Lyu *et al.* (2015) showed that MVs from unstimulated cardiac fibroblasts mediated cardiomyocyte hypertrophy by activating the cardiomyocyte RAS and increase the autocrine secretion of Ang II in cardiomyocytes (Lyu *et al.*, 2015). In this setting, stimulation with Ang II did not modulate the pro-hypertrophic effect and is in contrast to the results here where MVs from unstimulated fibroblasts did not affect cardiomyocyte cell size. While activation of the cardiomyocyte RAS has not been fully investigated here, a similar increase in the mRNA for the AT_1R and AT_2R was detected in H9c2 cells treated with MVs from cardiac fibroblasts irrespective of Ang II treatment. This receptor upregulation did not translate into a pro-hypertrophic effect with control MVs and was also not induced by stimulation with exogenous Ang II. This is in line with the observation that Ang II stimulation, either exogenously or via MVs, tended to decrease ACE mRNA. It is therefore plausible that the increase in AT_1R and AT_2R gene expression may be a result of the exosomal transfer of AT_1R and AT_2R as previously demonstrated (Pironti *et al.*, 2015). Nevertheless, these results demonstrate that induction of

cardiomyocyte hypertrophy by fibroblast-derived MVs is likely to be due to a multitude of factors and pathways that converge on the hypertrophic signalling pathways within cardiomyocytes.

Here, it was demonstrated that AngII packaged into fibroblast-derived MVs mediates cardiomyocyte hypertrophy in an AT_1R dependent manner. However, given results previously discussed, the location of these AT_1R remains elusive and there are several possibilities. MVs can either adhere to the cell membrane inducing outside-in signalling extracellularly or they can fuse with the plasma membrane releasing their cargo into the recipient cells or get internalised by endocytosis (Cocucci and Meldolesi, 2015). Additionally, some vesicles may break and release their contents into the extracellular space thereby freeing up Ang II to bind extracellular AT_1R (Cocucci and Meldolesi, 2015). An intracellular action of Ang II is supported by the observation that the AT_1R can be localised intracellularly in endosomes as part of its recycling process as well as in the nucleus and other yet unidentified cellular compartments (Li and Zhuo, 2008, Brailoiu *et al.*, 1999, Hein *et al.*, 1997). By binding to its receptors, intracellular Ang II has previously been shown to induce $TGF\beta_1$ and MCP1 gene expression by binding nuclear AT_1R (Li and Zhuo, 2008) and to mediate VSMC contraction by mediating Ca^{2+} influx (Brailoiu *et al.*, 1999). However, intracellular Ang II also demonstrated AT_1R-independent effects including the mobilisation of intracellular Ca^{2+} and the stimulation of cell growth as well as cardiomyocyte hypertrophy (Baker *et al.*, 2004, Baker and Kumar, 2006, Zhuo *et al.*, 2006). Although Losartan has been demonstrated to be taken up and transported by epithelial cells, in cardiomyocytes extracellularly applied losartan failed to cross the cell membrane to inhibit intracellular Ang II signalling (Soldner *et al.*, 2000, De Mello, 1998). It is therefore unlikely that Ang II contained in MVs is released into the cytosol to mediate intracellular effects. While Pironti *et al.* (2015) have demonstrated that the AT_1R is enriched in exosomes (Pironti *et al.*, 2015), the presence of Ang II regulated signalling molecules such as PLA_2, phospholipase D, Akt and PKC-α in MVs has also been confirmed (Subra *et al.*, 2010, Nazarewicz *et al.*, 2011). This raises the possibility that instead of the transfer of single molecules and peptides by MVs, MVs have the potential to transfer an entire "signalosome" to its recipient cells to modulate cell behaviour.

6.5 Summary

In summary, this study has shown that cardiomyocytes and cardiac fibroblasts can communicate *via* MVs and that cardiac fibroblasts stimulated with Ang II load Ang II into MVs. MVs loaded with Ang II mediated cardiomyocyte hypertrophy in a similar manner to exogenous Ang II which was dependent on binding to the AT_1R (Figure 6-10). Treatment with Brefeldin A and Proteinase K to inhibit MV release and digest membrane associated proteins, respectively, confirmed that the hypertrophic response was specific to Ang II loaded into MVs and therefore represents a novel pathway for cardiac fibroblasts to alter cardiomyocyte behaviour during cardiac disease. Moreover, Ang II was found to be present in circulating MVs from the serum and plasma of different animal models of HHD. Overall, these results demonstrate the presence of Ang II in MVs derived from isolated cardiac fibroblasts *in vitro* and serum and plasma *in vivo* which has important implications for our understanding of the RAS in cell–to-cell communication in health and disease.

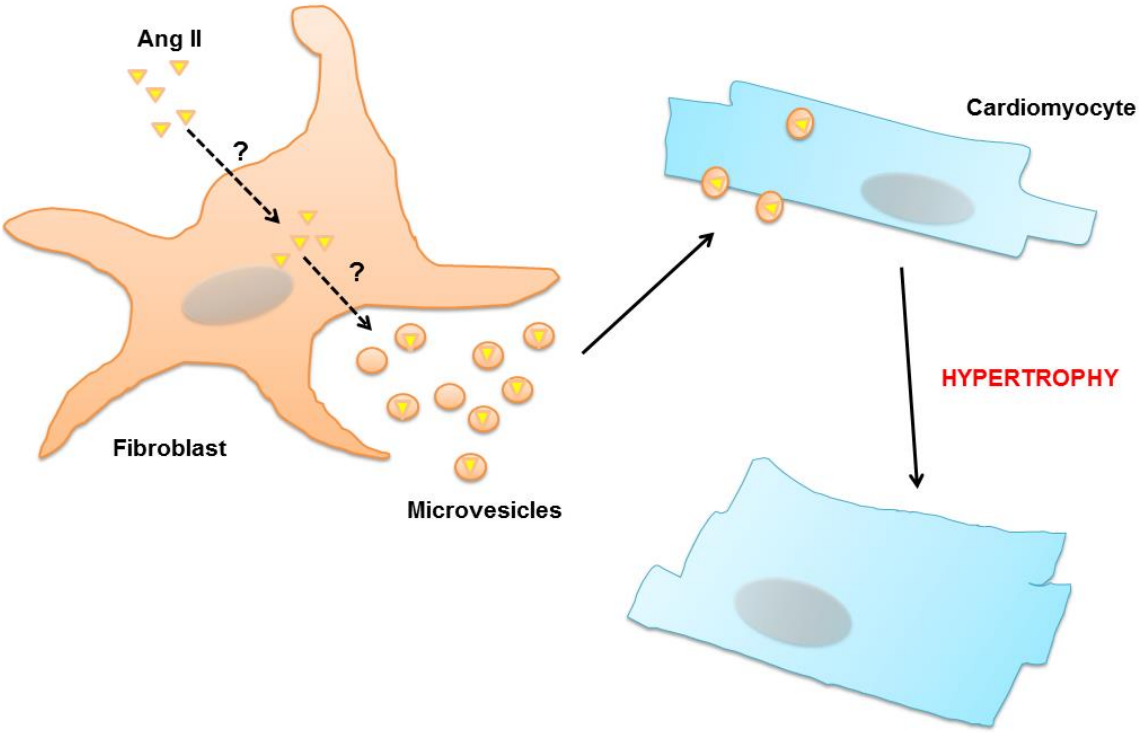

Figure 6-10. Schematic of fibroblast-derived MV-induced cardiomyocyte hypertrophy. Stimulation cardiac fibroblasts with Ang II leads to the internalisation of Ang II, potentially *via* the AT_1R. Ang II is subsequently loaded into MVs *via* a yet unidentified pathway and secreted back into the extracellular fluid where the fibroblast-derived MVs interact with cardiomyocytes. Ang II contained in MVs interacts with AT_1R of yet unknown location to initiate cardiomyocyte growth.

Chapter 7 – General Discussion

7.1 Overall summary

Activation of the RAS plays a key role in the development of hypertension and its associated adverse cardiac remodelling during HHD which eventually results in HF (Brooks *et al.*, 2010, Berk *et al.*, 2007). Understanding the underlying molecular mechanisms in Ang II-mediated structural remodelling in the heart is essential for the development of novel therapeutics targeting adverse cardiac remodelling. Activation of the counter-regulatory RAS has emerged as a potential novel therapeutic objective to treat adverse cardiac remodelling and maintain cardiac function in CVDs (McKinney *et al.*, 2014). The primary aim of this thesis was to investigate the potential therapeutic effects of the counter-regulatory peptide Ang-(1-9) in reversing chronic Ang II-induced cardiac remodelling and contractile dysfunction. Additionally, this thesis aimed to elucidate whether Ang II-induced cardiac remodelling involves the process of EndMT and cell-to-cell communication *via* MVs.

Initially, a mouse model of chronic Ang II infusion was characterised for structural and functional changes by infusion of either a low or high dose of Ang II for 6 weeks. Echocardiographic analysis revealed that low dose Ang II infusion resulted in a gradual decline in cardiac contractile function with dysfunction being evident after 4 weeks of infusion. In contrast, high dose Ang II infusion resulted in acute cardiac contractile dysfunction as early as 2 weeks after treatment. Cardiac hypertrophy and fibrosis were evident in the hearts of Ang II-infused mice which was not significantly different between either concentration. Gene expression analysis revealed no changes in components of the RAS but infusion of a high dose of Ang II exacerbated the expression of pro-fibrotic and pro-hypertrophic markers. The structural and functional changes occurring during chronic low dose infusion of Ang II closely mimic the development of hypertension in humans (Simon *et al.*, 1995) while high dose infusion provides an ideal model to study acute cardiac dysfunction. The Ang II-infusion model is therefore an ideal model to study the therapeutic potential of Ang-(1-9) in reversing Ang II-induced cardiac disease.

Next, the cardiovascular actions of Ang-(1-9) infusion in healthy normotensive mice were assessed. Ang-(1-9) infusion for 6 weeks did not significantly alter cardiac function and had no effect on cardiac remodelling processes. In the next

study, cardiac dysfunction and remodelling was induced by minipump infusion of a high dose of Ang II for 2 weeks before minipumps were replaced and Ang-(1-9) was co-infused with Ang II for a further 2-4 weeks. Ang-(1-9) did not significantly modulate Ang II-induced increases in BP. However, the addition of Ang-(1-9) significantly improved cardiac FS after 2 weeks of infusion before a further decline after 4 weeks. The recovery of FS by Ang-(1-9) after 2 weeks was independent of an effect on Ang II-induced cardiac remodelling and similarly, no differences were found after 4 weeks suggesting that Ang-(1-9) mediates direct effects on cardiac contractile function.

To investigate the transient effect observed for Ang-(1-9) on cardiac function in the *in vivo* reversal study, next its effects were assessed in the isolated Langendorff perfused rat heart in comparison to Ang II and Ang-(1-7). Perfusion of Ang-(1-9) in the isolated paced or spontaneously beating heart resulted in a significant increase in LVDP and dP/dt_{max} suggesting that Ang-(1-9) acts as a positive inotrope. In contrast, both Ang II and Ang-(1-7) had little to no effects on cardiac contractile function. The effects mediated by Ang-(1-9) were found to potentially be mediated by the activation of PKA but not CaMKII. Investigation into the receptor by which Ang-(1-9) mediates its effect was performed using the specific antagonists Losartan and PD123319 for the AT_1R and AT_2R, respectively. It was demonstrated that the effects of Ang-(1-9) were only partially mediated by the AT_2R and could be fully abolished by AT_1R blockade. This suggests a novel mechanism of Ang-(1-9) action and warrants further investigation.

Next, novel pathways that may contribute to Ang II-induced cardiac remodelling were investigated. EndMT has emerged as an important mechanism in the development of cardiac fibrosis (Zeisberg *et al.*, 2007b). The role of $TGF\beta_1$ in the induction of pathological EndMT is already well described (Yoshimatsu and Watabe, 2011). Here it was hypothesised that Ang II could contribute to microvascular rarefaction *in vivo* by the induction of EndMT. Microvascular density in the hearts of Ang II-infused mice was significantly reduced following the infusion of Ang II for 4-6 weeks. Furthermore, EndMT could be detected in the myocardium by significant co-localisation of endothelial and fibroblast markers *via* immunofluorescence (Murdoch *et al.*, 2014). To further elucidate the role of Ang II, a cell culture model of EndMT using HCAEC was established.

Stimulation of HCAEC with Ang II alone only marginally altered mesenchymal gene expression, however, when cells were co-stimulated with Ang II and TGFß$_1$, it was found that Ang II significantly exacerbated TGFß$_1$-induced expression of mesenchymal markers. The activation of SMAD2/3 and ERK1/2 are key mediators of TGFß-induced EndMT (Li *et al.*, 2010, Cooley *et al.*, 2014, Wylie-Sears *et al.*, 2014). To further elucidate a possible signalling pathway underlying the effect of Ang II, the acute activation of SMAD2/3 and ERK1/2 was assessed by Western immunoblot. AngII did not modulate TGFß$_1$-induced activation of either SMAD2/3 or ERK1/2. Measurements of superoxide production however revealed that Ang II significantly increased superoxide production in HCAEC through activation of Nox1. Further studies are required to elucidate whether Nox1 contributes to the exacerbation of TGFß$_1$-induced EndMT by Ang II *in vitro* and *in vivo*.

Extracellular vesicles have emerged as important paracrine mediators of cellular signalling and a role of MVs and exosomes has also been demonstrated in the cardiovascular system (Sluijter *et al.*, 2014). Because components of the RAS have previously been demonstrated in MVs (Gonzales *et al.*, 2009, Pisitkun *et al.*, 2004, Pironti *et al.*, 2015), a further study aimed to examine whether Ang II is present in fibroblast-derived MVs and their role in Ang II-induced cardiomyocyte hypertrophy. Measurements of Ang II concentration by ELISA revealed that fibroblast-derived MVs contain detectable amounts of Ang II which increased when fibroblasts were stimulated with Ang II suggesting that fibroblasts load exogenous Ang II into MVs. MVs from Ang II-stimulated fibroblasts were found to induce cardiomyocyte hypertrophy while control MVs from unstimulated fibroblasts had no effect. This pro-hypertrophic effect was maintained after proteinase K digestion of MVs to remove MV surface proteins but could be abolished by treatment of fibroblasts with BFA to inhibit endosomal trafficking. Identification of the receptor by which the fibroblast-derived MVs mediate their pro-hypertrophic effect was investigated using the ARB Losartan. It was found that Losartan fully blocked the pro-hypertrophic response to MVs from Ang II-stimulated fibroblasts. However the location of this receptor still needs to be determined. To further investigate the relevance of Ang II packaged into MVs, MVs were isolated from the serum and plasma of AngII-infused mice and SHRSP rats, respectively and Ang II content measured. Results demonstrate that MVs from control mice and WKY rats contain Ang II. Ang II content tended to

increase with Ang II infusion but was not significantly different in the SHRSP rat. The presence of Ang II in serum and plasma MVs correlates with the increased presence of ACE, ACE2 and the AT_1R in MVs in CVD (Pironti *et al.*, 2015, Pisitkun *et al.*, 2004, Gonzales *et al.*, 2009). However, the physiological and pharmacological importance of these observations needs to be established in future studies.

7.2 Considerations and future perspectives

This study is the first study to present evidence that the actions of Ang-(1-9) in cardiac pathology are dependent on its time of administration with it having no effect in normotensive healthy mice but beneficial when given to mice with established cardiac disease.

Here it was shown that when administered to mice with established Ang II-induced contractile dysfunction, Ang-(1-9) transiently improved cardiac contractile function by a direct effect on the heart. This was independent of an effect on cardiac remodelling and therefore suggests a direct effect of Ang-(1-9) on cardiac contractility. Transient improvement could be explained by a mismatch in cardiac energy demand/ nutrient supply. Thus, the increased cardiac energy demand due to the positive inotropic actions of Ang-(1-9) is not met by the significantly reduced myocardial capillary density while uncontrolled hypertension further favours adverse cardiac remodelling. It can therefore be hypothesised that if BP were controlled, Ang-(1-9) may mediate more favourable long-term effects on cardiac contractile function. This is demonstrated in another study which demonstrated the cardioprotective effects of Ang-(1-9) in a model of diabetic cardiomyopathy (Zheng *et al.*, 2015). This model lacks a hypertensive phenotype and when Ang-(1-9) was administered over 4 weeks it improved cardiac contractile function and reduced adverse cardiac remodelling (Zheng *et al.*, 2015). Therefore, it would be of interest to assess the functional effects of Ang-(1-9) in the Ang II-infusion model when BP is controlled with anti-hypertensive therapy. This provides a more clinical setting as it is appreciated that most hypertensive patients would be receiving at least one anti-hypertensive medication. Because both ARBs and ACE-I interfere with the RAS and therefore with AngI II and Ang-(1-9) metabolism, an alternative anti-hypertensive such as a diuretic which has been shown to lower BP without an

effect on cardiac remodelling (Kim *et al.*, 1995) would be the drug of choice to elucidate the direct effects of Ang-(1-9) on Ang II-induced cardiac dysfunction in the absence of hypertension.

Another process that has been suggested to be a key event in the early stages of Ang II-induced cardiac remodelling is the occurrence of myocyte apoptosis which has been demonstrated to occur within 3 days of Ang II-infusion (Tan *et al.*, 1991, Campbell *et al.*, 1995). Although this has not been assessed here *per se*, replacement fibrosis is clearly evident in Ang II infused mice after 4 and 6 weeks. Although there is so far no evidence linking Ang-(1-9) to apoptosis or necrosis, a role for the AT_2R has been clearly demonstrated in a variety of cell types, including cardiomyocytes, where activation of the AT_2R counteracted Ang II mediated stimulation of growth pathways resulting in inactivation of Bcl-2 and subsequent apoptosis (Yamada *et al.*, 1998b, Yamada *et al.*, 1996, Horiuchi *et al.*, 1997, Goldenberg *et al.*, 2001). Hence, Ang-(1-9) may directly contribute to cardiac dysfunction by exacerbating cardiomyocyte apoptosis. This could be assessed by Terminal deoxynucleotidyl transferase (TdT) dUTP Nick-End Labeling (TUNEL) staining of cardiac sections to identify apoptotic cells (Goldenberg *et al.*, 2001). However, cell necrosis is more difficult to determine because so far no distinct biochemical marker has been identified and cells may proceed from apoptosis into necrosis (Krysko *et al.*, 2008). Thus, identification of cell necrosis requires a combination of morphological and biochemical techniques including light microscopy, electron microscopy and Western blotting. Because apoptotic and necrotic cell death with Ang II infusion has been demonstrated to peak at 3 days before subsiding (Fiordaliso *et al.*, 2000) these investigations should be carried out at early time points rather than at 4 and 6 weeks where cardiac remodelling is well established and cardiomyocyte apoptosis will be very low which may lead to a false negative result. Another important aspect to consider is that if Ang II induces the loss of cardiomyocytes and Ang-(1-9) prevents Ang II-induced fibrosis (Flores-Munoz *et al.*, 2012), this will result in impaired wound healing where the dead myocytes are not equally replaced by a collagenous scar therefore altering cardiac ultrastructure and predisposing the myocardium to myocyte slippage resulting in contractile and electrical dysfunction.

The direct effect of Ang-(1-9) leading to improved contractile function was corroborated in the *ex vivo* Langendorff-perfused rat heart where Ang-(1-9)

mediated positive inotropic effects. This was in contrast to Ang II and Ang-(1-7) which had little to no effect and therefore provide evidence that Ang-(1-9) elicits its positive inotropic actions independent of its breakdown to either Ang II or Ang-(1-7). It is noteworthy that *ex vivo* studies were performed in rat hearts whereas *in vivo* assessments of Ang-(1-9) were performed in mice. Although rats and mice share similar mechanisms of EC coupling and Ca^{2+} homeostasis that differ from rabbits and humans (Berk *et al.*, 2007), it has been demonstrated that Ang II only mediates an increase in cardiac contractility in mice but not in rats (Masaki *et al.*, 1998, Lefroy *et al.*, 1996). Hence, despite similar molecular mechanisms, species differences may exist and it would therefore be of interest to corroborate the effects of Ang-(1-9) perfusion also in the *ex vivo* mouse heart. A previous study has already identified that Ang-(1-9) increases Ca^{2+} transient amplitude and fractional cell shortening in isolated mouse cardiomyocytes (Fattah *et al.*, 2014) and this supports the hypothesis that Ang-(1-9) has direct positive inotropic actions in the mouse heart. Additionally, it would be of interest to investigate this finding in more detail *in vivo* by employing pressure-volume (PV-loop) analysis. Using PV-loop analysis it has already been demonstrated that bolus infusion of Ang II leads to an acute increase in LV end systolic and end diastolic pressure and volume and an increase in dP/dt_{max} (Broomé *et al.*, 2001, Cheng *et al.*, 1996). However, the effects of chronic (>2 weeks) Ang II infusion on PV-loop parameters are relatively unknown (Murdoch *et al.*, 2014). PV-loop analysis would therefore provide invaluable information on the underlying pathophysiology of Ang II-induced contractile dysfunction (independent of pre-/afterload and how this is modulated by the infusion of Ang-(1-9).

The present study did not use receptor antagonists to determine the receptor by which Ang-(1-9) mediates its effect *in vivo*. However, previous evidence has demonstrated that Ang-(1-9) mediates its anti-hypertrophic, anti-fibrotic and more recently cardiac effects *via* the AT_2R (Flores-Muñoz *et al.*, 2011, Flores-Munoz *et al.*, 2012, Flores-Munoz *et al.*, 2013, Zheng *et al.*, 2015) and it can be assumed that in this study Ang-(1-9) mediates its effects *via* the AT_2R. While this may hold true for the anti-remodelling effect of Ang-(1-9) which was not demonstrated here, the data presented here in the isolated rat heart suggests that Ang-(1-9) is mediating its cardiac actions *via* the AT_1R. Although Ang-(1-9)

can bind the AT_2R and the AT_1R with equal affinities, this is the first report of Ang-(1-9) binding to the AT_1R to mediate its biological actions. It would be of interest to confirm these observations *in vivo* and assess whether the recovery in cardiac contractile function by Ang-(1-9) is indeed mediated *via* the AT_1R *in vivo*. This could be accomplished by the co-infusion of the receptor-specific antagonist Losartan and PD123319 for the AT_1R and AT_2R, respectively which have been employed successfully in previous studies (Flores-Munoz *et al.*, 2012, Ocaranza *et al.*, 2014, Zheng *et al.*, 2015). However, concerns have been raised about the specificity of PD123319 and off-target effects have been reported for example in Ang II-induced abdominal aortic aneurysms where PD123319 enhanced Ang II-induced aneurysm formation to a similar degree in wild type and AT_2R-null mice (Daugherty *et al.*, 2013). The AT_2R-null mice would therefore provide an ideal tool to investigate the contribution of the AT_2R in mediating the cardiac effects of Ang-(1-9). However, it has to be noted that AT_2R-null mice have been shown to respond differently to Ang II infusion and are protected against Ang II-induced cardiac hypertrophy (Senbonmatsu *et al.*, 2000, Ichihara *et al.*, 2001) and therefore care must be taken when interpreting results.

The identification that Losartan fully blocks the positive inotropic actions in the paced rat heart although Ang II itself has no direct cardiac actions allows the speculation that Ang-(1-9) acts as a biased agonist at the AT_1R. Previously, it has been demonstrated that Ang-(1-9) mediates its beneficial effects on cardiac remodelling via the AT_2R but not the AT_1R (Flores-Muñoz *et al.*, 2011, Flores-Munoz *et al.*, 2012) and the current results suggest a new tissue specific role for Ang-(1-9) in cardiomyocytes. Biased agonists at the AT_1R have previously been demonstrated to mediate an increase in cardiac contractility by selectively engaging the ß-arrestin-MAPK pathway strengthening the notion that Ang-(1-9) may activate ß-arrestin signalling at the AT_1R (Violin *et al.*, 2010). Identification of Ang-(1-9) as a natural biased agonist at the AT_1R would have important implications for its therapeutic potential as synthetic biased AT_1R agonists are currently in development to harness the beneficial effects of AT_1R signalling *via* ß-arrestin pathways while blocking the detrimental effects of Ang II-mediated G protein activation (Violin *et al.*, 2010, Kim *et al.*, 2012, Boerrigter *et al.*, 2011, Boerrigter *et al.*, 2012). Such biased agonism could be investigated in, for example, Chinese hamster ovary cells (which do not intrinsically express the

AT_1R) selectively expressing the AT_1R stimulated with Ang-(1-9) and subsequently probing for the activation of ERK1/2, Ca^{2+} mobilisation as well as measuring [^{35}S]GTPγS binding and ß-arrestin recruitment to the AT_1R (Wei *et al.*, 2003, Rajagopal *et al.*, 2006).

Using specific inhibitors, it was demonstrated that the positive inotropic effect induced by Ang-(1-9) in the isolated rat heart requires PKA but not CaMKII. However, phosphorylation of PKA was found to be unchanged in response to Ang-(1-9) stimulation. PKA is a unique enzyme which is fully phosphorylated *in vivo* and *in vitro* and is mainly regulated by binding of cAMP (Moore *et al.*, 2002). Hence PKA phosphorylation is not a prerequisite for PKA activation. It would be of interest to further confirm PKA activation *via* other experimental approaches. As such, commercial PKA activity assay kits are available employing a specific synthetic substrate for PKA the phosphorylated from of which can then be detected by a specific polyclonal antibody. One such PKA target is VASP which has been employed previously to probe for specific PKA activation (Dulin *et al.*, 2001). Alternatively, cAMP generation could be measured by ELISA to give an indirect measure of PKA activation. However, since neither the AT_1R or AT_2R have been linked to activation of the G protein G_s and instead it has been demonstrated that the AT_1R can activate PKA *via* cAMP independent pathways (Dulin *et al.*, 2001) it would not be unexpected if PKA activation occurs in the absence of cAMP generation when cardiomyocytes are stimulated with Ang-(1-9). Furthermore, it would be of interest to investigate the role of PKA in the positive inotropic effect in isolated cardiomyocytes. It has previously been demonstrated that Ang-(1-9) increases Ca^{2+} transient amplitude and fractional cell shortening *via* an increase in the L-type Ca^{2+} current (Fattah *et al.*, 2014). Since the L-type Ca^{2+} channel is regulated by PKA phosphorylation (Bünemann *et al.*, 1999, Kamp and Hell, 2000) it would be of interest to investigate whether PKA inhibition also abolishes this pathway in isolated cardiomyocytes stimulated with Ang-(1-9). Additionally, in this study, the phosphorylation of targets in the EC coupling machinery such as PLB, the L-type Ca^{2+} channel, RyR and SERCA were not investigated. Ang-(1-7) has previously been shown to stimulate PKA and enhance L-type Ca^{2+} currents in isolated cardiomyocytes while SERCA2A was found upregulated in transgenic mice with Ang-(1-7) overexpression in the heart (De Mello, 2015, Zhou *et al.*, 2015, Ferreira *et al.*, 2010). Phosphorylation of

these targets are the key mechanisms involved in the regulation of EC coupling on a beat-to-beat basis (Bers, 2002) and hence it would be important to investigate the phosphorylation and expression of these targets to better understand the molecular mechanisms by which Ang-(1-9) affects cardiomyocyte EC coupling and mediates positive inotropy.

Here it was demonstrated that Ang II infusion led to a significant reduction in myocardial capillary density which correlates with the development of cardiac hypertrophy. It has previously been demonstrated that vascular growth is tightly coupled to myocardial growth (Brutsaert, 2003, Zhang and Shah, 2014). Thus, inhibition or stimulation of cardiac angiogenesis promoted the development of cardiac hypertrophy and cardiac contractile dysfunction (Giordano *et al.*, 2001, Tirziu *et al.*, 2010). This suggests that when there is dysregulation of the angiogenic program the result is cardiac hypertrophy. More importantly, it has been suggested that the transition from a compensated to a decompensated state is accompanied by a significant loss in myocardial capillaries (Izumiya *et al.*, 2006, Shiojima *et al.*, 2005). This correlates with the observations made in this study where the loss in myocardial capillary density at 4 weeks strongly correlated with cardiac hypertrophy at the stage of cardiac decompensation. Moreover, it has been demonstrated that ECs prevent cardiomyocyte dedifferentiation and re-expression of foetal markers such as ßMHC and skeletal actin while endothelial ET-1 secretion mediates cardiomyocyte hypertrophy (Brutsaert, 2003, Adiarto *et al.*, 2012) highlighting the importance of adequate endothelial-cardiomyocyte cross-talk which is lost in the progression of cardiac remodelling. Although evidence has shown that Ang II contributes to microvascular rarefaction during hypertensive cardiac remodelling the underlying mechanisms remain unclear (Sabri *et al.*, 1998, Belabbas *et al.*, 2008). It has previously been suggested that Ang II reduces the proliferation of ECs and stimulates EC apoptosis (Graiani *et al.*, 2005, Li *et al.*, 1999). This was not investigated, however, Ang II induced EndMT *in vivo* and *in vitro* providing an alternative mechanism contributing to the loss in microvascular endothelium. Furthermore, this process contributes to the recruitment of activated cardiac fibroblasts in the heart participating in the extensive cardiac remodelling in response to Ang II infusion. In the pressure overloaded heart using endothelial-lineage tracing mice, it was previously demonstrated that up to 30 % of

fibroblasts are sourced from EndMT (Zeisberg *et al.*, 2007b). The total contribution of EndMT could not be quantified in the current study but it would be of interest to investigate Ang II-induced EndMT in endothelial lineage tracing mice to further delineate the contribution of EndMT to Ang II induced microvascular rarefaction and cardiac fibrosis.

While stimulation of HCAEC with Ang II *in vitro* only partially induced EndMT, Ang II significantly exacerbated TGFß$_1$-induced EndMT. Although this process could be abolished by an inhibitor of the SMAD2/3 pathway, the pathway by which Ang II exacerbates TGFß$_1$-induced EndMT remains unknown. This study has demonstrated that Ang II selectively stimulates O_2^- production *via* the activation of Nox1 in HCAEC. To further investigate the link between Nox and EndMT it will be important to determine the direct involvement of Nox1 in Ang II-induced EndMT *in vitro* by employing the specific Nox1 inhibitors ML171 and GKT137831 used in this study. Alternatively, to exclude potential off target effects of these inhibitors, siRNA against Nox1 may be used.

MVs have emerged as important paracrine mediators of cell signals throughout the body and they have also gained much attention in the physiological and pathophysiological regulation of the cardiovascular system (Sluijter *et al.*, 2014). Although members of the RAS have previously been demonstrated to be present in exosomes (Gonzales *et al.*, 2009, Pisitkun *et al.*, 2004) and that the RAS can modulate exosome secretion and *vice versa* (Lyu *et al.*, 2015, Bang *et al.*, 2014), this is the first report of the presence of Ang II in fibroblast-derived MVs which act as paracrine mediators to induce cardiomyocyte hypertrophy. Although the direct mechanism by which fibroblasts load Ang II was not investigated here, it has previously been demonstrated that cardiomyocyte-derived exosomes are enriched in AT$_1$R during pressure overload in a ß-arrestin dependent manner suggesting a role for the AT$_1$R recycling pathway (Pironti *et al.*, 2015). It would therefore be of interest to investigate whether loading of Ang II is dependent on binding to the AT$_1$R and its subsequent internalisation and processing through the cellular endosomal pathway (Hein *et al.*, 1997). This is supported by the observation that BFA treatment abolished the pro-hypertrophic effect of fibroblast-derived MV possibly by attenuating Ang II endosomal transport. If Ang II loading was dependent on the AT$_1$R, then this should be inhibited by an AT$_1$R antagonist such as Losartan. As such, an initial experiment should investigate

whether Ang II is loaded into fibroblast-derived MVs when they are stimulated with Ang II in the presence of Losartan. Further experiments could investigate the dependency on ß-arrestin in this pathway by using siRNA to ß-arrestin 1 and ß-arrestin 2 (Wei *et al.*, 2003). Since the experiments in this study have been performed in *in vitro* cell culture models it would be of interest to further evaluate the biological significance of Ang II in MVs. This could be assessed *ex vivo* by circulating Ang II-loaded MVs in the isolated Langendorff-perfused heart and measuring acute effects on cardiac contractile function (Vicencio *et al.*, 2015). It has to be noted however, that the rat heart would be unsuitable for the investigation due to the lack of a positive inotropic effect during Ang II infusion (Lefroy *et al.*, 1996) and hence, the mouse heart would be a better suited model. Alternatively, this could also be assessed *in vivo* by measuring the acute BP response to a bolus injection of Ang II-loaded MVs. It would be of further interest to study the homing of these MVs in the circulation by injecting fluorescently labelled MVs (Luketic *et al.*, 2007). This would not only help to identify whether these MVs preferentially accumulate in the heart but also to determine the approximate half-life of MVs in the circulation.

7.3 Conclusion

Overall, these studies demonstrate the potential therapeutic applications for Ang-(1-9) in the treatment of cardiac contractile dysfunction while highlighting the necessity to further elucidate Ang-(1-9) signalling in the heart. Furthermore, these studies provide insight into novel pathways contributing to Ang II-induced cardiac remodelling which may present a novel therapeutic target to treat adverse cardiac remodelling in hypertension.

Bibliography

AATONEN, M. T., OHMAN, T., NYMAN, T. A., LAITINEN, S., GRÖNHOLM, M. & SILJANDER, P. R. 2014. Isolation and characterization of platelet-derived extracellular vesicles. *J Extracell Vesicles,* 3.

ABADIR, P. M., PERIASAMY, A., CAREY, R. M. & SIRAGY, H. M. 2006. Angiotensin II type 2 receptor-bradykinin B_2 receptor functional heterodimerization. *Hypertension,* 48**,** 316-22.

ABDALLA, S., ABDEL-BASET, A., LOTHER, H., EL MASSIERY, A. & QUITTERER, U. 2005. Mesangial AT_1/B_2 receptor heterodimers contribute to angiotensin II hyperresponsiveness in experimental hypertension. *J Mol Neurosci,* 26**,** 185-92.

ABDALLA, S., LOTHER, H., ABDEL-TAWAB, A. M. & QUITTERER, U. 2001. The angiotensin II AT_2 receptor is an AT_1 receptor antagonist. *J Biol Chem,* 276**,** 39721-6.

ABDALLA, S., LOTHER, H., LANGER, A., EL FARAMAWY, Y. & QUITTERER, U. 2004. Factor XIIIA transglutaminase crosslinks AT_1 receptor dimers of monocytes at the onset of atherosclerosis. *Cell,* 119**,** 343-54.

ABDALLA, S., LOTHER, H. & QUITTERER, U. 2000. AT_1-receptor heterodimers show enhanced G-protein activation and altered receptor sequestration. *Nature,* 407**,** 94-8.

ADACHI, Y., SAITO, Y., KISHIMOTO, I., HARADA, M., KUWAHARA, K., TAKAHASHI, N., KAWAKAMI, R., NAKANISHI, M., NAKAGAWA, Y., TANIMOTO, K., SAITOH, Y., YASUNO, S., USAMI, S., IWAI, M., HORIUCHI, M. & NAKAO, K. 2003. Angiotensin II type 2 receptor deficiency exacerbates heart failure and reduces survival after acute myocardial infarction in mice. *Circulation,* 107**,** 2406-8.

ADAMS, J. A., MCGLONE, M. L., GIBSON, R. & TAYLOR, S. S. 1995. Phosphorylation modulates catalytic function and regulation in the cAMP-dependent protein kinase. *Biochemistry,* 34**,** 2447-54.

ADIARTO, S., HEIDEN, S., VIGNON-ZELLWEGER, N., NAKAYAMA, K., YAGI, K., YANAGISAWA, M. & EMOTO, N. 2012. ET-1 from endothelial cells is required for complete angiotensin II-induced cardiac fibrosis and hypertrophy. *Life Sci,* 91**,** 651-7.

AHUJA, P., SDEK, P. & MACLELLAN, W. R. 2007. Cardiac myocyte cell cycle control in development, disease, and regeneration. *Physiol Rev,* 87**,** 521-44.

AIELLO, E. A. & CINGOLANI, H. E. 2001. Angiotensin II stimulates cardiac L-type Ca^{2+} current by a Ca^{2+}- and protein kinase C-dependent mechanism. *Am J Physiol Heart Circ Physiol,* 280**,** H1528-36.

AISAGBONHI, O., RAI, M., RYZHOV, S., ATRIA, N., FEOKTISTOV, I. & HATZOPOULOS, A. K. 2011. Experimental myocardial infarction triggers canonical Wnt signaling and endothelial-to-mesenchymal transition. *Disease Models & Mechanisms,* 4**,** 469-483.

AKISHITA, M., IWAI, M., WU, L., ZHANG, L., OUCHI, Y., DZAU, V. J. & HORIUCHI, M. 2000. Inhibitory effect of angiotensin II type 2 receptor on coronary arterial remodeling after aortic banding in mice. *Circulation,* 102**,** 1684-9.

ALENINA, N., XU, P., RENTZSCH, B., PATKIN, E. L. & BADER, M. 2008. Genetically altered animal models for Mas and angiotensin-(1-7). *Exp Physiol,* 93**,** 528-37.

ALLEN, I. S., COHEN, N. M., DHALLAN, R. S., GAA, S. T., LEDERER, W. J. & ROGERS, T. B. 1988. Angiotensin II increases spontaneous contractile frequency and stimulates calcium current in cultured neonatal rat heart myocytes: insights into the underlying biochemical mechanisms. *Circ Res,* 62**,** 524-34.

ALMEIDA, A. P., FRÁBREGAS, B. C., MADUREIRA, M. M., SANTOS, R. J., CAMPAGNOLE-SANTOS, M. J. & SANTOS, R. A. 2000. Angiotensin-(1-7) potentiates the coronary vasodilatatory effect of bradykinin in the isolated rat heart. *Braz J Med Biol Res,* 33**,** 709-13.

ANBORGH, P. H., SEACHRIST, J. L., DALE, L. B. & FERGUSON, S. S. 2000. Receptor/beta-arrestin complex formation and the differential trafficking and resensitization of beta2-adrenergic and angiotensin II type 1A receptors. *Mol Endocrinol,* 14**,** 2040-53.

AOKI, H., RICHMOND, M., IZUMO, S. & SADOSHIMA, J. 2000. Specific role of the extracellular signal-regulated kinase pathway in angiotensin II-induced cardiac hypertrophy in vitro. *Biochem J,* 347 Pt 1**,** 275-84.

AOYAMA, T., PAIK, Y. H., WATANABE, S., LALEU, B., GAGGINI, F., FIORASO-CARTIER, L., MOLANGO, S., HEITZ, F., MERLOT, C., SZYNDRALEWIEZ, C., PAGE, P. & BRENNER, D. A. 2012. Nicotinamide adenine dinucleotide phosphate oxidase in experimental liver fibrosis: GKT137831 as a novel potential therapeutic agent. *Hepatology,* 56**,** 2316-27.

APLIN, M., CHRISTENSEN, G. L., SCHNEIDER, M., HEYDORN, A., GAMMELTOFT, S., KJØLBYE, A. L., SHEIKH, S. P. & HANSEN, J. L. 2007. The angiotensin type 1 receptor activates extracellular signal-regulated kinases 1 and 2 by G protein-dependent and -independent pathways in cardiac myocytes and langendorff-perfused hearts. *Basic Clin Pharmacol Toxicol,* 100**,** 289-95.

APPLIED BIOSYSTEMS. 2010. *Introduction to Gene Expression: Getting Started Guide* [Online]. Thermo Fisher Scientific. Available: https://www.thermofisher.com/uk/en/home/life-science/pcr/real-time-pcr/qpcr-education/what-can-you-do-with-qpcr/introduction-to-gene-expression.html [Accessed 01/03/ 2016].

ARCINIEGAS, E., SUTTON, A. B., ALLEN, T. D. & SCHOR, A. M. 1992. Transforming growth factor beta 1 promotes the differentiation of endothelial cells into smooth muscle-like cells *in vitro*. *J Cell Sci,* 103 (Pt 2)**,** 521-9.

ARIMA, S., ENDO, Y., YAOITA, H., OMATA, K., OGAWA, S., TSUNODA, K., ABE, M., TAKEUCHI, K., ABE, K. & ITO, S. 1997. Possible role of P-450 metabolite of arachidonic acid in vasodilator mechanism of angiotensin II type 2 receptor in the isolated microperfused rabbit afferent arteriole. *J Clin Invest,* 100**,** 2816-23.

ARUN, K. H., KAUL, C. L. & RAMARAO, P. 2005. AT_1 receptors and L-type calcium channels: functional coupling in supersensitivity to angiotensin II in diabetic rats. *Cardiovasc Res,* 65**,** 374-86.

ASSOIAN, R. K., FLEURDELYS, B. E., STEVENSON, H. C., MILLER, P. J., MADTES, D. K., RAINES, E. W., ROSS, R. & SPORN, M. B. 1987. Expression and

secretion of type beta transforming growth factor by activated human macrophages. *Proc Natl Acad Sci U S A,* 84**,** 6020-4.

ATLAS, S. A. 2007. The renin-angiotensin aldosterone system: pathophysiological role and pharmacologic inhibition. *J Manag Care Pharm,* 13**,** 9-20.

AVERILL, D. B., ISHIYAMA, Y., CHAPPELL, M. C. & FERRARIO, C. M. 2003. Cardiac angiotensin-(1-7) in ischemic cardiomyopathy. *Circulation,* 108**,** 2141-6.

BADENHORST, D., MASEKO, M., TSOTETSI, O. J., NAIDOO, A., BROOKSBANK, R., NORTON, G. R. & WOODIWISS, A. J. 2003. Cross-linking influences the impact of quantitative changes in myocardial collagen on cardiac stiffness and remodelling in hypertension in rats. *Cardiovasc Res,* 57**,** 632-41.

BAI, J., ZHANG, N., HUA, Y., WANG, B., LING, L., FERRO, A. & XU, B. 2013. Metformin inhibits angiotensin II-induced differentiation of cardiac fibroblasts into myofibroblasts. *PLoS One,* 8**,** e72120.

BAICU, C. F., STROUD, J. D., LIVESAY, V. A., HAPKE, E., HOLDER, J., SPINALE, F. G. & ZILE, M. R. 2003. Changes in extracellular collagen matrix alter myocardial systolic performance. *Am J Physiol Heart Circ Physiol,* 284**,** H122-32.

BAKER, K. M., CHERNIN, M. I., SCHREIBER, T., SANGHI, S., HAIDERZAIDI, S., BOOZ, G. W., DOSTAL, D. E. & KUMAR, R. 2004. Evidence of a novel intracrine mechanism in angiotensin II-induced cardiac hypertrophy. *Regul Pept,* 120**,** 5-13.

BAKER, K. M. & KUMAR, R. 2006. Intracellular angiotensin II induces cell proliferation independent of AT_1 receptor. *Am J Physiol Cell Physiol,* 291**,** C995-1001.

BALLIGAND, J. L., KELLY, R. A., MARSDEN, P. A., SMITH, T. W. & MICHEL, T. 1993. Control of cardiac muscle cell function by an endogenous nitric oxide signaling system. *Proc Natl Acad Sci U S A,* 90**,** 347-51.

BALTATU, O., SILVA, J. A., GANTEN, D. & BADER, M. 2000. The brain renin-angiotensin system modulates angiotensin II-induced hypertension and cardiac hypertrophy. *Hypertension,* 35**,** 409-12.

BANERJEE, I., FUSELER, J. W., INTWALA, A. R. & BAUDINO, T. A. 2009. IL-6 loss causes ventricular dysfunction, fibrosis, reduced capillary density, and dramatically alters the cell populations of the developing and adult heart. *Am J Physiol Heart Circ Physiol,* 296**,** H1694-H1704.

BANERJEE, I., FUSELER, J. W., PRICE, R. L., BORG, T. K. & BAUDINO, T. A. 2007. Determination of cell types and numbers during cardiac development in the neonatal and adult rat and mouse. *Am J Physiol Heart Circ Physiol,* 293**,** H1883-91.

BANG, C., BATKAI, S., DANGWAL, S., GUPTA, S. K., FOINQUINOS, A., HOLZMANN, A., JUST, A., REMKE, J., ZIMMER, K., ZEUG, A., PONIMASKIN, E., SCHMIEDL, A., YIN, X., MAYR, M., HALDER, R., FISCHER, A., ENGELHARDT, S., WEI, Y., SCHOBER, A., FIEDLER, J. & THUM, T. 2014. Cardiac fibroblast-derived microRNA passenger strand-enriched exosomes mediate cardiomyocyte hypertrophy. *J Clin Invest,* 124**,** 2136-46.

BARKI-HARRINGTON, L., LUTTRELL, L. M. & ROCKMAN, H. A. 2003. Dual inhibition of beta-adrenergic and angiotensin II receptors by a single

antagonist: a functional role for receptor-receptor interaction in vivo. *Circulation,* 108**,** 1611-8.

BARNABEI, M. S., PALPANT, N. J. & METZGER, J. M. 2010. Influence of genetic background on *ex vivo* and *in vivo* cardiac function in several commonly used inbred mouse strains. *Physiol Genomics,* 42A**,** 103-13.

BARONI, M., PIZZIRANI, C., PINOTTI, M., FERRARI, D., ADINOLFI, E., CALZAVARINI, S., CARUSO, P., BERNARDI, F. & DI VIRGILIO, F. 2007. Stimulation of P2 ($P2X_7$) receptors in human dendritic cells induces the release of tissue factor-bearing microparticles. *FASEB J,* 21**,** 1926-33.

BAROUCH, L. A., HARRISON, R. W., SKAF, M. W., ROSAS, G. O., CAPPOLA, T. P., KOBEISSI, Z. A., HOBAI, I. A., LEMMON, C. A., BURNETT, A. L., O'ROURKE, B., RODRIGUEZ, E. R., HUANG, P. L., LIMA, J. A., BERKOWITZ, D. E. & HARE, J. M. 2002. Nitric oxide regulates the heart by spatial confinement of nitric oxide synthase isoforms. *Nature,* 416**,** 337-9.

BARRY, S. P., DAVIDSON, S. M. & TOWNSEND, P. A. 2008. Molecular regulation of cardiac hypertrophy. *Int J Biochem Cell Biol,* 40**,** 2023-39.

BEDECS, K., ELBAZ, N., SUTREN, M., MASSON, M., SUSINI, C., STROSBERG, A. D. & NAHMIAS, C. 1997. Angiotensin II type 2 receptors mediate inhibition of mitogen-activated protein kinase cascade and functional activation of SHP-1 tyrosine phosphatase. *Biochem J,* 325 (Pt 2)**,** 449-54.

BELABBAS, H., ZALVIDEA, S., CASELLAS, D., MOLÈS, J. P., GALBES, O., MERCIER, J. & JOVER, B. 2008. Contrasting effect of exercise and angiotensin II hypertension on *in vivo* and *in vitro* cardiac angiogenesis in rats. *Am J Physiol Regul Integr Comp Physiol,* 295**,** R1512-8.

BELL, R. M., MOCANU, M. M. & YELLON, D. M. 2011. Retrograde heart perfusion: the Langendorff technique of isolated heart perfusion. *J Mol Cell Cardiol,* 50**,** 940-50.

BENDALL, J. K., CAVE, A. C., HEYMES, C., GALL, N. & SHAH, A. M. 2002. Pivotal role of a gp91(phox)-containing NADPH oxidase in angiotensin II-induced cardiac hypertrophy in mice. *Circulation,* 105**,** 293-6.

BENNDORF, R., BÖGER, R. H., ERGÜN, S., STEENPASS, A. & WIELAND, T. 2003. Angiotensin II type 2 receptor inhibits vascular endothelial growth factor-induced migration and *in vitro* tube formation of human endothelial cells. *Circ Res,* 93**,** 438-47.

BENTER, I. F., FERRARIO, C. M., MORRIS, M. & DIZ, D. I. 1995. Antihypertensive actions of angiotensin-(1-7) in spontaneously hypertensive rats. *Am J Physiol,* 269**,** H313-9.

BERK, B. C., FUJIWARA, K. & LEHOUX, S. 2007. ECM remodeling in hypertensive heart disease. *J Clin Invest,* 117**,** 568-75.

BERNSTEIN, K. E., ONG, F. S., BLACKWELL, W. L., SHAH, K. H., GIANI, J. F., GONZALEZ-VILLALOBOS, R. A., SHEN, X. Z., FUCHS, S. & TOUYZ, R. M. 2013. A modern understanding of the traditional and nontraditional biological functions of angiotensin-converting enzyme. *Pharmacol Rev,* 65**,** 1-46.

BERS, D. M. 2000. Calcium fluxes involved in control of cardiac myocyte contraction. *Circ Res,* 87**,** 275-81.

BERS, D. M. 2002. Cardiac excitation-contraction coupling. *Nature,* 415**,** 198-205.

BISHOP, J. E. & LAURENT, G. J. 1995. Collagen turnover and its regulation in the normal and hypertrophying heart. *Eur Heart J,* 16 Suppl C**,** 38-44.

BKAILY, G., EL-BIZRI, N., NADER, M., HAZZOURI, K. M., RIOPEL, J., JACQUES, D., REGOLI, D., D'ORLEANS-JUSTE, P., GOBEIL, F. & AVEDANIAN, L. 2005. Angiotensin II induced increase in frequency of cytosolic and nuclear calcium waves of heart cells via activation of AT_1 and AT_2 receptors. *Peptides,* 26**,** 1418-26.

BLACK, F. M., PACKER, S. E., PARKER, T. G., MICHAEL, L. H., ROBERTS, R., SCHWARTZ, R. J. & SCHNEIDER, M. D. 1991. The vascular smooth muscle alpha-actin gene is reactivated during cardiac hypertrophy provoked by load. *J Clin Invest,* 88**,** 1581-8.

BOERRIGTER, G., LARK, M. W., WHALEN, E. J., SOERGEL, D. G., VIOLIN, J. D. & BURNETT, J. C. 2011. Cardiorenal actions of TRV120027, a novel ß-arrestin-biased ligand at the angiotensin II type I receptor, in healthy and heart failure canines: a novel therapeutic strategy for acute heart failure. *Circ Heart Fail,* 4**,** 770-8.

BOERRIGTER, G., SOERGEL, D. G., VIOLIN, J. D., LARK, M. W. & BURNETT, J. C. 2012. TRV120027, a novel ß-arrestin biased ligand at the angiotensin II type I receptor, unloads the heart and maintains renal function when added to furosemide in experimental heart failure. *Circ Heart Fail,* 5**,** 627-34.

BOKEMEYER, D., SCHMITZ, U. & KRAMER, H. J. 2000. Angiotensin II-induced growth of vascular smooth muscle cells requires an Src-dependent activation of the epidermal growth factor receptor. *Kidney Int,* 58**,** 549-58.

BOLDT, A., SCHOLL, A., GARBADE, J., RESETAR, M. E., MOHR, F. W., GUMMERT, J. F. & DHEIN, S. 2006. ACE-inhibitor treatment attenuates atrial structural remodeling in patients with lone chronic atrial fibrillation. *Basic Res Cardiol,* 101**,** 261-7.

BOLTE, S. & CORDELIÈRES, F. P. 2006. A guided tour into subcellular colocalization analysis in light microscopy. *J Microsc,* 224**,** 213-32.

BOOZ, G. W., DAY, J. N. & BAKER, K. M. 2002. Interplay between the cardiac renin angiotensin system and JAK-STAT signaling: role in cardiac hypertrophy, ischemia/reperfusion dysfunction, and heart failure. *J Mol Cell Cardiol,* 34**,** 1443-53.

BOSNYAK, S., JONES, E. S., CHRISTOPOULOS, A., AGUILAR, M. I., THOMAS, W. G. & WIDDOP, R. E. 2011. Relative affinity of angiotensin peptides and novel ligands at AT_1 and AT_2 receptors. *Clin Sci (Lond),* 121**,** 297-303.

BOSNYAK, S., WELUNGODA, I. K., HALLBERG, A., ALTERMAN, M., WIDDOP, R. E. & JONES, E. S. 2010. Stimulation of angiotensin AT_2 receptors by the non-peptide agonist, Compound 21, evokes vasodepressor effects in conscious spontaneously hypertensive rats. *Br J Pharmacol,* 159**,** 709-16.

BOUDREAU, H. E., CASTERLINE, B. W., RADA, B., KORZENIOWSKA, A. & LETO, T. L. 2012. Nox4 involvement in TGF-beta and SMAD3-driven induction of the epithelial-to-mesenchymal transition and migration of breast epithelial cells. *Free Radic Biol Med,* 53**,** 1489-99.

BOULPAEP, E. L. 2009. Organization of the cardiovascular system. *In:* BORON, W. F. & BOULPAEP, E. L. (eds.) *Medical Physiology*. 2 ed.: Saunders Elsevier.

BRAILOIU, E., FILIPEANU, C. M., TICA, A., TOMA, C. P., DE ZEEUW, D. & NELEMANS, S. A. 1999. Contractile effects by intracellular angiotensin II via receptors with a distinct pharmacological profile in rat aorta. *Br J Pharmacol,* 126**,** 1133-8.

BRANCACCIO, M., FRATTA, L., NOTTE, A., HIRSCH, E., POULET, R., GUAZZONE, S., DE ACETIS, M., VECCHIONE, C., MARINO, G., ALTRUDA, F., SILENGO, L., TARONE, G. & LEMBO, G. 2003. Melusin, a muscle-specific integrin β_1-interacting protein, is required to prevent cardiac failure in response to chronic pressure overload. *Nat Med,* 9**,** 68-75.

BRILLA, C. G. 2000. Regression of myocardial fibrosis in hypertensive heart disease: diverse effects of various antihypertensive drugs. *Cardiovasc Res,* 46**,** 324-31.

BRILLA, C. G., PICK, R., TAN, L. B., JANICKI, J. S. & WEBER, K. T. 1990. Remodeling of the rat right and left ventricles in experimental hypertension. *Circ Res,* 67**,** 1355-64.

BRILLA, C. G., ZHOU, G., MATSUBARA, L. & WEBER, K. T. 1994. Collagen metabolism in cultured adult rat cardiac fibroblasts: response to angiotensin II and aldosterone. *J Mol Cell Cardiol,* 26**,** 809-20.

BROOKS, V. L., ELL, K. R. & WRIGHT, R. M. 1993. Pressure-independent baroreflex resetting produced by chronic infusion of angiotensin II in rabbits. *Am J Physiol,* 265**,** H1275-82.

BROOKS, W. W., SHEN, S. S., CONRAD, C. H., GOLDSTEIN, R. H. & BING, O. H. 2010. Transition from compensated hypertrophy to systolic heart failure in the spontaneously hypertensive rat: Structure, function, and transcript analysis. *Genomics,* 95**,** 84-92.

BROOMÉ, M., HANEY, M., HÄGGMARK, S., JOHANSSON, G., ANEMAN, A. & BIBER, B. 2001. Acute effects of angiotensin II on myocardial performance. *Acta Anaesthesiol Scand,* 45**,** 1147-54.

BROWER, G. L., GARDNER, J. D., FORMAN, M. F., MURRAY, D. B., VOLOSHENYUK, T., LEVICK, S. P. & JANICKI, J. S. 2006. The relationship between myocardial extracellular matrix remodeling and ventricular function. *Eur J Cardiothorac Surg,* 30**,** 604-10.

BROWN, A. J., CASALS-STENZEL, J., GOFFORD, S., LEVER, A. F. & MORTON, J. J. 1981. Comparison of fast and slow pressor effects of angiotensin II in the conscious rat. *Am J Physiol,* 241**,** H381-8.

BROWN, K. A., AAKRE, M. E., GORSKA, A. E., PRICE, J. O., ELTOM, S. E., PIETENPOL, J. A. & MOSES, H. L. 2004. Induction by transforming growth factor-beta1 of epithelial to mesenchymal transition is a rare event in vitro. *Breast Cancer Res,* 6**,** R215-31.

BROWN, R. D., AMBLER, S. K., MITCHELL, M. D. & LONG, C. S. 2005. The cardiac fibroblast: therapeutic target in myocardial remodeling and failure. *Annu Rev Pharmacol Toxicol,* 45**,** 657-87.

BRUTSAERT, D. L. 2003. Cardiac endothelial-myocardial signaling: its role in cardiac growth, contractile performance, and rhythmicity. *Physiol Rev,* 83**,** 59-115.

BUENO, O. F., DE WINDT, L. J., TYMITZ, K. M., WITT, S. A., KIMBALL, T. R., KLEVITSKY, R., HEWETT, T. E., JONES, S. P., LEFER, D. J., PENG, C. F., KITSIS, R. N. & MOLKENTIN, J. D. 2000. The MEK1-ERK1/2 signaling pathway promotes compensated cardiac hypertrophy in transgenic mice. *EMBO J,* 19**,** 6341-50.

BÜNEMANN, M., GERHARDSTEIN, B. L., GAO, T. & HOSEY, M. M. 1999. Functional regulation of L-type calcium channels via protein kinase A-mediated phosphorylation of the beta(2) subunit. *J Biol Chem,* 274**,** 33851-4.

BURGER, D., REUDELHUBER, T. L., MAHAJAN, A., CHIBALE, K., STURROCK, E. D. & TOUYZ, R. M. 2014. Effects of a domain-selective ACE inhibitor in a mouse model of chronic angiotensin II-dependent hypertension. *Clin Sci (Lond),* 127**,** 57-63.

BURGESS, M. L., BUGGY, J., PRICE, R. L., ABEL, F. L., TERRACIO, L., SAMAREL, A. M. & BORG, T. K. 1996. Exercise- and hypertension-induced collagen changes are related to left ventricular function in rat hearts. *Am J Physiol,* 270**,** H151-9.

BURNS, W. C., VELKOSKA, E., DEAN, R., BURRELL, L. M. & THOMAS, M. C. 2010. Angiotensin II mediates epithelial-to-mesenchymal transformation in tubular cells by ANG 1-7/MAS-1-dependent pathways. *Am J Physiol Renal Physiol,* 299**,** F585-93.

BURT, V. L., WHELTON, P., ROCCELLA, E. J., BROWN, C., CUTLER, J. A., HIGGINS, M., HORAN, M. J. & LABARTHE, D. 1995. Prevalence of hypertension in the US adult population. Results from the Third National Health and Nutrition Examination Survey, 1988-1991. *Hypertension,* 25**,** 305-13.

BYRNE, J. A., GRIEVE, D. J., BENDALL, J. K., LI, J. M., GOVE, C., LAMBETH, J. D., CAVE, A. C. & SHAH, A. M. 2003. Contrasting roles of NADPH oxidase isoforms in pressure-overload versus angiotensin II-induced cardiac hypertrophy. *Circ Res,* 93**,** 802-5.

CABALLERO, R., GÓMEZ, R., MORENO, I., NUÑEZ, L., GONZÁLEZ, T., ARIAS, C., GUIZY, M., VALENZUELA, C., TAMARGO, J. & DELPÓN, E. 2004. Interaction of angiotensin II with the angiotensin type 2 receptor inhibits the cardiac transient outward potassium current. *Cardiovasc Res,* 62**,** 86-95.

CABY, M. P., LANKAR, D., VINCENDEAU-SCHERRER, C., RAPOSO, G. & BONNEROT, C. 2005. Exosomal-like vesicles are present in human blood plasma. *Int Immunol,* 17**,** 879-87.

CAMM, A. J. & BUNCE, N. H. 2009. Cardiovascular Disease. *In:* KUMAR, P. & CLARK, M. (eds.) *Clinical Medicine.* 7 ed. Edinburgh: Elsevier Saunders.

CAMPBELL, S. E., JANICKI, J. S. & WEBER, K. T. 1995. Temporal differences in fibroblast proliferation and phenotype expression in response to chronic administration of angiotensin II or aldosterone. *J Mol Cell Cardiol,* 27**,** 1545-60.

CARDIN, S., SCOTT-BOYER, M. P., PRAKTIKNJO, S., JEIDANE, S., PICARD, S., REUDELHUBER, T. L. & DESCHEPPER, C. F. 2014. Differences in cell-type-specific responses to angiotensin II explain cardiac remodeling differences in C57BL/6 mouse substrains. *Hypertension,* 64**,** 1040-6.

CARRETERO, O. A. & OPARIL, S. 2000. Essential hypertension. Part I: definition and etiology. *Circulation,* 101**,** 329-35.

CARTLEDGE, J. E., KANE, C., DIAS, P., TESFOM, M., CLARKE, L., MCKEE, B., AL AYOUBI, S., CHESTER, A., YACOUB, M. H., CAMELLITI, P. & TERRACCIANO, C. M. 2015. Functional crosstalk between cardiac fibroblasts and adult cardiomyocytes by soluble mediators. *Cardiovasc Res,* 105**,** 260-70.

CARVAJAL, G., RODRÍGUEZ-VITA, J., RODRIGUES-DÍEZ, R., SÁNCHEZ-LÓPEZ, E., RUPÉREZ, M., CARTIER, C., ESTEBAN, V., ORTIZ, A., EGIDO, J., MEZZANO, S. A. & RUIZ-ORTEGA, M. 2008. Angiotensin II activates the Smad pathway during epithelial mesenchymal transdifferentiation. *Kidney Int,* 74**,** 585-95.

CASTOLDI, G., DI GIOIA, C. R., PIERUZZI, F., VAN DE GREEF, W. M., BUSCA, G., SPERTI, G. & STELLA, A. 2001. Angiotensin II modulates calponin gene expression in rat vascular smooth muscle cells *in vivo*. *J Hypertens,* 19**,** 2011-8.

CASTRO-CHAVES, P., SOARES, S., FONTES-CARVALHO, R. & LEITE-MOREIRA, A. F. 2008. Negative inotropic effect of selective AT_2 receptor stimulation and its modulation by the endocardial endothelium. *Eur J Pharmacol,* 578**,** 261-9.

CASTRO, C. H., SANTOS, R. A., FERREIRA, A. J., BADER, M., ALENINA, N. & ALMEIDA, A. P. 2005. Evidence for a functional interaction of the angiotensin-(1-7) receptor Mas with AT_1 and AT_2 receptors in the mouse heart. *Hypertension,* 46**,** 937-42.

CASTRO, C. H., SANTOS, R. A., FERREIRA, A. J., BADER, M., ALENINA, N. & ALMEIDA, A. P. 2006. Effects of genetic deletion of angiotensin-(1-7) receptor Mas on cardiac function during ischemia/reperfusion in the isolated perfused mouse heart. *Life Sci,* 80**,** 264-8.

CERVENKA, L., MITCHELL, K. D., OLIVERIO, M. I., COFFMAN, T. M. & NAVAR, L. G. 1999. Renal function in the AT_{1A} receptor knockout mouse during normal and volume-expanded conditions. *Kidney Int,* 56**,** 1855-62.

CHA, S. A., PARK, B. M., GAO, S. & KIM, S. H. 2013. Stimulation of ANP by angiotensin-(1-9) via the angiotensin type 2 receptor. *Life Sci,* 93**,** 934-40.

CHARGAFF F, E. & WEST, R. 1946. The biological significance of the thromboplastic protein of blood. *J Biol Chem,* 166**,** 189-97.

CHE, Z. Q., GAO, P. J., SHEN, W. L., FAN, C. L., LIU, J. J. & ZHU, D. L. 2008. Angiotensin II-stimulated collagen synthesis in aortic adventitial fibroblasts is mediated by connective tissue growth factor. *Hypertens Res,* 31**,** 1233-40.

CHEN, H., MOHUCZY, D., LI, D., KIMURA, B., PHILLIPS, M. I., MEHTA, P. & MEHTA, J. L. 2001. Protection against ischemia/reperfusion injury and myocardial dysfunction by antisense-oligodeoxynucleotide directed at angiotensin-converting enzyme mRNA. *Gene Ther,* 8**,** 804-10.

CHEN, L., KIM, S. M., EISNER, C., OPPERMANN, M., HUANG, Y., MIZEL, D., LI, L., CHEN, M., SEQUEIRA LOPEZ, M. L., WEINSTEIN, L. S., GOMEZ, R. A., SCHNERMANN, J. & BRIGGS, J. P. 2010. Stimulation of renin secretion by angiotensin II blockade is Gsalpha-dependent. *J Am Soc Nephrol,* 21**,** 986-92.

CHEN, L., LIU, B. C., ZHANG, X. L., ZHANG, J. D., LIU, H. & LI, M. X. 2006. Influence of connective tissue growth factor antisense oligonucleotide on angiotensin II-induced epithelial mesenchymal transition in HK2 cells. *Acta Pharmacol Sin,* 27**,** 1029-36.

CHEN, S. J., YUAN, W., MORI, Y., LEVENSON, A., TROJANOWSKA, M. & VARGA, J. 1999. Stimulation of type I collagen transcription in human skin fibroblasts by TGF-beta: involvement of Smad 3. *J Invest Dermatol,* 112**,** 49-57.

CHEN, X., LI, W., YOSHIDA, H., TSUCHIDA, S., NISHIMURA, H., TAKEMOTO, F., OKUBO, S., FOGO, A., MATSUSAKA, T. & ICHIKAWA, I. 1997. Targeting deletion of angiotensin type 1B receptor gene in the mouse. *Am J Physiol,* 272**,** F299-304.

CHEN, Y. W., PAT, B., GLADDEN, J. D., ZHENG, J., POWELL, P., WEI, C. C., CUI, X., HUSAIN, A. & DELL'ITALIA, L. J. 2011. Dynamic molecular and histopathological changes in the extracellular matrix and inflammation in the transition to heart failure in isolated volume overload. *Am J Physiol Heart Circ Physiol,* 300**,** H2251-60.

CHEN, Z., TAN, F., ERDÖS, E. G. & DEDDISH, P. A. 2005. Hydrolysis of angiotensin peptides by human angiotensin I-converting enzyme and the resensitization of B_2 kinin receptors. *Hypertension,* 46**,** 1368-73.

CHENG, C. P., SUZUKI, M., OHTE, N., OHNO, M., WANG, Z. M. & LITTLE, W. C. 1996. Altered ventricular and myocyte response to angiotensin II in pacing-induced heart failure. *Circ Res,* 78**,** 880-92.

CHINTALGATTU, V. & KATWA, L. C. 2009. Role of protein kinase C-delta in angiotensin II induced cardiac fibrosis. *Biochem Biophys Res Commun,* 386**,** 612-6.

COATES, D. 2003. The angiotensin converting enzyme (ACE). *Int J Biochem Cell Biol,* 35**,** 769-73.

COCUCCI, E. & MELDOLESI, J. 2015. Ectosomes and exosomes: shedding the confusion between extracellular vesicles. *Trends Cell Biol*.

COLLIER, P., WATSON, C. J., VAN ES, M. H., PHELAN, D., MCGORRIAN, C., TOLAN, M., LEDWIDGE, M. T., MCDONALD, K. M. & BAUGH, J. A. 2012. Getting to the heart of cardiac remodeling; how collagen subtypes may contribute to phenotype. *J Mol Cell Cardiol,* 52**,** 148-53.

COLOMBO, M., MOITA, C., VAN NIEL, G., KOWAL, J., VIGNERON, J., BENAROCH, P., MANEL, N., MOITA, L. F., THÉRY, C. & RAPOSO, G. 2013. Analysis of ESCRT functions in exosome biogenesis, composition and secretion highlights the heterogeneity of extracellular vesicles. *J Cell Sci,* 126**,** 5553-65.

COOLEY, B. C., NEVADO, J., MELLAD, J., YANG, D., ST HILAIRE, C., NEGRO, A., FANG, F., CHEN, G., SAN, H., WALTS, A. D., SCHWARTZBECK, R. L., TAYLOR, B., LANZER, J. D., WRAGG, A., ELAGHA, A., BELTRAN, L. E., BERRY, C., FEIL, R., VIRMANI, R., LADICH, E., KOVACIC, J. C. & BOEHM, M. 2014. TGF-β signaling mediates endothelial-to-mesenchymal transition (EndMT) during vein graft remodeling. *Sci Transl Med,* 6**,** 227ra34.

CRABOS, M., ROTH, M., HAHN, A. W. & ERNE, P. 1994. Characterization of angiotensin II receptors in cultured adult rat cardiac fibroblasts. Coupling to signaling systems and gene expression. *J Clin Invest,* 93**,** 2372-8.

CRACKOWER, M. A., SARAO, R., OUDIT, G. Y., YAGIL, C., KOZIERADZKI, I., SCANGA, S. E., OLIVEIRA-DOS-SANTOS, A. J., DA COSTA, J., ZHANG, L., PEI, Y., SCHOLEY, J., FERRARIO, C. M., MANOUKIAN, A. S., CHAPPELL, M. C., BACKX, P. H., YAGIL, Y. & PENNINGER, J. M. 2002. Angiotensin-converting enzyme 2 is an essential regulator of heart function. *Nature,* 417**,** 822-8.

CUCORANU, I., CLEMPUS, R., DIKALOVA, A., PHELAN, P. J., ARIYAN, S., DIKALOV, S. & SORESCU, D. 2005. NAD(P)H oxidase 4 mediates transforming growth factor-beta1-induced differentiation of cardiac fibroblasts into myofibroblasts. *Circ Res,* 97**,** 900-7.

D'AMORE, A., BLACK, M. J. & THOMAS, W. G. 2005. The angiotensin II type 2 receptor causes constitutive growth of cardiomyocytes and does not antagonize angiotensin II type 1 receptor-mediated hypertrophy. *Hypertension,* 46**,** 1347-54.

DAUGHERTY, A., RATERI, D. L., HOWATT, D. A., CHARNIGO, R. & CASSIS, L. A. 2013. PD123319 augments angiotensin II-induced abdominal aortic aneurysms through an AT_2 receptor-independent mechanism. *PLoS One,* 8**,** e61849.

DAUGHERTY, S. L., POWERS, J. D., MAGID, D. J., TAVEL, H. M., MASOUDI, F. A., MARGOLIS, K. L., O'CONNOR, P. J., SELBY, J. V. & HO, P. M. 2012. Incidence and prognosis of resistant hypertension in hypertensive patients. *Circulation,* 125**,** 1635-42.

DAVARE, M. A., HORNE, M. C. & HELL, J. W. 2000. Protein phosphatase 2A is associated with class C L-type calcium channels (Cav1.2) and antagonizes channel phosphorylation by cAMP-dependent protein kinase. *J Biol Chem,* 275**,** 39710-7.

DE ALMEIDA, P. W., MELO, M. B., LIMA, R. E. F., GAVIOLI, M., SANTIAGO, N. M., GRECO, L., JESUS, I. C., NOCCHI, E., PARREIRA, A., ALVES, M. N., MITRAUD, L., RESENDE, R. R., CAMPAGNOLE-SANTOS, M. J., DOS SANTOS, R. A. & GUATIMOSIM, S. 2015. Beneficial effects of angiotensin-(1-7) against deoxycorticosterone acetate-induced diastolic dysfunction occur independently of changes in blood pressure. *Hypertension,* 66**,** 389-95.

DE BOER, R. A., PINTO, Y. M., SUURMEIJER, A. J., POKHAREL, S., SCHOLTENS, E., HUMLER, M., SAAVEDRA, J. M., BOOMSMA, F., VAN GILST, W. H. & VAN VELDHUISEN, D. J. 2003. Increased expression of cardiac angiotensin II type 1 (AT(1)) receptors decreases myocardial microvessel density after experimental myocardial infarction. *Cardiovasc Res,* 57**,** 434-42.

DE LANNOY, L. M., DANSER, A. H., VAN KATS, J. P., SCHOEMAKER, R. G., SAXENA, P. R. & SCHALEKAMP, M. A. 1997. Renin-angiotensin system components in the interstitial fluid of the isolated perfused rat heart. Local production of angiotensin I. *Hypertension,* 29**,** 1240-51.

DE LANNOY, L. M., SCHUIJT, M. P., SAXENA, P. R., SCHALEKAMP, M. A. & DANSER, A. H. 2001. Angiotensin converting enzyme is the main contributor to angiotensin I-II conversion in the interstitium of the isolated perfused rat heart. *J Hypertens,* 19**,** 959-65.

DE MELLO, W. C. 1998. Intracellular angiotensin II regulates the inward calcium current in cardiac myocytes. *Hypertension,* 32**,** 976-82.

DE MELLO, W. C. 2004. Angiotensin (1-7) re-establishes impulse conduction in cardiac muscle during ischaemia-reperfusion. The role of the sodium pump. *J Renin Angiotensin Aldosterone Syst,* 5, 203-8.

DE MELLO, W. C. 2015. Intracellular angiotensin (1-7) increases the inward calcium current in cardiomyocytes. On the role of PKA activation. *Mol Cell Biochem,* 407, 9-16.

DE VRIES, L., REITZEMA-KLEIN, C. E., METER-ARKEMA, A., VAN DAM, A., RINK, R., MOLL, G. N. & AKANBI, M. H. 2010. Oral and pulmonary delivery of thioether-bridged angiotensin-(1-7). *Peptides,* 31, 893-8.

DEDDISH, P. A., MARCIC, B., JACKMAN, H. L., WANG, H. Z., SKIDGEL, R. A. & ERDÖS, E. G. 1998. N-domain-specific substrate and C-domain inhibitors of angiotensin-converting enzyme: angiotensin-(1-7) and keto-ACE. *Hypertension,* 31, 912-7.

DENZER, K., VAN EIJK, M., KLEIJMEER, M. J., JAKOBSON, E., DE GROOT, C. & GEUZE, H. J. 2000. Follicular dendritic cells carry MHC class II-expressing microvesicles at their surface. *J Immunol,* 165, 1259-65.

DER SARKISSIAN, S., GROBE, J. L., YUAN, L., NARIELWALA, D. R., WALTER, G. A., KATOVICH, M. J. & RAIZADA, M. K. 2008. Cardiac Overexpression of Angiotensin Converting Enzyme 2 Protects the Heart From Ischemia-Induced Pathophysiology. *Hypertension,* 51, 712-718.

DERUMEAUX, G., ICHINOSE, F., RAHER, M. J., MORGAN, J. G., COMAN, T., LEE, C., CUESTA, J. M., THIBAULT, H., BLOCH, K. D., PICARD, M. H. & SCHERRER-CROSBIE, M. 2008. Myocardial alterations in senescent mice and effect of exercise training: a strain rate imaging study. *Circ Cardiovasc Imaging,* 1, 227-34.

DESMOULIÈRE, A., REDARD, M., DARBY, I. & GABBIANI, G. 1995. Apoptosis mediates the decrease in cellularity during the transition between granulation tissue and scar. *Am J Pathol,* 146, 56-66.

DEVEREUX, R. B., DAHLÖF, B., GERDTS, E., BOMAN, K., NIEMINEN, M. S., PAPADEMETRIOU, V., ROKKEDAL, J., HARRIS, K. E., EDELMAN, J. M. & WACHTELL, K. 2004. Regression of hypertensive left ventricular hypertrophy by losartan compared with atenolol: the Losartan Intervention for Endpoint Reduction in Hypertension (LIFE) trial. *Circulation,* 110, 1456-62.

DEWALD, O., REN, G., DUERR, G. D., ZOERLEIN, M., KLEMM, C., GERSCH, C., TINCEY, S., MICHAEL, L. H., ENTMAN, M. L. & FRANGOGIANNIS, N. G. 2004. Of mice and dogs: species-specific differences in the inflammatory response following myocardial infarction. *Am J Pathol,* 164, 665-77.

DI GIOIA, C. R., VAN DE GREEF, W. M., SPERTI, G., CASTOLDI, G., TODARO, N., IERARDI, C., PIERUZZI, F. & STELLA, A. 2000. Angiotensin II increases calponin expression in cultured rat vascular smooth muscle cells. *Biochem Biophys Res Commun,* 279, 965-9.

DIAS-PEIXOTO, M. F., SANTOS, R. A., GOMES, E. R., ALVES, M. N., ALMEIDA, P. W., GRECO, L., ROSA, M., FAULER, B., BADER, M., ALENINA, N. & GUATIMOSIM, S. 2008. Molecular mechanisms involved in the angiotensin-(1-7)/Mas signaling pathway in cardiomyocytes. *Hypertension,* 52, 542-8.

DÍEZ-FREIRE, C., VÁZQUEZ, J., CORREA DE ADJOUNIAN, M. F., FERRARI, M. F., YUAN, L., SILVER, X., TORRES, R. & RAIZADA, M. K. 2006. ACE2 gene transfer attenuates hypertension-linked pathophysiological changes in the SHR. *Physiol Genomics,* 27**,** 12-9.

DÍEZ, J., QUEREJETA, R., LÓPEZ, B., GONZÁLEZ, A., LARMAN, M. & MARTÍNEZ UBAGO, J. L. 2002. Losartan-dependent regression of myocardial fibrosis is associated with reduction of left ventricular chamber stiffness in hypertensive patients. *Circulation,* 105**,** 2512-7.

DIKALOV, S. I., DIKALOVA, A. E., BIKINEYEVA, A. T., SCHMIDT, H. H., HARRISON, D. G. & GRIENDLING, K. K. 2008. Distinct roles of Nox1 and Nox4 in basal and angiotensin II-stimulated superoxide and hydrogen peroxide production. *Free Radic Biol Med,* 45**,** 1340-51.

DIMMELER, S., RIPPMANN, V., WEILAND, U., HAENDELER, J. & ZEIHER, A. M. 1997. Angiotensin II induces apoptosis of human endothelial cells. Protective effect of nitric oxide. *Circ Res,* 81**,** 970-6.

DINH, D. T., FRAUMAN, A. G., JOHNSTON, C. I. & FABIANI, M. E. 2001. Angiotensin receptors: distribution, signalling and function. *Clin Sci (Lond),* 100**,** 481-92.

DIWAN, A. & DORN, G. W. 2007. Decompensation of cardiac hypertrophy: cellular mechanisms and novel therapeutic targets. *Physiology (Bethesda),* 22**,** 56-64.

DOERING, C. W., JALIL, J. E., JANICKI, J. S., PICK, R., AGHILI, S., ABRAHAMS, C. & WEBER, K. T. 1988. Collagen network remodelling and diastolic stiffness of the rat left ventricle with pressure overload hypertrophy. *Cardiovasc Res,* 22**,** 686-95.

DOGGRELL, S. A. & BROWN, L. 1998. Rat models of hypertension, cardiac hypertrophy and failure. *Cardiovasc Res,* 39**,** 89-105.

DOMENIGHETTI, A. A., BOIXEL, C., CEFAI, D., ABRIEL, H. & PEDRAZZINI, T. 2007. Chronic angiotensin II stimulation in the heart produces an acquired long QT syndrome associated with IK1 potassium current downregulation. *J Mol Cell Cardiol,* 42**,** 63-70.

DOMENIGHETTI, A. A., WANG, Q., EGGER, M., RICHARDS, S. M., PEDRAZZINI, T. & DELBRIDGE, L. M. 2005. Angiotensin II-mediated phenotypic cardiomyocyte remodeling leads to age-dependent cardiac dysfunction and failure. *Hypertension,* 46**,** 426-32.

DONOGHUE, M., HSIEH, F., BARONAS, E., GODBOUT, K., GOSSELIN, M., STAGLIANO, N., DONOVAN, M., WOOLF, B., ROBISON, K., JEYASEELAN, R., BREITBART, R. E. & ACTON, S. 2000. A Novel Angiotensin-Converting Enzyme–Related Carboxypeptidase (ACE2) Converts Angiotensin I to Angiotensin 1-9. *Circ Res,* 87**,** e1-e9.

DONOGHUE, M., WAKIMOTO, H., MAGUIRE, C. T., ACTON, S., HALES, P., STAGLIANO, N., FAIRCHILD-HUNTRESS, V., XU, J., LORENZ, J. N., KADAMBI, V., BERUL, C. I. & BREITBART, R. E. 2003. Heart block, ventricular tachycardia, and sudden death in ACE2 transgenic mice with downregulated connexins. *J Mol Cell Cardiol,* 35**,** 1043-53.

DORN, G. W. & FORCE, T. 2005. Protein kinase cascades in the regulation of cardiac hypertrophy. *J Clin Invest,* 115**,** 527-37.

DOS SANTOS, A. F., ALMEIDA, C. B., BRUGNEROTTO, A. F., ROVERSI, F. M., PALLIS, F. R., FRANCO-PENTEADO, C. F., LANARO, C., ALBUQUERQUE, D. M., LEONARDO, F. C., COSTA, F. F. & CONRAN, N. 2014. Reduced plasma angiotensin II levels are reversed by hydroxyurea treatment in mice with sickle cell disease. *Life Sci,* 117**,** 7-12.

DRAZNER, M. H. 2011. The progression of hypertensive heart disease. *Circulation,* 123**,** 327-34.

DRUMMER, O. H., KOURTIS, S. & JOHNSON, H. 1988. Formation of angiotensin II and other angiotensin peptides from des-leu 10-angiotensin I in rat lung and kidney. *Biochem Pharmacol,* 37**,** 4327-33.

DRUMMOND, G. R. & SOBEY, C. G. 2014. Endothelial NADPH oxidases: which NOX to target in vascular disease? *Trends Endocrinol Metab,* 25**,** 452-63.

DULIN, N. O., ALEXANDER, L. D., HARWALKAR, S., FALCK, J. R. & DOUGLAS, J. G. 1998. Phospholipase A2-mediated activation of mitogen-activated protein kinase by angiotensin II. *Proc Natl Acad Sci U S A,* 95**,** 8098-102.

DULIN, N. O., NIU, J., BROWNING, D. D., YE, R. D. & VOYNO-YASENETSKAYA, T. 2001. Cyclic AMP-independent activation of protein kinase A by vasoactive peptides. *J Biol Chem,* 276**,** 20827-30.

DURIK, M., VAN VEGHEL, R., KUIPERS, A., RINK, R., HAAS JIMOH AKANBI, M., MOLL, G., DANSER, A. H. & ROKS, A. J. 2012. The effect of the thioether-bridged, stabilized Angiotensin-(1-7) analogue cyclic ang-(1-7) on cardiac remodeling and endothelial function in rats with myocardial infarction. *Int J Hypertens,* 2012**,** 536426.

EGOROVA, A. D., KHEDOE, P. P. S. J., GOUMANS, M.-J. T. H., YODER, B. K., NAULI, S. M., TEN DIJKE, P., POELMANN, R. E. & HIERCK, B. P. 2011. Lack of Primary Cilia Primes Shear-Induced Endothelial-to-Mesenchymal Transition. *Circulation Research,* 108**,** 1093-U142.

EVERETT, A. D., TUFRO-MCREDDIE, A., FISHER, A. & GOMEZ, R. A. 1994. Angiotensin receptor regulates cardiac hypertrophy and transforming growth factor-beta 1 expression. *Hypertension,* 23**,** 587-92.

FALCÓN, B. L., STEWART, J. M., BOURASSA, E., KATOVICH, M. J., WALTER, G., SPETH, R. C., SUMNERS, C. & RAIZADA, M. K. 2004. Angiotensin II type 2 receptor gene transfer elicits cardioprotective effects in an angiotensin II infusion rat model of hypertension. *Physiol Genomics,* 19**,** 255-61.

FANG, L., GAO, X. M., SAMUEL, C. S., SU, Y., LIM, Y. L., DART, A. M. & DU, X. J. 2008. Higher levels of collagen and facilitated healing protect against ventricular rupture following myocardial infarction. *Clin Sci (Lond),* 115**,** 99-106.

FATTAH, C., LOUGHREY, C. & NICKLIN, S. 2014. P013 Adenoviral delivery of angiotensin-(1–9) improves cardiac remodelling and function in a murine model of myocardial infarction (MI) (Abstract). *Human Gene Therapy,* 25**,** A1-A22.

FEDERMANN, M. & HESS, O. M. 1994. Differentiation between systolic and diastolic dysfunction. *Eur Heart J,* 15 Suppl D**,** 2-6.

FERRARIO, C. M. 2006. Role of angiotensin II in cardiovascular disease therapeutic implications of more than a century of research. *J Renin Angiotensin Aldosterone Syst,* 7**,** 3-14.

FERREIRA, A. J., CASTRO, C. H., GUATIMOSIM, S., ALMEIDA, P. W., GOMES, E. R., DIAS-PEIXOTO, M. F., ALVES, M. N., FAGUNDES-MOURA, C. R., RENTZSCH, B., GAVA, E., ALMEIDA, A. P., GUIMARÃES, A. M., KITTEN, G. T., REUDELHUBER, T., BADER, M. & SANTOS, R. A. 2010. Attenuation of isoproterenol-induced cardiac fibrosis in transgenic rats harboring an angiotensin-(1-7)-producing fusion protein in the heart. *Ther Adv Cardiovasc Dis,* 4**,** 83-96.

FERREIRA, A. J., SANTOS, R. A. & ALMEIDA, A. P. 2001. Angiotensin-(1-7): cardioprotective effect in myocardial ischemia/reperfusion. *Hypertension,* 38**,** 665-8.

FERREIRA, A. J., SANTOS, R. A. & ALMEIDA, A. P. 2002. Angiotensin-(1-7) improves the post-ischemic function in isolated perfused rat hearts. *Braz J Med Biol Res,* 35**,** 1083-90.

FERREIRA, A. J., SHENOY, V., QI, Y., FRAGA-SILVA, R. A., SANTOS, R. A., KATOVICH, M. J. & RAIZADA, M. K. 2011. Angiotensin-converting enzyme 2 activation protects against hypertension-induced cardiac fibrosis involving extracellular signal-regulated kinases. *Exp Physiol,* 96**,** 287-94.

FERREIRA, S. H. 1965. A BRADYKININ-POTENTIATING FACTOR (BPF) PRESENT IN THE VENOM OF BOTHROPS JARARCA. *Br J Pharmacol Chemother,* 24**,** 163-9.

FINCKENBERG, P., INKINEN, K., AHONEN, J., MERASTO, S., LOUHELAINEN, M., VAPAATALO, H., MÜLLER, D., GANTEN, D., LUFT, F. & MERVAALA, E. 2003. Angiotensin II induces connective tissue growth factor gene expression via calcineurin-dependent pathways. *Am J Pathol,* 163**,** 355-66.

FIORDALISO, F., LI, B., LATINI, R., SONNENBLICK, E. H., ANVERSA, P., LERI, A. & KAJSTURA, J. 2000. Myocyte death in streptozotocin-induced diabetes in rats in angiotensin II- dependent. *Lab Invest,* 80**,** 513-27.

FLEETWOOD, G., BOUTINET, S., MEIER, M. & WOOD, J. M. 1991. Involvement of the renin-angiotensin system in ischemic damage and reperfusion arrhythmias in the isolated perfused rat heart. *J Cardiovasc Pharmacol,* 17**,** 351-6.

FLESCH, M., KILTER, H., CREMERS, B., LENZ, O., SÜDKAMP, M., KUHN-REGNIER, F. & BÖHM, M. 1997. Acute effects of nitric oxide and cyclic GMP on human myocardial contractility. *J Pharmacol Exp Ther,* 281**,** 1340-9.

FLORES-MUNOZ, M., GRAHAM, D., BAKER, A. H., MILLIGAN, G. & A, N. S. 2013. Angiotensin-(1-9) antagonises cardiac remodelling via the angiotensin type 2 receptor (Abstract). *European Heart Journal* 34.

FLORES-MUÑOZ, M., SMITH, N. J., HAGGERTY, C., MILLIGAN, G. & NICKLIN, S. A. 2011. Angiotensin1-9 antagonises pro-hypertrophic signalling in cardiomyocytes via the angiotensin type 2 receptor. *J Physiol,* 589**,** 939-51.

FLORES-MUNOZ, M., WORK, L. M., DOUGLAS, K., DENBY, L., DOMINICZAK, A. F., GRAHAM, D. & NICKLIN, S. A. 2012. Angiotensin-(1-9) attenuates cardiac fibrosis in the stroke-prone spontaneously hypertensive rat via the angiotensin type 2 receptor. *Hypertension,* 59**,** 300-7.

FÖLDES, G., SUO, M., SZOKODI, I., LAKÓ-FUTÓ, Z., DECHÂTEL, R., VUOLTEENAHO, O., HUTTUNEN, P., RUSKOAHO, H. & TÓTH, M. 2001.

Factors derived from adrenals are required for activation of cardiac gene expression in angiotensin II-induced hypertension. *Endocrinology,* 142**,** 4256-63.

FRID, M. G., KALE, V. A. & STENMARK, K. R. 2002. Mature vascular endothelium can give rise to smooth muscle cells via endothelial-mesenchymal transdifferentiation: in vitro analysis. *Circ Res,* 90**,** 1189-96.

FROHLICH, E. D. 1999. State of the Art lecture. Risk mechanisms in hypertensive heart disease. *Hypertension,* 34**,** 782-9.

FROHLICH, E. D., APSTEIN, C., CHOBANIAN, A. V., DEVEREUX, R. B., DUSTAN, H. P., DZAU, V., FAUAD-TARAZI, F., HORAN, M. J., MARCUS, M. & MASSIE, B. 1992. The heart in hypertension. *N Engl J Med,* 327**,** 998-1008.

FUCHS, S., XIAO, H. D., HUBERT, C., MICHAUD, A., CAMPBELL, D. J., ADAMS, J. W., CAPECCHI, M. R., CORVOL, P. & BERNSTEIN, K. E. 2008. Angiotensin-converting enzyme C-terminal catalytic domain is the main site of angiotensin I cleavage *in vivo*. *Hypertension,* 51**,** 267-74.

FUJISAKI, H., ITO, H., HIRATA, Y., TANAKA, M., HATA, M., LIN, M., ADACHI, S., AKIMOTO, H., MARUMO, F. & HIROE, M. 1995. Natriuretic peptides inhibit angiotensin II-induced proliferation of rat cardiac fibroblasts by blocking endothelin-1 gene expression. *J Clin Invest,* 96**,** 1059-65.

GABBIANI, G. 2003. The myofibroblast in wound healing and fibrocontractive diseases. *J Pathol,* 200**,** 500-3.

GALLAGHER, P. E., FERRARIO, C. M. & TALLANT, E. A. 2008. Regulation of ACE2 in cardiac myocytes and fibroblasts. *Am J Physiol Heart Circ Physiol,* 295**,** H2373-9.

GALLAGHER, S. R. & DESJARDINS, P. R. 2006. Quantitation of DNA and RNA with absorption and fluorescence spectroscopy. *Curr Protoc Mol Biol,* Appendix 3**,** Appendix 3D.

GAO, S., HO, D., VATNER, D. E. & VATNER, S. F. 2011. Echocardiography in Mice. *Curr Protoc Mouse Biol,* 1**,** 71-83.

GARABELLI, P. J., MODRALL, J. G., PENNINGER, J. M., FERRARIO, C. M. & CHAPPELL, M. C. 2008. Distinct roles for angiotensin-converting enzyme 2 and carboxypeptidase A in the processing of angiotensins within the murine heart. *Exp Physiol,* 93**,** 613-21.

GARCIA-MENENDEZ, L., KARAMANLIDIS, G., KOLWICZ, S. & TIAN, R. 2013. Substrain specific response to cardiac pressure overload in C57BL/6 mice. *Am J Physiol Heart Circ Physiol,* 305**,** H397-402.

GARCÍA-VILLALÓN, A. L., FERNÁNDEZ, N., MONGE, L. & DIÉGUEZ, G. 2011. Coronary response to diadenosine tetraphosphate after ischemia-reperfusion in the isolated rat heart. *Eur J Pharmacol,* 660**,** 394-401.

GARDINER, C., FERREIRA, Y. J., DRAGOVIC, R. A., REDMAN, C. W. & SARGENT, I. L. 2013. Extracellular vesicle sizing and enumeration by nanoparticle tracking analysis. *J Extracell Vesicles,* 2.

GARSIDE, V. C., CHANG, A. C., KARSAN, A. & HOODLESS, P. A. 2013. Co-ordinating Notch, BMP, and TGF-β signaling during heart valve development. *Cell Mol Life Sci,* 70**,** 2899-917.

GASC, J. M., SHANMUGAM, S., SIBONY, M. & CORVOL, P. 1994. Tissue-specific expression of type 1 angiotensin II receptor subtypes. An in situ hybridization study. *Hypertension,* 24**,** 531-7.

GAUDESIUS, G., MIRAGOLI, M., THOMAS, S. P. & ROHR, S. 2003. Coupling of cardiac electrical activity over extended distances by fibroblasts of cardiac origin. *Circ Res,* 93**,** 421-8.

GAVRAS, H., KREMER, D., BROWN, J. J., GRAY, B., LEVER, A. F., MACADAM, R. F., MEDINA, A., MORTON, J. J. & ROBERTSON, J. I. 1975. Angiotensin- and norepinephrine-induced myocardial lesions: experimental and clinical studies in rabbits and man. *Am Heart J,* 89**,** 321-32.

GAVRAS, H., LEVER, A. F., BROWN, J. J., MACADAM, R. F. & ROBERTSON, J. I. 1971. Acute renal failure, tubular necrosis, and myocardial infarction induced in the rabbit by intravenous angiotensin II. *Lancet,* 2**,** 19-22.

GENNEBÄCK, N., HELLMAN, U., MALM, L., LARSSON, G., RONQUIST, G., WALDENSTRÖM, A. & MÖRNER, S. 2013. Growth factor stimulation of cardiomyocytes induces changes in the transcriptional contents of secreted exosomes. *J Extracell Vesicles,* 2.

GEORGAKOPOULOS, D. & KASS, D. 2001. Minimal force-frequency modulation of inotropy and relaxation of in situ murine heart. *J Physiol,* 534**,** 535-45.

GHOSH, A. K., BRADHAM, W. S., GLEAVES, L. A., DE TAEYE, B., MURPHY, S. B., COVINGTON, J. W. & VAUGHAN, D. E. 2010. Genetic deficiency of plasminogen activator inhibitor-1 promotes cardiac fibrosis in aged mice: involvement of constitutive transforming growth factor-beta signaling and endothelial-to-mesenchymal transition. *Circulation,* 122**,** 1200-9.

GIACOMELLI, F., ANVERSA, P. & WIENER, J. 1976. Effect of angiotensin-induced hypertension on rat coronary arteries and myocardium. *Am J Pathol,* 84**,** 111-38.

GIANI, J. F., MUÑOZ, M. C., MAYER, M. A., VEIRAS, L. C., ARRANZ, C., TAIRA, C. A., TURYN, D., TOBLLI, J. E. & DOMINICI, F. P. 2010. Angiotensin-(1–7) improves cardiac remodeling and inhibits growth-promoting pathways in the heart of fructose-fed rats. *Am J of Physiol Heart Circ Physiol,* 298**,** H1003-H1013.

GIANNI, D., TAULET, N., ZHANG, H., DERMARDIROSSIAN, C., KISTER, J., MARTINEZ, L., ROUSH, W. R., BROWN, S. J., BOKOCH, G. M. & ROSEN, H. 2010. A novel and specific NADPH oxidase-1 (Nox1) small-molecule inhibitor blocks the formation of functional invadopodia in human colon cancer cells. *ACS Chem Biol,* 5**,** 981-93.

GIORDANO, F. J., GERBER, H. P., WILLIAMS, S. P., VANBRUGGEN, N., BUNTING, S., RUIZ-LOZANO, P., GU, Y., NATH, A. K., HUANG, Y., HICKEY, R., DALTON, N., PETERSON, K. L., ROSS, J., CHIEN, K. R. & FERRARA, N. 2001. A cardiac myocyte vascular endothelial growth factor paracrine pathway is required to maintain cardiac function. *Proc Natl Acad Sci U S A,* 98**,** 5780-5.

GOLDENBERG, I., GROSSMAN, E., JACOBSON, K. A., SHNEYVAYS, V. & SHAINBERG, A. 2001. Angiotensin II-induced apoptosis in rat cardiomyocyte culture: a possible role of AT_1 and AT_2 receptors. *J Hypertens,* 19**,** 1681-9.

GOLDSMITH, E. C., HOFFMAN, A., MORALES, M. O., POTTS, J. D., PRICE, R. L., MCFADDEN, A., RICE, M. & BORG, T. K. 2004. Organization of fibroblasts in the heart. *Dev Dyn,* 230**,** 787-94.

GONANO, L. A., SEPÚLVEDA, M., RICO, Y., KAETZEL, M., VALVERDE, C. A., DEDMAN, J., MATTIAZZI, A. & VILA PETROFF, M. 2011. Calcium-calmodulin kinase II mediates digitalis-induced arrhythmias. *Circ Arrhythm Electrophysiol,* 4**,** 947-57.

GONZALES, P. A., PISITKUN, T., HOFFERT, J. D., TCHAPYJNIKOV, D., STAR, R. A., KLETA, R., WANG, N. S. & KNEPPER, M. A. 2009. Large-scale proteomics and phosphoproteomics of urinary exosomes. *J Am Soc Nephrol,* 20**,** 363-79.

GONZALEZ, L. J., GIBBONS, E., BAILEY, R. W., FAIRBOURN, J., NGUYEN, T., SMITH, S. K., BEST, K. B., NELSON, J., JUDD, A. M. & BELL, J. D. 2009. The influence of membrane physical properties on microvesicle release in human erythrocytes. *PMC Biophys,* 2**,** 7.

GOULTER, A. B., GODDARD, M. J., ALLEN, J. C. & CLARK, K. L. 2004. ACE2 gene expression is up-regulated in the human failing heart. *BMC Med,* 2**,** 19.

GOUMANS, M.-J., VAN ZONNEVELD, A. J. & TEN DIJKE, P. 2008. Transforming Growth Factor beta-Induced Endothelial-to-Mesenchymal Transition: A Switch to Cardiac Fibrosis? *Trends in Cardiovascular Medicine,* 18**,** 293-298.

GRAIANI, G., LAGRASTA, C., MIGLIACCIO, E., SPILLMANN, F., MELONI, M., MADEDDU, P., QUAINI, F., PADURA, I. M., LANFRANCONE, L., PELICCI, P. & EMANUELI, C. 2005. Genetic deletion of the $p66^{Shc}$ adaptor protein protects from angiotensin II-induced myocardial damage. *Hypertension,* 46**,** 433-40.

GRAY, M. O., LONG, C. S., KALINYAK, J. E., LI, H. T. & KARLINER, J. S. 1998. Angiotensin II stimulates cardiac myocyte hypertrophy via paracrine release of TGF-beta 1 and endothelin-1 from fibroblasts. *Cardiovasc Res,* 40**,** 352-63.

GRIENDLING, K. K., MINIERI, C. A., OLLERENSHAW, J. D. & ALEXANDER, R. W. 1994. Angiotensin II stimulates NADH and NADPH oxidase activity in cultured vascular smooth muscle cells. *Circ Res,* 74**,** 1141-8.

GROBE, J. L., MECCA, A. P., LINGIS, M., SHENOY, V., BOLTON, T. A., MACHADO, J. M., SPETH, R. C., RAIZADA, M. K. & KATOVICH, M. J. 2007. Prevention of angiotensin II-induced cardiac remodeling by angiotensin-(1–7). *Am J of Physiol Heart Circ Physiol,* 292**,** H736-H742.

GROHÉ, C., KAHLERT, S., LÖBBERT, K., NEYSES, L., VAN EICKELS, M., STIMPEL, M. & VETTER, H. 1998. Angiotensin converting enzyme inhibition modulates cardiac fibroblast growth. *J Hypertens,* 16**,** 377-84.

GUO, D. F., SUN, Y. L., HAMET, P. & INAGAMI, T. 2001. The angiotensin II type 1 receptor and receptor-associated proteins. *Cell Res,* 11**,** 165-80.

GUPTA, S. & KNOWLTON, A. A. 2007. HSP60 trafficking in adult cardiac myocytes: role of the exosomal pathway. *Am J Physiol Heart Circ Physiol,* 292**,** H3052-6.

GUSEV, K., DOMENIGHETTI, A. A., DELBRIDGE, L. M., PEDRAZZINI, T., NIGGLI, E. & EGGER, M. 2009. Angiotensin II-mediated adaptive and maladaptive

remodeling of cardiomyocyte excitation-contraction coupling. *Circ Res,* 105**,** 42-50.

HABER, P. K., YE, M., WYSOCKI, J., MAIER, C., HAQUE, S. K. & BATLLE, D. 2014. Angiotensin-converting enzyme 2-independent action of presumed angiotensin-converting enzyme 2 activators: studies *in vivo, ex vivo*, and *in vitro*. *Hypertension,* 63**,** 774-82.

HABUCHI, Y., LU, L. L., MORIKAWA, J. & YOSHIMURA, M. 1995. Angiotensin II inhibition of L-type Ca^{2+} current in sinoatrial node cells of rabbits. *Am J Physiol,* 268**,** H1053-60.

HAO, J., WANG, B., JONES, S. C., JASSAL, D. S. & DIXON, I. M. 2000. Interaction between angiotensin II and Smad proteins in fibroblasts in failing heart and *in vitro*. *Am J Physiol Heart Circ Physiol,* 279**,** H3020-30.

HASCHKE, M., SCHUSTER, M., POGLITSCH, M., LOIBNER, H., SALZBERG, M., BRUGGISSER, M., PENNINGER, J. & KRÄHENBÜHL, S. 2013. Pharmacokinetics and pharmacodynamics of recombinant human angiotensin-converting enzyme 2 in healthy human subjects. *Clin Pharmacokinet,* 52**,** 783-92.

HAUDEK, S. B., XIA, Y., HUEBENER, P., LEE, J. M., CARLSON, S., CRAWFORD, J. R., PILLING, D., GOMER, R. H., TRIAL, J., FRANGOGIANNIS, N. G. & ENTMAN, M. L. 2006. Bone marrow-derived fibroblast precursors mediate ischemic cardiomyopathy in mice. *Proc Natl Acad Sci U S A,* 103**,** 18284-9.

HAYWOOD, G. A., GULLESTAD, L., KATSUYA, T., HUTCHINSON, H. G., PRATT, R. E., HORIUCHI, M. & FOWLER, M. B. 1997. AT_1 and AT_2 angiotensin receptor gene expression in human heart failure. *Circulation,* 95**,** 1201-6.

HEID, C. A., STEVENS, J., LIVAK, K. J. & WILLIAMS, P. M. 1996. Real time quantitative PCR. *Genome Res,* 6**,** 986-94.

HEIJNEN, H. F., SCHIEL, A. E., FIJNHEER, R., GEUZE, H. J. & SIXMA, J. J. 1999. Activated platelets release two types of membrane vesicles: microvesicles by surface shedding and exosomes derived from exocytosis of multivesicular bodies and alpha-granules. *Blood,* 94**,** 3791-9.

HEIN, L., MEINEL, L., PRATT, R. E., DZAU, V. J. & KOBILKA, B. K. 1997. Intracellular trafficking of angiotensin II and its AT_1 and AT_2 receptors: evidence for selective sorting of receptor and ligand. *Mol Endocrinol,* 11**,** 1266-77.

HEINEKE, J. & MOLKENTIN, J. D. 2006. Regulation of cardiac hypertrophy by intracellular signalling pathways. *Nat Rev Mol Cell Biol,* 7**,** 589-600.

HERMANS, H., SWINNEN, M., POKREISZ, P., CALUWÉ, E., DYMARKOWSKI, S., HERREGODS, M. C., JANSSENS, S. & HERIJGERS, P. 2014. Murine pressure overload models: a 30-MHz look brings a whole new "sound" into data interpretation. *J Appl Physiol (1985),* 117**,** 563-71.

HERNÁNDEZ PRADA, J. A., FERREIRA, A. J., KATOVICH, M. J., SHENOY, V., QI, Y., SANTOS, R. A., CASTELLANO, R. K., LAMPKINS, A. J., GUBALA, V., OSTROV, D. A. & RAIZADA, M. K. 2008. Structure-based identification of small-molecule angiotensin-converting enzyme 2 activators as novel antihypertensive agents. *Hypertension,* 51**,** 1312-7.

HESCHELER, J., MEYER, R., PLANT, S., KRAUTWURST, D., ROSENTHAL, W. & SCHULTZ, G. 1991. Morphological, biochemical, and electrophysiological

characterization of a clonal cell (H9c2) line from rat heart. *Circ Res,* 69**,** 1476-86.

HEUSCH, G. 2008. Heart rate in the pathophysiology of coronary blood flow and myocardial ischaemia: benefit from selective bradycardic agents. *Br J Pharmacol,* 153**,** 1589-601.

HEYMANS, S., LUPU, F., TERCLAVERS, S., VANWETSWINKEL, B., HERBERT, J. M., BAKER, A., COLLEN, D., CARMELIET, P. & MOONS, L. 2005. Loss or inhibition of uPA or MMP-9 attenuates LV remodeling and dysfunction after acute pressure overload in mice. *Am J Pathol,* 166**,** 15-25.

HEYMANS, S., LUTTUN, A., NUYENS, D., THEILMEIER, G., CREEMERS, E., MOONS, L., DYSPERSIN, G. D., CLEUTJENS, J. P., SHIPLEY, M., ANGELLILO, A., LEVI, M., NÜBE, O., BAKER, A., KESHET, E., LUPU, F., HERBERT, J. M., SMITS, J. F., SHAPIRO, S. D., BAES, M., BORGERS, M., COLLEN, D., DAEMEN, M. J. & CARMELIET, P. 1999. Inhibition of plasminogen activators or matrix metalloproteinases prevents cardiac rupture but impairs therapeutic angiogenesis and causes cardiac failure. *Nat Med,* 5**,** 1135-42.

HIGASHI, M., SHIMOKAWA, H., HATTORI, T., HIROKI, J., MUKAI, Y., MORIKAWA, K., ICHIKI, T., TAKAHASHI, S. & TAKESHITA, A. 2003. Long-term inhibition of Rho-kinase suppresses angiotensin II-induced cardiovascular hypertrophy in rats *in vivo*: effect on endothelial NAD(P)H oxidase system. *Circ Res,* 93**,** 767-75.

HIGUCHI, S., OHTSU, H., SUZUKI, H., SHIRAI, H., FRANK, G. D. & EGUCHI, S. 2007. Angiotensin II signal transduction through the AT_1 receptor: novel insights into mechanisms and pathophysiology. *Clin Sci (Lond),* 112**,** 417-28.

HIGUCHI, Y., OTSU, K., NISHIDA, K., HIROTANI, S., NAKAYAMA, H., YAMAGUCHI, O., MATSUMURA, Y., UENO, H., TADA, M. & HORI, M. 2002. Involvement of reactive oxygen species-mediated NF-kappa B activation in TNF-alpha-induced cardiomyocyte hypertrophy. *J Mol Cell Cardiol,* 34**,** 233-40.

HINGTGEN, S. D., TIAN, X., YANG, J., DUNLAY, S. M., PEEK, A. S., WU, Y., SHARMA, R. V., ENGELHARDT, J. F. & DAVISSON, R. L. 2006. Nox2-containing NADPH oxidase and Akt activation play a key role in angiotensin II-induced cardiomyocyte hypertrophy. *Physiol Genomics,* 26**,** 180-91.

HOKIMOTO, S., YASUE, H., FUJIMOTO, K., YAMAMOTO, H., NAKAO, K., KAIKITA, K., SAKATA, R. & MIYAMOTO, E. 1996. Expression of angiotensin-converting enzyme in remaining viable myocytes of human ventricles after myocardial infarction. *Circulation,* 94**,** 1513-8.

HOLUBARSCH, C., HASENFUSS, G., SCHMIDT-SCHWEDA, S., KNORR, A., PIESKE, B., RUF, T., FASOL, R. & JUST, H. 1993. Angiotensin I and II exert inotropic effects in atrial but not in ventricular human myocardium. An *in vitro* study under physiological experimental conditions. *Circulation,* 88**,** 1228-37.

HOOD, S. G., COCHRANE, T., MCKINLEY, M. J. & MAY, C. N. 2007. Investigation of the mechanisms by which chronic infusion of an acutely subpressor dose of angiotensin II induces hypertension. *Am J Physiol Regul Integr Comp Physiol,* 292**,** R1893-9.

HORIUCHI, M., HAYASHIDA, W., KAMBE, T., YAMADA, T. & DZAU, V. J. 1997. Angiotensin type 2 receptor dephosphorylates Bcl-2 by activating mitogen-activated protein kinase phosphatase-1 and induces apoptosis. *J Biol Chem,* 272**,** 19022-6.

HUNYADY, L., BAUKAL, A. J., GABORIK, Z., OLIVARES-REYES, J. A., BOR, M., SZASZAK, M., LODGE, R., CATT, K. J. & BALLA, T. 2002. Differential PI 3-kinase dependence of early and late phases of recycling of the internalized AT_1 angiotensin receptor. *J Cell Biol,* 157**,** 1211-22.

HUNYADY, L. & CATT, K. J. 2006. Pleiotropic AT_1 receptor signaling pathways mediating physiological and pathogenic actions of angiotensin II. *Mol Endocrinol,* 20**,** 953-70.

IBRAHIM, A. & MARBÁN, E. 2015. Exosomes: Fundamental Biology and Roles in Cardiovascular Physiology. *Annu Rev Physiol*.

ICHIHARA, S., SENBONMATSU, T., PRICE, E., ICHIKI, T., GAFFNEY, F. A. & INAGAMI, T. 2001. Angiotensin II type 2 receptor is essential for left ventricular hypertrophy and cardiac fibrosis in chronic angiotensin II-induced hypertension. *Circulation,* 104**,** 346-51.

ICHIKI, T., TAKEDA, K., TOKUNOU, T., FUNAKOSHI, Y., ITO, K., IINO, N. & TAKESHITA, A. 2001. Reactive oxygen species-mediated homologous downregulation of angiotensin II type 1 receptor mRNA by angiotensin II. *Hypertension,* 37**,** 535-40.

IHARA, M., URATA, H., KINOSHITA, A., SUZUMIYA, J., SASAGURI, M., KIKUCHI, M., IDEISHI, M. & ARAKAWA, K. 1999. Increased chymase-dependent angiotensin II formation in human atherosclerotic aorta. *Hypertension,* 33**,** 1399-405.

IKEDA, Y., SATO, K., PIMENTEL, D. R., SAM, F., SHAW, R. J., DYCK, J. R. & WALSH, K. 2009. Cardiac-specific deletion of LKB1 leads to hypertrophy and dysfunction. *J Biol Chem,* 284**,** 35839-49.

IMAI, T., TAKAHASHI, Y., NISHIKAWA, M., KATO, K., MORISHITA, M., YAMASHITA, T., MATSUMOTO, A., CHAROENVIRIYAKUL, C. & TAKAKURA, Y. 2015. Macrophage-dependent clearance of systemically administered B16BL6-derived exosomes from the blood circulation in mice. *J Extracell Vesicles,* 4**,** 26238.

IMIG, J. D., NAVAR, G. L., ZOU, L. X., O'REILLY, K. C., ALLEN, P. L., KAYSEN, J. H., HAMMOND, T. G. & NAVAR, L. G. 1999. Renal endosomes contain angiotensin peptides, converting enzyme, and AT(1A) receptors. *Am J Physiol,* 277**,** F303-11.

ISHIHATA, A. & ENDOH, M. 1995. Species-related differences in inotropic effects of angiotensin II in mammalian ventricular muscle: receptors, subtypes and phosphoinositide hydrolysis. *Br J Pharmacol,* 114**,** 447-53.

ISHISAKI, A., HAYASHI, H., LI, A. J. & IMAMURA, T. 2003. Human umbilical vein endothelium-derived cells retain potential to differentiate into smooth muscle-like cells. *J Biol Chem,* 278**,** 1303-9.

ISHIYAMA, Y., GALLAGHER, P. E., AVERILL, D. B., TALLANT, E. A., BROSNIHAN, K. B. & FERRARIO, C. M. 2004. Upregulation of angiotensin-converting enzyme 2 after myocardial infarction by blockade of angiotensin II receptors. *Hypertension,* 43**,** 970-6.

ISLAM, A., SHEN, X., HIROI, T., MOSS, J., VAUGHAN, M. & LEVINE, S. J. 2007. The brefeldin A-inhibited guanine nucleotide-exchange protein, BIG2, regulates the constitutive release of TNFR1 exosome-like vesicles. *J Biol Chem,* 282**,** 9591-9.

ITO, H., HIRATA, Y., ADACHI, S., TANAKA, M., TSUJINO, M., KOIKE, A., NOGAMI, A., MURUMO, F. & HIROE, M. 1993. Endothelin-1 is an autocrine/paracrine factor in the mechanism of angiotensin II-induced hypertrophy in cultured rat cardiomyocytes. *J Clin Invest,* 92**,** 398-403.

ITO, M., OLIVERIO, M. I., MANNON, P. J., BEST, C. F., MAEDA, N., SMITHIES, O. & COFFMAN, T. M. 1995. Regulation of blood pressure by the type 1A angiotensin II receptor gene. *Proc Natl Acad Sci U S A,* 92**,** 3521-5.

IWAI, M. & HORIUCHI, M. 2009. Devil and angel in the renin-angiotensin system: ACE-angiotensin II-AT1 receptor axis vs. ACE2-angiotensin-(1-7)-Mas receptor axis. *Hypertens Res,* 32**,** 533-6.

IWAI, N. & INAGAMI, T. 1992. Identification of two subtypes in the rat type I angiotensin II receptor. *FEBS Lett,* 298**,** 257-60.

IWAI, N., SHIMOIKE, H. & KINOSHITA, M. 1995. Cardiac renin-angiotensin system in the hypertrophied heart. *Circulation,* 92**,** 2690-6.

IWANAGA, Y., AOYAMA, T., KIHARA, Y., ONOZAWA, Y., YONEDA, T. & SASAYAMA, S. 2002. Excessive activation of matrix metalloproteinases coincides with left ventricular remodeling during transition from hypertrophy to heart failure in hypertensive rats. *J Am Coll Cardiol,* 39**,** 1384-91.

IWANCIW, D., REHM, M., PORST, M. & GOPPELT-STRUEBE, M. 2003. Induction of connective tissue growth factor by angiotensin II: integration of signaling pathways. *Arterioscler Thromb Vasc Biol,* 23**,** 1782-7.

IWATA, M., COWLING, R. T., GURANTZ, D., MOORE, C., ZHANG, S., YUAN, J. X. J. & GREENBERG, B. H. 2005. Angiotensin-(1–7) binds to specific receptors on cardiac fibroblasts to initiate antifibrotic and antitrophic effects. *Am J of Physiol Heart Circ Physiol,* 289**,** H2356-H2363.

IZUMIYA, Y., KIM, S., IZUMI, Y., YOSHIDA, K., YOSHIYAMA, M., MATSUZAWA, A., ICHIJO, H. & IWAO, H. 2003. Apoptosis signal-regulating kinase 1 plays a pivotal role in angiotensin II-induced cardiac hypertrophy and remodeling. *Circ Res,* 93**,** 874-83.

IZUMIYA, Y., SHIOJIMA, I., SATO, K., SAWYER, D. B., COLUCCI, W. S. & WALSH, K. 2006. Vascular endothelial growth factor blockade promotes the transition from compensatory cardiac hypertrophy to failure in response to pressure overload. *Hypertension,* 47**,** 887-93.

JACKMAN, H. L., MASSAD, M. G., SEKOSAN, M., TAN, F., BROVKOVYCH, V., MARCIC, B. M. & ERDÖS, E. G. 2002. Angiotensin 1-9 and 1-7 release in human heart: role of cathepsin A. *Hypertension,* 39**,** 976-81.

JALIL, J. E., DOERING, C. W., JANICKI, J. S., PICK, R., SHROFF, S. G. & WEBER, K. T. 1989. Fibrillar collagen and myocardial stiffness in the intact hypertrophied rat left ventricle. *Circ Res,* 64**,** 1041-50.

JANICKI, J. S. & BROWER, G. L. 2002. The role of myocardial fibrillar collagen in ventricular remodeling and function. *J Card Fail,* 8**,** S319-25.

JHUND, P. S., MACINTYRE, K., SIMPSON, C. R., LEWSEY, J. D., STEWART, S., REDPATH, A., CHALMERS, J. W., CAPEWELL, S. & MCMURRAY, J. J. 2009.

Long-term trends in first hospitalization for heart failure and subsequent survival between 1986 and 2003: a population study of 5.1 million people. *Circulation,* 119**,** 515-23.

JOHNSTONE, R. M., ADAM, M., HAMMOND, J. R., ORR, L. & TURBIDE, C. 1987. Vesicle formation during reticulocyte maturation. Association of plasma membrane activities with released vesicles (exosomes). *J Biol Chem,* 262**,** 9412-20.

JOULIN, O., MARECHAUX, S., HASSOUN, S., MONTAIGNE, D., LANCEL, S. & NEVIERE, R. 2009. Cardiac force-frequency relationship and frequency-dependent acceleration of relaxation are impaired in LPS-treated rats. *Crit Care,* 13**,** R14.

JUILLERAT, L., NUSSBERGER, J., MÉNARD, J., MOOSER, V., CHRISTEN, Y., WAEBER, B., GRAF, P. & BRUNNER, H. R. 1990. Determinants of angiotensin II generation during converting enzyme inhibition. *Hypertension,* 16**,** 564-72.

KALRA, H., ADDA, C. G., LIEM, M., ANG, C. S., MECHLER, A., SIMPSON, R. J., HULETT, M. D. & MATHIVANAN, S. 2013. Comparative proteomics evaluation of plasma exosome isolation techniques and assessment of the stability of exosomes in normal human blood plasma. *Proteomics,* 13**,** 3354-64.

KAMBAYASHI, Y., NAGATA, K., ICHIKI, T. & INAGAMI, T. 1996. Insulin and insulin-like growth factors induce expression of angiotensin type-2 receptor in vascular-smooth-muscle cells. *Eur J Biochem,* 239**,** 558-65.

KAMP, T. J. & HELL, J. W. 2000. Regulation of cardiac L-type calcium channels by protein kinase A and protein kinase C. *Circ Res,* 87**,** 1095-102.

KANAIDE, H., ICHIKI, T., NISHIMURA, J. & HIRANO, K. 2003. Cellular mechanism of vasoconstriction induced by angiotensin II: it remains to be determined. *Circ Res,* 93**,** 1015-7.

KASCHINA, E., GRZESIAK, A., LI, J., FORYST-LUDWIG, A., TIMM, M., ROMPE, F., SOMMERFELD, M., KEMNITZ, U. R., CURATO, C., NAMSOLLECK, P., TSCHÖPE, C., HALLBERG, A., ALTERMAN, M., HUCKO, T., PAETSCH, I., DIETRICH, T., SCHNACKENBURG, B., GRAF, K., DAHLÖF, B., KINTSCHER, U., UNGER, T. & STECKELINGS, U. M. 2008. Angiotensin II type 2 receptor stimulation: a novel option of therapeutic interference with the renin-angiotensin system in myocardial infarction? *Circulation,* 118**,** 2523-32.

KASCHINA, E. & UNGER, T. 2003. Angiotensin AT_1/AT_2 receptors: regulation, signalling and function. *Blood Press,* 12**,** 70-88.

KAWADA, N., IMAI, E., KARBER, A., WELCH, W. J. & WILCOX, C. S. 2002. A mouse model of angiotensin II slow pressor response: role of oxidative stress. *J Am Soc Nephrol,* 13**,** 2860-8.

KAWANO, H., DO, Y. S., KAWANO, Y., STARNES, V., BARR, M., LAW, R. E. & HSUEH, W. A. 2000. Angiotensin II has multiple profibrotic effects in human cardiac fibroblasts. *Circulation,* 101**,** 1130-7.

KAWANO, H., TODA, G., NAKAMIZO, R., KOIDE, Y., SETO, S. & YANO, K. 2005a. Valsartan decreases type I collagen synthesis in patients with hypertrophic cardiomyopathy. *Circ J,* 69**,** 1244-8.

KAWANO, S., KUBOTA, T., MONDEN, Y., KAWAMURA, N., TSUTSUI, H., TAKESHITA, A. & SUNAGAWA, K. 2005b. Blockade of NF-kappaB ameliorates myocardial hypertrophy in response to chronic infusion of angiotensin II. *Cardiovasc Res,* 67**,** 689-98.

KAWASAKI, D., KOSUGI, K., WAKI, H., YAMAMOTO, K., TSUJINO, T. & MASUYAMA, T. 2007. Role of activated renin-angiotensin system in myocardial fibrosis and left ventricular diastolic dysfunction in diabetic patients--reversal by chronic angiotensin II type 1A receptor blockade. *Circ J,* 71**,** 524-9.

KEHAT, I. & MOLKENTIN, J. D. 2010. Molecular pathways underlying cardiac remodeling during pathophysiological stimulation. *Circulation,* 122**,** 2727-35.

KELLY, D. J., COX, A. J., GOW, R. M., ZHANG, Y., KEMP, B. E. & GILBERT, R. E. 2004. Platelet-derived growth factor receptor transactivation mediates the trophic effects of angiotensin II *in vivo*. *Hypertension,* 44**,** 195-202.

KEMP, B. A., HOWELL, N. L., GILDEA, J. J., KELLER, S. R., PADIA, S. H. & CAREY, R. M. 2014. AT_2 receptor activation induces natriuresis and lowers blood pressure. *Circ Res,* 115**,** 388-99.

KEMP, C. D. & CONTE, J. V. 2012. The pathophysiology of heart failure. *Cardiovasc Pathol,* 21**,** 365-71.

KIM, K. S., ABRAHAM, D., WILLIAMS, B., VIOLIN, J. D., MAO, L. & ROCKMAN, H. A. 2012. ß-Arrestin-biased AT_1R stimulation promotes cell survival during acute cardiac injury. *Am J Physiol Heart Circ Physiol,* 303**,** H1001-10.

KIM, S., OHTA, K., HAMAGUCHI, A., YUKIMURA, T., MIURA, K. & IWAO, H. 1995. Angiotensin II induces cardiac phenotypic modulation and remodeling *in vivo* in rats. *Hypertension,* 25**,** 1252-9.

KIM, Y. M., JEON, E. S., KIM, M. R., JHO, S. K., RYU, S. W. & KIM, J. H. 2008. Angiotensin II-induced differentiation of adipose tissue-derived mesenchymal stem cells to smooth muscle-like cells. *Int J Biochem Cell Biol,* 40**,** 2482-91.

KIRCHHEFER, U., BREKLE, C., ESKANDAR, J., ISENSEE, G., KUČEROVÁ, D., MÜLLER, F. U., PINET, F., SCHULTE, J. S., SEIDL, M. D. & BOKNIK, P. 2014. Cardiac function is regulated by B56α-mediated targeting of protein phosphatase 2A (PP2A) to contractile relevant substrates. *J Biol Chem,* 289**,** 33862-73.

KIRIBAYASHI, K., MASAKI, T., NAITO, T., OGAWA, T., ITO, T., YORIOKA, N. & KOHNO, N. 2005. Angiotensin II induces fibronectin expression in human peritoneal mesothelial cells via ERK1/2 and p38 MAPK. *Kidney Int,* 67**,** 1126-35.

KISCH, E. S., DLUHY, R. G. & WILLIAMS, G. H. 1976. Enhanced aldosterone response to angiotensin II in human hypertension. *Circ Res,* 38**,** 502-5.

KITAMURA, M., SHIMIZU, M., INO, H., OKEIE, K., YAMAGUCHI, M., FUNJNO, N., MABUCHI, H. & NAKANISHI, I. 2001. Collagen remodeling and cardiac dysfunction in patients with hypertrophic cardiomyopathy: the significance of type III and VI collagens. *Clin Cardiol,* 24**,** 325-9.

KITAZONO, T., PADGETT, R. C., ARMSTRONG, M. L., TOMPKINS, P. K. & HEISTAD, D. D. 1995. Evidence that angiotensin II is present in human monocytes. *Circulation,* 91**,** 1129-34.

KLUSKENS, L. D., NELEMANS, S. A., RINK, R., DE VRIES, L., METER-ARKEMA, A., WANG, Y., WALTHER, T., KUIPERS, A., MOLL, G. N. & HAAS, M. 2009. Angiotensin-(1-7) with thioether bridge: an angiotensin-converting enzyme-resistant, potent angiotensin-(1-7) analog. *J Pharmacol Exp Ther,* 328**,** 849-54.

KNÖLL, R., HOSHIJIMA, M., HOFFMAN, H. M., PERSON, V., LORENZEN-SCHMIDT, I., BANG, M. L., HAYASHI, T., SHIGA, N., YASUKAWA, H., SCHAPER, W., MCKENNA, W., YOKOYAMA, M., SCHORK, N. J., OMENS, J. H., MCCULLOCH, A. D., KIMURA, A., GREGORIO, C. C., POLLER, W., SCHAPER, J., SCHULTHEISS, H. P. & CHIEN, K. R. 2002. The cardiac mechanical stretch sensor machinery involves a Z disc complex that is defective in a subset of human dilated cardiomyopathy. *Cell,* 111**,** 943-55.

KOBAYASHI, K., IMANISHI, T. & AKASAKA, T. 2006. Endothelial progenitor cell differentiation and senescence in an angiotensin II-infusion rat model. *Hypertens Res,* 29**,** 449-55.

KOBAYASHI, N., KOBAYASHI, K., HARA, K., HIGASHI, T., YANAKA, H., YAGI, S. & MATSUOKA, H. 1999. Benidipine stimulates nitric oxide synthase and improves coronary circulation in hypertensive rats. *Am J Hypertens,* 12**,** 483-91.

KOITABASHI, N., DANNER, T., ZAIMAN, A. L., PINTO, Y. M., ROWELL, J., MANKOWSKI, J., ZHANG, D., NAKAMURA, T., TAKIMOTO, E. & KASS, D. A. 2011. Pivotal role of cardiomyocyte TGF-β signaling in the murine pathological response to sustained pressure overload. *J Clin Invest,* 121**,** 2301-12.

KOKKONEN, J. O., SAARINEN, J. & KOVANEN, P. T. 1997. Regulation of local angiotensin II formation in the human heart in the presence of interstitial fluid. Inhibition of chymase by protease inhibitors of interstitial fluid and of angiotensin-converting enzyme by Ang-(1-9) formed by heart carboxypeptidase A-like activity. *Circulation,* 95**,** 1455-63.

KORHONEN, J., POLVI, A., PARTANEN, J. & ALITALO, K. 1994. The mouse tie receptor tyrosine kinase gene: expression during embryonic angiogenesis. *Oncogene,* 9**,** 395-403.

KRAMKOWSKI, K., MOGIELNICKI, A., LESZCZYNSKA, A. & BUCZKO, W. 2010. Angiotensin-(1-9), the product of angiotensin I conversion in platelets, enhances arterial thrombosis in rats. *J Physiol Pharmacol,* 61**,** 317-24.

KREGE, J. H., HODGIN, J. B., HAGAMAN, J. R. & SMITHIES, O. 1995. A noninvasive computerized tail-cuff system for measuring blood pressure in mice. *Hypertension,* 25**,** 1111-5.

KRYSKO, D. V., VANDEN BERGHE, T., PARTHOENS, E., D'HERDE, K. & VANDENABEELE, P. 2008. Methods for distinguishing apoptotic from necrotic cells and measuring their clearance. *Methods Enzymol,* 442**,** 307-41.

KUPFAHL, C., PINK, D., FRIEDRICH, K., ZURBRÜGG, H. R., NEUSS, M., WARNECKE, C., FIELITZ, J., GRAF, K., FLECK, E. & REGITZ-ZAGROSEK, V. 2000. Angiotensin II directly increases transforming growth factor beta1 and osteopontin and indirectly affects collagen mRNA expression in the human heart. *Cardiovasc Res,* 46**,** 463-75.

KURISU, S., OZONO, R., OSHIMA, T., KAMBE, M., ISHIDA, T., SUGINO, H., MATSUURA, H., CHAYAMA, K., TERANISHI, Y., IBA, O., AMANO, K. & MATSUBARA, H. 2003. Cardiac angiotensin II type 2 receptor activates the kinin/NO system and inhibits fibrosis. *Hypertension,* 41**,** 99-107.

KUSCHEL, M., ZHOU, Y. Y., SPURGEON, H. A., BARTEL, S., KARCZEWSKI, P., ZHANG, S. J., KRAUSE, E. G., LAKATTA, E. G. & XIAO, R. P. 1999. ß2-adrenergic cAMP signaling is uncoupled from phosphorylation of cytoplasmic proteins in canine heart. *Circulation,* 99**,** 2458-65.

KUWAHARA, F., KAI, H., TOKUDA, K., KAI, M., TAKESHITA, A., EGASHIRA, K. & IMAIZUMI, T. 2002. Transforming growth factor-beta function blocking prevents myocardial fibrosis and diastolic dysfunction in pressure-overloaded rats. *Circulation,* 106**,** 130-5.

LAKÓ-FUTÓ, Z., SZOKODI, I., SÁRMÁN, B., FÖLDES, G., TOKOLA, H., ILVES, M., LESKINEN, H., VUOLTEENAHO, O., SKOUMAL, R., DECHÂTEL, R., RUSKOAHO, H. & TÓTH, M. 2003. Evidence for a functional role of angiotensin II type 2 receptor in the cardiac hypertrophic process *in vivo* in the rat heart. *Circulation,* 108**,** 2414-22.

LAMBERT, C. 1995. Mechanisms of angiotensin II chronotropic effect in anaesthetized dogs. *Br J Pharmacol,* 115**,** 795-800.

LAMBERT, D. W., HOOPER, N. M. & TURNER, A. J. 2008. Angiotensin-converting enzyme 2 and new insights into the renin-angiotensin system. *Biochem Pharmacol,* 75**,** 781-6.

LAMOUILLE, S., XU, J. & DERYNCK, R. 2014. Molecular mechanisms of epithelial-mesenchymal transition. *Nat Rev Mol Cell Biol,* 15**,** 178-96.

LANDMESSER, U., CAI, H., DIKALOV, S., MCCANN, L., HWANG, J., JO, H., HOLLAND, S. M. & HARRISON, D. G. 2002. Role of p47(phox) in vascular oxidative stress and hypertension caused by angiotensin II. *Hypertension,* 40**,** 511-5.

LAPLANTE, M. A., WU, R., EL MIDAOUI, A. & DE CHAMPLAIN, J. 2003. NAD(P)H oxidase activation by angiotensin II is dependent on p42/44 ERK-MAPK pathway activation in rat's vascular smooth muscle cells. *J Hypertens,* 21**,** 927-36.

LASSÈGUE, B., ALEXANDER, R. W., NICKENIG, G., CLARK, M., MURPHY, T. J. & GRIENDLING, K. K. 1995. Angiotensin II down-regulates the vascular smooth muscle AT_1 receptor by transcriptional and post-transcriptional mechanisms: evidence for homologous and heterologous regulation. *Mol Pharmacol,* 48**,** 601-9.

LAUER, D., SLAVIC, S., SOMMERFELD, M., THÖNE-REINEKE, C., SHARKOVSKA, Y., HALLBERG, A., DAHLÖF, B., KINTSCHER, U., UNGER, T., STECKELINGS, U. M. & KASCHINA, E. 2014. Angiotensin type 2 receptor stimulation ameliorates left ventricular fibrosis and dysfunction via regulation of tissue inhibitor of matrix metalloproteinase 1/matrix metalloproteinase 9 axis and transforming growth factor ß1 in the rat heart. *Hypertension,* 63**,** e60-7.

LAYLAND, J. & KENTISH, J. C. 1999. Positive force- and $[Ca^{2+}]_i$-frequency relationships in rat ventricular trabeculae at physiological frequencies. *Am J Physiol,* 276**,** H9-H18.

LAYLAND, J., LI, J. M. & SHAH, A. M. 2002. Role of cyclic GMP-dependent protein kinase in the contractile response to exogenous nitric oxide in rat cardiac myocytes. *J Physiol,* 540**,** 457-67.

LEASK, A. & ABRAHAM, D. J. 2004. TGF-beta signaling and the fibrotic response. *FASEB J,* 18**,** 816-27.

LEE, T. H., D'ASTI, E., MAGNUS, N., AL-NEDAWI, K., MEEHAN, B. & RAK, J. 2011. Microvesicles as mediators of intercellular communication in cancer--the emerging science of cellular 'debris'. *Semin Immunopathol,* 33**,** 455-67.

LEE, V. C., LLOYD, E. N., DEARDEN, H. C. & WONG, K. 2013. A systematic review to investigate whether Angiotensin-(1-7) is a promising therapeutic target in human heart failure. *Int J Pept,* 2013**,** 260346.

LEFROY, D. C., CRAKE, T., DEL MONTE, F., VESCOVO, G., DALLA LIBERA, L., HARDING, S. & POOLE-WILSON, P. A. 1996. Angiotensin II and contraction of isolated myocytes from human, guinea pig, and infarcted rat hearts. *Am J Physiol,* 270**,** H2060-9.

LEGAULT, F., ROULEAU, J. L., JUNEAU, C., ROSE, C. & RAKUSAN, K. 1990. Functional and morphological characteristics of compensated and decompensated cardiac hypertrophy in dogs with chronic infrarenal aorto-caval fistulas. *Circ Res,* 66**,** 846-59.

LEI, M., WANG, X., KE, Y. & SOLARO, R. J. 2015. Regulation of Ca(2+) transient by PP2A in normal and failing heart. *Front Physiol,* 6**,** 13.

LEITE-MOREIRA, A. F. & GILLEBERT, T. C. 1994. Nonuniform course of left ventricular pressure fall and its regulation by load and contractile state. *Circulation,* 90**,** 2481-91.

LEIVONEN, S. K., HÄKKINEN, L., LIU, D. & KÄHÄRI, V. M. 2005. Smad3 and extracellular signal-regulated kinase 1/2 coordinately mediate transforming growth factor-beta-induced expression of connective tissue growth factor in human fibroblasts. *J Invest Dermatol,* 124**,** 1162-9.

LEVY, B. I., DURIEZ, M. & SAMUEL, J. L. 2001. Coronary microvasculature alteration in hypertensive rats. Effect of treatment with a diuretic and an ACE inhibitor. *Am J Hypertens,* 14**,** 7-13.

LEVY, D., ANDERSON, K. M., SAVAGE, D. D., BALKUS, S. A., KANNEL, W. B. & CASTELLI, W. P. 1987. Risk of ventricular arrhythmias in left ventricular hypertrophy: the Framingham Heart Study. *Am J Cardiol,* 60**,** 560-5.

LEVY, D., GARRISON, R. J., SAVAGE, D. D., KANNEL, W. B. & CASTELLI, W. P. 1990. Prognostic implications of echocardiographically determined left ventricular mass in the Framingham Heart Study. *N Engl J Med,* 322**,** 1561-6.

LEWIS, J. L., SERIKAWA, T. & WARNOCK, D. G. 1993. Chromosomal localization of angiotensin II type 1 receptor isoforms in the rat. *Biochem Biophys Res Commun,* 194**,** 677-82.

LI, D., SALDEEN, T., ROMEO, F. & MEHTA, J. L. 2000. Oxidized LDL upregulates angiotensin II type 1 receptor expression in cultured human coronary artery endothelial cells: the potential role of transcription factor NF-kappaB. *Circulation,* 102**,** 1970-6.

LI, D., YANG, B., PHILIPS, M. I. & MEHTA, J. L. 1999. Proapoptotic effects of ANG II in human coronary artery endothelial cells: role of AT_1 receptor and PKC activation. *Am J Physiol,* 276**,** H786-92.

LI, J., LEE, Y., JOHANSSON, H. J., MÄGER, I., VADER, P., NORDIN, J. Z., WIKLANDER, O. P., LEHTIÖ, J., WOOD, M. J. & ANDALOUSSI, S. E. 2015. Serum-free culture alters the quantity and protein composition of neuroblastoma-derived extracellular vesicles. *J Extracell Vesicles,* 4**,** 26883.

LI, J., QU, X., YAO, J., CARUANA, G., RICARDO, S. D., YAMAMOTO, Y., YAMAMOTO, H. & BERTRAM, J. F. 2010. Blockade of Endothelial-Mesenchymal Transition by a Smad3 Inhibitor Delays the Early Development of Streptozotocin-Induced Diabetic Nephropathy. *Diabetes,* 59**,** 2612-2624.

LI, J. M. & SHAH, A. M. 2003. Mechanism of endothelial cell NADPH oxidase activation by angiotensin II. Role of the $p47^{phox}$ subunit. *J Biol Chem,* 278**,** 12094-100.

LI, J. M., WHEATCROFT, S., FAN, L. M., KEARNEY, M. T. & SHAH, A. M. 2004. Opposing roles of $p47^{phox}$ in basal versus angiotensin II-stimulated alterations in vascular O^{2-} production, vascular tone, and mitogen-activated protein kinase activation. *Circulation,* 109**,** 1307-13.

LI, Q., ZHANG, J., PFAFFENDORF, M. & VAN ZWIETEN, P. A. 1996. Direct positive chronotropic effects of angiotensin II and angiotensin III in pithed rats and in rat isolated atria. *Br J Pharmacol,* 118**,** 1653-8.

LI, X. C. & ZHUO, J. L. 2008. Intracellular ANG II directly induces in vitro transcription of TGF-beta1, MCP-1, and NHE-3 mRNAs in isolated rat renal cortical nuclei via activation of nuclear AT1a receptors. *Am J Physiol Cell Physiol,* 294**,** C1034-45.

LIANG, W., OUDIT, G. Y., PATEL, M. M., SHAH, A. M., WOODGETT, J. R., TSUSHIMA, R. G., WARD, M. E. & BACKX, P. H. 2010. Role of phosphoinositide 3-kinase {alpha}, protein kinase C, and L-type Ca2+ channels in mediating the complex actions of angiotensin II on mouse cardiac contractility. *Hypertension,* 56**,** 422-9.

LIP, G. Y. 2001. Regression of left ventricular hypertrophy and improved prognosis: some hope now . . . or hype? *Circulation,* 104**,** 1582-4.

LIU, F., GOMEZ GARCIA, A. M. & MEYSKENS, F. L. 2012. NADPH oxidase 1 overexpression enhances invasion via matrix metalloproteinase-2 and epithelial-mesenchymal transition in melanoma cells. *J Invest Dermatol,* 132**,** 2033-41.

LO, J., PATEL, V. B., WANG, Z., LEVASSEUR, J., KAUFMAN, S., PENNINGER, J. M. & OUDIT, G. Y. 2013. Angiotensin-converting enzyme 2 antagonizes angiotensin II-induced pressor response and NADPH oxidase activation in Wistar-Kyoto rats and spontaneously hypertensive rats. *Exp Physiol,* 98**,** 109-22.

LOOT, A. E., ROKS, A. J., HENNING, R. H., TIO, R. A., SUURMEIJER, A. J., BOOMSMA, F. & VAN GILST, W. H. 2002. Angiotensin-(1-7) attenuates the development of heart failure after myocardial infarction in rats. *Circulation,* 105**,** 1548-50.

LÓPEZ, B., GONZÁLEZ, A., QUEREJETA, R., LARMAN, M. & DÍEZ, J. 2006. Alterations in the pattern of collagen deposition may contribute to the deterioration of systolic function in hypertensive patients with heart failure. *J Am Coll Cardiol,* 48**,** 89-96.

LÓPEZ, B., QUEREJETA, R., VARO, N., GONZÁLEZ, A., LARMAN, M., MARTÍNEZ UBAGO, J. L. & DÍEZ, J. 2001. Usefulness of serum carboxy-terminal propeptide of procollagen type I in assessment of the cardioreparative ability of antihypertensive treatment in hypertensive patients. *Circulation,* 104**,** 286-91.

LÓPEZ, J. E., MYAGMAR, B. E., SWIGART, P. M., MONTGOMERY, M. D., HAYNAM, S., BIGOS, M., RODRIGO, M. C. & SIMPSON, P. C. 2011. ß-myosin heavy chain is induced by pressure overload in a minor subpopulation of smaller mouse cardiac myocytes. *Circ Res,* 109**,** 629-38.

LOUCH, W. E., SHEEHAN, K. A. & WOLSKA, B. M. 2011. Methods in cardiomyocyte isolation, culture, and gene transfer. *J Mol Cell Cardiol,* 51**,** 288-98.

LUCHNER, A., STEVENS, T. L., BORGESON, D. D., REDFIELD, M., WEI, C. M., PORTER, J. G. & BURNETT, J. C. 1998. Differential atrial and ventricular expression of myocardial BNP during evolution of heart failure. *Am J Physiol,* 274**,** H1684-9.

LUKETIC, L., DELANGHE, J., SOBOL, P. T., YANG, P., FROTTEN, E., MOSSMAN, K. L., GAULDIE, J., BRAMSON, J. & WAN, Y. 2007. Antigen presentation by exosomes released from peptide-pulsed dendritic cells is not suppressed by the presence of active CTL. *J Immunol,* 179**,** 5024-32.

LYU, L., WANG, H., LI, B., QIN, Q., QI, L., NAGARKATTI, M., NAGARKATTI, P., JANICKI, J. S., WANG, X. L. & CUI, T. 2015. A critical role of cardiac fibroblast-derived exosomes in activating renin angiotensin system in cardiomyocytes. *J Mol Cell Cardiol*.

MAHMOOD, T. & YANG, P. C. 2012. Western blot: technique, theory, and trouble shooting. *N Am J Med Sci,* 4**,** 429-34.

MAI, J., HU, Q., XIE, Y., SU, S., QIU, Q., YUAN, W., YANG, Y., SONG, E., CHEN, Y. & WANG, J. 2015. Dyssynchronous pacing triggers endothelial-mesenchymal transition through heterogeneity of mechanical stretch in a canine model. *Circ J,* 79**,** 201-9.

MALESZEWSKA, M., MOONEN, J. R., HUIJKMAN, N., VAN DE SLUIS, B., KRENNING, G. & HARMSEN, M. C. 2013. IL-1ß and TGFß2 synergistically induce endothelial to mesenchymal transition in an NFκB-dependent manner. *Immunobiology,* 218**,** 443-54.

MANDINOV, L., EBERLI, F. R., SEILER, C. & HESS, O. M. 2000. Diastolic heart failure. *Cardiovasc Res,* 45**,** 813-25.

MARCIC, B., DEDDISH, P. A., JACKMAN, H. L. & ERDÖS, E. G. 1999. Enhancement of bradykinin and resensitization of its B_2 receptor. *Hypertension,* 33**,** 835-43.

MARIJIANOWSKI, M. M., TEELING, P., MANN, J. & BECKER, A. E. 1995. Dilated cardiomyopathy is associated with an increase in the type I/type III collagen ratio: a quantitative assessment. *J Am Coll Cardiol,* 25**,** 1263-72.

MARQUES, F. D., MELO, M. B., SOUZA, L. E., IRIGOYEN, M. C., SINISTERRA, R. D., DE SOUSA, F. B., SAVERGNINI, S. Q., BRAGA, V. B., FERREIRA, A. J. &

SANTOS, R. A. 2012. Beneficial effects of long-term administration of an oral formulation of Angiotensin-(1-7) in infarcted rats. *Int J Hypertens,* 2012**,** 795452.

MARRERO, M. B., SCHIEFFER, B., PAXTON, W. G., HEERDT, L., BERK, B. C., DELAFONTAINE, P. & BERNSTEIN, K. E. 1995. Direct stimulation of Jak/STAT pathway by the angiotensin II AT_1 receptor. *Nature,* 375**,** 247-50.

MARTIN, M. M., WHITE, C. R., LI, H., MILLER, P. J. & ELTON, T. S. 1995. A functional comparison of the rat type-1 angiotensin II receptors ($AT_{1A}R$ and $AT_{1B}R$). *Regul Pept,* 60**,** 135-47.

MARTOS, R., BAUGH, J., LEDWIDGE, M., O'LOUGHLIN, C., CONLON, C., PATLE, A., DONNELLY, S. C. & MCDONALD, K. 2007. Diastolic heart failure: evidence of increased myocardial collagen turnover linked to diastolic dysfunction. *Circulation,* 115**,** 888-95.

MARTTILA, M., VUOLTEENAHO, O., GANTEN, D., NAKAO, K. & RUSKOAHO, H. 1996. Synthesis and secretion of natriuretic peptides in the hypertensive TGR(mREN-2)27 transgenic rat. *Hypertension,* 28**,** 995-1004.

MASAKI, H., KURIHARA, T., YAMAKI, A., INOMATA, N., NOZAWA, Y., MORI, Y., MURASAWA, S., KIZIMA, K., MARUYAMA, K., HORIUCHI, M., DZAU, V. J., TAKAHASHI, H., IWASAKA, T., INADA, M. & MATSUBARA, H. 1998. Cardiac-specific overexpression of angiotensin II AT_2 receptor causes attenuated response to AT_1 receptor-mediated pressor and chronotropic effects. *J Clin Invest,* 101**,** 527-35.

MASSAGUÉ, J. 2012. TGFβ signalling in context. *Nat Rev Mol Cell Biol,* 13**,** 616-30.

MASSION, P. B., FERON, O., DESSY, C. & BALLIGAND, J. L. 2003. Nitric oxide and cardiac function: ten years after, and continuing. *Circ Res,* 93**,** 388-98.

MASSON, R., NICKLIN, S. A., CRAIG, M. A., MCBRIDE, M., GILDAY, K., GREGOREVIC, P., ALLEN, J. M., CHAMBERLAIN, J. S., SMITH, G., GRAHAM, D., DOMINICZAK, A. F., NAPOLI, C. & BAKER, A. H. 2009. Onset of Experimental Severe Cardiac Fibrosis Is Mediated by Overexpression of Angiotensin-Converting Enzyme 2. *Hypertension,* 53**,** 694-700.

MASUYER, G., SCHWAGER, S. L., STURROCK, E. D., ISAAC, R. E. & ACHARYA, K. R. 2012. Molecular recognition and regulation of human angiotensin-I converting enzyme (ACE) activity by natural inhibitory peptides. *Sci Rep,* 2**,** 717.

MATSUI, Y., JIA, N., OKAMOTO, H., KON, S., ONOZUKA, H., AKINO, M., LIU, L., MORIMOTO, J., RITTLING, S. R., DENHARDT, D., KITABATAKE, A. & UEDE, T. 2004. Role of osteopontin in cardiac fibrosis and remodeling in angiotensin II-induced cardiac hypertrophy. *Hypertension,* 43**,** 1195-201.

MATSUMOTO, E., SASAKI, S., KINOSHITA, H., KITO, T., OHTA, H., KONISHI, M., KUWAHARA, K., NAKAO, K. & ITOH, N. 2013. Angiotensin II-induced cardiac hypertrophy and fibrosis are promoted in mice lacking Fgf16. *Genes Cells,* 18**,** 544-53.

MATSUMOTO, T., OZONO, R., OSHIMA, T., MATSUURA, H., SUEDA, T., KAJIYAMA, G. & KAMBE, M. 2000. Type 2 angiotensin II receptor is downregulated in cardiomyocytes of patients with heart failure. *Cardiovasc Res,* 46**,** 73-81.

MATSUSAKA, H., IDE, T., MATSUSHIMA, S., IKEUCHI, M., KUBOTA, T., SUNAGAWA, K., KINUGAWA, S. & TSUTSUI, H. 2006. Targeted deletion of matrix metalloproteinase 2 ameliorates myocardial remodeling in mice with chronic pressure overload. *Hypertension,* 47**,** 711-7.

MCCOLLUM, L. T., GALLAGHER, P. E. & ANN TALLANT, E. 2012a. Angiotensin-(1–7) attenuates angiotensin II-induced cardiac remodeling associated with upregulation of dual-specificity phosphatase 1. *Am J of Physiol Heart Circ Physiol,* 302**,** H801-H810.

MCCOLLUM, L. T., GALLAGHER, P. E. & TALLANT, E. A. 2012b. Angiotensin-(1-7) abrogates mitogen-stimulated proliferation of cardiac fibroblasts. *Peptides,* 34**,** 380-8.

MCEWAN, P. E., GRAY, G. A., SHERRY, L., WEBB, D. J. & KENYON, C. J. 1998. Differential Effects of Angiotensin II on Cardiac Cell Proliferation and Intramyocardial Perivascular Fibrosis *In Vivo*. *Circulation,* 98**,** 2765-2773.

MCKINNEY, C. A., FATTAH, C., LOUGHREY, C. M., MILLIGAN, G. & NICKLIN, S. A. 2014. Angiotensin-(1-7) and angiotensin-(1-9): function in cardiac and vascular remodelling. *Clin Sci (Lond),* 126**,** 815-27.

MEHTA, P. K. & GRIENDLING, K. K. 2007. Angiotensin II cell signaling: physiological and pathological effects in the cardiovascular system. *Am J Physiol Cell Physiol,* 292**,** C82-97.

MELO, S. A., SUGIMOTO, H., O'CONNELL, J. T., KATO, N., VILLANUEVA, A., VIDAL, A., QIU, L., VITKIN, E., PERELMAN, L. T., MELO, C. A., LUCCI, A., IVAN, C., CALIN, G. A. & KALLURI, R. 2014. Cancer exosomes perform cell-independent microRNA biogenesis and promote tumorigenesis. *Cancer Cell,* 26**,** 707-21.

MERCURE, C., YOGI, A., CALLERA, G. E., ARANHA, A. B., BADER, M., FERREIRA, A. J., SANTOS, R. A. S., WALTHER, T., TOUYZ, R. M. & REUDELHUBER, T. L. 2008. Angiotensin(1-7) Blunts Hypertensive Cardiac Remodeling by a Direct Effect on the Heart. *Circ Res,* 103**,** 1319-1326.

MESSAOUDI, S., MILLIEZ, P., SAMUEL, J.-L. & DELCAYRE, C. 2009. Cardiac aldosterone overexpression prevents harmful effects of diabetes in the mouse heart by preserving capillary density. *FASEB J,* 23**,** 2176-2185.

METCALFE, B. L., HUENTELMAN, M. J., PARILAK, L. D., TAYLOR, D. G., KATOVICH, M. J., KNOT, H. J., SUMNERS, C. & RAIZADA, M. K. 2004. Prevention of cardiac hypertrophy by angiotensin II type-2 receptor gene transfer. *Hypertension,* 43**,** 1233-8.

MIFUNE, M., SASAMURA, H., SHIMIZU-HIROTA, R., MIYAZAKI, H. & SARUTA, T. 2000. Angiotensin II type 2 receptors stimulate collagen synthesis in cultured vascular smooth muscle cells. *Hypertension,* 36**,** 845-50.

MIN, L. J., CUI, T. X., YAHATA, Y., YAMASAKI, K., SHIUCHI, T., LIU, H. W., CHEN, R., LI, J. M., OKUMURA, M., JINNO, T., WU, L., IWAI, M., NAHMIAS, C., HASHIMOTO, K. & HORIUCHI, M. 2004. Regulation of collagen synthesis in mouse skin fibroblasts by distinct angiotensin II receptor subtypes. *Endocrinology,* 145**,** 253-60.

MIRAGOLI, M., SALVARANI, N. & ROHR, S. 2007. Myofibroblasts induce ectopic activity in cardiac tissue. *Circ Res,* 101**,** 755-8.

MIURA, S. & KARNIK, S. S. 1999. Angiotensin II type 1 and type 2 receptors bind angiotensin II through different types of epitope recognition. *J Hypertens,* 17**,** 397-404.

MIURA, S. & KARNIK, S. S. 2000. Ligand-independent signals from angiotensin II type 2 receptor induce apoptosis. *EMBO J,* 19**,** 4026-35.

MÖBIUS, W., OHNO-IWASHITA, Y., VAN DONSELAAR, E. G., OORSCHOT, V. M., SHIMADA, Y., FUJIMOTO, T., HEIJNEN, H. F., GEUZE, H. J. & SLOT, J. W. 2002. Immunoelectron microscopic localization of cholesterol using biotinylated and non-cytolytic perfringolysin O. *J Histochem Cytochem,* 50**,** 43-55.

MOHAMMED, S. F., HUSSAIN, S., MIRZOYEV, S. A., EDWARDS, W. D., MALESZEWSKI, J. J. & REDFIELD, M. M. 2015. Coronary microvascular rarefaction and myocardial fibrosis in heart failure with preserved ejection fraction. *Circulation,* 131**,** 550-9.

MOHAN, P., BRUTSAERT, D. L., PAULUS, W. J. & SYS, S. U. 1996. Myocardial contractile response to nitric oxide and cGMP. *Circulation,* 93**,** 1223-9.

MONASKY, M. M. & JANSSEN, P. M. 2009. The positive force-frequency relationship is maintained in absence of sarcoplasmic reticulum function in rabbit, but not in rat myocardium. *J Comp Physiol B,* 179**,** 469-79.

MONTECALVO, A., LARREGINA, A. T., SHUFESKY, W. J., STOLZ, D. B., SULLIVAN, M. L., KARLSSON, J. M., BATY, C. J., GIBSON, G. A., ERDOS, G., WANG, Z., MILOSEVIC, J., TKACHEVA, O. A., DIVITO, S. J., JORDAN, R., LYONS-WEILER, J., WATKINS, S. C. & MORELLI, A. E. 2012. Mechanism of transfer of functional microRNAs between mouse dendritic cells via exosomes. *Blood,* 119**,** 756-66.

MONTORFANO, I., BECERRA, A., CERRO, R., ECHEVERRÍA, C., SÁEZ, E., MORALES, M. G., FERNÁNDEZ, R., CABELLO-VERRUGIO, C. & SIMON, F. 2014. Oxidative stress mediates the conversion of endothelial cells into myofibroblasts via a TGF-ß1 and TGF-ß2-dependent pathway. *Lab Invest,* 94**,** 1068-82.

MOONEN, J. R., LEE, E. S., SCHMIDT, M., MALESZEWSKA, M., KOERTS, J. A., BROUWER, L. A., VAN KOOTEN, T. G., VAN LUYN, M. J., ZEEBREGTS, C. J., KRENNING, G. & HARMSEN, M. C. 2015. Endothelial-to-mesenchymal transition contributes to fibro-proliferative vascular disease and is modulated by fluid shear stress. *Cardiovasc Res,* 108**,** 377-86.

MOORE, M. J., KANTER, J. R., JONES, K. C. & TAYLOR, S. S. 2002. Phosphorylation of the catalytic subunit of protein kinase A. Autophosphorylation versus phosphorylation by phosphoinositide-dependent kinase-1. *J Biol Chem,* 277**,** 47878-84.

MORI, T. & HASHIMOTO, A. 2006. Direct positive chronotropic action by angiotensin II in the isolated mouse atrium. *Life Sci,* 79**,** 637-40.

MORIGUCHI, Y., MATSUBARA, H., MORI, Y., MURASAWA, S., MASAKI, H., MARUYAMA, K., TSUTSUMI, Y., SHIBASAKI, Y., TANAKA, Y., NAKAJIMA, T., ODA, K. & IWASAKA, T. 1999. Angiotensin II-induced transactivation of epidermal growth factor receptor regulates fibronectin and transforming growth factor-beta synthesis via transcriptional and posttranscriptional mechanisms. *Circ Res,* 84**,** 1073-84.

MORII, I., KIHARA, Y., KONISHI, T., INUBUSHI, T. & SASAYAMA, S. 1996. Mechanism of the negative force-frequency relationship in physiologically intact rat ventricular myocardium--studies by intracellular Ca^{2+} monitor with indo-1 and by ^{31}P-nuclear magnetic resonance spectroscopy. *Jpn Circ J,* 60**,** 593-603.

MORITA, H., KIMURA, J. & ENDOH, M. 1995. Angiotensin II activation of a chloride current in rabbit cardiac myocytes. *J Physiol,* 483 (Pt 1)**,** 119-30.

MUKHERJEE, D. & SEN, S. 1993. Alteration of cardiac collagen phenotypes in hypertensive hypertrophy: role of blood pressure. *J Mol Cell Cardiol,* 25**,** 185-96.

MUKOYAMA, M., NAKAJIMA, M., HORIUCHI, M., SASAMURA, H., PRATT, R. E. & DZAU, V. J. 1993. Expression cloning of type 2 angiotensin II receptor reveals a unique class of seven-transmembrane receptors. *J Biol Chem,* 268**,** 24539-42.

MÜLLER, D. N., FISCHLI, W., CLOZEL, J. P., HILGERS, K. F., BOHLENDER, J., MÉNARD, J., BUSJAHN, A., GANTEN, D. & LUFT, F. C. 1998. Local angiotensin II generation in the rat heart: role of renin uptake. *Circ Res,* 82**,** 13-20.

MULSOW, J. J., WATSON, R. W., FITZPATRICK, J. M. & O'CONNELL, P. R. 2005. Transforming growth factor-beta promotes pro-fibrotic behavior by serosal fibroblasts via PKC and ERK1/2 mitogen activated protein kinase cell signaling. *Ann Surg,* 242**,** 880-7, discussion 887-9.

MUNCH, P. A. & LONGHURST, J. C. 1991. Bradykinin increases myocardial contractility: relation to the Gregg phenomenon. *Am J Physiol,* 260**,** R1095-103.

MUNK, V. C., SANCHEZ DE MIGUEL, L., PETRIMPOL, M., BUTZ, N., BANFI, A., ERIKSSON, U., HEIN, L., HUMAR, R. & BATTEGAY, E. J. 2007. Angiotensin II induces angiogenesis in the hypoxic adult mouse heart *in vitro* through an AT_2-B_2 receptor pathway. *Hypertension,* 49**,** 1178-85.

MURÇA, T. M., MORAES, P. L., CAPURUÇO, C. A., SANTOS, S. H., MELO, M. B., SANTOS, R. A., SHENOY, V., KATOVICH, M. J., RAIZADA, M. K. & FERREIRA, A. J. 2012. Oral administration of an angiotensin-converting enzyme 2 activator ameliorates diabetes-induced cardiac dysfunction. *Regul Pept,* 177**,** 107-15.

MURDOCH, C. E., CHAUBEY, S., ZENG, L., YU, B., IVETIC, A., WALKER, S. J., VANHOUTTE, D., HEYMANS, S., GRIEVE, D. J., CAVE, A. C., BREWER, A. C., ZHANG, M. & SHAH, A. M. 2014. Endothelial NADPH oxidase-2 promotes interstitial cardiac fibrosis and diastolic dysfunction through proinflammatory effects and endothelial-mesenchymal transition. *J Am Coll Cardiol,* 63**,** 2734-41.

MUTLAK, M. & KEHAT, I. 2015. Extracellular signal-regulated kinases 1/2 as regulators of cardiac hypertrophy. *Front Pharmacol,* 6**,** 149.

MYAT, A., REDWOOD, S. R., QURESHI, A. C., SPERTUS, J. A. & WILLIAMS, B. 2012. Resistant hypertension. *BMJ,* 345**,** e7473.

NABHAN, J. F., HU, R., OH, R. S., COHEN, S. N. & LU, Q. 2012. Formation and release of arrestin domain-containing protein 1-mediated microvesicles

(ARMMs) at plasma membrane by recruitment of TSG101 protein. *Proc Natl Acad Sci U S A,* 109**,** 4146-51.

NADELLA, V. & HOWELL, S. 2015. Hypertension: pathophysiology and perioperative implications. *BJA Education,* 15**,** 275-279.

NAKAGAMI, H., TAKEMOTO, M. & LIAO, J. K. 2003. NADPH oxidase-derived superoxide anion mediates angiotensin II-induced cardiac hypertrophy. *J Mol Cell Cardiol,* 35**,** 851-9.

NAKAYAMA, M., YAN, X., PRICE, R. L., BORG, T. K., ITO, K., SANBE, A., ROBBINS, J. & LORELL, B. H. 2005. Chronic ventricular myocyte-specific overexpression of angiotensin II type 2 receptor results in intrinsic myocyte contractile dysfunction. *Am J Physiol Heart Circ Physiol,* 288**,** H317-27.

NARAYAN, P., MCCUNE, S. A., ROBITAILLE, P. M., HOHL, C. M. & ALTSCHULD, R. A. 1995. Mechanical alternans and the force-frequency relationship in failing rat hearts. *J Mol Cell Cardiol,* 27**,** 523-30.

NAZAREWICZ, R. R., SALAZAR, G., PATRUSHEV, N., SAN MARTIN, A., HILENSKI, L., XIONG, S. & ALEXANDER, R. W. 2011. Early endosomal antigen 1 (EEA1) is an obligate scaffold for angiotensin II-induced, PKC-alpha-dependent Akt activation in endosomes. *J Biol Chem,* 286**,** 2886-95.

NHS. 2011. *Phase 1 study to investigate safety, tolerability, PK and PD of MP-157* [Online]. Available: http://www.hra.nhs.uk/news/research-summaries/phase-1-study-to-investigate-safety-tolerability-pk-and-pd-of-mp-157/#sthash.ekxjbjGX.dpuf [Accessed 13/03/2016].

NICHOLLS, M. G. & ROBERTSON, J. I. 2000. The renin-angiotensin system in the year 2000. *J Hum Hypertens,* 14**,** 649-66.

NICOL, R. L., FREY, N., PEARSON, G., COBB, M., RICHARDSON, J. & OLSON, E. N. 2001. Activated MEK5 induces serial assembly of sarcomeres and eccentric cardiac hypertrophy. *EMBO J,* 20**,** 2757-67.

NIO, Y., MATSUBARA, H., MURASAWA, S., KANASAKI, M. & INADA, M. 1995. Regulation of gene transcription of angiotensin II receptor subtypes in myocardial infarction. *J Clin Invest,* 95**,** 46-54.

NIU, J., VAISKUNAITE, R., SUZUKI, N., KOZASA, T., CARR, D. W., DULIN, N. & VOYNO-YASENETSKAYA, T. A. 2001. Interaction of heterotrimeric G_{13} protein with an A-kinase-anchoring protein 110 (AKAP110) mediates cAMP-independent PKA activation. *Curr Biol,* 11**,** 1686-90.

NOUET, S. & NAHMIAS, C. 2000. Signal transduction from the angiotensin II AT_2 receptor. *Trends Endocrinol Metab,* 11**,** 1-6.

OCARANZA, M. P., GODOY, I., JALIL, J. E., VARAS, M., COLLANTES, P., PINTO, M., ROMAN, M., RAMIREZ, C., COPAJA, M., DIAZ-ARAYA, G., CASTRO, P. & LAVANDERO, S. 2006. Enalapril attenuates downregulation of Angiotensin-converting enzyme 2 in the late phase of ventricular dysfunction in myocardial infarcted rat. *Hypertension,* 48**,** 572-8.

OCARANZA, M. P., LAVANDERO, S., JALIL, J. E., MOYA, J., PINTO, M., NOVOA, U., APABLAZA, F., GONZALEZ, L., HERNANDEZ, C., VARAS, M., LOPEZ, R., GODOY, I., VERDEJO, H. & CHIONG, M. 2010. Angiotensin-(1-9) regulates cardiac hypertrophy *in vivo* and *in vitro*. *J Hypertens,* 28**,** 1054-64.

OCARANZA, M. P., MOYA, J., BARRIENTOS, V., ALZAMORA, R., HEVIA, D., MORALES, C., PINTO, M., ESCUDERO, N., GARCÍA, L., NOVOA, U., AYALA, P., DÍAZ-ARAYA, G., GODOY, I., CHIONG, M., LAVANDERO, S., JALIL, J. E. & MICHEA, L. 2014. Angiotensin-(1-9) reverses experimental hypertension and cardiovascular damage by inhibition of the angiotensin converting enzyme/Ang II axis. *J Hypertens,* 32**,** 771-83.

OH, E., KIM, J. Y., CHO, Y., LEE, N., AN, H., KIM, J. S. & SEO, J. H. 2015. Abstract 1445: Overexpression of angiotensin II type 1 receptor induces epithelial-mesenchymal transition and promotes tumorigenesis of human breast cancer cells. *Cancer Research,* 75**,** 1445-1445.

OKAMOTO, K., TAJIMA, H., NAKANUMA, S., SAKAI, S., MAKINO, I., KINOSHITA, J., HAYASHI, H., NAKAMURA, K., OYAMA, K., NAKAGAWARA, H., FUJITA, H., TAKAMURA, H., NINOMIYA, I., KITAGAWA, H., FUSHIDA, S., FUJIMURA, T., HARADA, S., WAKAYAMA, T., ISEKI, S. & OHTA, T. 2012. Angiotensin II enhances epithelial-to-mesenchymal transition through the interaction between activated hepatic stellate cells and the stromal cell-derived factor-1/CXCR4 axis in intrahepatic cholangiocarcinoma. *Int J Oncol,* 41**,** 573-82.

OKOSHI, M. P., YAN, X., OKOSHI, K., NAKAYAMA, M., SCHULDT, A. J., O'CONNELL, T. D., SIMPSON, P. C. & LORELL, B. H. 2004. Aldosterone directly stimulates cardiac myocyte hypertrophy. *J Card Fail,* 10**,** 511-8.

OKUNISHI, H., OKA, Y., SHIOTA, N., KAWAMOTO, T., SONG, K. & MIYAZAKI, M. 1993. Marked species-difference in the vascular angiotensin II-forming pathways: humans versus rodents. *Jpn J Pharmacol,* 62**,** 207-10.

OLSON, E. R., SHAMHART, P. E., NAUGLE, J. E. & MESZAROS, J. G. 2008. Angiotensin II-induced extracellular signal-regulated kinase 1/2 activation is mediated by protein kinase Cdelta and intracellular calcium in adult rat cardiac fibroblasts. *Hypertension,* 51**,** 704-11.

OPIE, L. H. 1965. Coronary flow rate and perfusion pressure as determinants of mechanical function and oxidative metabolism of isolated perfused rat heart. *J Physiol,* 180**,** 529-41.

ORTIZ, M. C., MANRIQUEZ, M. C., ROMERO, J. C. & JUNCOS, L. A. 2001. Antioxidants block angiotensin II-induced increases in blood pressure and endothelin. *Hypertension,* 38**,** 655-9.

OUALI, R., BERTHELON, M. C., BÉGEOT, M. & SAEZ, J. M. 1997. Angiotensin II receptor subtypes AT_1 and AT_2 are down-regulated by angiotensin II through AT_1 receptor by different mechanisms. *Endocrinology,* 138**,** 725-33.

OWEN, C. A. & CAMPBELL, E. J. 1998. Angiotensin II generation at the cell surface of activated neutrophils: novel cathepsin G-mediated catalytic activity that is resistant to inhibition. *J Immunol,* 160**,** 1436-43.

PAN, C. H., WEN, C. H. & LIN, C. S. 2008. Interplay of angiotensin II and angiotensin(1-7) in the regulation of matrix metalloproteinases of human cardiocytes. *Exp Physiol,* 93**,** 599-612.

PANDYA, K., KIM, H. S. & SMITHIES, O. 2006. Fibrosis, not cell size, delineates beta-myosin heavy chain reexpression during cardiac hypertrophy and normal aging in vivo. *Proc Natl Acad Sci U S A,* 103**,** 16864-9.

PASSOS-SILVA, D. G., VERANO-BRAGA, T. & SANTOS, R. A. 2013. Angiotensin-(1-7): beyond the cardio-renal actions. *Clin Sci (Lond),* 124**,** 443-56.

PAUL, M., POYAN MEHR, A. & KREUTZ, R. 2006. Physiology of local renin-angiotensin systems. *Physiol Rev,* 86**,** 747-803.

PAULIS, L., STECKELINGS, U. M. & UNGER, T. 2012. Key advances in antihypertensive treatment. *Nat Rev Cardiol,* 9**,** 276-85.

PAZ, Y., GUREVITCH, J., FROLKIS, I., MATSA, M., KRAMER, A., LOCKER, C., MOHR, R. & KEREN, G. 1998. Effects of an angiotensin II antagonist on ischemic and nonischemic isolated rat hearts. *Ann Thorac Surg,* 65**,** 474-9.

PEI, Z., MENG, R., LI, G., YAN, G., XU, C., ZHUANG, Z., REN, J. & WU, Z. 2010. Angiotensin-(1-7) ameliorates myocardial remodeling and interstitial fibrosis in spontaneous hypertension: role of MMPs/TIMPs. *Toxicol Lett,* 199**,** 173-81.

PELLEGRINO, D., SHIVA, S., ANGELONE, T., GLADWIN, M. T. & TOTA, B. 2009. Nitrite exerts potent negative inotropy in the isolated heart via eNOS-independent nitric oxide generation and cGMP-PKG pathway activation. *Biochim Biophys Acta,* 1787**,** 818-27.

PENG, H., YANG, X. P., CARRETERO, O. A., NAKAGAWA, P., D'AMBROSIO, M., LEUNG, P., XU, J., PETERSON, E. L., GONZÁLEZ, G. E., HARDING, P. & RHALEB, N. E. 2011. Angiotensin II-induced dilated cardiomyopathy in Balb/c but not C57BL/6J mice. *Exp Physiol,* 96**,** 756-64.

PENG, K., TIAN, X., QIAN, Y., SKIBBA, M., ZOU, C., LIU, Z., WANG, J., XU, Z., LI, X. & LIANG, G. 2016. Novel EGFR inhibitors attenuate cardiac hypertrophy induced by angiotensin II. *J Cell Mol Med,* 20**,** 482-94.

PENG, X., KRAUS, M. S., WEI, H., SHEN, T. L., PARIAUT, R., ALCARAZ, A., JI, G., CHENG, L., YANG, Q., KOTLIKOFF, M. I., CHEN, J., CHIEN, K., GU, H. & GUAN, J. L. 2006. Inactivation of focal adhesion kinase in cardiomyocytes promotes eccentric cardiac hypertrophy and fibrosis in mice. *J Clin Invest,* 116**,** 217-27.

PEREIRA, M. G., SOUZA, L. L., BECARI, C., DUARTE, D. A., CAMACHO, F. R., OLIVEIRA, J. A., GOMES, M. D., OLIVEIRA, E. B., SALGADO, M. C., GARCIA-CAIRASCO, N. & COSTA-NETO, C. M. 2013. Angiotensin II-independent angiotensin-(1-7) formation in rat hippocampus: involvement of thimet oligopeptidase. *Hypertension,* 62**,** 879-85.

PESHAVARIYA, H. M., CHAN, E. C., LIU, G. S., JIANG, F. & DUSTING, G. J. 2014. Transforming growth factor-ß1 requires NADPH oxidase 4 for angiogenesis *in vitro* and *in vivo*. *J Cell Mol Med,* 18**,** 1172-83.

PHARMA, V. 2016. *Clinical development* [Online]. Available: http://www.vicorepharma.com/en/research.aspx [Accessed 17/03/2016].

PIERA-VELAZQUEZ, S., LI, Z. & JIMENEZ, S. A. 2011. Role of endothelial-mesenchymal transition (EndoMT) in the pathogenesis of fibrotic disorders. *The American journal of pathology,* 179**,** 1074-80.

PIMENTA, E. & CALHOUN, D. A. 2012. Resistant hypertension: incidence, prevalence, and prognosis. *Circulation,* 125**,** 1594-6.

PINTO, A. R., ILINYKH, A., IVEY, M. J., KUWABARA, J. T., D'ANTONI, M. L., DEBUQUE, R., CHANDRAN, A., WANG, L., ARORA, K., ROSENTHAL, N. A. &

TALLQUIST, M. D. 2016. Revisiting Cardiac Cellular Composition. *Circ Res,* 118**,** 400-9.

PIRONTI, G., STRACHAN, R. T., ABRAHAM, D., MON-WEI YU, S., CHEN, M., CHEN, W., HANADA, K., MAO, L., WATSON, L. J. & ROCKMAN, H. A. 2015. Circulating Exosomes Induced by Cardiac Pressure Overload Contain Functional Angiotensin II Type 1 Receptors. *Circulation,* 131**,** 2120-30.

PISITKUN, T., SHEN, R. F. & KNEPPER, M. A. 2004. Identification and proteomic profiling of exosomes in human urine. *Proc Natl Acad Sci U S A,* 101**,** 13368-73.

PIZZIRANI, C., FERRARI, D., CHIOZZI, P., ADINOLFI, E., SANDONÀ, D., SAVAGLIO, E. & DI VIRGILIO, F. 2007. Stimulation of P2 receptors causes release of IL-1beta-loaded microvesicles from human dendritic cells. *Blood,* 109**,** 3856-64.

PÖRSTI, I., HECKER, M., BASSENGE, E. & BUSSE, R. 1993. Dual action of angiotensin II on coronary resistance in the isolated perfused rabbit heart. *Naunyn Schmiedebergs Arch Pharmacol,* 348**,** 650-8.

PORTER, K. E. & TURNER, N. A. 2009. Cardiac fibroblasts: at the heart of myocardial remodeling. *Pharmacol Ther,* 123**,** 255-78.

PROGATZKY, F., DALLMAN, M. J. & LO CELSO, C. 2013. From seeing to believing: labelling strategies for *in vivo* cell-tracking experiments. *Interface Focus,* 3**,** 20130001.

PU, Q., LAROUCHE, I. & SCHIFFRIN, E. L. 2003. Effect of dual angiotensin converting enzyme/neutral endopeptidase inhibition, angiotensin converting enzyme inhibition, or AT_1 antagonism on coronary microvasculature in spontaneously hypertensive rats. *Am J Hypertens,* 16**,** 931-7.

PURI, P. L., AVANTAGGIATI, M. L., BURGIO, V. L., CHIRILLO, P., COLLEPARDO, D., NATOLI, G., BALSANO, C. & LEVRERO, M. 1995. Reactive oxygen intermediates mediate angiotensin II-induced c-Jun.c-Fos heterodimer DNA binding activity and proliferative hypertrophic responses in myogenic cells. *J Biol Chem,* 270**,** 22129-34.

QIN, H., FROHMAN, M. A. & BOLLAG, W. B. 2010. Phospholipase D2 mediates acute aldosterone secretion in response to angiotensin II in adrenal glomerulosa cells. *Endocrinology,* 151**,** 2162-70.

QU, Y., RAMACHANDRA, L., MOHR, S., FRANCHI, L., HARDING, C. V., NUNEZ, G. & DUBYAK, G. R. 2009. P2X7 receptor-stimulated secretion of MHC class II-containing exosomes requires the ASC/NLRP3 inflammasome but is independent of caspase-1. *J Immunol,* 182**,** 5052-62.

RABELO, L. A., XU, P., TODIRAS, M., SAMPAIO, W. O., BUTTGEREIT, J., BADER, M., SANTOS, R. A. & ALENINA, N. 2008. Ablation of angiotensin (1-7) receptor Mas in C57Bl/6 mice causes endothelial dysfunction. *J Am Soc Hypertens,* 2**,** 418-24.

RAJAGOPAL, K., WHALEN, E. J., VIOLIN, J. D., STIBER, J. A., ROSENBERG, P. B., PREMONT, R. T., COFFMAN, T. M., ROCKMAN, H. A. & LEFKOWITZ, R. J. 2006. ß-arrestin2-mediated inotropic effects of the angiotensin II type 1A receptor in isolated cardiac myocytes. *Proc Natl Acad Sci U S A,* 103**,** 16284-9.

RAJAGOPAL, S., RAJAGOPAL, K. & LEFKOWITZ, R. J. 2010. Teaching old receptors new tricks: biasing seven-transmembrane receptors. *Nat Rev Drug Discov,* 9**,** 373-86.

RAM, R., MICKELSEN, D. M., THEODOROPOULOS, C. & BLAXALL, B. C. 2011. New approaches in small animal echocardiography: imaging the sounds of silence. *Am J Physiol Heart Circ Physiol,* 301**,** H1765-80.

RAPOSO, G. & STOORVOGEL, W. 2013. Extracellular vesicles: exosomes, microvesicles, and friends. *J Cell Biol,* 200**,** 373-83.

REGAN, J. A., MAURO, A. G., CARBONE, S., MARCHETTI, C., GILL, R., MEZZAROMA, E., VALLE RALEIGH, J., SALLOUM, F. N., VAN TASSELL, B. W., ABBATE, A. & TOLDO, S. 2015. A mouse model of heart failure with preserved ejection fraction due to chronic infusion of a low subpressor dose of angiotensin II. *Am J Physiol Heart Circ Physiol,* 309**,** H771-8.

REHMAN, A., LEIBOWITZ, A., YAMAMOTO, N., RAUTUREAU, Y., PARADIS, P. & SCHIFFRIN, E. L. 2012. Angiotensin type 2 receptor agonist compound 21 reduces vascular injury and myocardial fibrosis in stroke-prone spontaneously hypertensive rats. *Hypertension,* 59**,** 291-9.

REKKER, K., SAARE, M., ROOST, A. M., KUBO, A. L., ZAROVNI, N., CHIESI, A., SALUMETS, A. & PETERS, M. 2014. Comparison of serum exosome isolation methods for microRNA profiling. *Clin Biochem,* 47**,** 135-8.

RHYU, D. Y., YANG, Y., HA, H., LEE, G. T., SONG, J. S., UH, S. T. & LEE, H. B. 2005. Role of reactive oxygen species in TGF-ß1-induced mitogen-activated protein kinase activation and epithelial-mesenchymal transition in renal tubular epithelial cells. *J Am Soc Nephrol,* 16**,** 667-75.

RICE, G. I., THOMAS, D. A., GRANT, P. J., TURNER, A. J. & HOOPER, N. M. 2004. Evaluation of angiotensin-converting enzyme (ACE), its homologue ACE2 and neprilysin in angiotensin peptide metabolism. *Biochem J,* 383**,** 45-51.

RIEDER, F., KESSLER, S. P., WEST, G. A., BHILOCHA, S., DE LA MOTTE, C., SADLER, T. M., GOPALAN, B., STYLIANOU, E. & FIOCCHI, C. 2011. Inflammation-induced endothelial-to-mesenchymal transition: a novel mechanism of intestinal fibrosis. *Am J Pathol,* 179**,** 2660-73.

RIPLEY, E. & HIRSCH, A. 2010. Fifteen years of losartan: what have we learned about losartan that can benefit chronic kidney disease patients? *Int J Nephrol Renovasc Dis,* 3**,** 93-8.

RIVARD, K., GRANDY, S. A., DOUILLETTE, A., PARADIS, P., NEMER, M., ALLEN, B. G. & FISET, C. 2011. Overexpression of type 1 angiotensin II receptors impairs excitation-contraction coupling in the mouse heart. *Am J Physiol Heart Circ Physiol,* 301**,** H2018-27.

RIVARD, K., PARADIS, P., NEMER, M. & FISET, C. 2008. Cardiac-specific overexpression of the human type 1 angiotensin II receptor causes delayed repolarization. *Cardiovasc Res,* 78**,** 53-62.

RIVIÈRE, G., MICHAUD, A., BRETON, C., VANCAMP, G., LABORIE, C., ENACHE, M., LESAGE, J., DELOOF, S., CORVOL, P. & VIEAU, D. 2005. Angiotensin-converting enzyme 2 (ACE2) and ACE activities display tissue-specific sensitivity to undernutrition-programmed hypertension in the adult rat. *Hypertension,* 46**,** 1169-74.

ROBINET, A., HOIZEY, G. & MILLART, H. 2005. PI 3-kinase, protein kinase C, and protein kinase A are involved in the trigger phase of beta1-adrenergic preconditioning. *Cardiovasc Res,* 66**,** 530-42.

RODRIGUES-DÍEZ, R., CARVAJAL-GONZÁLEZ, G., SÁNCHEZ-LÓPEZ, E., RODRÍGUEZ-VITA, J., RODRIGUES DÍEZ, R., SELGAS, R., ORTIZ, A., EGIDO, J., MEZZANO, S. & RUIZ-ORTEGA, M. 2008. Pharmacological modulation of epithelial mesenchymal transition caused by angiotensin II. Role of ROCK and MAPK pathways. *Pharm Res,* 25**,** 2447-61.

RODRÍGUEZ-VITA, J., SÁNCHEZ-LÓPEZ, E., ESTEBAN, V., RUPÉREZ, M., EGIDO, J. & RUIZ-ORTEGA, M. 2005. Angiotensin II activates the Smad pathway in vascular smooth muscle cells by a transforming growth factor-beta-independent mechanism. *Circulation,* 111**,** 2509-17.

ROIG, E., PEREZ-VILLA, F., MORALES, M., JIMÉNEZ, W., ORÚS, J., HERAS, M. & SANZ, G. 2000. Clinical implications of increased plasma angiotensin II despite ACE inhibitor therapy in patients with congestive heart failure. *Eur Heart J,* 21**,** 53-7.

ROMPE, F., ARTUC, M., HALLBERG, A., ALTERMAN, M., STRÖDER, K., THÖNE-REINEKE, C., REICHENBACH, A., SCHACHERL, J., DAHLÖF, B., BADER, M., ALENINA, N., SCHWANINGER, M., ZUBERBIER, T., FUNKE-KAISER, H., SCHMIDT, C., SCHUNCK, W. H., UNGER, T. & STECKELINGS, U. M. 2010. Direct angiotensin II type 2 receptor stimulation acts anti-inflammatory through epoxyeicosatrienoic acid and inhibition of nuclear factor kappaB. *Hypertension,* 55**,** 924-31.

ROSENKRANZ, S. 2004. TGF-ß1 and angiotensin networking in cardiac remodeling. *Cardiovasc Res,* 63**,** 423-432.

ROSENKRANZ, S., FLESCH, M., AMANN, K., HAEUSELER, C., KILTER, H., SEELAND, U., SCHLÜTER, K. D. & BÖHM, M. 2002. Alterations of beta-adrenergic signaling and cardiac hypertrophy in transgenic mice overexpressing TGF-beta(1). *Am J Physiol Heart Circ Physiol,* 283**,** H1253-62.

ROSS, J., MIURA, T., KAMBAYASHI, M., EISING, G. P. & RYU, K. H. 1995. Adrenergic control of the force-frequency relation. *Circulation,* 92**,** 2327-32.

ROTTMAN, J. N., NI, G. & BROWN, M. 2007. Echocardiographic evaluation of ventricular function in mice. *Echocardiography,* 24**,** 83-9.

ROWE, B. P., SAYLOR, D. L., SPETH, R. C. & ABSHER, D. R. 1995. Angiotensin-(1-7) binding at angiotensin II receptors in the rat brain. *Regul Pept,* 56**,** 139-46.

RUCKLIDGE, G. J., MILNE, G., MCGAW, B. A., MILNE, E. & ROBINS, S. P. 1992. Turnover rates of different collagen types measured by isotope ratio mass spectrometry. *Biochim Biophys Acta,* 1156**,** 57-61.

RUECKSCHLOSS, U., QUINN, M. T., HOLTZ, J. & MORAWIETZ, H. 2002. Dose-dependent regulation of NAD(P)H oxidase expression by angiotensin II in human endothelial cells: protective effect of angiotensin II type 1 receptor blockade in patients with coronary artery disease. *Arterioscler Thromb Vasc Biol,* 22**,** 1845-51.

RUPÉREZ, M., LORENZO, O., BLANCO-COLIO, L. M., ESTEBAN, V., EGIDO, J. & RUIZ-ORTEGA, M. 2003. Connective tissue growth factor is a mediator of angiotensin II-induced fibrosis. *Circulation,* 108**,** 1499-505.

RUZICKA, M., SKARDA, V. & LEENEN, F. H. 1995. Effects of ACE inhibitors on circulating versus cardiac angiotensin II in volume overload-induced cardiac hypertrophy in rats. *Circulation,* 92**,** 3568-73.

RYKL, J., THIEMANN, J., KURZAWSKI, S., POHL, T., GOBOM, J., ZIDEK, W. & SCHLÜTER, H. 2006. Renal cathepsin G and angiotensin II generation. *J Hypertens,* 24**,** 1797-807.

SABRI, A., SAMUEL, J.-L., MAROTTE, F., POITEVIN, P., RAPPAPORT, L. & LEVY, B. I. 1998. Microvasculature in Angiotensin II–Dependent Cardiac Hypertrophy in the Rat. *Hypertension,* 32**,** 371-375.

SADOSHIMA, J. & IZUMO, S. 1993a. Molecular characterization of angiotensin II--induced hypertrophy of cardiac myocytes and hyperplasia of cardiac fibroblasts. Critical role of the AT_1 receptor subtype. *Circ Res,* 73**,** 413-23.

SADOSHIMA, J. & IZUMO, S. 1993b. Signal transduction pathways of angiotensin II--induced c-fos gene expression in cardiac myocytes in vitro. Roles of phospholipid-derived second messengers. *Circ Res,* 73**,** 424-38.

SAKURAI, K., NOROTA, I., TANAKA, H., KUBOTA, I., TOMOIKE, H. & ENDO, M. 2002. Negative inotropic effects of angiotensin II, endothelin-1 and phenylephrine in indo-1 loaded adult mouse ventricular myocytes. *Life Sci,* 70**,** 1173-84.

SALAS, M. A., VALVERDE, C. A., SÁNCHEZ, G., SAID, M., RODRIGUEZ, J. S., PORTIANSKY, E. L., KAETZEL, M. A., DEDMAN, J. R., DONOSO, P., KRANIAS, E. G. & MATTIAZZI, A. 2010. The signalling pathway of CaMKII-mediated apoptosis and necrosis in the ischemia/reperfusion injury. *J Mol Cell Cardiol,* 48**,** 1298-306.

SALAS, M. A., VILA-PETROFF, M. G., PALOMEQUE, J., AIELLO, E. A. & MATTIAZZI, A. 2001. Positive inotropic and negative lusitropic effect of angiotensin II: intracellular mechanisms and second messengers. *J Mol Cell Cardiol,* 33**,** 1957-71.

SALES, V. L., SUKHOVA, G. K., LOPEZ-ILASACA, M. A., LIBBY, P., DZAU, V. J. & PRATT, R. E. 2005. Angiotensin type 2 receptor is expressed in murine atherosclerotic lesions and modulates lesion evolution. *Circulation,* 112**,** 3328-36.

SAMPAIO, W. O., HENRIQUE DE CASTRO, C., SANTOS, R. A., SCHIFFRIN, E. L. & TOUYZ, R. M. 2007a. Angiotensin-(1-7) counterregulates angiotensin II signaling in human endothelial cells. *Hypertension,* 50**,** 1093-8.

SAMPAIO, W. O., SOUZA DOS SANTOS, R. A., FARIA-SILVA, R., DA MATA MACHADO, L. T., SCHIFFRIN, E. L. & TOUYZ, R. M. 2007b. Angiotensin-(1-7) through receptor Mas mediates endothelial nitric oxide synthase activation via Akt-dependent pathways. *Hypertension,* 49**,** 185-92.

SANNA, B., BUENO, O. F., DAI, Y. S., WILKINS, B. J. & MOLKENTIN, J. D. 2005. Direct and indirect interactions between calcineurin-NFAT and MEK1-extracellular signal-regulated kinase 1/2 signaling pathways regulate cardiac gene expression and cellular growth. *Mol Cell Biol,* 25**,** 865-78.

SANO, M., FUKUDA, K., KODAMA, H., PAN, J., SAITO, M., MATSUZAKI, J., TAKAHASHI, T., MAKINO, S., KATO, T. & OGAWA, S. 2000a. Interleukin-6 family of cytokines mediate angiotensin II-induced cardiac hypertrophy in rodent cardiomyocytes. *J Biol Chem,* 275**,** 29717-23.

SANO, M., FUKUDA, K., KODAMA, H., TAKAHASHI, T., KATO, T., HAKUNO, D., SATO, T., MANABE, T., TAHARA, S. & OGAWA, S. 2000b. Autocrine/Paracrine secretion of IL-6 family cytokines causes angiotensin II-induced delayed STAT3 activation. *Biochem Biophys Res Commun,* 269**,** 798-802.

SANO, M., MINAMINO, T., TOKO, H., MIYAUCHI, H., ORIMO, M., QIN, Y., AKAZAWA, H., TATENO, K., KAYAMA, Y., HARADA, M., SHIMIZU, I., ASAHARA, T., HAMADA, H., TOMITA, S., MOLKENTIN, J. D., ZOU, Y. & KOMURO, I. 2007. p53-induced inhibition of Hif-1 causes cardiac dysfunction during pressure overload. *Nature,* 446**,** 444-8.

SANTOS, R. A., BROSNIHAN, K. B., JACOBSEN, D. W., DICORLETO, P. E. & FERRARIO, C. M. 1992. Production of angiotensin-(1-7) by human vascular endothelium. *Hypertension,* 19**,** II56-61.

SANTOS, R. A., CASTRO, C. H., GAVA, E., PINHEIRO, S. V., ALMEIDA, A. P., PAULA, R. D., CRUZ, J. S., RAMOS, A. S., ROSA, K. T., IRIGOYEN, M. C., BADER, M., ALENINA, N., KITTEN, G. T. & FERREIRA, A. J. 2006. Impairment of i*n vitro* and *in vivo* heart function in angiotensin-(1-7) receptor MAS knockout mice. *Hypertension,* 47**,** 996-1002.

SANTOS, R. A., SIMOES E SILVA, A. C., MARIC, C., SILVA, D. M., MACHADO, R. P., DE BUHR, I., HERINGER-WALTHER, S., PINHEIRO, S. V., LOPES, M. T., BADER, M., MENDES, E. P., LEMOS, V. S., CAMPAGNOLE-SANTOS, M. J., SCHULTHEISS, H. P., SPETH, R. & WALTHER, T. 2003. Angiotensin-(1-7) is an endogenous ligand for the G protein-coupled receptor Mas. *Proc Natl Acad Sci U S A,* 100**,** 8258-63.

SARKAR, S., VELLAICHAMY, E., YOUNG, D. & SEN, S. 2004. Influence of cytokines and growth factors in ANG II-mediated collagen upregulation by fibroblasts in rats: role of myocytes. *Am J Physiol Heart Circ Physiol,* 287**,** H107-17.

SASAGURI, M., IDEISHI, M., OGATA, S., MIURA, S., IKEDA, M. & ARAKAWA, K. 1995. Human urinary kallikrein can generate angiotensin II from homologous renin substrates. *Hypertens Res,* 18**,** 33-7.

SATO, M., SHEGOGUE, D., GORE, E. A., SMITH, E. A., MCDERMOTT, P. J. & TROJANOWSKA, M. 2002. Role of p38 MAPK in transforming growth factor beta stimulation of collagen production by scleroderma and healthy dermal fibroblasts. *J Invest Dermatol,* 118**,** 704-11.

SAVIO-GALIMBERTI, E., FRANK, J., INOUE, M., GOLDHABER, J. I., CANNELL, M. B., BRIDGE, J. H. & SACHSE, F. B. 2008. Novel features of the rabbit transverse tubular system revealed by quantitative analysis of three-dimensional reconstructions from confocal images. *Biophys J,* 95**,** 2053-62.

SCHEEL, C., EATON, E. N., LI, S. H., CHAFFER, C. L., REINHARDT, F., KAH, K. J., BELL, G., GUO, W., RUBIN, J., RICHARDSON, A. L. & WEINBERG, R. A. 2011. Paracrine and autocrine signals induce and maintain mesenchymal and stem cell states in the breast. *Cell,* 145**,** 926-40.

SCHIAFFINO, S., SAMUEL, J. L., SASSOON, D., LOMPRÉ, A. M., GARNER, I., MAROTTE, F., BUCKINGHAM, M., RAPPAPORT, L. & SCHWARTZ, K. 1989. Nonsynchronous accumulation of alpha-skeletal actin and beta-myosin heavy chain mRNAs during early stages of pressure-overload--induced cardiac hypertrophy demonstrated by in situ hybridization. *Circ Res,* 64**,** 937-48.

SCHMITTGEN, T. D. & LIVAK, K. J. 2008. Analyzing real-time PCR data by the comparative C(T) method. *Nat Protoc,* 3**,** 1101-8.

SCHMITTGEN, T. D., ZAKRAJSEK, B. A., MILLS, A. G., GORN, V., SINGER, M. J. & REED, M. W. 2000. Quantitative reverse transcription-polymerase chain reaction to study mRNA decay: comparison of endpoint and real-time methods. *Anal Biochem,* 285**,** 194-204.

SCHORB, W., BOOZ, G. W., DOSTAL, D. E., CONRAD, K. M., CHANG, K. C. & BAKER, K. M. 1993. Angiotensin II is mitogenic in neonatal rat cardiac fibroblasts. *Circ Res,* 72**,** 1245-54.

SCHULTZ, J. L. J., WITT, S. A., GLASCOCK, B. J., NIEMAN, M. L., REISER, P. J., NIX, S. L., KIMBALL, T. R. & DOETSCHMAN, T. 2002. TGF-beta1 mediates the hypertrophic cardiomyocyte growth induced by angiotensin II. *J Clin Invest,* 109**,** 787-96.

SCHUNKERT, H., SADOSHIMA, J., CORNELIUS, T., KAGAYA, Y., WEINBERG, E. O., IZUMO, S., RIEGGER, G. & LORELL, B. H. 1995. Angiotensin II-induced growth responses in isolated adult rat hearts. Evidence for load-independent induction of cardiac protein synthesis by angiotensin II. *Circ Res,* 76**,** 489-97.

SCHWARTZKOPFF, B., BREHM, M., MUNDHENKE, M. & STRAUER, B. E. 2000. Repair of coronary arterioles after treatment with perindopril in hypertensive heart disease. *Hypertension,* 36**,** 220-5.

SEKINE, T., KUSANO, H., NISHIMARU, K., TANAKA, Y., TANAKA, H. & SHIGENOBU, K. 1999. Developmental conversion of inotropism by endothelin I and angiotensin II from positive to negative in mice. *Eur J Pharmacol,* 374**,** 411-5.

SENBONMATSU, T., ICHIHARA, S., PRICE, E., GAFFNEY, F. A. & INAGAMI, T. 2000. Evidence for angiotensin II type 2 receptor-mediated cardiac myocyte enlargement during *in vivo* pressure overload. *J Clin Invest,* 106**,** R25-9.

SENBONMATSU, T., SAITO, T., LANDON, E. J., WATANABE, O., PRICE, E., ROBERTS, R. L., IMBODEN, H., FITZGERALD, T. G., GAFFNEY, F. A. & INAGAMI, T. 2003. A novel angiotensin II type 2 receptor signaling pathway: possible role in cardiac hypertrophy. *EMBO J,* 22**,** 6471-82.

SERNERI, G. G., BODDI, M., CECIONI, I., VANNI, S., COPPO, M., PAPA, M. L., BANDINELLI, B., BERTOLOZZI, I., POLIDORI, G., TOSCANO, T., MACCHERINI, M. & MODESTI, P. A. 2001. Cardiac angiotensin II formation in the clinical course of heart failure and its relationship with left ventricular function. *Circ Res,* 88**,** 961-8.

SETA, K. & SADOSHIMA, J. 2003. Phosphorylation of tyrosine 319 of the angiotensin II type 1 receptor mediates angiotensin II-induced trans-activation of the epidermal growth factor receptor. *J Biol Chem,* 278**,** 9019-26.

SHAH, A. M. & MANN, D. L. 2011. In search of new therapeutic targets and strategies for heart failure: recent advances in basic science. *Lancet,* 378**,** 704-12.

SHAH, A. P., SIEDLECKA, U., GANDHI, A., NAVARATNARAJAH, M., AL-SAUD, S. A., YACOUB, M. H. & TERRACCIANO, C. M. 2010. Genetic background affects function and intracellular calcium regulation of mouse hearts. *Cardiovasc Res,* 87**,** 683-93.

SHAI, S. Y., HARPF, A. E., BABBITT, C. J., JORDAN, M. C., FISHBEIN, M. C., CHEN, J., OMURA, M., LEIL, T. A., BECKER, K. D., JIANG, M., SMITH, D. J., CHERRY, S. R., LOFTUS, J. C. & ROSS, R. S. 2002. Cardiac myocyte-specific excision of the beta1 integrin gene results in myocardial fibrosis and cardiac failure. *Circ Res,* 90**,** 458-64.

SHALITIN, N., FRIEDMAN, M., SCHLESINGER, H., BARHUM, Y., LEVY, M. J., SCHAPER, W. & KESSLER-ICEKSON, G. 1996. The effect of angiotensin II on myosin heavy chain expression in cultured myocardial cells. *In Vitro Cell Dev Biol Anim,* 32**,** 573-8.

SHELKE, G. V., LÄSSER, C., GHO, Y. S. & LÖTVALL, J. 2014. Importance of exosome depletion protocols to eliminate functional and RNA-containing extracellular vesicles from fetal bovine serum. *J Extracell Vesicles,* 3.

SHEN, B., WU, N., YANG, J. M. & GOULD, S. J. 2011. Protein targeting to exosomes/microvesicles by plasma membrane anchors. *J Biol Chem,* 286**,** 14383-95.

SHENG, J. W., WANG, W. Y. & XU, Y. F. 2011. Angiotensin II decreases spontaneous firing rate of guinea-pig sino-atrial node cells. *Eur J Pharmacol,* 660**,** 387-93.

SHIOJIMA, I., SATO, K., IZUMIYA, Y., SCHIEKOFER, S., ITO, M., LIAO, R., COLUCCI, W. S. & WALSH, K. 2005. Disruption of coordinated cardiac hypertrophy and angiogenesis contributes to the transition to heart failure. *J Clin Invest,* 115**,** 2108-18.

SHUTES, A., ONESTO, C., PICARD, V., LEBLOND, B., SCHWEIGHOFFER, F. & DER, C. J. 2007. Specificity and mechanism of action of EHT 1864, a novel small molecule inhibitor of Rac family small GTPases. *J Biol Chem,* 282**,** 35666-78.

SIMON, G., ABRAHAM, G. & CSEREP, G. 1995. Pressor and subpressor angiotensin II administration. Two experimental models of hypertension. *Am J Hypertens,* 8**,** 645-50.

SKEGGS, L. T., KAHN, J. R. & SHUMWAY, N. P. 1956. The preparation and function of the hypertensin-converting enzyme. *J Exp Med,* 103**,** 295-9.

SKEGGS, L. T., MARSH, W. H., KAHN, J. R. & SHUMWAY, N. P. 1954. The existence of two forms of hypertensin. *J Exp Med,* 99**,** 275-82.

SKRZYPIEC-SPRING, M., GROTTHUS, B., SZELAG, A. & SCHULZ, R. 2007. Isolated heart perfusion according to Langendorff---still viable in the new millennium. *J Pharmacol Toxicol Methods,* 55**,** 113-26.

SLUIJTER, J. P., VERHAGE, V., DEDDENS, J. C., VAN DEN AKKER, F. & DOEVENDANS, P. A. 2014. Microvesicles and exosomes for intracardiac communication. *Cardiovasc Res,* 102**,** 302-11.

SMITH, N. J., BENNETT, K. A. & MILLIGAN, G. 2011. When simple agonism is not enough: emerging modalities of GPCR ligands. *Mol Cell Endocrinol,* 331**,** 241-7.

SOLDNER, A., BENET, L. Z., MUTSCHLER, E. & CHRISTIANS, U. 2000. Active transport of the angiotensin-II antagonist losartan and its main metabolite EXP 3174 across MDCK-MDR1 and caco-2 cell monolayers. *Br J Pharmacol,* 129**,** 1235-43.

SOPEL, M. J., ROSIN, N. L., LEE, T. D. & LÉGARÉ, J. F. 2011. Myocardial fibrosis in response to Angiotensin II is preceded by the recruitment of mesenchymal progenitor cells. *Lab Invest,* 91**,** 565-78.

SORESCU, D., WEISS, D., LASSÈGUE, B., CLEMPUS, R. E., SZÖCS, K., SORESCU, G. P., VALPPU, L., QUINN, M. T., LAMBETH, J. D., VEGA, J. D., TAYLOR, W. R. & GRIENDLING, K. K. 2002. Superoxide production and expression of nox family proteins in human atherosclerosis. *Circulation,* 105**,** 1429-35.

SOUDERS, C. A., BOWERS, S. L. & BAUDINO, T. A. 2009. Cardiac fibroblast: the renaissance cell. *Circ Res,* 105**,** 1164-76.

STACY, L. B., YU, Q., HORAK, K. & LARSON, D. F. 2007. Effect of angiotensin II on primary cardiac fibroblast matrix metalloproteinase activities. *Perfusion,* 22**,** 51-5.

STAWSKI, L., HAN, R., BUJOR, A. M. & TROJANOWSKA, M. 2012. Angiotensin II induces skin fibrosis: a novel mouse model of dermal fibrosis. *Arthritis Res Ther,* 14**,** R194.

STECKELINGS, U. M., LARHED, M., HALLBERG, A., WIDDOP, R. E., JONES, E. S., WALLINDER, C., NAMSOLLECK, P., DAHLÖF, B. & UNGER, T. 2011. Non-peptide AT_2-receptor agonists. *Curr Opin Pharmacol,* 11**,** 187-92.

STRATTON, D., MOORE, C., ZHENG, L., LANGE, S. & INAL, J. 2015. Prostate cancer cells stimulated by calcium-mediated activation of protein kinase C undergo a refractory period before re-releasing calcium-bearing microvesicles. *Biochem Biophys Res Commun,* 460**,** 511-7.

STRUTZ, F., OKADA, H., LO, C. W., DANOFF, T., CARONE, R. L., TOMASZEWSKI, J. E. & NEILSON, E. G. 1995. Identification and characterization of a fibroblast marker: FSP1. *J Cell Biol,* 130**,** 393-405.

STUDER, R., REINECKE, H., MÜLLER, B., HOLTZ, J., JUST, H. & DREXLER, H. 1994. Increased angiotensin-I converting enzyme gene expression in the failing human heart. Quantification by competitive RNA polymerase chain reaction. *J Clin Invest,* 94**,** 301-10.

STUFFERS, S., SEM WEGNER, C., STENMARK, H. & BRECH, A. 2009. Multivesicular endosome biogenesis in the absence of ESCRTs. *Traffic,* 10**,** 925-37.

SUBRA, C., GRAND, D., LAULAGNIER, K., STELLA, A., LAMBEAU, G., PAILLASSE, M., DE MEDINA, P., MONSARRAT, B., PERRET, B., SILVENTE-POIROT, S., POIROT, M. & RECORD, M. 2010. Exosomes account for vesicle-mediated transcellular transport of activatable phospholipases and prostaglandins. *J Lipid Res,* 51**,** 2105-20.

SUO, M., HAUTALA, N., FÖLDES, G., SZOKODI, I., TÓTH, M., LESKINEN, H., UUSIMAA, P., VUOLTEENAHO, O., NEMER, M. & RUSKOAHO, H. 2002. Posttranscriptional control of BNP gene expression in angiotensin II-induced hypertension. *Hypertension,* 39**,** 803-8.

SUZUKI, J., MATSUBARA, H., URAKAMI, M. & INADA, M. 1993. Rat angiotensin II (type 1A) receptor mRNA regulation and subtype expression in myocardial growth and hypertrophy. *Circ Res,* 73**,** 439-47.

SWANEY, J. S., ROTH, D. M., OLSON, E. R., NAUGLE, J. E., MESZAROS, J. G. & INSEL, P. A. 2005. Inhibition of cardiac myofibroblast formation and collagen synthesis by activation and overexpression of adenylyl cyclase. *Proc Natl Acad Sci U S A,* 102**,** 437-42.

TALLANT, E. A., FERRARIO, C. M. & GALLAGHER, P. E. 2005. Angiotensin-(1–7) inhibits growth of cardiac myocytes through activation of the mas receptor. *Am J of Physiol Heart Circ Physiol,* 289**,** H1560-H1566.

TAMARAT, R., SILVESTRE, J. S., DURIE, M. & LEVY, B. I. 2002. Angiotensin II angiogenic effect *in vivo* involves vascular endothelial growth factor- and inflammation-related pathways. *Lab Invest,* 82**,** 747-56.

TAMURA, T., SAID, S. & GERDES, A. M. 1999. Gender-related differences in myocyte remodeling in progression to heart failure. *Hypertension,* 33**,** 676-80.

TAN, L. B., JALIL, J. E., PICK, R., JANICKI, J. S. & WEBER, K. T. 1991. Cardiac myocyte necrosis induced by angiotensin II. *Circ Res,* 69**,** 1185-95.

TANG, H. T., CHENG, D. S., JIA, Y. T., BEN, D. F., MA, B., LV, K. Y., WEI, D., SHENG, Z. Y. & XIA, Z. F. 2009. Angiotensin II induces type I collagen gene expression in human dermal fibroblasts through an AP-1/TGF-beta1-dependent pathway. *Biochem Biophys Res Commun,* 385**,** 418-23.

TANG, R., LI, Q., LV, L., DAI, H., ZHENG, M., MA, K. & LIU, B. 2010. Angiotensin II mediates the high-glucose-induced endothelial-to-mesenchymal transition in human aortic endothelial cells. *Cardiovasc Diabetol,* 9.

TANG, R. N., LV, L. L., ZHANG, J. D., DAI, H. Y., LI, Q., ZHENG, M., NI, J., MA, K. L. & LIU, B. C. 2013. Effects of angiotensin II receptor blocker on myocardial endothelial-to-mesenchymal transition in diabetic rats. *Int J Cardiol,* 162**,** 92-9.

TARIGOPULA, M., DAVIS, R. T., MUNGAI, P. T., RYBA, D. M., WIECZOREK, D. F., COWAN, C. L., VIOLIN, J. D., WOLSKA, B. M. & SOLARO, R. J. 2015. Cardiac myosin light chain phosphorylation and inotropic effects of a biased ligand, TRV120023, in a dilated cardiomyopathy model. *Cardiovasc Res,* 107**,** 226-34.

TATSUKAWA, Y., KIYOSUE, T. & ARITA, M. 1997. Mechanical stretch increases intracellular calcium concentration in cultured ventricular cells from neonatal rats. *Heart Vessels,* 12**,** 128-35.

TAYLOR, D. G., PARILAK, L. D., LEWINTER, M. M. & KNOT, H. J. 2004. Quantification of the rat left ventricle force and Ca^{2+} -frequency relationships: similarities to dog and human. *Cardiovasc Res,* 61**,** 77-86.

TERENTYEV, D., VIATCHENKO-KARPINSKI, S., GYORKE, I., TERENTYEVA, R. & GYORKE, S. 2003. Protein phosphatases decrease sarcoplasmic reticulum calcium content by stimulating calcium release in cardiac myocytes. *J Physiol,* 552**,** 109-18.

THEEUWES, F. & YUM, S. I. 1976. Principles of the design and operation of generic osmotic pumps for the delivery of semisolid or liquid drug formulations. *Ann Biomed Eng,* 4**,** 343-53.

THÉRY, C., AMIGORENA, S., RAPOSO, G. & CLAYTON, A. 2006. Isolation and characterization of exosomes from cell culture supernatants and biological fluids. *Curr Protoc Cell Biol,* Chapter 3**,** Unit 3.22.

TIAN, J., GUO, X., LIU, X. M., LIU, L., WENG, Q. F., DONG, S. J., KNOWLTON, A. A., YUAN, W. J. & LIN, L. 2013a. Extracellular HSP60 induces inflammation through activating and up-regulating TLRs in cardiomyocytes. *Cardiovasc Res,* 98**,** 391-401.

TIAN, T., ZHU, Y. L., HU, F. H., WANG, Y. Y., HUANG, N. P. & XIAO, Z. D. 2013b. Dynamics of exosome internalization and trafficking. *J Cell Physiol,* 228**,** 1487-95.

TIGERSTEDT, R. & BERGMAN, P. Q. 1898. Niere und Kreislauf (in German). *Skandinavisches Archiv Für Physiologie,* 8**,** 223-271.

TILLEY, D. G., NGUYEN, A. D. & ROCKMAN, H. A. 2010. Troglitazone stimulates beta-arrestin-dependent cardiomyocyte contractility via the angiotensin II type 1A receptor. *Biochem Biophys Res Commun,* 396**,** 921-6.

TIPNIS, S. R., HOOPER, N. M., HYDE, R., KARRAN, E., CHRISTIE, G. & TURNER, A. J. 2000. A Human Homolog of Angiotensin-converting Enzyme: cloning and functional expression as a captopril-insensitive carboxypeptidase. *J Biol Chem,* 275**,** 33238-33243.

TIRZIU, D., GIORDANO, F. J. & SIMONS, M. 2010. Cell communications in the heart. *Circulation,* 122**,** 928-37.

TOHGO, A., PIERCE, K. L., CHOY, E. W., LEFKOWITZ, R. J. & LUTTRELL, L. M. 2002. ß-Arrestin scaffolding of the ERK cascade enhances cytosolic ERK activity but inhibits ERK-mediated transcription following angiotensin AT_{1a} receptor stimulation. *J Biol Chem,* 277**,** 9429-36.

TOKUDA, K., KAI, H., KUWAHARA, F., YASUKAWA, H., TAHARA, N., KUDO, H., TAKEMIYA, K., KOGA, M., YAMAMOTO, T. & IMAIZUMI, T. 2004. Pressure-independent effects of angiotensin II on hypertensive myocardial fibrosis. *Hypertension,* 43**,** 499-503.

TOUYZ, R. M. & BERRY, C. 2002. Recent advances in angiotensin II signaling. *Braz J Med Biol Res,* 35**,** 1001-15.

TOUYZ, R. M., CRUZADO, M., TABET, F., YAO, G., SALOMON, S. & SCHIFFRIN, E. L. 2003. Redox-dependent MAP kinase signaling by Ang II in vascular smooth muscle cells: role of receptor tyrosine kinase transactivation. *Can J Physiol Pharmacol,* 81**,** 159-67.

TOUYZ, R. M., FAREH, J., THIBAULT, G., TOLLOCZKO, B., LARIVIÈRE, R. & SCHIFFRIN, E. L. 1996a. Modulation of Ca^{2+} transients in neonatal and adult rat cardiomyocytes by angiotensin II and endothelin-1. *Am J Physiol,* 270**,** H857-68.

TOUYZ, R. M., SVENTEK, P., LARIVIÈRE, R., THIBAULT, G., FAREH, J., REUDELHUBER, T. & SCHIFFRIN, E. L. 1996b. Cytosolic calcium changes induced by angiotensin II in neonatal rat atrial and ventricular cardiomyocytes are mediated via angiotensin II subtype 1 receptors. *Hypertension,* 27**,** 1090-6.

TRAJKOVIC, K., HSU, C., CHIANTIA, S., RAJENDRAN, L., WENZEL, D., WIELAND, F., SCHWILLE, P., BRÜGGER, B. & SIMONS, M. 2008. Ceramide triggers

budding of exosome vesicles into multivesicular endosomes. *Science,* 319**,** 1244-7.

TSUKAMOTO, Y., MANO, T., SAKATA, Y., OHTANI, T., TAKEDA, Y., TAMAKI, S., OMORI, Y., IKEYA, Y., SAITO, Y., ISHII, R., HIGASHIMORI, M., KANEKO, M., MIWA, T., YAMAMOTO, K. & KOMURO, I. 2013. A novel heart failure mice model of hypertensive heart disease by angiotensin II infusion, nephrectomy, and salt loading. *Am J Physiol Heart Circ Physiol,* 305**,** H1658-67.

TSUTSUMI, Y., MATSUBARA, H., MASAKI, H., KURIHARA, H., MURASAWA, S., TAKAI, S., MIYAZAKI, M., NOZAWA, Y., OZONO, R., NAKAGAWA, K., MIWA, T., KAWADA, N., MORI, Y., SHIBASAKI, Y., TANAKA, Y., FUJIYAMA, S., KOYAMA, Y., FUJIYAMA, A., TAKAHASHI, H. & IWASAKA, T. 1999. Angiotensin II type 2 receptor overexpression activates the vascular kinin system and causes vasodilation. *J Clin Invest,* 104**,** 925-35.

TSUTSUMI, Y., MATSUBARA, H., OHKUBO, N., MORI, Y., NOZAWA, Y., MURASAWA, S., KIJIMA, K., MARUYAMA, K., MASAKI, H., MORIGUCHI, Y., SHIBASAKI, Y., KAMIHATA, H., INADA, M. & IWASAKA, T. 1998. Angiotensin II type 2 receptor is upregulated in human heart with interstitial fibrosis, and cardiac fibroblasts are the major cell type for its expression. *Circ Res,* 83**,** 1035-46.

TZIMA, E., IRANI-TEHRANI, M., KIOSSES, W. B., DEJANA, E., SCHULTZ, D. A., ENGELHARDT, B., CAO, G., DELISSER, H. & SCHWARTZ, M. A. 2005. A mechanosensory complex that mediates the endothelial cell response to fluid shear stress. *Nature,* 437**,** 426-31.

URATA, H., HEALY, B., STEWART, R. W., BUMPUS, F. M. & HUSAIN, A. 1990a. Angiotensin II-forming pathways in normal and failing human hearts. *Circ Res,* 66**,** 883-90.

URATA, H., KINOSHITA, A., MISONO, K. S., BUMPUS, F. M. & HUSAIN, A. 1990b. Identification of a highly specific chymase as the major angiotensin II-forming enzyme in the human heart. *J Biol Chem,* 265**,** 22348-57.

VAN ESCH, J. H., GEMBARDT, F., STERNER-KOCK, A., HERINGER-WALTHER, S., LE, T. H., LASSNER, D., STIJNEN, T., COFFMAN, T. M., SCHULTHEISS, H. P., DANSER, A. H. & WALTHER, T. 2010. Cardiac phenotype and angiotensin II levels in AT_{1a}, AT_{1b}, and AT_2 receptor single, double, and triple knockouts. *Cardiovasc Res,* 86**,** 401-9.

VAN ESCH, J. H., SCHUIJT, M. P., SAYED, J., CHOUDHRY, Y., WALTHER, T. & JAN DANSER, A. H. 2006. AT_2 receptor-mediated vasodilation in the mouse heart depends on AT_{1A} receptor activation. *Br J Pharmacol,* 148**,** 452-8.

VAN KATS, J. P., DE LANNOY, L. M., JAN DANSER, A. H., VAN MEEGEN, J. R., VERDOUW, P. D. & SCHALEKAMP, M. A. 1997. Angiotensin II type 1 (AT_1) receptor-mediated accumulation of angiotensin II in tissues and its intracellular half-life *in vivo*. *Hypertension,* 30**,** 42-9.

VAN KATS, J. P., SCHALEKAMP, M. A., VERDOUW, P. D., DUNCKER, D. J. & DANSER, A. H. 2001. Intrarenal angiotensin II: interstitial and cellular levels and site of production. *Kidney Int,* 60**,** 2311-7.

VANDERHEYDEN, M., GOETHALS, M., VERSTREKEN, S., DE BRUYNE, B., MULLER, K., VAN SCHUERBEECK, E. & BARTUNEK, J. 2004. Wall stress modulates

brain natriuretic peptide production in pressure overload cardiomyopathy. *J Am Coll Cardiol,* 44**,** 2349-54.

VASAN, R. S., BEISER, A., SESHADRI, S., LARSON, M. G., KANNEL, W. B., D'AGOSTINO, R. B. & LEVY, D. 2002. Residual lifetime risk for developing hypertension in middle-aged women and men: The Framingham Heart Study. *JAMA,* 287**,** 1003-10.

VASAN, R. S. & LEVY, D. 1996. The role of hypertension in the pathogenesis of heart failure. A clinical mechanistic overview. *Arch Intern Med,* 156**,** 1789-96.

VEGA, R. B., HARRISON, B. C., MEADOWS, E., ROBERTS, C. R., PAPST, P. J., OLSON, E. N. & MCKINSEY, T. A. 2004. Protein kinases C and D mediate agonist-dependent cardiac hypertrophy through nuclear export of histone deacetylase 5. *Mol Cell Biol,* 24**,** 8374-85.

VERDECCHIA, P., PORCELLATI, C., REBOLDI, G., GATTOBIGIO, R., BORGIONI, C., PEARSON, T. A. & AMBROSIO, G. 2001. Left ventricular hypertrophy as an independent predictor of acute cerebrovascular events in essential hypertension. *Circulation,* 104**,** 2039-44.

VICENCIO, J. M., YELLON, D. M., SIVARAMAN, V., DAS, D., BOI-DOKU, C., ARJUN, S., ZHENG, Y., RIQUELME, J. A., KEARNEY, J., SHARMA, V., MULTHOFF, G., HALL, A. R. & DAVIDSON, S. M. 2015. Plasma exosomes protect the myocardium from ischemia-reperfusion injury. *J Am Coll Cardiol,* 65**,** 1525-36.

VILAS-BOAS, W. W., RIBEIRO-OLIVEIRA, A., PEREIRA, R. M., RIBEIRO, R. A. C., ALMEIDA, J., NADU, A. P., SIMÕES E SILVA, A. C. & DOS SANTOS, R. A. 2009. Relationship between angiotensin-(1-7) and angiotensin II correlates with hemodynamic changes in human liver cirrhosis. *World J Gastroenterol,* 15**,** 2512-9.

VIOLIN, J. D., DEWIRE, S. M., YAMASHITA, D., ROMINGER, D. H., NGUYEN, L., SCHILLER, K., WHALEN, E. J., GOWEN, M. & LARK, M. W. 2010. Selectively engaging β-arrestins at the angiotensin II type 1 receptor reduces blood pressure and increases cardiac performance. *J Pharmacol Exp Ther,* 335**,** 572-9.

VLIEGEN, H. W., VAN DER LAARSE, A., CORNELISSE, C. J. & EULDERINK, F. 1991. Myocardial changes in pressure overload-induced left ventricular hypertrophy. A study on tissue composition, polyploidization and multinucleation. *Eur Heart J,* 12**,** 488-94.

VON THUN, A. M., VARI, R. C., EL-DAHR, S. S. & NAVAR, L. G. 1994. Augmentation of intrarenal angiotensin II levels by chronic angiotensin II infusion. *Am J Physiol,* 266**,** F120-8.

WAGNER, S., DANTZ, C., FLEBBE, H., AZIZIAN, A., SAG, C. M., ENGELS, S., MÖLLENCAMP, J., DYBKOVA, N., ISLAM, T., SHAH, A. M. & MAIER, L. S. 2014. NADPH oxidase 2 mediates angiotensin II-dependent cellular arrhythmias via PKA and CaMKII. *J Mol Cell Cardiol,* 75**,** 206-15.

WALDENSTRÖM, A., GENNEBÄCK, N., HELLMAN, U. & RONQUIST, G. 2012. Cardiomyocyte microvesicles contain DNA/RNA and convey biological messages to target cells. *PLoS One,* 7**,** e34653.

WALKER, J. M. 1994. The bicinchoninic acid (BCA) assay for protein quantitation. *Methods Mol Biol,* 32**,** 5-8.

WALTHER, T., MENRAD, A., ORZECHOWSKI, H. D., SIEMEISTER, G., PAUL, M. & SCHIRNER, M. 2003. Differential regulation of *in vivo* angiogenesis by angiotensin II receptors. *FASEB J,* 17**,** 2061-7.

WANG, J. M., BAUDHUIN, P., COURTOY, P. J. & DE POTTER, W. 1995. Conversion of angiotensin II into active fragments by an endosomal pathway in bovine adrenal medullary cells in primary culture. *Endocrinology,* 136**,** 5274-82.

WANG, R., WANG, Y., LIN, W. K., ZHANG, Y., LIU, W., HUANG, K., TERRAR, D. A., SOLARO, R. J., WANG, X., KE, Y. & LEI, M. 2014. Inhibition of angiotensin II-induced cardiac hypertrophy and associated ventricular arrhythmias by a p21 activated kinase 1 bioactive peptide. *PLoS One,* 9**,** e101974.

WANG, W., HUANG, X. R., CANLAS, E., OKA, K., TRUONG, L. D., DENG, C., BHOWMICK, N. A., JU, W., BOTTINGER, E. P. & LAN, H. Y. 2006. Essential role of Smad3 in angiotensin II-induced vascular fibrosis. *Circ Res,* 98**,** 1032-9.

WANG, Z. Q., MOORE, A. F., OZONO, R., SIRAGY, H. M. & CAREY, R. M. 1998. Immunolocalization of subtype 2 angiotensin II (AT_2) receptor protein in rat heart. *Hypertension,* 32**,** 78-83.

WATKINS, S. J., BORTHWICK, G. M., OAKENFULL, R., ROBSON, A. & ARTHUR, H. M. 2012. Angiotensin II-induced cardiomyocyte hypertrophy in vitro is TAK1-dependent and Smad2/3-independent. *Hypertens Res,* 35**,** 393-8.

WEBER, K. T., JANICKI, J. S., SHROFF, S. G., PICK, R., CHEN, R. M. & BASHEY, R. I. 1988. Collagen remodeling of the pressure-overloaded, hypertrophied nonhuman primate myocardium. *Circ Res,* 62**,** 757-65.

WEBER, K. T., PICK, R., JALIL, J. E., JANICKI, J. S. & CARROLL, E. P. 1989. Patterns of myocardial fibrosis. *J Mol Cell Cardiol,* 21 Suppl 5**,** 121-31.

WEBER, K. T., SUN, Y., BHATTACHARYA, S. K., AHOKAS, R. A. & GERLING, I. C. 2013. Myofibroblast-mediated mechanisms of pathological remodelling of the heart. *Nat Rev Cardiol,* 10**,** 15-26.

WEI, H., AHN, S., SHENOY, S. K., KARNIK, S. S., HUNYADY, L., LUTTRELL, L. M. & LEFKOWITZ, R. J. 2003. Independent ß-arrestin 2 and G protein-mediated pathways for angiotensin II activation of extracellular signal-regulated kinases 1 and 2. *Proc Natl Acad Sci U S A,* 100**,** 10782-7.

WEI, L., ALHENC-GELAS, F., CORVOL, P. & CLAUSER, E. 1991. The two homologous domains of human angiotensin I-converting enzyme are both catalytically active. *J Biol Chem,* 266**,** 9002-8.

WEINBERG, E. O., LEE, M. A., WEIGNER, M., LINDPAINTNER, K., BISHOP, S. P., BENEDICT, C. R., HO, K. K., DOUGLAS, P. S., CHAFIZADEH, E. & LORELL, B. H. 1997. Angiotensin AT_1 receptor inhibition. Effects on hypertrophic remodeling and ACE expression in rats with pressure-overload hypertrophy due to ascending aortic stenosis. *Circulation,* 95**,** 1592-600.

WELCH-REARDON, K. M., WU, N. & HUGHES, C. C. 2015. A role for partial endothelial-mesenchymal transitions in angiogenesis? *Arterioscler Thromb Vasc Biol,* 35**,** 303-8.

WESTERMANN, D., LINDNER, D., KASNER, M., ZIETSCH, C., SAVVATIS, K., ESCHER, F., VON SCHLIPPENBACH, J., SKURK, C., STEENDIJK, P., RIAD, A., POLLER, W., SCHULTHEISS, H. P. & TSCHÖPE, C. 2011. Cardiac inflammation contributes to changes in the extracellular matrix in patients with heart failure and normal ejection fraction. *Circ Heart Fail,* 4**,** 44-52.

WHELAN, R. S., KAPLINSKIY, V. & KITSIS, R. N. 2010. Cell death in the pathogenesis of heart disease: mechanisms and significance. *Annu Rev Physiol,* 72**,** 19-44.

WHO. 2013. *World Health Organisation: A global brief on hypertension* [Online]. Available: http://apps.who.int/iris/bitstream/10665/79059/1/WHO_DCO_WHD_2013.2_eng.pdf [Accessed 01/05/2013].

WHO. 2014a. *World Health Organization: Raised blood pressure data by WHO region* [Online]. Available: http://apps.who.int/gho/data/view.main.2540?lang=en [Accessed 14/03/2016].

WHO. 2014b. *World Health Organization: Global Status Report on noncommunicable diseases 2014* [Online]. Available: http://apps.who.int/iris/bitstream/10665/148114/1/9789241564854_eng.pdf?ua=1 [Accessed 14/03/2016].

WIDDOP, R. E., MATROUGUI, K., LEVY, B. I. & HENRION, D. 2002. AT_2 receptor-mediated relaxation is preserved after long-term AT_1 receptor blockade. *Hypertension,* 40**,** 516-20.

WIDYANTORO, B., EMOTO, N., NAKAYAMA, K., ANGGRAHINI, D. W., ADIARTO, S., IWASA, N., YAGI, K., MIYAGAWA, K., RIKITAKE, Y., SUZUKI, T., KISANUKI, Y. Y., YANAGISAWA, M. & HIRATA, K.-I. 2010. Endothelial Cell-Derived Endothelin-1 Promotes Cardiac Fibrosis in Diabetic Hearts Through Stimulation of Endothelial-to-Mesenchymal Transition. *Circulation,* 121**,** 2407-U88.

WILLEMS, I. E., HAVENITH, M. G., DE MEY, J. G. & DAEMEN, M. J. 1994. The alpha-smooth muscle actin-positive cells in healing human myocardial scars. *Am J Pathol,* 145**,** 868-75.

WITWER, K. W., BUZÁS, E. I., BEMIS, L. T., BORA, A., LÄSSER, C., LÖTVALL, J., NOLTE-'T HOEN, E. N., PIPER, M. G., SIVARAMAN, S., SKOG, J., THÉRY, C., WAUBEN, M. H. & HOCHBERG, F. 2013. Standardization of sample collection, isolation and analysis methods in extracellular vesicle research. *J Extracell Vesicles,* 2.

WOLF, K., DELLA BRUNA, R., BRUCKSCHLEGEL, G., SCHUNKERT, H., RIEGGER, G. A. & KURTZ, A. 1996. Angiotensin II receptor gene expression in hypertrophied left ventricles of rat hearts. *J Hypertens,* 14**,** 349-54.

WOLF, P. 1967. The nature and significance of platelet products in human plasma. *Br J Haematol,* 13**,** 269-88.

WOLLERT, T. & HURLEY, J. H. 2010. Molecular mechanism of multivesicular body biogenesis by ESCRT complexes. *Nature,* 464**,** 864-9.

WRIGHT, C. S. 1984. Structural comparison of the two distinct sugar binding sites in wheat germ agglutinin isolectin II. *J Mol Biol,* 178**,** 91-104.

WRIGHT, M. 2012. Nanoparticle tracking analysis for the multiparameter characterization and counting of nanoparticle suspensions. *Methods Mol Biol,* 906**,** 511-24.

WU, X., ZHANG, T., BOSSUYT, J., LI, X., MCKINSEY, T. A., DEDMAN, J. R., OLSON, E. N., CHEN, J., BROWN, J. H. & BERS, D. M. 2006. Local InsP3-dependent perinuclear Ca^{2+} signaling in cardiac myocyte excitation-transcription coupling. *J Clin Invest,* 116**,** 675-82.

WYLIE-SEARS, J., LEVINE, R. A. & BISCHOFF, J. 2014. Losartan inhibits endothelial-to-mesenchymal transformation in mitral valve endothelial cells by blocking transforming growth factor-ß-induced phosphorylation of ERK. *Biochem Biophys Res Commun,* 446**,** 870-5.

WYSOCKI, J., YE, M., RODRIGUEZ, E., GONZÁLEZ-PACHECO, F. R., BARRIOS, C., EVORA, K., SCHUSTER, M., LOIBNER, H., BROSNIHAN, K. B., FERRARIO, C. M., PENNINGER, J. M. & BATLLE, D. 2010. Targeting the degradation of angiotensin II with recombinant angiotensin-converting enzyme 2: prevention of angiotensin II-dependent hypertension. *Hypertension,* 55**,** 90-8.

XIA, Y., LEE, K., LI, N., CORBETT, D., MENDOZA, L. & FRANGOGIANNIS, N. G. 2009. Characterization of the inflammatory and fibrotic response in a mouse model of cardiac pressure overload. *Histochem Cell Biol,* 131**,** 471-81.

XIAO, F., PUDDEFOOT, J. R. & VINSON, G. P. 2000. The expression of renin and the formation of angiotensin II in bovine aortic endothelial cells. *J Endocrinol,* 164**,** 207-14.

XIAO, R. P. & LAKATTA, E. G. 1993. Beta 1-adrenoceptor stimulation and beta 2-adrenoceptor stimulation differ in their effects on contraction, cytosolic Ca2+, and Ca2+ current in single rat ventricular cells. *Circ Res,* 73**,** 286-300.

XU, J., SUN, Y., CARRETERO, O. A., ZHU, L., HARDING, P., SHESELY, E. G., DAI, X., RHALEB, N. E., PETERSON, E. & YANG, X. P. 2014. Effects of Cardiac Overexpression of the Angiotensin II Type 2 Receptor on Remodeling and Dysfunction in Mice Post-Myocardial Infarction. *Hypertension,* 63**,** 1251-9.

XU, P., COSTA-GONCALVES, A. C., TODIRAS, M., RABELO, L. A., SAMPAIO, W. O., MOURA, M. M., SANTOS, S. S., LUFT, F. C., BADER, M., GROSS, V., ALENINA, N. & SANTOS, R. A. 2008. Endothelial dysfunction and elevated blood pressure in MAS gene-deleted mice. *Hypertension,* 51**,** 574-80.

XU, X., FRIEHS, I., ZHONG HU, T., MELNYCHENKO, I., TAMPE, B., ALNOUR, F., IASCONE, M., KALLURI, R., ZEISBERG, M., DEL NIDO, P. J. & ZEISBERG, E. M. 2015. Endocardial fibroelastosis is caused by aberrant endothelial to mesenchymal transition. *Circ Res,* 116**,** 857-66.

YAMADA, K., IYER, S. N., CHAPPELL, M. C., GANTEN, D. & FERRARIO, C. M. 1998a. Converting Enzyme Determines Plasma Clearance of Angiotensin-(1–7). *Hypertension,* 32**,** 496-502.

YAMADA, T., AKISHITA, M., POLLMAN, M. J., GIBBONS, G. H., DZAU, V. J. & HORIUCHI, M. 1998b. Angiotensin II type 2 receptor mediates vascular smooth muscle cell apoptosis and antagonizes angiotensin II type 1 receptor action: an *in vitro* gene transfer study. *Life Sci,* 63**,** PL289-95.

YAMADA, T., HORIUCHI, M. & DZAU, V. J. 1996. Angiotensin II type 2 receptor mediates programmed cell death. *Proc Natl Acad Sci U S A,* 93**,** 156-60.

YAMAMOTO, K., CHAPPELL, M. C., BROSNIHAN, K. B. & FERRARIO, C. M. 1992. *In vivo* metabolism of angiotensin I by neutral endopeptidase (EC 3.4.24.11) in spontaneously hypertensive rats. *Hypertension,* 19**,** 692-6.

YAMAZAKI, T., KOMURO, I., KUDOH, S., ZOU, Y., NAGAI, R., AIKAWA, R., UOZUMI, H. & YAZAKI, Y. 1998. Role of ion channels and exchangers in mechanical stretch-induced cardiomyocyte hypertrophy. *Circ Res,* 82**,** 430-7.

YAN, X., PRICE, R. L., NAKAYAMA, M., ITO, K., SCHULDT, A. J., MANNING, W. J., SANBE, A., BORG, T. K., ROBBINS, J. & LORELL, B. H. 2003. Ventricular-specific expression of angiotensin II type 2 receptors causes dilated cardiomyopathy and heart failure in transgenic mice. *Am J Physiol Heart Circ Physiol,* 285**,** H2179-87.

YANG, B., LARSON, D. F. & RANGER-MOORE, J. 2013a. Biphasic change of tau (τ) in mice as arterial load acutely increased with phenylephrine injection. *PLoS One,* 8**,** e60580.

YANG, B. C., PHILLIPS, M. I., AMBUEHL, P. E., SHEN, L. P., MEHTA, P. & MEHTA, J. L. 1997. Increase in angiotensin II type 1 receptor expression immediately after ischemia-reperfusion in isolated rat hearts. *Circulation,* 96**,** 922-6.

YANG, F., CHUNG, A. C., HUANG, X. R. & LAN, H. Y. 2009. Angiotensin II induces connective tissue growth factor and collagen I expression via transforming growth factor-beta-dependent and -independent Smad pathways: the role of Smad3. *Hypertension,* 54**,** 877-84.

YANG, F., HUANG, X. R., CHUNG, A. C., HOU, C. C., LAI, K. N. & LAN, H. Y. 2010. Essential role for Smad3 in angiotensin II-induced tubular epithelial-mesenchymal transition. *J Pathol,* 221**,** 390-401.

YANG, J., ZHU, H. H., CHEN, G. P., YE, Y., ZHAO, C. Z., MOU, Y. & HU, S. J. 2013b. Inhibition of farnesyl pyrophosphate synthase attenuates angiotensin II-induced cardiac hypertrophy and fibrosis *in vivo*. *Int J Biochem Cell Biol,* 45**,** 657-66.

YANG, X. H., WANG, Y. H., WANG, J. J., LIU, Y. C., DENG, W., QIN, C., GAO, J. L. & ZHANG, L. Y. 2012. Role of angiotensin-converting enzyme (ACE and ACE2) imbalance on tourniquet-induced remote kidney injury in a mouse hindlimb ischemia-reperfusion model. *Peptides,* 36**,** 60-70.

YOKOTA, N., BRUNEAU, B. G., FERNANDEZ, B. E., DE BOLD, M. L., PIAZZA, L. A., EID, H. & DE BOLD, A. J. 1995. Dissociation of cardiac hypertrophy, myosin heavy chain isoform expression, and natriuretic peptide production in DOCA-salt rats. *Am J Hypertens,* 8**,** 301-10.

YOSHIDA, L. S. & TSUNAWAKI, S. 2008. Expression of NADPH oxidases and enhanced H(2)O(2)-generating activity in human coronary artery endothelial cells upon induction with tumor necrosis factor-alpha. *Int Immunopharmacol,* 8**,** 1377-85.

YOSHIMATSU, Y. & WATABE, T. 2011. Roles of TGF-ß signals in endothelial-mesenchymal transition during cardiac fibrosis. *Int J Inflam,* 2011**,** 724080.

YU, H., GAO, J., WANG, H., WYMORE, R., STEINBERG, S., MCKINNON, D., ROSEN, M. R. & COHEN, I. S. 2000. Effects of the renin-angiotensin system on the current I(to) in epicardial and endocardial ventricular myocytes from the canine heart. *Circ Res,* 86**,** 1062-8.

YUSUF, S., SLEIGHT, P., POGUE, J., BOSCH, J., DAVIES, R. & DAGENAIS, G. 2000. Effects of an angiotensin-converting-enzyme inhibitor, ramipril, on cardiovascular events in high-risk patients. The Heart Outcomes Prevention Evaluation Study Investigators. *N Engl J Med,* 342**,** 145-53.

ZAMAN, M. A., OPARIL, S. & CALHOUN, D. A. 2002. Drugs targeting the renin-angiotensin-aldosterone system. *Nat Rev Drug Discov,* 1**,** 621-36.

ZANKOV, D. P., OMATSU-KANBE, M., ISONO, T., TOYODA, F., DING, W. G., MATSUURA, H. & HORIE, M. 2006. Angiotensin II potentiates the slow component of delayed rectifier K^+ current via the AT_1 receptor in guinea pig atrial myocytes. *Circulation,* 113**,** 1278-86.

ZEISBERG, E. M., POTENTA, S., XIE, L., ZEISBERG, M. & KALLURI, R. 2007a. Discovery of endothelial to mesenchymal transition as a source for carcinoma-associated fibroblasts. *Cancer Research,* 67**,** 10123-10128.

ZEISBERG, E. M., POTENTA, S. E., SUGIMOTO, H., ZEISBERG, M. & KALLURI, R. 2008. Fibroblasts in Kidney Fibrosis Emerge via Endothelial-to-Mesenchymal Transition. *Journal of the American Society of Nephrology,* 19**,** 2282-2287.

ZEISBERG, E. M., TARNAVSKI, O., ZEISBERG, M., DORFMAN, A. L., MCMULLEN, J. R., GUSTAFSSON, E., CHANDRAKER, A., YUAN, X., PU, W. T., ROBERTS, A. B., NEILSON, E. G., SAYEGH, M. H., IZUMO, S. & KALLURI, R. 2007b. Endothelial-to-mesenchymal transition contributes to cardiac fibrosis. *Nature Medicine,* 13**,** 952-961.

ZEISBERG, M., YANG, C., MARTINO, M., DUNCAN, M. B., RIEDER, F., TANJORE, H. & KALLURI, R. 2007c. Fibroblasts derive from hepatocytes in liver fibrosis via epithelial to mesenchymal transition. *J Biol Chem,* 282**,** 23337-47.

ZENTILIN, L., PULIGADDA, U., LIONETTI, V., ZACCHIGNA, S., COLLESI, C., PATTARINI, L., RUOZI, G., CAMPORESI, S., SINAGRA, G., PEPE, M., RECCHIA, F. A. & GIACCA, M. 2010. Cardiomyocyte VEGFR-1 activation by VEGF-B induces compensatory hypertrophy and preserves cardiac function after myocardial infarction. *FASEB J,* 24**,** 1467-78.

ZHAI, P., GALEOTTI, J., LIU, J., HOLLE, E., YU, X., WAGNER, T. & SADOSHIMA, J. 2006. An angiotensin II type 1 receptor mutant lacking epidermal growth factor receptor transactivation does not induce angiotensin II-mediated cardiac hypertrophy. *Circ Res,* 99**,** 528-36.

ZHANG, H., SCHMEISSER, A., GARLICHS, C. D., PLÖTZE, K., DAMME, U., MÜGGE, A. & DANIEL, W. G. 1999. Angiotensin II-induced superoxide anion generation in human vascular endothelial cells: role of membrane-bound NADH-/NADPH-oxidases. *Cardiovasc Res,* 44**,** 215-22.

ZHANG, M. & SHAH, A. M. 2014. ROS signalling between endothelial cells and cardiac cells. *Cardiovasc Res,* 102**,** 249-57.

ZHANG, W., LAVINE, K. J., EPELMAN, S., EVANS, S. A., WEINHEIMER, C. J., BARGER, P. M. & MANN, D. L. 2015. Necrotic myocardial cells release damage-associated molecular patterns that provoke fibroblast activation

in vitro and trigger myocardial inflammation and fibrosis *in vivo*. *J Am Heart Assoc,* 4**,** e001993.

ZHAO, Q., ISHIBASHI, M., HIASA, K., TAN, C., TAKESHITA, A. & EGASHIRA, K. 2004. Essential role of vascular endothelial growth factor in angiotensin II-induced vascular inflammation and remodeling. *Hypertension,* 44**,** 264-70.

ZHENG, H., PU, S. Y., FAN, X. F., LI, X. S., ZHANG, Y., YUAN, J., ZHANG, Y. F. & YANG, J. L. 2015. Treatment with angiotensin-(1-9) alleviates the cardiomyopathy in streptozotocin-induced diabetic rats. *Biochem Pharmacol,* 95**,** 38-45.

ZHONG, J., BASU, R., GUO, D., CHOW, F. L., BYRNS, S., SCHUSTER, M., LOIBNER, H., WANG, X. H., PENNINGER, J. M., KASSIRI, Z. & OUDIT, G. Y. 2010. Angiotensin-converting enzyme 2 suppresses pathological hypertrophy, myocardial fibrosis, and cardiac dysfunction. *Circulation,* 122**,** 717-28, 18 p following 728.

ZHOU, L., XUE, H., YUAN, P., NI, J., YU, C., HUANG, Y. & LU, L. M. 2010. Angiotensin AT_1 receptor activation mediates high glucose-induced epithelial-mesenchymal transition in renal proximal tubular cells. *Clin Exp Pharmacol Physiol,* 37**,** e152-7.

ZHOU, P., CHENG, C. P., LI, T., FERRARIO, C. M. & CHENG, H. J. 2015. Modulation of cardiac L-type Ca^{2+} current by angiotensin-(1-7): normal versus heart failure. *Ther Adv Cardiovasc Dis,* 9**,** 342-53.

ZHUO, J. L., IMIG, J. D., HAMMOND, T. G., ORENGO, S., BENES, E. & NAVAR, L. G. 2002. Ang II accumulation in rat renal endosomes during Ang II-induced hypertension: role of AT(1) receptor. *Hypertension,* 39**,** 116-21.

ZHUO, J. L., LI, X. C., GARVIN, J. L., NAVAR, L. G. & CARRETERO, O. A. 2006. Intracellular ANG II induces cytosolic Ca^{2+} mobilization by stimulating intracellular AT_1 receptors in proximal tubule cells. *Am J Physiol Renal Physiol,* 290**,** F1382-90.

ZILE, M. R., BAICU, C. F. & GAASCH, W. H. 2004. Diastolic heart failure--abnormalities in active relaxation and passive stiffness of the left ventricle. *N Engl J Med,* 350**,** 1953-9.

ZISMAN, L. S., MEIXELL, G. E., BRISTOW, M. R. & CANVER, C. C. 2003. Angiotensin-(1-7) formation in the intact human heart: *in vivo* dependence on angiotensin II as substrate. *Circulation,* 108**,** 1679-81.

ZOU, L. X., IMIG, J. D., HYMEL, A. & NAVAR, L. G. 1998. Renal uptake of circulating angiotensin II in Val^5-angiotensin II infused rats is mediated by AT_1 receptor. *Am J Hypertens,* 11**,** 570-8.

ZOU, L. X., IMIG, J. D., VON THUN, A. M., HYMEL, A., ONO, H. & NAVAR, L. G. 1996. Receptor-mediated intrarenal angiotensin II augmentation in angiotensin II-infused rats. *Hypertension,* 28**,** 669-77.

ZOU, Y., AKAZAWA, H., QIN, Y., SANO, M., TAKANO, H., MINAMINO, T., MAKITA, N., IWANAGA, K., ZHU, W., KUDOH, S., TOKO, H., TAMURA, K., KIHARA, M., NAGAI, T., FUKAMIZU, A., UMEMURA, S., IIRI, T., FUJITA, T. & KOMURO, I. 2004. Mechanical stress activates angiotensin II type 1 receptor without the involvement of angiotensin II. *Nat Cell Biol,* 6**,** 499-506.

ZOU, Z., YAN, Y., SHU, Y., GAO, R., SUN, Y., LI, X., JU, X., LIANG, Z., LIU, Q., ZHAO, Y., GUO, F., BAI, T., HAN, Z., ZHU, J., ZHOU, H., HUANG, F., LI, C., LU, H., LI, N., LI, D., JIN, N., PENNINGER, J. M. & JIANG, C. 2014. Angiotensin-converting enzyme 2 protects from lethal avian influenza A H5N1 infections. *Nat Commun,* 5**,** 3594.